Loughborough
University

University Library

Author/Filing Title ....HO..........

....

Class Mark ....T..........

Please note that fines are charged on ALL overdue items.

FOR REFERENCE ONLY

0402889452

DYNAMIC RUGGEDIZING OF PRINTED CIRCUIT BOARDS IN HARSH ENVIRONMENTAL CONDITIONS USING A WIDE-BAND DYNAMIC ABSORBER

by

VAN CUONG HO

Doctoral Thesis submitted in partial fulfilment of the requirements for the award of Doctor of Philosophy of Loughborough University

May 2003

© by V C Ho 2003

Loughborough
University
Pilkington Library

Date Feb 04

Class

Acc
No. 040288945

ACKNOWLEDGEMENTS

I wish to express my gratitude to Engineering Faculty of Loughborough University for its financial support. I am also deeply indebted to Dr Veprik and Professor Babitsky for their help comments, suggestions and continued encouragement during the development of this project. Their aid in the furthering of my understanding in the field of dynamics is greatly appreciated and has given me a real interest in this area of engineering.

Finally, I would like to thank Mechanical Department of Loughborough University for carrying out a series of specialist tests and its laboratory technicians for providing me with technical assistance and using the test equipment

ABSTRACT

The existing approaches to ruggedizing inherently fragile and sensitive critical components of electronic equipment such as printed circuit boards (PCB) for use in hostile industrial and military environment are either insufficient or quite expensive.

This Thesis addresses a novel approach towards ruggedizing commercially-off-the-shelf PCBs using a miniature wide-band dynamic absorber aimed at essential suppressing of the resonant responses of the original structure. The development of an optimisation technique is based on the dynamic properties of the original system, where the mass, stiffness and damping properties of the dynamic absorber are chosen in such a fashion to minimise the level of vibration experienced by the system.

The optimisation procedure relies on the analytical solution and computational resources. The results of the proposed single-mode and full-mode approximation are proven experimentally under random vibration. Further study of the dynamic absorber is achieved by considering the system under swept-sine and shock excitations. This approach eventually focuses on the universal performance of the optimal dynamic absorber.

The unprotected PCB shows a power spectrum density of relative deflection of 312 μm RMS When exposed to a typical excitation level of 14 g RMS. The analytical testing shows that a value of 78 μm RMS is theoretically achievable, while experimental work is achieved a value of 79 μm RMS. The same optimal absorber has also achieved the reduction of the resonant peak value from 4617 μm down to 190 μm for the relative deflection under 10 g peak swept-sine excitation while the time settling under half-sine shock (200 g peak at 3 ms) is improved by 90% which are close to theoretical prediction. In addition, the optimal design dynamic absorber that designed for the critical area is also suppressed almost critical resonances of the entire PCB. This work is also backed up by comparison between analytical solutions and experimental results under random vibration.

Further study of the dynamic absorber is achieved by using Matlab/ Simulink to model the system in time domain. This approach focuses on the improvement in the endurance life and reliability of the PCB under random vibration.

In this Thesis, the author considers the performance delivered by the linear and nonlinear vibroimpact wide-band dynamic absorbers or impact damper under typical wide-band random, swept-sine and shock excitation. The attractions of these simple devices and computer resources have brought in the attention of additional work. The effective, predictability, robustness and sensitivity of impact damper are discussed through the illustration of numerical simulation performed by Matlab/Simulink. The interesting results are based on realistic model of visco-elastic collision. A similar performance is achieved in terms of overall relative deflection, peak deflection and time settling in the corresponding of random vibration, swept-sine and shock excitation, respectively as compared to the performance of dynamic absorber

The results of the analytical study are backed up by the full-scale experiment. The experimental work is carried out with the use of a rattling ball bearing to illustrate the universal performance and simplicity of the impact damper. A close correlation between numerically simulated predictions and experimental results increases the validity and accuracy of modelling of an actual system. As it is shown, the performance of impact damper is almost similar to the performance of the optimal dynamic absorber. This indicates that the lowest cost solution can also achieve the same performance as compared to linear dynamic absorber.

CONTENT

1.0 INTRODUCTION 1
1.1 VIBRATION ISOLATION 2
1.2 DAMPING TREATMENT 3
1.3 STIFFENING FRAME 3
1.4 BUMPERED VIBRATION CONTROL 4
1.5 LINEAR DYNAMIC ABSORBER 5
1.6 IMPACT DYNAMIC ABSORBER 8
1.7 OBJECTIVES 9
2.0 DYNAMIC PROPERTIES OF A PCB 12
2.1 PCB AND MOUNTING 12
2.2 EXPERIMENTAL RIG 13
2.3 CURVE-FITTING OF RESULTS 19
2.4 DETERMINING THE EFFECTIVE MASS OF PCB 25
2.5 ADDITIONAL MEASUREMENT 26
2.6 MEASUREMENT OF RECEPTANCE 29
2.6.1 Local receptance 29
2.6.2 Transient receptance measurement 31
2.8 CONCLUDING REMARKS 35
3.0 SINGLE-MODE MODEL OF PCB WITH DYNAMIC ABSORBER ATTACHED 36
3.1 MATHEMATICAL MODEL 36
3.2 RANDOM VIBRATION 38
3.2.1 Designing MS®Excel worksheet for minimising overall relative deflection 39
3.2.2 Sensitivity analysis 49
3.2.3 Fatigue analysis 51
3.2.4 Numerical simulation 54
3.3 SINE VIBRATION 63
3.3.1 Designing MS®Excel worksheet for minisming peak relative deflection 64
3.3.2 Sensitivity analysis 69
3.3.3 Numerical simulation 71
3.4 SHOCK 76
3.5 CONCLUDING REMARKS 81
4.0 FULL-MODE MODEL OF PCB WITH DYNAMIC ABSORBER ATTACHED 83
4.1 MATHEMATICAL MODEL 84
4.2 RANDOM VIBRATION 85

4.2.1 Designing MS$^{®}$Excel worksheet for minimising overall relative deflection *85*
4.2.2 Sensitivity analysis *90*
4.2.3 Additional measurement *96*
4.2.4 Global curve-fitting of results *101*
4.2.5 Numerical simulation *108*
4.3 SINE VIBRATION 115
4.3.1 Designing MS$^{®}$Excel worksheet for minimising peak relative deflection *115*
4.3.2 Sensitivity analysis *120*
4.3.3 Numerical simulation *122*
4.4 SHOCK 126
4.5 CONCLUDING REMARKS 129
5.0 IMPACT DYNAMIC ABSORBER 130
5.1 MODELLING OF VISCO-ELASTIC IMPACT 130
5.2 RANDOM VIBRATION 134
5.2.1 Dynamics of PCB in a |SDOF approximation with impact damper *134*
5.2.2 Minimising the overall relative deflection of the PCB *138*
5.2.3 Sensitivity analysis *143*
5.2.4 PCB with impact damper (full-mode model) *151*
5.3 SINE VIBRATION 157
5.3.1 Sensitivity analysis *159*
5.4 SHOCK 164
5.5 CONCLUDING REMARKS 167
6.0 EXPERIMENTAL VALIDATION 169
6.1 DYNAMIC PROPERTIES OF DYNAMIC ABSORBER 169
6.2 COMBINED SYSTEM 173
6.2.1 Random vibration *175*
Additional measurement *180*
6.2.2 Sine vibration *183*
6.2.3 Shock *189*
6.3 CONCLUDING REMARKS 194
6.4 SOME PRACTICAL CONSIDERATIONS 194
6.5 EXPERIMENTAL VALIDATION FOR IMPACT DAMPER 197
7.0 CONCLUSIONS 205
8.0 SUGGESTIONS FOR FURTHER WORK 206
9.0 REFERENCES 207

LIST OF FIGURES AND TABLES

Figure 2.0. Typical PCB mounting 12
Figure 2.1. Vibration test Rig 15
Figure 2.2. Random vibration profile from vibration control screen 17
Figure 2.3. Analyser screenshot of universal absolute transmissibility of PCB 17
Figure 2.4. Experimentally measured transmissibilities of PCB 19
Figure 2.5. Finite Element Analysis of PCB with supported corners 20
Figure 2.6. SDOF system 21
Figure 2.7. Curve-fitting using the Solver function. 23
Figure 2.8. Comparison absolute transmissibility of first-mode PCB 24
Figure 2.9. Experimentally measured modulus of absolute transmissibility of PCB 25
Figure 2.10. Schematic layout of the PCB marked with observation point 26
Figure 2.11a. Experimentally measured modulus of universal transmissibilities at different observation points on PCB 27
Figure 2.11b. Experimentally measured phase of absolute transmissibility at different observation points on PCB 28
Figure 2.12. Experimental rig for measuring local receptance of PCB 30
Figure 2.13.Experimentally measured receptance and absolute transmissibility of PCB 31
Figure 2.14. Schematic layout of measuring transient receptance on PCB 31
Figure 2.15a. Experimental measured modulus of receptance at different observation points on PCB 32
Figure 2.15b. Experimental measured phase of receptance at different observation points on PCB 33
Figure 3.0. Model of PCB in a single-mode approximation with attached dynamic absorber 37
Figure 3.1. Spreadsheet for calculation of dynamic response and for optimisation 40
Figure 3.2. Dynamic response of PCB at different mass ratios 41
Figure 3.3. Optimal overall relative deflection of PCB at different mass ratios 42
Figure 3.4. Ratio of optimal overall relative deflection of PCB at different mass ratios 43
Figure 3.5. Optimal parameters of dynamic absorber at different mass ratios 43
Figure 3.6. Dynamic response of the original and ruggedized PCB 44
Figure 3.7. Comparison of traditional and novel optimal parameters of dynamic absorber 45
Figure 3.8. Dynamic response of the PCB at different mass ratio 46
Figure 3.9. Comparison of dynamic response in the case of traditional and novel design 47
Figure 4.10. Comparison of dynamic response in the case of traditional and novel design 48
Figure 3.11. Sensitivity analysis 50
Figure 3.12. Fatigue analysis using simple cycles technique 53
Figure 3.13. Simulink diagram for random excitation 55
Figure 3.14. Random vibration excitation 56
Table 3.0. Comparison of the increased life factor between the simple cycle and overall technique 57
Figure 3.15a. Simulated time history of original and ruggedized PCB (with η=65%) 58

Figure 3.15b. Simulated time history of original and ruggedized PCB (with η=35%)....................................59
Figure 3.16. Simulated PSD of base acceleration 60
Figure 3.17. Simulated dynamic response of original and ruggedized PCB (η=65%) 61
Figure 3.18. Comparison of dynamic response of ruggedized PCB (η=65%)..62
Figure 3.19. Spreadsheet for calculation of dynamic response and for optimisation.......................................64
Figure 3.20. Dynamic response of PCB with different mass ratios 65
Figure 3.21. Peak response of PCB with different mass ratios 66
Figure 3.22. Optimal parameters of dynamic absorber at different mass ratios..67
Figure 3.23. Comparison of peak relative deflection in the case of traditional and novel design....................68
Figure 3.24. Comparison of relative deflection in the case of traditional and novel design 69
Figure 3.25. Sensitivity analysis 70
Figure 3.26. Dynamic response of original and ruggedized PCB 71
Figure 3.27. Simulink diagram for swept-sine excitation 72
Figure 3.28. Signal processing "tool box" 73
Figure 3.29. Simulated relative deflection 74
Figure 3.30. Simulated absolute acceleration of original and ruggedized PCB 75
Figure 3.31. Simulated relative deflection of original and ruggedized PCB...75
Figure 3.32. Custom design for half-sine shock...77
Figure 3.33. Simulink diagram for shock excitation 78
Figure 3.34. Shock response of original and ruggedized PCB (η=65%) 79
Figure 3.35. Shock response of original and ruggedized PCB (η=35%) 80
Table 3.1. Comparison results in the case of novel and traditional designs...81
Figure 4.0. Dynamic model of generic PCB and with attached dynamic absorber..84
Figure 4.1. Spreadsheet showing Solver for calculation and optimising dynamic absorber..............................86
Figure 4.2. Dynamic response of ruggedized PCB with different mass ratios...88
Figure 4.3. Optimal parameters of dynamic absorber at different mass ratios...89
Figure 4.4. Sensitivity analysis 92
Figure 4.5. Dynamic response of original and ruggedized PCB 92
Figure 4.6. Comparison of overall relative deflection in the case of traditional and novel design 93
Figure 4.7. Comparison of overall absolute acceleration in the case of traditional and novel design 94
Figure 4.8. Comparison of PSD of absolute acceleration in the case of traditional and novel design.............95
Figure 4.9. Dynamic model of generic PCB and with attached dynamic absorber..96
Figure 4.10. Spreadsheet showing Solver for calculation and optimising dynamic absorber............................98
Table 4.0. Optimal parameters 99
Table 4.1. Optimal response..99
Figure 4.11. Dynamic response of original and ruggedized PCB at different observation point...................100
Figure 4.12. Worksheet for curve-fitting..103
Figure 4.13. SDOF modal contribution...104
Table 4.2. SDOF modal parameters 104

Figure 4.14. Universal absolute transmissibility of PCB 105
Table 4.3. SDOF modal parameters 106
Figure 4.15. Local receptance 107
Figure 4.16. Simulink diagram for random vibration excitation 109
Figure 4.17. Sub-system Simulink block diagram of original PCB 109
Figure 4.18. Simulated time history response of original and ruggedized PCB (η=35%) 110
Figure 4.19. Simulated time history response of original and ruggedized PCB (η=65%) 111
Table 4.4. Comparison of the increased life factor between the simple cycle and overall technique 112
Figure 4.20. Simulated absolute transmissibility of original and ruggedized PCB 113
Figure 4.21. Simulated PSD of absolute acceleration of original and ruggedized PCB 113
Figure 4.22. Simulated PSD of relative deflection of original and ruggedized PCB 114
Figure 4.23. Comparison dynamic response of ruggedized PCB (η=35%) 114
Figure 4.24. Comparison dynamic response of ruggedized PCB (η=65%) 115
Figure 4.25. Spreadsheet showing Solver for calculation and optimising dynamic absorber 116
Figure 4.26. Dynamic response of ruggedized PCB at different mass ratios 117
Figure 4.27. Peak relative deflection of the PCB at different mass ratios 118
Figure 4.28. Optimal parameters of dynamic absorber at different mass ratios 120
Figure 4.29. Sensitivity analysis 121
Figure 4.30. Dynamic response of original and ruggedized PCB 122
Figure 4.31. Simulink diagram for swept-sine excitation 123
Figure 4.32. Simulated absolute acceleration of original and ruggedized PCB 124
Figure 4.33. Simulated relative deflection of original and ruggedized PCB 124
Figure 4.34. Comparison dynamic response of ruggedized PCB 125
Figure 4.35. Simulink diagram for shock excitation 126
Figure 4.36. Shock response of original and ruggedized PCB (65%mass ratio) 127
Figure 4.37. Shock response of original and ruggedized PCB (35% mass ratio) 128
Figure 5.0. Dynamic model of visco-elastic impact 131
Figure 5.1. Simulink model of visco-elastic impact 132
Figure 5.2. Time histories of visco-elastic impact 134
Figure 5.3. Mathematical model of impact damper 135
Figure 5.4. Simulink diagram for studying impact damper (single-mode model PCB) 136
Figure 5.5. Impact force subsystem 137
Figure 5.6. Time history of impact damper under random vibration excitation 138
Figure 5.7. Matlab script for random variable method 139
Figure 5.8. Overall relative deflection versus parameters of impact damper 141
Figure 5.9. Simulated PSD of relative deflection of ruggedized PCB at different clearances 142
Figure 5.10. Sensitivity analysis of natural frequency dependence on clearance 143
Figure 5.11. A closer look of sensitivity analysis on natural frequency 144
Figure 5.12. Sensitivity analysis of loss factor dependence on clearance 144

Figure 5.13. Sensitivity analysis on clearance 146
Figure 5.14. Simulated time response of original and modified PCB 147
Figure 5.15. Simulated PSD of original and modified PCB 148
Figure 5.16. Simulated time response of original and modified PCB 149
Figure 5.17. Simulated PSD of original and modified PCB 150
Figure 5.18. Simulink model for random vibration 152
Figure 5.19. Simulated time response of original and modified PCB (η=65%) 153
Figure 5.20. Simulated PSD of original and modified PCB (η=65%) 154
Figure 5.21. Simulated time response of original and modified PCB (η=35%) 156
Figure 5.22. Simulated PSD of original and modified PCB (η=35%) 157
Figure 5.23. Simulink diagram for swept-sine excitation 158
Figure 5.24. Time history of impact damper under swept-sine excitation 159
Figure 5.25. Sensitivity analysis on natural frequency 160
Figure 5.26. Sensitivity analysis on loss factor 160
Figure 5.27. Simulated dynamic response of original and modified PCB (η=65%) 162
Figure 5.28. Simulated dynamic response of original and modified PCB (η=35%) 163
Figure 5.29. Simulink diagram for shock excitation 164
Figure 5.30. Shock response of original and modified PCB (η=65%) 166
Figure 5.31. Shock response of original and modified PCB (η=35%) 167
Figure 6.0. Dynamic absorber 170
Figure 6.1. Experimental rig for tuning dynamic properties of dynamic absorber 171
Figure 6.2. Comparison of absolute transmissibility of optimal dynamic absorbers 172
Figure 6.3. Experimental rig for studying dynamic of PCB combined with dynamic absorber 174
Figure 6.4 Analyser screenshot of absolute transmissibility of the original and ruggedized PCB at different mass ratio and their input excitation 176
Figure 6.5. Experimentally measured absolute transmissibility of PCB with different mass ratios 177
Table 6.0. Comparison between measured and predicted results 178
Figure 6.6. Experimentally measured PSD of absolute acceleration of PCB with different mass ratios 178
Figure 6.7. Experimentally measured PSD of relative deflection of original and ruggedized PCB at different mass ratios 179
Figure 6.8. Comparison of PSD of relative deflection of ruggedized PCB at different mass ratios 180
Table 6.1. Comparison between measured and predicted results 180
Figure 6.9. Experimentally measured absolute transmissibility of original and ruggedized PCB at different observation points 181
Figure 6.10. Comparison of PSD of relative deflection of original and ruggedized PCB at different observation points 182
Figure 6.11. Swept-sine vibration profile from vibration control screen 184
Figure 6.12. Analyser screenshot of absolute transmissibility of original and ruggedized PCB 185

Figure 6.13. Experimentally measured absolute transmissibility and acceleration of original and ruggedized PCB 186
Figure 6.14. Comparison of relative deflection of ruggedized PCB at different mass ratios 187
Figure 6.15. Experimentally measured relative deflection of original and ruggedized PCB 188
Figure 6.16. Shock profile from vibration control screen 189
Figure 6.17. Analyser screenshot of absolute acceleration response of original PCB 190
Figure 6.18. Analyser screenshot of absolute acceleration response of the ruggedized PCB with different mass ratios 191
Figure 6.19. Experimentally measured of original and ruggedized PCB with 65% mass ratio 192
Figure 6.20. Experimentally measured of original and ruggedized PCB with 35% mass ratio 193
Figure 6.21. All-metal dynamic absorber 195
Figure 6.22. Absolute transmissibility of all-metal dynamic absorber 195
Figure 6.23. Comparison of dynamic response of the modified PCB in the case all-metal and grommet dynamic absorber 196
Figure 6.24. Ball bearing mounted on PCB for studying impact damper behaviour 198
Figure 6.25. All-metal impact damper 198
Figure 6.26. Analyser screenshot of absolute transmissibility under random vibration 199
Figure 6.27. Experimentally measured absolute transmissibility of original and modified PCB 200
Figure 6.28. Experimentally measured PSD of absolute acceleration of original and modified PCB 200
Figure 6.29. Experimentally measured PSD of relative deflection of original and modified PCB 201
Figure 6.30. Analyser screenshot of absolute transmissibility of original and modified PCB under swept-sine vibration 202
Figure 6.31. Experimentally measured absolute transmissibility and acceleration of original and modified PCB 203
Figure 6.32. Experimentally measured relative of original and modified PCB 204

SYMBOL and NOTATION

Symbols	Descriptions	Units
t	Time	s
τ	Impact duration	s
T	Period of excitation	s
$x(t)$	Absolute deflection	m
$\dot{x}(t)$	Absolute velocity	m/s
$\ddot{x}(t)$	Absolute acceleration	m/s^2
$z(t)$	Relative deflection	m
$\dot{z}(t)$	Relative velocity	m/s
$\ddot{z}(t)$	Relative acceleration	m/s^2
$\ddot{y}(t)$	Absolute base acceleration	m/s^2
Δ	Clearance	m
σ	Magnitude of the stress	m
N	The number of simple cycles	Dimensionless
R	Restitution ratio	Dimensionless
g	Acceleration due to gravity	9.81 m/s^2
f	Frequency	Hz
ω	Angular frequency	rad/s
$Z(j\omega)$	Relative deflection, complex spectrum	m
$\dot{Z}(j\omega)$	Relative velocity, complex spectrum	m/s
$\ddot{Z}(j\omega)$	Relative acceleration, complex spectrum	m/s^2
$X(j\omega)$	Absolute deflection, complex spectrum	m
$\dot{X}(j\omega)$	Absolute velocity, complex spectrum	m/s
$\ddot{X}(j\omega)$	Absolute acceleration, complex spectrum	m/s^2
$\ddot{Y}(j\omega)$	Absolute base acceleration, complex spectrum	m/s^2
$T_a(j\omega)$	Complex universal absolute transmissibility	Dimensionless
$T_r(j\omega)$	Complex universal relative transmissibility	Dimensionless
$H(j\omega)$	Complex Receptance	m/N
$T_a(s)$	Universal absolute transfer function	Dimensionless
$T_r(s)$	Universal relative transfer function	Dimensionless
$H(s)$	Receptance transfer function	m/N
$S_Z(\omega)$	Power Spectrum Density of relative deflection	m^2/Hz
$S_{\ddot{x}}(\omega)$	Power Spectrum Density of absolute acceleration	(m/s^2)^2/Hz

$S_{\ddot{y}}(\omega)$	Power Spectrum Density of base acceleration	$(m/s^2)^2/Hz$
σ_{S_z}	Overall RMS relative deflection	m
$\sigma_{S_{\ddot{x}}}$	Overall RMS absolute acceleration	m/s^2

System parameters

Symbols	**Descriptions**	**Units**
M, m	Mass	kg
K, k	Stiffness	N/m
C, c	Damping	Ns/m
η	Mass ratio	Dimensionless

Modal parameters

Symbol	**Description**	**Units**
Ω	Natural frequency	rad/s
ξ	Loss factor	Dimensionless
Θ	Transmissibility form factor	Dimensionless
Ψ	Receptance form factor	Dimensionless

Subscripts and Superscripts

1	Primary sub-system is PCB mounted inside the electronic box
2	Secondary sub-system is dynamic absorber mounted upon the PCB
opt	Optimal parameter
res	Resonant frequency
~	Combined system

Abbreviations

COTS	Commercial off the Shelf
PCB	Printed Circuit Board
PSD	Power Spectrum Density
SDOF	Single Degree of Freedom
2DOF	Two Degree of Freedom
MDOF	Multi Degree of Freedom
FRF	Frequency Response Function
DSP	Digital Signal Processing
RMS	Root Mean Square
FH	Fundamental Harmonic
G-Force	Constant acceleration

Math Symbols

$\lvert\ \rvert$	Magnitude
$\approx$	Approximately equal to

$\propto$	Proportional
∞	Infinity
$\sqrt{\ }$	Square root
$\rightarrow$	Approaching to
$\sum$	Sum
j	Imaginary unity
s	Laplace domain
min	Minimum
max	Maximum
γ, λ	Co-ordinate axes

Chapter 1

1.0 Introduction

Modern integrated military systems, which are used for reconnaissance, targeting, navigating, control and communication, rely widely on electronic equipment containing delicate internal components such as printed circuit boards (PCBs). This equipment is inherently fragile and sensitive to harsh environmental conditions to which military applications are normally exposed.

Designing embedded "military" electronics presents a significant technical challenge. An increase in the reliability of the electronics in a demanding environment of the global battlefield, where elevated levels of stresses are developed due to shock and vibration, requires special design and packaging approaches.

The typical price of the bespoke hardware designed to military specs is legendary and military budgets were traditionally equal to the need. Since the end of the Cold War, military forces have been undergoing significant changes while downsizing. At the same time, the reliability of the relatively cheap commercially graded electronics has greatly improved. At this time military contractors realised that the commercial-off-the-shelf (COTS) electronics may potentially be an effective substitute to the expensive and quick to out date military hardware.

This approach, which allows not only for cost saving manufacturing and maintaining, but also for rapid access to advanced technologies and faster time to market, was initiated in the mid nineties by the then US Secretary of Defence, William Perry [1]. The main objective of the COTS initiative was to create a wide market of low-cost commercially graded electronics capable of withstanding the demand of military environments.

It is now becoming clear that the COTS initiative is achieving the above objectives. The extensive and dynamic market of COTS electronics allows the military subcontractor the widest choice of modern and reliable electronic hardware.

Nevertheless, significant challenges still remain. Commercially graded hardware typically shows a shorter life as compared with "made-for-military" components and often cannot stand the increasing rigors of military life. When reliability becomes a critical factor, the industry moves back towards designs based on the strict military guidelines.

Plug-in PCBs are typically plate-like structures, which are made of Epoxy Fibreglass, and carry soldered microchips along with lumped components which are interconnected using lead or copper wiring. The PCBs are supported by edge-guides and connectors from an electronic enclosure.

The dynamic properties of the commercially graded, unframed, PCBs are such, that the fundamental natural frequency and loss factor are inherently low [2]. During operation, PCBs encounter exposure to harsh environmental conditions such as shock and wide-band random vibration, the spectrum of which contains essential frequency components up to 2000 Hz [3,4]. As a result, the excessive narrow-band quasi-resonant dynamic response is built-up and resulting accumulated fatigue leads to the failure of the above wiring and soldered joints.

Today vendors develop their own approaches to ruggedizing, do their own screening and even manufacturing. At the bottom line, developing the effective, miniature and cheap product means that shock and vibration control of electronic hardware has became a critical issue for the commercial and technical success of the COTS manufacturer.

To improve the reliability of PCBs, the designers are looking now for different methods of protecting the PCBs, such as: the *vibration isolation* of the entire electronic box and *ruggedizing* on the PCB level.

This Thesis analyses the response of a PCB held by screws at the sides and external wide-band random vibration transmitted directly from the base. Resulting from harsh environmental conditions, a need for a vibration protection system has been addressed. Sometimes the endurance of the COTS PCB is lower than required, thus slight modification is practised in order to protect the sensitive internal components in the electronic box. Currently, there are several existing methods of protection. However, this Thesis introduces a new concept for a "dynamic ruggedizing" which is based on the principle of wide-band dynamic absorber. This is applied to the wide-band suppressing of the dynamic response in terms of overall value of the relative deflection for PCB mounted inside the electronic box. In addition, this dynamic absorber is cheap, lightweight and small in size

1.1 Vibration isolation

To get around this problem, designers often use standard shock and vibration products such as wire rope isolators, elastomeric mounts, and hydraulic dampers. The single and multiple stage *vibration isolation* are the most effective way of reducing the transmission of vibratory energy to the PCBs.

This method is based on the placement of the compliant member (vibration isolator) between the vibrating structure and electronic box [4,5,6, see also examples at http://www.rtdusa.com/images/movie/IDAN_VIB.PDF]. The properties of such a vibration isolator have to be chosen to minimise the relative deflection and absolute acceleration of the plug-in PCBs while maintaining the peak deflection of the electronic box within allowed tolerances under the worst combination of *G-loads* and wide-band random vibration [5,6].

However, if the above tolerances are tight, this method calls for a stiff isolator and is only applicable for the electronic box containing PCBs, the resonant frequencies of which are relatively high (the 2-octave rule is explained in [2], [5] and [7]). These are framed PCBs with the resonant frequencies well above 200 Hz.

1.2 Damping treatment

The PCBs inside the electronic box might be ruggedized using some kind of *resin foam*, which is applied to fill all the interior of the box and even tiny gaps between PCBs. This method is extremely efficient for vibration protection of critical electronic equipment; however, this complicates heat sinking and replacement.

The reliability of the PCB may also be increased by *damping being added at the board level* [7,8] using, say, dampening strips. In spite of the apparent simplicity of this method, the attainable performance is not very impressive. The explanation of this surprising fact is simple. The overall RMS response of the system under random wide-band excitation is reciprocal to the loss factor of the system [9]. The dampening strips operate effectively only if their bending stiffness is comparable with that of the PCB. That is why the dampening strips in the form of a sandwiched structure were proposed [8,9]. Taking into account the mass added by such a dampening strip, the effective loss factor of the combined system cannot be altered significantly. Extra problems arise due to the outgassing and ageing of the plastic components along with bonding properties at elevated temperatures. This explains why dampening strips are not currently widely used.

1.3 Stiffening frame

To improve stability in severe shock and vibration conditions, board vendors use a variety of combinations of *stiffening of the PCB* by using ribs and frames as used in old-fashion military designs. It is aimed at increasing the resonant frequency of the PCB to above the excitation range. The obvious pitfall of this approach is the essential increase in the overall weight, dimension and reduction of the useful surface available for the placing of electronic components and wiring.

It is a widespread opinion among the manufacturers of the modern electronic hardware that making the PCB stiffer could reduce the level of stresses involved. This opinion is based on the fact that the stiffening of the PCB leads to a decreased level of deflection [11].

Unfortunately, this conclusion is not applicable to stresses. Moreover, stiffening of the PCB leads to a decrease of the loss factor (increase of Q-factor). Since it is impossible to manufacture the PCB with the resonant frequency outside the excitation range, the increase of the dynamic quasi-resonant response and stress level is most likely. In addition to this, the increased level of acceleration experienced by the PCB with increased Q-factor leads to the increased level of acceleration forces applied to the lumped components and fatigue of the soldered joints [7].

A novel solution - Ruggedizer was offered recently by the Thomson-CSF, CETIA (see http://www.cetia.com/product/whitepapers/prod_bds_whitepap_ruggedizer_000_0e.pdf) as a standard optional accessory to their commercially graded PCBs. The Ruggedizer is a board level heat sink designed to add mechanical stiffening and protection. As the Ruggedizer covers the entire top face of the board, the vibration and shock characteristics of the latter are drastically improved. The "sandwich" structure of the Ruggedizer-equipped PCB reduces the effects of harsh shock and vibration by eliminating the most dangerous low-frequency resonances and, thus, reduces the risks of physical-failure fatigue. However, such a design eventually leads to high-cost mechanical manufacturing, long re-design time, added weight, increased dimensions and price.

1.4 Bumpered vibration control

Nonlinear vibration control has been introduced in [2] to protect PCBs in extreme environmental condition with a reasonable cost. This method relies on using *snubbers*, sometime called *bumpers* [20], which are small devices that can be attached to adjacent PCBs so they hit each other in dynamic conditions. According to [2], there are two types which can be employed depending on the natural frequency of PCB. Soft rubber snubbers work best for PCBs with natural frequencies below 50 Hz; PCBs with higher natural frequencies above 100 Hz must use more rigid materials for effective reduction of the PCBs relative motion. The best location for snubbers or bumpers is close to the centres of the various PCBs, where the maximum displacements are expected.

However, the analytical solution of such a nonlinear vibration problem is not discussed and experimental descriptions are not available. To our knowledge, the dynamic behaviour of such an arrangement may be classified as strongly nonlinear or vibroimpact system [20]. The best performance of the proposed solution strongly depends on clearance between bumpers and their dynamic properties. The dynamic properties of the PCBs and types of excitation, and G-loads also have great influence on optimal performance. In modern literature, a closed form solution for this similar type of vibration control has not been obtained. In a general sense, under dynamic conditions, this vibration control is only effective when both PCBs are moving out of phase to each other so that "head on" collision takes place. In a worse situation, both PCBs are moving in the same phase and have the same dynamic properties then this method does not provide any mean of vibration control. In addition, soft bumpers rely on the use of elastomeric or rubber. These materials have a poor history of maintaining their mechanical properties in extreme temperature conditions which increase the risk of noise level and nonlinear resonant phenomena.

1.5 Linear dynamic absorber

La Malfa et al [12] recently considered an application of the *tuned dynamic absorber* for vibration control of PCB under constant frequency excitation. Design of such a dynamic absorber has a long history. As a practical application of the 2DOF system, it may consider here the spring-mass system. By tuning the system to the frequency of the excitation force, an undamped absorber can reduce the unwanted deflections to zero.

However, for military application, wide-band random, dwell-sine vibration and shock are of primary importance. In many installations for military electronic equipment, random vibration tests have became very commonplace and primary military specifications for the testing of this type of equipment [3] have placed heavy emphasis on random vibration, tailored to the actual application.

Under such an excitation, the above undamped dynamic absorber can make matters worse due to the excitation of resonant responses and even cause damage, which would not otherwise occur. Due to the excitation being experienced by the PCB being harsh random vibration the absorber has to protect against a wide-band excitation. This can be achieved by adding damping to the absorber. With damping, the absorber can no longer completely absorb the deflections at particular frequencies but with careful optimisation they can be greatly reduced.

In this study, we are making an attempt to accommodate the idea of using a wide-band damped dynamic absorber for controlling the dynamic response of lightly damped and extremely responsive PCB under the wide-band random vibration. The proposed approach focuses primarily on the design of an optimal dynamic absorber tailored for avionics military specification. This new design concept will achieve higher reliability and fatigue life, greater shock and vibration resistance, lower cost and maintenance.

Generally speaking, a damped dynamic absorber is a secondary sub-system consisting of a mass attached at the appropriate point of the structure under treatment using a visco-elastic member. The inertia and visco-elastic properties of dynamic absorber have to be carefully "tuned" for the best performance in minimising the dynamic response of the modified system in the specified environment. The market for these devices is large and covers a wide range of applications, from spaceborne structure to sports equipment and from heavy construction to transport industries. These devices show their superiority by means of controlling either torsional or rectilinear vibratory motion. Their size varies from as large as an engine flywheel to small size like as a fingertip, depending on natural existence of the base structure.

Several authors have investigated different strategies for choosing the optimal parameters of dynamic absorber using either time domain or frequency domain performance indices. The first attempt to optimise the dynamic absorber for suppression of the undamped primary single-degree-freedom system (SDOF) structure under force harmonic excitation with frequency which was varied in a wide range was carried out by Den Hartog and Ormondroyd [13]. Warburton [14] has presented an expression for optimum absorber parameters for undamped SDOF primary systems, considering harmonic and white noise random force excitations. The effect of damping in the primary system on optimum absorber parameters has been also investigated by Wang and Cheng [15]. They have compared four optimisation methods (the equal peak method, the minimal variance method, the energy method and the area ratio method).

Korenev [16] has addressed the problem of optimal design of dynamic absorber as applied to the vibration control of a SDOF system under the force and base-induced excitation. Analytical solutions were obtained for a specific type of excitation, e.g. white noise.

When applied to the SDOF system with primary damping to the original system, Nishimura et al [17] addressed the optimisation of a dynamic absorber for a multiple-degree-of-freedom (MDOF) system subjected to random force input with a dominant frequency, using an optimisation method based on the optimal control theory. In reference [18], Kitis et al. proposed an efficient optimal design algorithm for minimising the vibratory response of MDOF systems under sinusoidal loading over several excitation frequencies. The method explores mass, stiffness and damping matrices provided by an analytical model and incorporates an effective time-saving analysis approach to compute the cost function and its derivatives. More recently, a modal theory for visco-elastic dynamic absorber was developed and associated to different optimisation techniques for the optimal over a wide frequency band [19].

This study will address the application of wide-band dynamic absorber to the vibration control of the PCB under typical random vibration, dwell-sine and shock test per MIL-STD [3]. Since the purpose of the dynamic absorber is to make the PCB more rugged using the dynamic effect, we introduce here the term *dynamic ruggedizer* which reflects the objective and method of its achievement.

In this work, in the first approximation, we deal with the single-mode model of PCB, as proposed by Steinberg [2]. The improved solution is then obtained using full-mode model of

PCB, where the dynamic properties of the latter are given through the experimentally measured complex frequency response functions (FRFs), namely local receptance and universal absolute transmissibility.

In general, the analysis of an uniform plate-wise structure, if in the right condition, a single dynamic absorber has the capability of suppressing not only the critical resonant frequency where it is tuned but almost all neighbouring resonances if it is not placed at a node point. The influence of damped dynamic absorber, as long as it does not mounted in a node point, is an extremely powerful tool of vibration suppression. As well as suppressing all resonant responses where it is attached it also suppresses almost all resonant frequencies of other locations of the base structure without disturbing their anti-resonances even if it is a single attachment point. These positive features are explained why the damped dynamic absorber is a very popular device in the vibration control category for complex dynamic structures.

However, making the right choice of dynamic absorber and its desired location are critical for this vibration control strategy. Due to the large amount of literature and algorithms currently available for optimising parameters of dynamic absorber, it has been rather difficult to determine the exact need for each method and which method is best. There is no ideal solution and the common methods are only approximations. Also, many methods are very similar to each other and in some cases, simply extensions of a few basic techniques. Selecting a “right” method for optimising the response of a COTS PCB is of primary concern of this study. Also, most of the above references, the FRFs of the MDOF-primary system are directly formulated from traditional methods and the vibratory motion is caused by force excitation in which inapplicable for this study.

Additionally, PCBs are far more complex than the simple plate model, they can be very flexible or can be stiffened in multiple ways, and components can significantly affect the stiffness. Moreover, stiffeners, screws, standoffs, board cutouts, or other components can act as “stress risers”. Under random vibration, stresses from multiple mode shapes combine. All these complexities affect component life, thus, there can be huge errors in predicting life capabilities using only the traditional method.

To overcome these problems, in the analysis of the full-mode model of PCB with base support motion, as here, we attempt to build a new radical optimising technique with the use of computational resources and experimentally measured FRFs of the original PCB design. The optimal design of such a damped dynamic system is independently investigated in different vibration environments, with the aim of minimising the relative deflection of the PCB.

1.6 Impact dynamic absorber

An interesting approach to the nonlinear vibration control of a linear lightly damped SDOF system to the harmonically excited primary structure was initially proposed by Ormondroyd and Den Hartog [13]. It is the simplest case when both the primary and the secondary sub-structures are lightly damped SDOF systems. The frequency response of such a combined two-degree-of-freedom (2DOF) system display two sharp resonant peaks and one anti-resonant notch that is located exactly at the natural frequency of the secondary sub-structure. The appearance of such a notch is used for the essential suppression of vibration of the primary system caused by harmonic force with a constant frequency. However, some variation, for instance, in speed of rotating machinery it is unavoidable. In addition, the first resonance frequency always has to be traversed before a steady speed of operation is achieved (at the tuning frequency) during the start-up and slow-down. Running through the first resonance frequency will inevitability induce large transient vibration. In order to avoid resonance peaks in the system containing such a dynamic absorber, the authors have proposed to limit the relative motion of the absorber to the primary structure by means of elastic stops. They also suggested designing the sway space of the dynamic absorber in such a manner as to provide impactless linear motions for both masses in the desired vicinity of the anti-resonant frequency. Such a design allows for maintaining the desired feature of linear dynamic suppression of harmonic vibration. As soon as the relative motion between the dynamic absorber and the primary structure exceeds the pre-deigned clearance the stops come in to play, thus limiting the relative motion of the absorber.

Since then, numerous researchers [22-27] have been attracted by this elegant engineering solution and have studied such an approach numerically in a simpler version, it is known as *impact damper*. In this class of dynamic absorbers, the secondary mass is unsupported by either a spring or a damper; it is constrained to move unidirectional in a container attached to the primary vibrating system, the ends of the container limiting its movement. When the primary system is vibrating the secondary mass moves back and forth impacting, alternatively, either end of the container. The amplitude of vibration of the main system is reduced by the mechanism of the transfer of momentum between the primary and the secondary system and by the conversion of mechanical energy into noise and heat. Early publications described the damper as an acceleration damper, because the damping force is proportional to the absolute acceleration of the secondary mass. But since energy is also converted into noise and heat in this class of damper, a more accurate description is *impact dynamic absorber*.

There is a strong opinion [22-26] that the application of impact dynamic absorber is more superior as compared to a conventional damped dynamic absorber, in terms of performance, design, reliability and immune to environmental condition. This is despite the fact that a closed form of analytical solution has not yet been established and no comparison has been made. This conclusion may not be true for different vibration environments. In reality, designing for optimal performance using impact dynamic absorber will take a labour task [27], however, the optimal parameters have not been shown. It should be noted that although an impact dynamic absorber may improve the performance of primary structure under certain specified conditions, in general, they will degrade system performance under other operation conditions, such as a short duration shock. Under this condition, the impact dynamic absorber can make matters worse for other components even cause damage, which would not otherwise happen.

The first publication describing a practical application of the impact dynamic absorber was that by Paget in 1937 [28] referring to the damper used to reduce turbine blade vibration. A similar application was described by Hahn [29] for damping the vibration of boring quills. Recently, impact dynamic absorber is used to control lightly damped structure such as street lampposts and suspended pipeline.

In spite of their success, there is little known about the response of these absorbers to random excitation and shock. Probably the main reason for the lack of analytical studies is that this problem does not lend itself to treatment by the standard analytical techniques for determining the response of nonlinear systems to random excitation. The difficulty lies in the fact that the systems as a highly nonlinear dissipative 2DOF system in which the nonlinearity involves the relative displacement as well as the relative velocity of the two masses.

Although the impact dynamic absorber has been long used in consumer products. The lack of demonstrated performance and relevant structure and the inability to predict behaviour has limited the application of impact dynamic absorber solutions to aerospace and other technology intensive application. Therefore in this study, we directly use the numerical solution based on the realistic model of non-momentary visco-elastic impact suggested [20]. A design of view of such an impact dynamic absorber is based on its universal performance as compared to its damped dynamic absorber subjected to different external excitations. This includes its optimal performance, sensitivity and robustness of the full-mode model of PCB despite its natural complexity.

1.7 Objectives

According to the above, the main aim of this project is to develop the theory and design a linear wide-band dynamic absorber for dynamic ruggedizing of PCB under wide-band vibration. All analytical and numerical modelling were completed prior to the experimental testing with the goal of minimising the overall relative response of the critical point in PCB under the influence of damped dynamic absorber. This dynamic absorber was optimised based upon the dynamic properties of a particular PCB operating under wide-band vibration excitation. As an additional work of this project, the numerical solution of impact damper was developed to see how much difference there was in terms of optimal performance as compared to damped dynamic absorber. The appropriate experimental work was carried out to support its numerical solution.

The complete route to completion of the project developed into the following series of steps:

Step1

The experimental rig was set-up to identify the dynamic properties of the chosen PCB under actual working condition. All the necessary information was obtained and presented in terms of modal parameters and frequency response functions.

Step 2

The PCB carried the damped dynamic absorber which was modelled as a 2DOF system in a simplified approach. Mathematical modelling of the system was built in the frequency domain, using MS®Excel Solver function to optimise the response under random and swept-sine vibration to give the minimum deflection of the PCB. The system was modelled in the time domain using Matlab/Simulink to analyse the vibration fatigue and to check the shock response.

Step 3

To improve the result of designing an optimal damped dynamic absorber, the analytical solution of the full-mode model PCB was set-up with the use of experimentally obtained FRFs from step 1 and optimisation technique from step 2. The curve-fitting technique was used for extracting all modal parameters of the PCB for numerical simulation purposes.

Step 4

The numerical solution for impact dynamic absorber was developed with the main concern of optimal performance under random and swept-sine vibration for the single-mode and full-mode model of PCB as compared to the damped dynamic absorber.

Step 5

Experimental validation was carried out for both types of dynamic absorber under Mil-STD-810 test to support its analytical and numerical solution. The test rig from Step 1 was tailored to install the dynamic absorber. Prior to that, there was various experimental testing to obtain the required universal absolute transmissibility of the damped dynamic absorber. The prediction and experimental results were compared to obtain a suitable dynamic absorber. Due to space constraint in the electronic box, there was a stage for designing and manufacturing a miniature dynamic absorber. This dynamic absorber was able to perform well in a small sway space.

Chapter 2

2.0 Dynamic properties of a PCB

There are several methods that can be implemented to determine the dynamic characteristics of a PCB. One of the most popular procedures involves random vibration testing. With random vibration testing one is able to measure the response of a PCB to a wide-band of frequency excitations. The vibration test is fast and convenient. Once the frequency response is measured, the data can be further processed to build a mathematical model in terms of modal parameters. The choice of optimal dynamic absorber depends strongly on dynamic properties of PCB.

2.1 PCB and mounting

The PCB is typically constructed of a series of laminated, tracking and preimpregnated (insulating layers) in a vertical stack. Within the stack is often a series of drilled holes, plated forming vias (interconnecting between layers) between tracking or plated through holes between surfaces. Furthermore the components on the PCB are mounted through holes and soldered on the adjacent sides. This type of mounting has better mechanical properties compared to surface mounted component PCB.

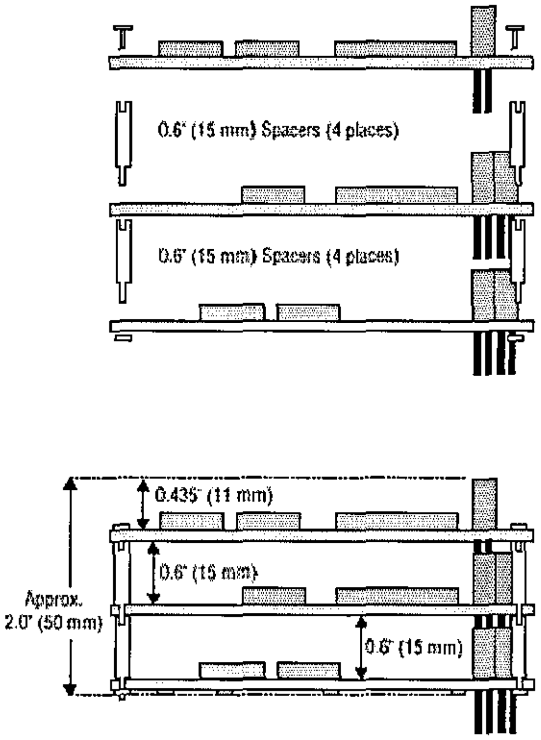
0.6" (15 mm) Spacers (4 places)
0.6" (15 mm) Spacers (4 places)
0.435" (11 mm)
0.6" (15 mm)
Approx. 2.0" (50 mm)
0.6" (15 mm)

Figure 2.0. Typical PCB mounting (image adopted from http://www.rtcgroup.com/cotsjournal)

The manner in which the PCB is supported in the electronic box can be an important factor in determining how the boards will respond to vibration and shock. During vibration, high G-load or resonant phenomena will cause the PCB to bend back and forth in the vertical axis. This would eventually lead to fatigue and failure of the components due to dynamic stress that are developed because of the relative motion. In more severe applications, board edge guides are used to reduce rotation and translational forces and in contrast, increasing the natural frequency and loss factor.

The electronic industry manufactures a wide variety of PCB with different sizes and shapes along with many different mounting arrangements. A simple PCB with typical electronic component parts such as integrated circuits, resistors, capacitors and flat-pack chips was chosen to demonstrate the principle of vibration protection system. There are various ways of mounting PCB, however, the common practice in military applications is to mount a PCB using pillars and screws allowing for high-pressure interfaces. This would allow the PCB to develop an excessive vibration at its fundamental resonant frequency [2].

2.2 Experimental Rig

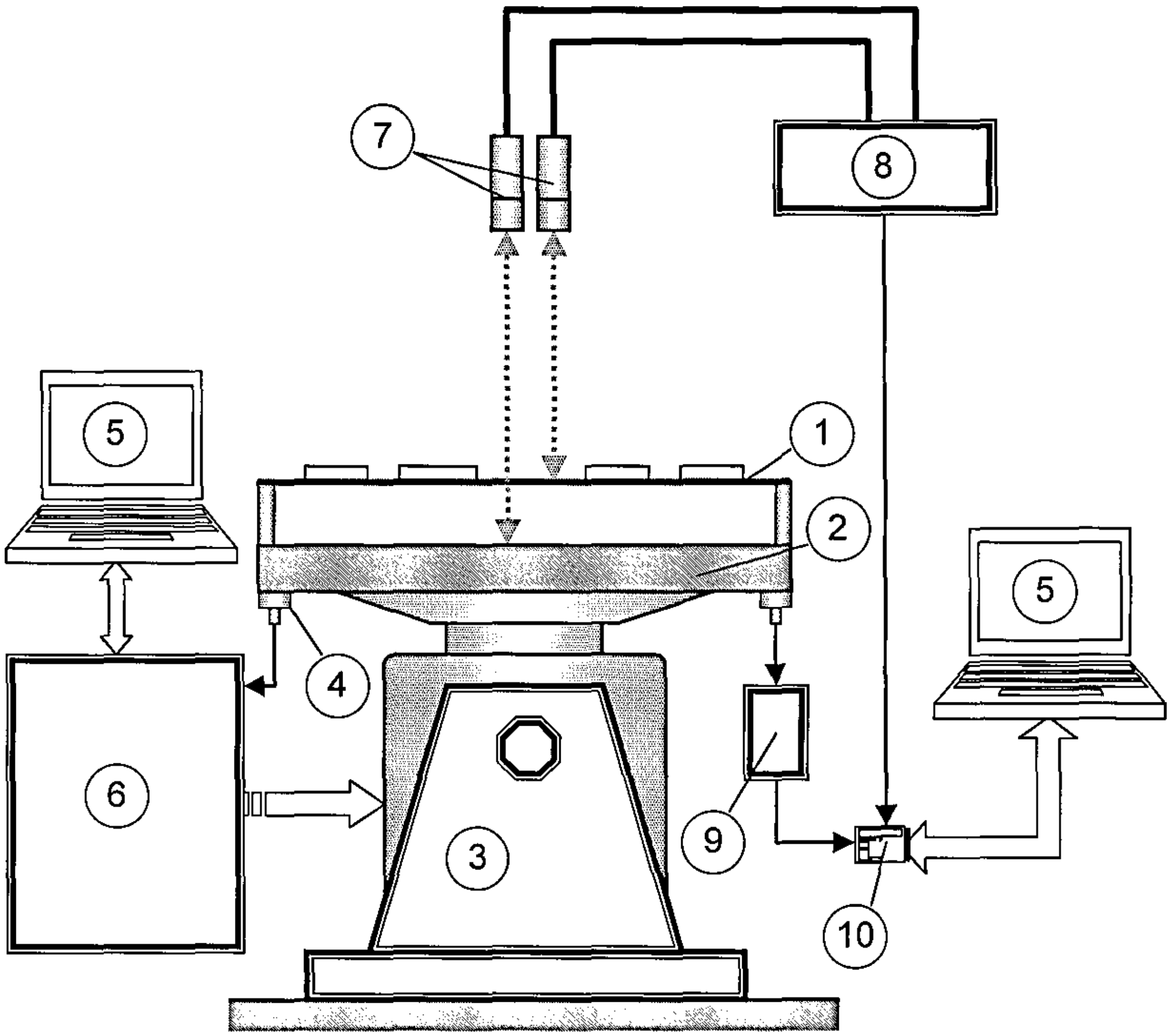

a) Schematic layout

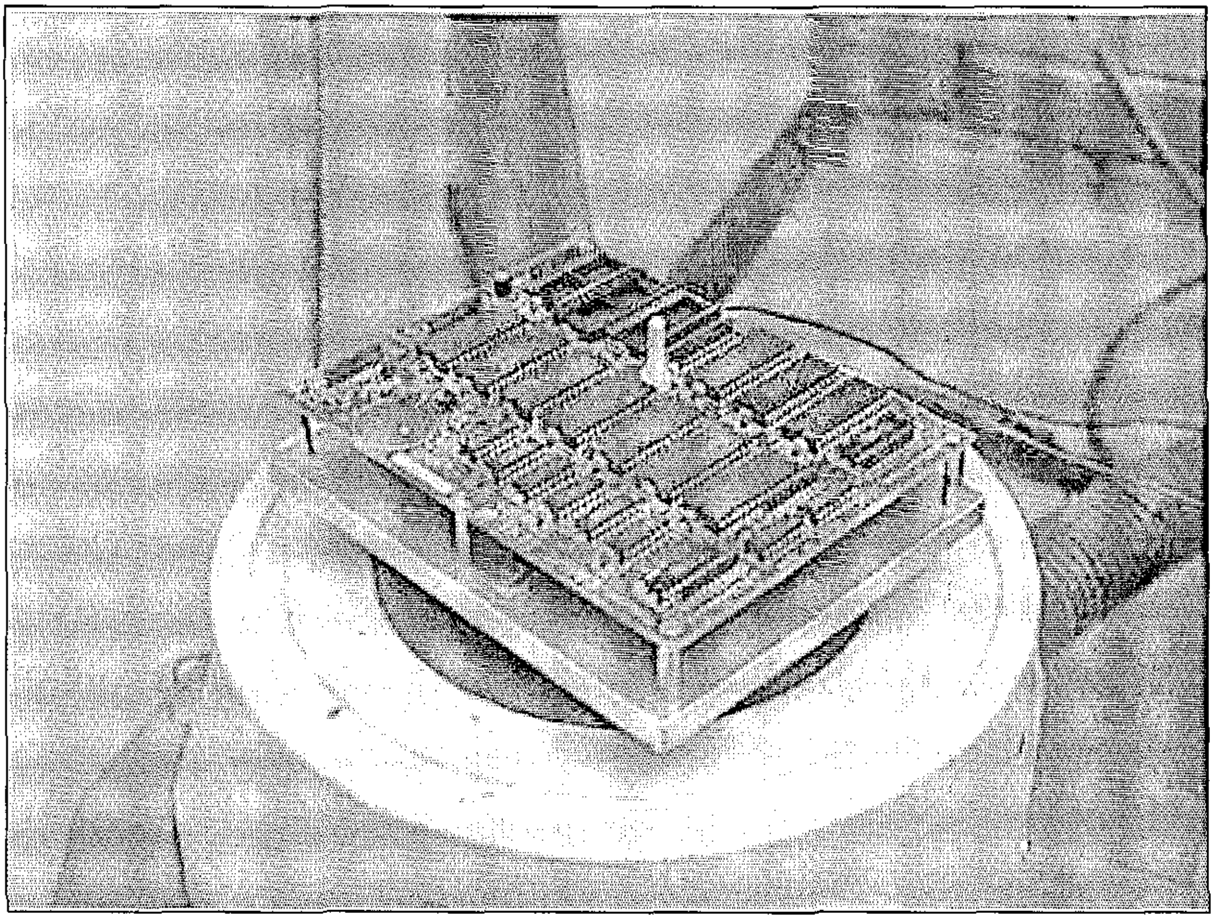

b) PCB mounted on the shaker

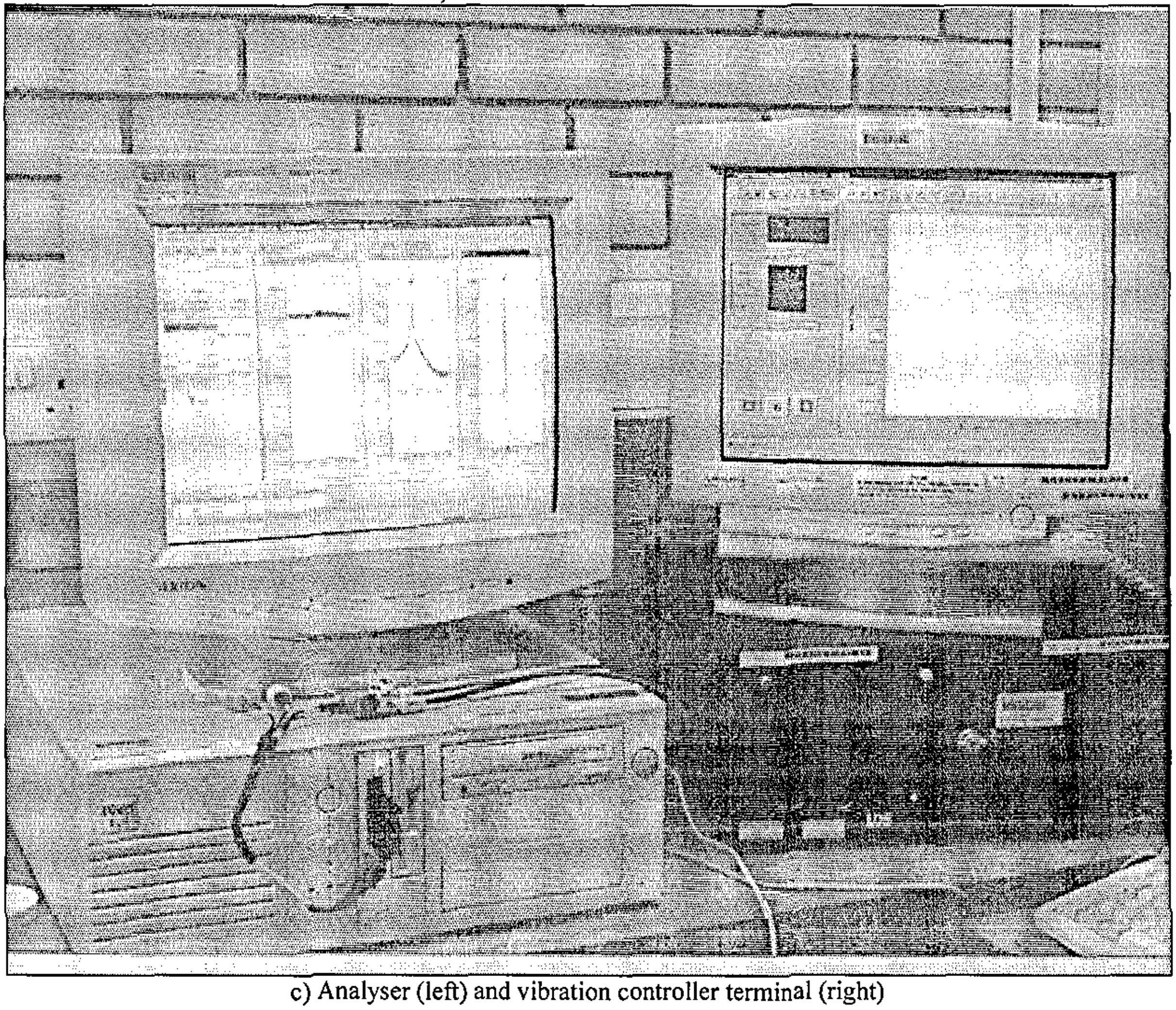

c) Analyser (left) and vibration controller terminal (right)

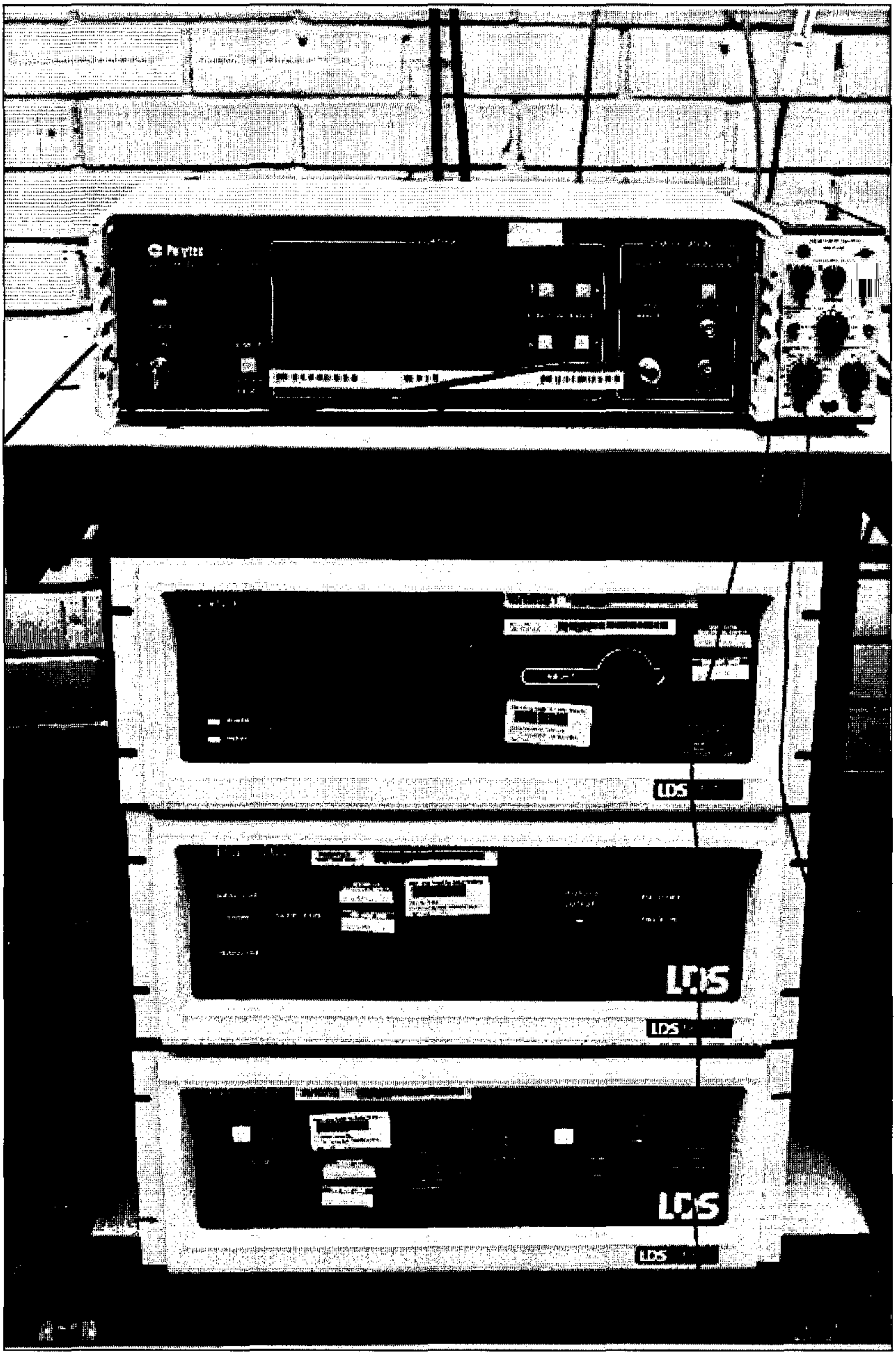

d) Vibration controller (bottom) and laser Vibrometer (top)

Figure 2.1. Vibration test Rig

Figure 2.1a shows the typical rig for studying the dynamic properties of the PCB. The Epoxy Fibreglass PCB ① is mounted upon fixture ②, which is attached to the vibration test system ③ (V550 Series, Ling Dynamic System). The miniature accelerometer ④ (Bruel and Kjaer, Type 4393) is mounted upon the fixture and provides the signal for the internal feedback loop for the System Controller ⑥ (DVC-48, Ling Dynamic System Ltd). The controller is connected to the Terminal ⑤. Vibration test system is programmed to provide the close-loop controllable wide-band random, sweep-sine vibration and shock. Dual Beam Polytec OFV 512 Fibre Interferometer and Polytec OFV 3001 Vibrometer Controller ⑦, ⑧ are used to measure the absolute or relative velocity of the PCB. The second miniature accelerometer (Bruel and Kjaer, Type 4393) is bonded to the fixture and produces the reference signal of the absolute acceleration. The Charge Amplifier (Bruel and Kjaer, Type 2635) is used for signal conditioning. The above two signals (absolute acceleration of the base and relative velocity of PCB) are then passed to Signal Cal Ace ⑩ (Data Physics Corporation, Vibration Analyser, DP104 -100) providing for the appropriate data acquisition and DSP using terminal ⑤.

The heart of this vibration test is non-contact laser vibrometry with the advantages of avoiding unnecessary additional mass or interference and it can be either configured to measure the relative or absolute motion of the PCB to the supported fixture.

To simulate the dynamic response of the PCB to the actual working environment, the vibration test system is programmed to reproduce a wide-band random vibration with uniform power spectral density (PSD) $0.1g^2/Hz$ in the frequency range 20-2000 Hz (overall level 14g RMS, typical military specification in accordance with [3]). Figure 2.2 shows the random vibration spectrum to which the PCB was exposed.

The latest generation signal analysers and their companion Window base software contain all features for data acquisition and DSP. The input channel can be interfaced in several formats (force, acceleration, velocity and displacement) each of which depends on the receiving signal. Measurement functions such as windowing, averaging and Fast Fourier Transforms (FFT) computation are available within the software and readily to process the measuring signals. The analyser also enables of exporting of the relevant data to MS®Excel for further analysis or a screenshot to MS®Word document. Regarding random vibration testing, a Hanning window is used. Figure 2.3 shows a screenshot of the analyser, a typical FRF display.

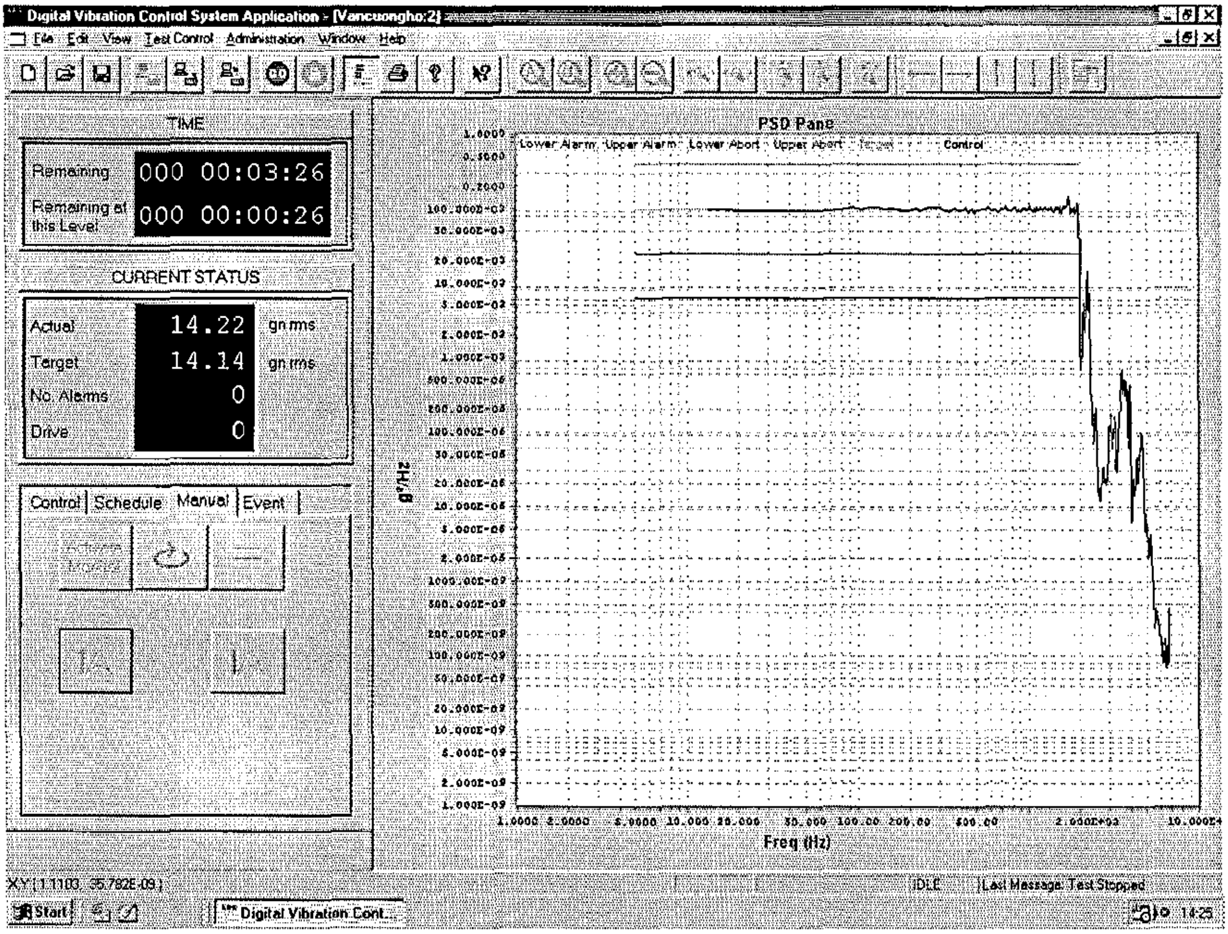

Digital Vibration Control System Application - [Vancuongho:2]

TIME

Remaining: 000 00:03:26

Remaining at this Level: 000 00:00:26

CURRENT STATUS

Actual	14.22	gn rms
Target	14.14	gn rms
No. Alarms	0	
Drive	0	

XY [1.1103, 35.782E-09]

IDLE

Last Message: Test Stopped

File Edit View Test Control Administration Window Help
Control
Schedule
Manual
Event
PSD Pane
Lower Alarm
Upper Alarm
Lower Abort
Upper Abort
Target
Control
G²/Hz
Freq (Hz)
1.0000
2.0000
5.0000
10.000
20.000
50.000
100.00
200.00
500.00
2.000E+03
10.000E+
Start
Digital Vibration Cont...
14:25

Figure 2.2. Random vibration profile from vibration control screen

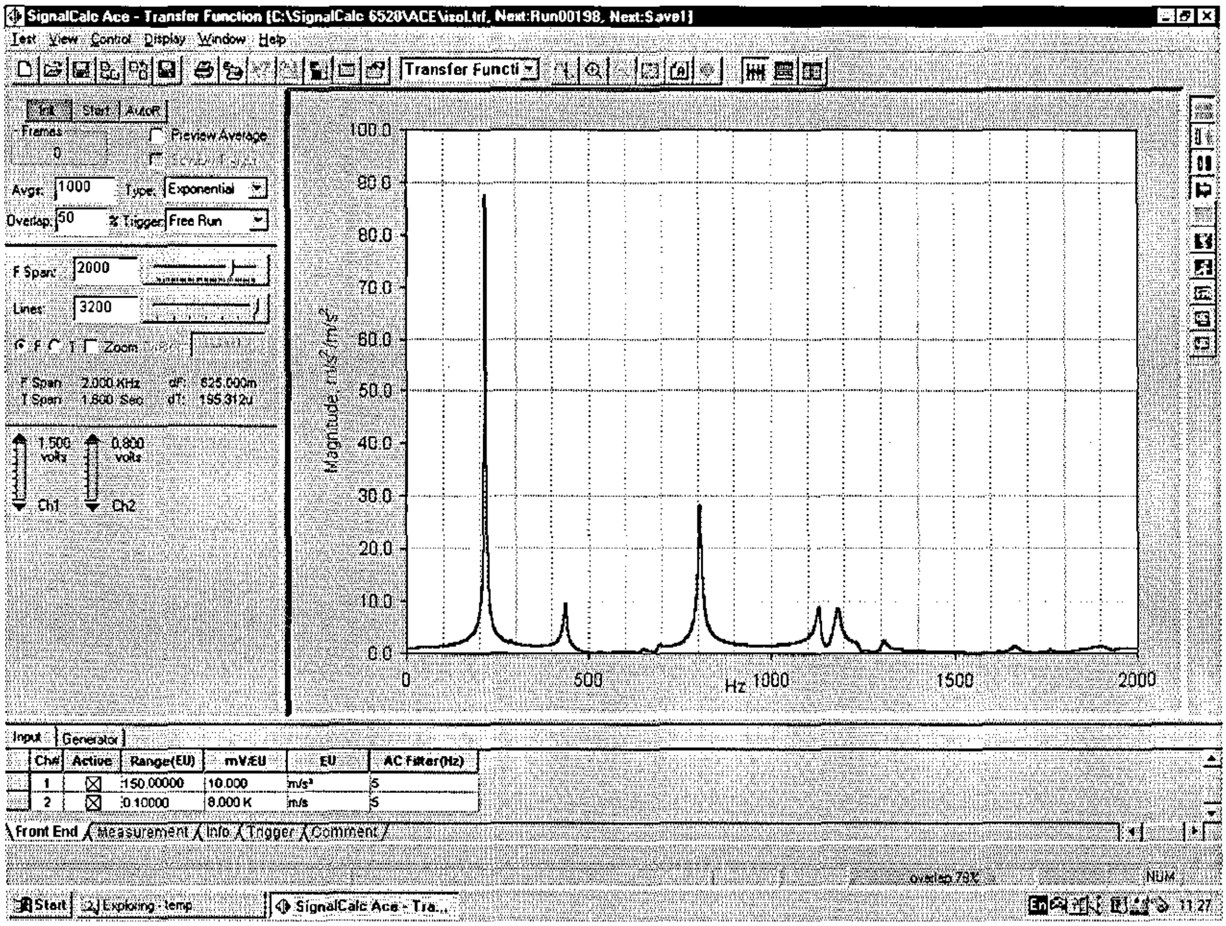

SignalCalc Ace - Transfer Function [C:\SignalCalc 6520\ACE\isol.trf, Next:Run00198, Next:Save1]

Frames: 0

☐ Preview Average

Avgs: 1000 Type: Exponential

Overlap: 50 % Trigger: Free Run

F Span: 2000

Lines: 3200

● F ○ T ☐ Zoom

F Span 2.000 KHz dF: 625.000m

T Span 1.600 Sec dT: 195.312u

1.500 volts Ch1

0.800 volts Ch2

Ch#	Active	Range(EU)	mV/EU	EU	AC Filter(Hz)
1	☒	150.00000	10.000	m/s²	5
2	☒	0.10000	8.000 K	m/s	5

overlap 79%

Test View Control Display Window Help
Transfer Functi
Init
Start
AutoR
Input
Generator
Front End
Measurement
Info
Trigger
Comment
Magnitude, m/s²/m/s²
100.0
90.0
80.0
70.0
60.0
50.0
40.0
30.0
20.0
10.0
0.0
0
500
Hz 1000
1500
2000
NUM
Start
Exploring - temp
SignalCalc Ace - Tra...
11:27

Figure 2.3. Analyser screenshot of universal absolute transmissibility of PCB

The complex frequency response function (FRF) or more specifically *universal* transmissibility as we are loosely using in this study is a mathematical model defining the input-output dimensionless relationship of a dynamic system. In this test, the PCB response (output) is caused by vibration excitation (input) from the shaker. Mathematically, the FRF is defined as the complex Fourier transform of the output divided by the complex Fourier transform of the input. Because it is a complex quantity, the frequency response function cannot be fully displayed on a single-two dimensional plot. It can however, be represented in several formats, one method of presenting the data is magnitude and phase versus frequency.

Figure 2.4 shows the experimentally obtained modulus and phase of the universal transmissibilities at the origin location of the PCB. By plotting the magnitude in logarithmic scale versus logarithmic frequency, it is possible to distinguish the natural frequency and conveniently display the amplitude of the first mode in the response spectrum. From Figure 2.4, the PCB may be thought of as a lightly damped MDOF, the first natural frequency of which is 220 Hz, which is typical for COTS PCBs. The amplification ratio at this frequency is about 90. This indicates that the amount of damping is extremely small and explains why the PCB is so susceptive to wide-band random vibration.

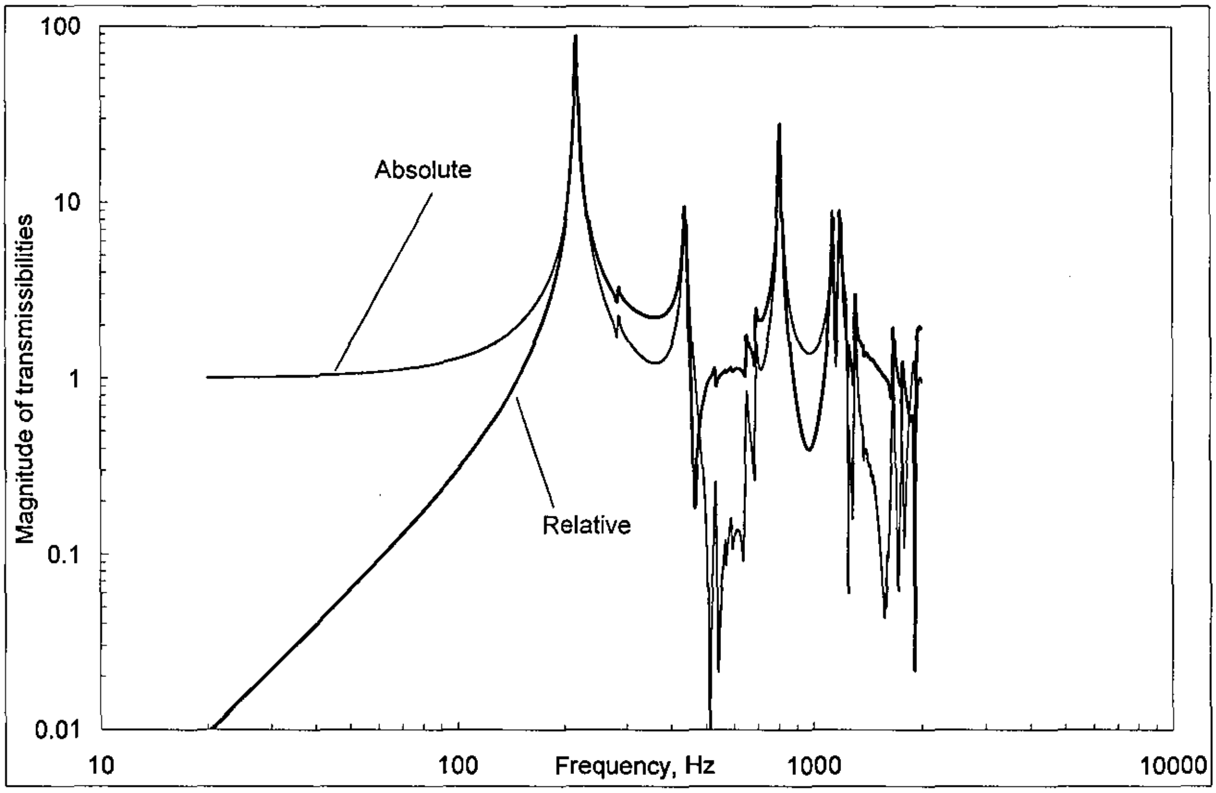

a) Moduli

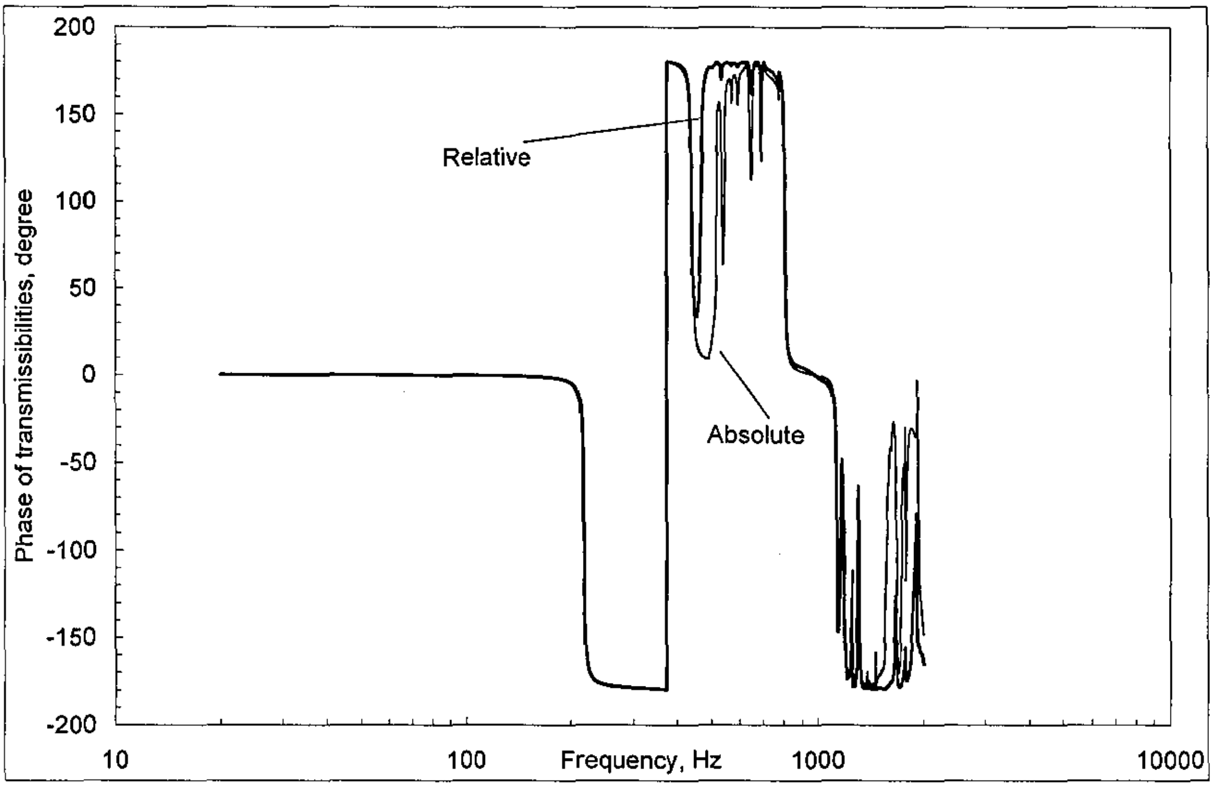

b) Phase

Figure 2.4. Experimentally measured transmissibilities of PCB

It is clearly seen that contribution of the first vibration mode associated with this frequency will cause most of the accumulated fatigue to the PCB, as here the deflection of the PCB is greatest.

2.3 Curve-fitting of results

Curve-fitting or *Parameter Estimation* is a numerical process that is typically used to represent a set of experimental data by assuming analytical function. The results of this curve-fitting process are the coefficients, or parameters, that are used in defining the analytical function. With regard to the FRF, the parameters that are calculated are its so-called modal parameters (i.e. modal frequency, loss factor and form factor). The curve-fitting process can also be thought of as a data compression process since a large number of experimental values can be represented by a much smaller number of modal parameters. For the results to be of any use in designing an optimal dynamic absorber, values for the natural frequency and loss factor of the PCB need to be obtained from the experimental results.

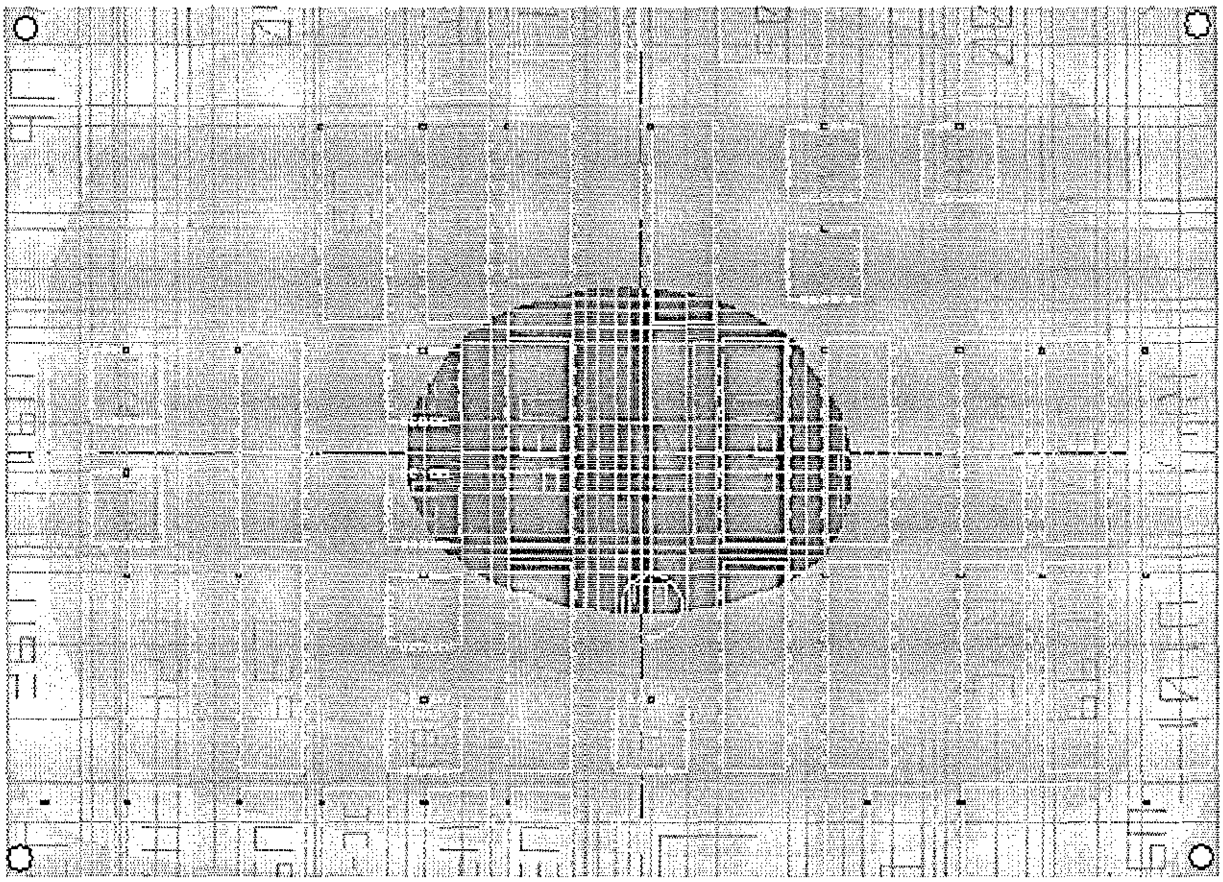

Figure 2.5. Finite Element Analysis of PCB with supported corners (image adopted from http://www.indirect.com/www/pacnum/vibplus.html)

Normally the typical PCB mounting in Figure 2.0, the relative deflection of the PCB at its central region would be maximum. Figure 2.5 shows the different relative deflection boundaries of the PCB using Finite Element Analysis for the above type of mounting. The critical area in black shows where the failure of mounted components normally occurs. In a worse situation, a crack may occur on the board level itself. In terms of vibration, it is often convenient to represent this type of mounting as a simple mass and spring, so then the approximate response characteristics can be evaluated. This type of analysis yields fast results, but the accuracy is reduced, since it is impossible to accurately represent a complex PCB with a few masses and springs. A real electronic system typically has many major resonant frequencies. The purpose of the simplified analysis is to try to simulate the first resonance where most of the damage normally occurs. Dynamic displacements, stresses and accelerations are usually maximum under these conditions [2]. Therefore, in this arrangement, the PCB might be mathematically approximated as a SDOF with base supporting motion, $y(t)$ as shown in Figure 2.6. This system is said to undergo base induced vibration and the motion of the system is described using only single absolute co-ordinate $x(t)$. In practice, this model is used to get a quick insight into the overall behaviour of the system.

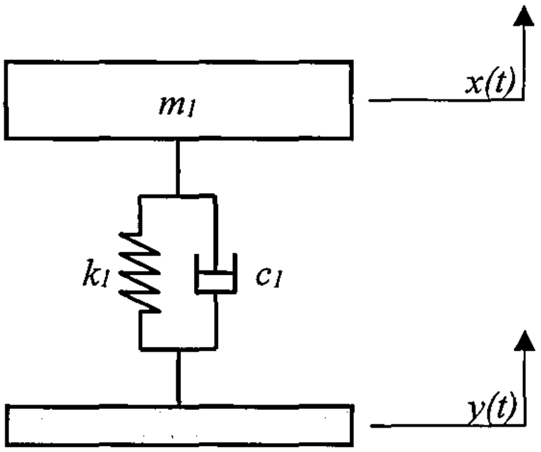

Figure 2.6. SDOF system

Figure 2.6 shows a simple mass-spring-damper system for simplification representing the PCB. Here m_1 is the apparent mass involved in motion of the PCB, k_1 and c_1 is the stiffness and damping characteristics of the PCB. The equation of motion is:

$$m_1\ddot{x} + c_1(\dot{x} - \dot{y}) + k_1(x - y) = 0 \tag{2.0}$$

The Laplace Transform changes the domain of the function from the positive real number line (t) to the complex number plane (s) [31]. That is:

$$x(t) \Leftrightarrow X(s)\,;\dot{x}(t) \Leftrightarrow sX(s)\,;\ddot{x}(t) \Leftrightarrow s^2X(s)\,;y(t) \Leftrightarrow Y(s) \tag{2.1}$$

This yields the equation of motion in the operator form:

$$m_1s^2X(s) + c_1s\left[X(s) - Y(s)\right] + k_1\left[X(s) - Y(s)\right] = 0 \tag{2.2}$$

or

$$X(s)\left(m_1s^2 + c_1s + k_1\right) = Y(s)\left(c_1s + k_1\right) \tag{2.3}$$

From (2.3), the universal absolute and relative transfer function are given by:

$$T_a(s) = \frac{X(s)}{Y(s)} = \frac{c_1s + k_1}{m_1s^2 + c_1s + k_1}, \tag{2.4}$$

$$T_r(s) = \frac{X(s) - Y(s)}{Y(s)} = \frac{c_1s + k_1}{m_1s^2 + c_1s + k} - 1 = \frac{-m_1s^2}{m_1s^2 + c_1s + k}. \tag{2.5}$$

We further express the above transfer functions in terms of natural frequency and loss factor $\Omega_1 = \sqrt{k_1/m_1}$, $\xi_1 = c_1/(2m_1\Omega_1)$. Each of the above expressions also the defines frequency response function, by the formal substitution of $s = j\omega$. Here s is restricted to lie along the imaginary axis in the complex plane and $j = \sqrt{-1}$, imaginary unit and ω is the angular frequency in radians per second. This yields universal absolute complex transmissibility:

$$T_a(j\omega)=\frac{\Omega_1{}^2+2j\omega\xi_1\Omega_1}{\Omega_1{}^2-\omega^2+2j\omega\xi_1\Omega_1}, \tag{2.6}$$

and universal relative complex transmissibility:

$$T_r(j\omega)=\frac{\omega^2}{\Omega_1{}^2-\omega^2+2j\omega\xi_1\Omega_2}, \tag{2.7}$$

Various forms of the analytical transmissibility functions can be used to curve fit the FRF measurement. From experiment, the above PCB might be modelled as a first approximation, as a lightly damped SDOF system. As recognised, the modulus of the universal absolute transmissibility may be expressed in terms of undamped natural frequency, Ω_1, and loss factor, ξ_1 that is:

$$|T_a(j\omega)|=\sqrt{\frac{\Omega_1^4+4\omega^2\xi_1^2\Omega_1^2}{\left(\Omega_1^2-\omega^2\right)^2+4\omega^2\xi_1^2\Omega_1^2}}. \tag{2.8}$$

The MS®Excel worksheet shown in Figure 2.7 describes this process being carried out with the experimentally measured data. The estimated values for natural frequency and loss factor are inputted into the boxes, B3 and B4, and are used in Equation 2.8 to calculate the universal absolute transmissibility of column F. The square difference between the experimental, column H, and analytical data, column F is calculated in column I, and summed in the box in the figure, B7 within the frequency range of 20-400 Hz for first mode. This value should be zero for the two curves to be matched. This brings in the use of the Solver function in which the summed cell, B7, is minimised by the Solver by altering the parameters of the PCB. The embedded graphs show the superimposed experimental data and curve-fitted one of the corresponding universal absolute transmissibility and relative transmissibility within the entire measured frequency range. The worksheet shows how the two curves are made to closely match the first vibration mode, giving numerical values for the properties for the first mode PCB. It is also used to verify that the Solver has performed properly as the difference could be minimised by large positive and negative differences cancelling each other out. This technique can be later used for extracting all modal parameters of the full-mode model of PCB.

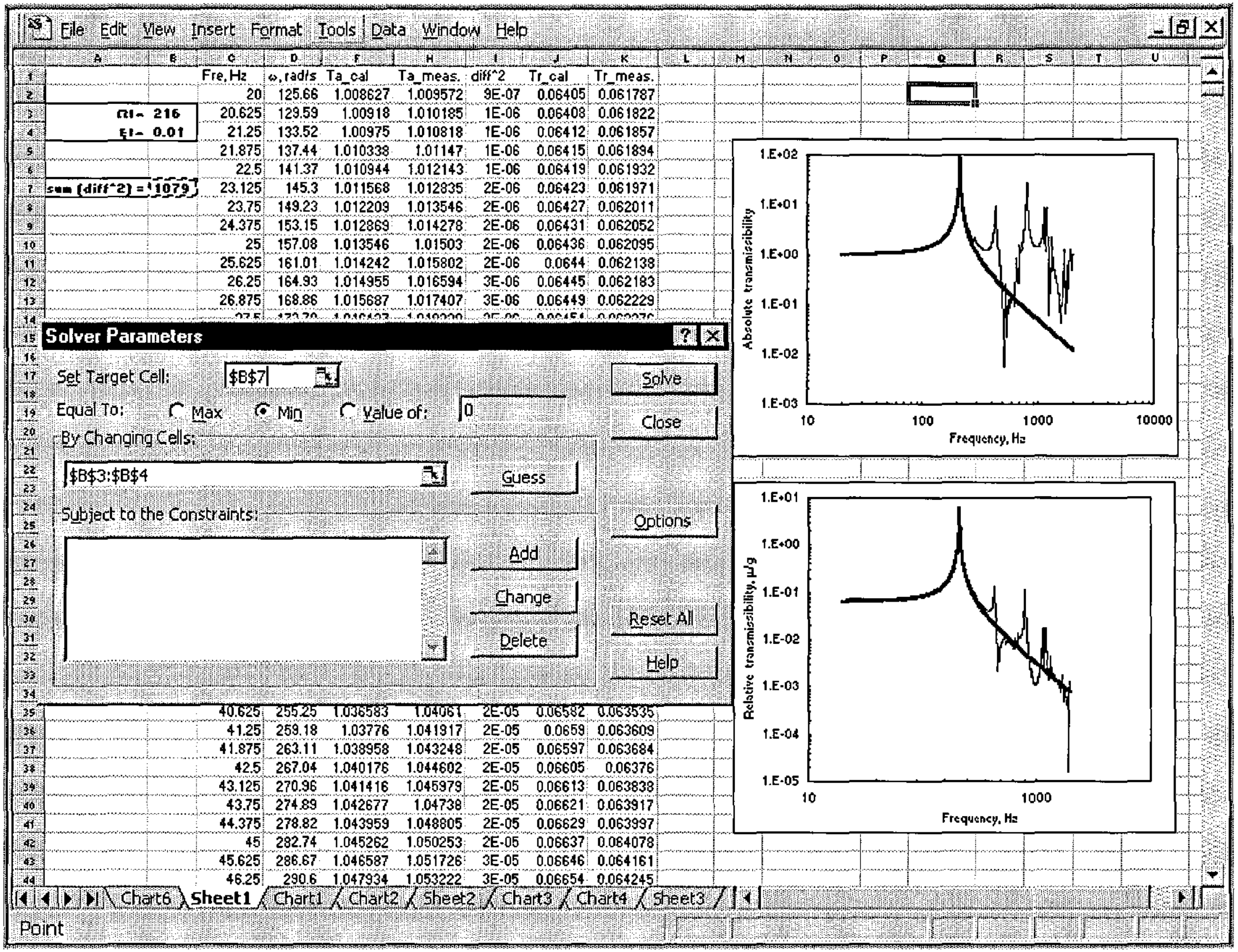
File Edit View Insert Format Tools Data Window Help
Chart6 Sheet1 Chart1 Chart2 Sheet2 Chart3 Chart4 Sheet3
Point
Absolute transmissibility
1.E+02
1.E+01
1.E+00
1.E-01
1.E-02
1.E-03
10
100
1000
10000
Frequency, Hz
Relative transmissibility, μ/g
1.E+01
1.E+00
1.E-01
1.E-02
1.E-03
1.E-04
1.E-05
10
1000
Frequency, Hz

	A	B	C	D	F	H	I	J	K
1			Fre, Hz	ω, rad/s	Ta_cal	Ta_meas.	diff^2	Tr_cal	Tr_meas.
2			20	125.66	1.008627	1.009572	9E-07	0.06405	0.061787
3	ω1=	216	20.625	129.59	1.00918	1.010185	1E-06	0.06408	0.061822
4	ξ1=	0.01	21.25	133.52	1.00975	1.010818	1E-06	0.06412	0.061857
5			21.875	137.44	1.010338	1.01147	1E-06	0.06415	0.061894
6			22.5	141.37	1.010944	1.012143	1E-06	0.06419	0.061932
7	sum (diff^2) =	1079	23.125	145.3	1.011568	1.012835	2E-06	0.06423	0.061971
8			23.75	149.23	1.012209	1.013546	2E-06	0.06427	0.062011
9			24.375	153.15	1.012869	1.014278	2E-06	0.06431	0.062052
10			25	157.08	1.013546	1.01503	2E-06	0.06436	0.062095
11			25.625	161.01	1.014242	1.015802	2E-06	0.0644	0.062138
12			26.25	164.93	1.014955	1.016594	3E-06	0.06445	0.062183
13			26.875	168.86	1.015687	1.017407	3E-06	0.06449	0.062229
35			40.625	255.25	1.036583	1.04061	2E-05	0.06582	0.063535
36			41.25	259.18	1.03776	1.041917	2E-05	0.0659	0.063609
37			41.875	263.11	1.038958	1.043248	2E-05	0.06597	0.063684
38			42.5	267.04	1.040176	1.044602	2E-05	0.06605	0.06376
39			43.125	270.96	1.041416	1.045979	2E-05	0.06613	0.063838
40			43.75	274.89	1.042677	1.04738	2E-05	0.06621	0.063917
41			44.375	278.82	1.043959	1.048805	2E-05	0.06629	0.063997
42			45	282.74	1.045262	1.050253	2E-05	0.06637	0.064078
43			45.625	286.67	1.046587	1.051726	3E-05	0.06646	0.064161
44			46.25	290.6	1.047934	1.053222	3E-05	0.06654	0.064245

Solver Parameters

Set Target Cell: $B$7

Equal To: ○ Max ● Min ○ Value of: 0

By Changing Cells: $B$3:$B$4

Subject to the Constraints:

Solve
Close
Guess
Options
Add
Change
Delete
Reset All
Help

Figure 2.7. Curve-fitting using the Solver function.

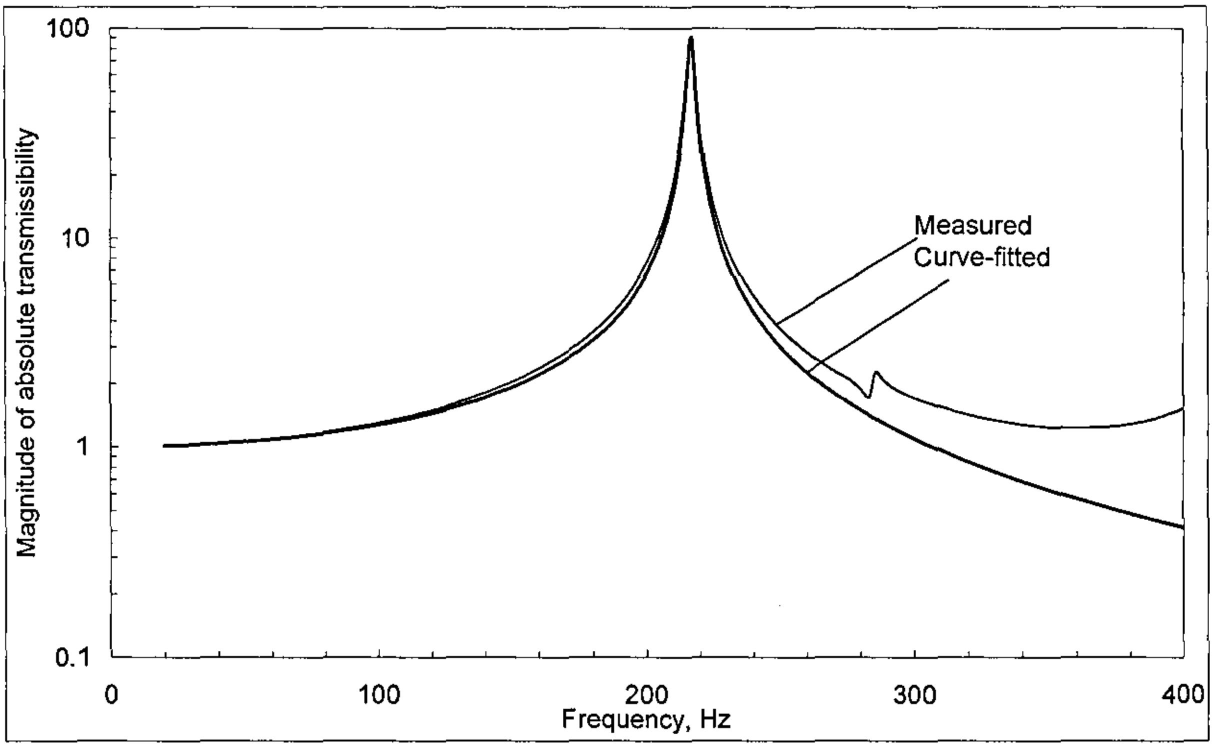

a) Modulus

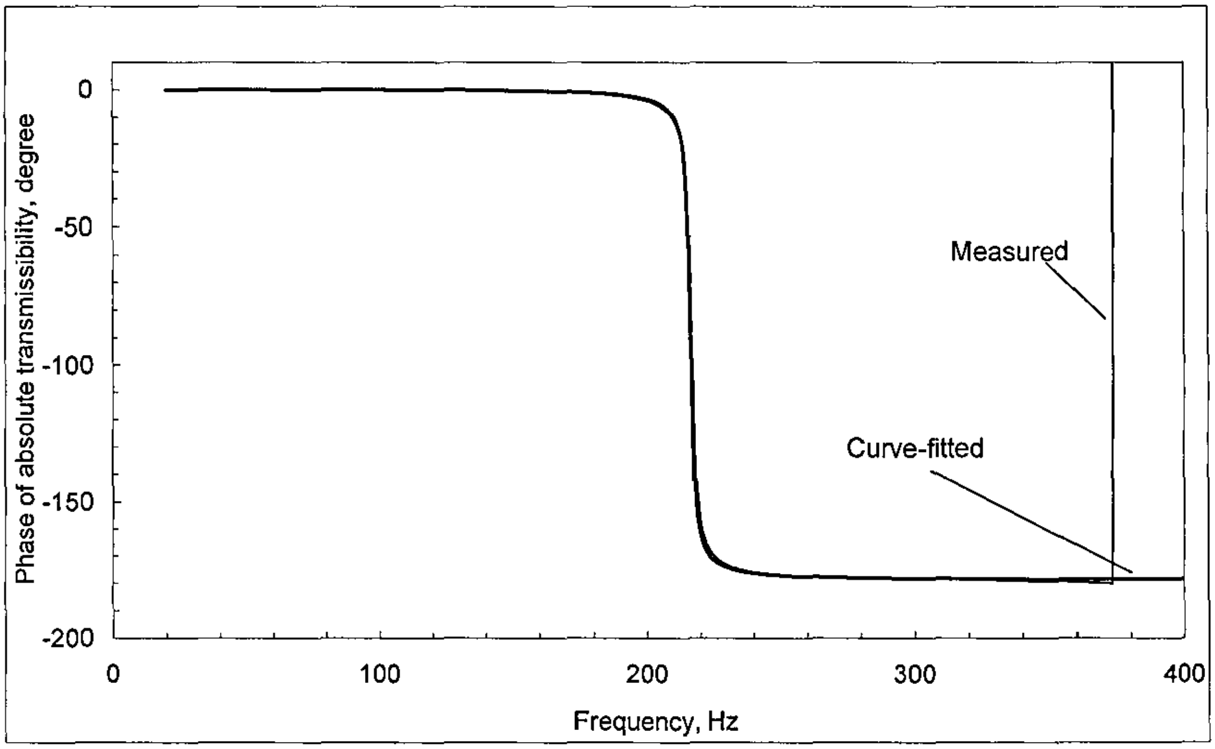

b) Phase

Figure 2.8. Comparison absolute transmissibility of first-mode PCB

In Figure 2.8, curve-fitting is applied to the experimental data in the vicinity of the first resonant frequency. From curve-fitting, $\xi_1 = 0.0065$, $\Omega_1/2\pi = 216.25$ Hz are found. Figure 2.8 shows the superimposed original transmissibility of the PCB and curve-fitted one in the frequency range of 20-400 Hz.

2.4 Determining the effective mass of PCB

The mass of the PCB, required for further analysis, can not be found by weighting the whole PCB. Only certain parts of the PCB vibrate when it is shaken, as the edges are screwed firmly to the pillars. This means that the mass of the board actually moving part will be less than the mass of the whole board.

Since $|T_a(j\omega)|$ from (2.8) does not contain a mass explicitly, a new experiment has to be carried out. The effective mass of the first mode of the PCB will be of a great importance in the further development of a dynamic absorber. The effective mass can be estimated by defining the modified value of the natural frequency, Ω_a by attaching the trial mass, m_a at the point where dynamic absorber to be attached. In accordance with [31]:

$$m_1 = m_a \Big/ \left[(\Omega_1 / \Omega_a)^2 - 1 \right]. \tag{2.9}$$

A trial mass of 9.3 gr was attached to the PCB, and modified natural frequency is estimated to be 206.25 Hz as shown in Figure 2.9. From (2.9), the first mode mass is m_1=90 gr whilst the total mass of the PCB is 175.5 gr.

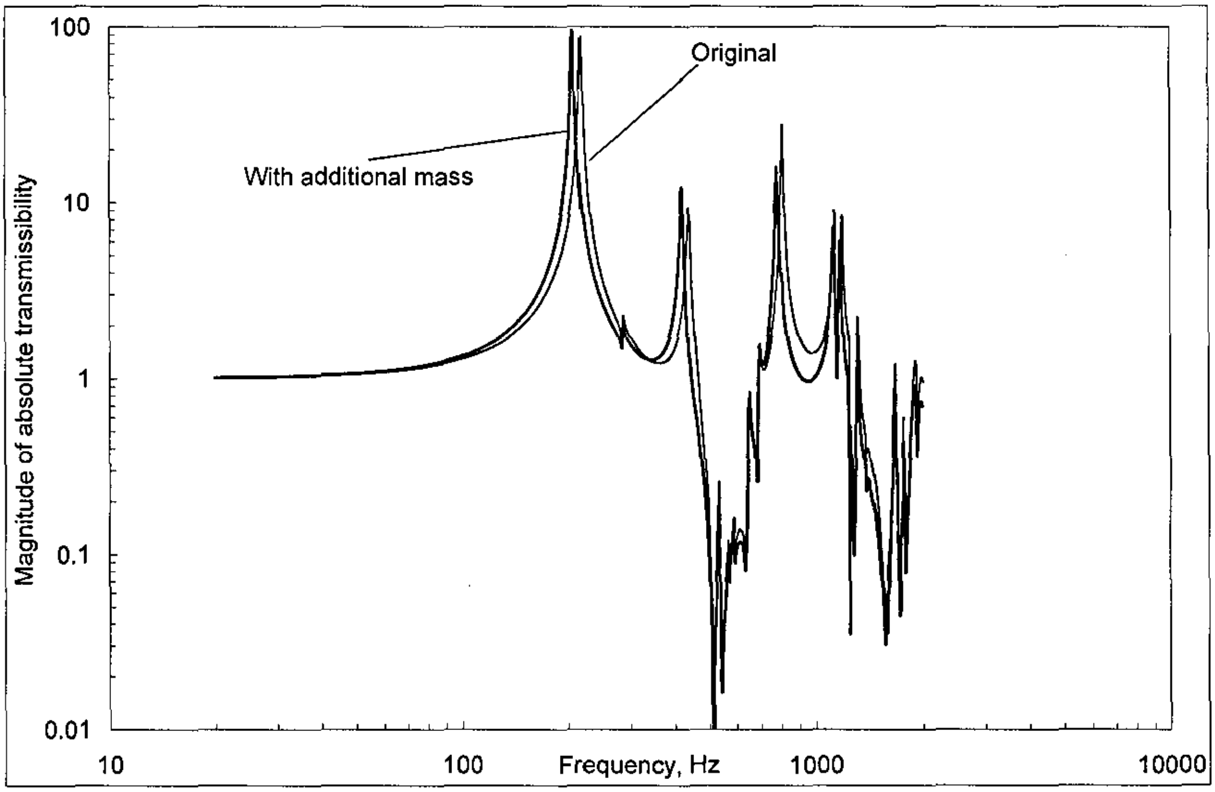

Figure 2.9. Experimentally measured modulus of absolute transmissibility of PCB

2.5 Additional measurement

The dynamic properties of the complex plate-wise structured PCB might not be the same, typically FRF and effective mass if the above measuring technique is also to be considered for different locations on the PCB. Unlike a simple mass and spring system, a single point measurement might not be sufficient to represent the entire dynamic properties of the PCB for further analysis and comparison purposes. Although, the above measurements were made in the area where the relative deflection of the PCB is assumed to be maximum. It is clear that additional experimental data (universal transmissibilities) on different areas of the original PCB must be carried out at this stage. For this reason, observation point ①, ②, ③ and ④ are marked symmetrically from the origin, observation point ⓪ on the PCB which represents in the schematic layout in Figure 2.10 as reference. In this figure, observation point ⓪ at the centre of PCB might be treated as a critical measurement and calculation point for appropriate vibration control method. Additionally, such an observation point ensures that the major nodal points will not be involved, the dynamic properties of the PCB are already obtained; the experimentally measured data and detailed analysis have been discussed above.

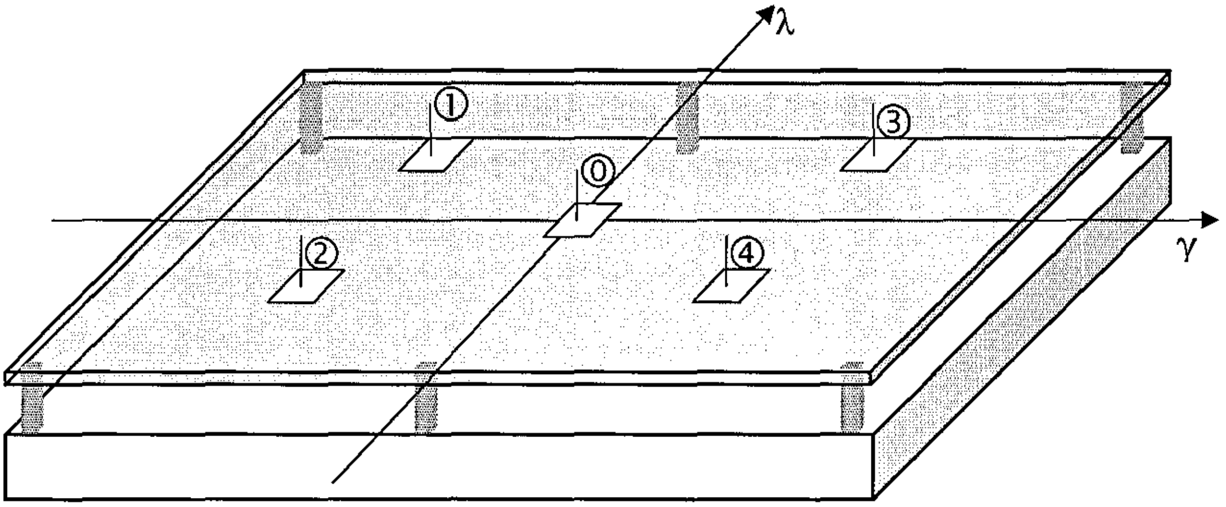

Figure 2.10. Schematic layout of the PCB marked with observation point

Figure 2.11 shows the experimentally obtained moduli of universal transmissibilities of the corresponding observation point on the PCB. As would be expected the responses are different from each other, although these points are observed symmetrically from the origin. This could explain why traditional methods normally fail to predict the actual FRF of the PCB. However, the first natural frequency is about 220 Hz at which the peak amplification is steepest.

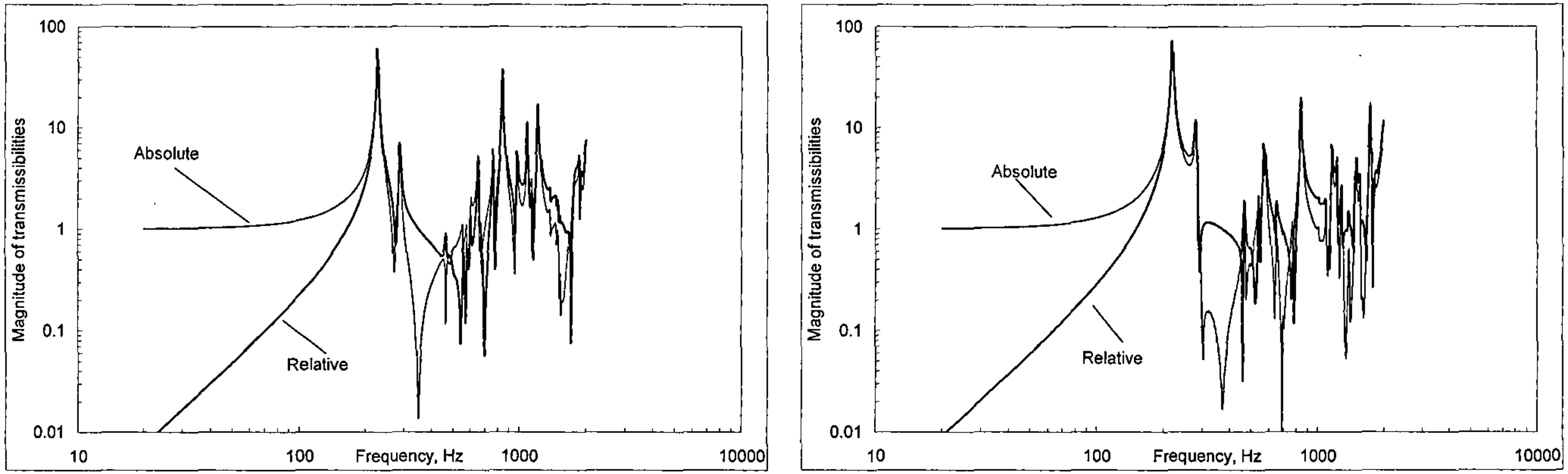

a) Observation point ①

b) Observation point ②

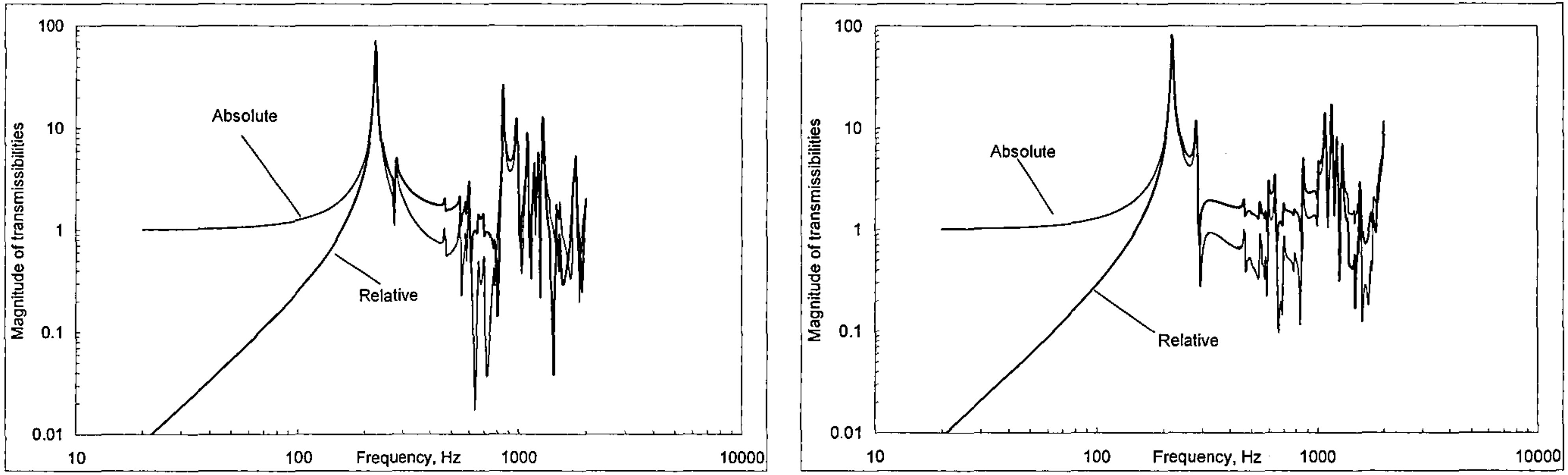

c) Observation point ③

d) Observation point ④

Figure 2.11a. Experimentally measured modulus of universal transmissibilities at different observation points on PCB

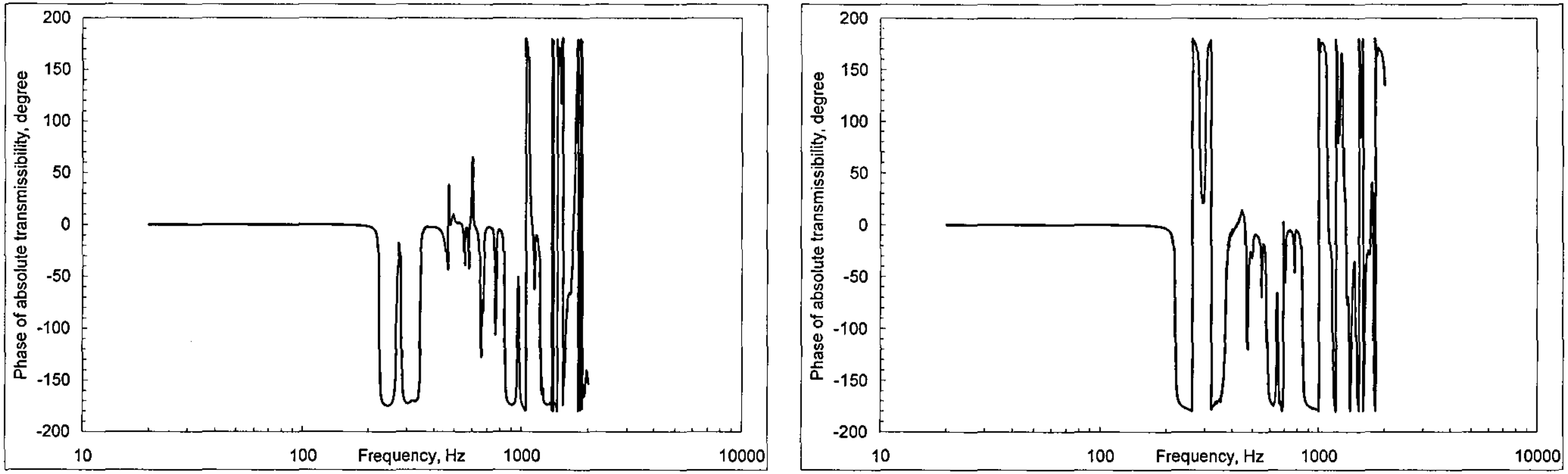

a) Observation point ①

b) Observation point ②

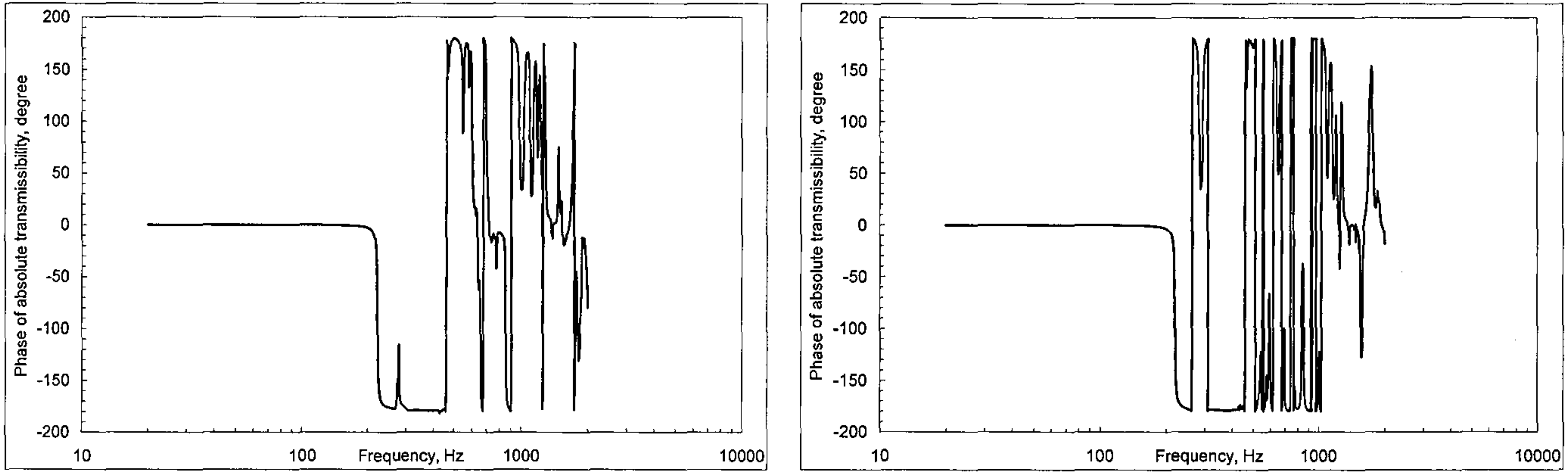

c) Observation point ③

d) Observation point ④

Figure 2.11b. Experimentally measured phase of absolute transmissibility at different observation points on PCB

2.6 Measurement of receptance

For single-mode approximation, the dynamic properties at observation point ⓪ might be sufficient to represent dynamic properties of the PCB and experimentation with dynamic absorber can begin. However, for analysis of the full-mode model of PCB, it is necessary at this stage, to obtain the local and transient receptances of those corresponding observation points.

2.6.1 Local receptance

Figure 2.12 shows an experimental rig where the fixture ② supports the PCB ① and was rigidly clamped to the rigid and massive isolated table ③ to avoid unwanted interference. The instrumented impact hamper ④ (PCB Piezotronics) contains a piezoceramic force transducer ⑤ providing the assessable force excitation to the PCB. To concentrate the whole energy in the frequency range up to 2000 Hz, a hard hammer tip was used. Through the Charge Amplifier ⑨, the signal of the excitation force is passed firstly to channel of Signal Analyser ⑩. Simultaneously, the dual beam laser Vibrometer ⑦ measures the velocity of PCB relative to the fixture. This relative signal is then passed to the second channel of the Signal Analyser via the Vibrometer Controller ⑧.

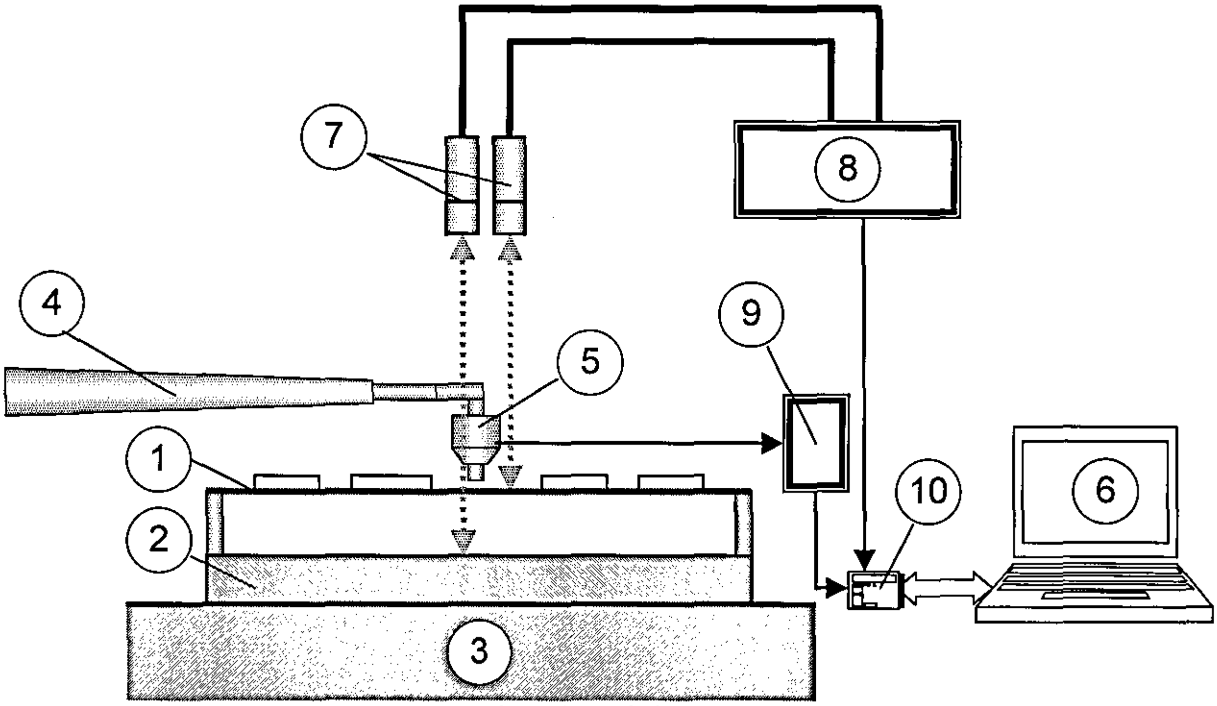

a) Schematic layout

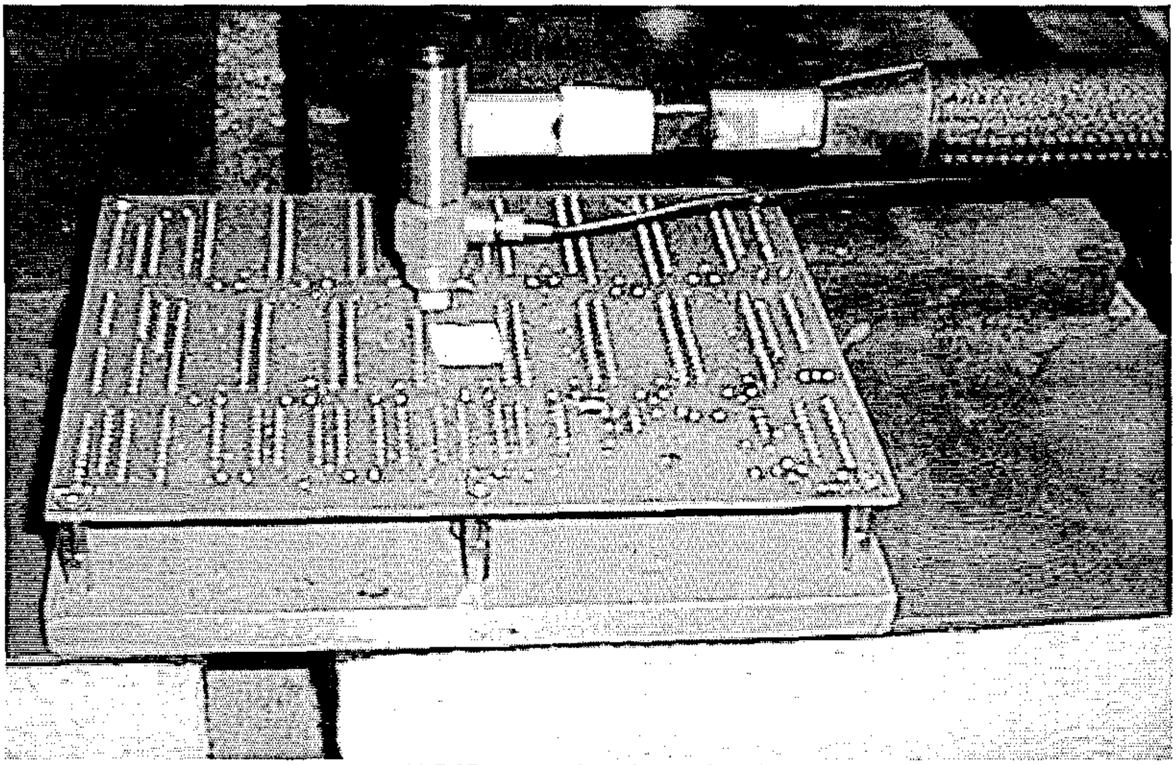

b) PCB mounted on the test bench

Figure 2.12. Experimental rig for measuring local receptance of PCB

The first test was carried out at observation point ◎ on the PCB, where the dynamic absorber was to be attached. At this location, the impact hammer was struck on the PCB and the laser beam is positioned nearby. The pick up signals are determined as local receptance, expressed as the ratio of the displacement at a response point divided by the force at the input point at any frequency.

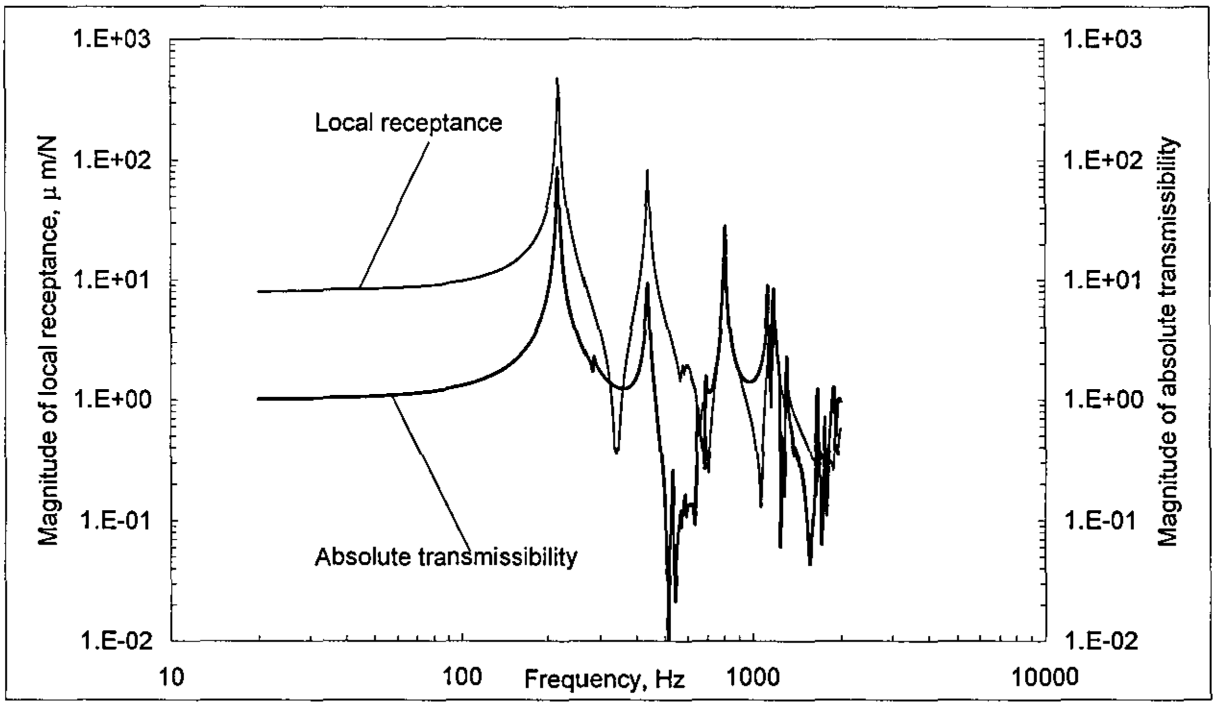

a) Moduli

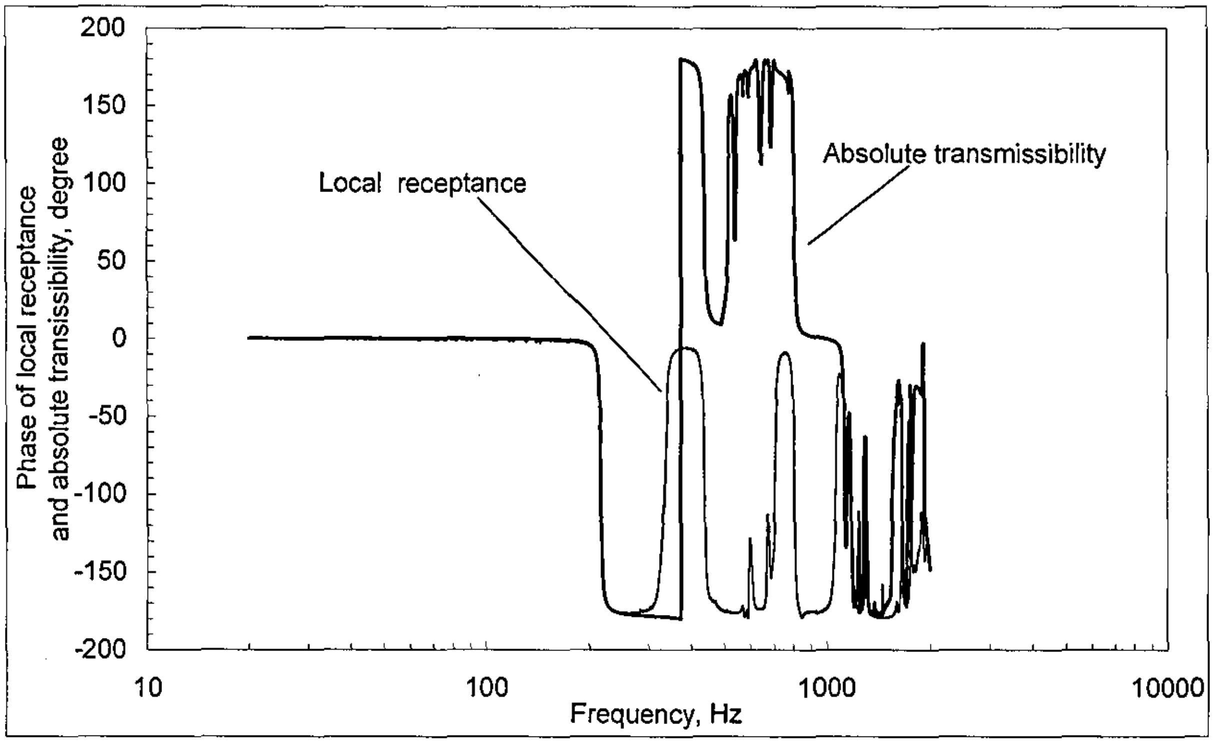

b) Phase

Figure 2.13.Experimentally measured receptance and absolute transmissibility of PCB

Figure 2.13 shows the superimposed local receptance and absolute transmissibility of the PCB. From Figure 2.13, the resonant sequence is consistent for absolute transmissibility and local receptance.

2.6.2 Transient receptance measurement

Regarding the calculation of observation point ①, ②, ③ and ④ for the modified PCB using a dynamic absorber and its designed location, it clearly indicates the transient receptance for these observation points of the original PCB must be obtained before the analysis can begin. The experimental procedure for measuring these data is the same as that in Figure 2.12.

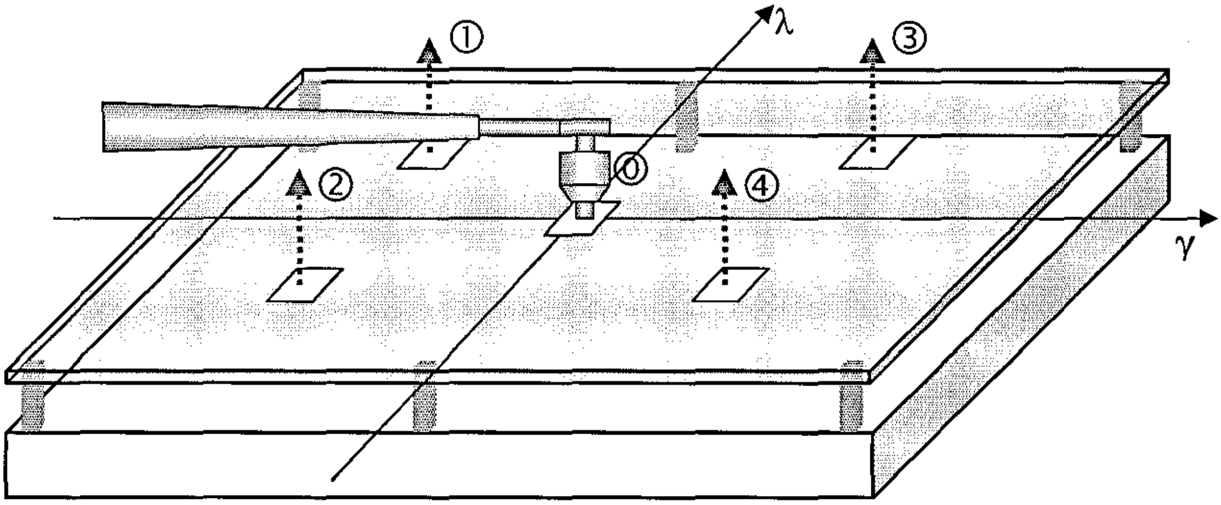

Figure 2.14. Schematic layout of measuring transient receptance on PCB

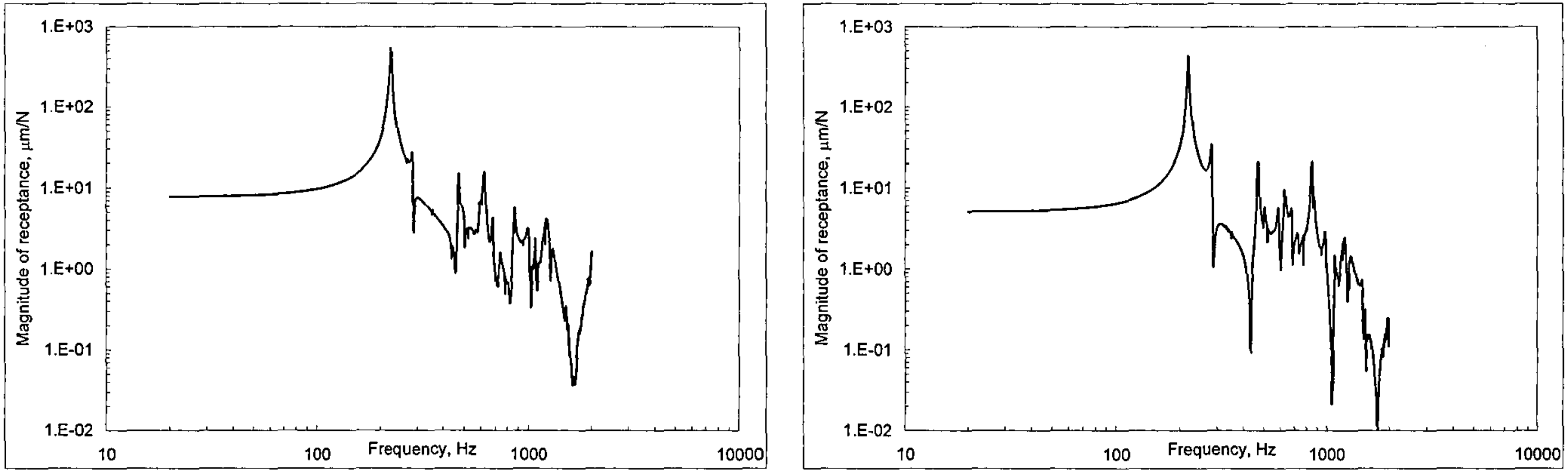

a) Observation point ①

b) Observation point ②

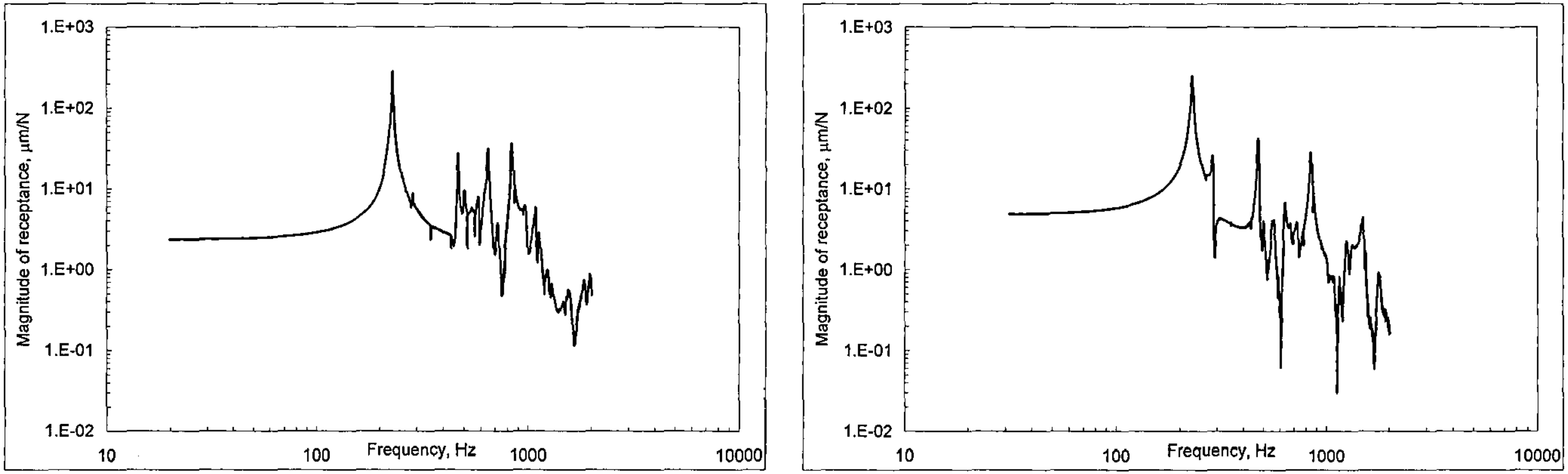

c) Observation point ③

d) Observation point ④

Figure 2.15a. Experimental measured modulus of receptance at different observation points on PCB

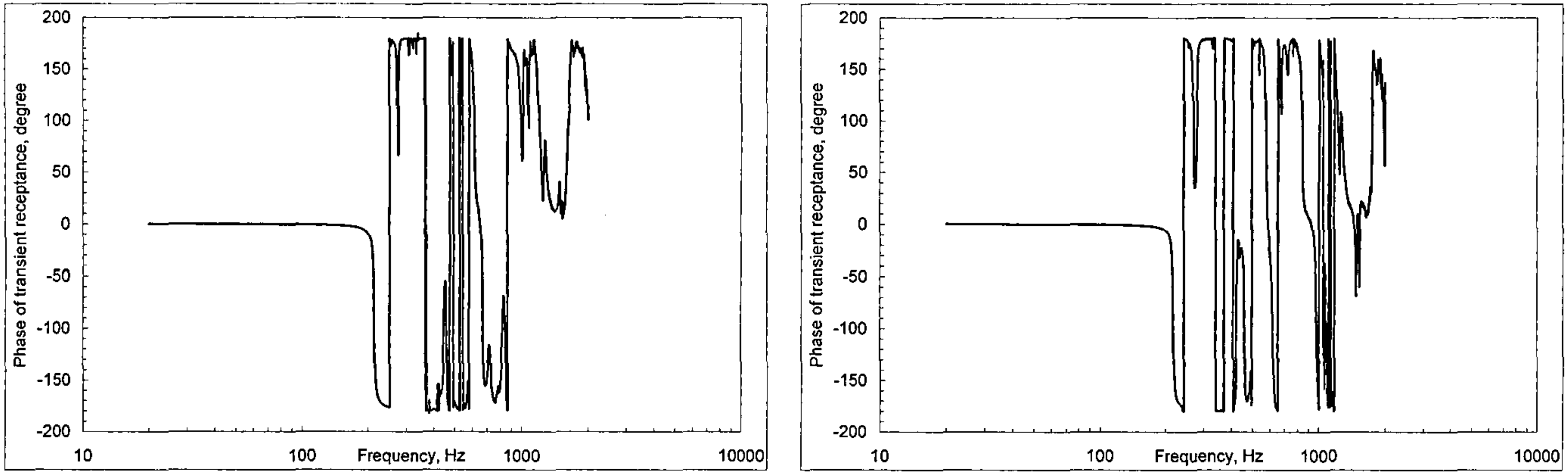

a) Observation point ①

b) Observation point ②

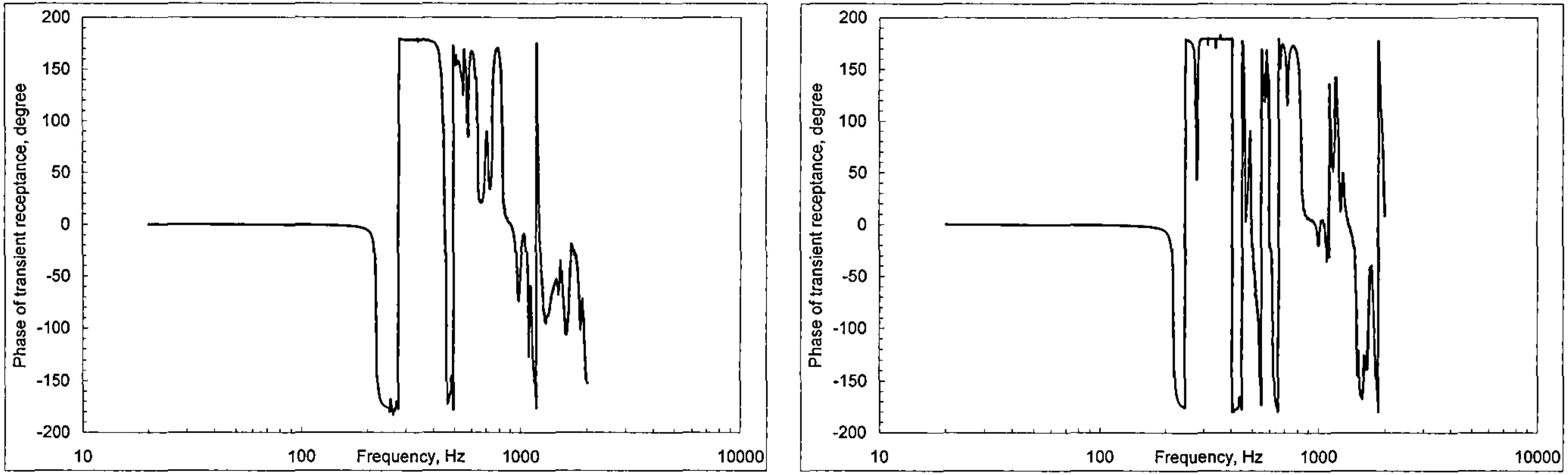

c) Observation point ③

d) Observation point ④

Figure 2.15b. Experimental measured phase of receptance at different observation points on PCB

Figure 2.14 describes schematically a method of measuring transient receptance of different observation points. In this test, the hammer is struck at observation point ◎ (where the dynamic absorber is to be attached) and the responses of these observation points are obtained accordingly.

Figure 2.15a and Figure 2.15b show the experimental modulus and phase of transient receptance in μm/N of the corresponding observation point on the original PCB. From a magnitude response perspective, they are quite consistent with each other and they all show the dominance of first-mode natural frequency of the PCB. Since effective mass of these observation points is partially embedded in the measured receptances, the method of determining effective mass for these locations is no longer needed.

2.8 Concluding remarks

Results obtained with experimental measurement proved to be quantitatively consistent. The experimental rig was set-up in accordance to the PCB mounting configuration, although it does not represent the actual PCB system mounting, but still has the desired properties of mass, natural frequency and damping ratio. As usual for this kind of analysis and its obtained results, the task was logically followed:

- Preparation of the PCB was made in such a way to reduce the inevitable experimental errors
- By appropriately exciting the PCB and measuring its dynamic response, and then these signals were treated to get information in the frequency domain
- Collection of frequency response function measurements with several different locations on the PCB for future purposes
- The reliability of modal parameter extraction methods using Least Squares is accepted, the PCB's constraints responds to good modal analysis practice requirements. Obviously, the high quality MS®Excel and its companion built-in Solver opens a whole new class of vibration design aspects, typically those that are concerned with optimal performance and graphical presentation
- The observability of the PCB was good, the information content of excitation and response signal was abundantly sufficient and the PCB proved to be time invariant and linear
- The analytical solution of the single-mode and full-mode model of PCB with dynamic absorber can be relied upon according to the above experimental information.

Chapter 3

3.0 Single-mode model of PCB with dynamic absorber attached

In this chapter, we are introducing a damped dynamic absorber as a new radical vibration control method for the PCB. In general, designing dynamic absorbers have a number of very attractive features:

- They are inherently compact, modular devices that can have a simple attachment to the base structure without external interface
- They can be readily added to a base structure that is already designed or even built
- The dynamic absorber does not impact the static strength or stiffness of the base structure
- For designing the dynamic absorber, it is often possible to characterise the base structure by inexpensive testing or analysis. Additionally, a dynamic absorber can be designed for any frequency resonance of the base structure, and there is no constraint of its design parameters.

However, the practical challenge in designing and implementing a dynamic absorber is usually concerned with the optimal performance in different environment conditions. This means that a universal dynamic absorber for the PCB application must be capable of withstanding random, swept-sine vibration and even shock. For this purpose, we are accommodating single dynamic absorber in the development of the mathematical model. The investigation of optimal parameters of the dynamic absorber depends on its operational environment, random vibration, followed by swept-sine and shock excitation with the aim of minimising the relative deflection of the modified system. In order to achieve these tasks, first, we used MS®Excel and its Solver to find an appropriate optimal parameters set of the dynamic absorber. Once these parameters are known then a numerical simulation is built using Matlab/Simulink environment to verify its analytical solution.

3.1 Mathematical model

In this approach, the primary system (PCB) is thought of as a SDOF system with a mass, m_1, stiffness, k_1, and damping c_1. The secondary system is a dynamic absorber mounted upon the PCB with mass, m_2, stiffness, k_2, and damping c_2. The excitation is due to the motion of the base, $y(t)$. Figure 3.0 shows this model.

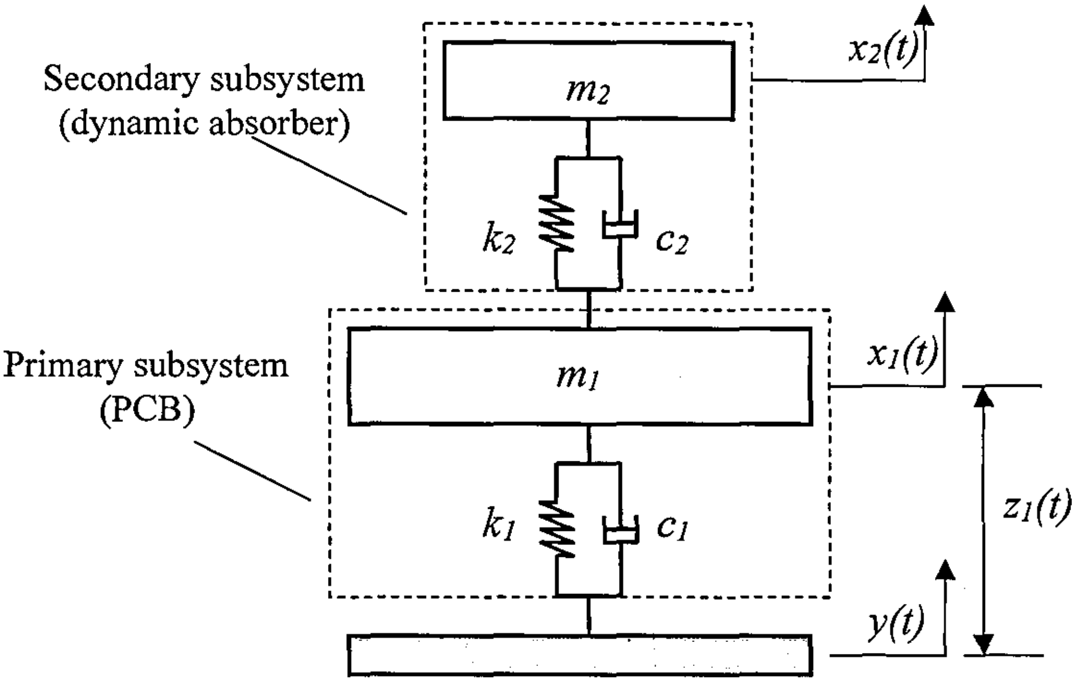

Figure 3.0. Model of PCB in a single-mode approximation with attached dynamic absorber

The equations of motion take the form:

$$m_1\ddot{x}_1 + c_1(\dot{x}_1 - \dot{y}) + k_1(x_1 - y) + k_2(x_1 - x_2) + c_2(\dot{x}_1 - \dot{x}_2) = 0\,, \tag{3.0}$$

$$m_2\ddot{x}_2 + c_2(\dot{x}_2 - \dot{x}_1) + k_2(x_2 - x_1) = 0\,. \tag{3.1}$$

The values for stiffness and damping may be expressed through the appropriate values of mass ratio $\eta = \frac{m_2}{m_1}$, partial undamped frequencies Ω_1, Ω_2 and partial loss factors ξ_1, ξ_2. These are:

$$c_1 = 2m_1\Omega_1\xi_1,\ k_1 = m_1\Omega_1^2,\ c_2 = 2\eta m_1\Omega_2\xi_2 \text{ and } k_2 = \eta m_1\Omega_2^2\,.$$

In Figure 3.0, x_1, x_2 and y are the absolute deflections of the PCB, dynamic absorber and the base, respectively, and z_1 is the motion of the PCB relative to the base. Taking the Laplace transform, yields:

$$x_{1,2}(t) \Leftrightarrow X_{1,2}(s)\,;\dot{x}_{1,2}(t) \Leftrightarrow sX_{1,2}(s)\,;\ddot{x}_{1,2}(t) \Leftrightarrow s^2X_{1,2}(s)\,;y(t) \Leftrightarrow Y(s)\,;z_1(t) \Leftrightarrow Z_1(s)\,,$$

where *s* is the Laplace variable.

Expressing the equations of motion in the matrix form yields:

$$\begin{bmatrix} m_1s^2 + (c_1 + c_2)s + k_1 + k_2 & -(c_2s + k_2) \\ -(c_2s + k_2) & (m_2s^2 + c_2s + k_2) \end{bmatrix} \begin{bmatrix} X_1 \\ X_2 \end{bmatrix} = \begin{bmatrix} c_1s + k_1 \\ 0 \end{bmatrix} Y\,. \tag{3.2}$$

From the matrix equation, absolute transfer function of the combined system is:

$$\widetilde{T}_a(s)=\frac{(c_1 s+k_1)(m_2 s^2+c_2 s+k_2)}{\left[m_1 s^2+(c_1+c_2)s+k_1+k_2\right](m_2 s^2+c_2 s+k_2)-(c_2 s+k_2)^2}. \tag{3.3}$$

By the formal substitution, $s=j\omega$, where $j=\sqrt{-1}$ and ω is the angular frequency, we find the appropriate FRF i.e. complex universal absolute transmissibility

$$\widetilde{T}_a(j\omega)=\frac{(k_2-m_2\omega^2+c_2 j\omega)(c_1 j\omega+k_1)}{\left[k_1+k_2-m_1\omega^2+(c_1+c_2)j\omega\right](k_2-m_2\omega^2+c_2 j\omega)-(c_2 j\omega+k_2)^2}, \tag{3.4}$$

For the universal relative transmissibility, we find:

$$\widetilde{T}_r(j\omega)=\widetilde{T}_a(j\omega)-1. \tag{3.5}$$

3.2 Random vibration

Flight dynamics deal with the motion of an aircraft under the influence of forces, which contributes to the caustic environment. Resulting from these harsh environmental conditions, a need for a vibration protection system has been addressed. Sometimes the endurance of the COTS PCB is lower than required, thus slight modification is practised in order to protect the sensitive internal components in the electronic box.

A wide-band random process is a stationary process whose spectral density function has significant values over a range or band of frequency [32]. Random vibration closely represents the true environment in which the electronic equipment operates. Random vibration tests have become very commonplace in many installations for military electronics equipment. Primary military specifications for the testing of this type of equipment (such as MIL-STD-810) have placed heavy emphasis on random vibration, tailored to the actual application. By designing, developing and producing a cost-effective and lightweight structure, the equipment is capable of operating in the desired environment with a high degree of reliability.

A Gaussian distribution curve is used to represent the probability value of the instantaneous acceleration level expected for random vibration. The maximum acceleration levels considered for random vibration are the 3σ levels because the instantaneous acceleration is between $+3\sigma$ and -3σ levels corresponds to 99.73% of the time which is close to 100% [32].

The relationship between power spectral density (PSD) of excitation and relative response is [32]:

$$S_{Z_1}(\omega)=\left(\frac{\left|\widetilde{T}_r(j\omega)\right|}{\omega^2}\right)^2 S_{\ddot{y}}(\omega), \tag{3.6}$$

where $S_{\ddot{y}}(\omega)$ is PSD of the base acceleration and $S_{Z_1}(\omega)$ is PSD of relative deflection, $\omega \in [0,\infty[$. It is important to reduce the overall stresses in the system, and the mean square value of the relative deflection [32]:

$$\sigma_{Z_1} = \sqrt{\frac{1}{2\pi}\int_0^\infty S_{Z_1}(\omega)d\omega} \tag{3.7}$$

may be thought of as a measure of these.

3.2.1 Designing MS®Excel worksheet for minimising overall relative deflection

In theory, most of the approaches presented in reference [13-19] may be used to find the optimal response for this particular problem. However, it has been rather difficult to select the right method, obviously, a high degree of accuracy in results is very time-consuming. Additionally, in their approaches the vibratory motion is caused by force excitation in which inapplicable for this study.

With the increase in computational power, there are now a number of packages available to solve such problems without time-consuming and mathematical complication. One of the most popular packages is MS®Excel with the built-in Solver allowing for simplest optimisation. This package can handle complex numbers. Unlike other packages, MS®Excel is widely available and does not require high programming skills.

The equation for the damped 2DOF system discussed earlier can be now set-up in MS®Excel worksheet. All the transfer functions are to be in complex numbers as a function of frequency. It is much easier to work in terms of a complex transfer function rather than absolute values of the latter. This is because as the degree of freedom increases from SDOF to 2DOF, the terms get more complicated and it is much more difficult to obtain the analytical expression for the modulus of the transfer function. Since most of the complex terms are often used more than once, the calculation of the complex resultant transfer function can be eased by breaking it into smaller "pieces" and formulating them in appropriate columns. These smaller terms can be conveniently "submerged" inside the worksheet to "give way" for the resultant equation. Summing the values of PSD over the frequency spectrum and multiplying by the frequency step to produce an appropriate RMS value.

To make practical use of these resultant equations, a MS®Excel worksheet has been developed to calculate the RMS value of the power spectrum density of the relative deflection. The worksheet, shown in Figure 3.1, takes predetermined parameters for the primary system and evaluates the relative response to excitation over a frequency range, taking into account the parameters of the dynamic absorber.

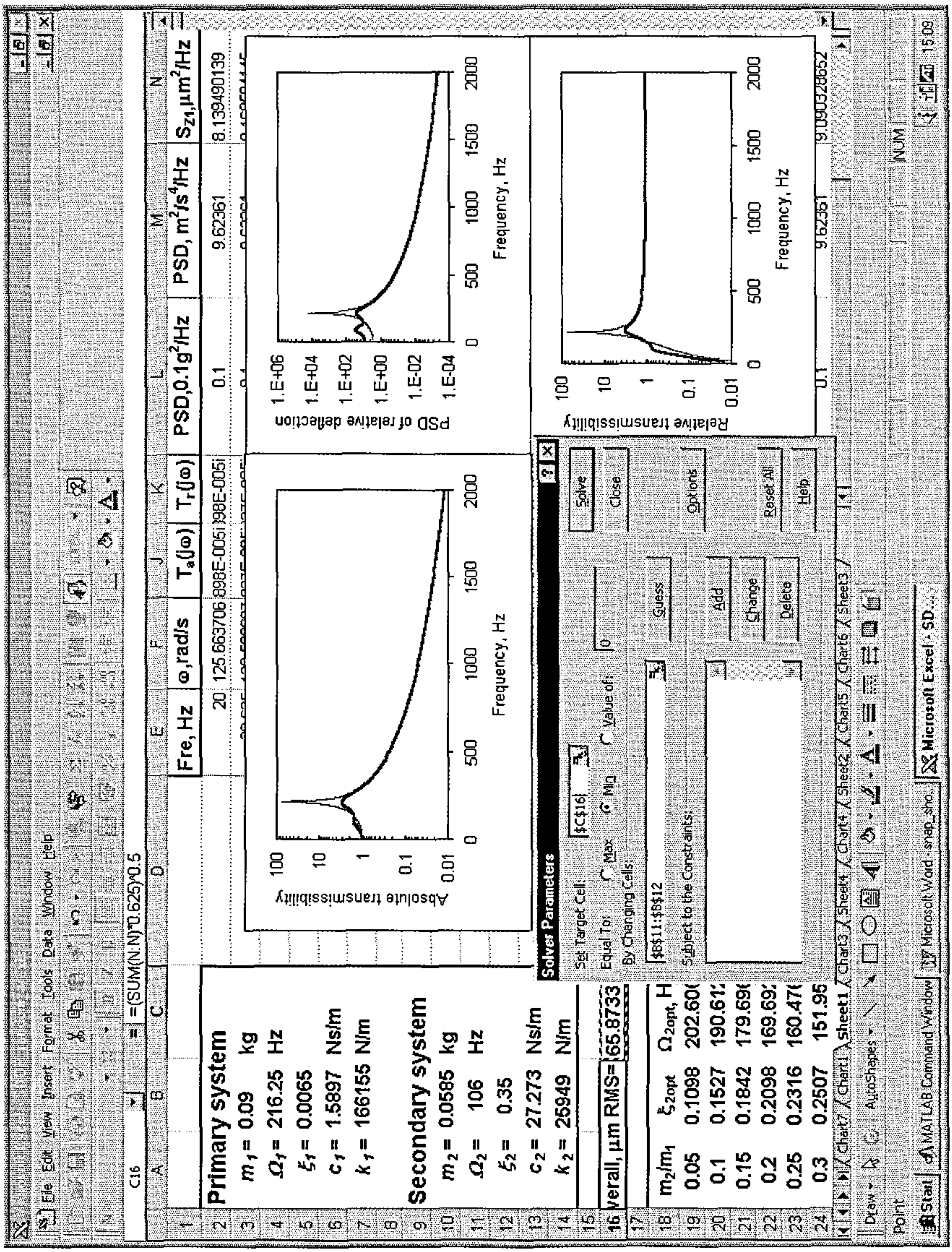

C16 = =(SUM(N:N)*0.625)^0.5

Fre, Hz	ω,rad/s	$T_a(j\omega)$	$T_r(j\omega)$	PSD,0.1g^2/Hz	PSD, m^2/s^4/Hz	S_{Z1},μm^2/Hz
20	125.663706	898E-005i	98E-005i	0.1	9.62361	8.139490139

Primary system

m_1 = 0.09 kg

Ω_1 = 216.25 Hz

ξ_1 = 0.0065

c_1 = 1.5897 Ns/m

k_1 = 166155 N/m

Secondary system

m_2 = 0.0585 kg

Ω_2 = 106 Hz

ξ_2 = 0.35

c_2 = 27.273 Ns/m

k_2 = 25949 N/m

verall, μm RMS= 65.8733

m_2/m_1	ξ_{2opt}	Ω_{2opt}, H
0.05	0.1098	202.60
0.1	0.1527	190.61
0.15	0.1842	179.69
0.2	0.2098	169.69
0.25	0.2316	160.47
0.3	0.2507	151.95

Solver Parameters

Set Target Cell: $C$16

Equal To: ○ Max ● Min ○ Value of: 0

By Changing Cells: $B$11:$B$12

Subject to the Constraints:

File Edit View Insert Format Tools Data Window Help
Absolute transmissibility
100
10
1
0.1
0.01
0
500
1000
1500
2000
Frequency, Hz
PSD of relative deflection
1.E+06
1.E+04
1.E+02
1.E+00
1.E-02
1.E-04
Relative transmissibility
Solve
Close
Guess
Options
Add
Change
Delete
Reset All
Help
Chart7
Chart1
Sheet1
Chart3
Sheet4
Chart4
Sheet2
Chart5
Chart6
Sheet3
Draw
AutoShapes
Point
NUM
Start
MATLAB Command Window
Microsoft Word - snap_sho...
Microsoft Excel - SD...
15:09

Figure 3.1. Spreadsheet for calculation of dynamic response and for optimisation

The various parameters describing the complete system, including the dynamic absorber, are placed in the **Primary System** and **Secondary System** area. Columns E and F contain the frequency range in Hz and rad/s respectively. In column J, the universal absolute transmissibility is calculated using Equation 3.4 followed by universal relative transmissibility, column K using Equation 3.5 with embedded graphs (superimposed of the original and the modified system) to make it easier to spot mistakes. The excitation experienced by the system is given in columns L and M in units of g^2/Hz and m^2/s^4/Hz respectively.

With the establishment of the PSD value for relative deflection, in column N, using Equation 3.6 this spreadsheet will then calculate the overall RMS response of the PCB using Equation 3.7. By manually varying the mass ratio, η, in the range from 0 to 1, the Solver is then set to minimise the overall relative deflection response of the PCB (3.7) by varying the values Ω_2 and ξ_2.

Figure 3.1 features a built-in Solver function which can be found under the "Tools" drop menu. The Solver allows the minimisation or maximisation of a target cell by varying other cells related to the target. The program runs through trial and error iterations in a feedback loop within certain boundaries to optimise the solution. The boundaries consist of a period of time before the user is questioned before the computer continues and tolerance limits that can be altered depending on the desired result.

The values obtained can be irrelevant for the particular problem, especially with negative numbers being returned. This can be clearly seen as the visualising graph which shows the curve as the incorrect shape. This problem can be overcome by altering the initial guesses inputted into the variable boxes. The Solver can then be rerun with the iterations taking a different path until the visualising graph looks closer to the expected shape.

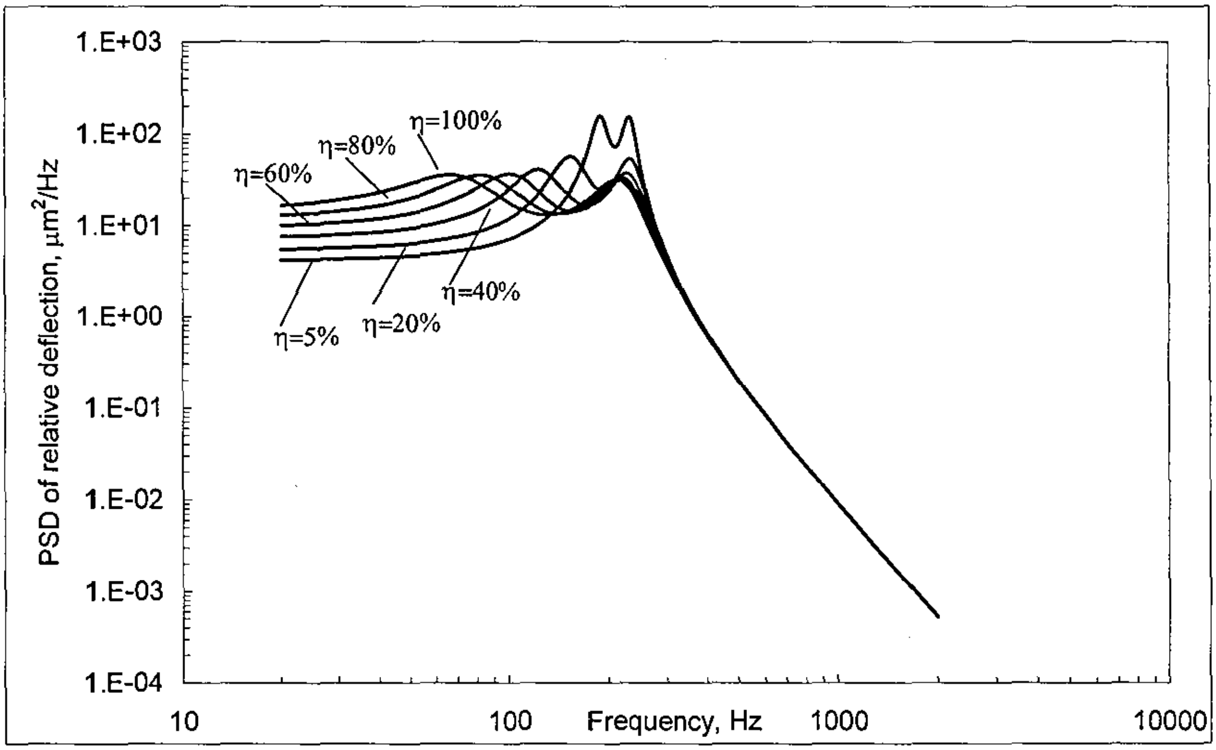

Figure 3.2. Dynamic response of PCB at different mass ratios

Figure 3.2 highlights the calculation results of optimal dynamic response of the PCB at different masses of the dynamic absorber, the results of the findings are best expressed in this graphical manner. It shows that the optimal tuning of the dynamic absorber is capable of modifying the lightly damped SDOF to a heavily damped 2DOF system. As the mass ratio is increased, the peak PSD at resonant frequency is reduced significantly, oppositely, the area at low frequency range (20-150 Hz) is increased, however, the peak value is not important for this analysis whereas the overall response (area under the curve) is critical. Thus a heavier mass could not produce a better performance in this case.

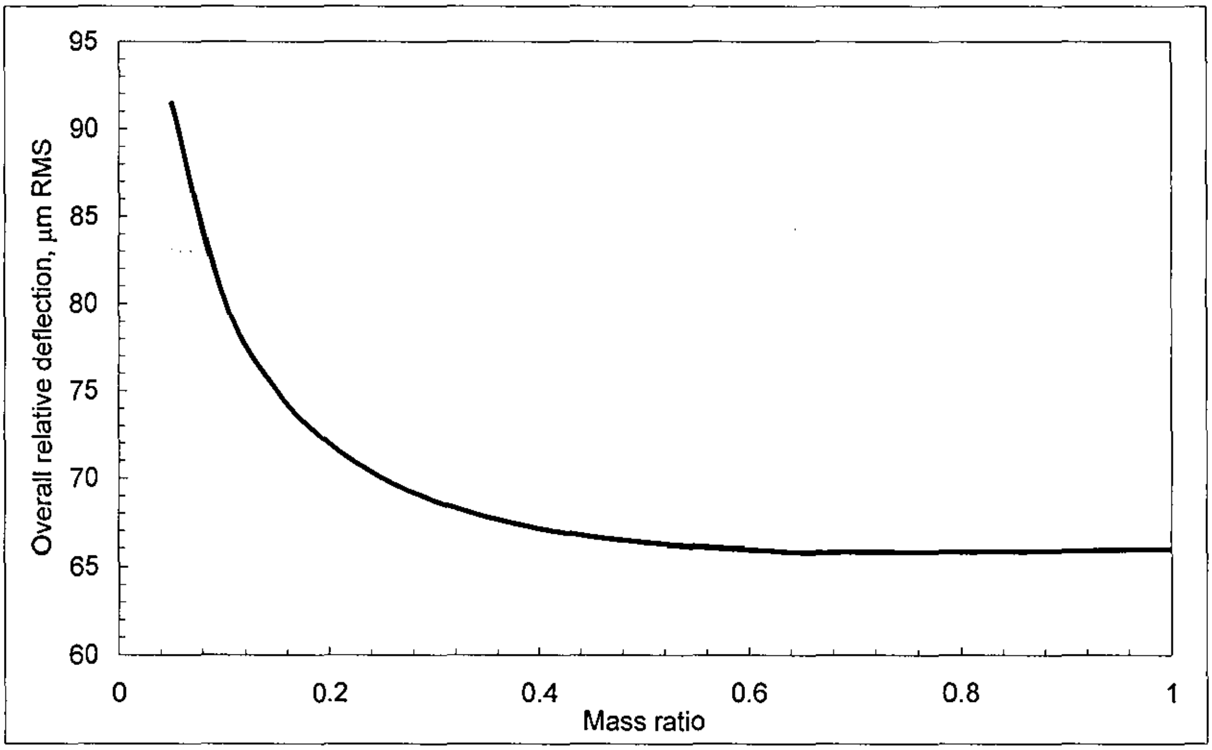

Figure 3.3. Optimal overall relative deflection of PCB at different mass ratios

Figure 3.3 shows the dependence of the overall level of deflection (in µm RMS) on the value of mass ratio. Figure 3.3 shows that the mass ratio of 65% corresponds to its optimal natural frequency and loss factor gives the lowest level for the overall relative deflection of PCB. Hence, the optimal mass of the dynamic absorber must be 58.5 gr (which indicates only 30% for the actual mass ratio relative to the overall mass of the PCB) for this particular application. Figure 3.4 shows the dependence of the normalised overall level of deflection on the value of mass ratio (the optimal value of the overall response is used for the normalisation).

It should be noted here that the overall deflection decreases as the mass ratio is varied between 5% to 65%. The overall dynamic response is said to be minimal when mass ratio is 65%. Beyond this optimal point, the overall deflection increases marginally.

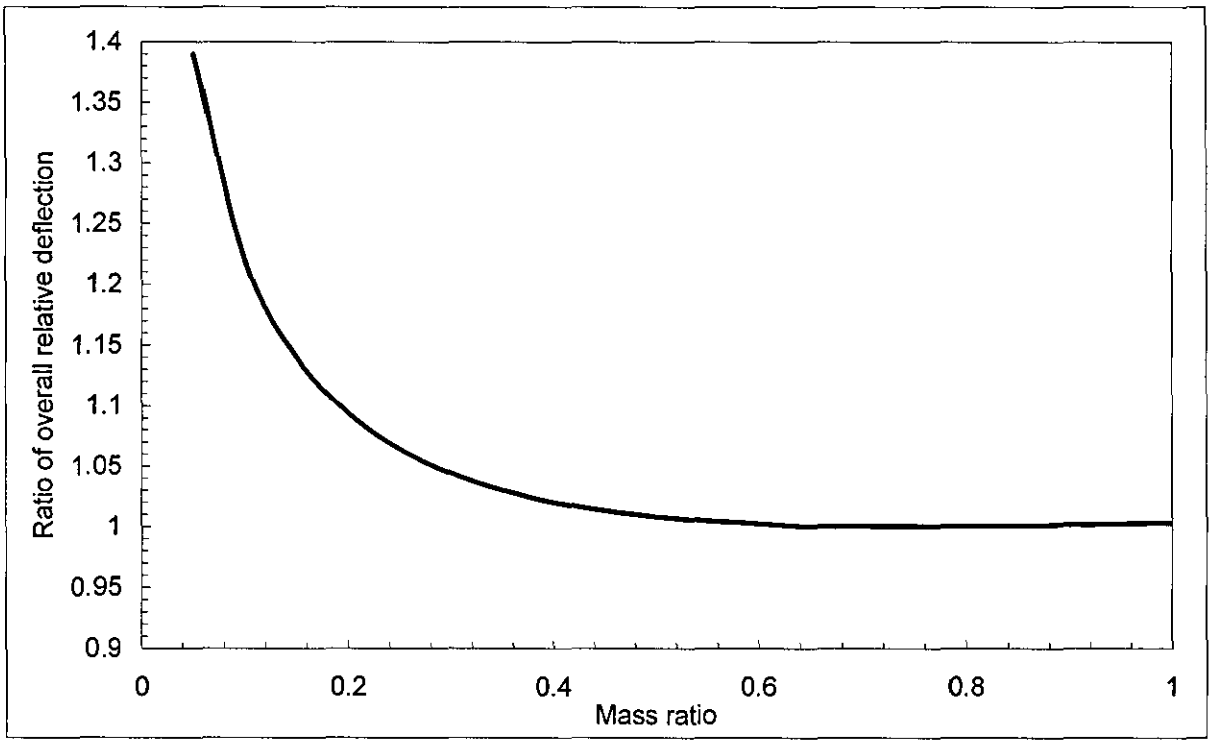

Figure 3.4. Ratio of optimal overall relative deflection of PCB at different mass ratios

Figure 3.4 shows 5% difference in the performance of the dynamic absorber between mass ratios of 25% and 65%. As far as the weight, space and performance are concerned, it would be reasonable to choose an appropriate mass of the dynamic absorber in this range. For this purpose, the mass ratio of 35% and 65% are chosen in which the optimal performance is only 2% different whereas the mass ratio is 46% different.

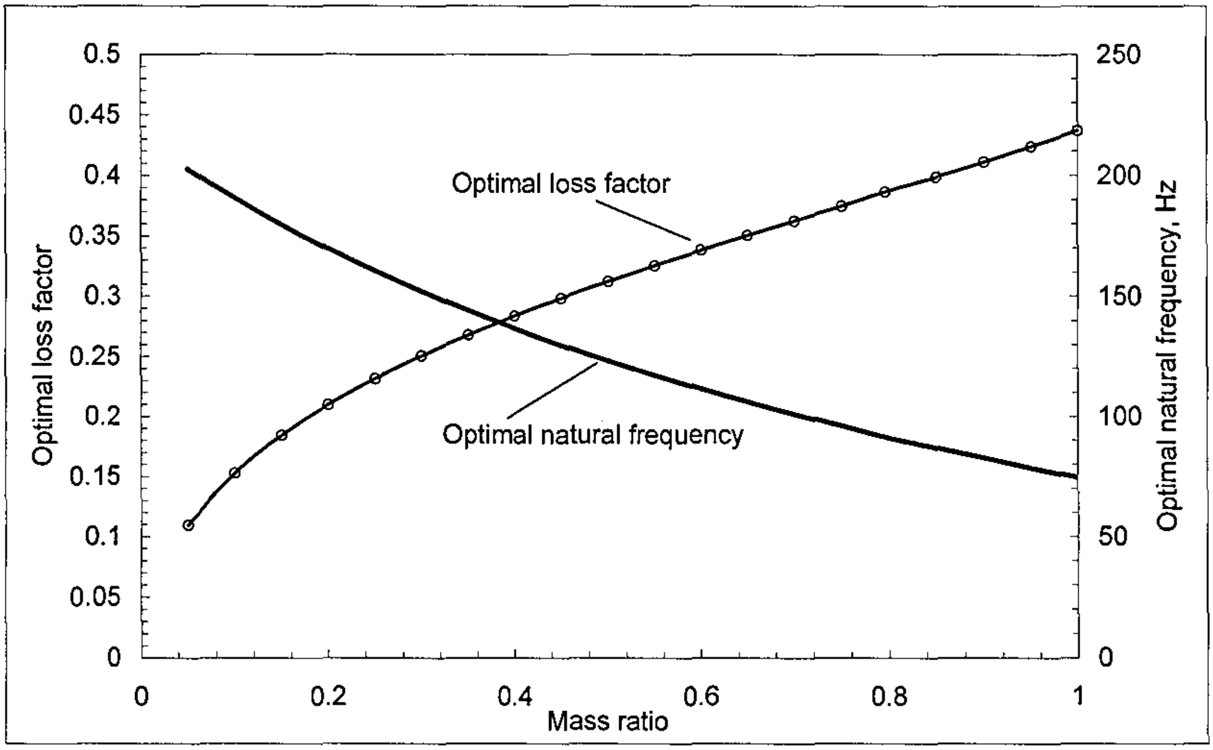

Figure 3.5. Optimal parameters of dynamic absorber at different mass ratios

Figure 3.5 shows the dependence of the optimal loss factor and natural frequency of the dynamic absorber at different mass ratios:

- At a mass ratio of 65%, the optimal natural frequency and optimal loss factor are found to be 106 Hz and 0.35, respectively
- At mass ratio of 35%, the optimal natural frequency and optimal loss factor are found to be 144 Hz and 0.267, respectively.

With reference to the actual mass of the PCB (175.5 gr), both dynamic absorbers would produce a 30% and 18% mass ratio, respectively.

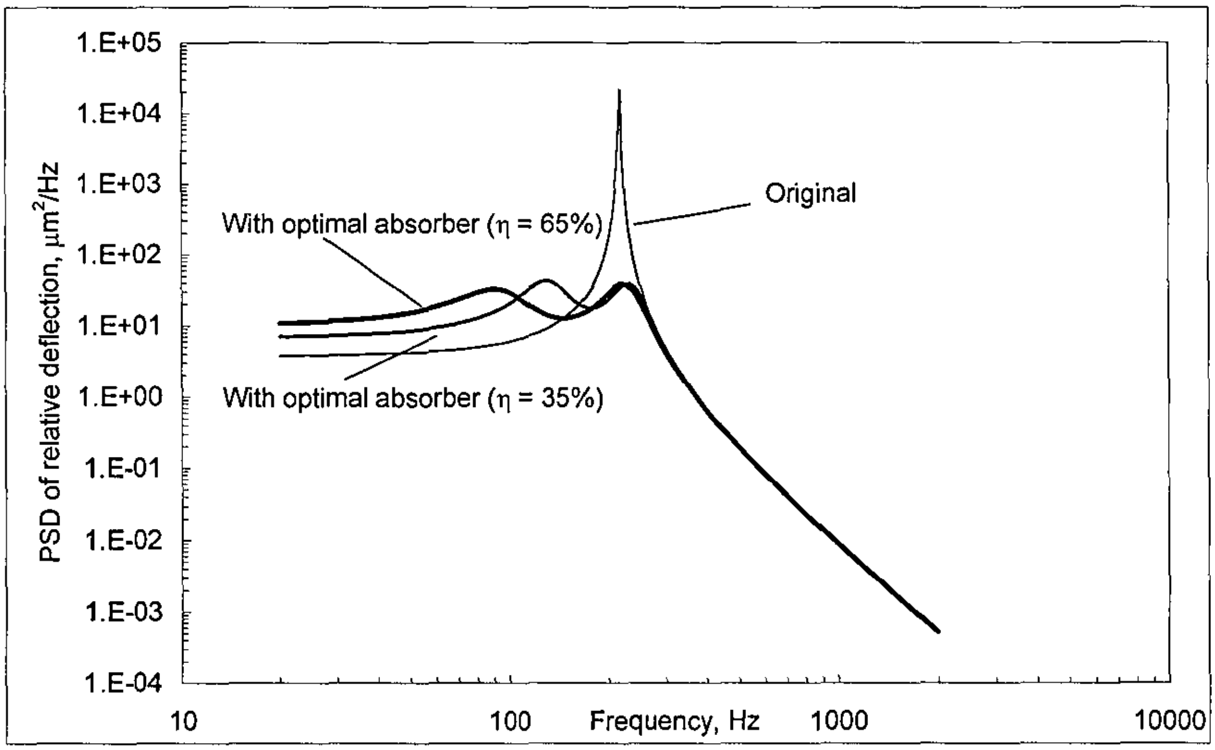

Figure 3.6. Dynamic response of the original and ruggedized PCB

Figure 3.6 shows the superimposed PSD of relative deflection of the original PCB (overall response 271.5 μm RMS) with the optimised dynamic absorber at 65% and 35% mass ratio (overall response 65.9 μm RMS and 68.1 μm RMS), thus the optimal design gives a reduction ratio of 4.1 and 3.9 respectively.

The novel optimal absorber design can be verified by using the conventional approach, say, [13]. A classical design method for wide-band frequency applications, known as the equal-peak method. The optimal natural frequency and loss factor of dynamic absorber at any given mass ratio can be found from the following expression [13]:

$$\Omega_{2opt} = \frac{1}{1+\eta}\Omega_1, \qquad \xi_{2opt} = \sqrt{\frac{3\eta}{8(1+\eta)^3}} \tag{3.7a}$$

For comparison purposes, the above expressions are best expressed in a graphical manner as shown in Figure 3.7 (see the curve labelled as **Traditional optimal design**). Also, in this figure the corresponding parameters of the new optimal absorber design are superimposed for reference (see the curve labelled as **Optimal design**). As can be clearly seen, both designs have a different natural frequency and loss factor at any mass ratio, these values are significant departed as the mass ratio increased.

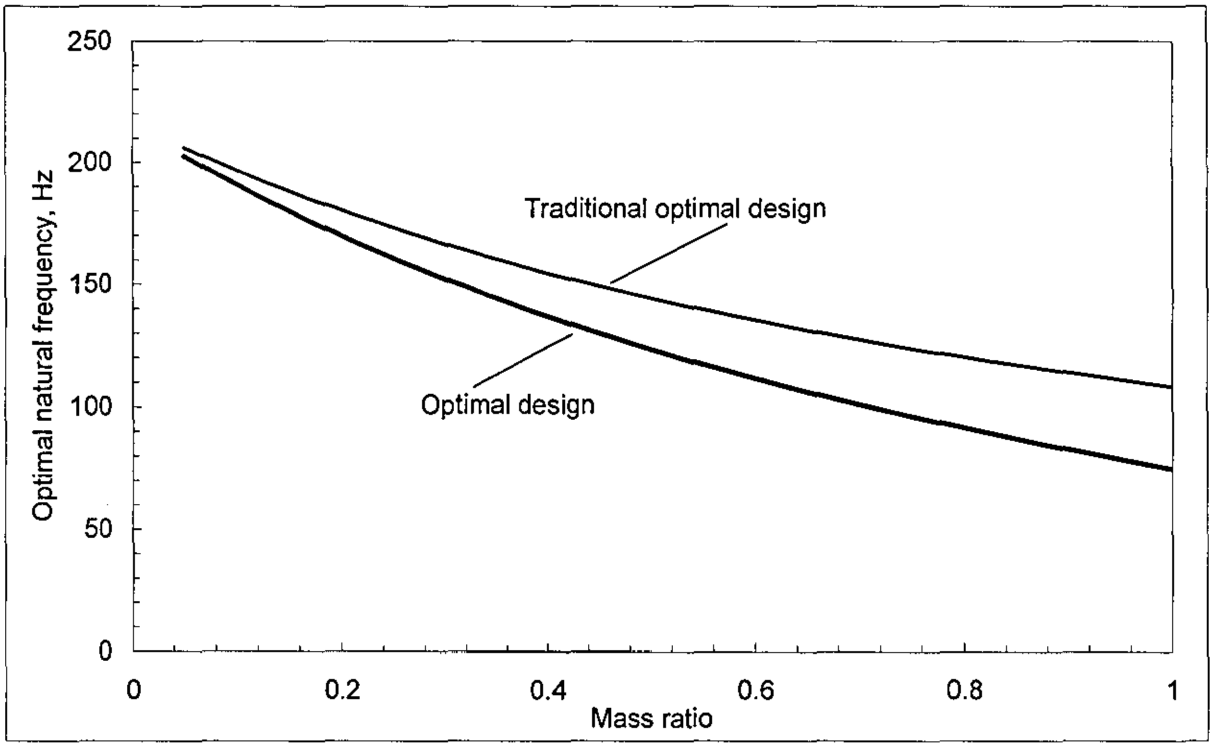

a) Natural frequency

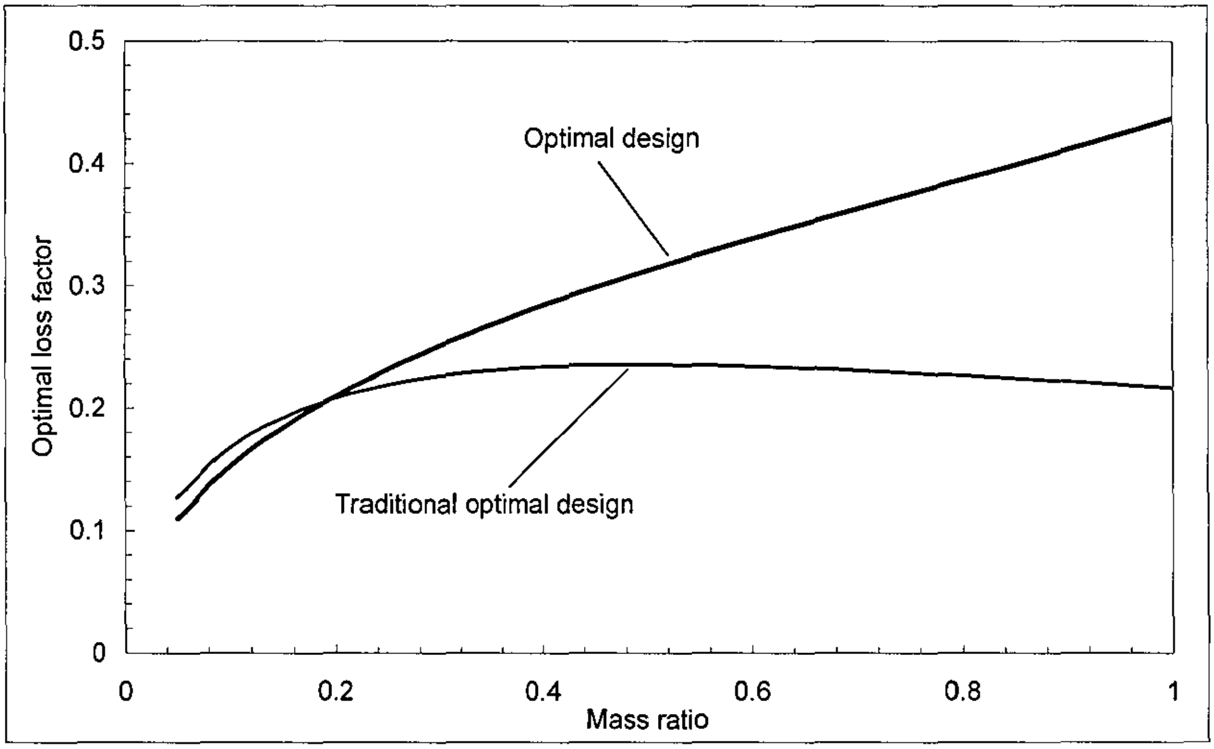

b) Loss factor

Figure 3.7. Comparison of traditional and novel optimal parameters of dynamic absorber

Using the traditional approach for the PCB application, as a result, Figure 3.8a highlights the traditional optimal dynamic response of the PCB, whereas Figure 3.8b shows its optimal overall relative deflection on the value of mass ratio. Also in Figure 3.8b the optimal response curve from Figure 3.3 is superimposed for comparison. It is clearly shown, the novel dynamic absorber design (see the curve labelled as **Optimal design**) produces a better performance than the traditional one (see the curve labelled as **Traditional optimal design**) at a higher mass ratio.

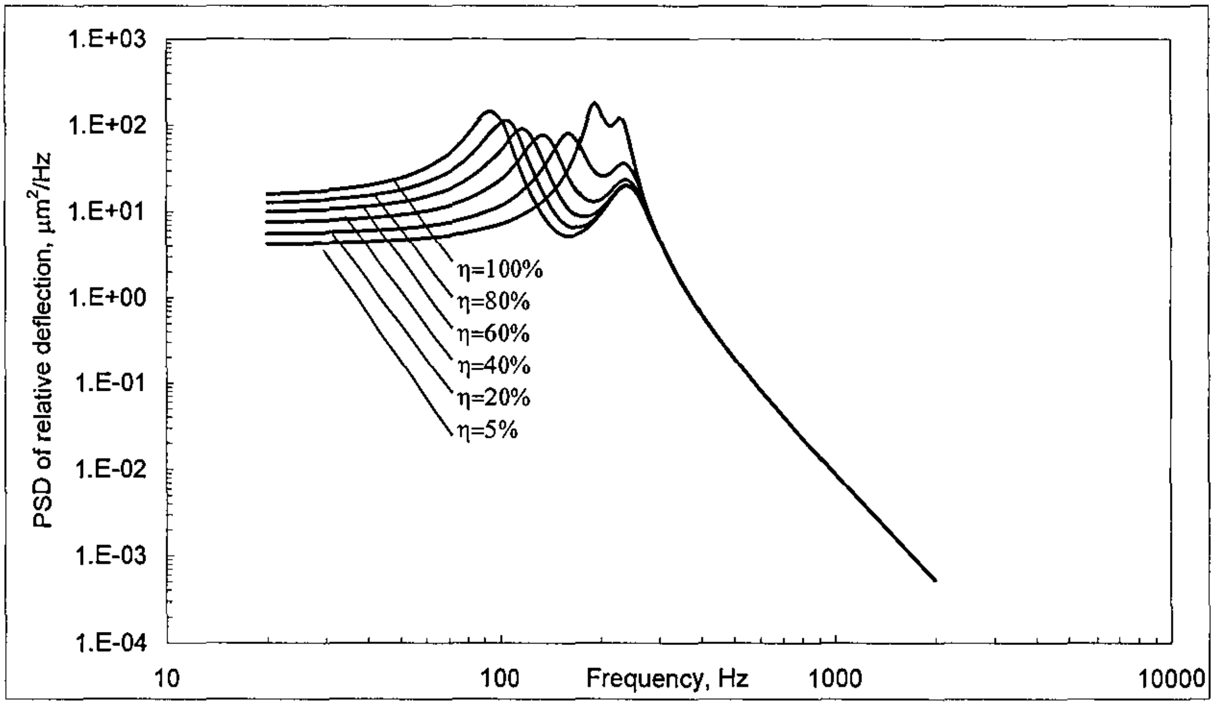

a) PSD of relative deflection in the case of traditional optimal design

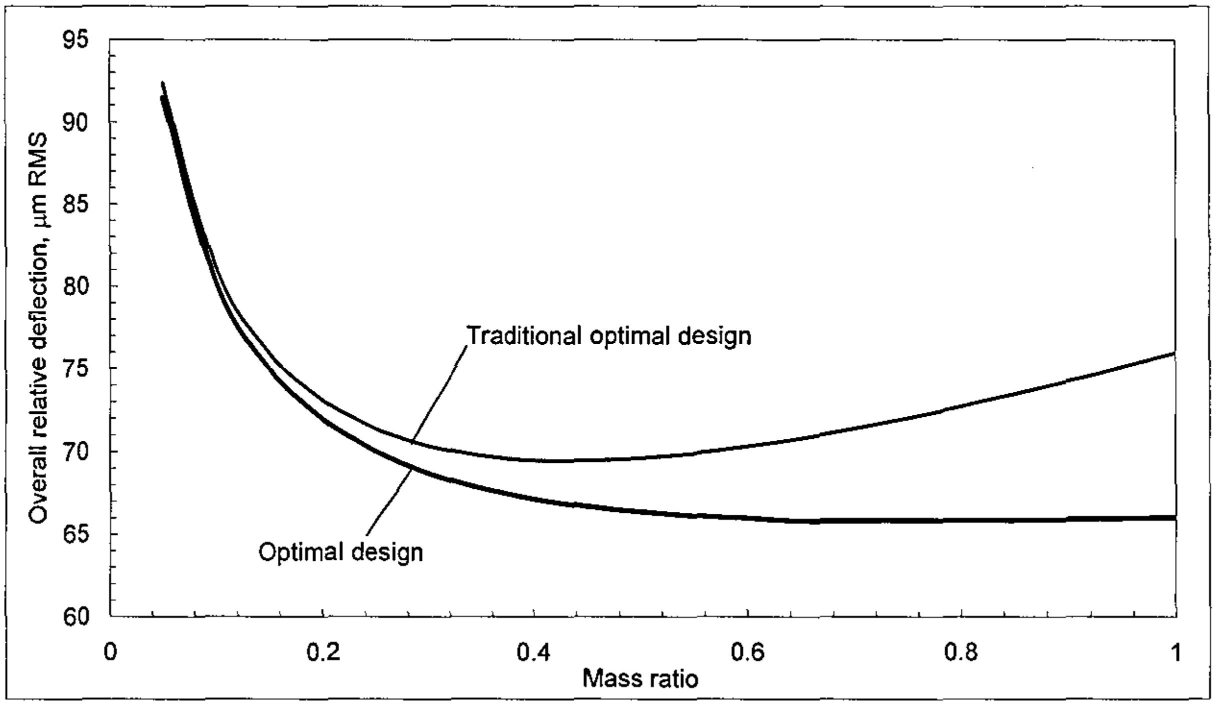

b) Comparison of overall relative deflection in the case of optimal traditional and novel design

Figure 3.8. Dynamic response of the PCB at different mass ratio

It should be noted that in Figure 3.8b, the curve labelled as **Traditional optimal design**, at the mass ratio of 45% corresponds to its optimal natural frequency, 149 Hz and optimal loss factor, 0.235 gives the lowest level for the overall relative deflection, 69.5 μm RMS of PCB. However, it is not said to be an optimal dynamic absorber for this study, since a better performance can be achieved at this mass ratio, the evidence is clearly shown in Figure 3.8b.

Figure 3.9 shows the superimposed optimal dynamic response of the PCB with the influence of novel design dynamic absorber (overall response 65.9 μm RMS) and traditional one (overall response 69.5 μm RMS) which corresponding to their optimal mass ratio.

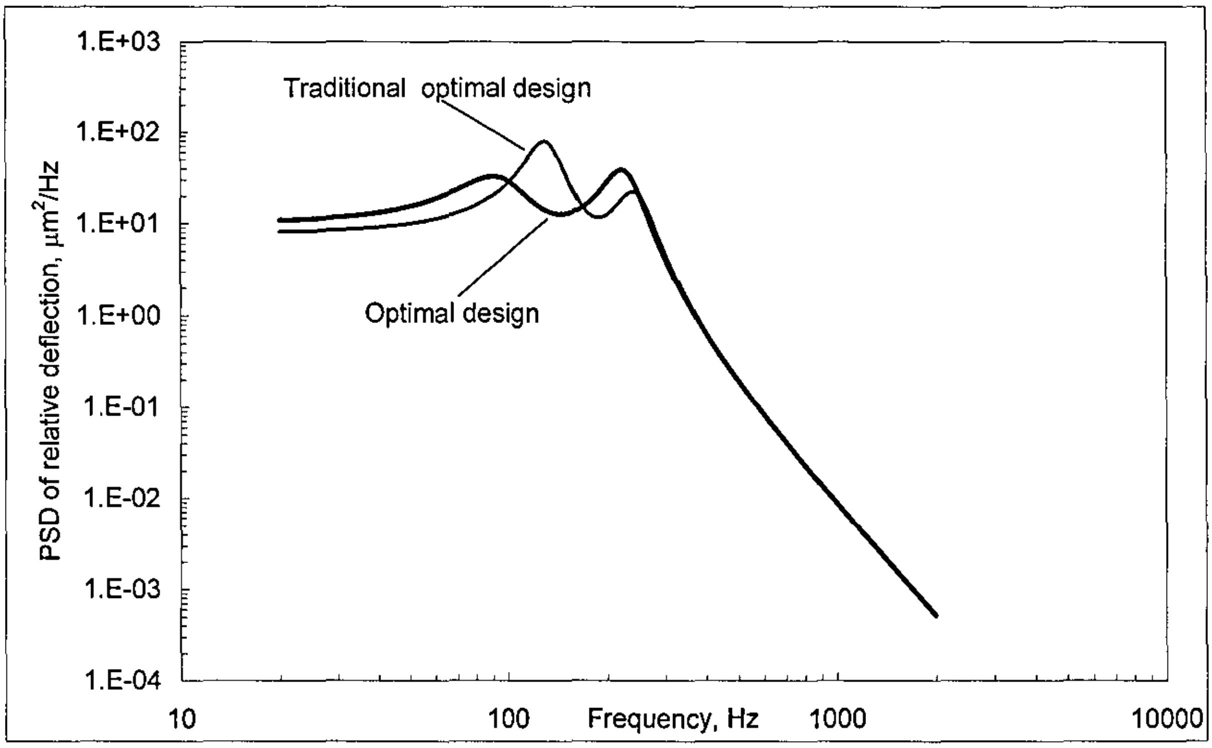

Figure 3.9. Comparison of dynamic response in the case of traditional and novel design

In this figure the equal-peak response does not seem to exist due to the fact that the peak PSD at first resonant frequency is much higher than that of the second one (see the curve labelled as **Traditional optimal design**) even it is thought of the equal-peak method. The explanation is rather simple, the traditional optimal parameters set is only applied for the system with force induced directly to the primary system whereas it does not apply for system with base supported motion.

From [13], the optimal parameters set of absorber design for peak deflection, in a general sense, does not provide the optimal peak acceleration response at any given mass ratio for the system under swept-sine excitation and vice versa where the primary system is subjected to force excitation. This is also true for the system with base supported motion under swept-sine or random vibration. The dynamic absorber that design for optimal overall relative deflection would not provide optimal overall absolute acceleration under random vibration. Keeping in mind, the aim of this study is to design an optimal dynamic absorber to suppress the overall relative deflection of the PCB, therefore, an optimal design for overall absolute acceleration is not an intention. However, with the same worksheet and the Solver, such an optimal dynamic absorber can be designed if a target cell of overall absolute acceleration is generated. For this instance, Figure 3.10 shows the comparison PSD of absolute acceleration of the PCB with the influence of different optimal dynamic absorber designs. At 65% mass ratio the optimal overall absolute acceleration 8.73 g RMS (see the curve labelled as **Independent optimal design**) is found which corresponding to the optimal natural frequency, 151 Hz and optimal loss factor, 0.33 of dynamic absorber. Regarding to the novel dynamic absorber that design for optimal overall relative deflection (i.e. $\eta = 65\%$, $\frac{\Omega_{2opt}}{2\pi} = 106\text{Hz}$ and $\zeta_{2opt} = 0.35$) gives 10.1 g RMS in terms of overall absolute acceleration (see the curve labelled as **Optimal design**) whereas traditional one (i.e. $\eta = 45\%$ $\frac{\Omega_{2opt}}{2\pi} = 149\text{Hz}$ and $\zeta_{2opt} = 0.235$) produces 10.1 g RMS (see the curve labelled as **Traditional Optimal design**) which give about the same reduction ratio, a factor of 5.1 with reference to the original PCB (overall response 51.10 g RMS), see the curve labelled as **Original**).

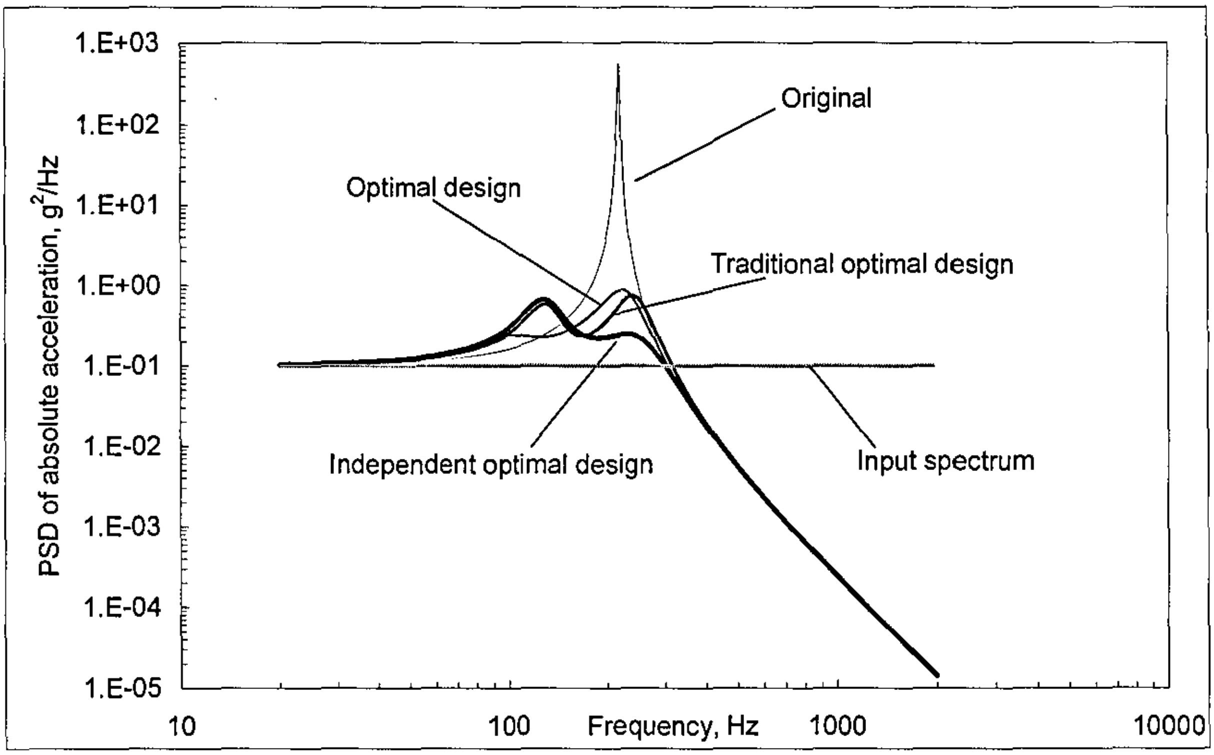

Figure 3.10. Comparison of dynamic response in the case of traditional and novel design

This study enhances the author's ideas in which the theory of optimal dynamic absorber for random vibration application does not appear to exist. Using a common dynamic absorber for the specific application, such the PCB, may not prove to be consistence, typically those that are concerned with optimal performance.

3.2.2 Sensitivity analysis

Nonetheless, during fabrication or operation, the desired loss factor and natural frequency may vary due to manufacturing tolerances, temperature and ageing, therefore it is very important to carry out the sensitivity analysis with the aim of finding out how differences in the dynamic absorber's properties affect its performance. This is performed by taking the optimal values for minimising the overall relative deflection response and varying optimal natural frequency and optimal loss factor separately. If the system proves not to be sensitive to an imperfect dynamic absorber there will be more freedom when designing it.

Figure 3.11a shows the typical dynamic response of the PCB at the mass ratio, 65% and optimal frequency, 106 Hz whilst the loss factor is varied in the range from 0 to 1. The corresponding Figure 3.11b shows a variation of its overall relative deflection together with sensitivity analysis for the mass ratio, 35% at its optimal frequency, 144 Hz.

Figure 3.11c shows the dynamic response of the PCB at the same mass ratio, 65%, and optimal loss factor, 0.35, where the natural frequency is varied in the range from 50 to 200 Hz. The corresponding Figure 3.11d shows a variation of its overall relative deflection together with sensitivity analysis for the mass ratio, 35% at its optimal loss factor, 0.267 for reference.

From sensitivity analysis in Figure 3.11 reasonably small variations in optimal natural frequency and loss factor have little effect on the overall relative deflection of the PCB. The dynamic response of the PCB is very large when the loss factor approaches zero (see Figure 3.11b). At a loss factor of between 0.2 and 0.5, the overall dynamic response only changes by 20%. It is important to maintain the loss factor and natural frequency of the dynamic absorber in discrepancy of 10% in terms of overall dynamic response. This would be sufficient to maintain a fail-safe vibration environment for electronic equipment and obviously, this allows for a lot of freedom when designing a real dynamic absorber.

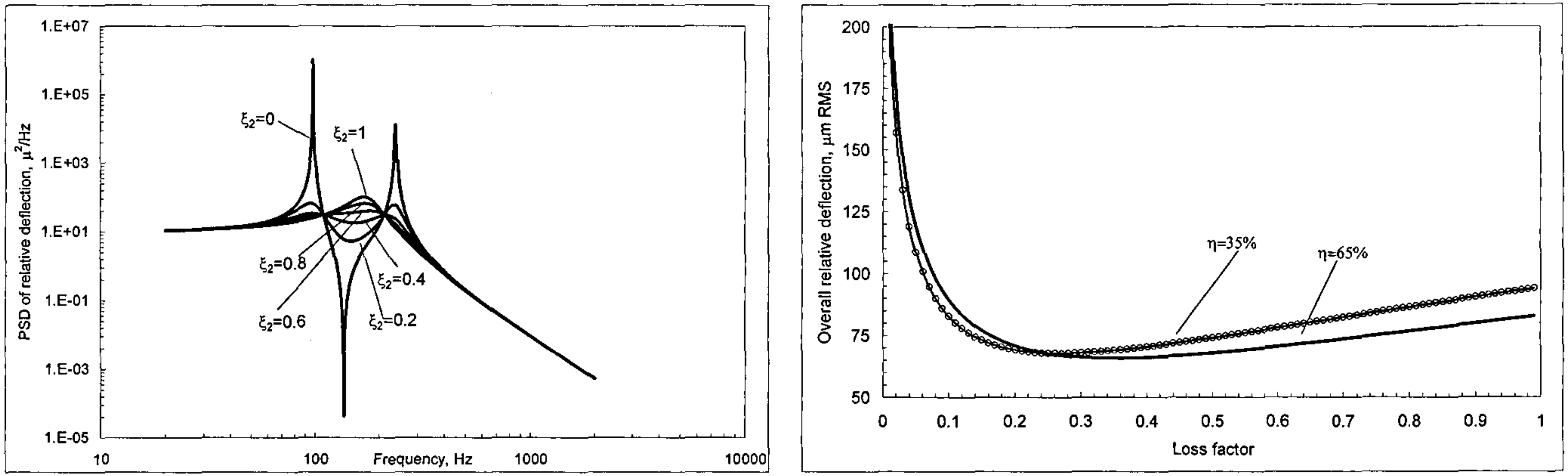

a) Dynamic response of PCB at different loss factors

b) Overall response of PCB at different loss factors

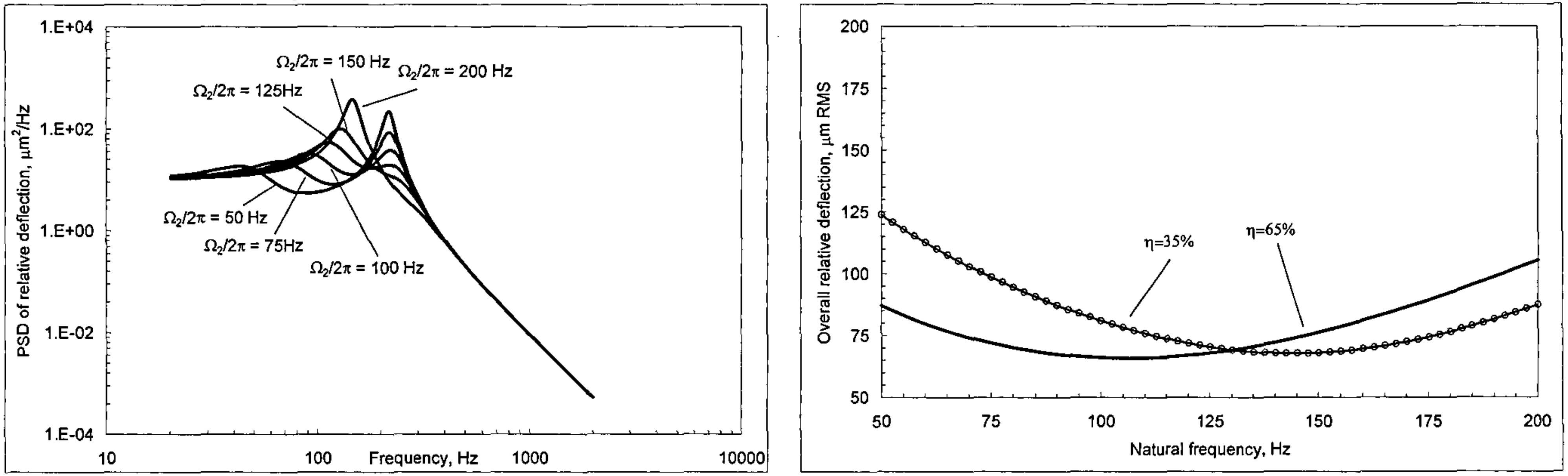

c) Dynamic response of PCB at different natural frequencies

d) Overall response of PCB at different natural frequencies

Figure 3.11. Sensitivity analysis

3.2.3 Fatigue analysis

The most obvious results are that there is lower relative transmissibility at the resonant frequency, which means lower relative deflection and acceleration of the PCB. Additionally, the overall RMS deflection of the system is reduced. According to Sloan [33], the endurance limit is given by:

$$N = c\sigma^{b}$$

where c is experimental constant and the fatigue exponent b=6.4 is given by [2] for the PCBs, σ is the RMS level of deflection or stresses. In the conservative estimation, therefore, the lifetime of PCB is increased by a factor of:

$$\left(\frac{\sigma_{original}}{\sigma_{ruggedized}}\right)^{b} = \left(\frac{271.5}{65.9}\right)^{6.4} = 8615 \text{ times (mass ratio of 65\%)},$$

and $$\left(\frac{\sigma_{original}}{\sigma_{ruggedized}}\right)^{b} = \left(\frac{271.5}{68.1}\right)^{6.4} = 6982 \text{ times (mass ratio of 35\%)}.$$

The calculation shows that the lifetime of the ruggedized PCB will be increased several thousand times as compared to its original design.

The fatigue accumulated by the PCB under wide-band random vibration may be estimated more accurately using the method, which is schematically described by Bolotin [34]. This method is based on counting the amount of simple cycles that are characterised by the particular magnitude over the length of the analysed time history. Upon carrying out the simulation and obtaining the relative deflection, the cumulative fatigue is determined using the formula suggested by [33]

$$Fatigue \propto \sum_{i=1}^{K} N_i \sigma_i^{\alpha} \qquad (3.8)$$

In this formula:

σ_i is the magnitude of the stress of the i-indexed simple cycles,

N_i is the number of simple cycles with the magnitude of stress σ_i,

$\alpha = 6.4$ is the experimental parameter that defines the fatigue properties of glass epoxy, which is used in the typical PCB design by [2].

K is the number of levels.

The amount of simple cycles, N_i, is counted along the simulated time history through the amount of the crossings of the level σ_i minus the amount of the crossings of the level σ_{i+1}. When calculating we start from the highest levels of the stresses.

At times, both vibration and fatigue analysis are of concern because specific frequencies can cause unexpected fatigue damage. The fatigue life of a component is generally made of a crack initiation phase. The stress and strain distributions are not evenly distributed due to the significant variation in the geometry of the PCB.

A program performing the calculation of the number of stress cycle by the logic of zero crossing intersection in the stress-time graph is developed and is shown in Figure 3.12a. Steady decrement from the peak until the *x*-axis, results in the number of levels, K. At each level, the number of zero crossing is determined. There are various methods of obtaining these values, the most efficient and timesaving is by carrying-out the product rule at each intersection.

If the product of the values on adjacent sides of the zero crossings (i.e. point of intersection) is negative, then there is a zero crossing. It should be noted here that, there is a more positive product than negative. These values are later set up in an array, and assigned to zero. The zero crossings are later determined by using the function '**find**'. These values are set to 1 and summed to determine the number of cycles N_i. This program is run using the M-File and the data is collected for comparison purpose. The fatigue parameter is defined in the M-file script as shown in Figure 3.12b. With reference to the block diagram shown in Section 3.2.4, and the Matlab script, the RMS value and fatigue level is calculated for both relative deflection and absolute acceleration. For the purpose of this program, a Simulink modelling of the dynamic system with the parameters is considered. This model is able to simulate the dynamic response of the system. A general assessment on the accuracy of the theoretical analysis will also be carried out based on the results of the simulation.

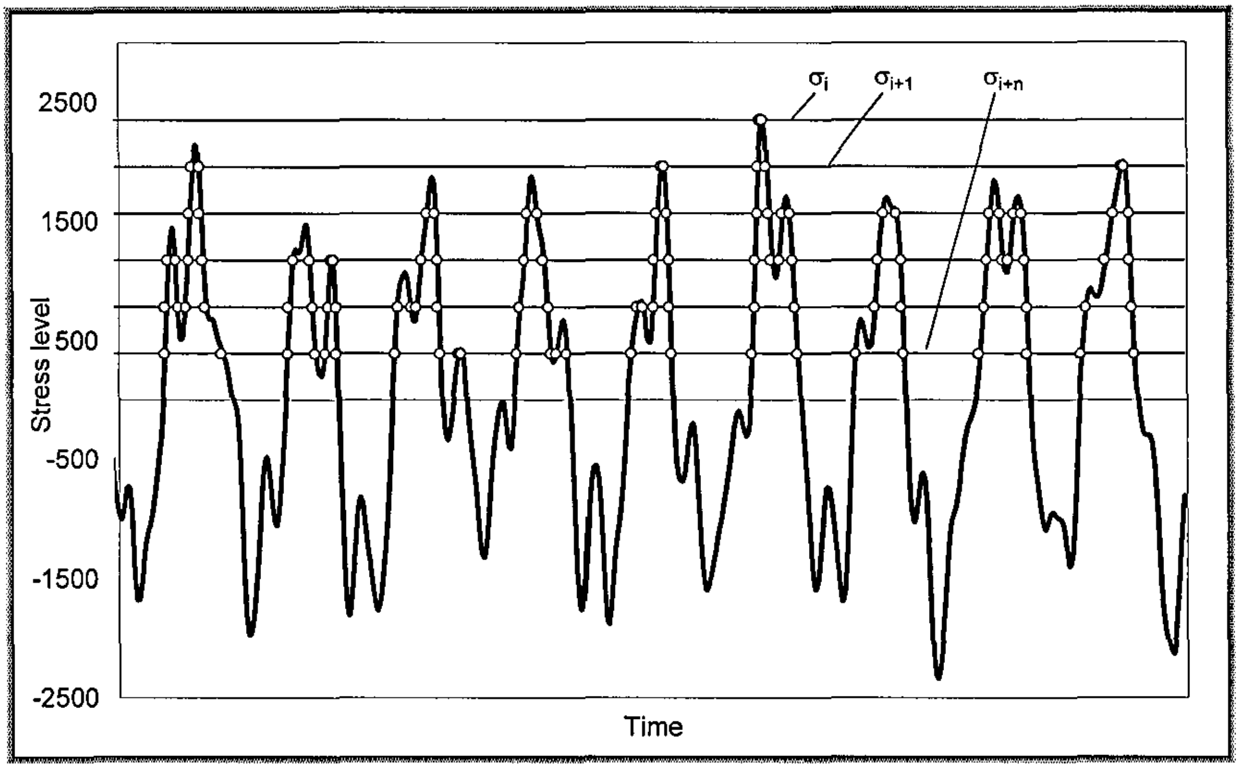

a) Stress-time graph

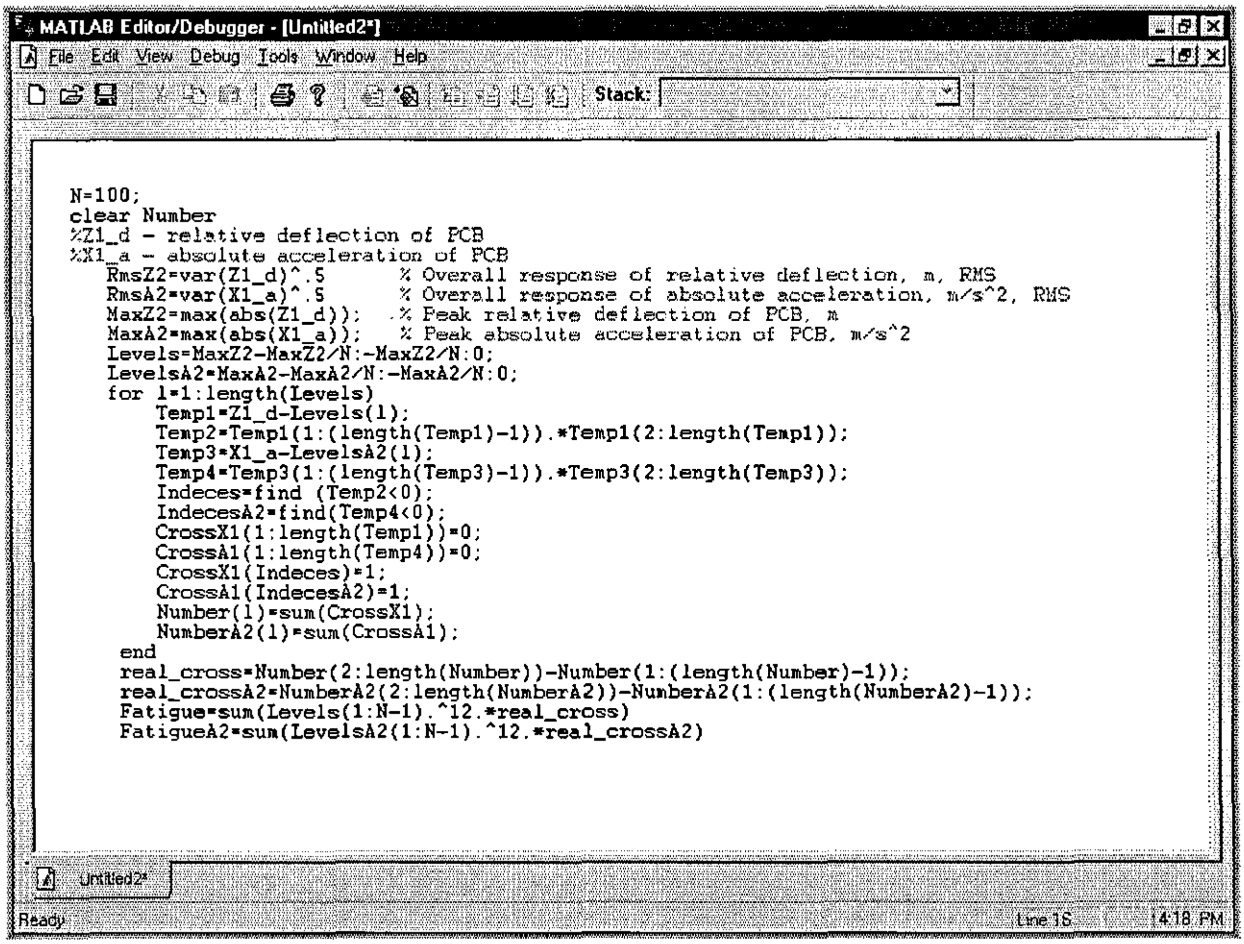
MATLAB Editor/Debugger - [Untitled2*]
File Edit View Debug Tools Window Help
Stack:
Untitled2*
Ready
Line 15
4:18 PM

```
N=100;
clear Number
%Z1_d - relative deflection of PCB
%X1_a - absolute acceleration of PCB
   RmsZ2=var(Z1_d)^.5       % Overall response of relative deflection, m, RMS
   RmsA2=var(X1_a)^.5       % Overall response of absolute acceleration, m/s^2, RMS
   MaxZ2=max(abs(Z1_d));    % Peak relative deflection of PCB, m
   MaxA2=max(abs(X1_a));    % Peak absolute acceleration of PCB, m/s^2
   Levels=MaxZ2-MaxZ2/N:-MaxZ2/N:0;
   LevelsA2=MaxA2-MaxA2/N:-MaxA2/N:0;
   for l=1:length(Levels)
       Temp1=Z1_d-Levels(l);
       Temp2=Temp1(1:(length(Temp1)-1)).*Temp1(2:length(Temp1));
       Temp3=X1_a-LevelsA2(l);
       Temp4=Temp3(1:(length(Temp3)-1)).*Temp3(2:length(Temp3));
       Indeces=find (Temp2<0);
       IndecesA2=find(Temp4<0);
       CrossX1(1:length(Temp1))=0;
       CrossA1(1:length(Temp4))=0;
       CrossX1(Indeces)=1;
       CrossA1(IndecesA2)=1;
       Number(l)=sum(CrossX1);
       NumberA2(l)=sum(CrossA1);
    end
    real_cross=Number(2:length(Number))-Number(1:(length(Number)-1));
    real_crossA2=NumberA2(2:length(NumberA2))-NumberA2(1:(length(NumberA2)-1));
    Fatigue=sum(Levels(1:N-1).^12.*real_cross)
    FatigueA2=sum(LevelsA2(1:N-1).^12.*real_crossA2)
```

b) Matlab scrip

Figure 3.12. Fatigue analysis using simple cycles technique

3.2.4 Numerical simulation

Traditional approaches to system design typically include building a prototype followed by extensive testing and revision. This method can be both time-consuming and expensive. As an effective and widely accepted alternative, simulation is now the preferred approach to engineering design. Simulink is a powerful simulation software tool that enables one to quickly build and test virtual prototypes so that one can explore design concepts at any level of detail with minimal effort. By using Simulink to iterate and refine designs before building the first prototype, engineers can benefit from a faster, more efficient design process.

Simulink provides an interactive, block diagram environment for modelling and simulating dynamic systems. It includes an extensive library of predefined blocks that can be used to build graphical models using drag-and-drop operations. Supported model types include linear, nonlinear, continuous-time, discrete-time, multirate, conditionally executed, and hybrid systems. Models can be grouped into hierarchies to create a simplified view of components or sub-systems. High-level information is clearly and concisely presented, while detailed information is easily hidden in sub-systems within the model hierarchy. Simulink has many features that allow customisation, especially with regard to incorporating existing user C codes. In addition, simulations can be run interactively or in batch mode from the Matlab command line.

Firstly, a simulation based on the dynamic model in for single-mode PCB is carried out using a Simulink block diagram and M-File. The simulation model here is run to obtain a solution containing peak deflection, the overall RMS value and subsequent endurance limit. The system parameter is defined in the M-file script. The Matlab/ Simulink diagram is defined by means of expressing the equation of motion in terms of relative motion. Where, $z_1 = x_1 - y$ is the relative motion for the primary system and $z_2 = x_2 - y$ is the relative motion for secondary system. Upon substituting these expressions into the primary and secondary equation obtained from (3.0) and (3.1) yields:

for the primary system

$$m_1\ddot{z}_1 + c_1\dot{z}_1 + k_1 z_1 + k_2(z_1 - z_2) + c_2(\dot{z}_1 - \dot{z}_2) = -m_1\ddot{y}, \tag{3.9}$$

for the secondary system

$$m_2\ddot{z}_2 + k_2(z_2 - z_1) + c_2(\dot{z}_2 - \dot{z}_1) = -m_2\ddot{y}. \tag{3.10}$$

Based on the above manipulation, elements performing operation of integration, multiplication, derivation, summation and signal representing the force are readily available on Matlab/ Simulink environment. With reference to the equation of motion above, in terms of relative motion, the simulation diagram is shown below.

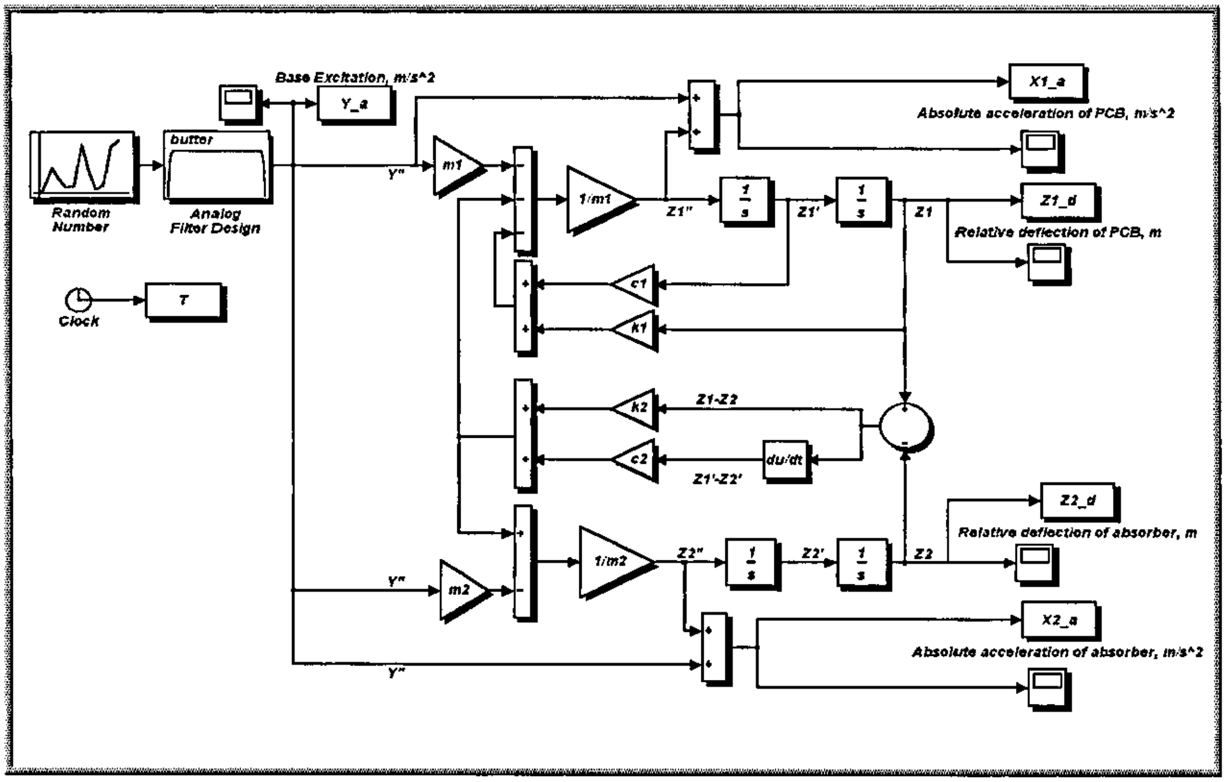
Random Number
butter
Analog Filter Design
Base Excitation, m/s^2
Y_a
Clock
T
Y"
m1
1/m1
Z1"
1/s
Z1'
1/s
Z1
X1_a
Absolute acceleration of PCB, m/s^2
Z1_d
Relative deflection of PCB, m
c1
k1
k2
Z1-Z2
du/dt
c2
Z1'-Z2'
Z2_d
Relative deflection of absorber, m
Y"
m2
1/m2
Z2"
1/s
Z2'
1/s
Z2
X2_a
Absolute acceleration of absorber, m/s^2
Y"

Figure 3.13. Simulink diagram for random excitation

Figure 3.13 shows the simulation model of PCB with the dynamic absorber attached. The corresponding gain block (marked with system parameters) generates its output by multiplying its input by a specified expression. The integrator blocks perform the transformation of acceleration to velocity and then to displacement using **ode45 (Dormand-Prince)** with an auto variable step time integration routine. This method is an effective timesaving approach of computing the derivative. The appropriate label scopes and workspaces records their corresponding response signal. It should be noted that in this model, any signal could be viewed by connecting a scope on the connected line.

The internal structure of this Simulink model contains all the necessary algorithms of 2DOF and bookkeeping routines to provide an appropriate framework for simulating the system under random, swept-sine vibration or shock load. At will, these excitation signals can be simultaneously superimposed with G-loads for studying the time history of deflection, absolute acceleration responses and hence fatigue failure of the system under this extreme condition.

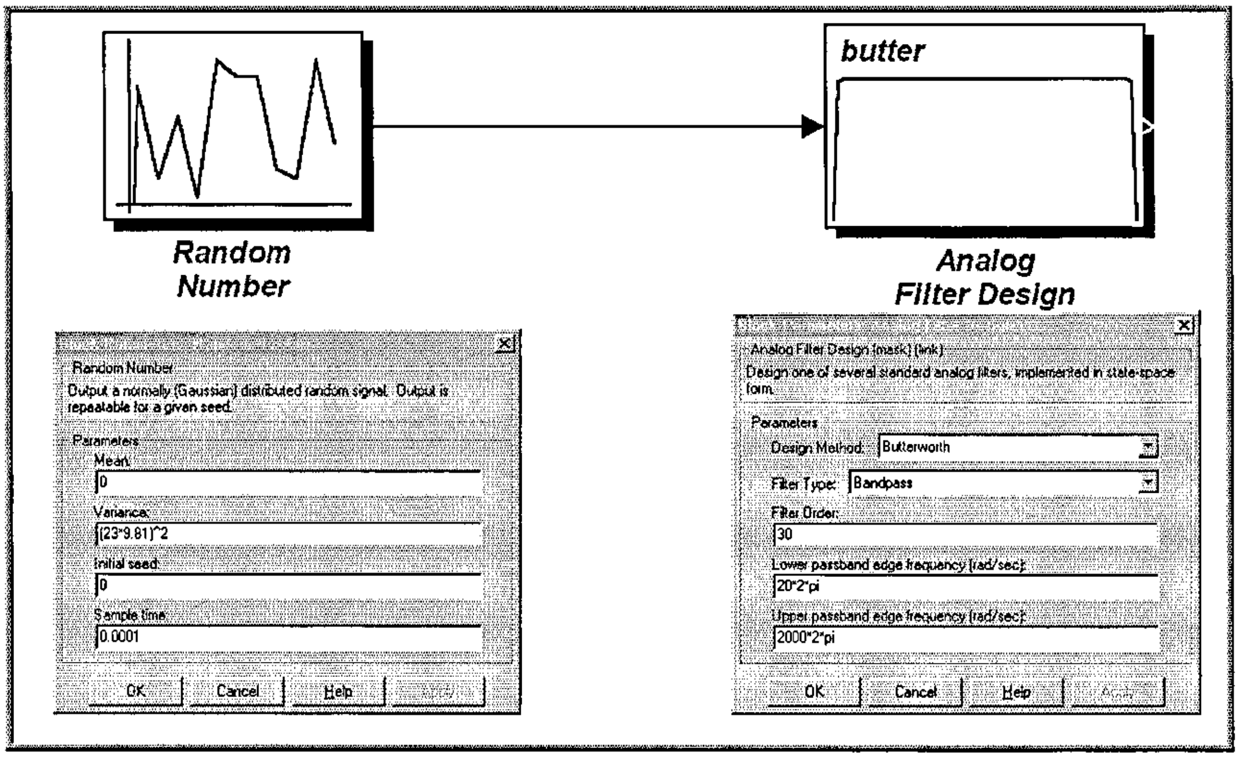

Random Number

Output a normally (Gaussian) distributed random signal. Output is repeatable for a given seed.

Parameters

Mean:
0

Variance:
(23*9.81)^2

Initial seed:
0

Sample time:
0.0001

Analog Filter Design (mask) (link)

Design one of several standard analog filters, implemented in state-space form.

Parameters

Design Method: Butterworth

Filter Type: Bandpass

Filter Order:
30

Lower passband edge frequency (rad/sec):
20*2*pi

Upper passband edge frequency (rad/sec):
2000*2*pi

a) Tuning value.

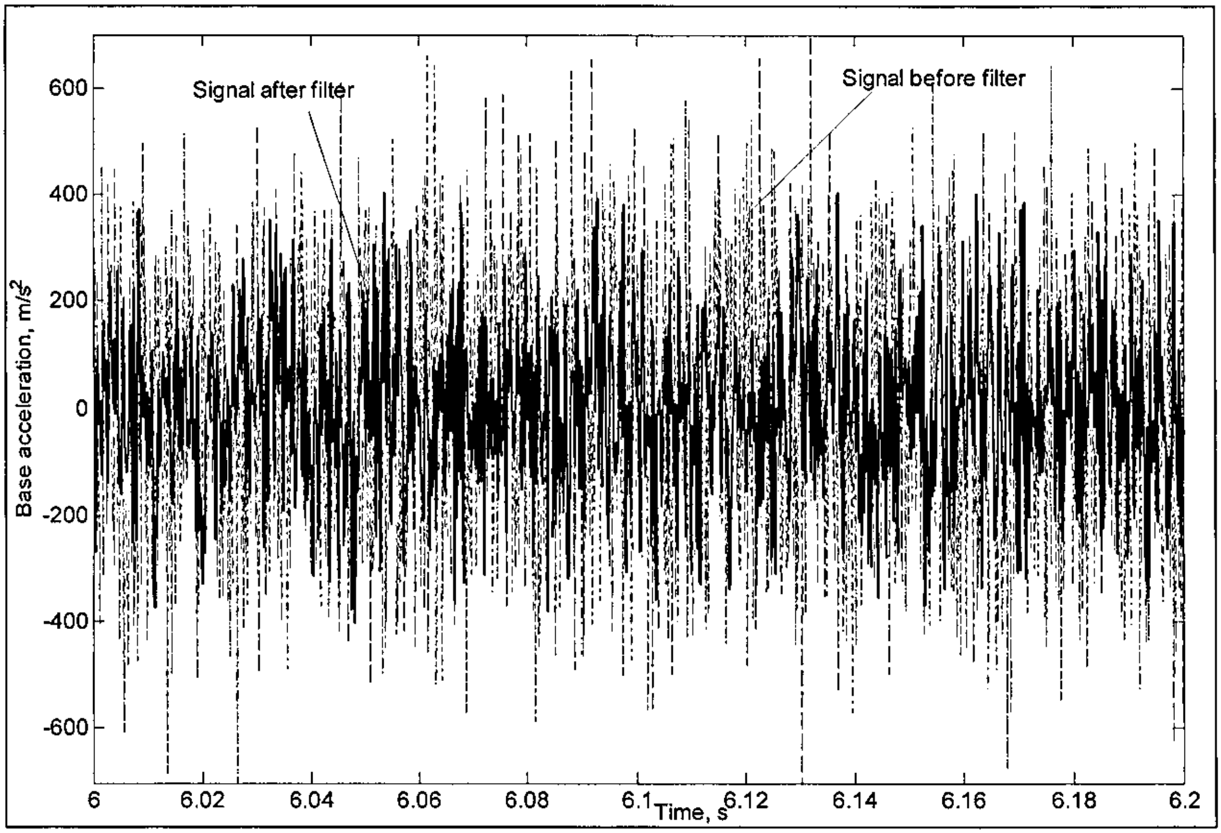

b) Time history of base acceleration

Figure 3.14. Random vibration excitation

Random vibration is of primary concern at this stage, therefore force signal is designed using the Random Number, which is available from Simulink's library. The level and spectrum are controlled by the values of variance and time discrete of the Random Number block and cross-frequency of the band-pass Filter block as shown in Figure 3.14a. The signal parameter is expressed in terms of variance at a specified sample time where it is tuned to match the required excitation signal of 14g RMS. In this design, a sampling time of 0.1ms is used in the **Random Number** dialog box which corresponds to a sampling frequency of 10000 Hz. The maximum frequency in this case is 5000 Hz. The cutoff frequencies are designed from the **Analog Filter Design** dialog box. In order to match the requirement, the setting starts from 20 Hz and has a cutoff frequency of 2000 Hz. The order of the filter in this block determines the sharpness of the cutoff. The higher the order, the sharper the cutoff, for this reason a 30th order filter is chosen.

The signal from the simulation is recorded (see Figure 3.14b) with a time step of 0.1ms in a matrix form using the workspace labelled **Y_a**, the overall RMS value is calculated by using **var** command from Matlab, after 3s of simulation, the value shows its stability.

Figure 3.15 shows the superimposed time domain of original and modified PCB with different mass ratios of dynamic absorber, the corresponding absolute acceleration and relative deflection are plotted at the vicinity of maximum magnitude response. Comparing the results obtained in Figure 3.15, it can be clearly seen that the relative deflection and absolute acceleration have reduced significantly. Furthermore, the obtained results are an acceptable base on which to predict results. Nonetheless, a simple verification check is carried on the above results. This is done by comparing the predicted reduction factor of the overall response from the Simulink model through the general methodology developed in Section 3.2.3. Table 3.0 shows the simulation results together with its theoretical calculation.

	Overall relative deflection, μm RMS (analytical)	Overall relative deflection, μm RMS (Simulation)	Improvement in Endurance limit (Overall technique)	Improvement in Endurance limit (Simple cycles technique)
Original	271.5	271.9	-	-
35% mass ratio	68.1	68.3	6,982 times	7,820 times
65% mass ratio	65.9	65.5	8,615 times	10,030 times

Table 3.0. Comparison of the increased life factor between the simple cycle and overall technique

In order to illustrate the validity of this approach, the improvement in the endurance limit was calculated from the Simulink analysis. The increase in the endurance limit under which the PCB operates with the optimal dynamic absorber was found to be 10,030 times. It should be noted that the overall reduction factor of RMS value for the predicted and simulated results are almost similar, but the effective endurance limit differs significantly. This is due to the more adequate method of calculation used in the program. With reference to the endurance limit, the fatigue life of the structure is predicted by a computational approach. The high endurance limit refers to low dynamic stress and strain when subjected to wide-band dynamic response.

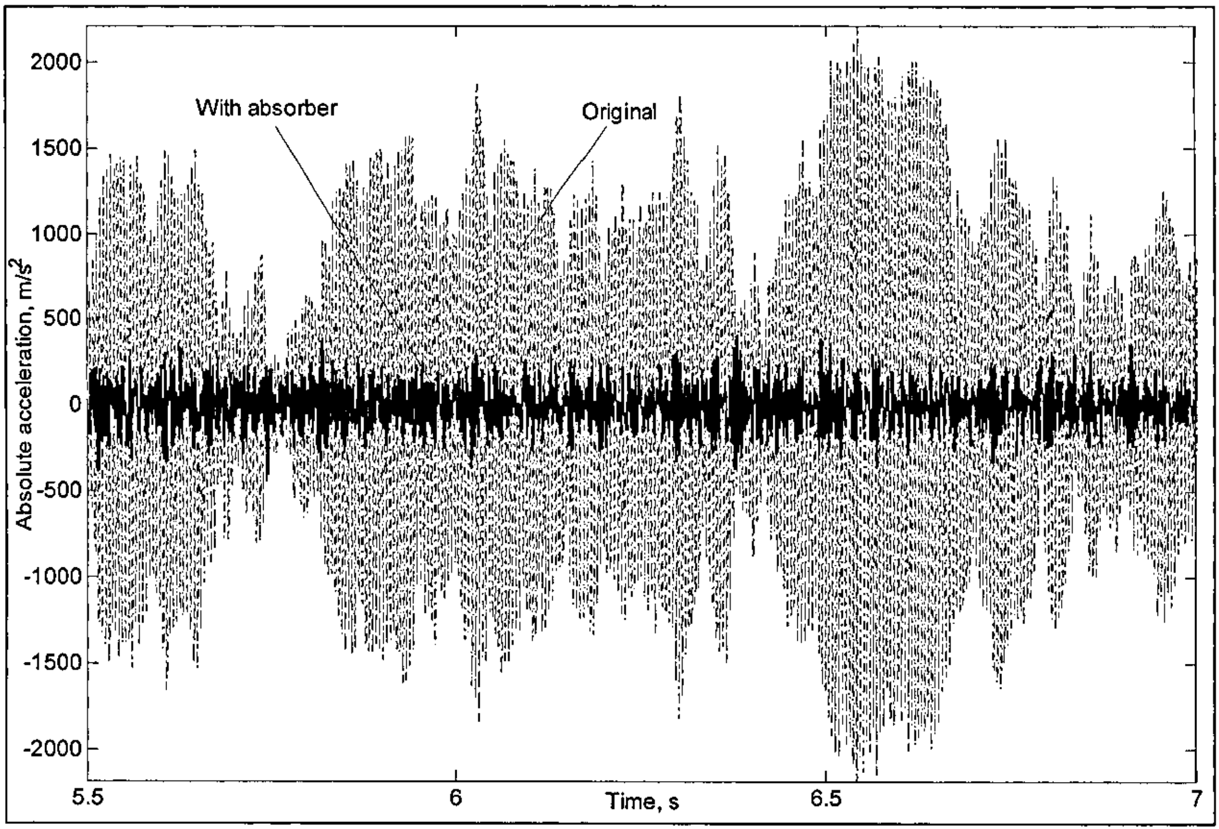

a) Absolute acceleration

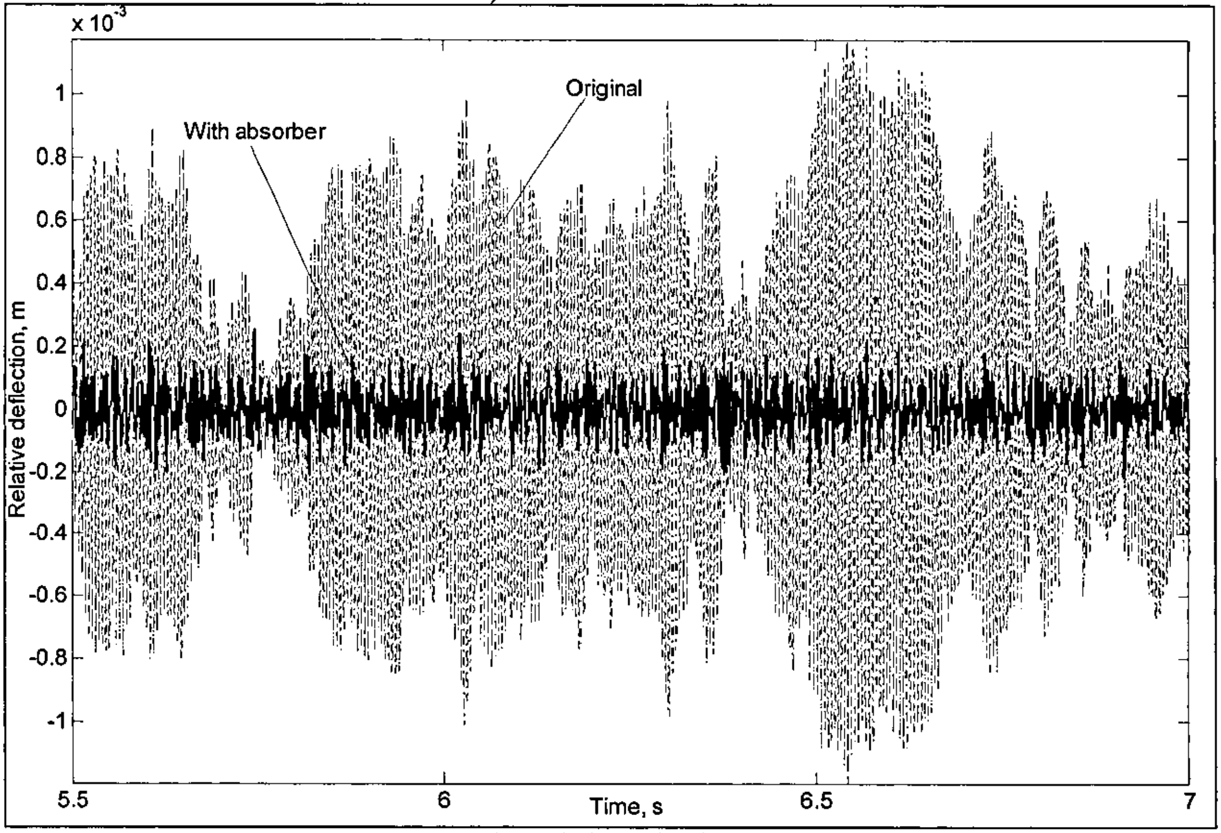

a) Relative deflection

Figure 3.15a. Simulated time history of original and ruggedized PCB (with η=65%)

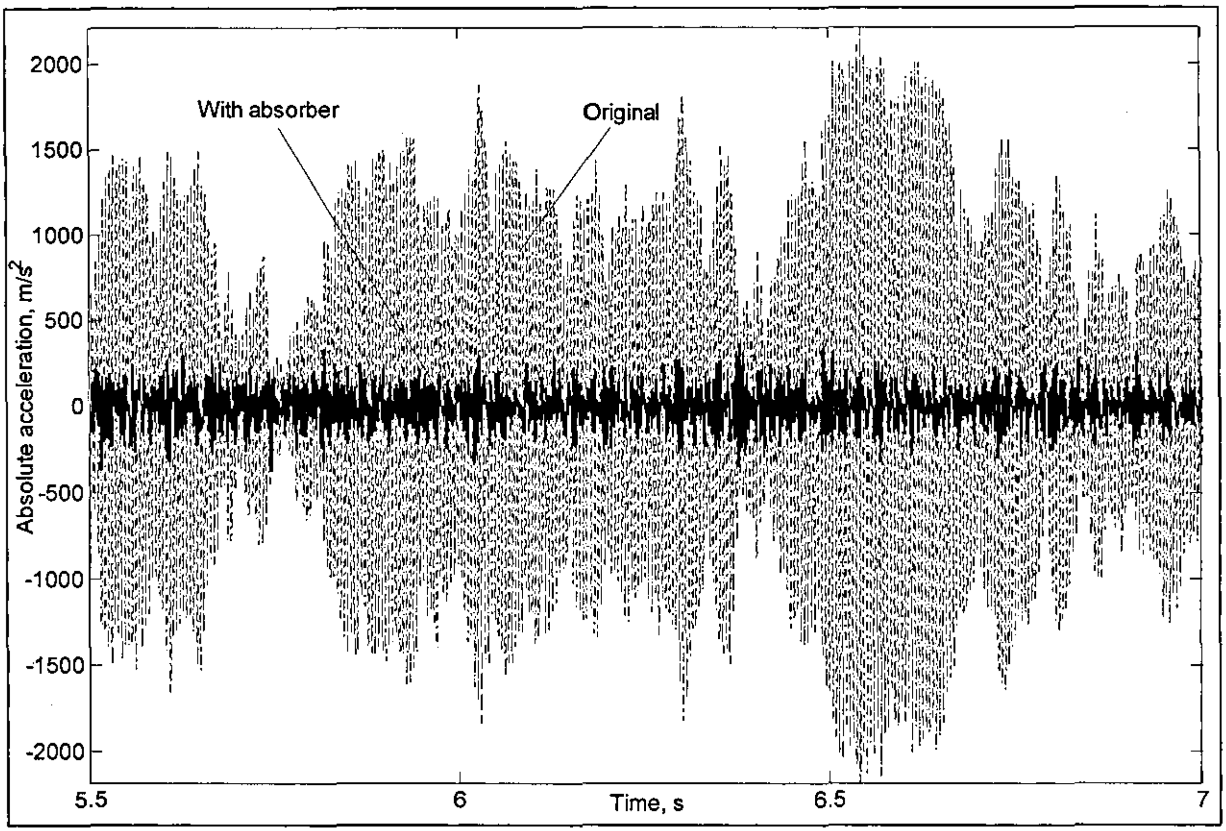

a) Absolute acceleration

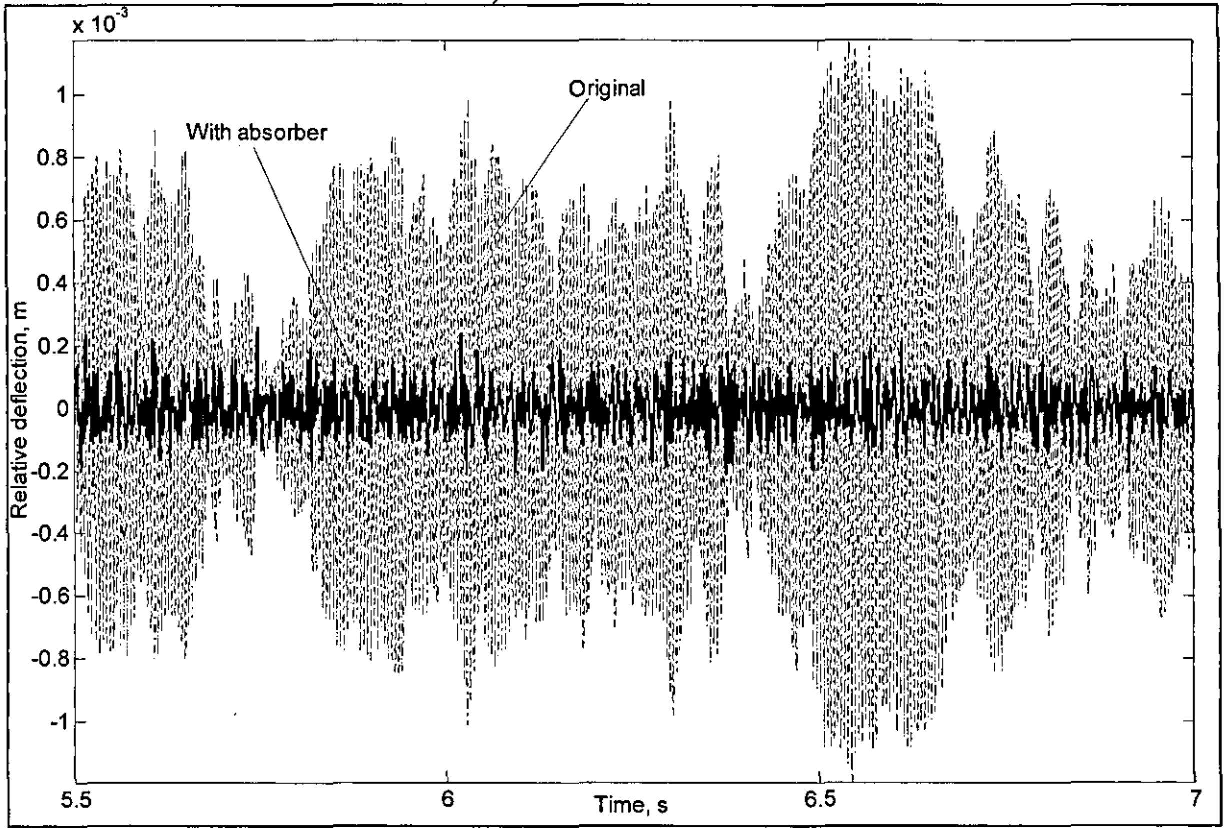

b) Relative deflection

Figure 3.15b. Simulated time history of original and ruggedized PCB (with η=35%)

The above simulation result can be further analysed by using Fast Fourier Transform (FFT). This technique would allow transformation of filter coefficient and white noise to the frequency domain for comparing it to its theoretical solution. Matlab itself provides a useful command known as **pwelch (signal, FFTs, Fs, window, Noverleap)** which is capable of automatically transforming a stationary time signal to PSD without mathematical complication or being time-consuming.

To verify the result of simulation to that appropriate analytical frequency response, an ensemble of 100,000 time points are generated by running the Simulink model up to 10s with a recording time step of 0.1ms in its workspace. Using the **pwelch** command for this configuration would provide an appropriate PSD response in the frequency range of 0-5000 Hz. Figure 3.16 shows the transformation of time domain (Figure 3.14b) to PSD, the desired response shape is almost similar to that experimental excitation spectrum in which the “flat” spectrum has a magnitude of 0.1g^2/Hz in the frequency range of 20-2000 Hz. Thus, the response outside this frequency range has no effect on overall RMS value due to the sharp cutoff frequency. This enhances further the close findings between numerical and analytical results as shown in Table 3.0.

A similar procedure is carried out to transform time domain of absolute acceleration and relative deflection of Figure 3.15 to frequency domain. As a result of the transformation, Figure 3.17 show the PSD of the original and ruggedized PCB (see appropriate label for reference). The differences between these curves and analytical ones are “smoothness” as shown in Figure 3.18.

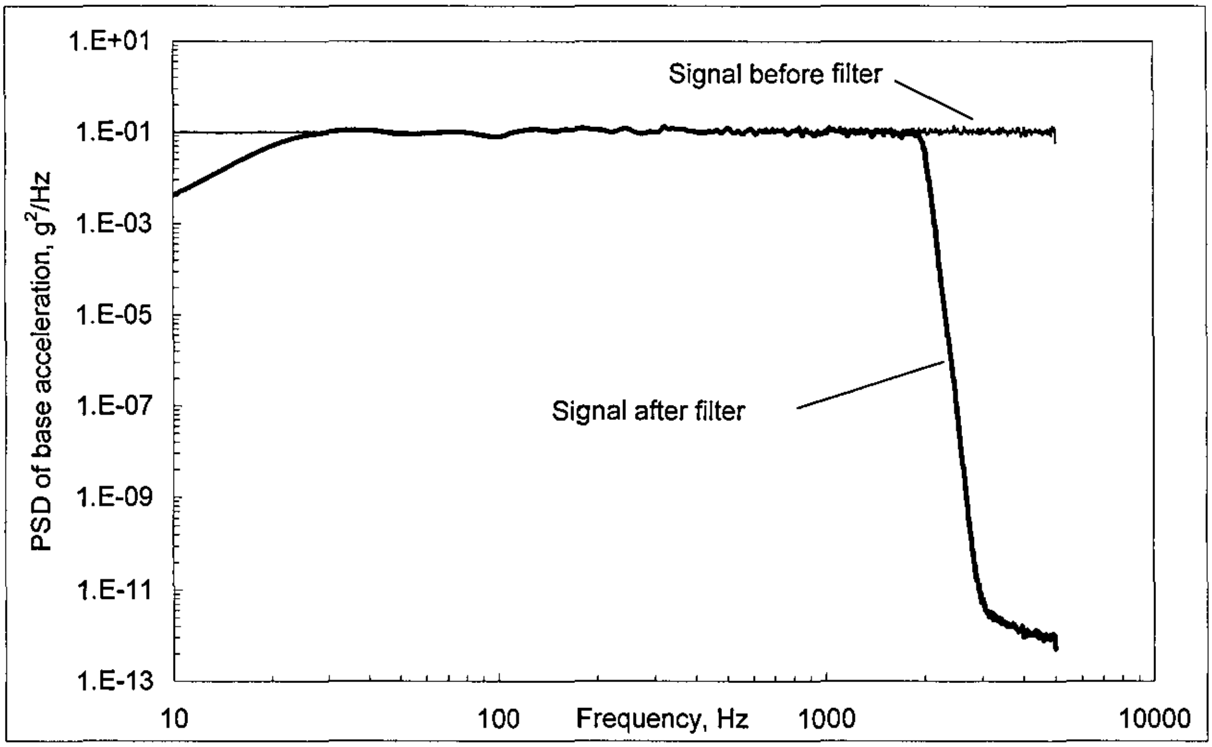

Figure 3.16. Simulated PSD of base acceleration

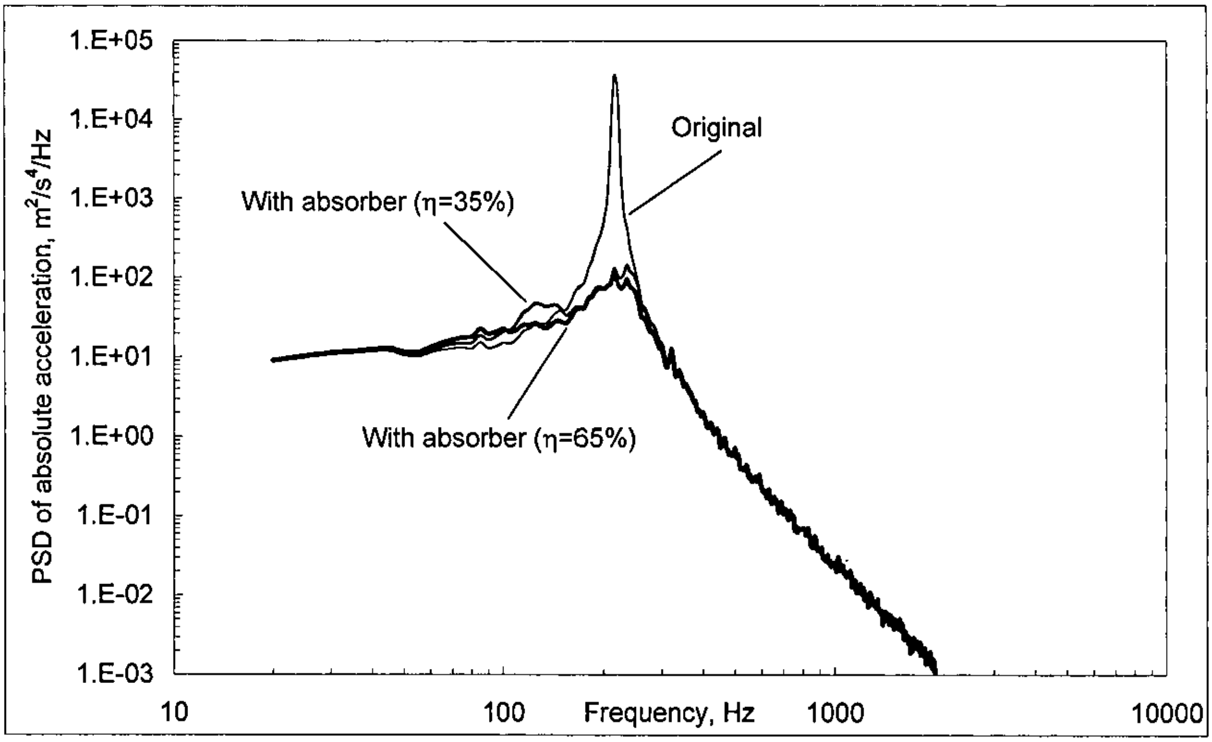

a) PSD of absolute acceleration

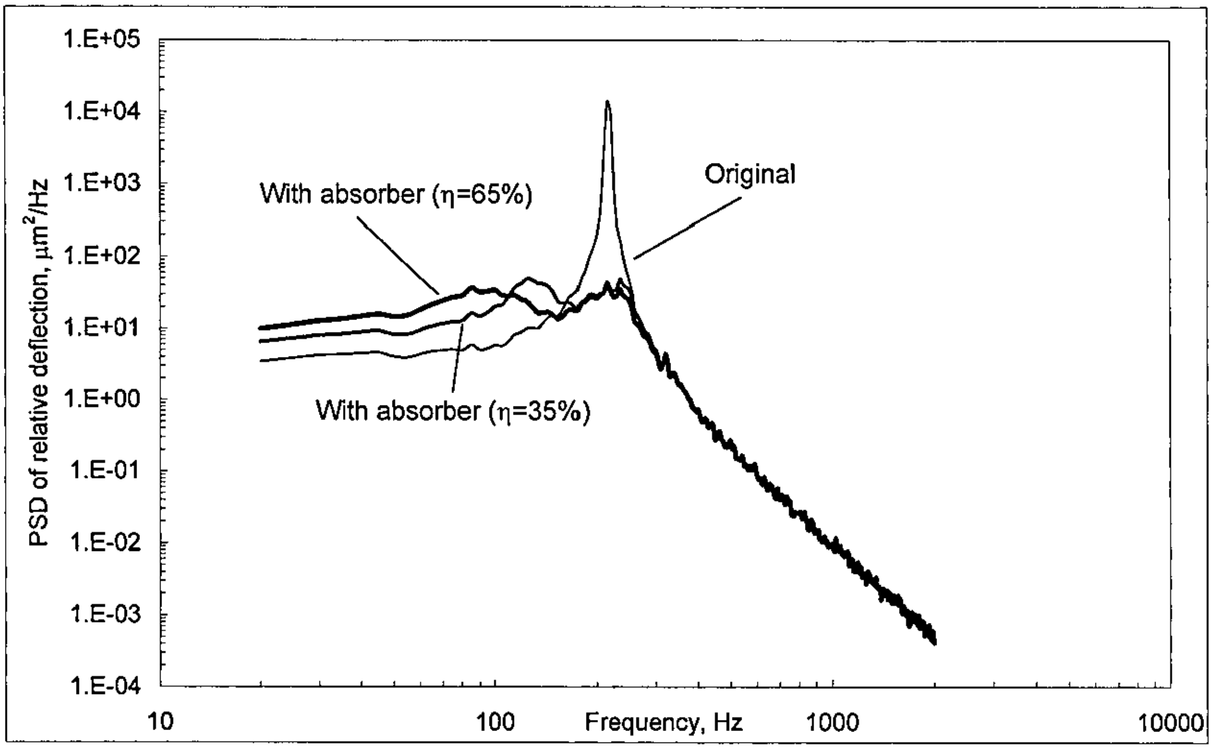

b) PSD of relative deflection

Figure 3.17. Simulated dynamic response of original and ruggedized PCB (η=65%)

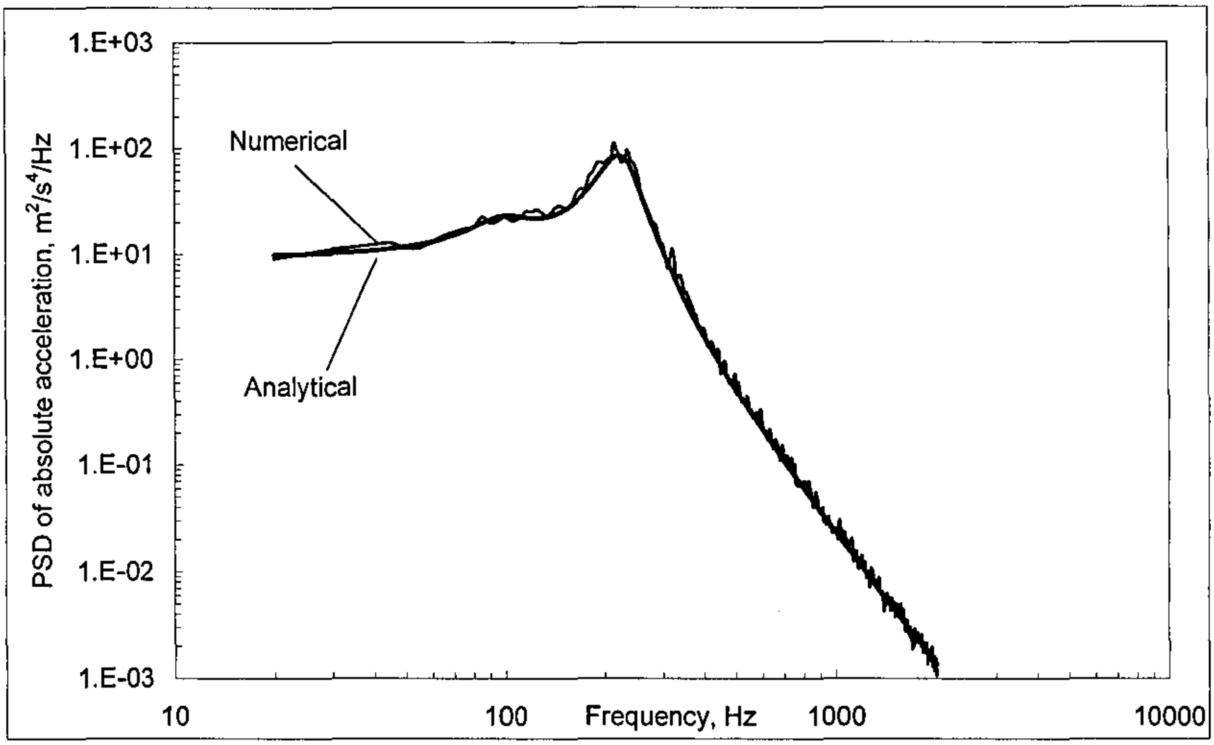

a) PSD of absolute acceleration

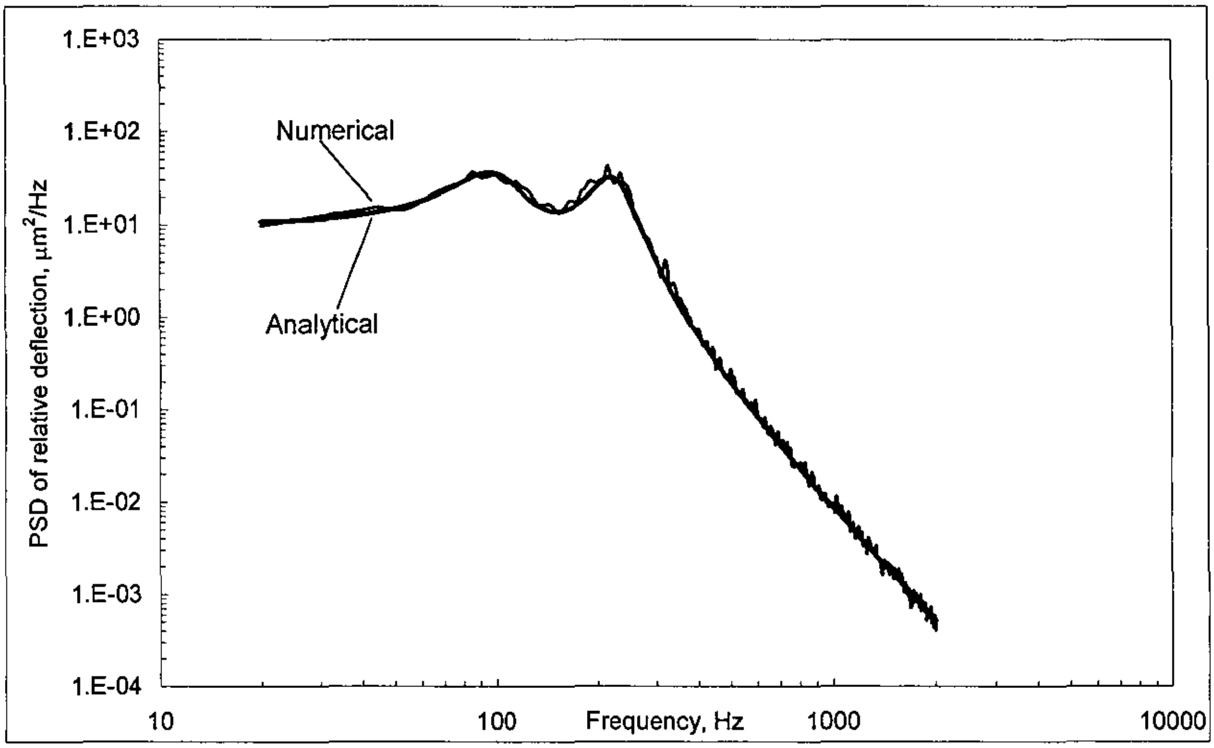

b) PSD of relative deflection

Figure 3.18. Comparison of dynamic response of ruggedized PCB (η=65%)

The "roughness" of these simulation curves can be removed if an alternative FFT command from Matlab is used, a typical one is known as: **tfe (input-signal, output-signal, FFTs, Fs, window, Noverleap).** This command is basically defines the input-output relationship by producing an appropriate FRF, formally known as transfer function estimation. The analytical expression is applied in order to produce a relevant PSD and additional calculation is probably required. In general, if in the right configuration, this technique would produce a "perfect" curve compared to its analytical one for any linear dynamic system under random vibration excitation.

The Simulink model was built for studying the fatigue analysis using a simple cycles technique through its simulation response. The technique of building the Simulink model is entirely based on the equation of motions of 2DOF system, in addition, the time response combines with the signal processing command from the Matlab yields frequency response which produce identical results compared to analytical solution. In general, this method gives a full view of both time and frequency domain of any dynamic system under study which may be a useful tool to the study of nonlinear systems i.e. Vibro-Impact systems.

3.3 Sine vibration

Today, numerous COTS manufacturers require sweep-sine and resonant dwell tests to be carried out as essential parts of qualification testing and screening of critical electronic systems. This kind of vibration testing is much more artificial as opposed to, say, a wide-band random vibration test which is considered in Section 3.2 of this study. However, while not completely representing true loading conditions, swept-sine and resonant dwell tests are important for testing the dynamic behaviour and fatigue of sensitive components of electronic equipment at resonance.

In Section 3.2 we show that a wide-band dynamic absorber is a powerful tool for modifying the dynamic properties and ruggedizing of the sensitive components of electronic equipment such as PCBs. In this instance, the properties of a dynamic absorber were chosen with the purpose of minimising the overall RMS response of the PCB under wide-band random vibration.

In this case, the base motion is given by the acceleration, $\ddot{y} = A\sin\omega t$, where A is acceleration magnitude and ω is driving angular frequency. In this study, we use the typical military specification in accordance with [3], where $A = 10g$, and driving frequency is swept linearly from 20 to 500 Hz. The magnitude of relative deflection of the PCB at frequency ω is [35]:

$$|Z_1(j\omega)| = \frac{A}{\omega^2}\left|\widetilde{T}_r(j\omega)\right| . \tag{3.11}$$

3.3.1 Designing MS®Excel worksheet for minisming peak relative deflection

As in Section 3.2.1, all the calculations were carried out using the MS®Excel spreadsheet. The optimisation procedure involves variation of the natural frequency and loss factor of dynamic absorber, Ω_2 and ξ_2, at a given mass ratio, in such a fashion as to minimise the resonant relative deflection of PCB, Z_1:

$$\left\{\max\left[\left|Z_1(j\omega)\right|\right]\right\} \rightarrow \min . \qquad (3.12)$$

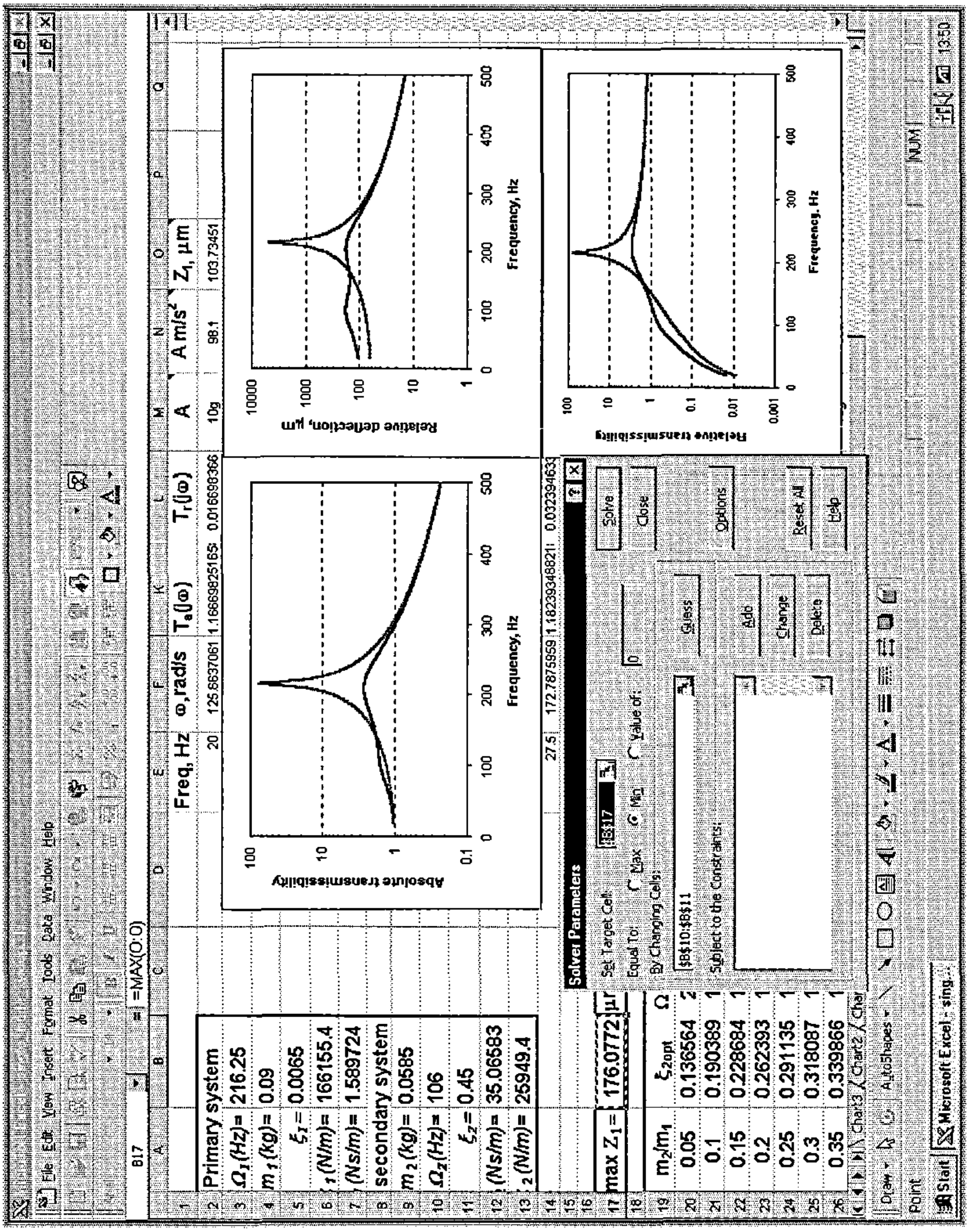
File Edit View Insert Format Tools Data Window Help
A B C D E F K L M N O P Q
Absolute transmissibility
100
10
1
0.1
0 100 200 300 400 500
Frequency, Hz
Relative deflection, μm
10000
1000
100
10
1
0 100 200 300 400 500
Frequency, Hz
Relative transmissibility
100
10
1
0.1
0.01
0.001
0 100 200 300 400 500
Frequency, Hz
Solver Parameters
Solve
Close
Guess
Options
Add
Change
Delete
Reset All
Help
Chart3 Chart2 Char
Draw AutoShapes
Point
NUM
Start
Microsoft Excel - sing...
13:50

B17 =MAX(O:O)

Freq, Hz	ω,rad/s	$T_a(j\omega)$	$T_r(j\omega)$	A	A m/s²	Z_1, μm
20	125.6637061	1.16669825165	0.016698366	10g	98.1	103.73451
27.5	172.7875959	1.18239348821	0.032394633			

Primary system	
$\Omega_1(Hz)$=	216.25
$m_1(kg)$=	0.09
ξ_1=	0.0065
$_1(N/m)$=	166155.4
(Ns/m)=	1.589724
secondary system	
$m_2(kg)$=	0.0585
$\Omega_2(Hz)$=	106
ξ_2=	0.45
(Ns/m)=	35.06583
$_2(N/m)$=	25949.4

max Z_1= 176.0772 μr

m_2/m_1	ξ_{2opt}	Ω
0.05	0.136564	2
0.1	0.190389	1
0.15	0.228684	1
0.2	0.262393	1
0.25	0.291135	1
0.3	0.318087	1
0.35	0.339866	1

Set Target Cell: $B$17

Equal To: ○ Max ● Min ○ Value of: 0

By Changing Cells: $B$10:$B$11

Subject to the Constraints:

Figure 3.19. Spreadsheet for calculation of dynamic response and for optimisation

Figure 3.19 shows the screen snapshot, where the add-in Solver is used for solving the optimal problem (3.12). It should be noted here, the FRFs have a similar feature to random vibration designed worksheet (see the embedded transmissibility graphs). This is due to the involvement of the same universal transmissibility formulations and probably from the same worksheet. For any linear dynamic system, MS®Excel worksheet proves to be the most convenient software for analysing frequency response under either random or swept-sine vibration, typically those that are concerned with optimal performance and quality graphical presentation.

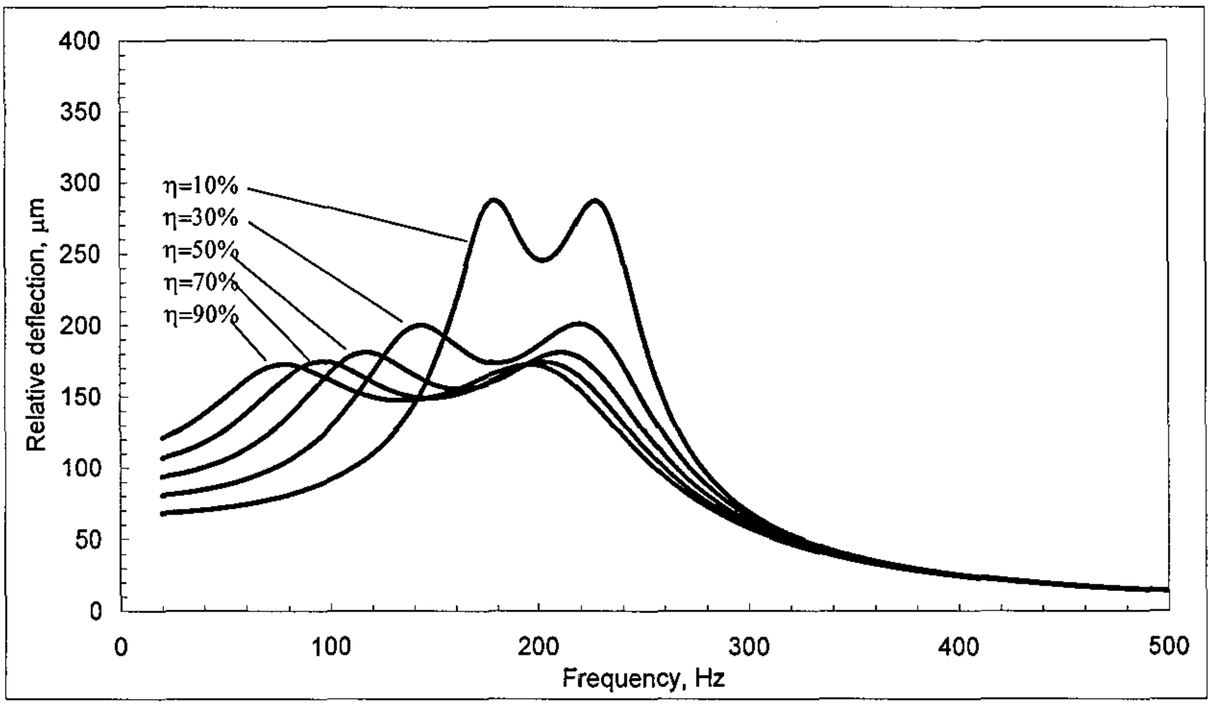

a) Swept-sine

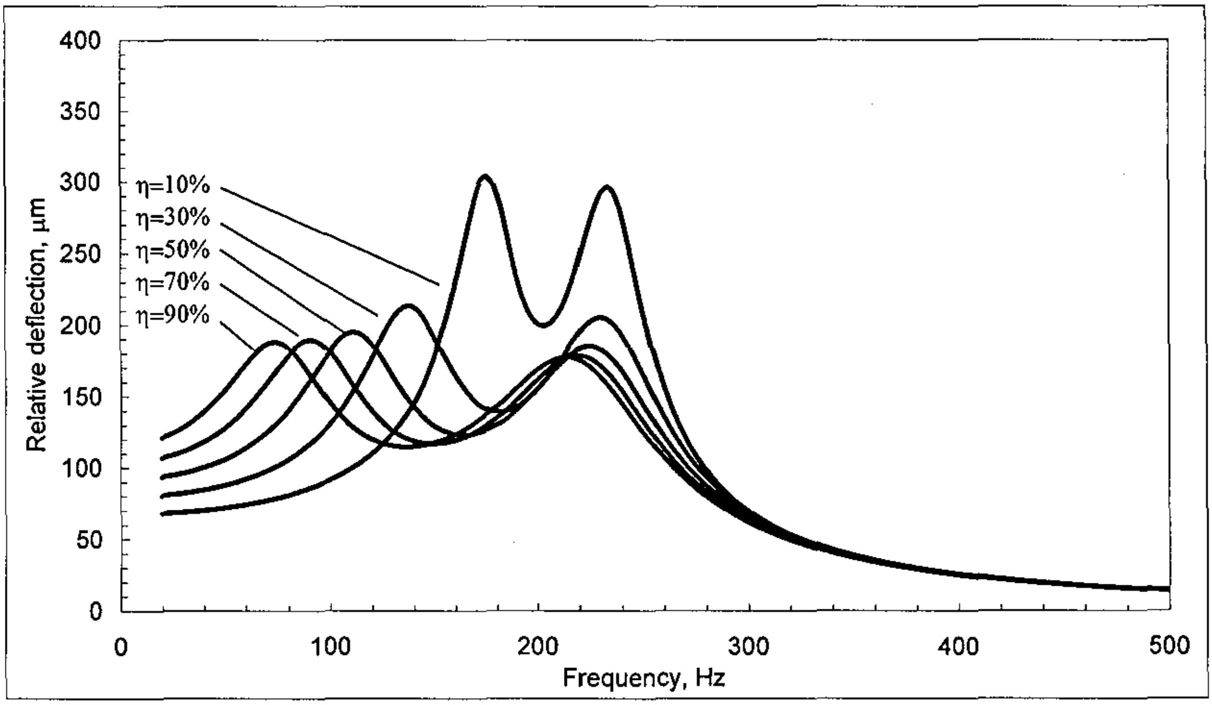

b) Random

Figure 3.20. Dynamic response of PCB with different mass ratios

Figure 3.20a highlights the relative deflection of the dynamically ruggedized PCB under swept-sine excitation where the dynamic absorber was optimised for the swept-sine excitation at different mass ratios. It should be noted in this figure the peak value is the same at first and second resonance at any mass ratio, a classical optimal response shape of a SDOF primary system with the influence of an optimal dynamic absorber, formally known as the equal-peak response. Figure 3.20b shows the relative deflection of the dynamically ruggedized PCB under swept-sine excitation where the dynamic absorber was optimised for the wide-band random excitation at different mass ratios.

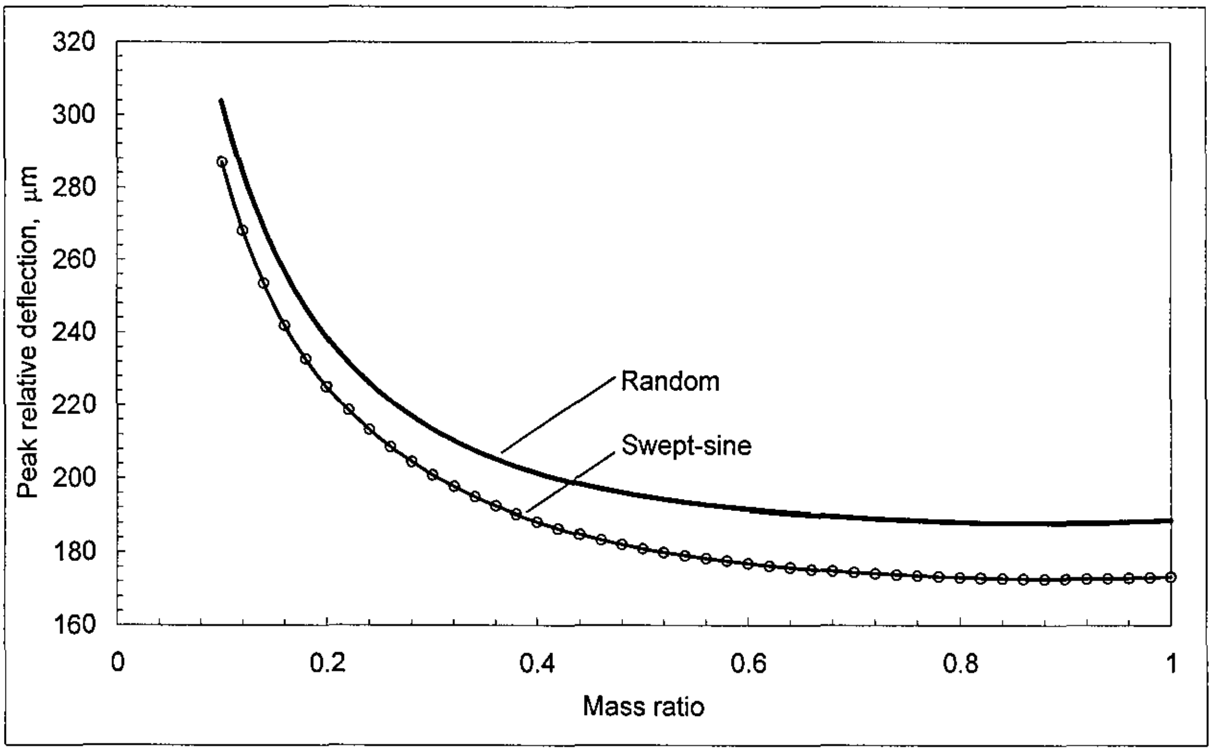

Figure 3.21. Peak response of PCB with different mass ratios

Figure 3.21 shows the dependence of the minimised peak response on the mass ratio. For comparison, the similar curve obtained for the dynamic absorber optimised for the random excitation in Section 3.2.1 in this study is superimposed. The difference obtained is reasonably small. This result would further enhance the design of the universal dynamic absorber, as the mass, loss factor and natural frequency is slightly altered without significantly affecting the performance of the PCB. This criterion is an important factor in designing the dynamic absorber due to the space constraint in an electronic box. From Figure 3.21, for the mass ratios greater then 65% ($\eta > 65\%$) the performance of the dynamic absorber cannot be significantly improved. Hence, it would be reasonable to have single dynamic absorber which suits equally well both cases of wide-band random and swept-sine excitation, where the optimal parameters of an dynamic absorber would be based on results of random vibration:

$$\eta = 65\%\,,\ \frac{\Omega_{2opt}}{2\pi} = 106\text{Hz and } \zeta_{2opt} = 0.35\,,$$

where the peak deflection 190 μm is found as slightly higher compared to the case of swept-sine (max peak deflection 175 μm) at the same mass ratio.

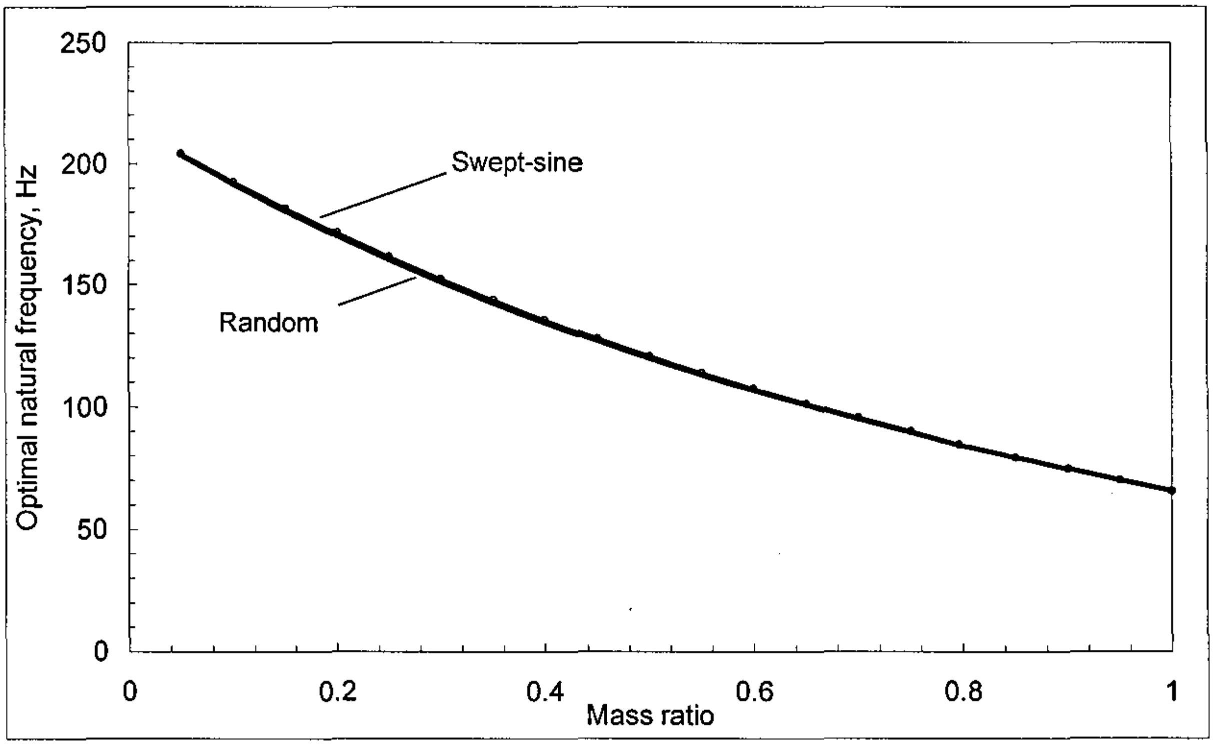

b) Optimal frequency

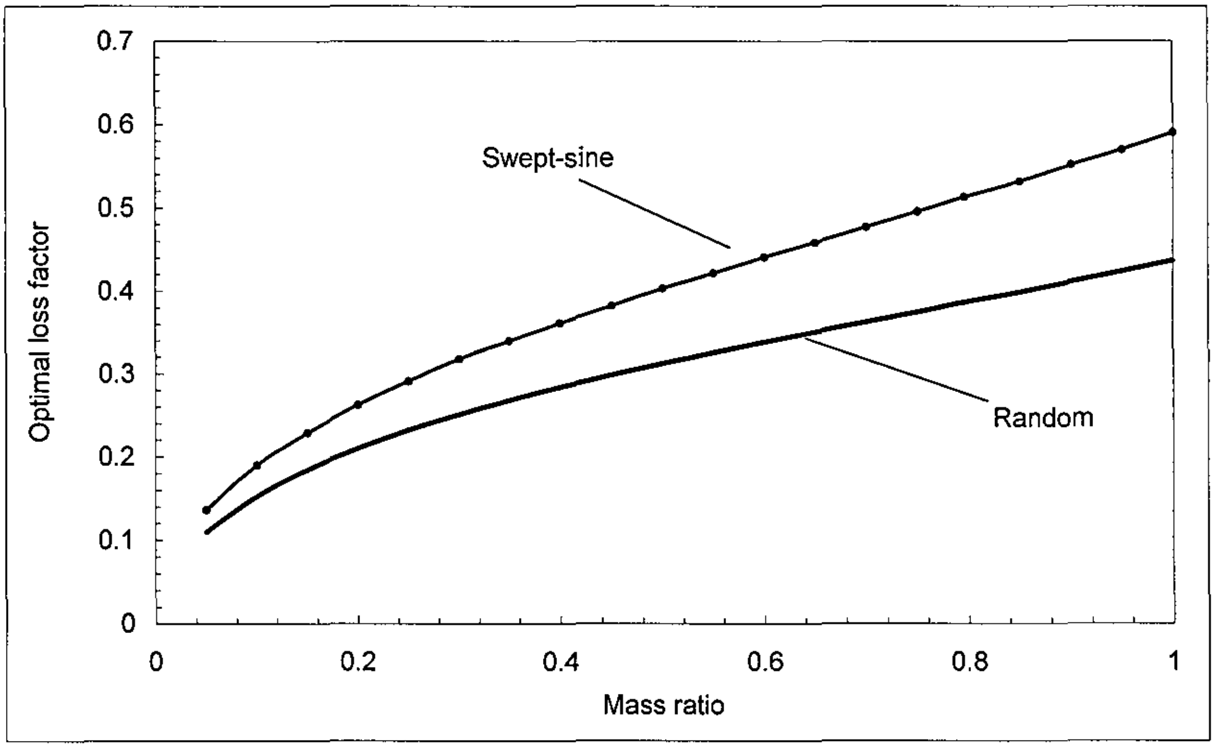

a) Optimal loss factor

Figure 3.22. Optimal parameters of dynamic absorber at different mass ratios

Figure 3.22 shows the dependencies of the optimal natural frequency (a) and loss factor (b) of the dynamic absorber at different mass ratios. In the same figures, the corresponding curves reflecting the case of the dynamic absorber obtained for the case of random excitation are superimposed. It appears that the optimal natural frequency of dynamic absorber is exactly the same for both types of excitations (see Figure 3.22b). However, the optimal loss factor is slightly different, as shown in Figure 3.22a.

Similarly, using the traditional design [13] for the PCB application under swept-sine excitation, as a result, Figure 3.23 shows the peak relative deflection on the value of mass ratio (see the curve labelled as **Traditional optimal design**) also the novel optimal curves from Figure 3.21 is superimposed for reference. As can be clearly seen the traditional optimal dynamic absorber design does not gives any better results as compared to the above novel optimal ones at any given mass ratio, see appropriate curve in Figure 3.23 for reference. Regarding to the traditional design, 30% mass ratio gives a lowest value of peak deflection, 275 μm and it seems to be very sensitive as the mass ratio increased.

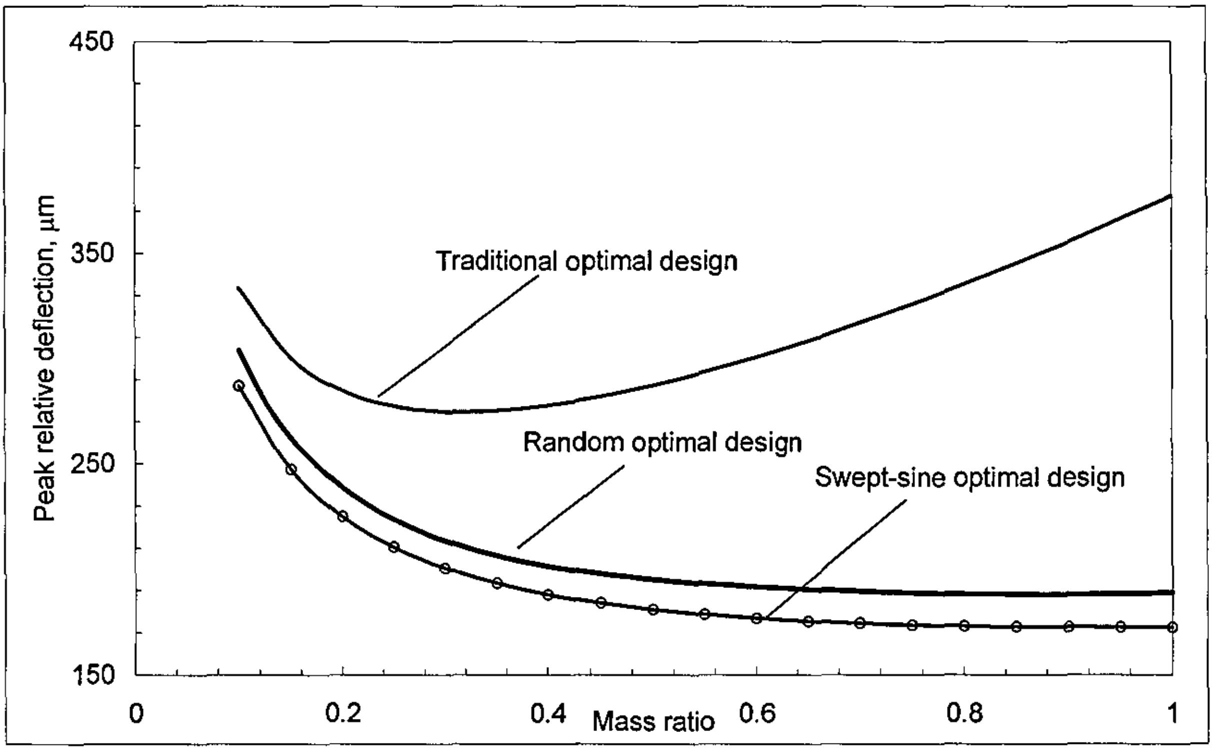

Figure 3.23. Comparison of peak relative deflection in the case of traditional and novel design

However, the aim of this study is to design a single dynamic absorber for both wide-band random and swept-sine excitations, as shown from the novel optimal approach, the chosen optimal dynamic absorber (i.e. $\eta = 65\%$, $\frac{\Omega_{2opt}}{2\pi} = 106\text{Hz}$ and $\zeta_{2opt} = 0.35$) for random excitation is also suitable for swept-sine excitation. To see the differences between the novel design and the traditional one therefore the traditional dynamic absorber (i.e. $\eta = 0.45\%$,

$\frac{\Omega_{2opt}}{2\pi} = 149\,\text{Hz}$ and $\zeta_{2opt} = 0.23\,5$) that design for optimal overall relative deflection is chosen.

As a result, Figure 3.24 shows the comparison of relative deflection of the PCB.

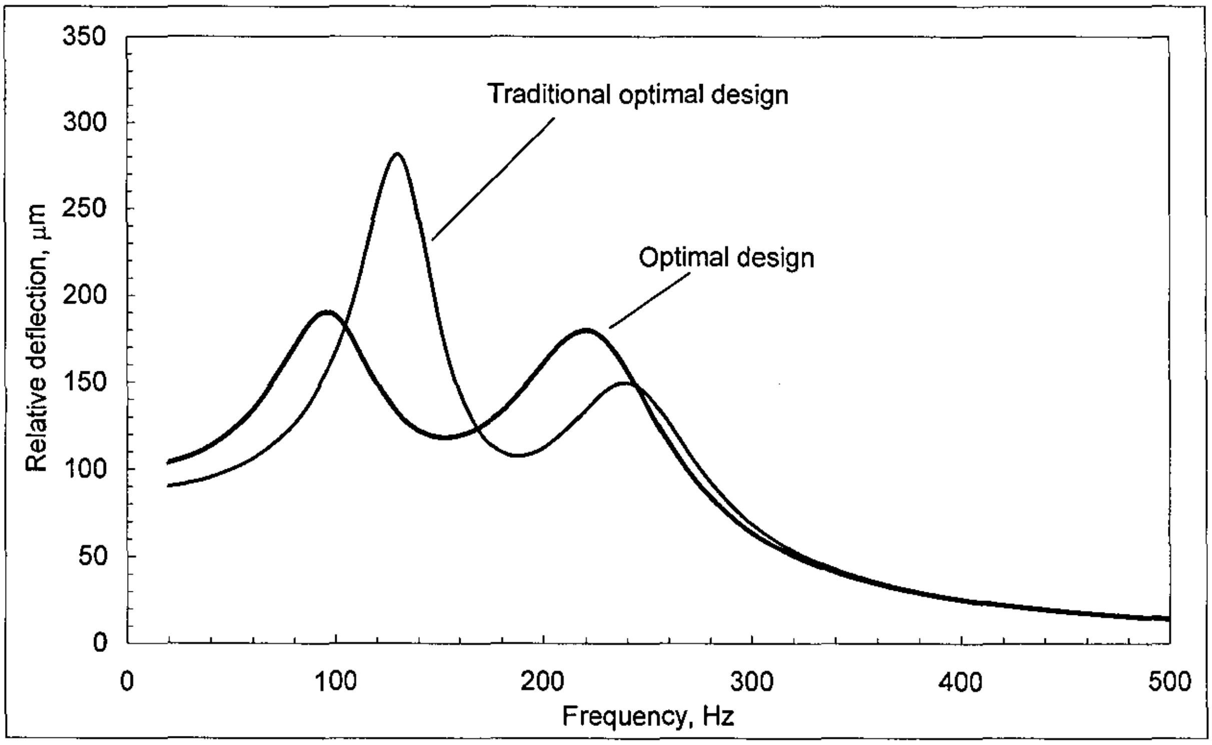

Figure 3.24. Comparison of relative deflection in the case of traditional and novel design

As here the novel optimal design produces the peak relative deflection, 190 µm whereas the traditional one produces 281 µm at the same excitation level. These huge differences give the design improvement by 32% whereas there is only 5% improvement in term of overall deflection under random vibration. Although, swept-sine is not critical factor for the PCB application, however, as here we demonstrate a better performance can be achieved using novel design.

3.3.2 Sensitivity analysis

Similar to Section 3.2.3, the sensitivity analysis was carried out. For this purpose the mass ratios were fixed at values of 65% and 35% respectively. Figure 3.25a shows the corresponding optimal loss factors 0.35 and 0.267 as being fixed, whilst the value of the natural frequency varies from 50 Hz to 200 Hz.

Figure 3.25b shows the same mass ratios of 35% and 65% with correspondent optimal natural frequencies 106 Hz and 144 Hz are fixed, whilst the loss factor varies from 0 to 1.

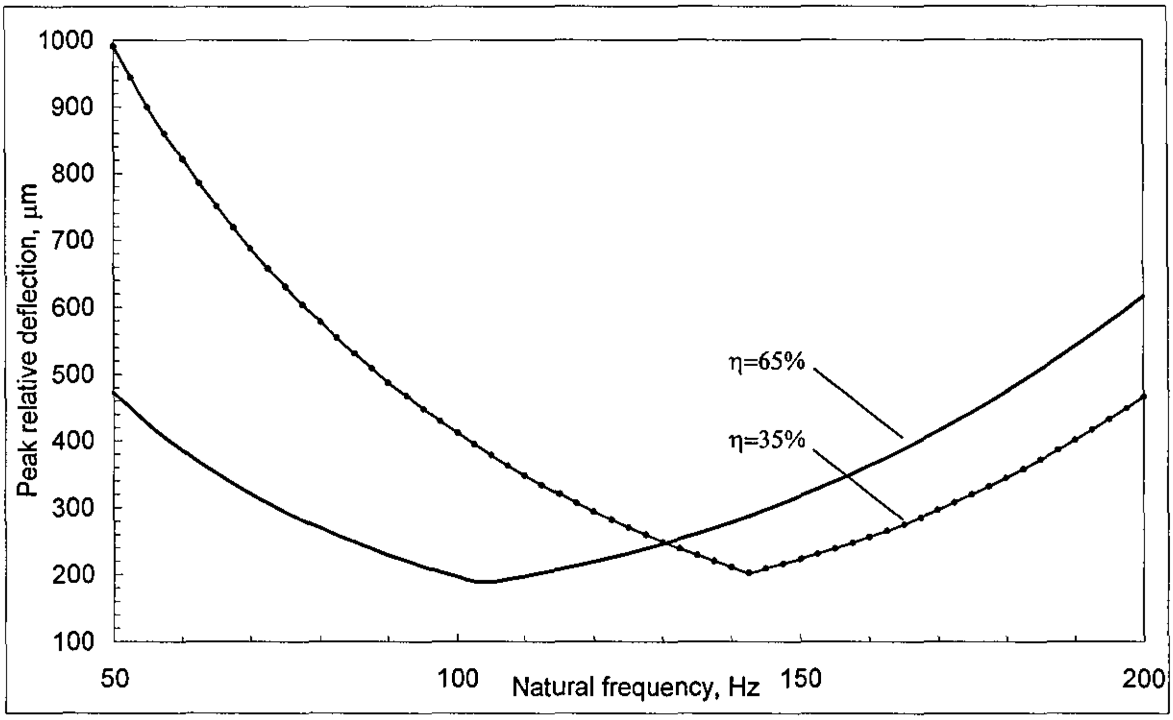

a) Peak relative deflection at different natural frequencies

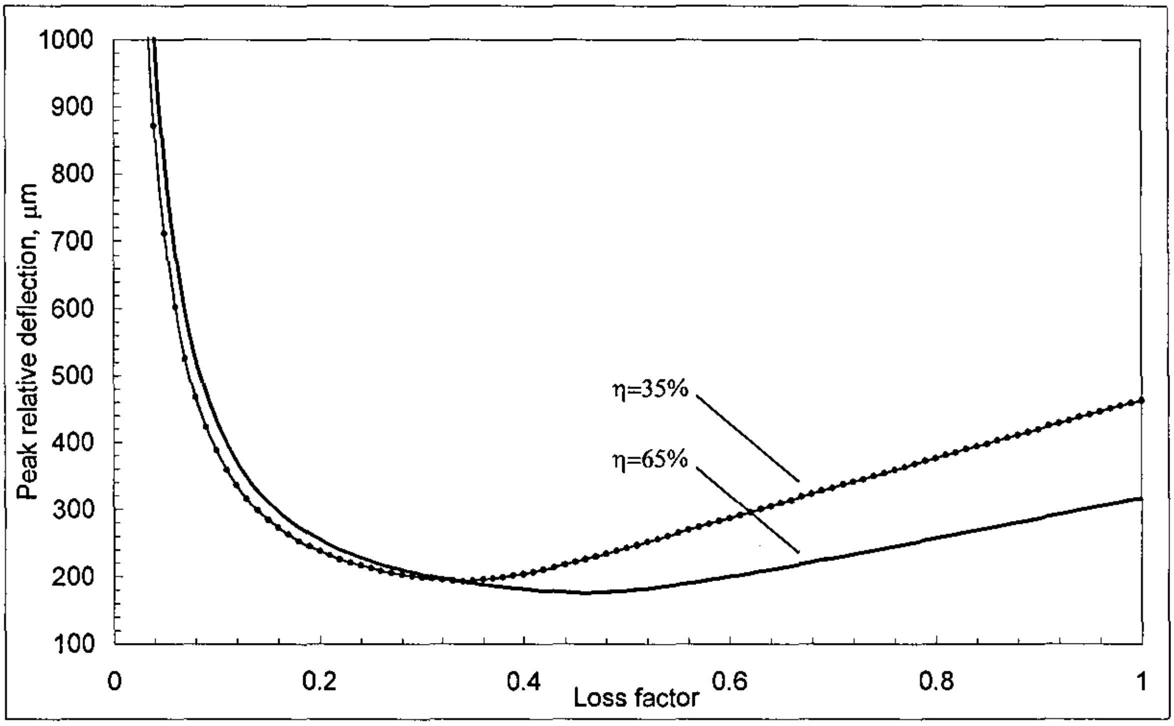

b) Peak relative deflection at different loss factors

Figure 3.25. Sensitivity analysis

From sensitivity analysis in Figure 3.25, a reasonably small variation of the loss factor and natural frequency around their optimal values would have little impact on the peak deflection of the PCB.

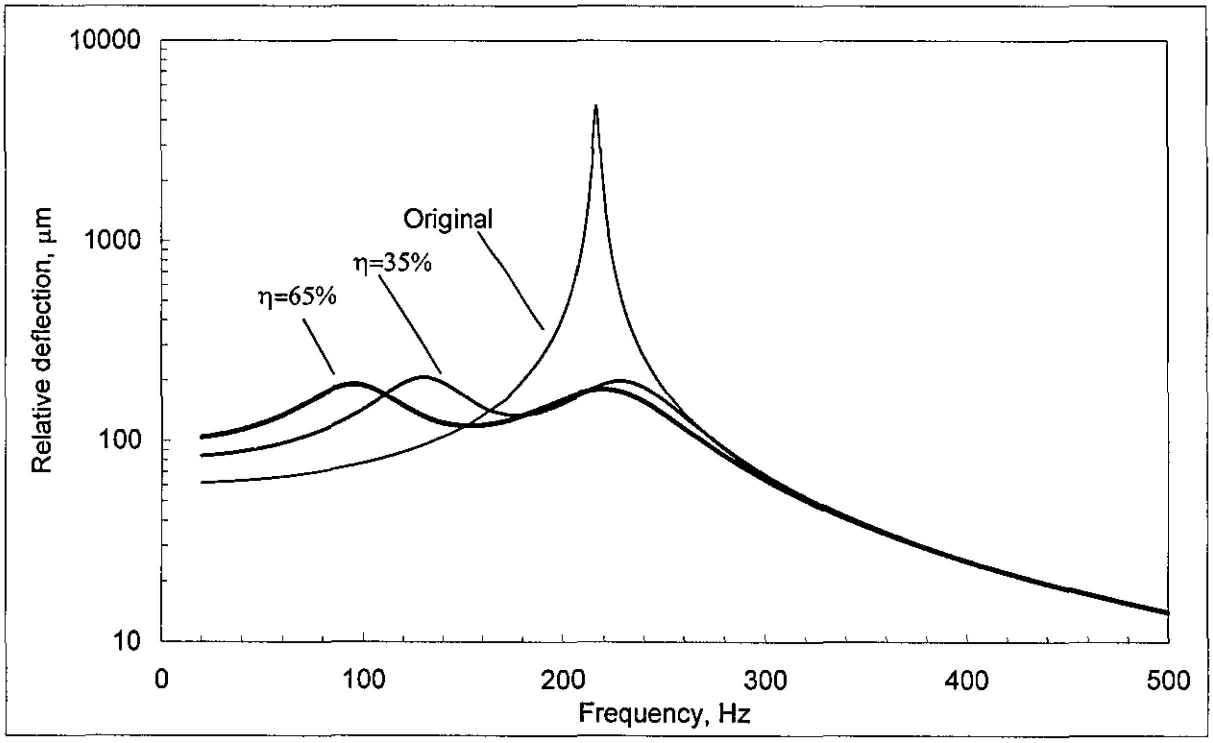

Figure 3.26. Dynamic response of original and ruggedized PCB

Figure 3.26 illustrates the dynamic response of the dynamically ruggedized PCB, where the dynamic absorber with the loss factor of 0.35, natural frequency of 106 Hz and mass ratio of 65%, yields 24-fold vibration suppression at resonance as compared with original design (from 4617 µm to 190 µm).

In the same figure, the dynamic absorber with the mass ratio of 35%, natural frequency 144 Hz and loss factor 0.29 yields 22-fold vibration suppression at resonance as compared with original design (from 4617 µm to 205 µm). It appears that the peak deflection of the ruggedized PCB has little impact on the selection of mass ratio between 35% and 65%.

3.3.3 Numerical simulation

As in random vibration study, the numerical simulation is carried for swept-sine excitation. The Simulink model is identical to that model of random vibration, however, in this model the random excitation (combination of **Random Number** and **Analog Filter Design**) is now replaced by harmonic excitation, the **Swept-sine** sub-system. It produces two signals, these are $\sin\omega t$ and $\cos\omega t$ with a linearly increasing frequency $\omega = \omega(t) = 2\pi\alpha t$, where α is sweep rate, Hz/s. This model also features a direct built-in signal processing, **Statistics** sub-system, this reduces the use of computational memory and the time being involved. The signal obtained via **Statistics** sub-system and instantly combined signal from **Swept-sine** sub-system could be either produced RMS value of peak-to-peak or the peak value of the fundamental harmonic process in frequency domain. In general, it would produce a corresponding "live" envelope of the current time history response. The signal can be recorded in workspace for comparison with its analytical solution. The structures of these sub-systems are shown in Figure 3.28.

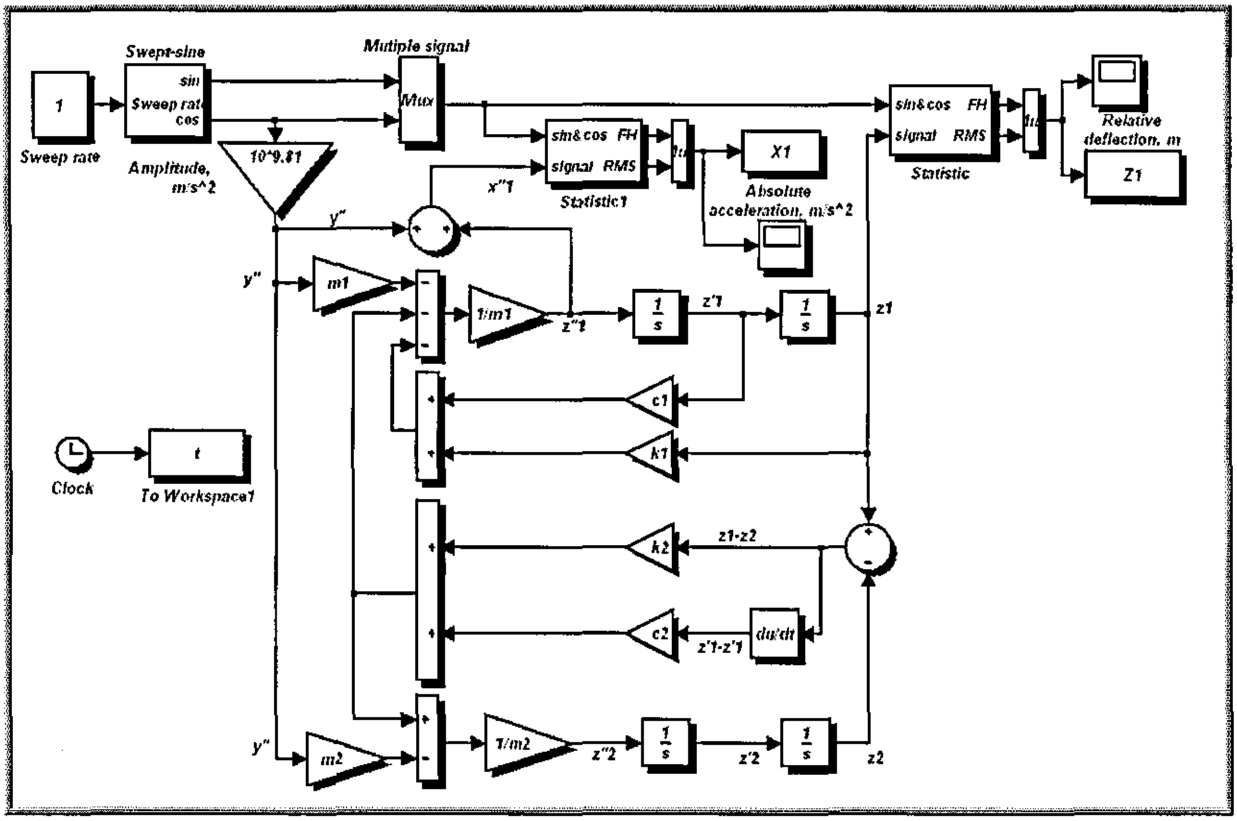
Swept-sine
sin
Sweep rate
cos
1
Sweep rate
Amplitude, m/s^2
10*9.81
Mutiple signal
Mux
sin&cos FH
signal RMS
Statistic1
x"1
X1
Absolute acceleration, m/s^2
y"
m1
1/m1
z"1
1/s
z'1
z1
c1
k1
Clock
t
To Workspace1
k2
z1-z2
c2
du/dt
z'1-z'1
m2
1/m2
z"2
z'2
z2
sin&cos FH
signal RMS
Statistic
Relative deflection, m
Z1

Figure 3.27. Simulink diagram for swept-sine excitation

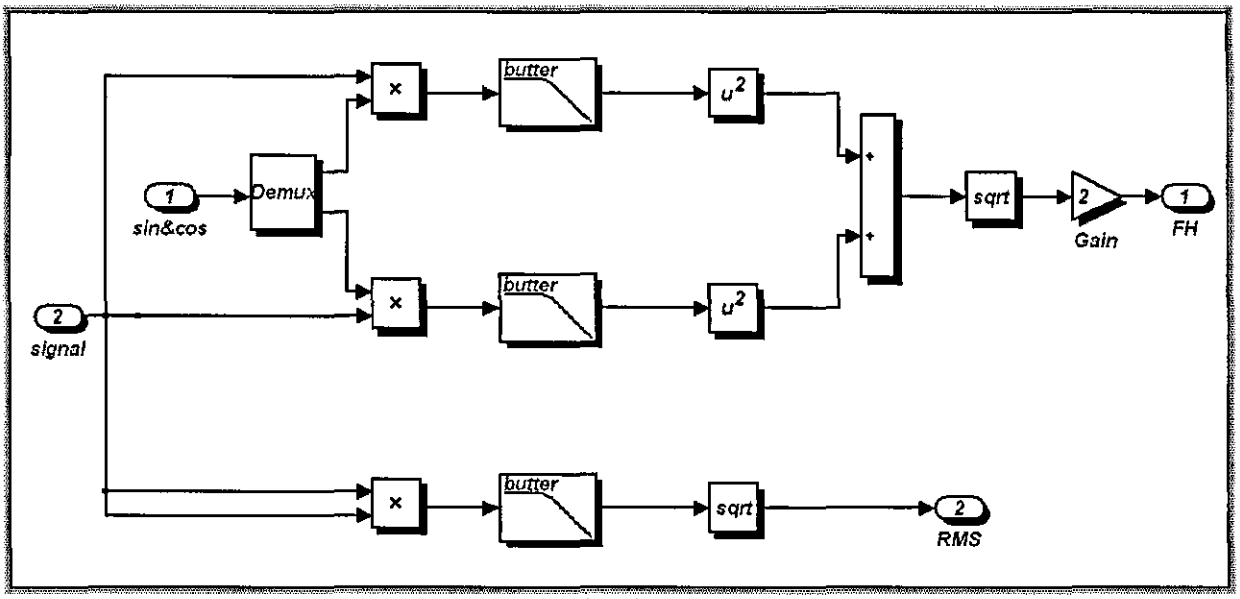
×
butter
u^2
1
sin&cos
Demux
2
signal
+
sqrt
2
Gain
1
FH
2
RMS

a) Statistic sub-system

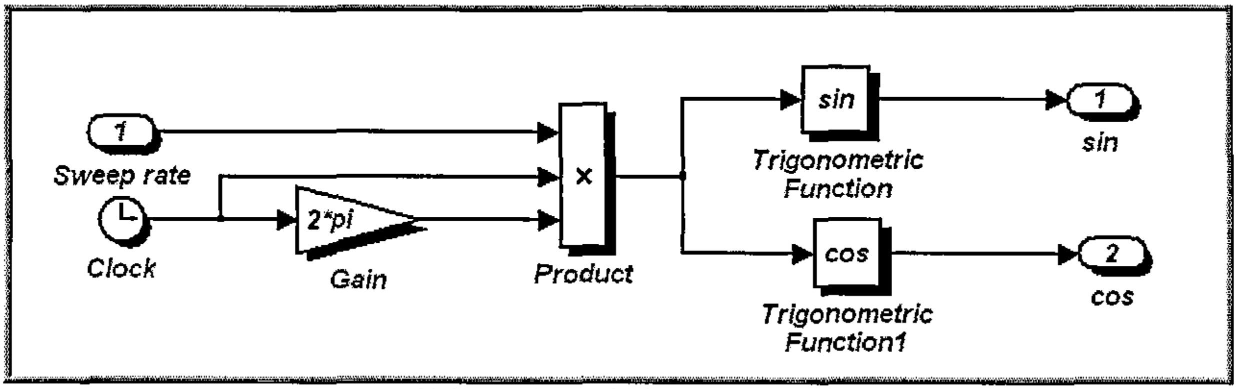

b) Swept-sine excitation sub-system

Figure 3.28. Signal processing "tool box"

There is a critical point in this numerical simulation, the value of sweep rate has great influence on the accuracy of the response signal. If the chosen value were high then the "beat phenomena" would occur. It would behave like a real system, especially in systems with low loss factor, the response signal will be distorted at the resonant frequency area. If the sweep rate is too small for the system with the high resonant frequency, then the simulation process will take time to complete each run and overload the computational memory. From this reason, a sweep rate of 1 Hz/s is chosen to sweep up from 0 Hz to 500 Hz. The whole integration routine is still used **ode45 (Dormand-Prince)** with auto variable step time.

Figure 3.29a shows a typical time history as it was swept through the frequency range of 216.5 Hz to 217.5 Hz, about resonant frequency of the original PCB. As can been seen from the plot, the recorded response in 1 s required a lot of computational memory and normally Simulink is automatically stopped if the workspace is overloading. Therefore the direct built-in signal processing, **Statistics** sub-system was used at this instance in order to avoid these problems and at the same time, the RMS or FH signals are shown as primarily of interest for this swept-sine vibration.

Figure 3.29b shows the superimposition of **RMS** and **FH** curve from simulation of the modified PCB. It clearly shows that the **FH** signal is the peak envelope of the time signal. Since the response of the system is linear where the positive and negative peak of the time signal response is symmetrical, then **FH** signal is equal to $\sqrt{2}$ **RMS** signal at any excitation frequency.

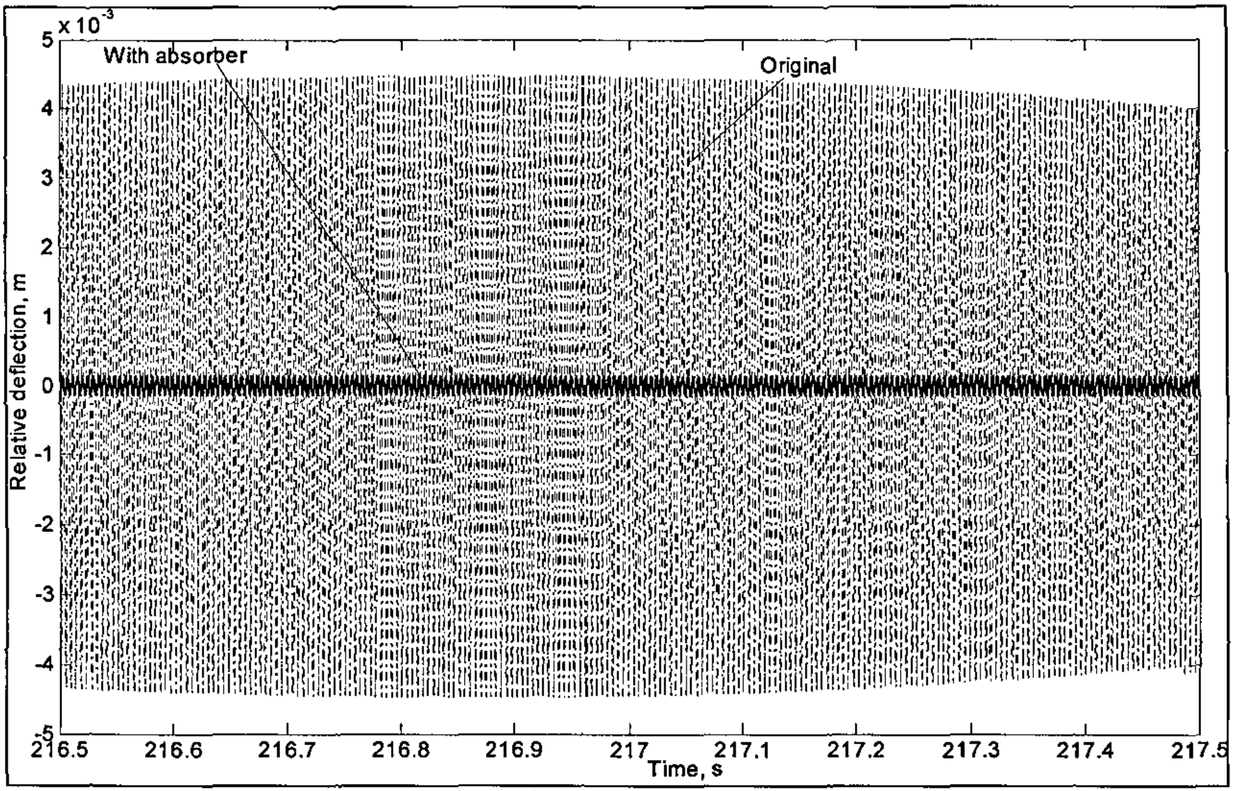

a) Time response

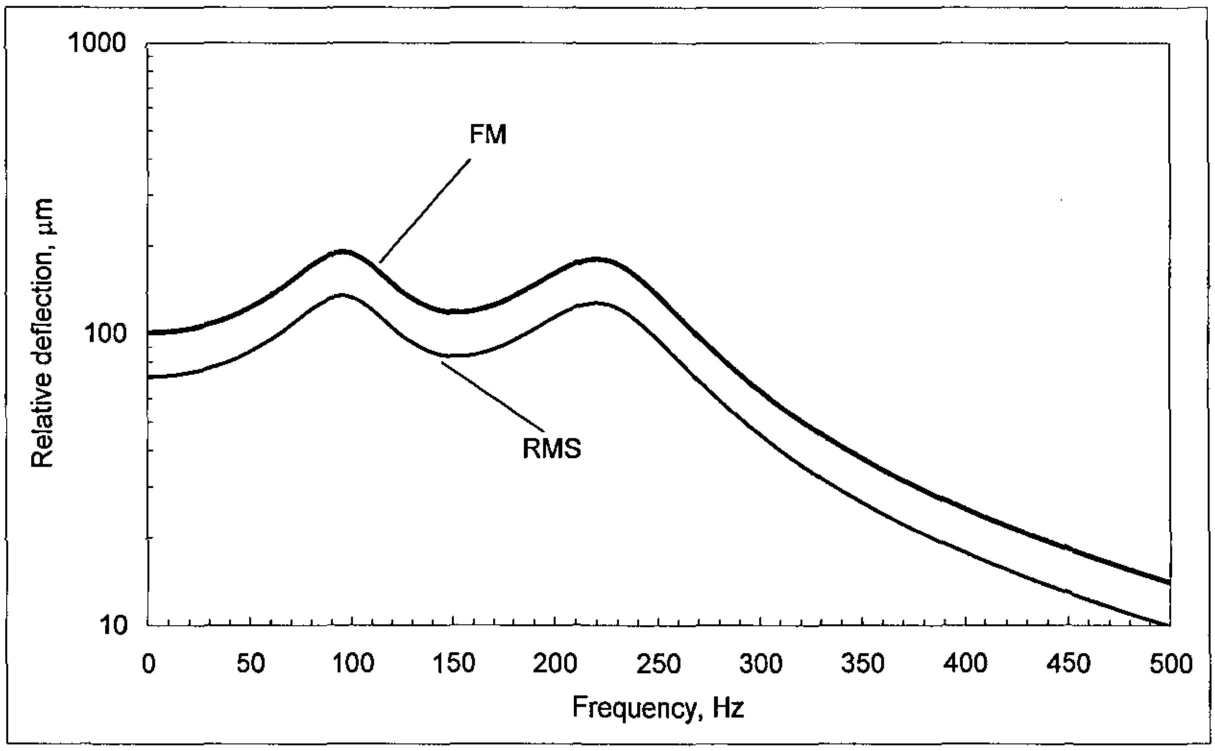

b) Frequency response

Figure 3.29. Simulated relative deflection

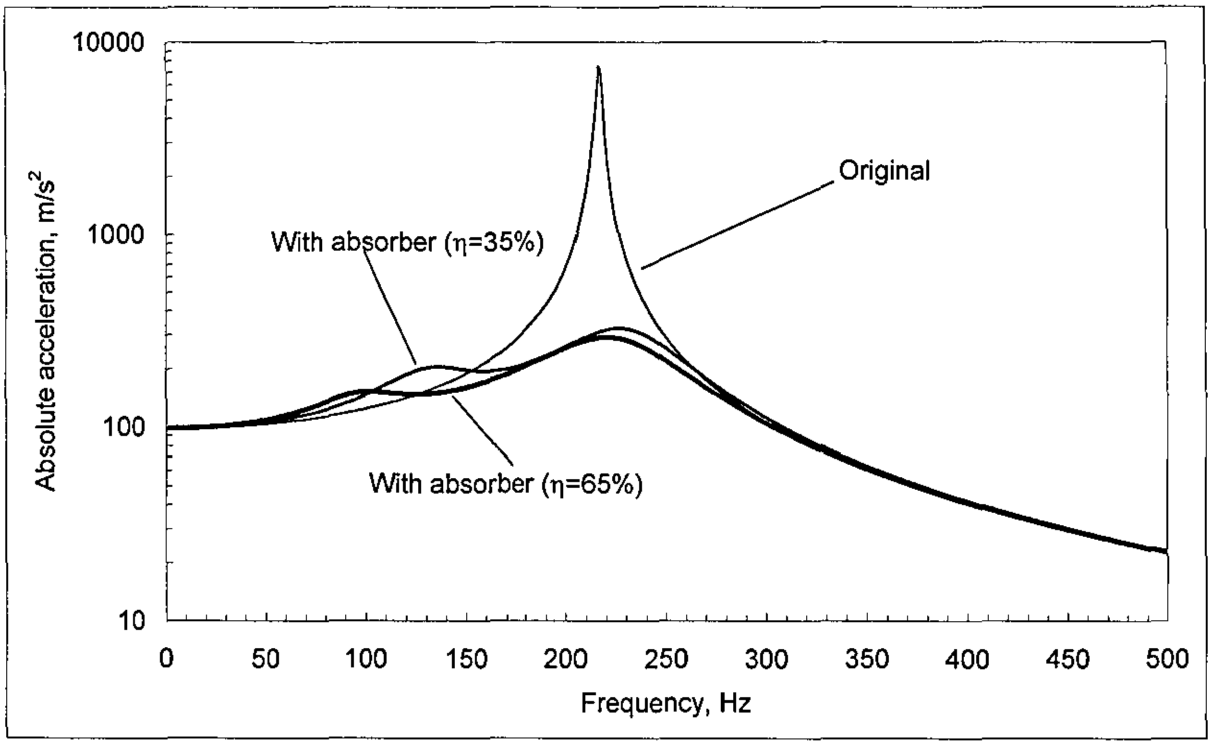

Figure 3.30. Simulated absolute acceleration of original and ruggedized PCB

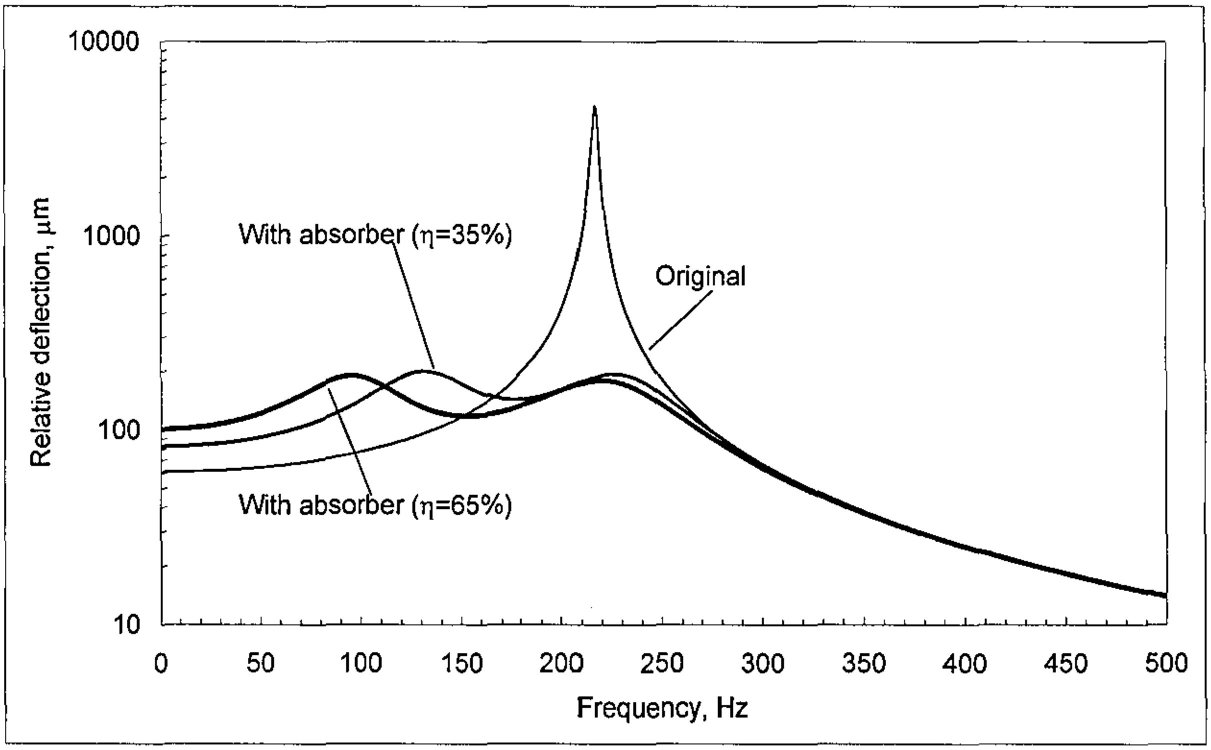

Figure 3.31. Simulated relative deflection of original and ruggedized PCB

As would be expected, the response shape of numerical solution using Simulink is close to that theoretical solution (see theoretical curve from Figure 3.31 for reference), where the peak value is the same in both cases.

The fatigue calculation base on the peak relative reduction ratio between the original and ruggedized PCB is vague compared to that of random vibration in which the expected life of the ruggedized PCB is increased tremendously. Since, sine vibration environment does not normally exist in a true vibration environment where normal electronic equipment would be used, the value of an increased lifetime factor for the PCB is not calculated in this case. However, in this section we show that the dynamic absorber, which has been optimised to dynamically ruggedize the PCB for application under severe wide-band random vibration, is still suitable for effective suppression of the PCB's resonant responses under swept-sine excitation. The investigation was carried out both analytically and numerically which produced identical results. In addition, the built-in signal processing sub-system design for calculating the frequency response during numerical simulation can apply in future research, say Vibro-Impact system with harmonic excitation. Finally, some potential problems associated with the use of this numerical integration have been identified.

3.4 Shock

Various types of shock pulses are often used to excite electronic assemblies to simulate transport environments, bench handling conditions, weapon application and operating environments. The manner in which the various electronic components respond to these shocks will determine if the components will survive the environments.

Shock is often defined as a rapid transfer of energy to a mechanical system, which results in a significant increase in stress, velocity, acceleration or displacement within the system. The time in which energy transfer takes place is usually related to resonant frequency of the system and excites many natural frequencies in a complex structure. Fatigue is usually not an important consideration in shock, unless a million or more stress cycles are involved. When less than a few thousand stress cycles are expected, fatigue stress concentrations can be ignored because they do not have great influence on how or when the structure will fail.

Many different methods have been used to specify shock motion or its effect. The most popular method is pulse shock. Pulse shock deals with acceleration or displacement in the form of well-known shapes such as square wave, half sine wave and various triangular (saw-tooth) waves. Pulse shocks are easy to work with because of their mathematical simplicity and convenience. However, pulse shocks do not represent the real world. The true shock is seldom a simple pulse. Nevertheless, simple pulses are often effective in revealing weak areas in many different types of structures.

Pulse shocks are often specified for electronics equipment, and many military specifications such as MIL-STD-810 which defines types of shock pulses and detailed methods for testing with these pulses. The half-sine shock pulse (200g peak @ 3ms) is the most common shock pulse used for testing almost any kind of commercial, industrial or military product.

The purpose of the simplified analysis is to try to simulate the response of the first mode where most of the damage normally occurs. Dynamic displacements, stresses and accelerations are usually maximum under these conditions. Therefore, it is necessary to analyse how single-mode PCB responds to shock pulse.

The dynamic model given in Figure 3.0 cannot be solved in a closed form for shock load, even if simplified by an excluding dynamic absorber. However, a numerical solution is possible in all cases. The simulation model from Figure 3.13 is reapplied with custom design of the half-sine shock sub-system in which it is required to generate a single shock pulse. In this design, a **Sine Wave** block would produce a pure single frequency excitation, π/0.003 rad/s at amplitude of 200 g for the entire simulation process, therefore a **step** block (step down 0.003 s) is designed in a manner to capture a first single pulse only. Figure 3.32 and 3.33 show the detail of this design.

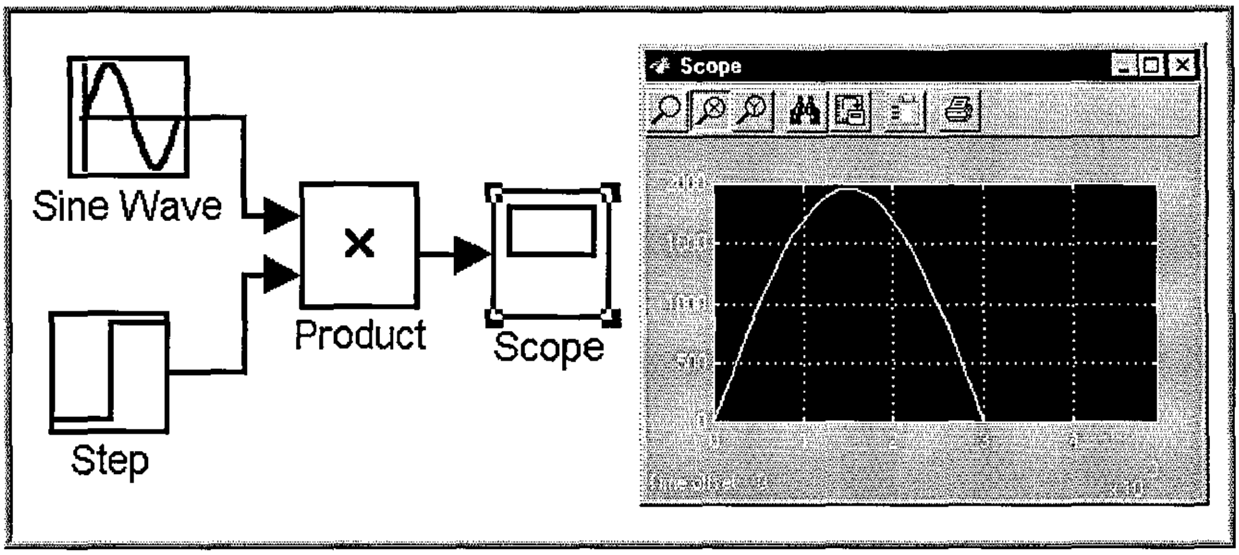

Figure 3.32. Custom design for half-sine shock

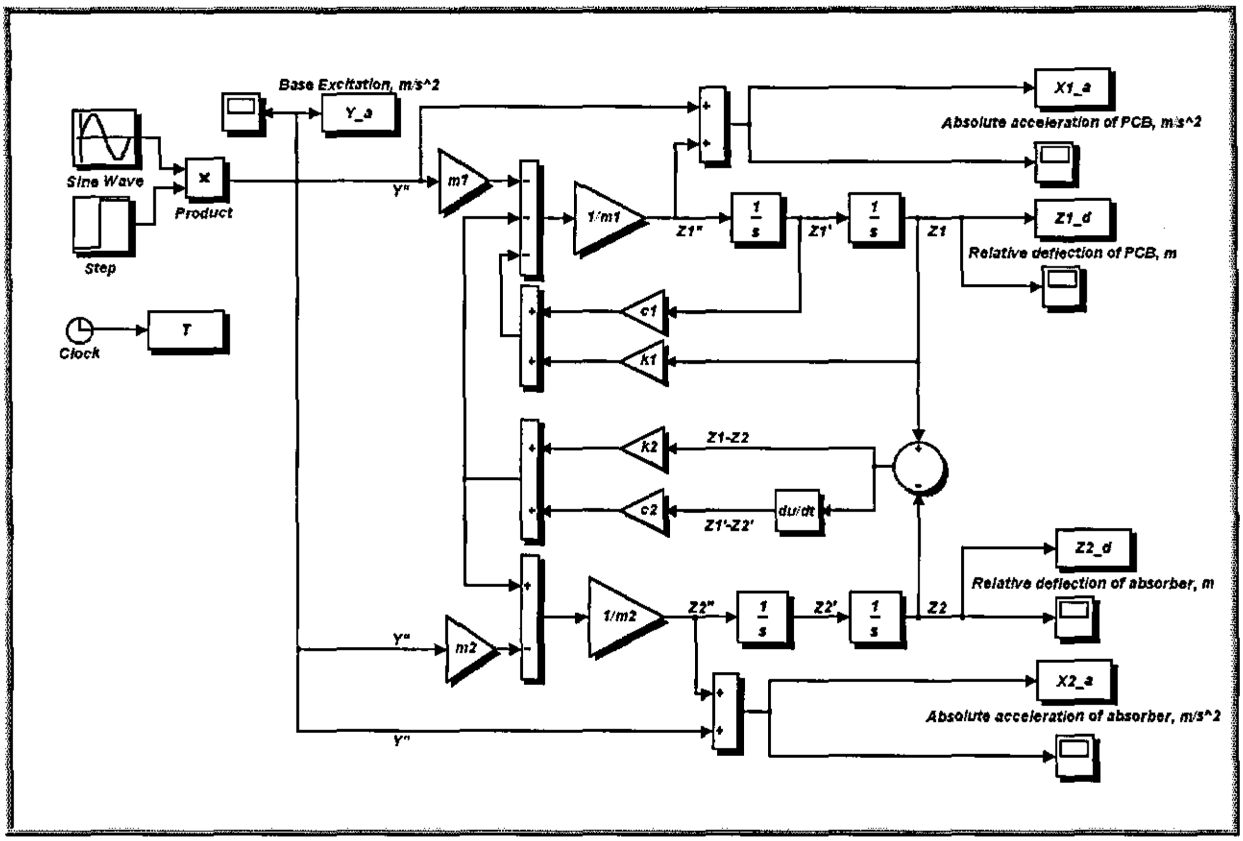
Base Excitation, m/s^2
Y_a
Sine Wave
Step
Product
Clock
T
Y"
m1
1/m1
Z1"
1/s
Z1'
1/s
Z1
X1_a
Absolute acceleration of PCB, m/s^2
Z1_d
Relative deflection of PCB, m
c1
k1
k2
Z1-Z2
c2
Z1'-Z2'
du/dt
Z2_d
Relative deflection of absorber, m
Y"
m2
1/m2
Z2"
1/s
Z2'
1/s
Z2
X2_a
Absolute acceleration of absorber, m/s^2
Y"

Figure 3.33. Simulink diagram for shock excitation

The numerical solution approach entails a laborious task to find a possible optimal dynamic absorber in which there are many possible combinations of natural frequency, loss factor and mass ratio. Also, type of shock and its duration are not always the same in nature, therefore finding an independent optimal parameter set for the dynamic absorber is excluded from this investigation. Section 3.2 and 3.3 presented a new vibration protection of PCB, a wide-band dynamic absorber was studied in both analytical and numerical for random and sine vibration. It shows that the chosen optimal tuned dynamic absorber is suitable for both applications. To complete this study, this section examines further the influence of dynamic absorber mounted on PCB subjected to a shock test with the primary concern of peak absolute acceleration, overall relative deflection and time settling. For this reason, the recommend half-sine shock pulse (200g peak @ 3ms) and the optimal dynamic absorber designed for random vibration are implemented in this numerical simulation:

$$\eta = 65\%, \ \frac{\Omega_{2opt}}{2\pi} = 106\text{Hz} \ \text{and} \ \zeta_{2opt} = 0.35,$$

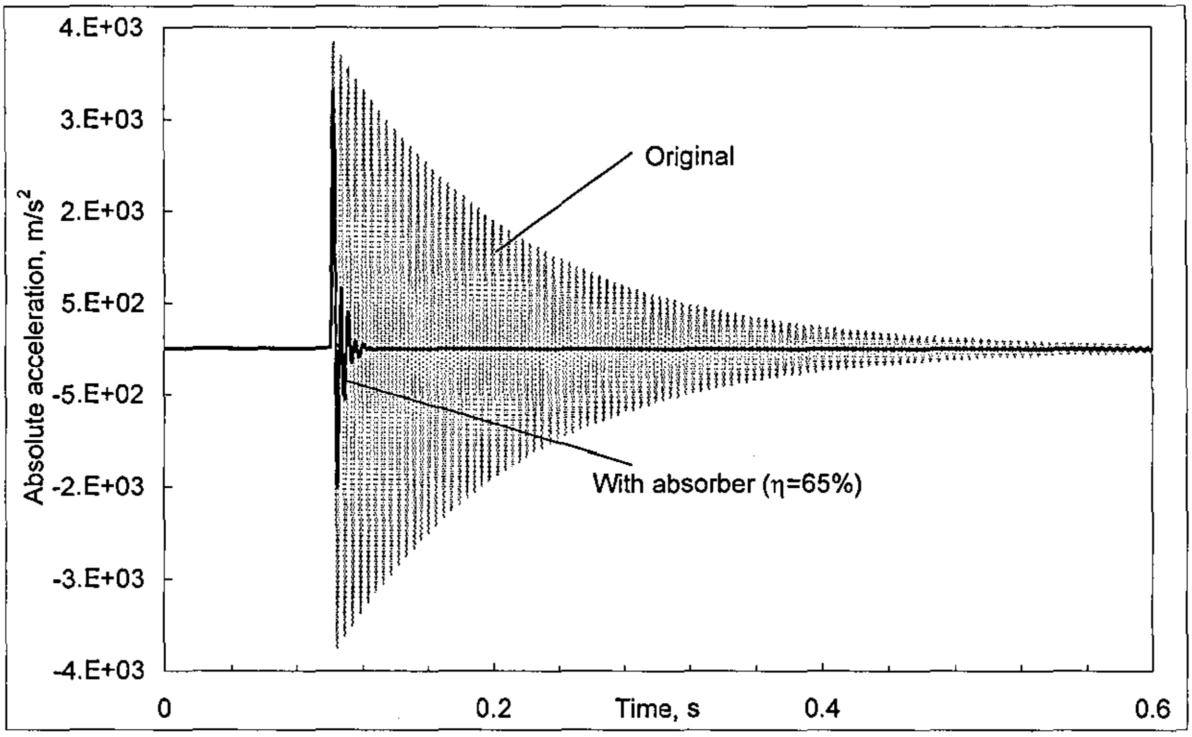

a) Absolute acceleration

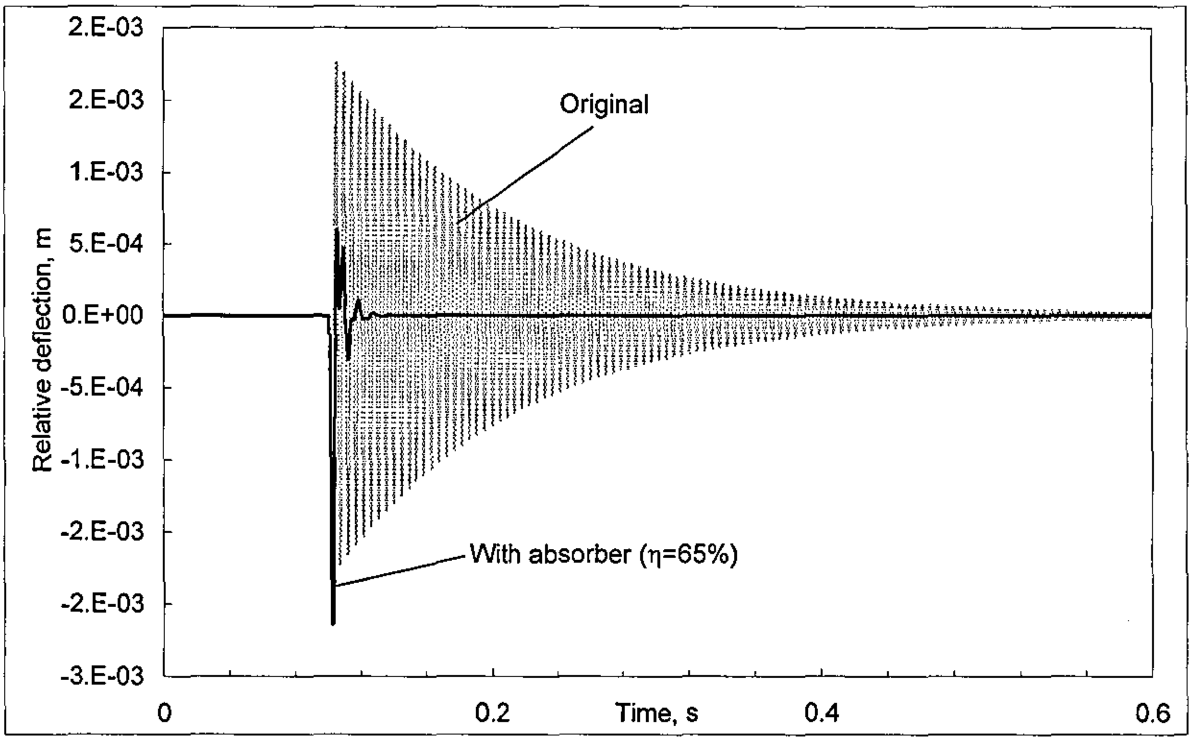

b) Relative deflection

Figure 3.34. Shock response of original and ruggedized PCB (η=65%)

Figure 3.34 shows the superimposed time history of PCB response with and without an optimal dynamic absorber. In terms of peak absolute acceleration, the ruggedized PCB response shows its reduction ratio of 18% compared to its original design whereas the peak relative deflection is deteriorated by 10%. However, in terms of overall response and vibration time settling, both absolute acceleration and relative deflection show a significant improvement. The evidence is clearly shown with appropriate labels in Figure 3.34.

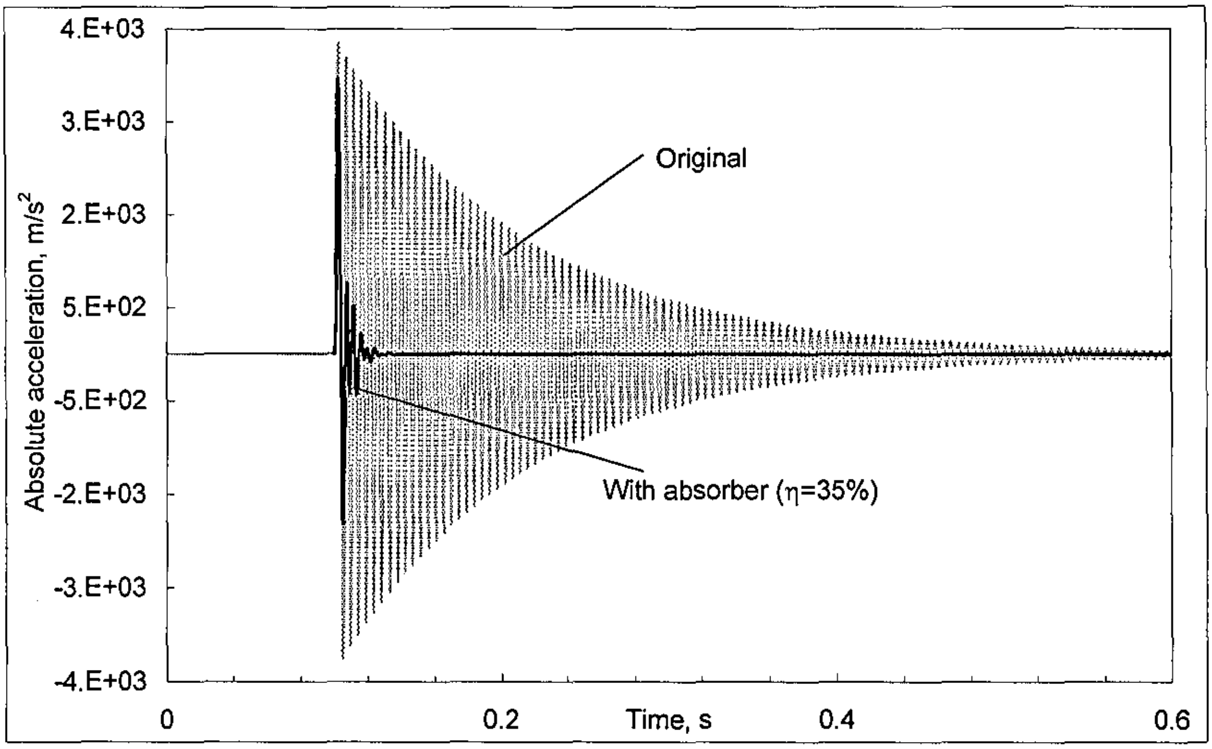

a) Absolute acceleration

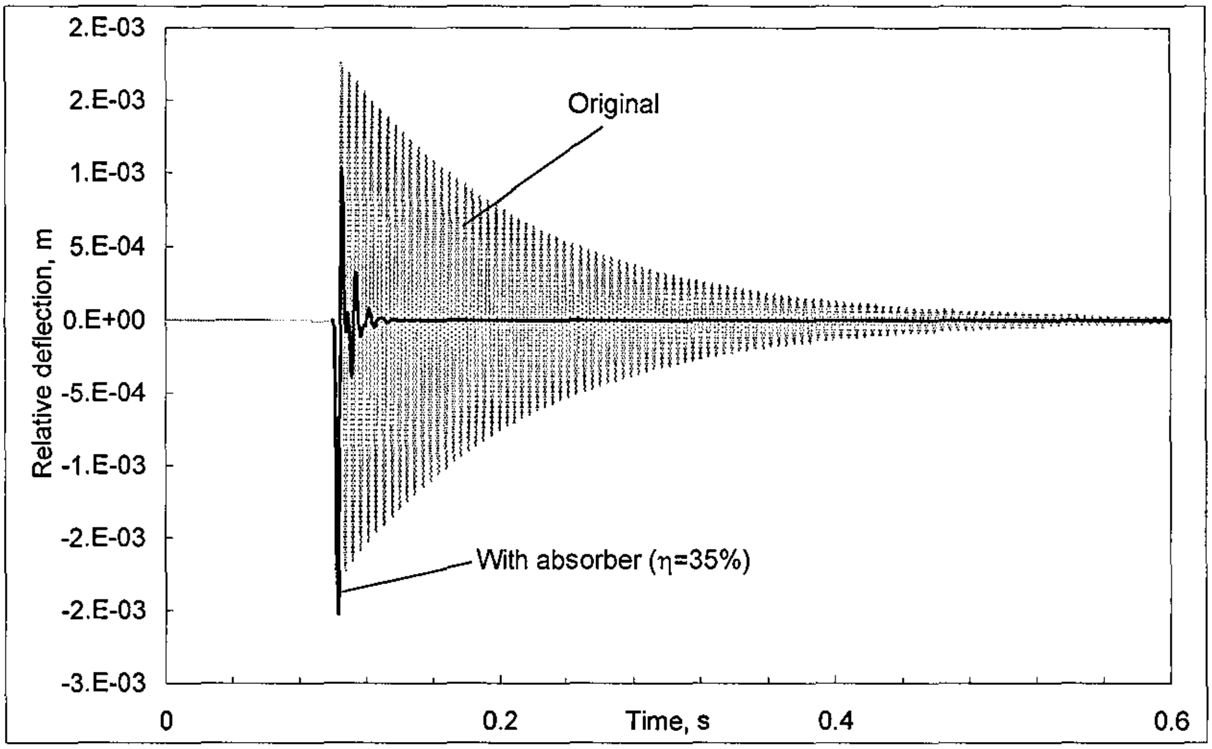

b) Relative deflection

Figure 3.35. Shock response of original and ruggedized PCB (η=35%)

Figure 3.35 shows the results of simulation for mass ratio of $\eta = 35\%$ (optimal dynamic absorber that designed for random vibration); the condition of improvement is almost the same from the case of mass ratio $\eta = 65\%$ with its corresponding optimal parameters.

The above simulation model is designed for the half-sine shock test for studying the effect of a dynamic absorber mounted on the PCB, such a design shows dynamic response in a qualitative result. Using this model, the optimal dynamic absorber can be found if a specific shock profile in nature is known. In this study, we show that the optimal dynamic absorber designed for random vibration is still capable of suppressing vibration of the PCB per MIL-STD shock test.

3.5 Concluding remarks

- A new optimisation novel has been developed for the single-mode PCB with dynamic absorber for random vibration. The optimal mass of dynamic absorber is 65% as compared with the effective mass, 90 gr of the PCB where its actual mass is 175.5 gr.
- The optimal dynamic absorber with 35% mass ratio is also provided a similar performance as compared to 65% mass ratio. However, this gives 46% mass ratio advantage.
- The optimal dynamic absorber chosen for random vibration is suitable for vibration suppression of PCB in sine vibration and shock, and it has a better performance than traditional one in term of relative deflection.

	Random vibration		Swept-sine vibration
	Overall absolute acceleration	Overall relative deflection	Peak relative deletion
Original response	51.10 g RMS	271.5 μm RMS	4617 μm
With traditional optimal absorber	10.1 g RMS	69.5 μm RMS	281 μm
With novel optimal absorber	10. 1 g RMS	65.9 μm RMS	190 μm
Design improvement	0%	5%	32%

Table 3.1. Comparison results in the case of novel and traditional designs

- Sensitivity analysis was carried out corresponding to its optimal values. It shows that a small variation of dynamic absorber has little effect on optimal dynamic absorber design
- The designed MS®Excel worksheet and its companion Solver allow instant access to find optimal parameters set of the dynamic absorber for both random and swept-sine vibration without being too time-consuming and fully supported from the numerical simulation. For shock loading, the analytical study was substituted by a numerical solution due to complexity time response of the combined system.

- The method of fatigue analysis using a simple cycles technique was numerically studied which indicated that the endurance of the ruggedized PCB was improved compared to its conventional approach, say overall response
- The Simulink model allowed an accurate prediction of the dynamic behaviour of the original and ruggedized PCB under extreme conditions. As in any simulation, this model provides definite advantages such as predicting fatigue failure of the PCB during the early design stage, repeatable quick and inexpensive numerical testing before carry out actual test.
- From the unique results of the numerical solution, this indicates that Matlab/Simulink can be implemented to study nonlinear vibration control of the PCB as mentioned in Chapter1.

Chapter 4

4.0 Full-mode model of PCB with dynamic absorber attached

From experiment, the frequency response function of the actual PCB indicates the presence of higher modes, although it was approximated as the SDOF system mainly for mathematical simplicity. This type of analysis yields fast results, but accuracy is reduced, therefore the above optimised dynamic absorber might not be optimal in a very general sense. The accuracy of analysis may be improved considerably by using the full-mode model of PCB.

This section deals with the new modal theory developed for the full-mode approximation. The methodology of the full-mode approximation is based on FRF of the primary system (PCB) obtained experimentally as well as the analytical approximation of the secondary system (dynamic absorber). This novel theory has coalesced of both experimentally and analytically obtained information, which makes it more accurate. Additionally, using this technique to analyse the dynamic response of the plate-wise structure like the PCB with multiple resonant frequencies, one must keep in mind these factors:

- The influence of optimal dynamic absorber would not only suppress the resonant frequency where it is tuned but almost all neighbouring resonances of the full-mode model of PCB would also be influenced as long as the dynamic absorber was not mounted in the node point
- The process of designing an optimal dynamic absorber is directly involved with experimental FRFs in which the modal parameters of the PCB are no longer required, therefore the methods of determining effective mass and parameter estimation may not be needed
- This type of analysis not only allows the study of the influence of dynamic absorbers where they are attached but it also allows the study of the dynamic response of the entire PCB if necessary
- Traditional methods have failed to predict the actual FRFs of the PCB therefore the degree of accuracy in designing an optimal dynamic absorber is entirely relies on the measured data and linearity of the original PCB.

Designing an optimal dynamic absorber at the point where it is located may not give optimal response for different areas on the PCB. Therefore in this approach, we still accommodate a single dynamic absorber in which the major work would be carried out in the area where the relative deflection is assumed to be maximum. Similar to that single-mode approximation, the optimal dynamic absorber design is independently investigated for random, swept-sine and shock application. Additionally, we attempt to find optimal performance for different observation points on the PCB.

4.1 Mathematical model

The primary limitation of the single-mode analysis is its single point measurement whereas all point measurements on the plate-wise structure of the PCB can be made which lead to unfair agreement in designing an optimal response. To narrow down the differences between them, in the improved approach, the dynamic properties of the original PCB are given through the universal absolute transfer function, $T_a(\gamma_o,\lambda_o,s)$, and local receptance, $H(\gamma_o,\lambda_o,s)$, in the point of observation and in the point (γ_o,λ_o) where the dynamic absorber should be attached, respectively. The corresponding frequency response functions are as follows; $T_a(\gamma_o,\lambda_o,j\omega)$ is the complex universal absolute transmissibility and $H(\gamma_o,\lambda_o,j\omega)$ is the local receptance of the original PCB. These data may be directly obtained from the experiment as shown in Chapter 2.

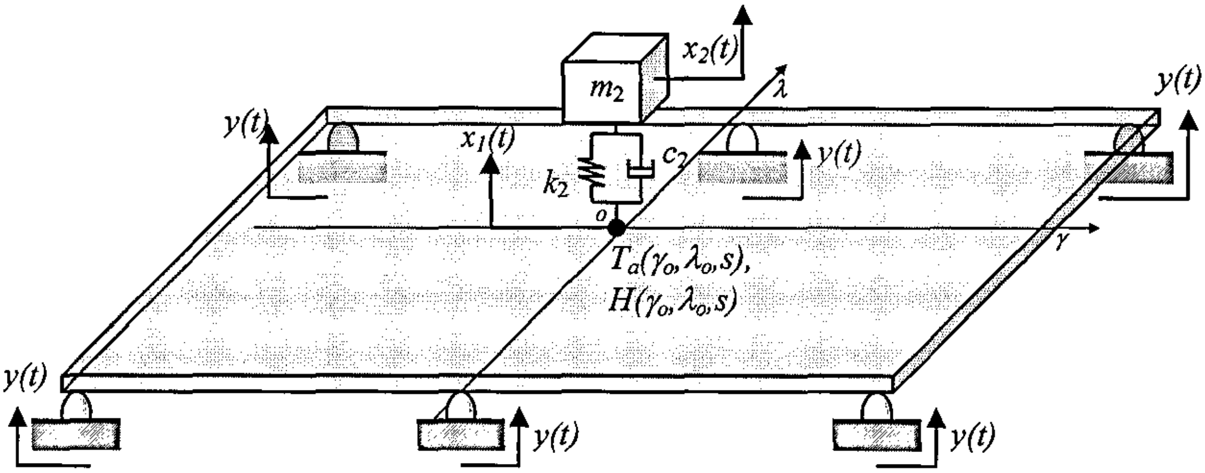

Figure 4.0. Dynamic model of generic PCB and with attached dynamic absorber

Figure 4.0 shows the schematic model of such a combined system. The equation of motion for the primary system, using operator method and superposition principle takes the form [40]:

$$X_1(\gamma_o,\lambda_o,s) = T_a(\gamma_o,\lambda_o,s)Y(s) - H(\gamma_o,\lambda_o,s)(c_2 s + k_2)(X_1(\gamma_o,\lambda_o,s) - X_2(s)) \tag{4.0}$$

Equation 4.0 reflects the fact that the motion of the primary system is due to the base excitation (first term in the right-hand side of the equation) and due to the force of reaction of the dynamic absorber (second add-end in the right-hand side of the equation).

For the secondary system, we have

$$X_2(s) = \frac{c_2 s + k_2}{m_2 s^2 + c_2 s + k_2} X_1(\gamma_o,\lambda_o,s)\,. \tag{4.1}$$

Equation (4.1) reflects the fact that the motion of dynamic absorber is due to the motion of its attachment. Substituting Equation (4.1) into (4.0) yields an absolute transfer function of the combined system:

$$\tilde{T}_a(\gamma,\lambda,s)=\frac{X_1(\gamma_o,\lambda_o,s)}{Y(s)}=\frac{T_a(\gamma_o,\lambda_o,s)}{1+\dfrac{m_2 s^2 H(\gamma_o,\lambda_o,s)(c_2 s+k_2)}{m_2 s^2+c_2 s+k_2}}. \tag{4.2}$$

The formal substitution, $s=j\omega$, yields universal absolute transmissibility of the combined system:

$$\tilde{T}_a(\gamma_o,\lambda_o,j\omega)=\frac{T_a(\gamma_o,\lambda_o,j\omega)}{1-\dfrac{m_2\omega^2(c_2 j\omega+k_2)}{-m_2\omega^2+c_2 j\omega+k_2}H(\gamma_o,\lambda_o,j\omega)}. \tag{4.3}$$

The corresponding universal relative transmissibility can be calculated using Equation 3.5.

From Equation 4.3, at the antiresonant frequency of the original system, as $H(\gamma_o,\lambda_o,j\omega)\to 0$, $\tilde{T}_a(\gamma_o,\lambda_o,j\omega)\to T_a(\gamma_o,\lambda_o,j\omega)$. This means that for any value of mass, damping and stiffness of the dynamic absorber, the antiresonant notches of original system would not be altered.

At the same time, the damped dynamic absorber suppresses the resonant peaks of the even undamped original system if it is not mounted in the node point. At resonant frequencies of the original undamped system, $\omega=\omega_{res}$, the transmissibility becomes infinite, $T_a(\gamma_o,\lambda_o,j\omega)\big|_{\omega=\omega_{res}}\to\infty$. From the general theory of linear systems, receptance and absolute transmissibility show the same resonant frequencies. Hence, at resonant frequencies the receptance also becomes infinite, $H(\gamma_o,\lambda_o,j\omega)\big|_{\omega=\omega_{res}}\to\infty$. Since the term $\dfrac{m_2\omega^2(c_2 j\omega+k_2)}{-m_2\omega^2+c_2 j\omega+k_2}$ in Equation 4.3, which reflects the presence of the damped dynamic absorber and cannot be zero or infinity, the ratio in Equation 4.3 and, therefore, the transmissibility of the combined system is finite.

4.2 Random vibration

4.2.1 Designing MS®Excel worksheet for minimising overall relative deflection

This new design method is to combine the analytical approximation of dynamic absorber and the experimentally measured FRFs of the original PCB. A design for optimal performance using the conventional method [13] might not be possible, since the modal parameters of the original PCB are "hidden" in this design. However, MS®Excel is capable of handling imported complex numbers, therefore the quest for optimal dynamic absorber is possible for the full-mode model PCB.

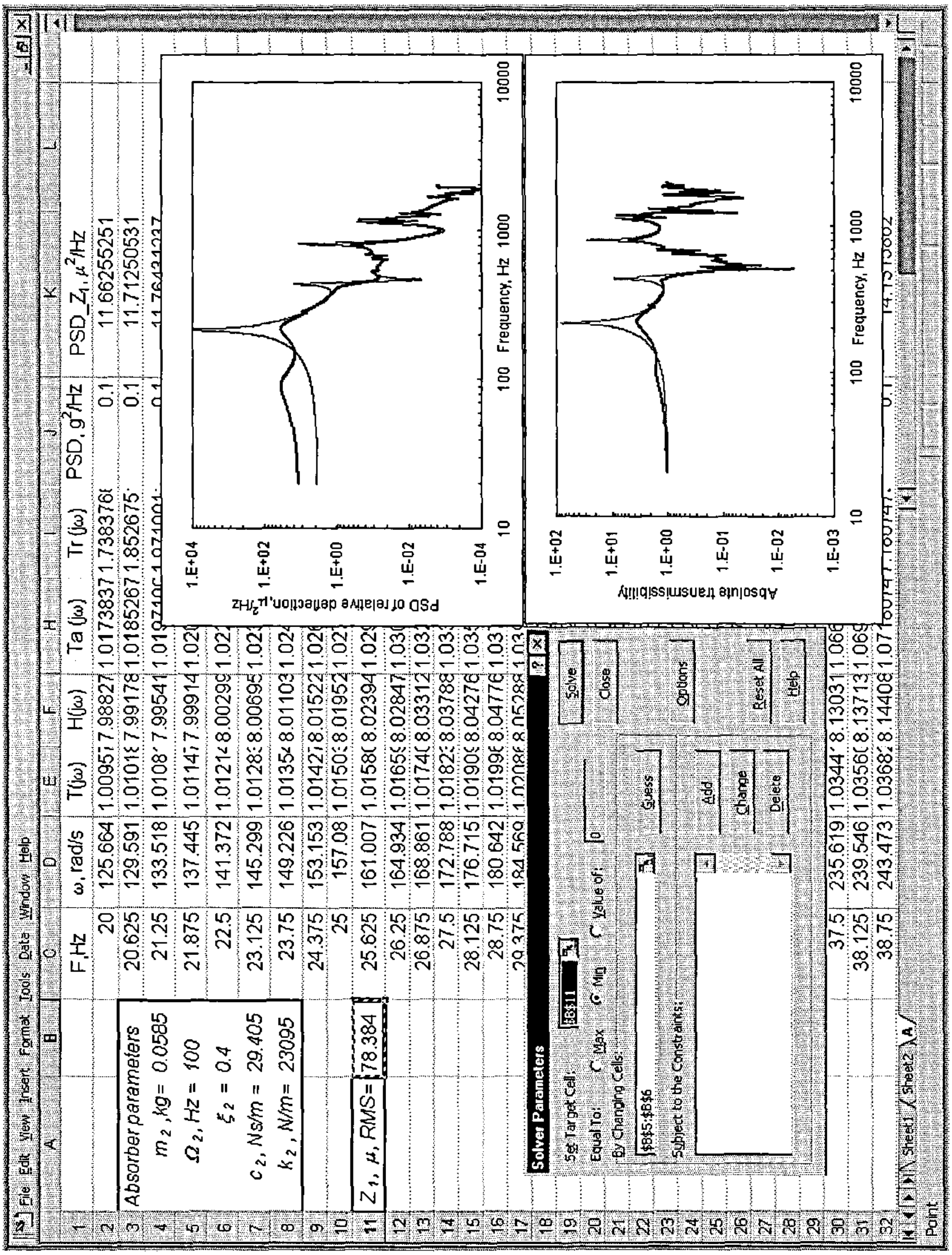
File Edit View Insert Format Tools Data Window Help
PSD of relative deflection, μ^2/Hz
1.E+04
1.E+02
1.E+00
1.E-02
1.E-04
10
100
Frequency, Hz
1000
10000
Absolute transmissibility
1.E+02
1.E+01
1.E+00
1.E-01
1.E-02
1.E-03
Solver Parameters
Solve
Close
Guess
Options
Add
Change
Delete
Reset All
Help
Sheet1
Sheet2
A
Point

Absorber parameters
m_2, kg= 0.0585
Ω_2, Hz = 100
ξ_2 = 0.4
c_2, Ns/m = 29.405
k_2, N/m= 23095

Z_1, μ, RMS= 78.384

Set Target Cell: $B$11
Equal To: ○ Max ● Min ○ Value of: 0
By Changing Cells: $B$5:$B$6
Subject to the Constraints:

	F,Hz	ω, rad/s	T(jω)	H(jω)	Ta (jω)	Tr (jω)	PSD, g^2/Hz	PSD_Z_1, μ^2/Hz
2	20	125.664	1.00957	7.98827	1.0173837	1.738376	0.1	11.66255251
3	20.625	129.591	1.01018	7.99178	1.0185267	1.852675	0.1	11.71250531
4	21.25	133.518	1.0108	7.99541				
5	21.875	137.445	1.01147	7.99914	1.02			
6	22.5	141.372	1.01214	8.00299	1.02			
7	23.125	145.299	1.01283	8.00695	1.02			
8	23.75	149.226	1.01354	8.01103	1.02			
9	24.375	153.153	1.01427	8.01522	1.02			
10	25	157.08	1.01503	8.01952	1.02			
11	25.625	161.007	1.01580	8.02394	1.02			
12	26.25	164.934	1.01659	8.02847	1.03			
13	26.875	168.861	1.01740	8.03312	1.03			
14	27.5	172.788	1.01823	8.03788	1.03			
15	28.125	176.715	1.01909	8.04276	1.03			
16	28.75	180.642	1.01996	8.04776	1.03			
17	29.375	184.569	1.02086	8.05288	1.03			
30	37.5	235.619	1.0344	8.13031	1.06			
31	38.125	239.546	1.03560	8.13713	1.06			
32	38.75	243.473	1.03682	8.14408	1.07		0.1	

Figure 4.1. Spreadsheet showing Solver for calculation and optimising dynamic absorber

The aim of this optimisation is to see how much the difference in optimal parameters design of the dynamic absorber and its influence on the overall performance compared to its single-mode model PCB design is. Therefore the optimisation procedure has to be carried out in a similar manner as mentioned in Section 3.2. Figure 4.1 shows the snapshot of appropriate MS®Excel worksheet. The calculation is straightforward, all the data captured from experiment are directly exported into spreadsheet in terms of complex numbers (absolute transmissibility in column E and receptance in column F) against frequency (column C in Hz and column D in rad/s). Once the combined universal transmissibilities, column H and column I are calculated using Equation 4.3 and 3.5 then a few necessary columns are added to compute the PSD response of the PCB. The design of this spreadsheet is less complicated than the single-mode approximation because there are fewer variables involved. However, there is a critical factor when considering this design technique, that is frequency resolution. Since the combined absolute transmissibility contains two sets of experimental data of the original PCB, therefore it is very important to verify the frequency resolution between them prior to experimental measurements or building a spreadsheet.

Since the information on the inertia properties of the PCB is "embedded" in the local receptance, the appropriate worksheet contains the value for the dynamic absorber's mass instead of the mass ratio as above. However, the effective mass of PCB is still assumed to be 90 gr for comparison purposes only whereas the actual mass of the PCB is 175.5 gr.

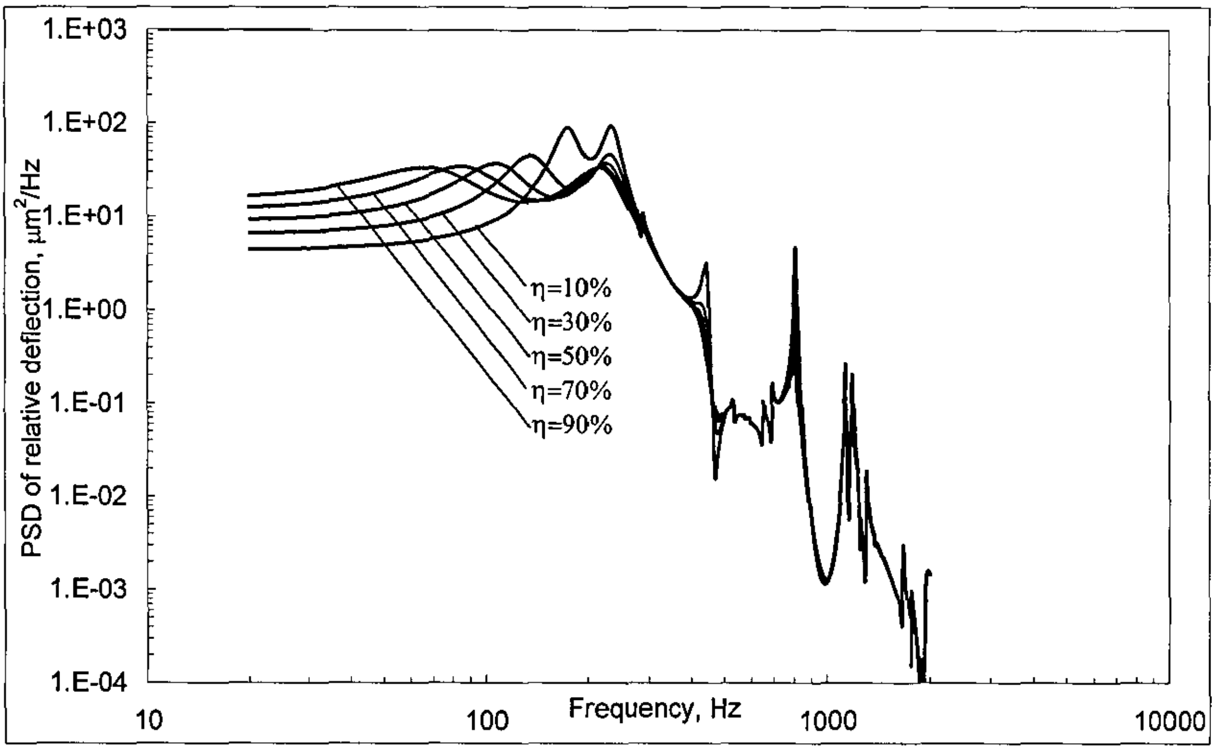

a) PSD response

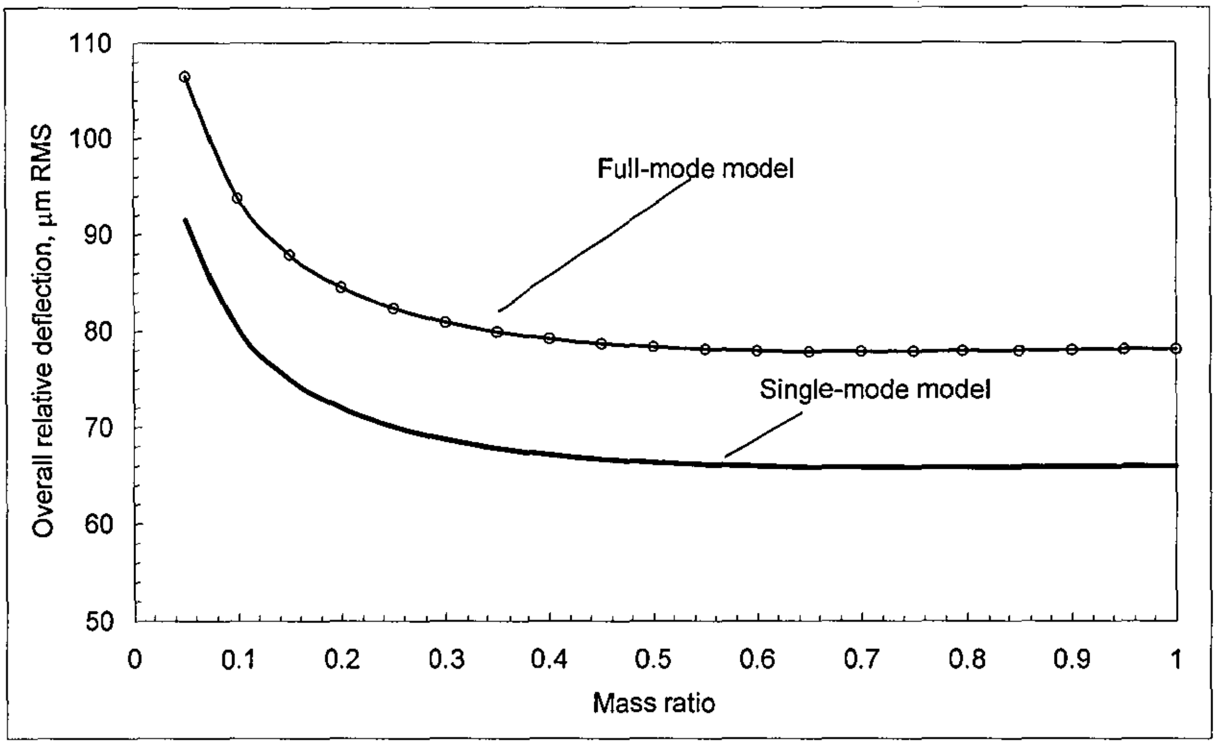

b) Overall response

Figure 4.2. Dynamic response of ruggedized PCB with different mass ratios

Figure 4.2a shows the superimposed PSD of relative deflection at different mass ratios and optimised dynamic absorber. The peak value of PSD of relative deflection is reduced significantly as mass ratio is increased. However, the peak value itself is not important for random vibration application, since the area under the curve (overall response) is critical. Figure 4.2b highlights the results of optimisation for full-mode model compared with that carried out for the single-mode approximation of PCB.

As a result of the optimisation procedure, the optimal mass is 59 gr. The value produces a mass ratio close to 65% (relative to 90 gr), which yields the lowest overall relative deflection 77.8 µm RMS. However, there is a significant difference of optimal overall deflection as compared to a single-mode approximation due to the contribution of higher frequency components. In this case, the overall deflection of the original full-mode model is 312 µm RMS. This yields a reduction ratio of 4.0, which is only slightly lower when compared to single-mode approximation.

From Figure 4.2 it is clear that the accuracy of the mass factor has relatively little effect on the response of the system. With a mass factor ranging from 35% to 100%, the response only varies by 3 µm RMS. This means that the dynamic absorber's mass does not have to be exactly optimal to still achieve the desired result.

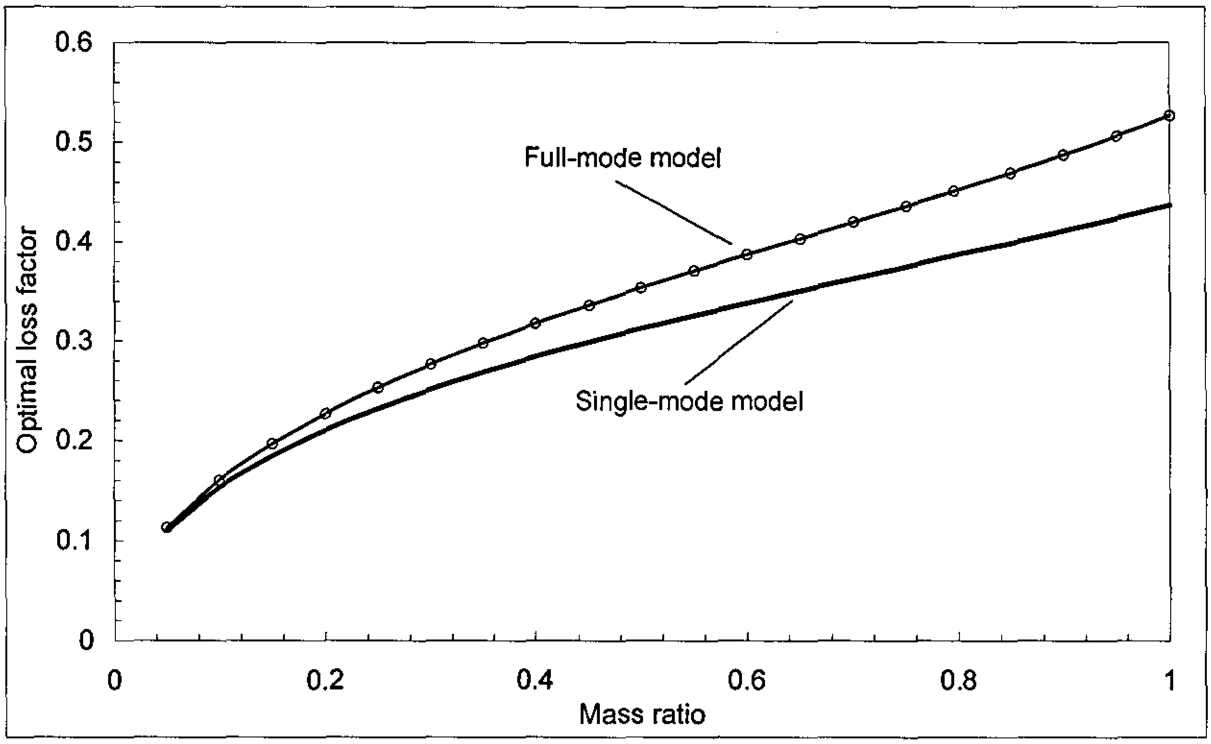

a) Optimal loss factor

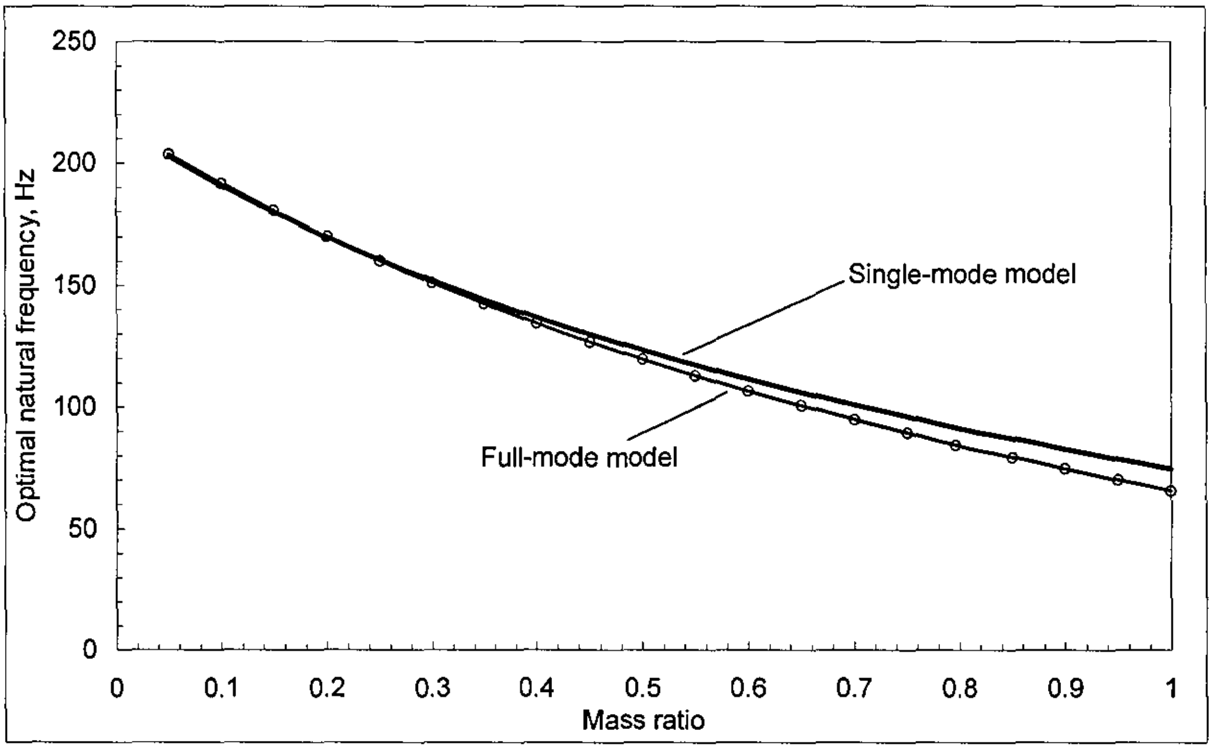

b) Optimal natural frequency

Figure 4.3. Optimal parameters of dynamic absorber at different mass ratios

Figure 4.3 shows the dependence of the optimal loss factor and natural frequency of the dynamic absorber at different mass ratios for the full-mode model compared to that single-mode approximation of PCB, the difference is small. With reference to this figure, two dynamic absorbers with their optimal parameters are chosen:

- At mass ratio of 65%, the optimal natural frequency and optimal loss factor are found to be 100 Hz and 0.4, respectively;

- At mass ratio of 35%, the optimal natural frequency and optimal loss factor are found to be 144 Hz and 0.29, respectively.

The above mass ratios are calculated with reference to the effective mass of the PCB (90 gr). Based on the actual mass of the PCB (175.5 gr) both dynamic absorbers would produce an actual mass ratio of 18% and 30%, respectively. Again, these are still miniature vibration control devices compared to all means of vibration protections of PCB. If they were compact enough then only a small amount of room on the PCB is required to accommodate them.

4.2.2 Sensitivity analysis

The sensitivity analysis is carried out in the same manner as mentioned in Section 3.2.2. Obviously, the optimal loss factor, 0.4 and optimal mass ratio, 65% are fixed as is the mass ratio, 35% with its optimal loss factor 0.29 whilst the natural frequency is varied in the range from 50 to 200 Hz. The characteristics of the behaviour are shown in Figure 4.4a and 4.4b, the sensitivity analysis of single-mode approximation is superimposed for reference.

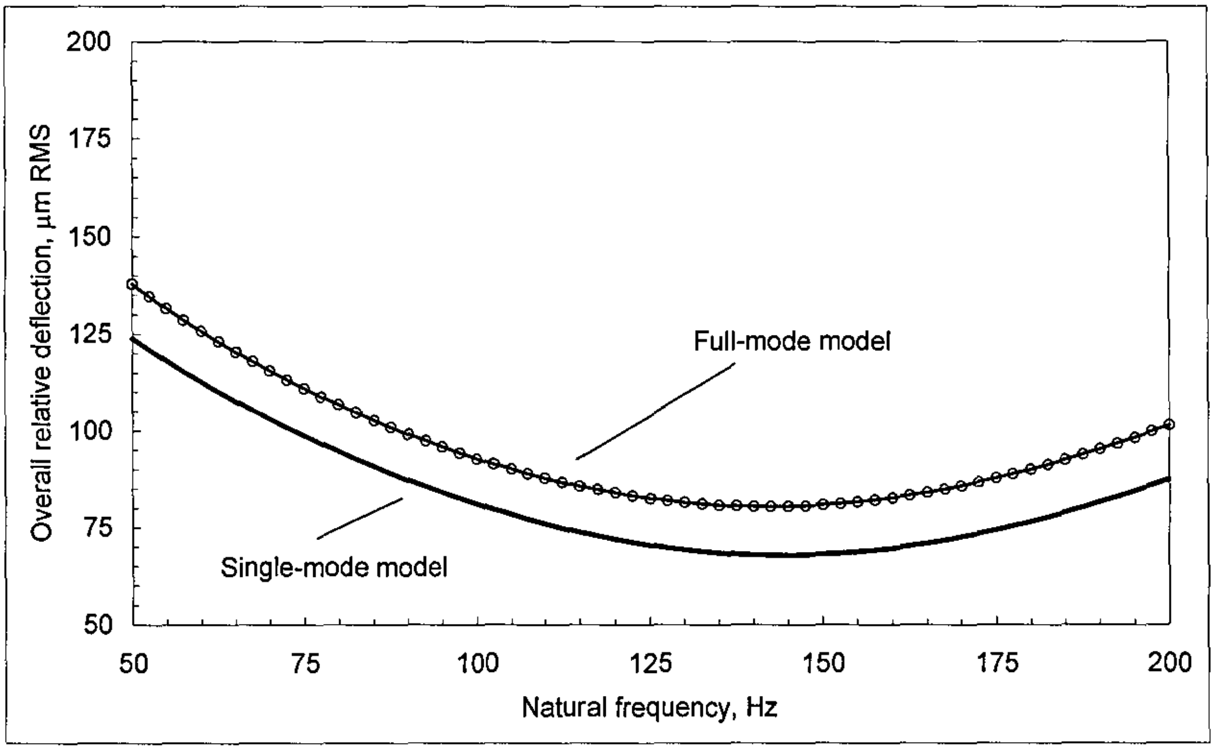

a) At 35% mass ratio

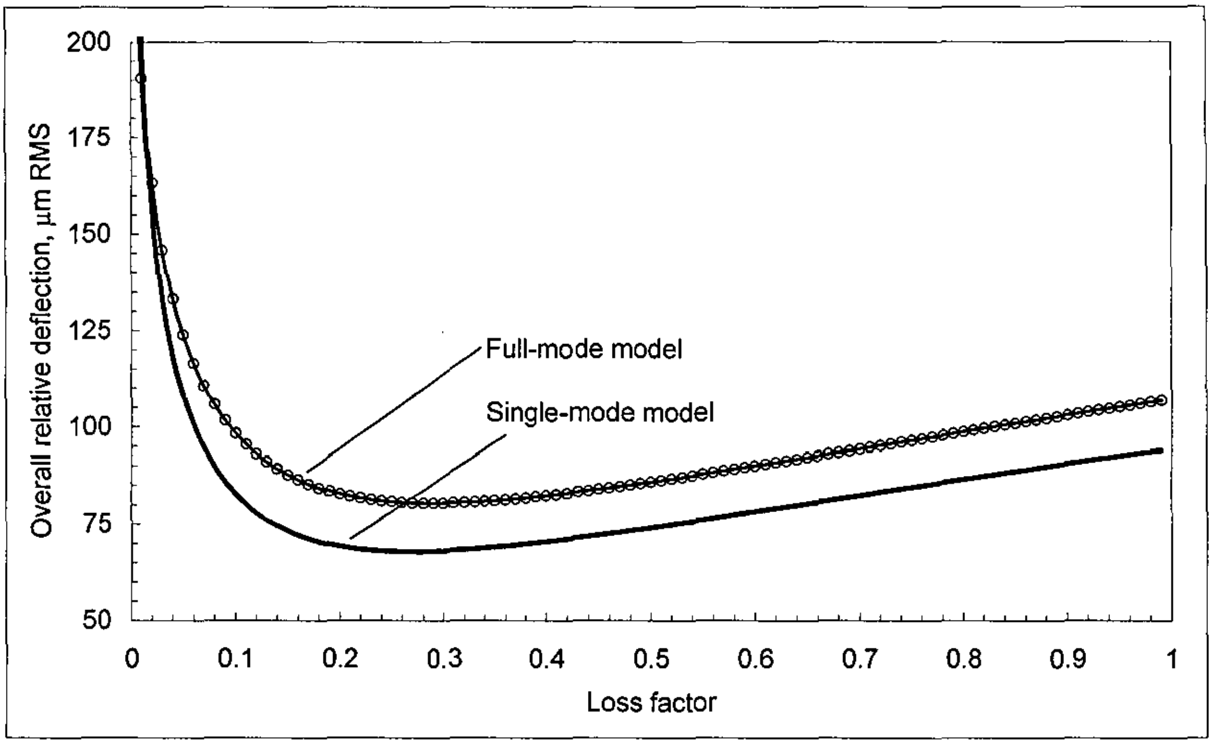

b) At 35% mass ratio

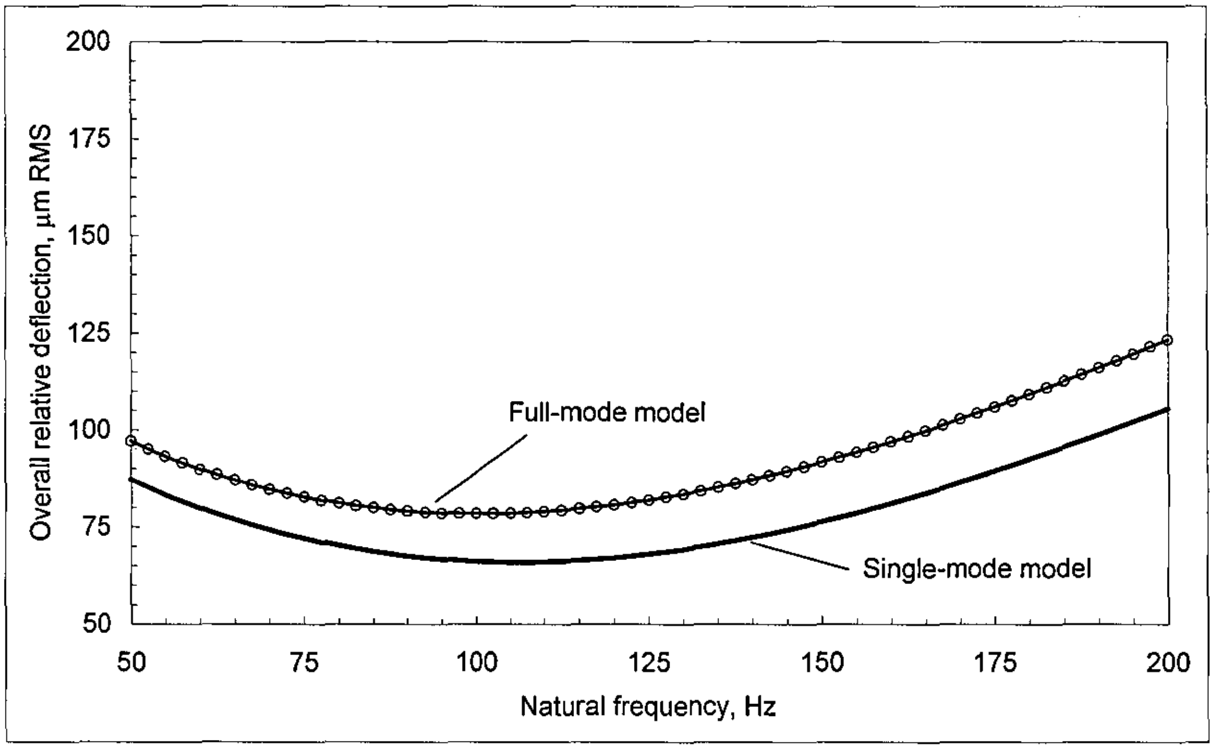

c) At 65% mass ratio

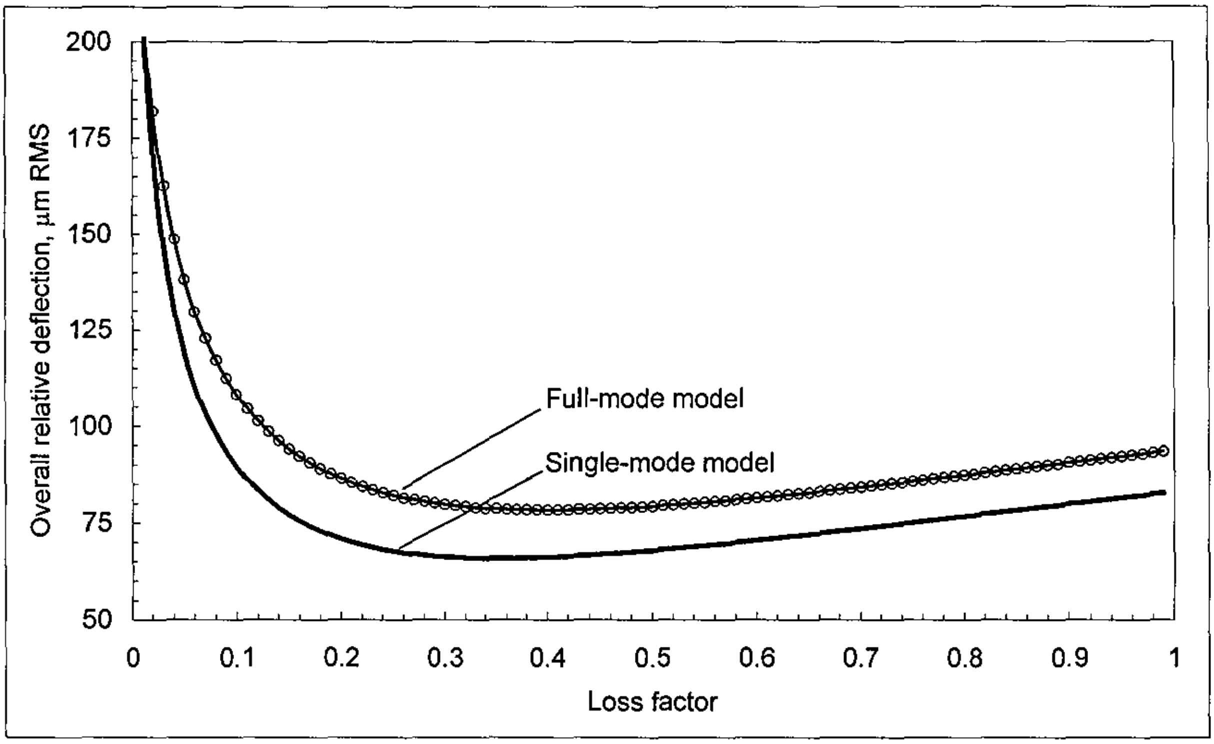

d) At 65% mass ratio

Figure 4.4. Sensitivity analysis

Similarly, Figure 4.4c and 4.4d show the variation of overall response when the loss factor is varied from 0 to 1 for the mass ratio of 35% and 65% with their corresponding optimal natural frequency, respectively also sensitivity analysis of single-mode is shown for reference.

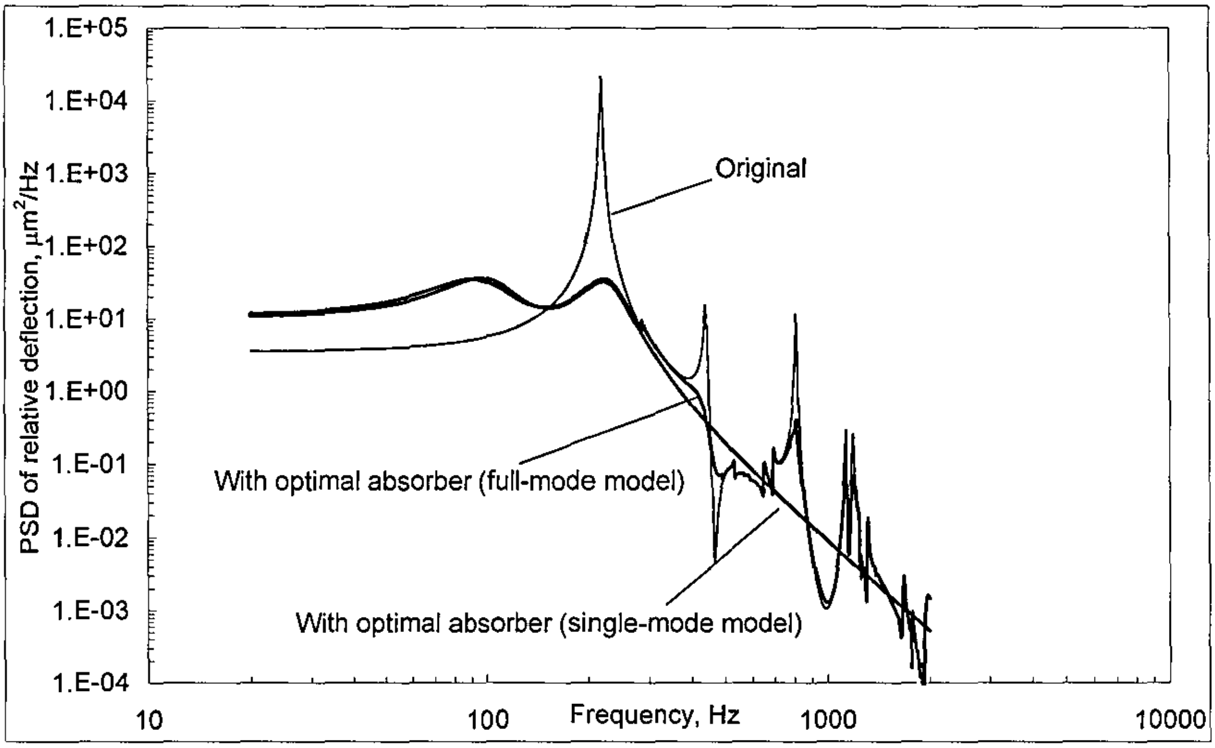

Figure 4.5. Dynamic response of original and ruggedized PCB

Figure 4.5 shows the superimposed dynamic responses of the PCB with dynamic ruggedizer optimised in a single-mode approximation (overall deflection 65.8 μm RMS) and full-mode model (overall deflection 77.8 μm RMS). The dynamic response of the original PCB is also shown for reference. From Figure 4.5, the influence of the dynamic absorber is that almost all resonances of the original PCB are suppressed significantly, while the antiresonant notches remain practically unaffected, as theoretically predicted above.

Figure 4.6 summaries the result of findings in both single-mode and full-mode approximation using the traditional approach and the novel ones. Since the modal parameters of primary system is not presented, for the full-mode approximation using the traditional approach where the dynamic properties of the absorber is calculated with to reference (and $m_1 = 90$ gr and ${}^{\Omega_1}\!/_{2\pi} = 216.25$ Hz) as they were used in the single mode approximation. As can be seen again, the novel approaches produce a better result than the traditional one at a higher value of mass ratio with respect to the case of single-mode and full-mode model approximation. It should be noted that in this figure the curve labelled as **Full-mode model (traditional optimal design),** at the value of mass ratio, 45% it also produces a lowest value of relative deflection 83 μm RMS which is about 5μm RMS higher than that of the novel one (77.8 μm RMS) with respect to its optimal mass ratio, 65%, see the curve labelled as **Full-mode model (optimal design)** in which the novel approach give an improvement by 5.4% compared to the traditional one.

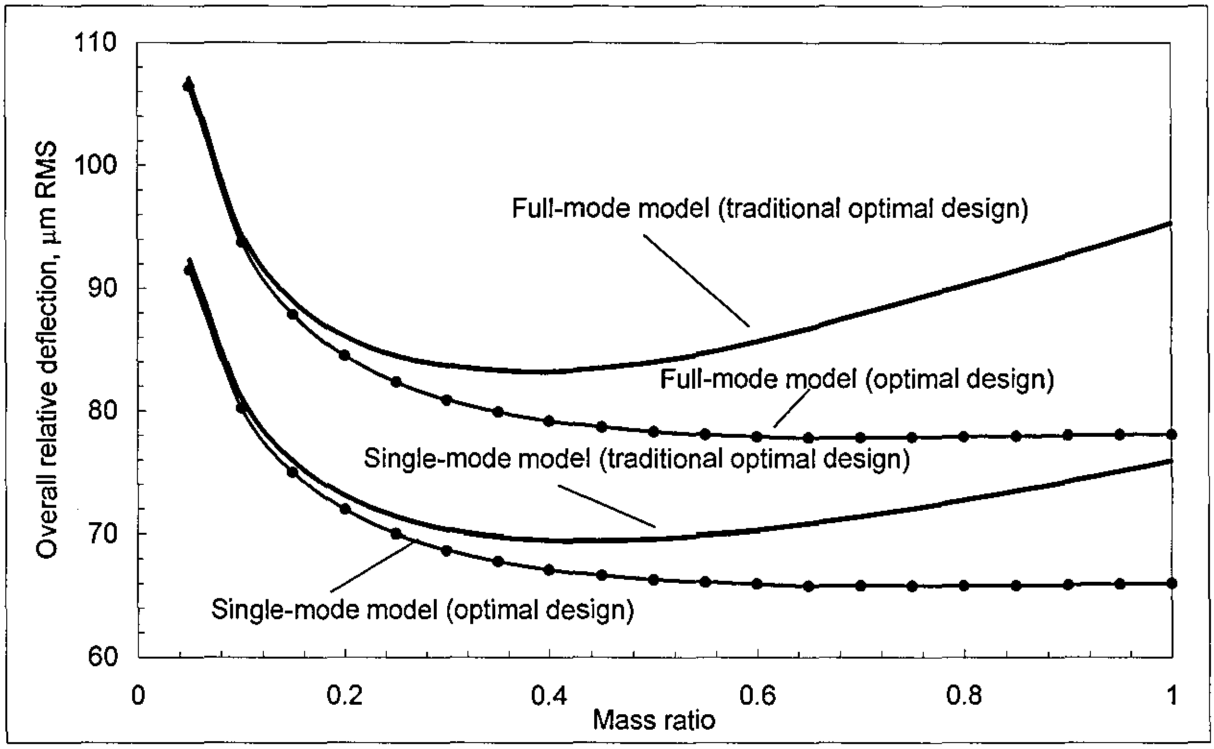

Figure 4.6. Comparison of overall relative deflection in the case of traditional and novel design

Keeping in mind the aim of this work is to design an optimal dynamic absorber to suppress the over relative deflection of the PCB. In Chapter 2, the work was focused mainly on the comparison of overall relative deflection under random vibration between the novel technique and the traditional one in the single-mode approximation, as shown, the traditional optimal design provides the same performance than novel one in terms of overall absolute acceleration where the dynamic absorbers were chosen to optimise the overall relative deflection. However, the studied mathematical model was insufficient to reflect on the true response of the PCB in term of absolution acceleration due to the presence of higher mode, therefore, it was unfair at that stage to compare the performance between the traditional and novel design. Since the mathematical full-mode model of PCB with attached dynamic absorber is presented in this study, it is an opportunity to justify the performance between them further.

For "fair play", the parameters of dynamic absorber design for the optimal overall relative deflection of the full-mode model PCB are considered. As a result, Figure 4.7 compares the overall absolute acceleration on the value of mass ratio between the traditional and novel design. At a lower value mass ratio the performance between them are almost the same. The novel design shows its superior performance as the mass ratio increased and no optimal mass ratio is shown for both cases.

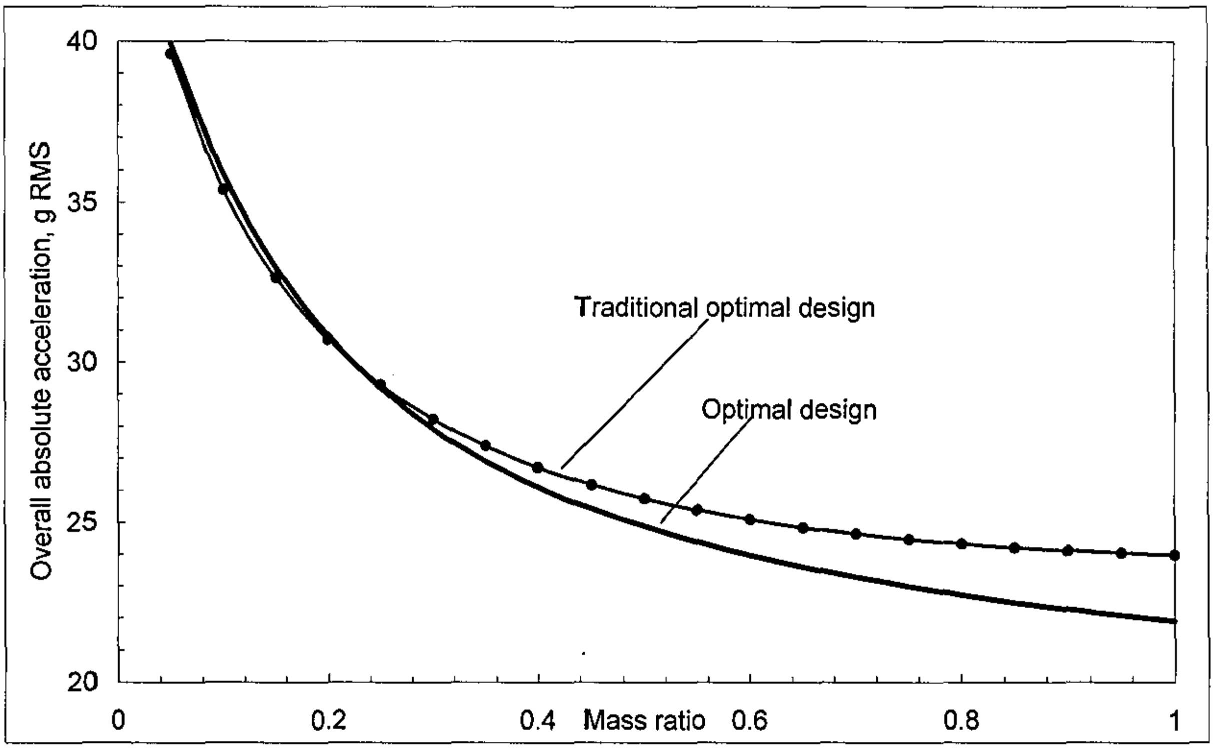

Figure 4.7. Comparison of overall absolute acceleration in the case of traditional and novel design

To justify further, Figure 4.8 shows the superimposed power PSD of absolute acceleration of the original and modified PCB with the influence between optimal dynamic absorbers (see the curve with appropriate label) whereas they are chosen from the case of designing the optimal overall relative deflection i.e.

traditional optimal dynamic absorber; $\eta_{opt} = 45\%$, $\Omega_{2opt}/2\pi = 149$ Hz and $\xi_{2opt} = 0.235$

novel optimal dynamic absorber; $\eta_{opt} = 65\%$, $\Omega_{2opt}/2\pi = 106$ and $\xi_{2opt} = 0.4$

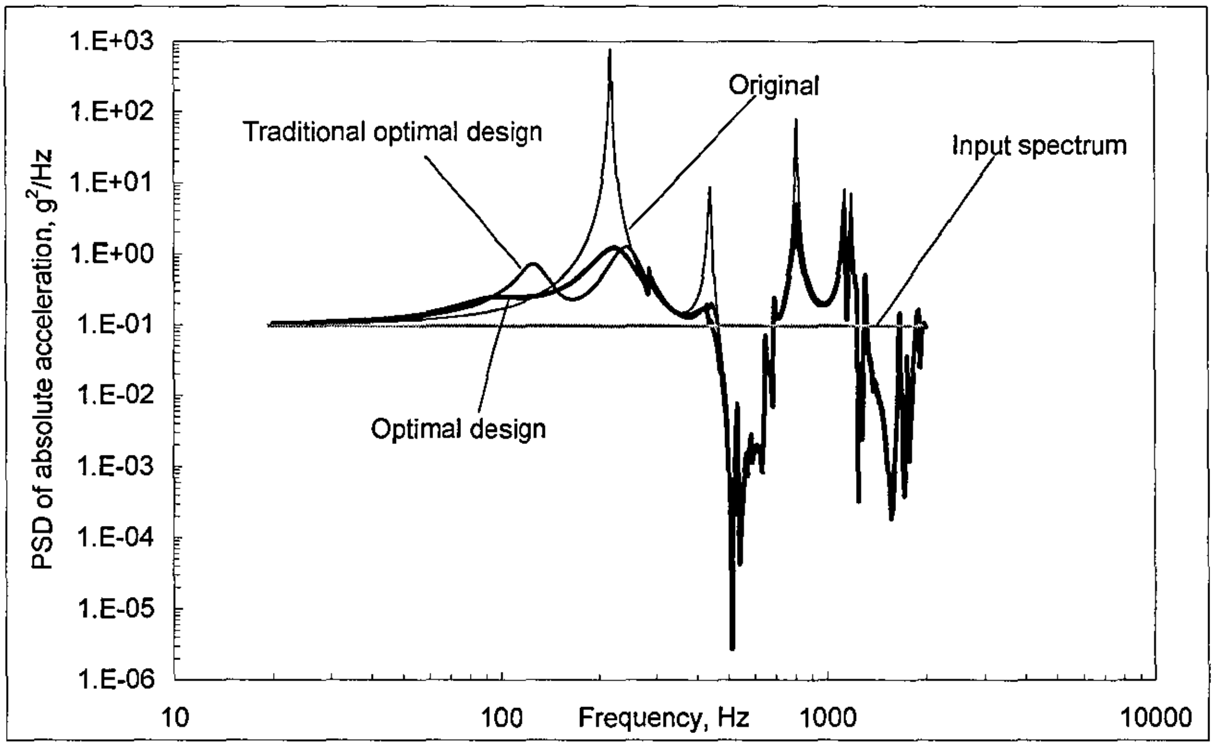

Figure 4.8. Comparison of PSD of absolute acceleration in the case of traditional and novel design

In term of reduction ratio as compared to the original PCB response (68.9 g RMS), the traditional design (26.2 g RMS) gives a factor of 2.3 whereas the novel one (23.6 g RMS) gives a factor of 2.6 in which the performance is improved by 12%. This improvement factor would be increased considerably as compared to the traditional approach if the dynamic absorber were designed for optimal overall absolute acceleration, however, it is not an intention of this study.

The above study shows that the absorber tuned for the optimal overall relative is only able to suppress the overall absolute acceleration by factor of 2.6 whereas for the overall relative deflection yields 4-fold vibration suppression. However, at will, the above worksheet and its Solver can be used to tune for an universal dynamic absorber which would be suitable for both overall relative deflection and absolute acceleration i.e. the same reduction ratio for both applications with respect to its original response.

In a general conclusion, the novel optimal dynamic absorber provides a better performance than the traditional one in terms of overall relative deflection and absolute acceleration under random vibration. The improvement seems to be small in this particular application, however, using a common approach for a specific application, as shown, is not the case in this study.

4.2.3 Additional measurement

The following analysis will reflect on the effect of the dynamic absorber on different observation points. In this approach, the dynamic properties of the original PCB are given again through the universal absolute transfer function, $T_a(\gamma,\lambda,s)$ at any observation γ,λ and transient receptance, $H(\gamma,\gamma_o;\lambda,\lambda_o;s)$ of that observation to the point γ_o,λ_o where the dynamic absorber is mounted, respectively. Taking into account the influence of the combined universal absolute transfer function, $\widetilde{T}_a(\gamma_o,\lambda_o,s)$ at the dynamic absorber's attachment point.

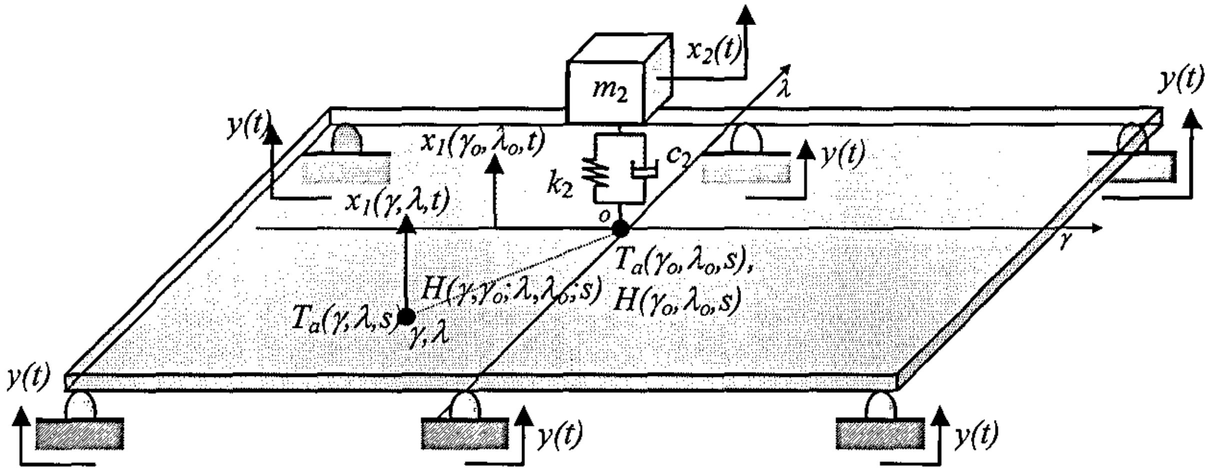

Figure 4.9. Dynamic model of generic PCB and with attached dynamic absorber

Figure 4.9 shows the schematic model of such a combined system which is similar to that in Figure 4.0. A new co-ordinate (γ,λ) marked on the PCB to analyse the response of this point in relation with the point where the dynamic absorber is mounted. Equation of motion for the primary system, using operator method and superposition principle takes the form of [40]:

$$X_1(\gamma,\lambda,s) = T_a(\gamma,\lambda,s)Y(s) - H(\gamma,\gamma_o;\lambda,\lambda_o;s)(c_2 s + k_2)(X_1(\gamma_o,\lambda_o,s) - X_2(s)), \tag{4.4}$$

for the secondary system:
$$X_2(s) = \frac{c_2 s + k_2}{m_2 s^2 + c_2 s + k_2} X_1(\gamma_o,\lambda_o,s), \tag{4.5}$$

or
$$X_1(\gamma_o,\lambda_o,s) - X_2(s) = \frac{m_2 s^2}{m_2 s^2 + c_2 s + k_2} X_1(\gamma_o,\lambda_o,s). \tag{4.6}$$

The absolute motion of the primary system at co-ordinate, γ_o,λ_o has the form:

$$X_1(\gamma_o,\lambda_o,s) = \frac{T_a(\gamma_o,\lambda_o,s)}{1 + \dfrac{m_2 s^2 H(\gamma_o,\lambda_o,s)(c_2 s + k_2)}{m_2 s^2 + c_2 s + k_2}} Y(s). \tag{4.7}$$

Substituting Equation 4.7 and 4.6 into Equation 4.4 yields an absolute transfer function of the combined system:

$$\tilde{T}_a(\gamma,\lambda,s)=\frac{X_1(\gamma,\lambda,s)}{Y(s)}=T_a(\gamma,\lambda,s)-\frac{H(\gamma,\gamma_o;\lambda,\lambda_o;s)T_a(\gamma_o,\lambda_o,s)}{H(\gamma_o,\lambda_o,s)+\dfrac{m_2s^2+c_2s+k_2)}{m_2s^2(c_2s+k_2)}}. \tag{4.8}$$

The formal substitution, $s=j\omega$, yields universal absolute transmissibility of the combined system:

$$\tilde{T}_a(\gamma,\lambda,j\omega)=T_a(\gamma,\lambda,j\omega)-\frac{H(\gamma,\gamma_o;\lambda,\lambda_o;j\omega)T_a(\gamma_o,\lambda_o,j\omega)}{H(\gamma_o,\lambda_o,j\omega)-\dfrac{-m_2\omega^2+c_2j\omega+k_2}{m_2\omega^2(c_2j\omega+k_2)}}. \tag{4.9}$$

The corresponding universal relative transmissibility might be calculated using Equation 3.5.

Equation 4.9 describes, in general, for the combined absolute transmissibility $\tilde{T}_a(\gamma,\lambda,j\omega)$ at observation point, γ,λ on the PCB can be calculated from the original universal absolute transmissibility, $T_o(\gamma_o,\lambda_o,j\omega)$ and local receptance, $H_o(\gamma_o,\lambda_o,j\omega)$ at the point of dynamic absorber is mounted in connection with transient receptance $H(\gamma,\gamma_o;\lambda,\lambda_o;j\omega)$.

Equation 4.9 can be verified by assuming the combined universal absolute transmissibility at the observation point is in the same co-ordinate with the dynamic absorber, γ_o,λ_o, which is:

$$\tilde{T}_a(\gamma_o,\lambda_o,j\omega)=T_a(\gamma_o,\lambda_o,j\omega)-\frac{H(\gamma_o,\lambda_o,j\omega)T_a(\gamma_o,\lambda_o,j\omega)}{H(\gamma_o,\lambda_o,j\omega)-\dfrac{-m_2\omega^2+c_2j\omega+k_2}{m_2\omega^2(c_2j\omega+k_2)}}. \tag{4.10}$$

Expressing the right hand side of Equation 4.10 in a common denominator and simplifying, gives:

$$\tilde{T}_a(\gamma_o,\lambda_o,j\omega)=\frac{T_a(\gamma_o,\lambda_o,j\omega)}{1-\dfrac{m_2\omega^2(c_2j\omega+k_2)}{-m_2\omega^2+c_2j\omega+k_2}H(\gamma_o,\lambda_o,j\omega)}. \tag{4.11}$$

The expression of Equation 4.11 is identical to that given by Equation 4.3.

Similarly, the calculation procedure was used MS®Excel. Figure 4.10 describes the process being carried out with the experimentally measured data. The measured absolute transmissibility and local receptance of observation point ◎ are placed in column E and F versus frequency, respectively, as a reference worksheet. The absolute transmissibility and transient receptance of the corresponding observation point are directly imported to column G and column H, respectively. Once the combined transmissibility using Equation 4.9 is calculated, then all standard calculation procedure is carried out identical to that in Figure 4.1 to produce the overall relative deflection value.

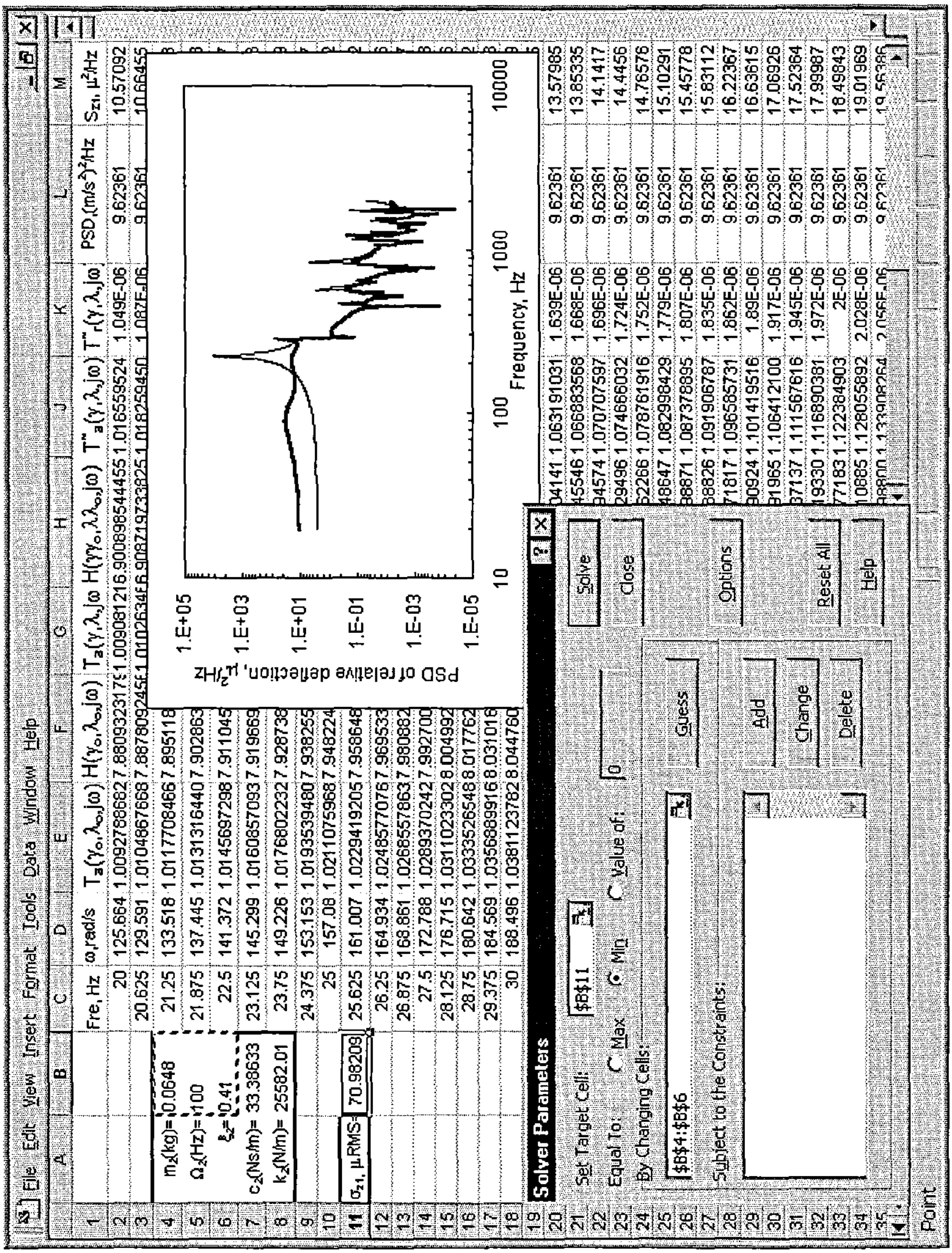

	A	B	C	D	E	F	G	H	J	K	L	M
1			Fre, Hz	ω,rad/s	$T_a(\gamma_o,\lambda_o,j\omega)$	$H(\gamma_o,\lambda_o,j\omega)$	$T_a(\gamma,\lambda,j\omega$	$H(\gamma\gamma_o,\lambda\lambda_o,j\omega)$	$T''_a(\gamma,\lambda,j\omega)$	$T''_r(\gamma,\lambda,j\omega$	PSD,(m/s²)²/Hz	S_{z1}, μ²/Hz
2			20	125.664	1.0092788682	7.880932317	1.00908121	6.900898544455	1.016559524	1.049E-06	9.62361	10.57092
3			20.625	129.591	1.0104867668	7.887809245	1.0102634	6.908719733825	1.018259450	1.087E-06	9.62361	10.66455
4	m_2(kg)=	0.0648	21.25	133.518	1.0117708466	7.895118						
5	Ω_2(Hz)=	100	21.875	137.445	1.0131316440	7.902863						
6	ξ_2=	0.41	22.5	141.372	1.0145697298	7.911045						
7	c_2(Ns/m)=	33.38633	23.125	145.299	1.0160857093	7.919669						
8	k_2(N/m)=	25582.01	23.75	149.226	1.0176802232	7.928738						
9			24.375	153.153	1.0193539480	7.938255						
10			25	157.08	1.0211075968	7.948224						
11	σ_{z1}, μRMS=	70.98209	25.625	161.007	1.0229419205	7.958648						
12			26.25	164.934	1.0248577076	7.969533						
13			26.875	168.861	1.0268557863	7.980882						
14			27.5	172.788	1.0289370242	7.992700						
15			28.125	176.715	1.0311023302	8.004992						
16			28.75	180.642	1.0333526548	8.017762						
17			29.375	184.569	1.0356889916	8.031016						
18			30	188.496	1.0381123782	8.044760						
19												
20								04141	1.063191031	1.639E-06	9.62361	13.57985
21								45546	1.066883568	1.668E-06	9.62361	13.85335
22								94574	1.070707597	1.696E-06	9.62361	14.1417
23								29496	1.074666032	1.724E-06	9.62361	14.4456
24								52266	1.078761916	1.752E-06	9.62361	14.76576
25								48647	1.082998429	1.779E-06	9.62361	15.10291
26								88671	1.087378895	1.807E-06	9.62361	15.45778
27								88826	1.091906787	1.835E-06	9.62361	15.83112
28								71817	1.096585731	1.862E-06	9.62361	16.22367
29								90924	1.101419516	1.89E-06	9.62361	16.63615
30								91965	1.106412100	1.917E-06	9.62361	17.06926
31								37137	1.111567616	1.945E-06	9.62361	17.52364
32								19330	1.116890381	1.972E-06	9.62361	17.99987
33								77183	1.122384903	2E-06	9.62361	18.49843
34								10885	1.128055892	2.028E-06	9.62361	19.01969

Set Target Cell: $B$11

Equal To: ○ Max ● Min ○ Value of: 0

By Changing Cells: $B$4:$B$6

Subject to the Constraints:

Figure 4.10. Spreadsheet showing Solver for calculation and optimising dynamic absorber

This worksheet contains four independent sets of measured data, they are all in complex form. The accuracy of calculation results are entirely dependent on the consistency of experimental data. Nevertheless, the aim of this analysis is to see how much difference there is in optimal parameters design for each observation point. Therefore, the Solver is independently set to minimise the overall relative deflection response of that corresponding observation point by simultaneously altering the natural frequency, loss factor and mass of the dynamic absorber. This optimising technique would allow a reduced workload, although, the calculation for these additional observation points is not as critical as for observation point ◎, where the deflection of the PCB is assumed maximum.

Optimal parameters	Observation point ①	Observation point ②	Observation point ③	Observation point ④
Mass ratio	57 %	92%	78%	72%
Natural frequency, Hz	115.45	91.22	93.13	100.03
Loss Factor	0.318	0.406	0.412	0.414

Table 4.0. Optimal parameters

Table 4.0 highlights the independent optimal parameters of the dynamic absorber for each observation point, bearing in mind that the attached location of the dynamic absorber is still at observation point ◎, and the effective mass of the PCB is still assumed to be 90 gr for comparison purpose only. As a result of optimising; the optimal mass ratio, loss factor and frequency are different from each other even though these points are observed symmetrically from the origin of the PCB. This can be explained from the complex plate-wise structure of the PCB and designed location of the dynamic absorber.

Overall relative deflection	Observation point ①	Observation point ②	Observation point ③	Observation point ④
Original response, μm RMS	234.43	260.82	301.31	305.45
Local design response, μm RMS	56.50	64.37	70.98	71.99
Universal design response, μm RMS	56.84	65.74	71.42	72.58

Table 4.1. Optimal response

Table 4.1 highlights the overall relative deflection of each observation point, the influence of an universal dynamic absorber ($\eta = 65\%$, $\Omega_2 = 100$ Hz, $\xi_2 = 0.4$) design shows little difference in terms of reduction ratio compared to local design. This table also shows that the overall relative deflection of these observation points is not as critical as from observation point ◎, therefore, the analysis of these observation points under swept-sine and shock can be neglected. Besides, obtaining the full modal parameters for numerical simulation purposes seems to be impossible in this case.

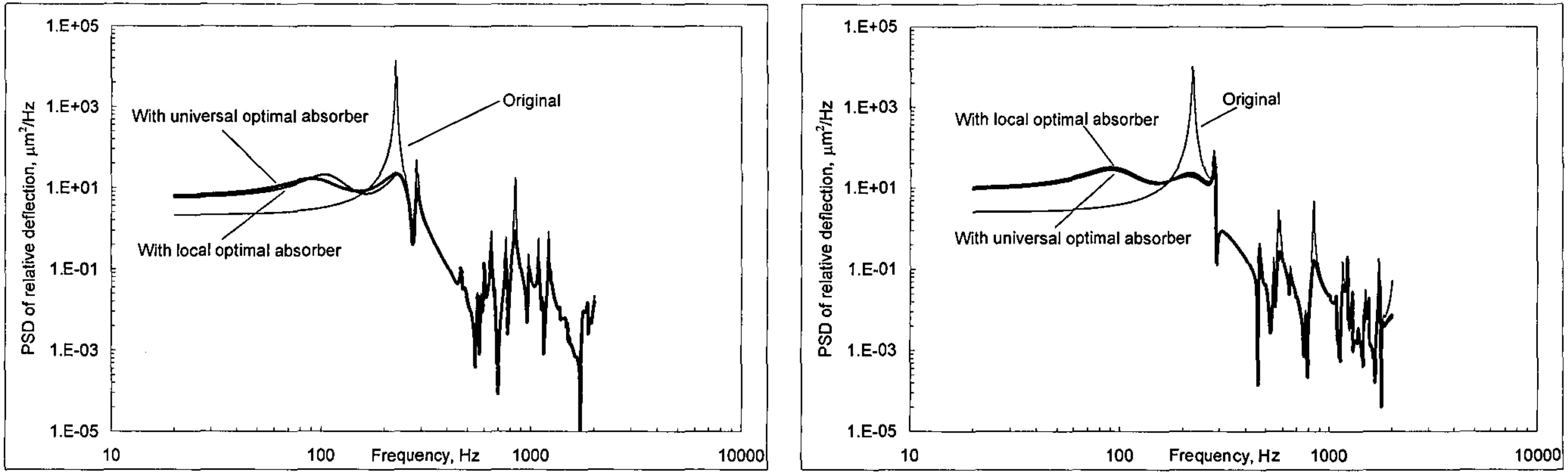

a) Observation point ①

b) Observation point ②

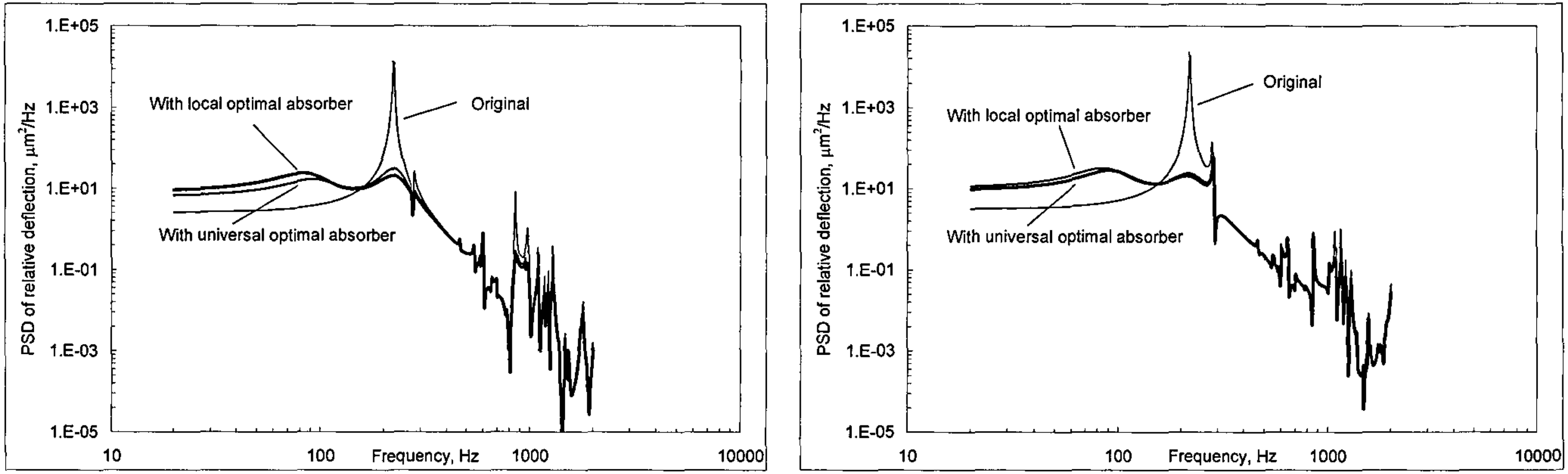

c) Observation point ③

d) Observation point ④

Figure 4.11. Dynamic response of original and ruggedized PCB at different observation point

Figure 4.11 shows the optimal dynamic response of the corresponding observation point. In these figures, the curve labelled as **With local optimal dynamic absorber** to represent the local optimal response design in accompany with the localised optimal parameters set of the dynamic absorber. The curve labelled as **With universal optimal dynamic absorber** where the optimal parameters of the dynamic absorber are chosen as: Ω_2 = 100 Hz, ξ_2 =0.4 and η=65%, the differences between them are really small. Since the overall relative deflection of the PCB is dictated by its first resonant frequency and its resonant peaks at high frequency range are not particularly strong at those observation points. Therefore, the major influence of the optimal dynamic absorber took place at the first mode as is clearly shown with the reference of original response curve.

The analysis of full-mode model seems to be more practical as oppose to the single-mode approximation. However, the degree of accuracy still entirely depends on the experimental data and linearity of PCB and the dynamic absorber.

4.2.4 Global curve-fitting of results

The relative deflection at observation point ◎ is the primary concern for numerical simulation. As from analytical solutions, there are two critical transfer functions are required for practising with the dynamic absorber, namely, the universal absolute transmissibility and local receptance of the original PCB involved in a process of building a numerical model with full modal parameters. Since the PCB used for the experimental purposes is an off-the-shelf product, using Finite Element Analysis (FEA) to extract modal parameters (natural frequency, damping and form factor) might not be relevant. From the experimental results, the random excitation in the frequency range of 20-2000 Hz excites all critical resonances of the PCB. This causes all the modes to be activated and therefore, the response is, in general, the linear superposition of all modes which are activated by this input excitation. Figures 2.4 shows modes that are well separated and lightly damped. These types of modes can be approximated with SDOF fit for each mode [37], the technique of curve-fitting is similar to that in Section 2.3.1. However, in this typical case, the universal absolute transmissibility of the PCB shows 10 modes system which can be described by the following frequency domain representation of the system as

$$T_a(j\omega) = \sum_{i=1}^{10} \Theta_i \frac{\Omega_i^2 + 2j\omega\xi_i\Omega_i}{\left(\Omega_i^2 - \omega^2\right) + 2j\omega\xi_i\Omega_i} \tag{4.12}$$

Here, Θ_i is form factor, Ω_i is natural frequency and ξ_i is loss factor of the corresponding mode.

In this system, each mode poses 3 unknown variables, it is too obvious if a full-mode model curve-fitted is used to estimate parameters of this case, 10 modes, then the total of 30 unknown parameters must be simultaneously identified during the curve-fitting process. However, the primary limitation of the Solver function is the number of variables in which it is set to perform. This means that fewer variables in the worksheet are the more accurate result that the Solver would produce and less time consuming.

The accurate loss factor and form factor estimate are, in general more difficult to obtain than accurate frequency estimates. Loss factor is the most difficult parameter to estimate accurately from FRF measurements, and the form factor is often tightly coupled with the loss factor. That is, if the loss factor is in large error, the form factor estimate will be in large error even though the curve-fitting function closely matches the experimental data.

These problems can be overcome by reducing the number of variables in the worksheet, this can be achieved by manually estimating the sequence natural frequency of each mode which corresponds to the experimental transmissibility. Also, properly guessed parameters of loss factor and form factor could reduce errors.

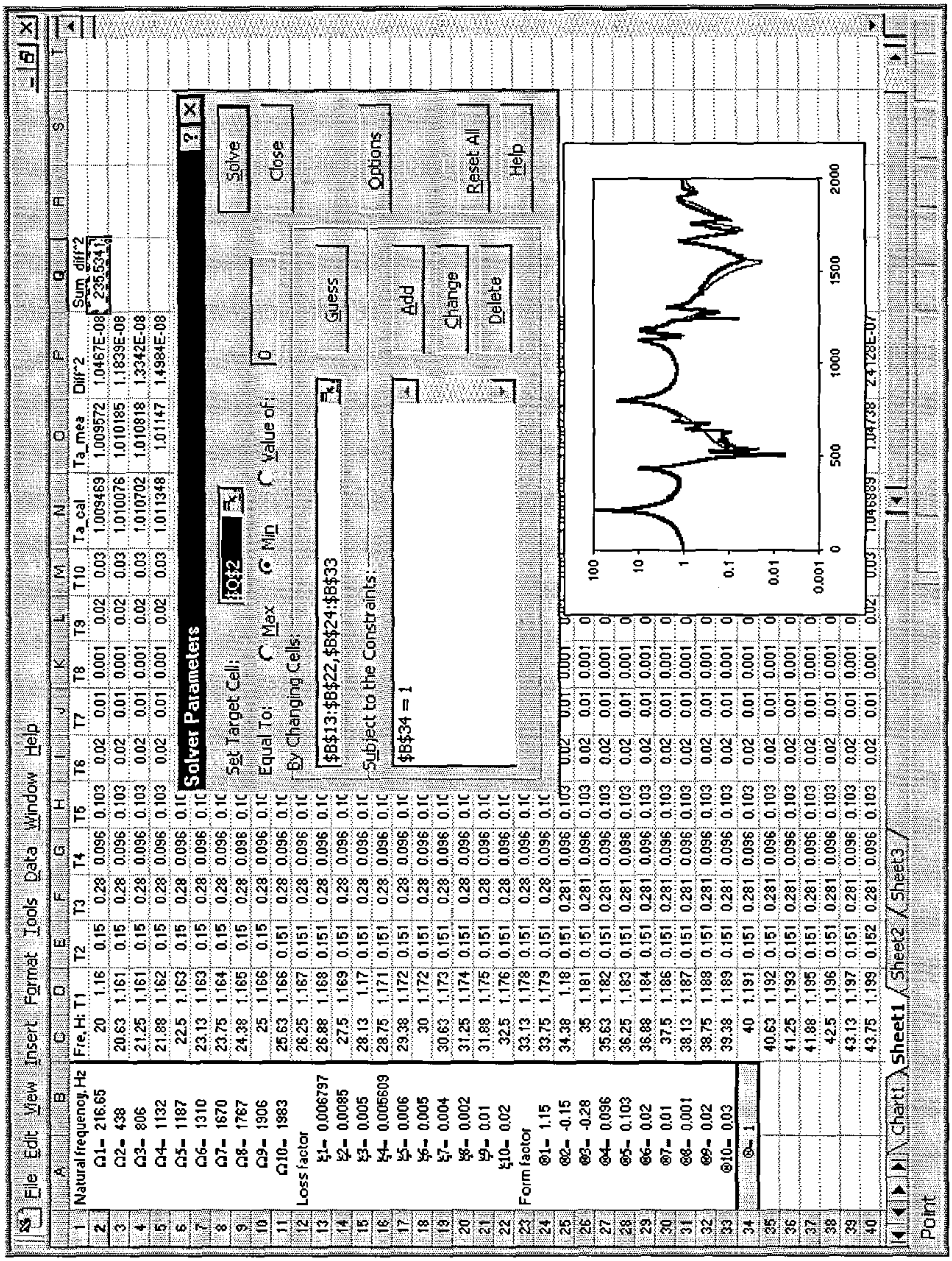

	A	B	C	D	E	F	G	H	I	J	K	L	M	N	O	P	Q
1	Natural frequency, Hz		Fre, H:	T1	T2	T3	T4	T5	T6	T7	T8	T9	T10	Ta_cal	Ta_mea	Diff^2	Sum_diff^2
2	Ω1=	216.65	20	1.16	0.15	0.28	0.096	0.103	0.02	0.01	0.001	0.02	0.03	1.009469	1.009572	1.0467E-08	235.5341
3	Ω2=	438	20.63	1.161	0.15	0.28	0.096	0.103	0.02	0.01	0.001	0.02	0.03	1.010076	1.010185	1.1839E-08	
4	Ω3=	806	21.25	1.161	0.15	0.28	0.096	0.103	0.02	0.01	0.001	0.02	0.03	1.010702	1.010818	1.3342E-08	
5	Ω4=	1132	21.88	1.162	0.15	0.28	0.096	0.103	0.02	0.01	0.001	0.02	0.03	1.011348	1.01147	1.4984E-08	
6	Ω5=	1187	22.5	1.163	0.15	0.28	0.096	0.1									
7	Ω6=	1310	23.13	1.163	0.15	0.28	0.096	0.1									
8	Ω7=	1670	23.75	1.164	0.15	0.28	0.096	0.1									
9	Ω8=	1767	24.38	1.165	0.15	0.28	0.096	0.1									
10	Ω9=	1906	25	1.166	0.15	0.28	0.096	0.1									
11	Ω10=	1983	25.63	1.166	0.151	0.28	0.096	0.1									
12	Loss factor		26.25	1.167	0.151	0.28	0.096	0.1									
13	ξ1=	0.006797	26.88	1.168	0.151	0.28	0.096	0.1									
14	ξ2=	0.0085	27.5	1.169	0.151	0.28	0.096	0.1									
15	ξ3=	0.005	28.13	1.17	0.151	0.28	0.096	0.1									
16	ξ4=	0.005609	28.75	1.171	0.151	0.28	0.096	0.1									
17	ξ5=	0.006	29.38	1.172	0.151	0.28	0.096	0.1									
18	ξ6=	0.005	30	1.172	0.151	0.28	0.096	0.1									
19	ξ7=	0.004	30.63	1.173	0.151	0.28	0.096	0.1									
20	ξ8=	0.002	31.25	1.174	0.151	0.28	0.096	0.1									
21	ξ9=	0.01	31.88	1.175	0.151	0.28	0.096	0.1									
22	ξ10=	0.02	32.5	1.176	0.151	0.28	0.096	0.1									
23	Form factor		33.13	1.178	0.151	0.28	0.096	0.1									
24	Φ1=	1.15	33.75	1.179	0.151	0.28	0.096	0.1									
25	Φ2=	-0.15	34.38	1.18	0.151	0.281	0.096	0.103	0.02	0.01	0.001	0					
26	Φ3=	-0.28	35	1.181	0.151	0.281	0.096	0.103	0.02	0.01	0.001	0					
27	Φ4=	0.096	35.63	1.182	0.151	0.281	0.096	0.103	0.02	0.01	0.001	0					
28	Φ5=	0.103	36.25	1.183	0.151	0.281	0.096	0.103	0.02	0.01	0.001	0					
29	Φ6=	0.02	36.88	1.184	0.151	0.281	0.096	0.103	0.02	0.01	0.001	0					
30	Φ7=	0.01	37.5	1.186	0.151	0.281	0.096	0.103	0.02	0.01	0.001	0					
31	Φ8=	0.001	38.13	1.187	0.151	0.281	0.096	0.103	0.02	0.01	0.001	0					
32	Φ9=	0.02	38.75	1.188	0.151	0.281	0.096	0.103	0.02	0.01	0.001	0					
33	Φ10=	0.03	39.38	1.189	0.151	0.281	0.096	0.103	0.02	0.01	0.001	0					
34	Φ=	1	40	1.191	0.151	0.281	0.096	0.103	0.02	0.01	0.001	0					
35			40.63	1.192	0.151	0.281	0.096	0.103	0.02	0.01	0.001	0					
36			41.25	1.193	0.151	0.281	0.096	0.103	0.02	0.01	0.001	0					
37			41.88	1.195	0.151	0.281	0.096	0.103	0.02	0.01	0.001	0					
38			42.5	1.196	0.151	0.281	0.096	0.103	0.02	0.01	0.001	0					
39			43.13	1.197	0.151	0.281	0.096	0.103	0.02	0.01	0.001	0					
40			43.75	1.199	0.152	0.281	0.096	0.103	0.02	0.01	0.001	0.02	0.03	1.046889	1.04738	2.4128E-07	

Set Target Cell: $Q$2

Equal To: ○ Max ● Min ○ Value of: 0

By Changing Cells: $B$13:$B$22,$B$24:$B$33

Subject to the Constraints: $B$34 = 1

Figure 4.12. Worksheet for curve-fitting

The designed worksheet to extract all necessary modal parameters is shown in Figure 4.12. The appropriate complex transmissibility expression of SDOF modal contribution is in place accordingly and the sum of these modes is calculated in column N, using Equation 4.12. In this situation, the Solver in is now tested to its limit, it is set to minimise the overall square difference between the measured transmissibility, column O and the fitted one, column N by simultaneously altering the form factor and loss factor of all modes, subjected to constrain $\sum \Theta_i = 1$, [38].

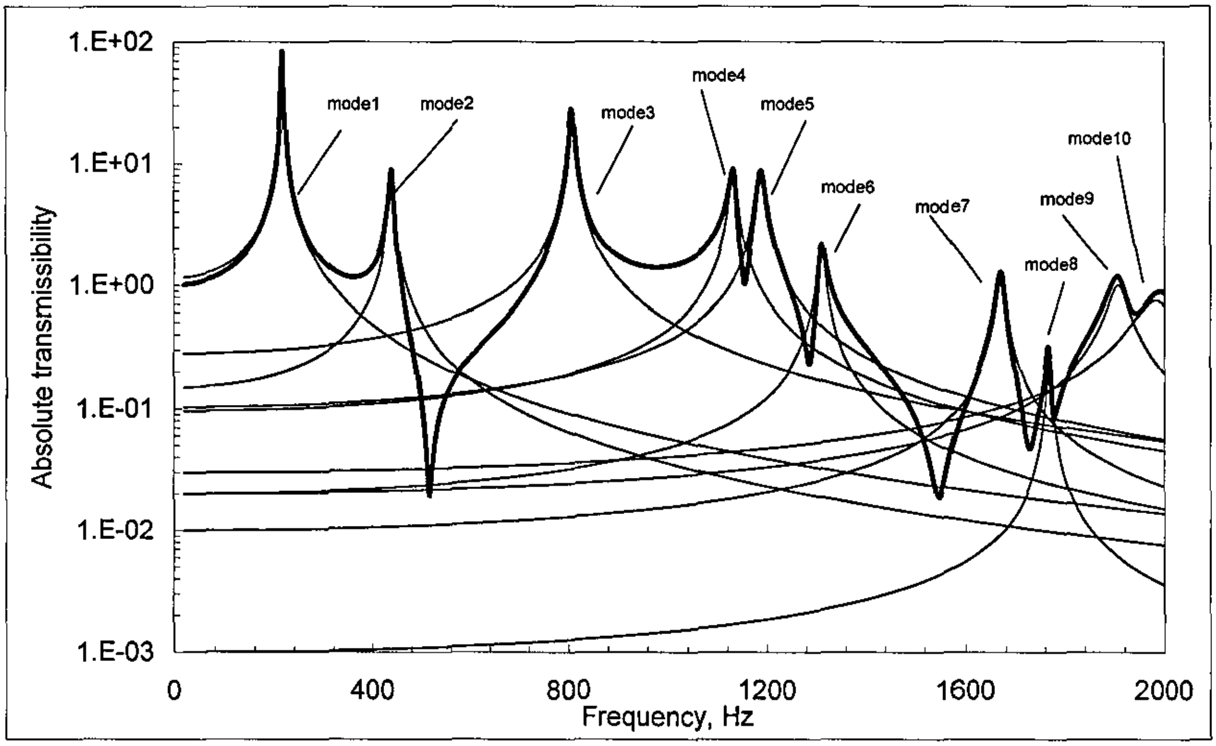

Figure 4.13. SDOF modal contribution

Mode	Θ	Natural frequency, Hz	Loss factor
Mode1	1.150	216.65	0.0067
Mode2	-0.150	438.67	0.0085
Mode3	-0.280	806.23	0.0050
Mode4	0.096	1132.78	0.0056
Mode5	0.103	1187.59	0.0063
Mode6	0.020	1310.59	0.0054
Mode7	0.010	1670.38	0.0043
Mode8	0.001	1767.56	0.0021
Mode9	0.020	1906.22	0.0111
Mode10	0.030	1983.12	0.0212

Table 4.2. SDOF modal parameters

Figure 4.13 and Table 4.2 review the results of each mode through the curve-fitting technique, as can be seen, the form factor of this complex structure can be either positive or negative which make up $\sum \Theta_i = 1$, this unity is very critical when considering numerical simulation.

These results have been used to create the graph of Figures 4.14 to more clearly illustrate what they mean as regards finding the closer match to experimental data.

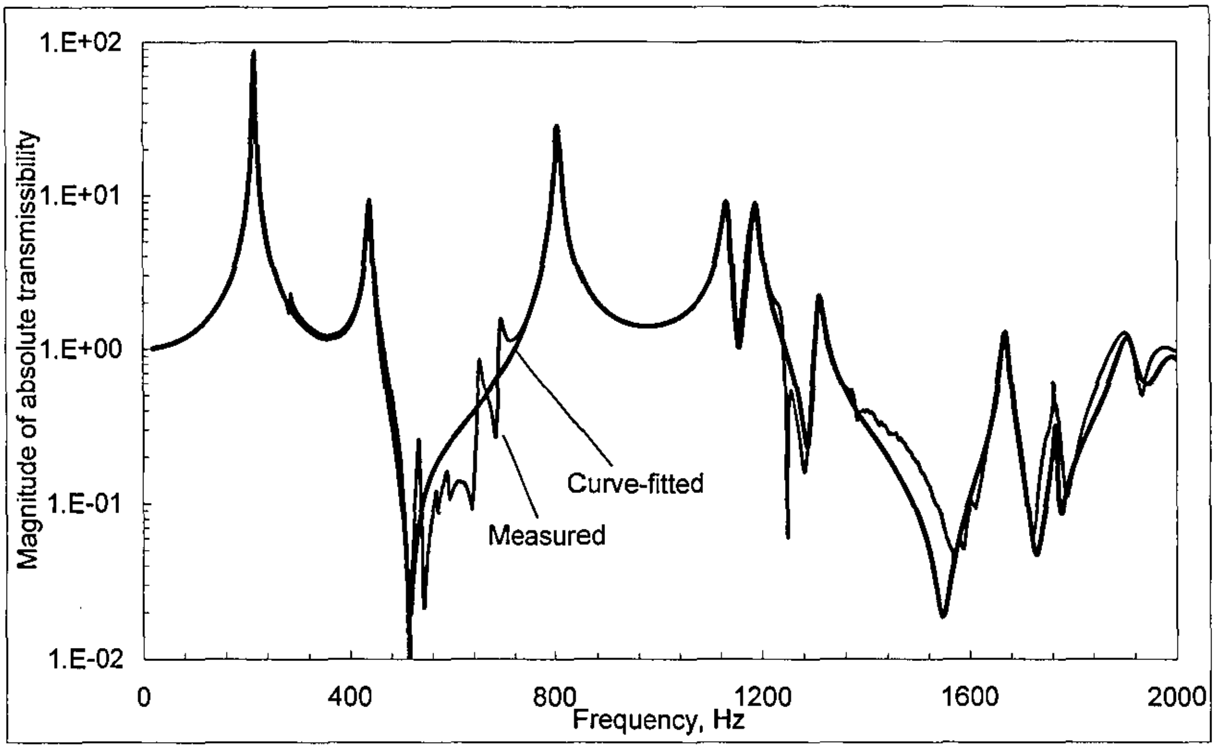

a) Modulus

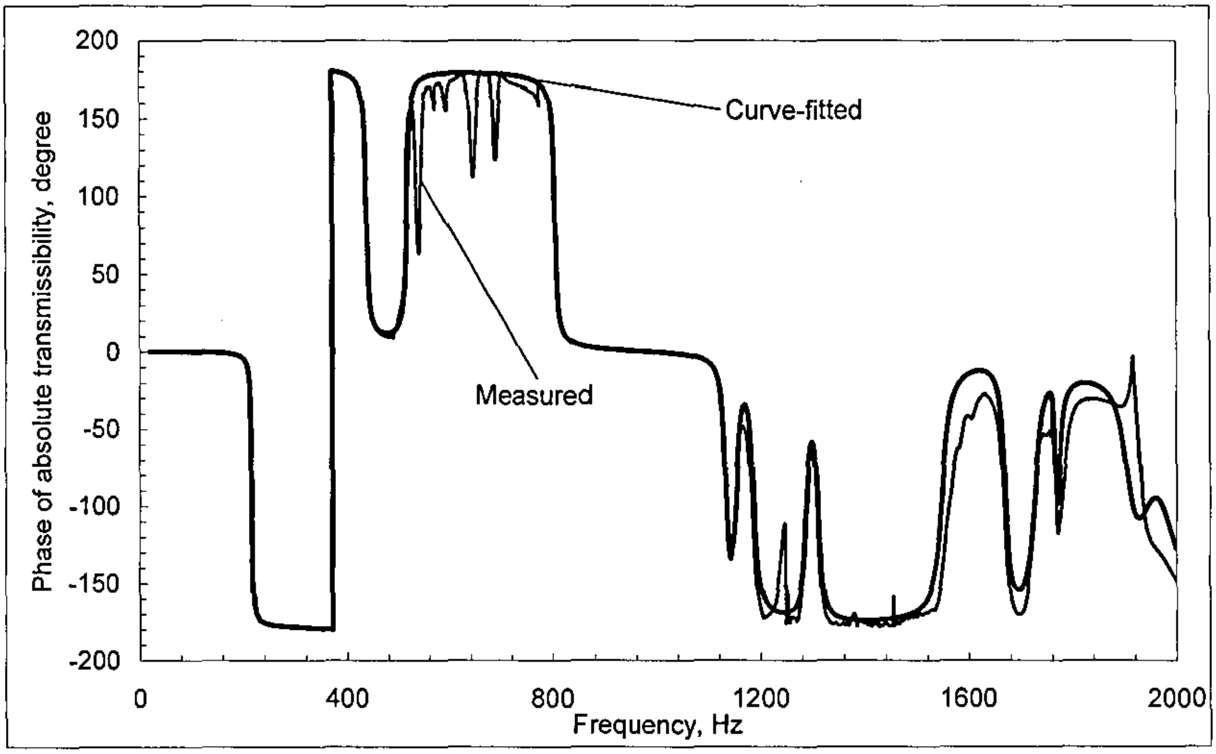

b) Phase angle

Figure 4.14. Universal absolute transmissibility of PCB

Figure 4.14 shows the superimposition of curve-fitted and experimental transmissibility. As shown, a simple curve-fitting technique can be applied to extract all modal parameters for such a complex system such as PCB.

Since the natural frequency and loss factor of each mode have already been obtained and are ready for use as shown in Table 4.2. The design worksheet for receptance curve-fitting is the same as Figure 4.12 only involving Equation 4.13

$$H(j\omega)=\sum_{i=1}^{10}\Psi_i\frac{1}{\left(\Omega_i^2-\omega^2\right)+2j\omega\xi_i\Omega_i}. \tag{4.13}$$

The task of the Solver is now set to match the curve-fitted and experimental local receptance by altering its form factors only.

Mode	Θ	Ψ	Natural frequency, Hz	Loss factor
Mode1	1.150	11.233	216.65	0.0067
Mode2	-0.150	10.900	438.67	0.0085
Mode3	-0.280	7.789	806.23	0.0050
Mode4	0.096	2.789	1132.78	0.0056
Mode5	0.103	4.556	1187.59	0.0063
Mode6	0.020	1.011	1310.59	0.0054
Mode7	0.010	0.789	1670.38	0.0043
Mode8	0.001	0.578	1767.56	0.0021
Mode9	0.020	0.356	1906.22	0.0111
Mode10	0.030	0.356	1983.12	0.0212

Table 4.3. SDOF modal parameters

Table 4.3 shows the completed modal parameters from curve-fitted of both local receptance and absolute transmissibility. In this table, the value of Θ_i is different from Ψ_i at their corresponding mode. These differences can be explained from different techniques of exciting the PCB and its mathematical expression [39].

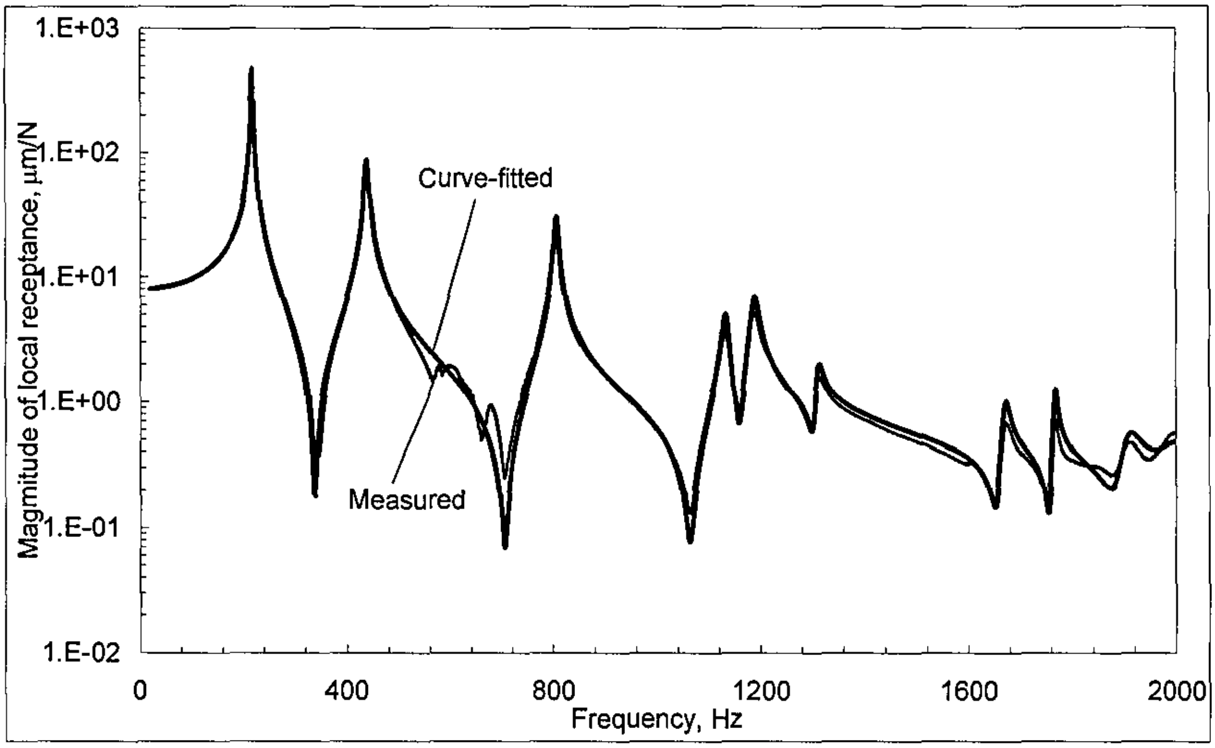

a) Magnitude

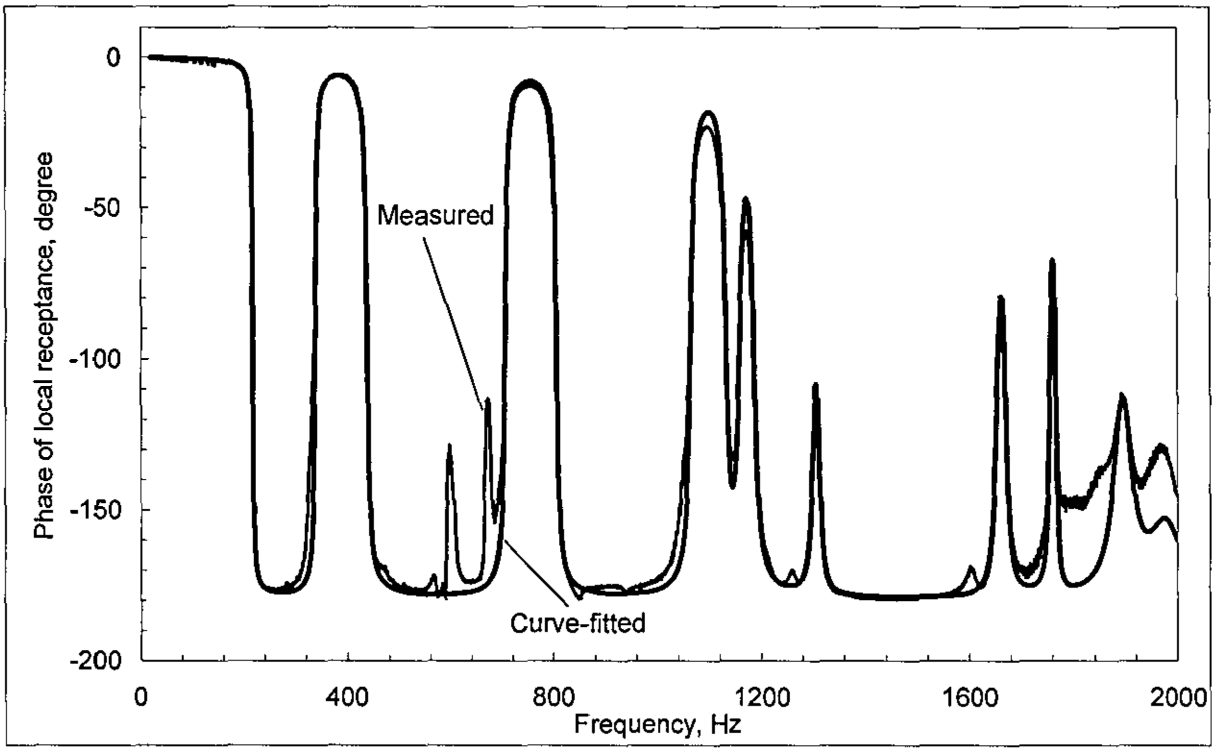

b) Phase

Figure 4.15. Local receptance

The optimisation for full-mode model based on curve-fitted results could carry on using standard procedure as mentioned in Section 4.3.1. However, this could duplicate work due to the fact that the mode shape of curve-fitted ones are almost the same as the experimental results.

4.2.5 Numerical simulation

The aim of this numerical simulation is to calculate the fatigue level using the Matlab-Script from Figure 3.12 of Section 3.2.3 for full-mode model of PCB. Since the program file is expressed in terms of relative motion, a formal substitution $z_1 = x_1 - y$, the relative motion for the primary system and $z_2 = x_2 - y$, the relative motion for secondary system into Equation 4.0 and 4.1 are required. This yields for the secondary system:

$$m_2\ddot{z}_2 + c_2(\dot{z}_2 - \dot{z}_1) + k_2(z_2 - z_1) = -m_2\ddot{y}, \tag{4.14}$$

and for the primary system

$$\ddot{z}_1 - s^2H(s)\left[c_2(\dot{z}_1 - \dot{z}_2) + k_2(z_1 - z_2)\right] = T_a(s)\ddot{y} - \ddot{y} \tag{4.15}$$

Here, $H(s)$ is local receptance transfer function and $T_a(s)$ is universal absolute transfer function of the original PCB.

Equation 4.14 and 4.15 are manipulated for simulation model as shown in Figure 4.16. This model contains 10 separated absolute transfer functions, $T_{a,i}(s)$ and 10 separated accelerance transfer functions, $s^2H_i(s)$ along with their corresponding form factors which are conveniently grouped in **Original PCB** sub-system. As for the single-mode PCB Simulink model, all the standard procedures are carried out to produce the corresponding signal for further analysis. Similarly, this simulation model can be either subjected to swept-sine or shock excitation at will.

For convenience of using Simulink's transfer function, the modal parameters of the PCB per Equation 4.12 and 4.13 are now expressed in terms of system parameters (stiffness, damping and mass), i.e.

universal absolute transfer function

$$T_a(s) = \sum_{i=1}^{10} \Theta \frac{c_i s + k_i}{ms^2 + c_i s + k_i}, \tag{4.17}$$

and acclerance transfer function

$$s^2H(s) = \sum_{i=1}^{10} m\Psi_i \frac{s^2}{ms^2 + c_i s + k_i}. \tag{4.18}$$

Here, we use *m* = 90 gr to calculate *c* and *k* from its modal parameters for all the modes. In terms of SDOF modal contribution, the value of *m* does not have any effect on the dynamic properties of the PCB whereas its form factors are of greater importance. The corresponding parameters of each mode are calculated and installed in Matlab m-file.

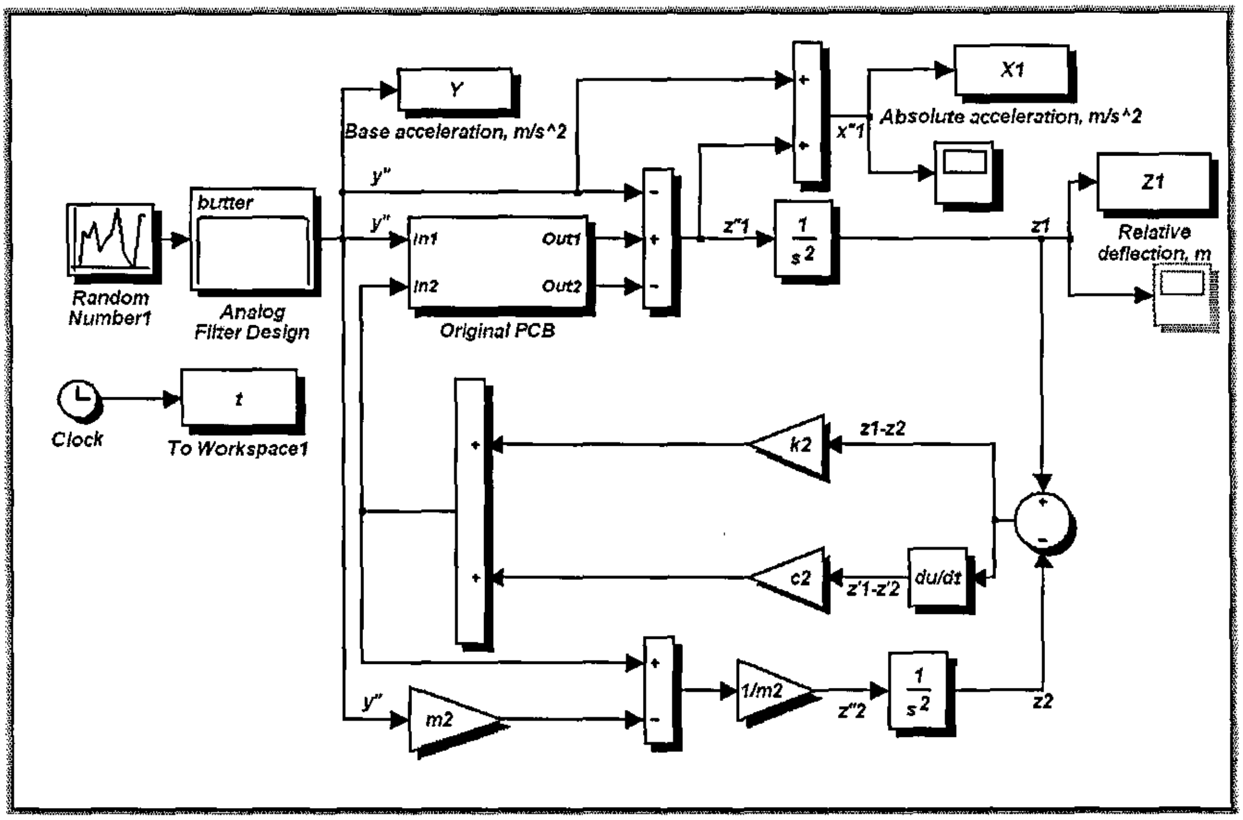
Y
Base acceleration, m/s^2
y"
butter
Random Number1
Analog Filter Design
In1
Out1
In2
Out2
Original PCB
x"1
X1
Absolute acceleration, m/s^2
Z1
Relative deflection, m
z"1
1/s2
z1
Clock
t
To Workspace1
k2
z1-z2
c2
z'1-z'2
du/dt
m2
1/m2
z"2
1/s2
z2

Figure 4.16. Simulink diagram for random vibration excitation

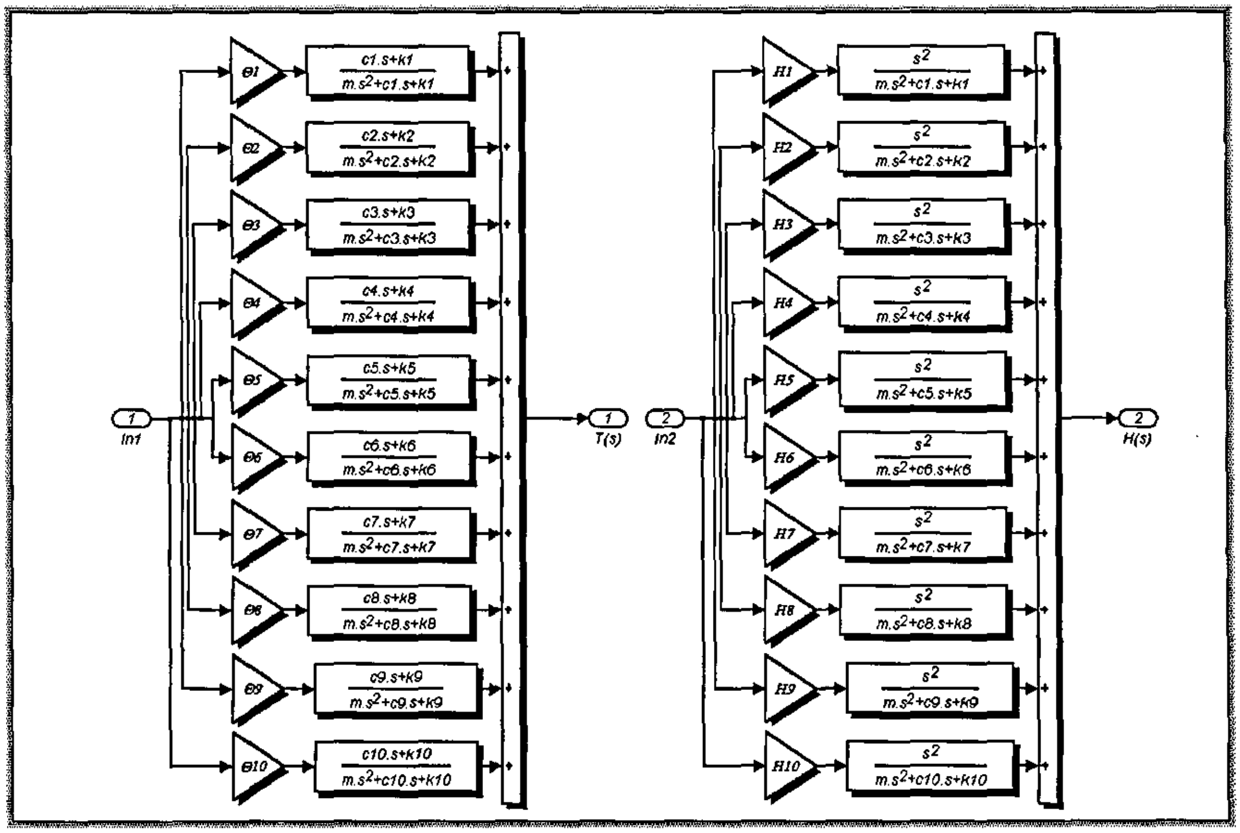
In1
θ1
c1.s+k1 / m.s2+c1.s+k1
θ2
c2.s+k2 / m.s2+c2.s+k2
θ3
c3.s+k3 / m.s2+c3.s+k3
θ4
c4.s+k4 / m.s2+c4.s+k4
θ5
c5.s+k5 / m.s2+c5.s+k5
θ6
c6.s+k6 / m.s2+c6.s+k6
θ7
c7.s+k7 / m.s2+c7.s+k7
θ8
c8.s+k8 / m.s2+c8.s+k8
θ9
c9.s+k9 / m.s2+c9.s+k9
θ10
c10.s+k10 / m.s2+c10.s+k10
T(s)
In2
H1
s2 / m.s2+c1.s+k1
H2
s2 / m.s2+c2.s+k2
H3
s2 / m.s2+c3.s+k3
H4
s2 / m.s2+c4.s+k4
H5
s2 / m.s2+c5.s+k5
H6
s2 / m.s2+c6.s+k6
H7
s2 / m.s2+c7.s+k7
H8
s2 / m.s2+c8.s+k8
H9
s2 / m.s2+c9.s+k9
H10
s2 / m.s2+c10.s+k10
H(s)

Figure 4.17. Sub-system Simulink block diagram of original PCB

The base excitation level is still assumed to be 14g RMS, where the sub-system bock diagram of random excitation is identical to that Figure 3.14a. As a result of simulation, the plot of time history of the original system is still maximum at the typical time range from 5.5 s to 7 s in which the response patterns are almost the same as the simulation result of the single-mode model. However, in this case, the time history of the absolute acceleration response is denser in both original and ruggedized PCB compared to single-mode approximation (see Figure 4.18 and 4.19 with appropriate label). This seems to be a more realistic approach.

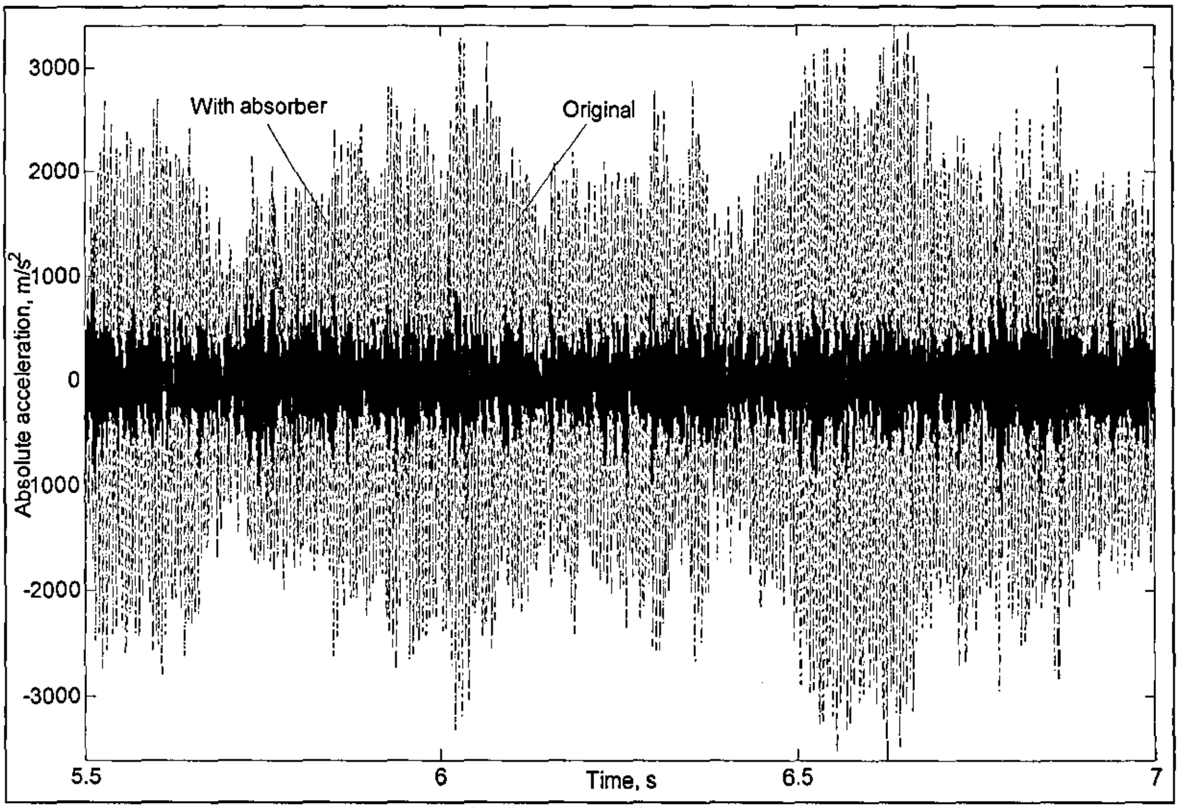

a) Absolute acceleration

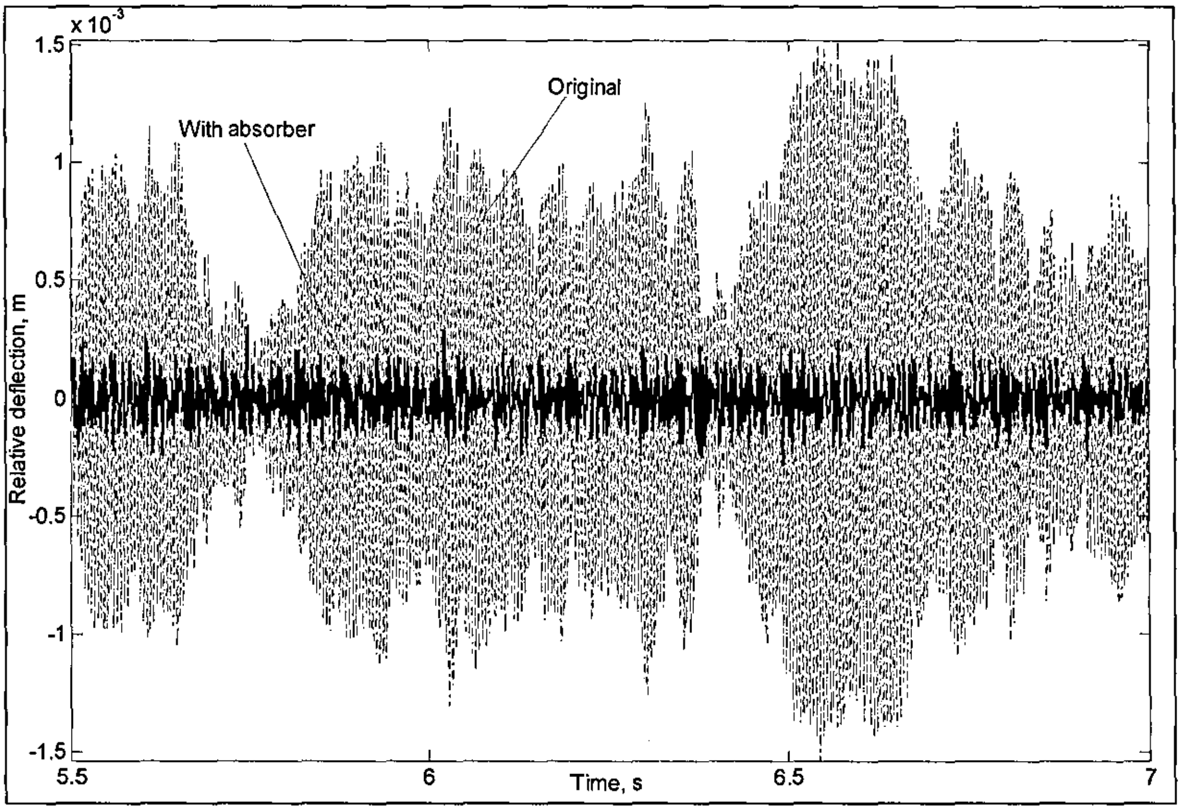

b) Relative deflection

Figure 4.18. Simulated time history response of original and ruggedized PCB (η=35%)

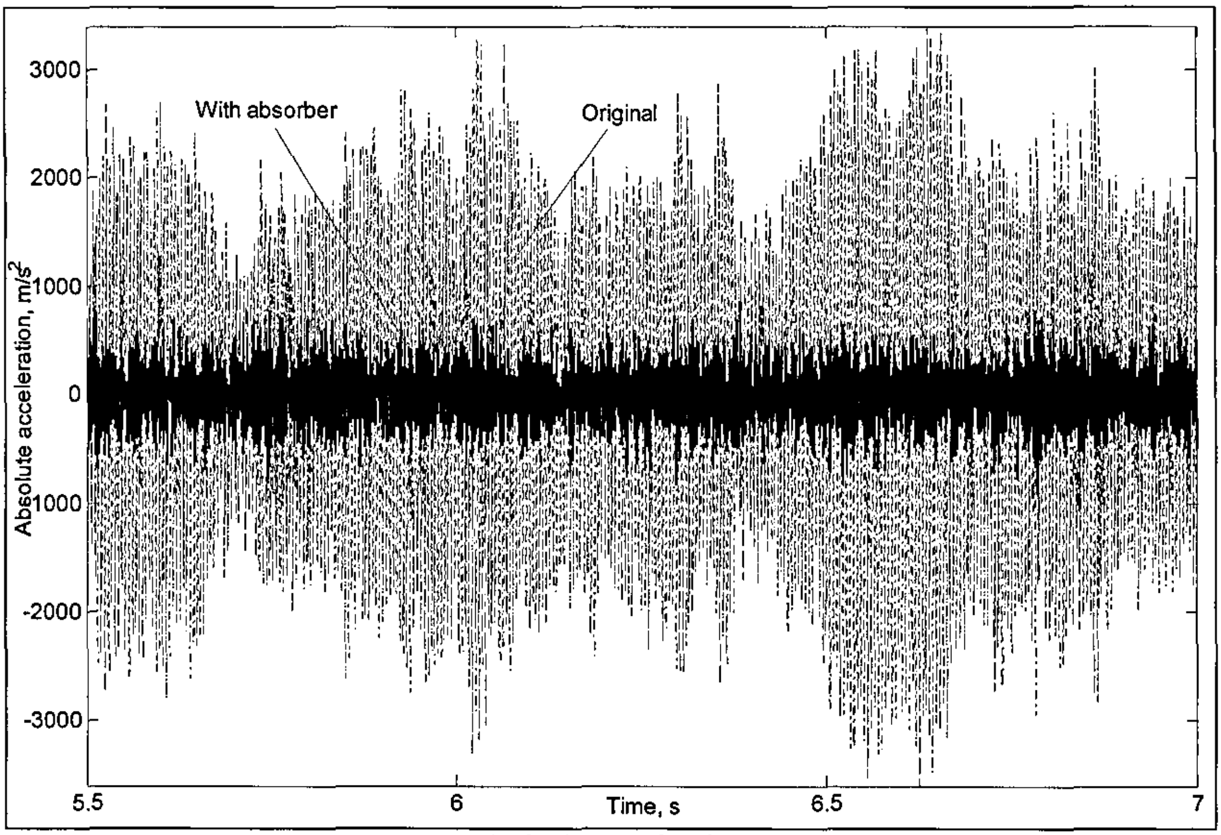

a) Absolute acceleration

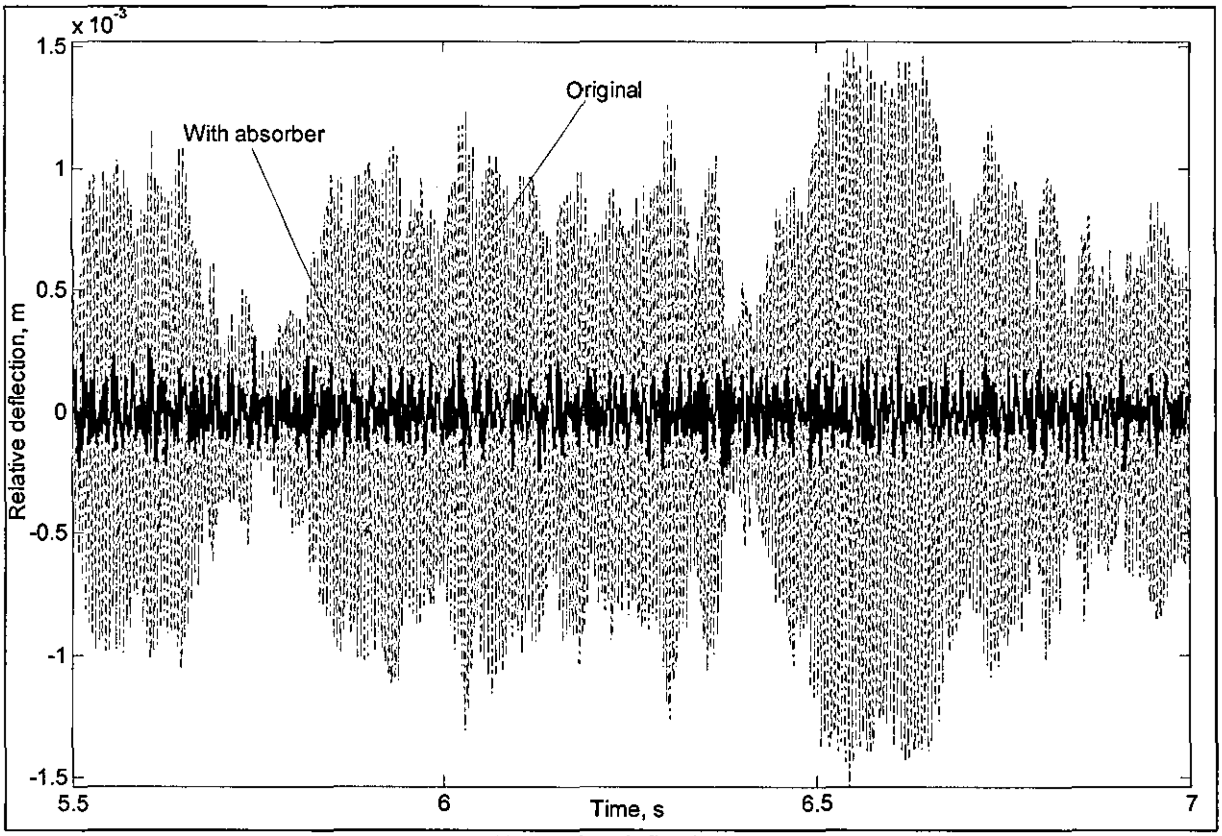

b) Relative deflection

Figure 4.19. Simulated time history response of original and ruggedized PCB (η=65%)

Based on these results, the parameters of the dynamic absorber are designed for optimal performance in terms of overall absolute acceleration for the single-mode approximation might not be as closed as the optimal design for the full-mode model of PCB. For a better result of prediction or simulation using a dynamic absorber in vibration control, it is necessary not to force the system to be as simple as possible.

Nonetheless, a simple verification check is carried out on the above relative results. This is done by comparing the predicted reduction factor of the overall response from the simulation model through the general methodology developed in Section 3.2.3 for different dynamic absorber's mass ratios. Table 4.4 shows the simulation results together with their theoretical calculation for both single-mode and full-mode models

Type of prediction	Overall relative deflection, μm RMS, (Analytical),		Overall relative deflection, μm RMS, (Simulation)		Increase life factor (Overall technique), times		Increase life factor (Simple cycles technique), times	
	Single-mode	Full-mode	Single-mode	Full-mode	Single-mode	Full-mode	Single-mode	Full-mode
Original	271.5	312	271.9	314				
35% mass ratio	68.1	79.8	68.3	80.2	6,982	5,968	7,820	7,095
65% mass ratio	65.9	77.8	65.5	77.5	8,615	7,249	10,030	9,216

Table 4.4. Comparison of the increased life factor between the simple cycle and overall technique

The transformation of time signal to frequency domain for both absolute acceleration and relative are further carried out for the above simulation results. For a better match with analytical results, it is necessary to compensate the response signal through the "roughness" input excitation. Using **tfe (input-signal, output-signal, FFTs, Fs, window, Noverleap)** command from Matlab, the absolute transmissibility is obtained as shown in Figure 4.20. Since the dynamic characteristic of the system is said to be linear, then the PSD may be calculated using the appropriate expression to produce the desired curve. Figure 4.21 and 4.22 show the PSD of absolute acceleration and relative deflection of the original and ruggedized PCB, respectively. As can be seen again, the influence of the dynamic absorber suppresses almost all resonances of the original PCB, while the antiresonant notches remain practically unaffected.

In general these "perfect" PSD curves can be directly obtained from the analytical solution, providing modal parameters. However, here, we demonstrate the resourcefulness of Matlab/Simulink and the technique of building a MDOF system using transfer functions. The obtained results from numerical simulations are in time domain and hence frequency domain in a reasonable time without mathematical complication. This package obviously shows its superiority for studying any dynamic systems.

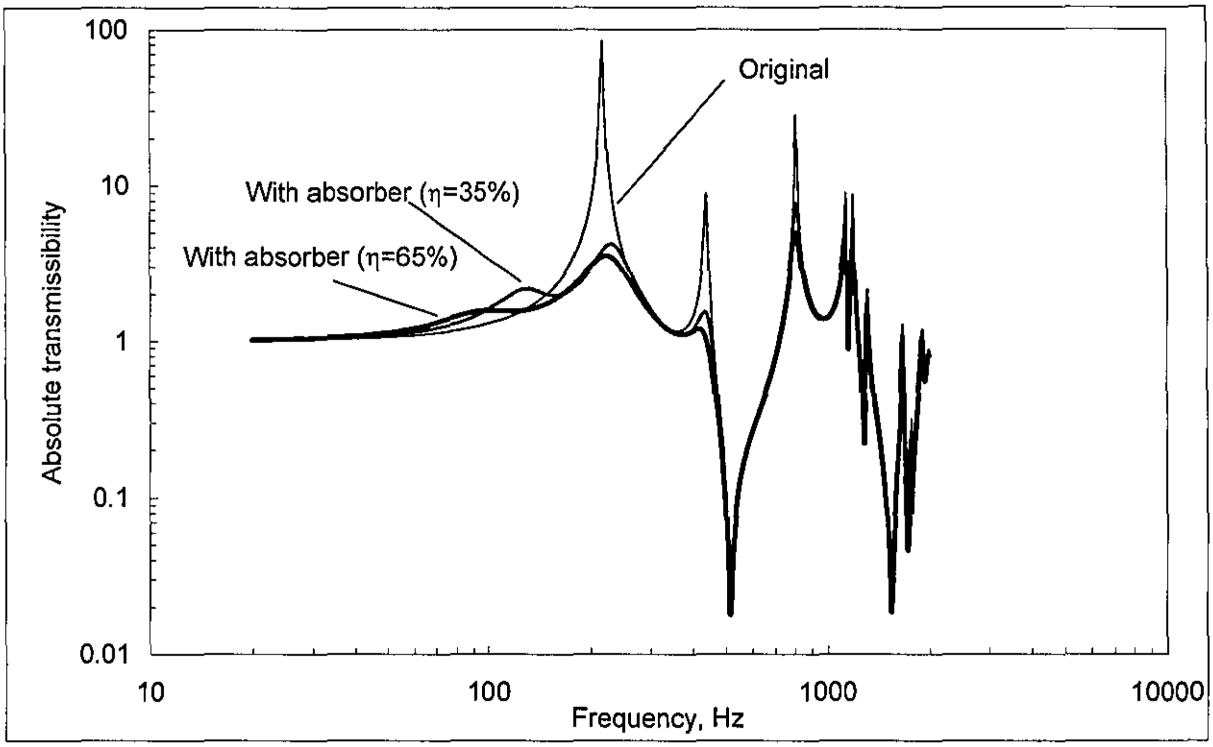

Figure 4.20. Simulated absolute transmissibility of original and ruggedized PCB

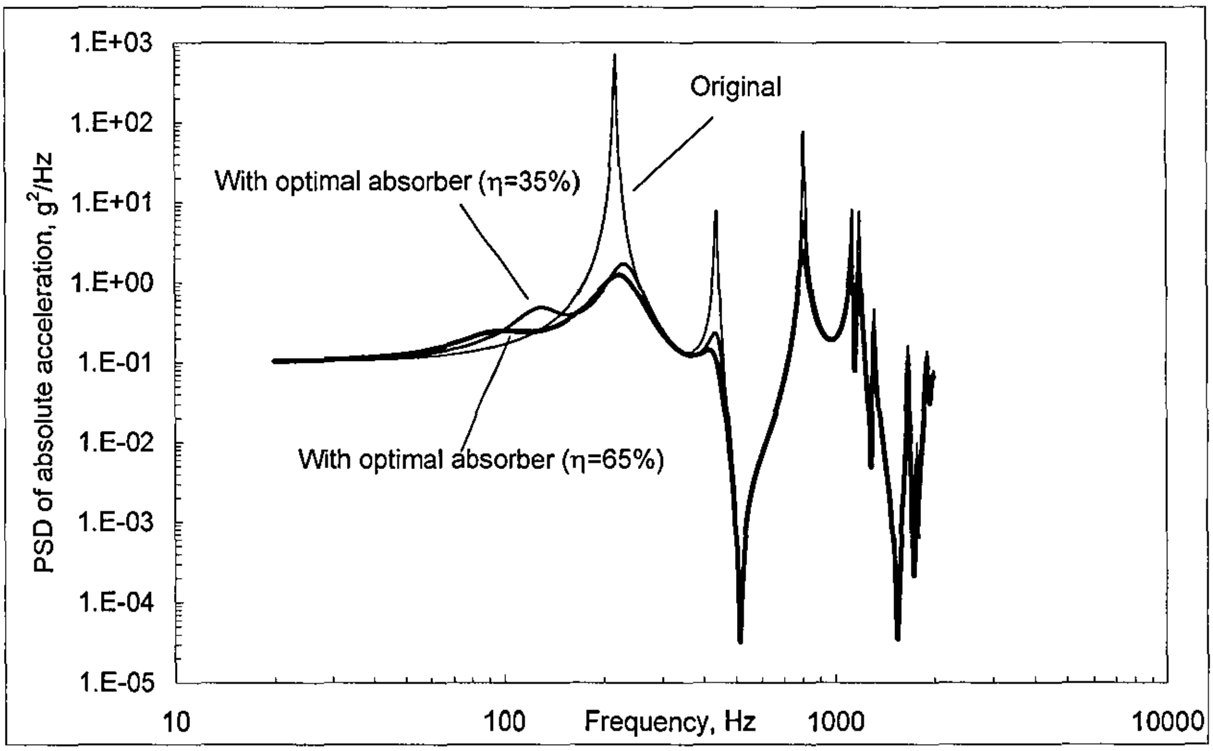

Figure 4.21. Simulated PSD of absolute acceleration of original and ruggedized PCB

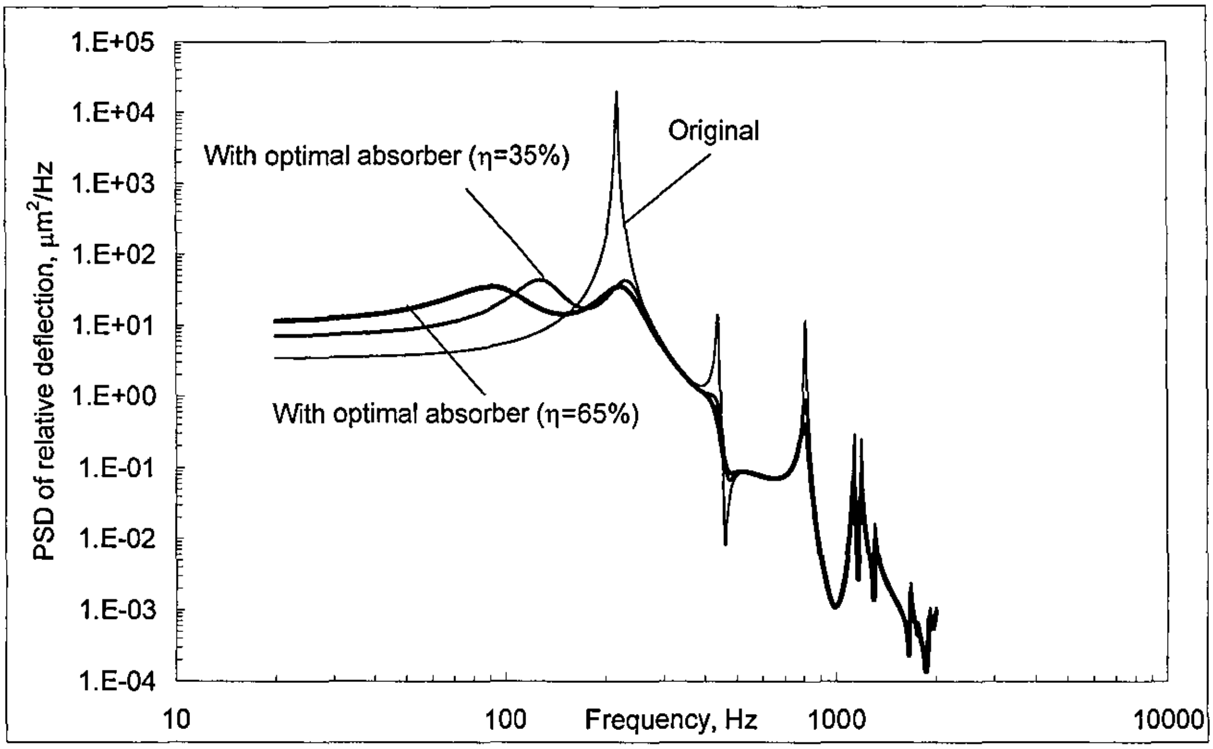

Figure 4.22. Simulated PSD of relative deflection of original and ruggedized PCB

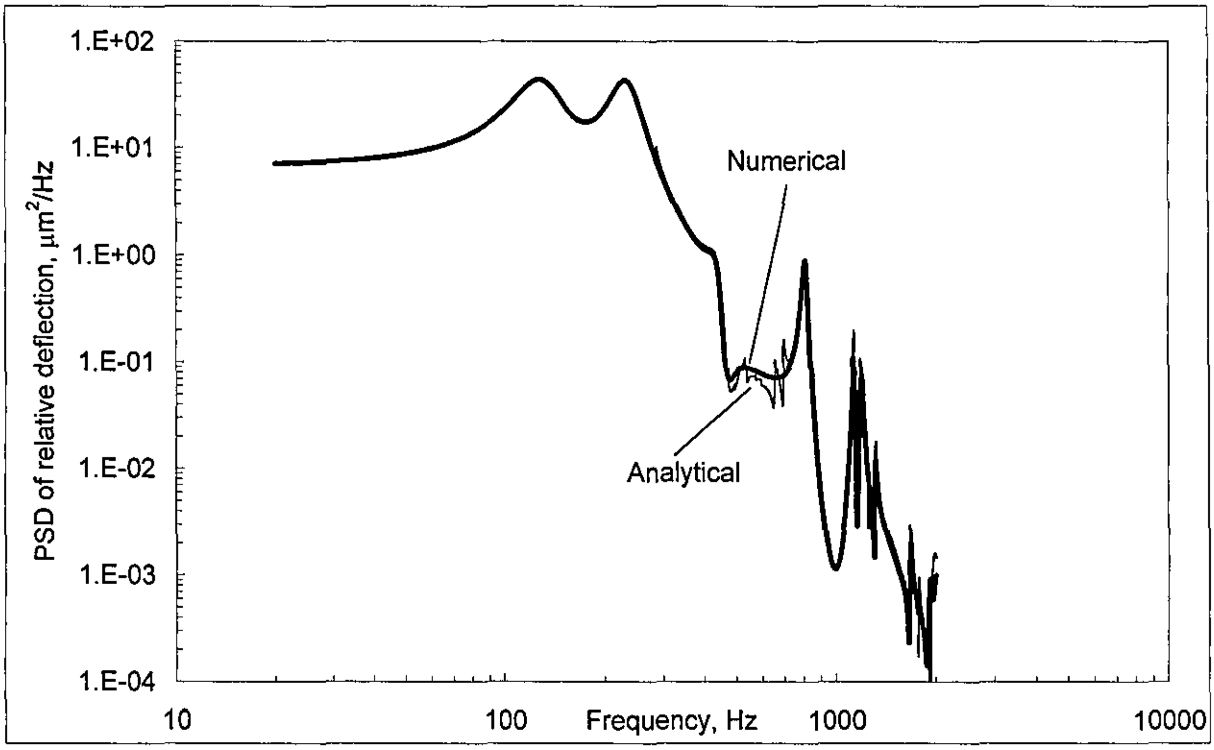

Figure 4.23. Comparison dynamic response of ruggedized PCB (η=35%)

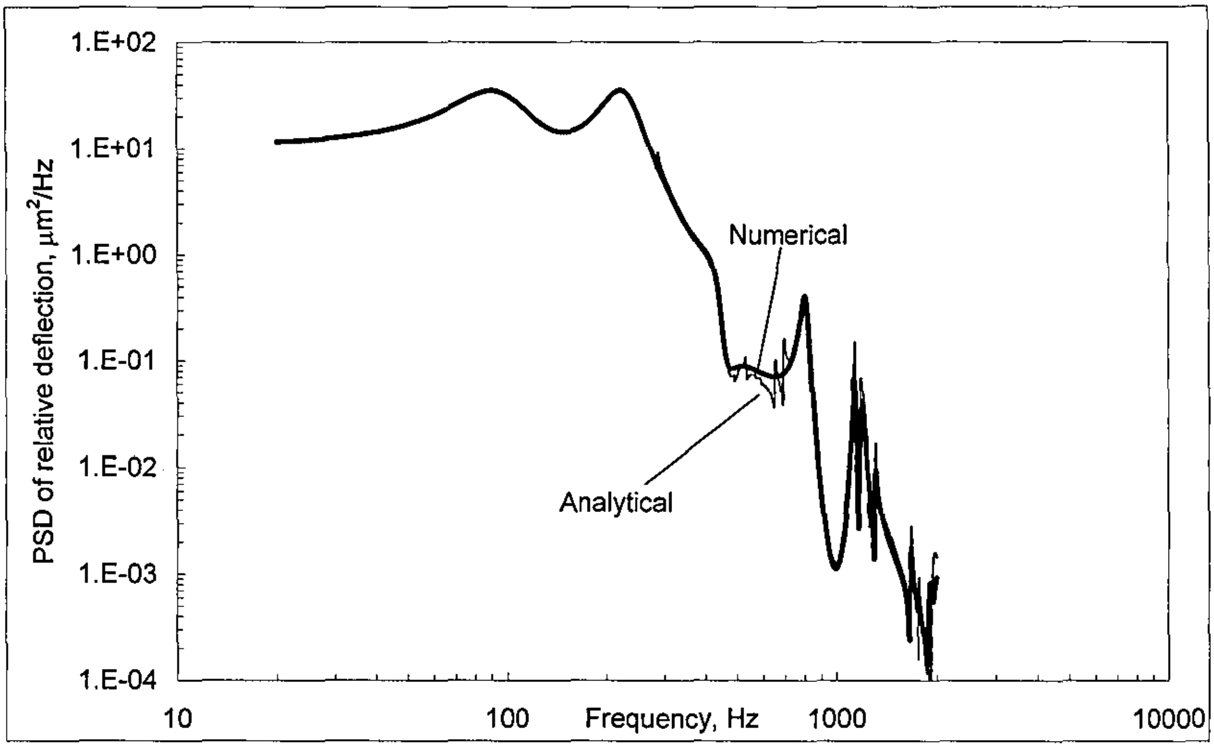

Figure 4.24. Comparison dynamic response of ruggedized PCB (η=65%)

Nonetheless, the simulation results can be justified by comparing the results obtained analytically. As shown in Figure 4.23 and 4.24 the close match results are reflected on the accurate results of the curve-fitting procedure. This indicates that using numerical simulations and hence fatigue analysis for the full-mode PCB, one must keep in mind the initial design stage, that is the method of extracting modal parameters.

4.3 Sine vibration

4.3.1 Designing MS®Excel worksheet for minimising peak relative deflection

The proceeding section deals with the optimal design of dynamic ruggedizer where the PCB was represented using the single-mode model. The application of the full-mode model gives more realistic results, especially when the frequency response function of the PCB contains essential high-frequency components.

The spreadsheet in Figure 4.25 is set up based upon the measured data as used in Section 4.3.1. Similarly, the MS®Excel Solver add-in is set to minimise the peak value calculated using Equation 3.11 by varying the natural frequency and loss factor of dynamic absorber at different mass ratios, where the input excitation is still assumed to be 10 g.

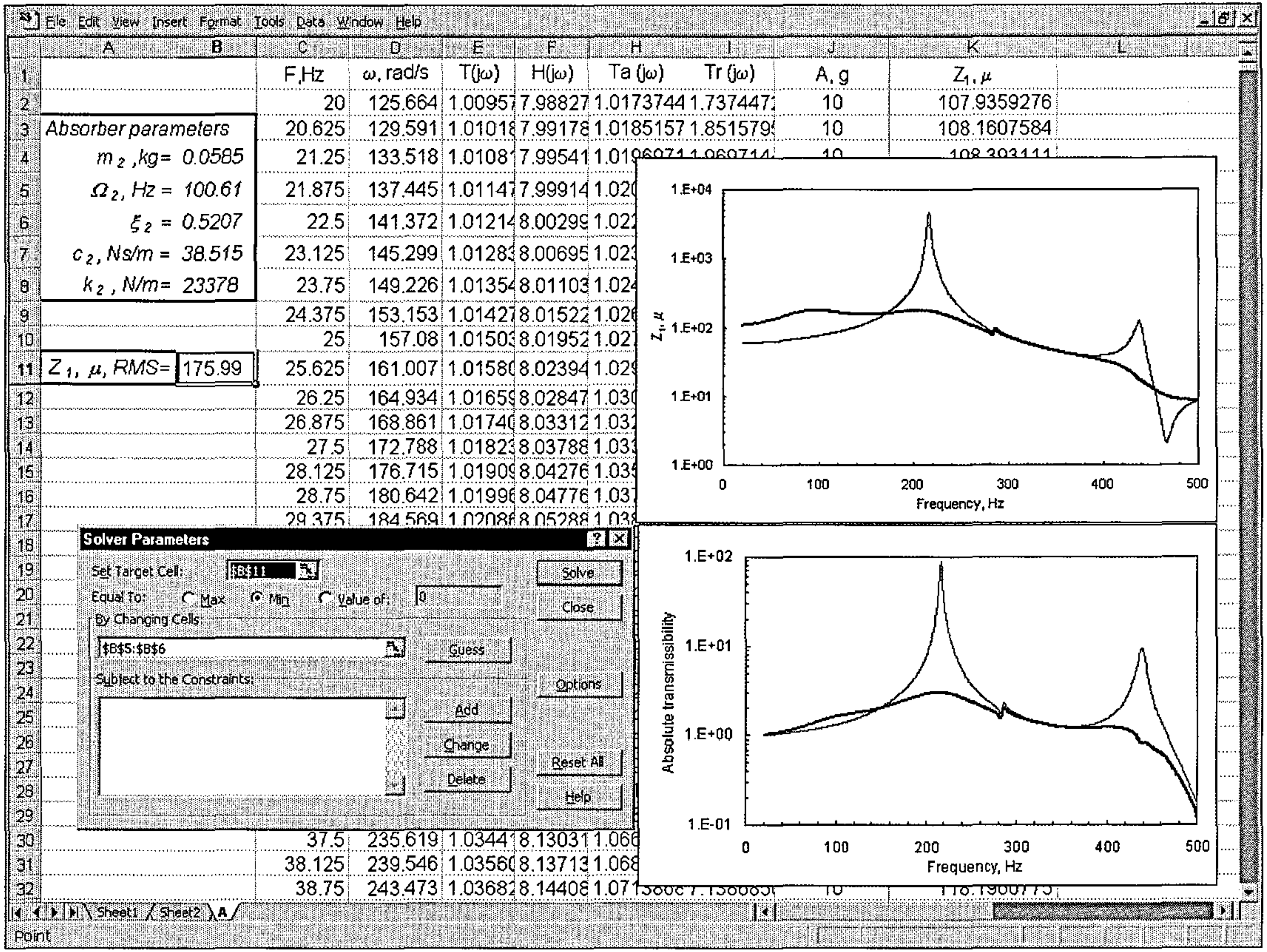
File Edit View Insert Format Tools Data Window Help
Sheet1
Sheet2
A
Point
Solve
Close
Guess
Options
Add
Change
Delete
Reset All
Help
1.E+04
1.E+03
1.E+02
1.E+01
1.E+00
Z1, μ
0
100
200
300
400
500
Frequency, Hz
1.E+02
1.E+01
1.E+00
1.E-01
Absolute transmissibility
0
100
200
300
400
500
Frequency, Hz

	A	B	C	D	E	F	H	I	J	K
1			F,Hz	ω, rad/s	T(jω)	H(jω)	Ta (jω)	Tr (jω)	A, g	Z_1, μ
2			20	125.664	1.00957	7.98827	1.0173744	1.737447	10	107.9359276
3	*Absorber parameters*		20.625	129.591	1.01018	7.99178	1.0185157	1.851579	10	108.1607584
4	*m_2 ,kg=*	*0.0585*	21.25	133.518	1.0108	7.99541	1.019			
5	*Ω_2, Hz =*	*100.61*	21.875	137.445	1.01147	7.99914	1.020			
6	*ξ_2 =*	*0.5207*	22.5	141.372	1.01214	8.00299	1.022			
7	*c_2, Ns/m =*	*38.515*	23.125	145.299	1.01283	8.00695	1.023			
8	*k_2 , N/m=*	*23378*	23.75	149.226	1.01354	8.01103	1.024			
9			24.375	153.153	1.01427	8.01522	1.026			
10			25	157.08	1.01503	8.01952	1.027			
11	*Z_1, μ, RMS=*	175.99	25.625	161.007	1.01580	8.02394	1.029			
12			26.25	164.934	1.01659	8.02847	1.030			
13			26.875	168.861	1.01740	8.03312	1.032			
14			27.5	172.788	1.01823	8.03788	1.033			
15			28.125	176.715	1.01909	8.04276	1.035			
16			28.75	180.642	1.01996	8.04776	1.037			
17			29.375	184.569	1.02086	8.05288	1.038			
30			37.5	235.619	1.03441	8.13031	1.066			
31			38.125	239.546	1.03560	8.13713	1.068			
32			38.75	243.473	1.03682	8.14408	1.07		10	

Solver Parameters

Set Target Cell: $B$11

Equal To: ○ Max ● Min ○ Value of: 0

By Changing Cells:

$B$5:$B$6

Subject to the Constraints:

Figure 4.25. Spreadsheet showing Solver for calculation and optimising dynamic absorber

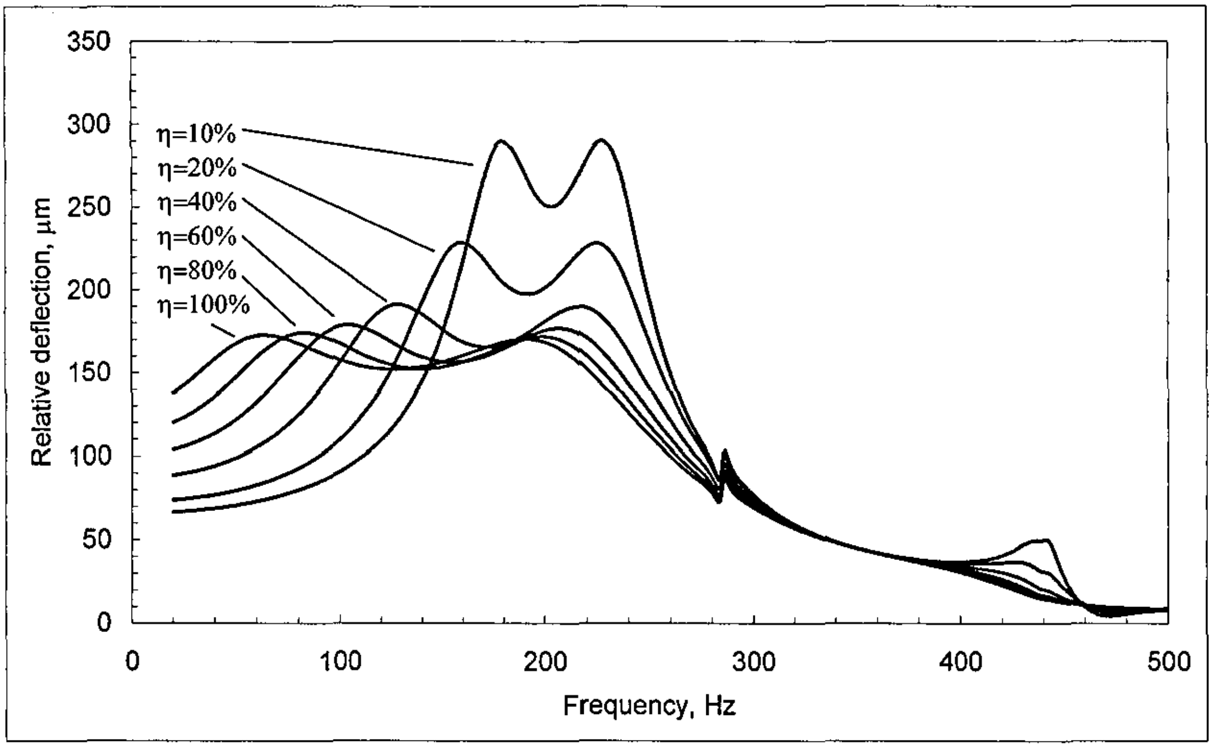

a) Swept-sine vibration

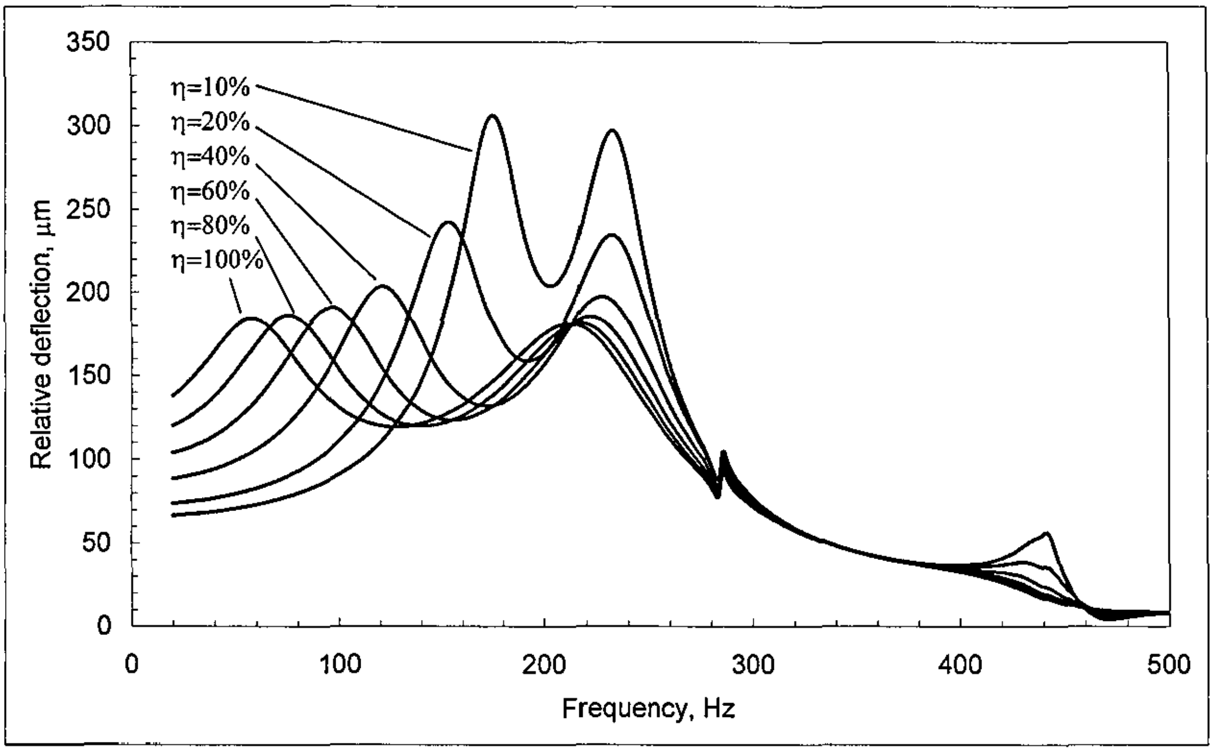

b) Swept-sine vibration

Figure 4.26. Dynamic response of ruggedized PCB at different mass ratios

Figure 4.26a highlights the relative deflection of the dynamically ruggedized PCB under swept-sine excitation where the dynamic absorber was optimised for the swept-sine excitation at different mass ratios. Again, in this figure the equal-peak response is shown at any mass ratio even the modal parameters of the PCB is not presented. This indicates the highly accuracy of MS®Excel Solver add-in for solving complex problem whereas the conventional approaches may prove to be impossible. Figure 4.23b shows the relative deflection of the dynamically ruggedized PCB under swept-sine excitation where the dynamic absorber was optimised for the wide-band random excitation at different mass ratios.

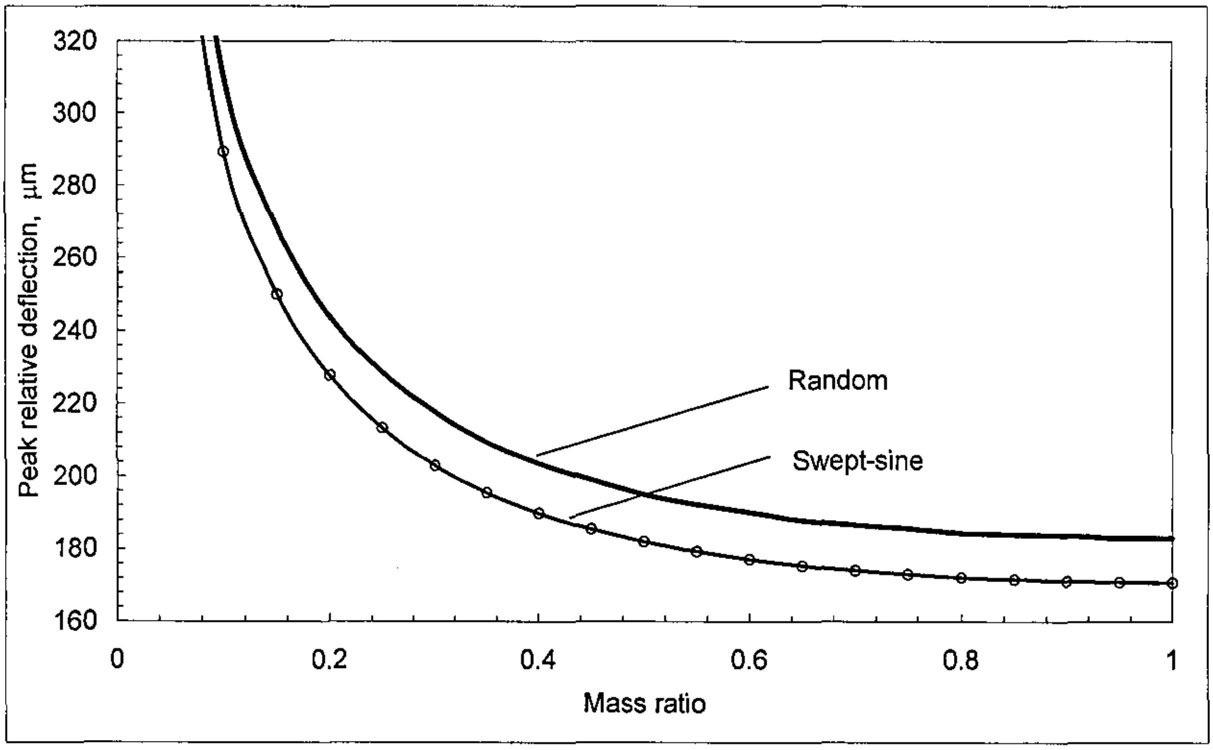

Figure 4.27. Peak relative deflection of the PCB at different mass ratios

Figure 4.27 shows the dependence of the minimised peak resonant response of the full-mode PCB in the swept-sine test on the mass ratio, where the dynamic absorber has been optimised for the swept-sine test (curve **Swept-sine**). For comparison, a similar dependence (curve **Random**) was obtained for the full-mode PCB with the dynamic absorber being optimised for the case of wide-band random excitation per Section 4.3.1. The departure obtained is reasonably small.

Since the information about the inertia properties of the PCB is already imbedded in the appropriate complex receptance, the effective mass is assumed to be 90 gr for reference purpose only. As a result of the optimisation procedure, it is also found that there is no optimal mass ratio.

From Figure 4.27, for the mass ratios greater than 65% ($\eta > 65\%$) the performance of the dynamic absorber could not be improved significantly. Hence, we can use a single design of dynamic absorber which suits practically equally well both cases of wide-band random and swept-sine excitation, where the optimal parameters of an dynamic absorber would be based on the results of Section 4.3.1, namely:

$$\eta = 65\%,\ \frac{\Omega_{2opt}}{2\pi} = 100\text{Hz and } \zeta_{2opt} = 0.40.$$

From Figure 4.27, the dynamic absorber with the above parameters yields the peak resonant deflection of the PCB to be 189 μm in the specified swept-sine test instead of 175 μm, as compared to the case when the dynamic absorber is especially optimised for the case of the swept-sine test. However, this difference is reasonably small.

Figure 4.28 shows the dependencies of the optimal natural frequency (a) and loss factor (b) of the dynamic absorber on mass ratio. In these figures, the corresponding curves reflecting the case of the dynamic absorber obtained for the case of random excitation are superimposed. It appears that the optimal natural frequency of the dynamic absorber is exactly the same for both types of excitations (see Figure 4.28a). However, the optimal loss factor is slightly different, as shown in Figure 4.28b.

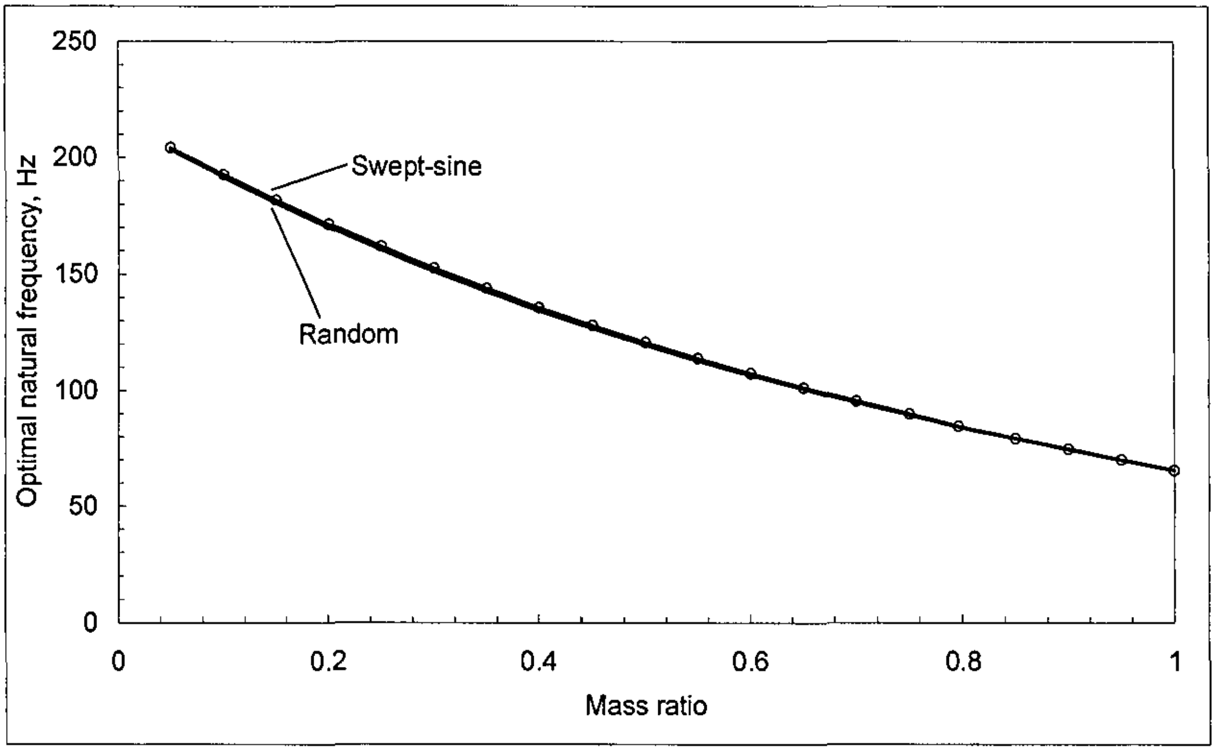

a) Optimal natural frequency of dynamic absorber at different mass ratios

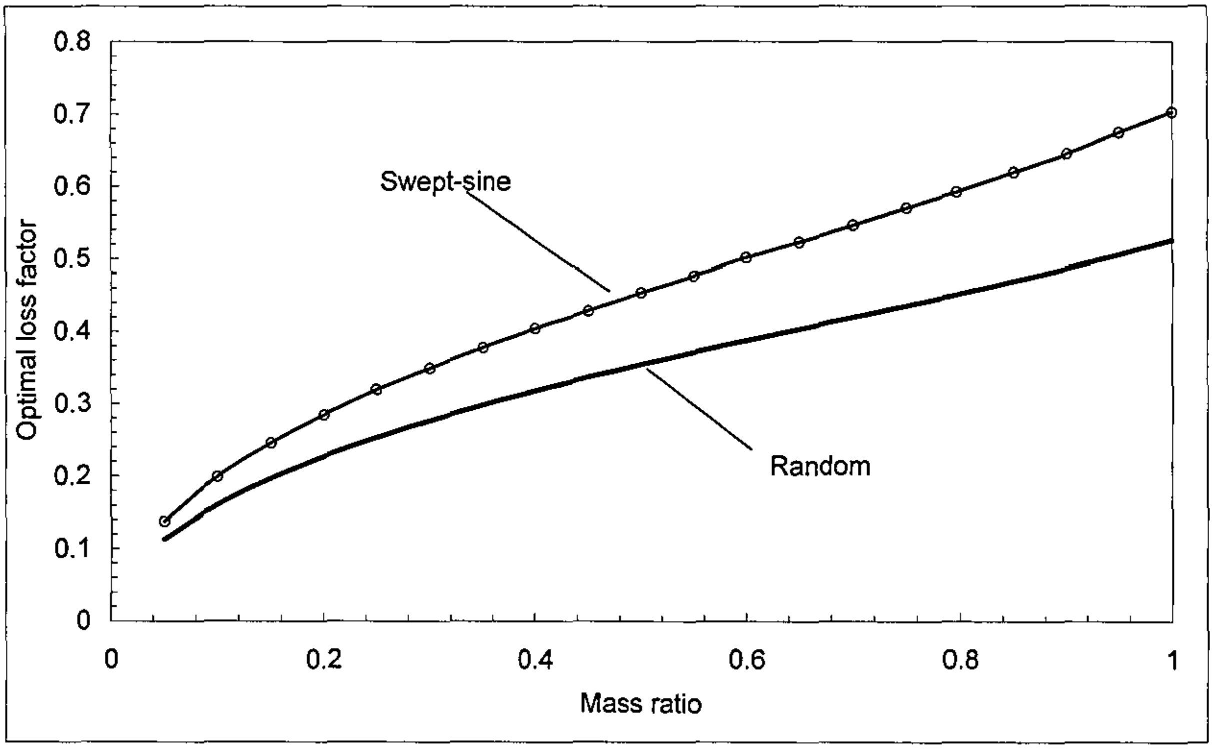

b) Optimal loss factor of dynamic absorber at different mass ratio

Figure 4.28. Optimal parameters of dynamic absorber at different mass ratios

From the above figures, a little difference in the performance of the dynamic absorber optimised for wide-band random and swept-sine vibration is found in the swept-sine test. Hence, the optimal dynamic absorber obtained from the optimal design random vibration would be fully adequate in swept-sine excitation.

4.3.2 Sensitivity analysis

The sensitivity analysis is carried out as in Section 4.2.2. For this purpose the mass ratios are fixed at values of 65% and 35%, respectively.

Figure 4.29a shows, where the loss factors are also fixed at their optimal values, 0.4 and 0.29 respectively where as their nature frequency varied from 50 to 200 Hz

Figure 4.29b shows the dependence of the peak resonant response on the value of the loss factor of the dynamic absorber in the range from 0 to 1, where the natural frequencies are fixed at their optimal values, 100 Hz and 144 Hz, respectively.

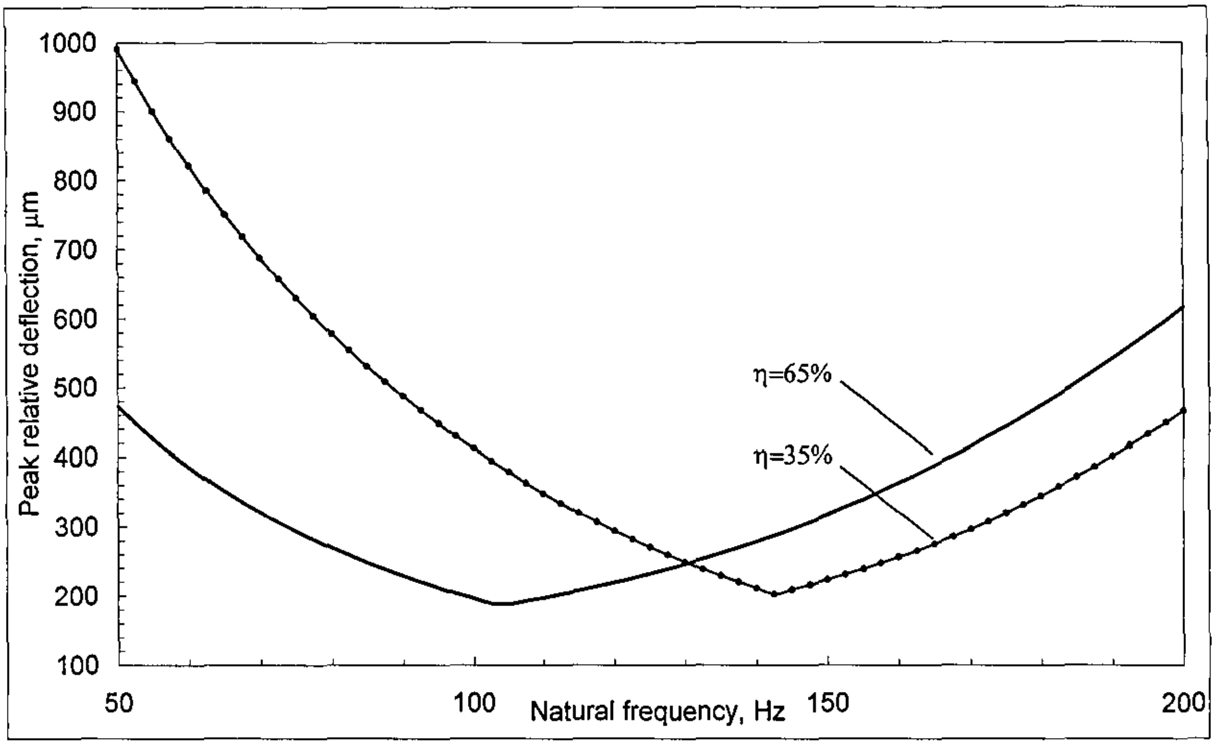

a) Peak relative deflection at different natural frequencies

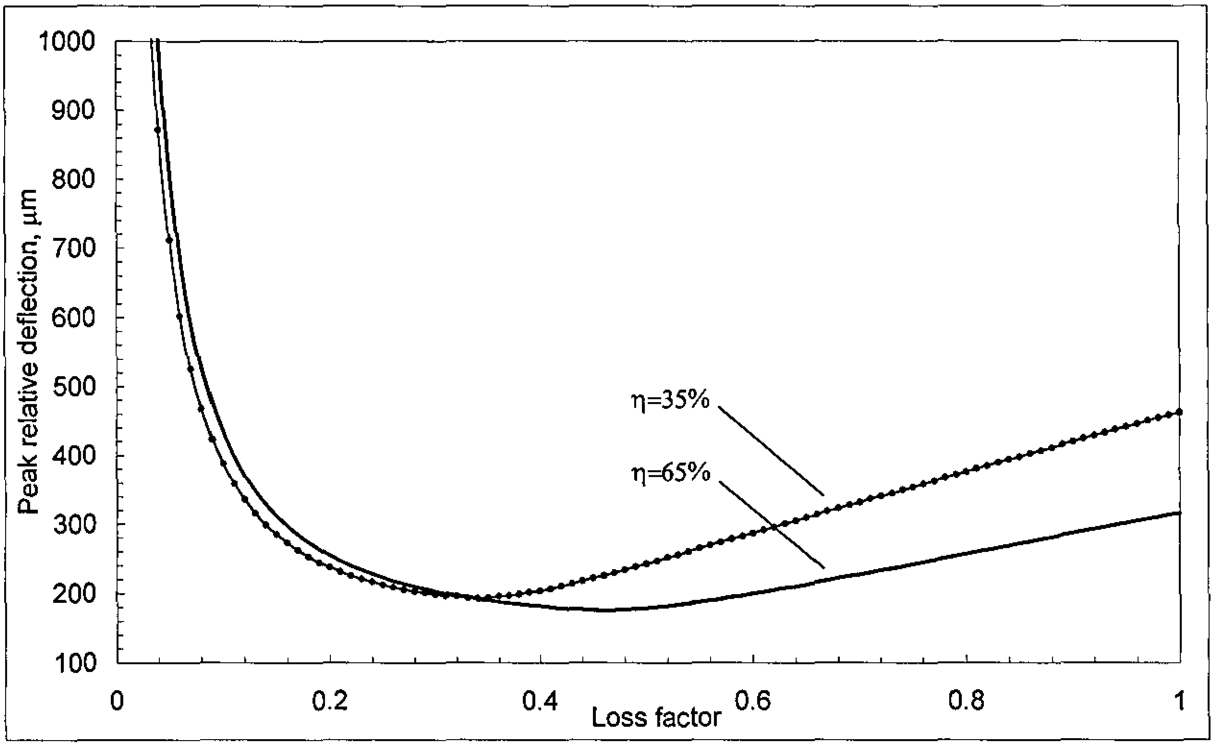

b) Peak relative deflection at different loss factors

Figure 4.29. Sensitivity analysis

From Figure 4.29, a small departure of the dynamic absorber's parameters from their optimal values has little impact on the overall performance.

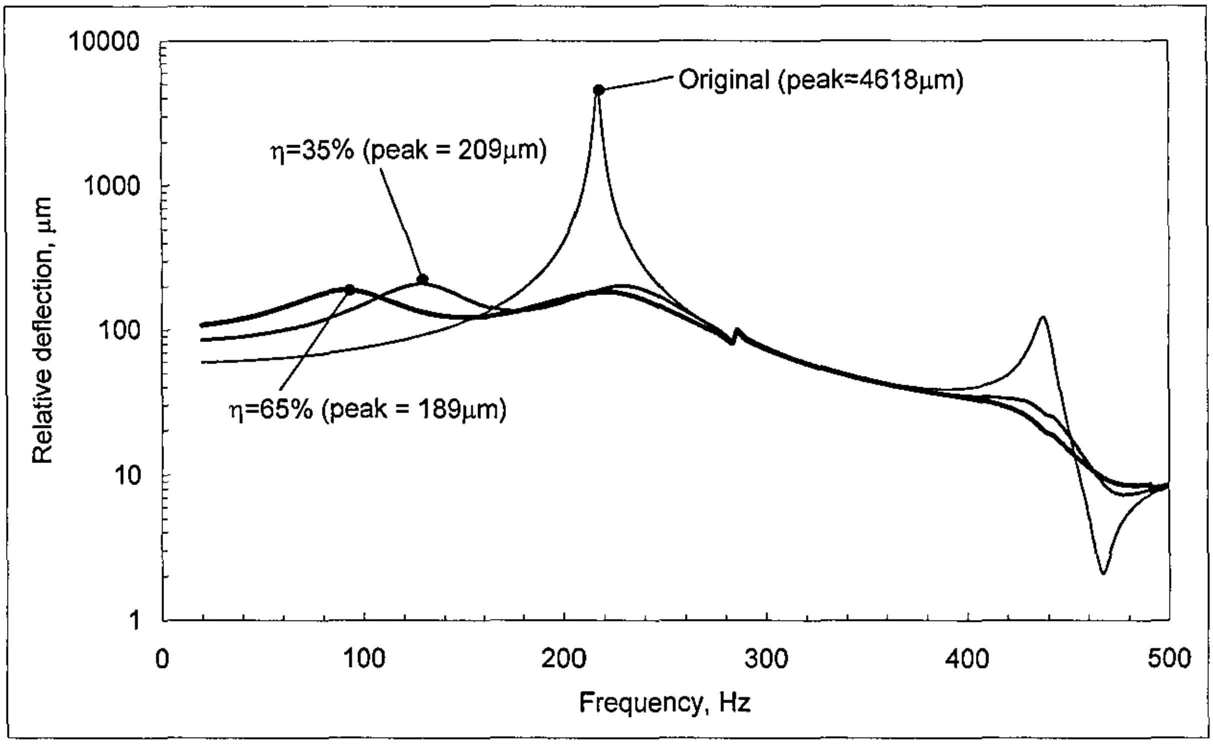

Figure 4.30. Dynamic response of original and ruggedized PCB

Figure 4.30 shows the dynamic responses of the original PCB (curve **Original**) and those for the dynamically ruggedized PCB under swept-sine test. The dynamic absorber with 35% mass ratio (curve labelled $\eta = 35\%$) yields the peak relative deflection of the PCB of 209 µm. The dynamic absorber with 65% mass ratio (curve labelled $\eta = 65\%$) yields the peak relative deflection of the PCB of 189 µm. Compared with the peak relative deflection of the original PCB (4617 µm), the suppression ratios are 23 and 24 respectively.

4.3.3 Numerical simulation

Similarly, numerical simulation is carried for the full-mode model of PCB. This gave a closer look at analytical and numerical design and definitely, the reliability of the global curve-fitting technique can be further justified. The Simulink model from Figure 4.16 is implemented with appropriate **Swept-sine** sub-system and **Statistics** sub-system to produce **FH** value of relative deflection and absolute acceleration of the PCB. Figure 4.28 shows the details of design of this numerical solution.

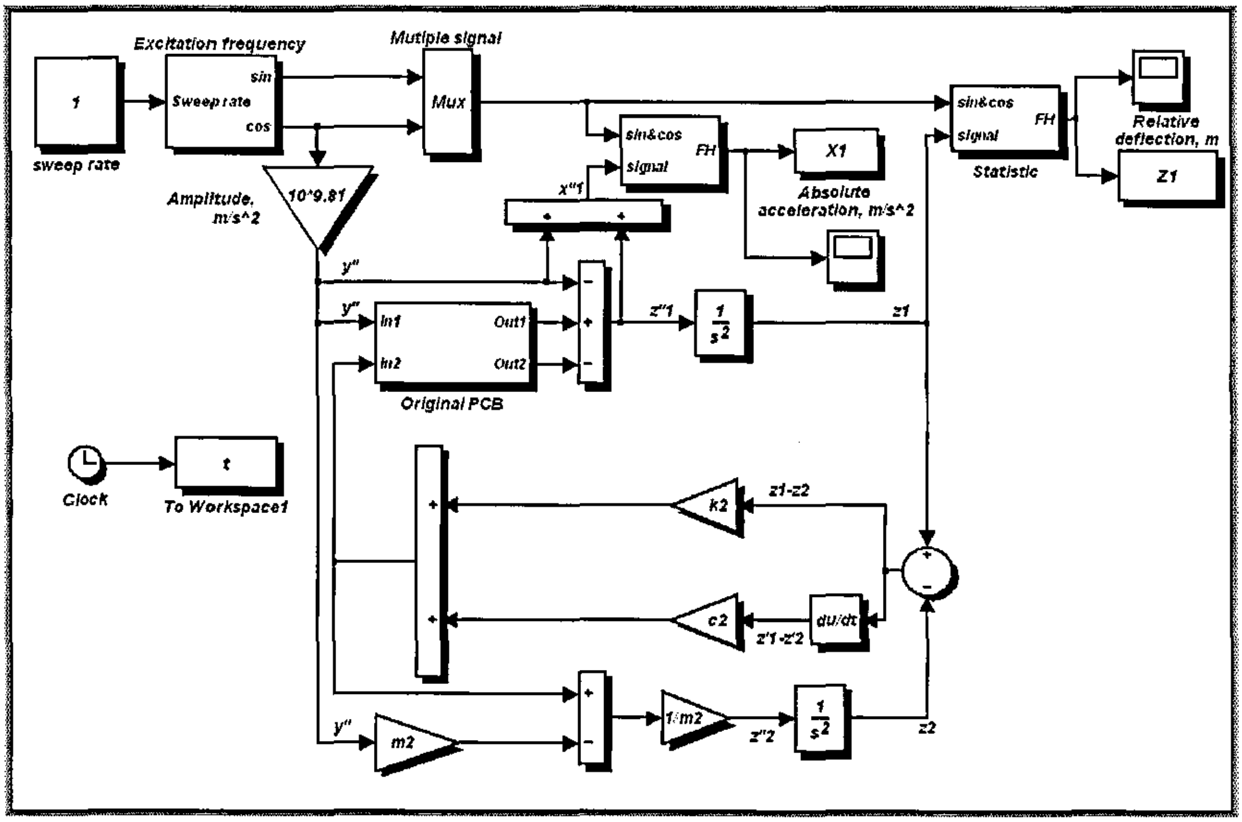
Excitation frequency
Mutiple signal
1
sweep rate
sin
Sweep rate
cos
Mux
Amplitude, m/s^2
10*9.81
sin&cos
signal
FH
X1
Absolute acceleration, m/s^2
x"1
y"
In1
In2
Out1
Out2
Original PCB
z"1
1/s^2
z1
sin&cos
signal
FH
Statistic
Relative deflection, m
Z1
Clock
t
To Workspace1
z1-z2
k2
c2
du/dt
z'1-z'2
m2
1/m2
z"2
1/s^2
z2

Figure 4.31. Simulink diagram for swept-sine excitation

For comparison purposes, the dynamic absorbers with their optimal parameters are chosen as:

$$\eta = 65\%,\ \frac{\Omega_{2opt}}{2\pi} = 100\text{Hz and } \zeta_{2_{opt}} = 0.40$$

and

$$\eta = 35\%\ \frac{\Omega_{2opt}}{2\pi} = 144\text{Hz and } \zeta_{2_{opt}} = 0.29,$$

which corresponds to 30% and 18% to the actual mass of the PCB (175.5 gr).

The constant sweep rate is still used to be 1 Hz/s and its amplitude is 10g, and all the necessary features of the integration procedure still remain the same for this numerical simulation. As a result of simulation, Figure 4.32 and 4.33 show the corresponding superimposed results of the original and ruggedized PCB (see appropriate label for reference).

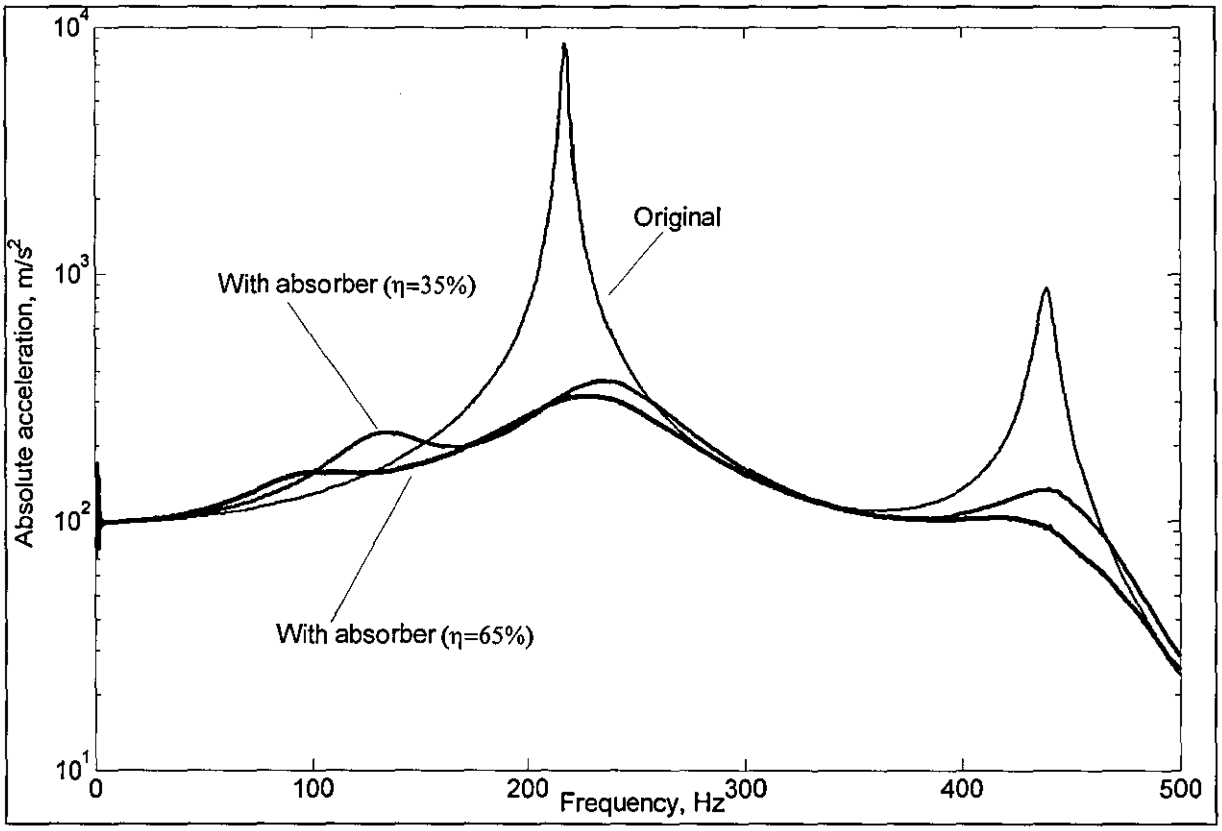

Figure 4.32. Simulated absolute acceleration of original and ruggedized PCB

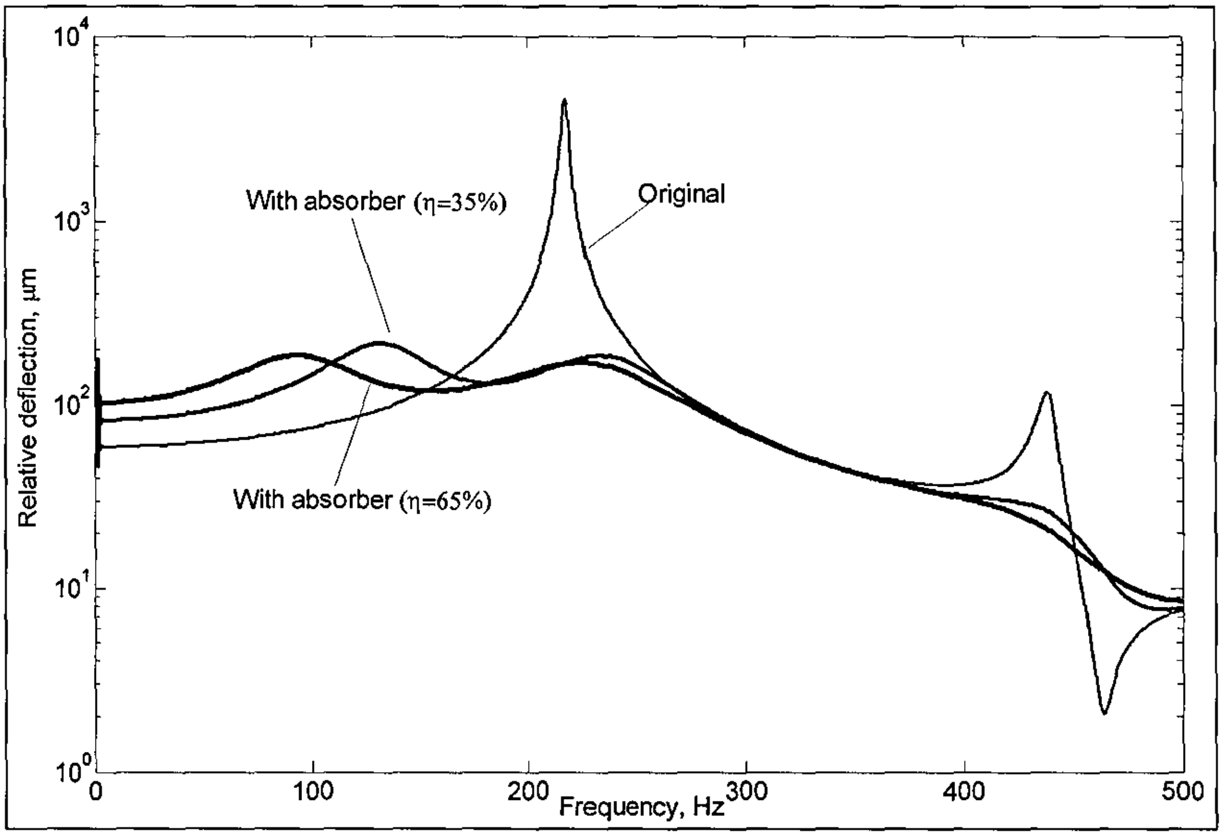

Figure 4.33. Simulated relative deflection of original and ruggedized PCB

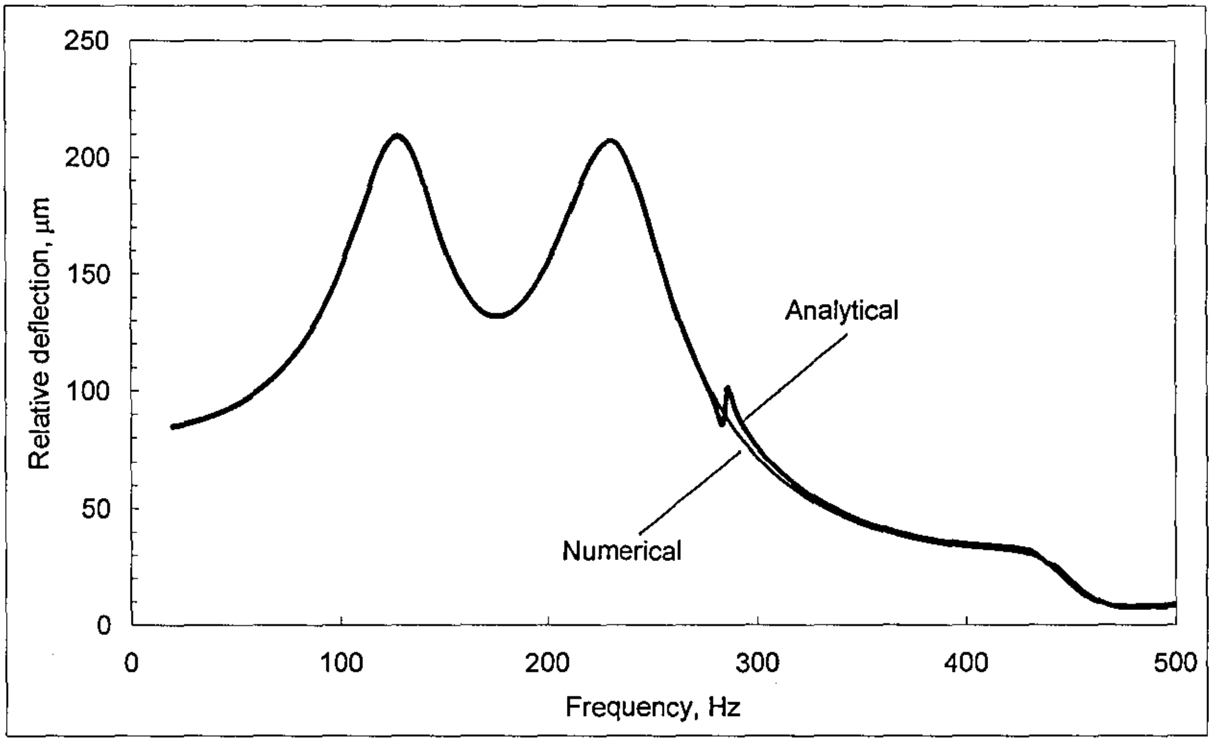

a) At 35% mass ratio

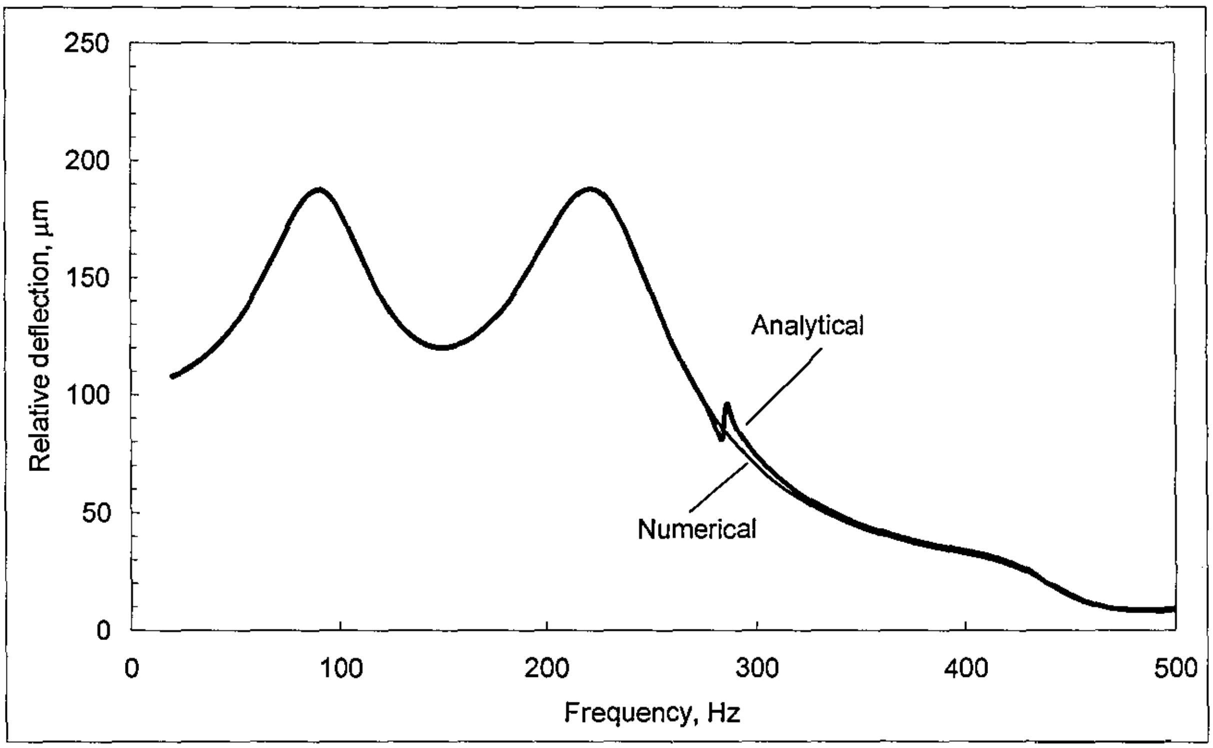

b) At 65% mass ratio

Figure 4.34. Comparison dynamic response of ruggedized PCB

The results of peak relative deflection or general dynamic response of swept-sine vibration between analytical and numerical simulation in general are identical (see Figure 4.34). However, using Simulink alone to design optimal parameters of dynamic absorber would be a laborious task. For this reason, first, we used the advantages of MS®Excel and its Solver to design the optimal parameters set of dynamic absorber before practising a numerical simulation. In reality, Simulink is still regarded as the most powerful tool to solve many dynamic systems because of its capability of handling complex and nonlinear systems. In addition, it does not require solving complex mathematics only a simple set of equations of motion of a dynamic system are required, in context it produces "perfect" results in both time and frequency domains. The evidence was clearly shown in all our linear vibration studies.

4.4 Shock

Since the full-mode model of PCB has been developed for numerical simulation, this section is proceeding further by studying the dynamic response of the PCB subjected to half-sine shock pulse at 200g @ 3ms. Additionally, the following dynamic absorbers designed for random vibration were implemented in order to see their influence on the PCB, they are:

$$\eta = 65\%,\ \frac{\Omega_{2opt}}{2\pi} = 100\text{Hz and } \zeta_{2opt} = 0.40$$

and

$$\eta = 35\%\ \frac{\Omega_{2opt}}{2\pi} = 144\text{Hz and } \zeta_{2opt} = 0.29$$

The simulation model is similar to that in Figure 4.16 with custom designed shock pulse being applied, Figure 4.35 shows detail of the model. In this numerical simulation, the primary concern is still peak absolute acceleration, settling time and overall relative deflection in time domain, therefore, all the necessary scope and workspace blocks are placed to capture the response signal.

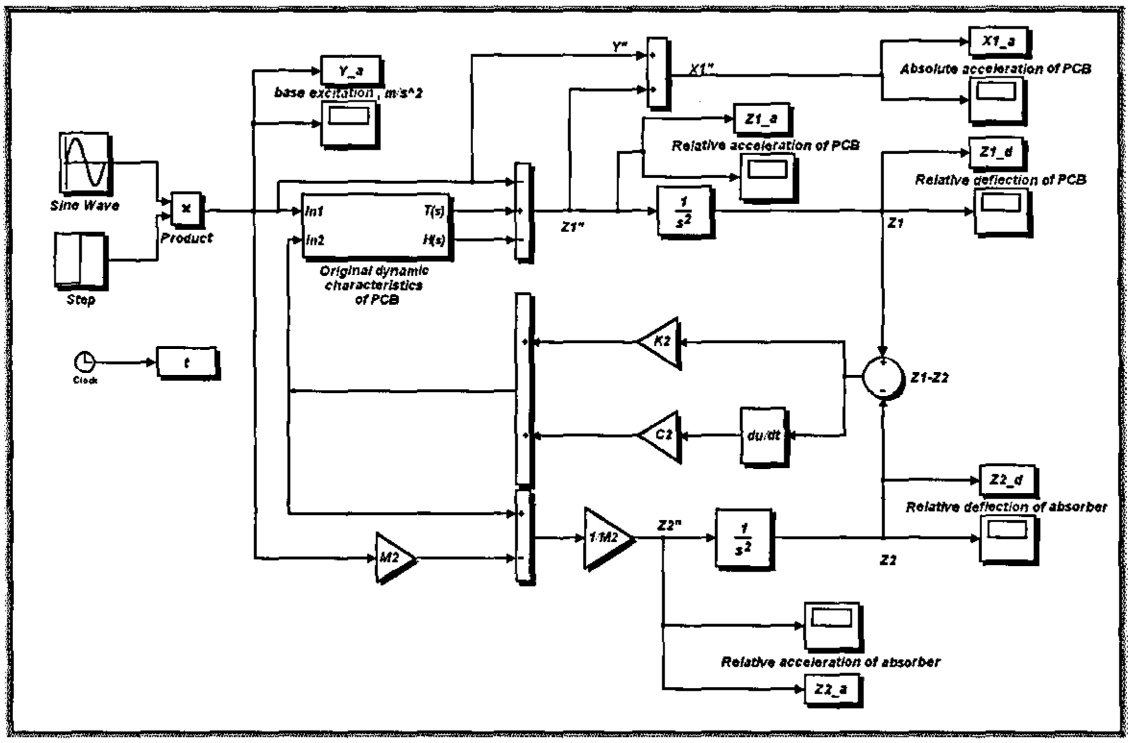
Y_a
base excitation , m/s^2
Sine Wave
Product
Step
Clock
t
In1
In2
T(s)
H(s)
Original dynamic characteristics of PCB
Y"
X1"
Z1"
1/s^2
Z1
X1_a
Absolute acceleration of PCB
Z1_a
Relative acceleration of PCB
Z1_d
Relative deflection of PCB
K2
C2
du/dt
Z1-Z2
Z2_d
Relative deflection of absorber
M2
1/M2
Z2"
1/s^2
Z2
Relative acceleration of absorber
Z2_a

Figure 4.35. Simulink diagram for shock excitation

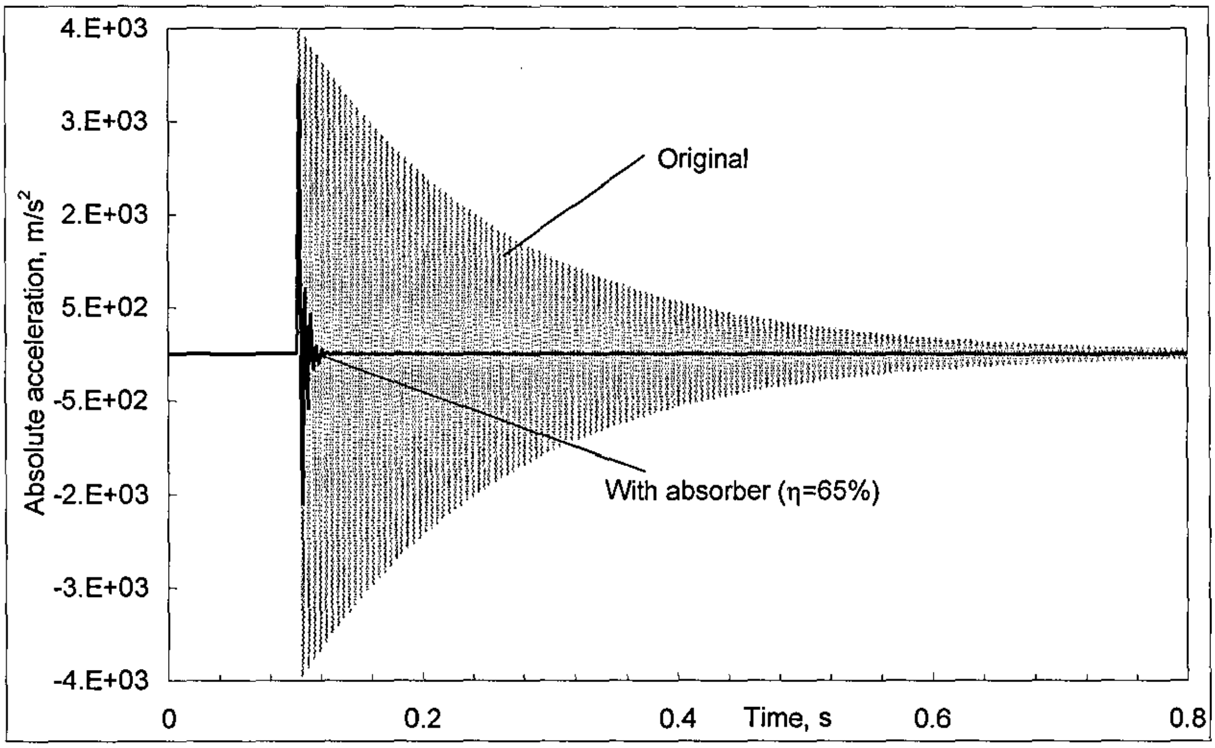

a) Absolute acceleration

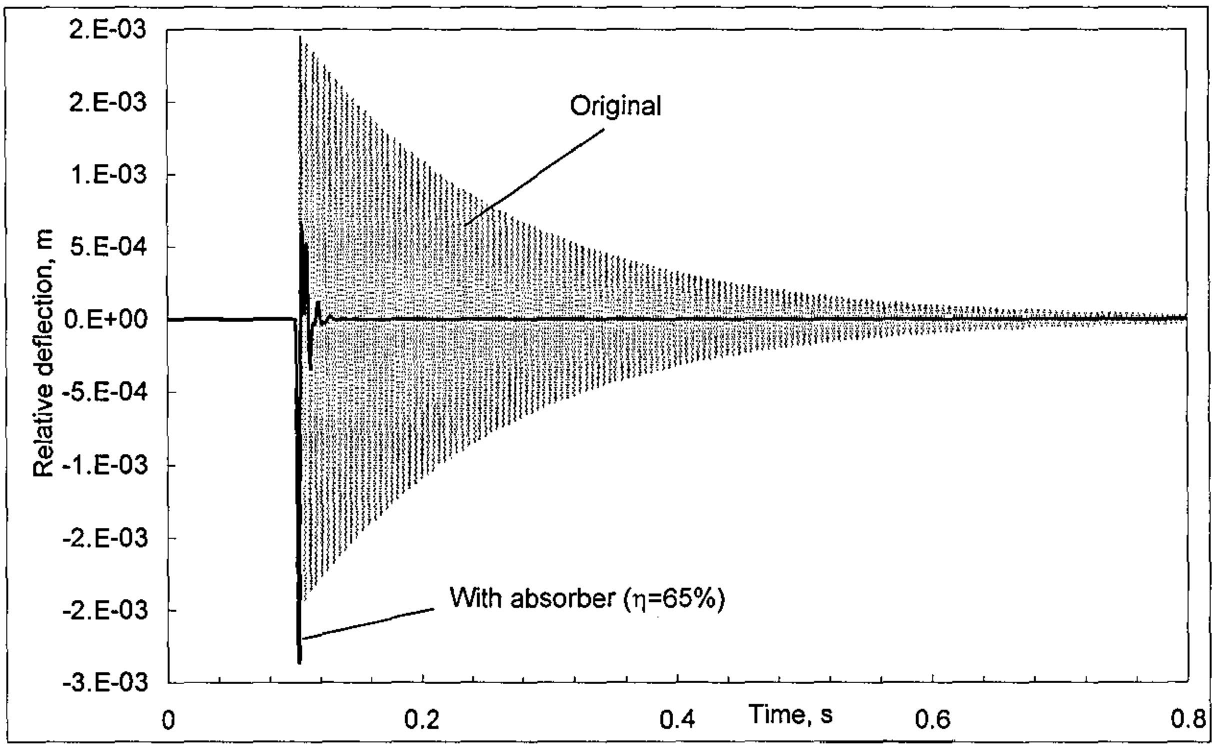

b) Relative deflection

Figure 4.36. Shock response of original and ruggedized PCB (65%mass ratio)

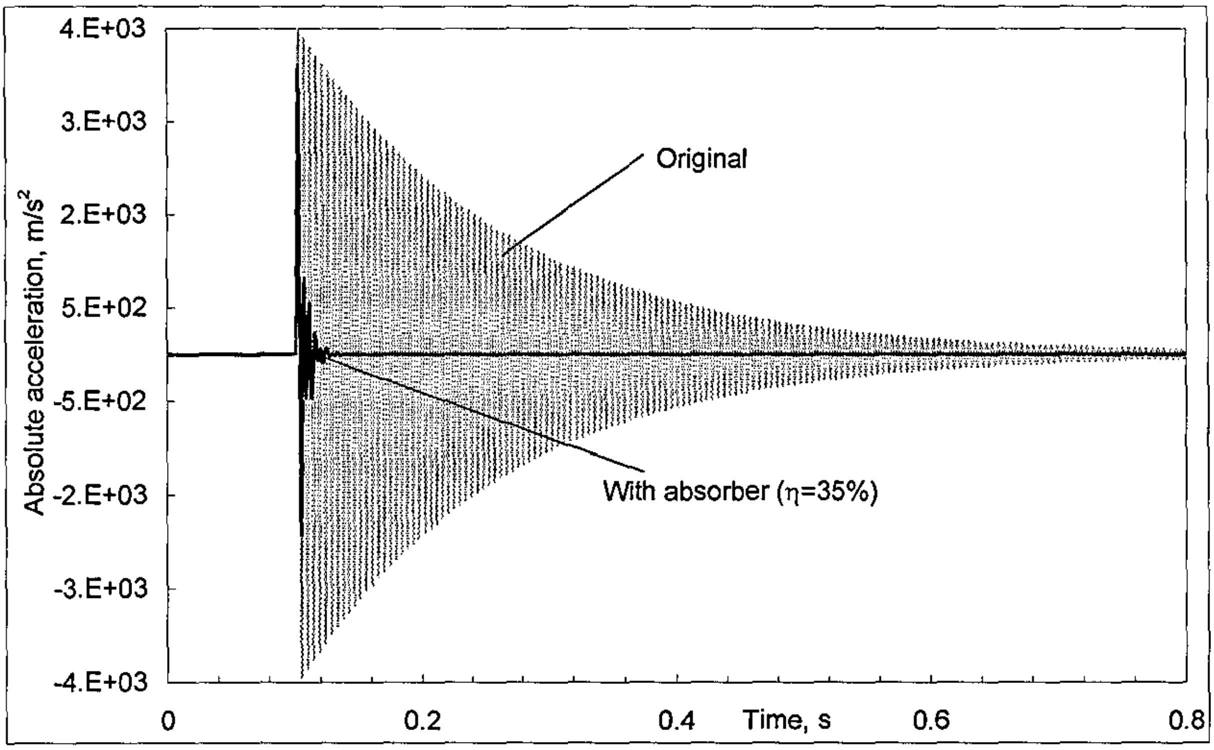

a) Absolute acceleration

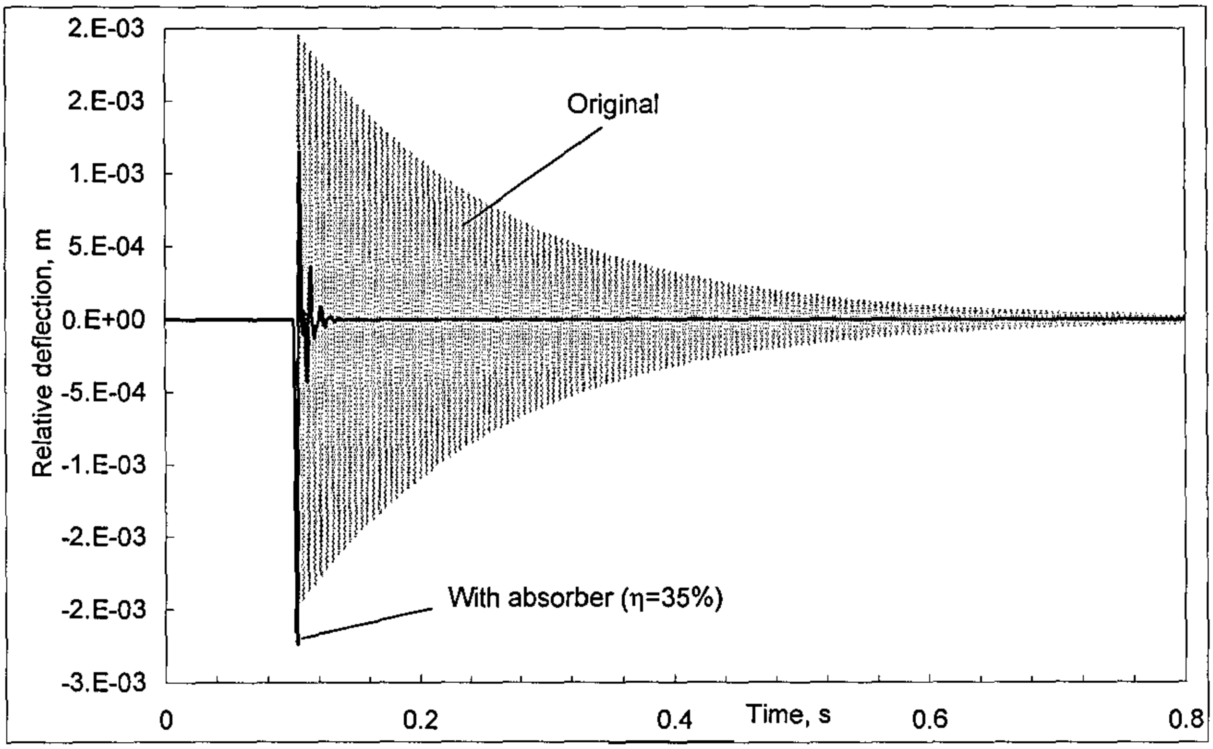

b) Relative deflection

Figure 4.37. Shock response of original and ruggedized PCB (35% mass ratio)

As a result of simulation, the dynamic behaviour of the full-mode PCB without or with optimal dynamic absorbers subjected to shock is almost similar to single-mode PCB (see Figure 3.34 and 3.35). The influence of optimal dynamic absorbers in this design still have a great impact on suppressing the vibration of the PCB in a shock environment.

4.5 Concluding remarks

- A new method has been developed for all point measurements on the full-mode PCB with the dynamic absorber based on measured FRFs. The optimising procedure was carried out using MS®Excel and its Solver which produced an optimal mass, 58.5 gr of dynamic absorber whereas the actual mass of the PCB is 175.5 gr which gives 30% mass ratio.
- For convenience, the effective mass of the PCB is assumed to be 90 gr which gives 65%, the same mass ratio compared to single-mode PCB design with a slight difference in optimal natural frequency and loss factor.
- The influence of this optimal dynamic absorber design shows all the locations of the PCB very close to their optimal response condition.
- The optimal dynamic absorber chosen for random vibration is again suitable for vibration suppression of PCB under sine vibration and shock.
- Sensitivity analysis was carried out corresponding to its optimal values. It shows that a small variation of dynamic absorber had a little effect on optimal dynamic absorber design. This means that under any operation conditions or qualification tests, the dynamic absorber would be one of the best candidates providing fail-safe vibration control of the PCB and was very simple to design.
- A numerical solution was developed to back up its analytical prediction even though it was an excessive work. However, the unique characteristics of the numerical model based on the actual dynamic properties of the PCB opens new opportunities for nonlinear analysis of MODF system where the traditional approach might not be possible.

Chapter 5

5.0 Impact dynamic absorber

In this section we consider an application of strongly nonlinear – vibroimpact – dynamic absorber for the close control of dynamic response of the PCB under the action of different environmental excitations, namely: wide-band random vibration, swept sine vibration and shock.

The behaviour of impact dynamic absorber is complex in nature. Using this technique to design an optimal performance for the PCB one must consider the critical parameters: restitution ratio, types of impacting (symmetrical or asymmetrical) and clearance. Furthermore, the degree of sensitivity will be involved on a number of linear parameters that introduced into the system despite the fact there is being problems in designing a real device and testing it. From this reason, the study of impact dynamic absorber will be considered of a loosened mass placed in a container which is then mounted upon the structure under treatment. The goals of the following analysis are:

- Development of numerical approaches for optimal design of the vibroimpact dynamic absorber to suppress the dynamic response of the above PCB
- Comparison of attainable performance delivered by the vibroimpact absorber with that delivered by the linear dynamic absorber considered above
- Manufacturing and experimental testing of the optimal vibroimpact dynamic absorber.

The numerical analysis will be based on the realistic model of visco-elastic impact developed in [20] and carried out in the Matlab/Simulink environment where the PCB will be represented using the above single-mode and full-mode approximations.

5.1 Modelling of visco-elastic impact

The mostly used model of vibroimpact interaction relies on the theory of momentary impact where the restitution ratio reflects the energy losses associated with impact. This approach, however, produces an infinite value for impact force and acceleration in the instance of collision and, therefore, is hardly applicable for numerical simulations. As an alternative, the experimentally proven [20] model of non-momentary visco-elastic impact is the most adequate choice for a systematically and computationally efficient way of determining the impact force and peak acceleration when the system comes in to contact with a stop or stops.

The model of a symmetrical impact shown in Figure 5.0 consists of a free mass, *m*. The movement of the mass is limited by the symmetrical visco-elastic stop which models schematically as parallel combination of spring, *K* and dashpot, *C* at a distance *Δ* from static equilibrium.

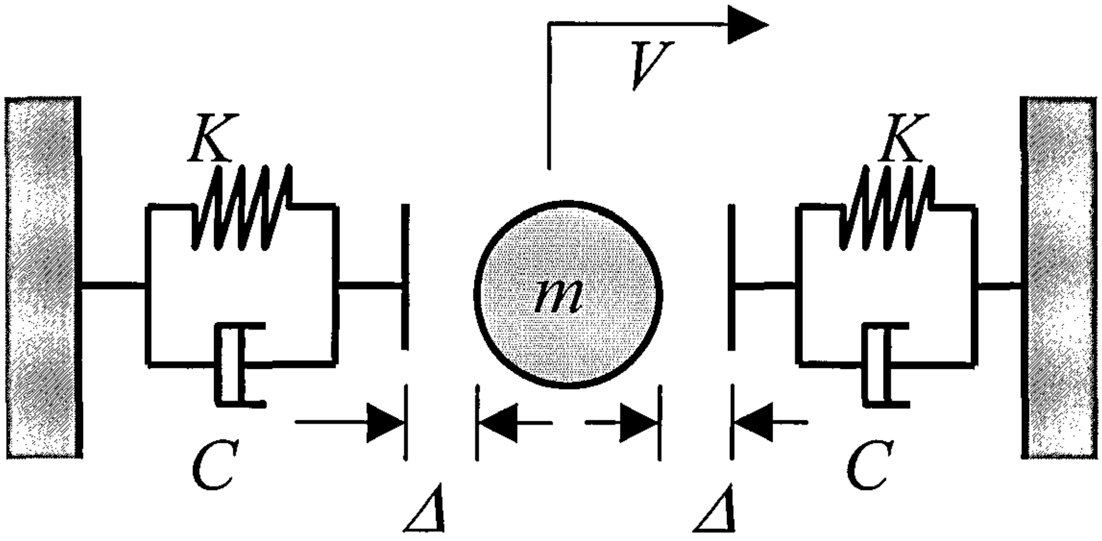

Figure 5.0. Dynamic model of visco-elastic impact

The equation of motion takes the form:

$$m\ddot{x} + \Phi(\dot{x}, x) = 0 \tag{5.0}$$

where $\Phi(\dot{x}, x)$ is threshold-type force of impact [20]:

$$\Phi(\dot{x}, x) = \begin{Bmatrix} C\dot{x} + K(|x| - \Delta) & \text{if} & |x| \geq \Delta & \text{and} & \Phi(\dot{x}, x) > 0 \\ 0 & \text{if} & |x| \geq \Delta & \text{and} & \Phi(\dot{x}, x) < 0 \\ 0 & \text{if} & & |x| \leq \Delta & \end{Bmatrix} \tag{5.1}$$

In accordance with equation of motion (5.0), the Simulink block diagram will be as shown in Figure 5.1. The lower loops on the grey background are details of the logical operation of the function, $\Phi(\dot{x}, x)$ per (5.1). The upper and lower limit of the **Dead Zone** block is set at clearance, Δ. The **Relational Operator** block produces unity if the displacement and impact force are of the same sign and null otherwise.

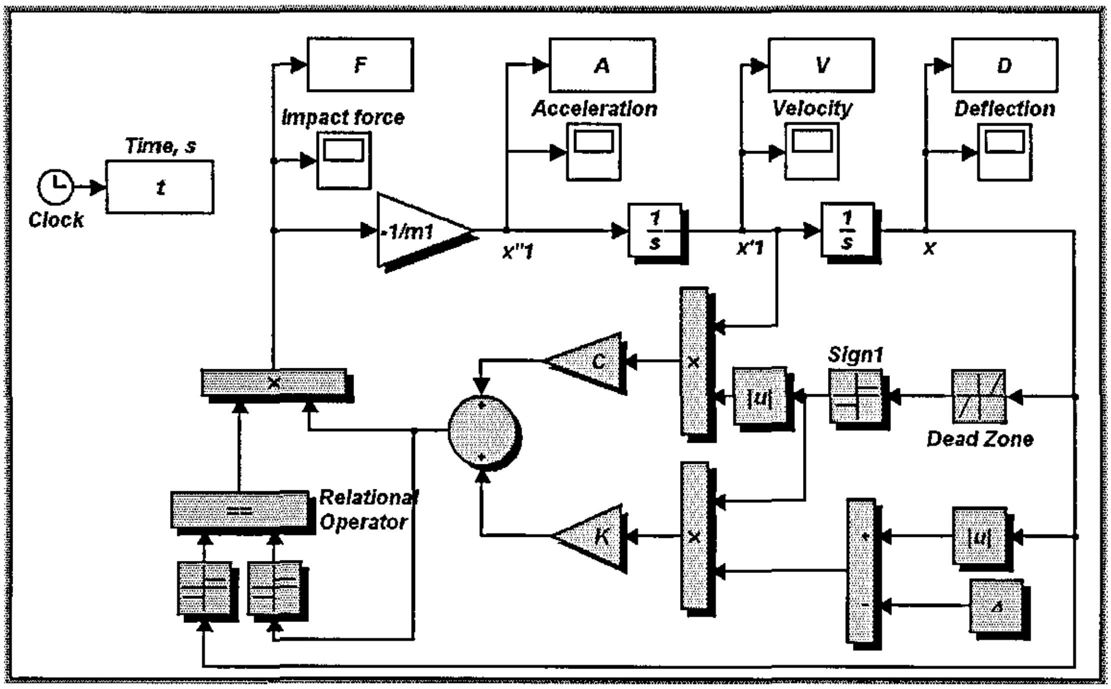
F
Impact force
A
Acceleration
V
Velocity
D
Deflection
Time, s
t
Clock
-1/m1
x''1
1/s
x'1
1/s
x
×
C
×
|u|
Sign1
Dead Zone
Relational Operator
==
K
×
|u|
Δ

Figure 5.1. Simulink model of visco-elastic impact

Here, the stiffness, K and damping, C of the visco-elastic stop are expressed in terms of their apparent loss factor ξ and natural frequency Ω in conjunction with the free moving mass, m (i.e. $K = m\Omega^2$ and $C = 2m\Omega\xi$).

For numerical purposes, the natural frequency, $\Omega / 2\pi$ =80 Hz and loss factor, $\xi = 0.2$ of the symmetrical stops were used. The mass, $m = 0.05$ kg is excited by the initial velocity, $V = 10$ m/s and limited by the stops at $\Delta = 0.02$ mm from the position of static equilibrium.

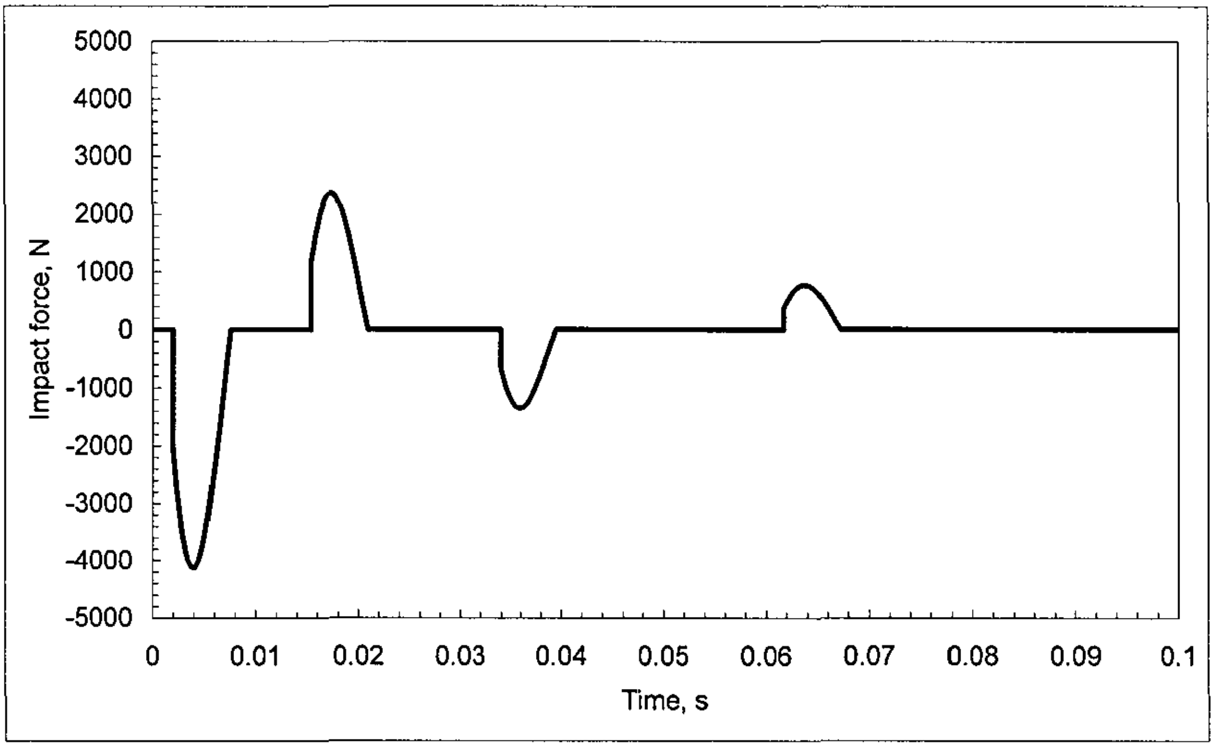

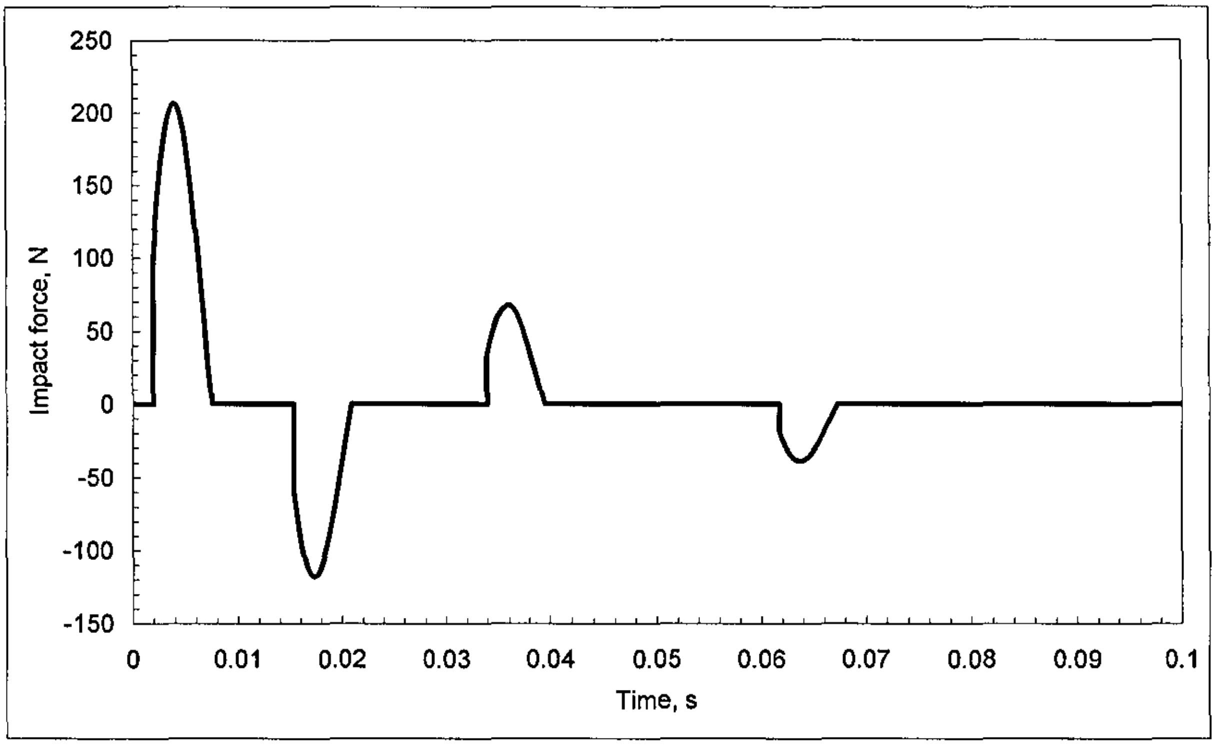

a) Impact force and acceleration

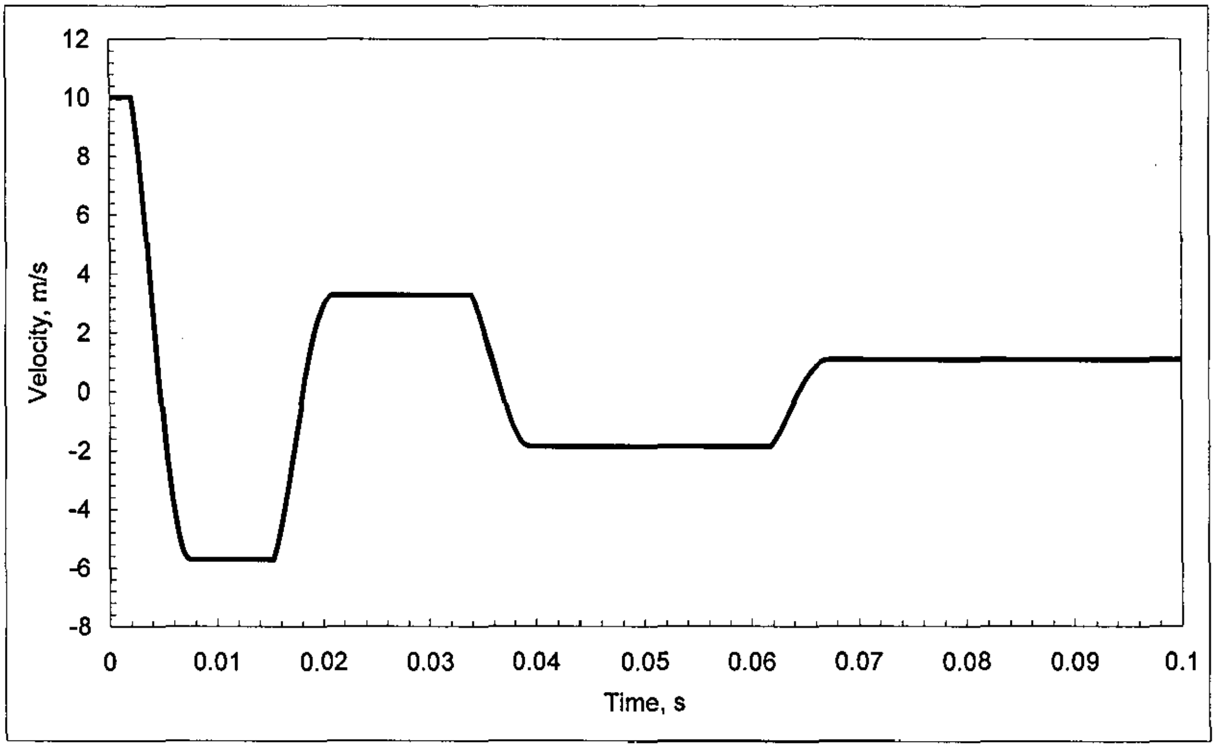

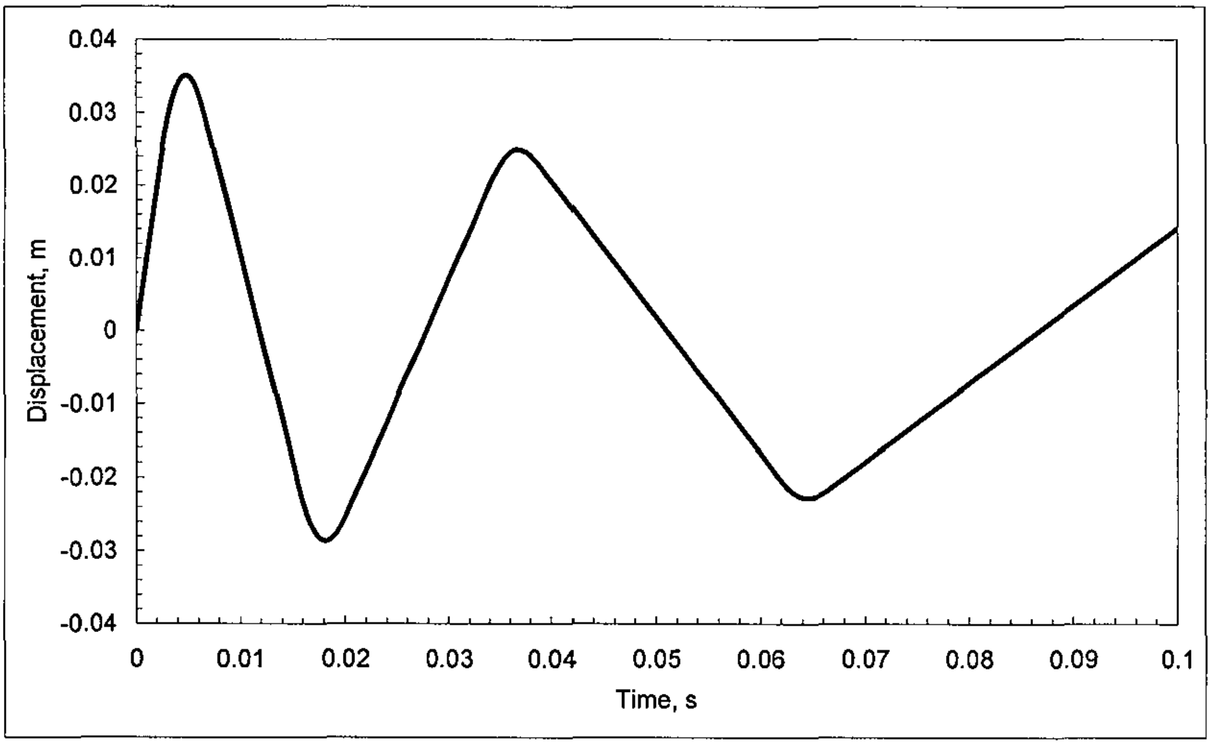

b) Velocity and displacement

Figure 5.2. Time histories of visco-elastic impact

Figure 5.2a shows the time histories of impact force and acceleration of visco-elastic impact, whereas Figure 5.2b shows the corresponding velocity and displacement of the free moving mass. The response shape of the impact force is strongly dominated by the amount of damping in visco-elastic stop, it can be very sharp when heavily damped bumper is used or it can be symmetrical with undamped one. In general, the amount of energy lost during collision would be associated with the damping of the stop.

The above simulation highlights one of the possible types of impact force that would be used in nonlinear vibration suppression of the PCB. The technique of obtaining such useful information is based on the equation of motion, condition of impact and computational resources. The impact force subsystem can be systematically implemented for studying the nonlinear vibration suppression of the PCB.

5.2 Random Vibration

5.2.1 Dynamics of PCB in a |SDOF approximation with impact damper

For simplicity of analysis, Figure 5.3 shows the model of the primary PCB represented as a mass-spring-dashpot (m_1, k_1, c_1) SDOF combination. The impact dynamic absorber is a secondary mass which is unsupported by either a spring or damper, formally known as impact damper. The relative motion of the above two bodies is limited by symmetrical visco-elastic limiter which is modelled as parallel combination of linear spring, K and the dashpot, C at a distance Δ. In Figure 5.3, x_1, x_2 and y are the absolute deflections of the PCB, impact damper and the base, respectively. The system is subjected to base-induced vibration in which z_1 and z_2 are the motion of the PCB and the impact damper relative to the base, respectively. This arrangement could transform the impact damper response to a linear dynamic absorber if the gap is closed, the analytical solution can be obtained directly using a traditional method for either random or swept-sine excitation.

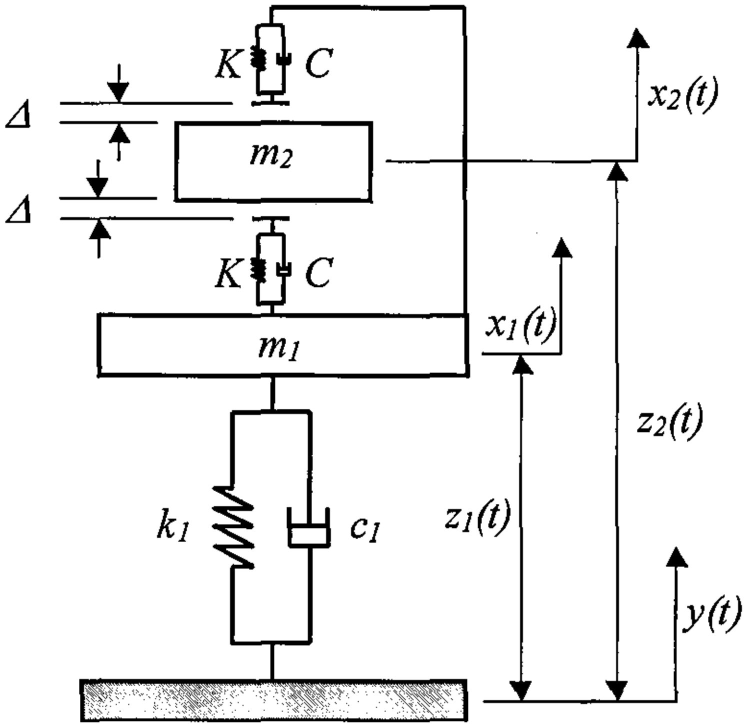

Figure 5.3. Mathematical model of impact damper

The equations of motion which account for the collision take the form:

for the primary sub-system

$$m_1\ddot{z}_1 + c_1\dot{z}_1 + k_1 z_1 + \Phi(\dot{z}_r, z_r) = -m_1\ddot{y}, \tag{5.2}$$

and for the secondary sub-system.

$$m_2\ddot{z}_2 - \Phi(\dot{z}_r, z_r) = -m_2\ddot{y}. \tag{5.3}$$

The symmetrical impact force takes the form:

$$\Phi(\dot{z}_r, z_r) = \left\{\begin{array}{ccc} C\dot{z}_r + K(|z_r| - \Delta) & \text{if} & |z_r| \geq \Delta \quad \text{and} \quad \Phi(\dot{z}_r, z_r) > 0 \\ 0 & \text{if} & |z_r| \geq \Delta \quad \text{and} \quad \Phi(\dot{z}_r, z_r) < 0 \\ 0 & \text{if} & |z_r| \leq \Delta \end{array}\right\}. \tag{5.4}$$

The presence of the symmetrical impact force function in the 2DOF system does not allow a general method of attack. Exact solutions can be found only in a few simple cases under specified excitation [30]. As an alternative, Matlab/Simulink has lead to new methods for solving this problem. A numerical simulation technique by use of Simulink's library is very powerful in analysing and designing nonlinear dynamic systems. It is possible to handle rather complicated nonlinear systems in a reasonable amount of time. Where the complexity of a system precludes the use of any analytical approach, typically under random vibration excitation, Simulink may prove to be the most advantageous in obtaining the necessary information for design purposes.

The Simulink model shown in Figure 5.4 is built identical to that in Figure 3.13 of Section 3.2.4 with an extra feature of **Impact Force** sub-systems to represent the vibroimpact model as shown in Figure 5.5. It contains the diagram for simulation in which it transforms the relative velocity (input ①) and relative displacement (input ②) between the primary and the secondary systems into the impact force (output ①). It only operates when the relative deflection between masses exceeds clearance, where in this diagram, the upper and lower limit of the **Dead Zone** block subsystem is set as Δ. These sub-systems reflect on Equation 5.4

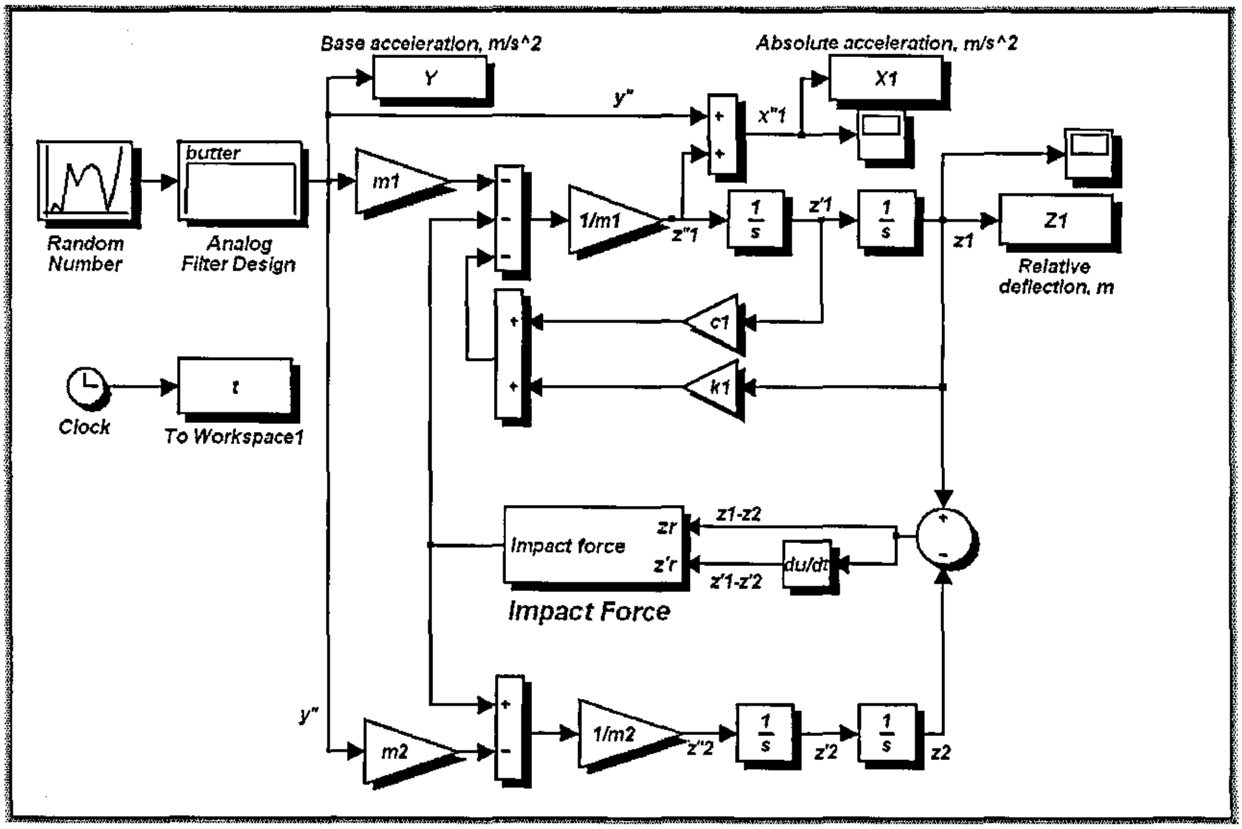
Base acceleration, m/s^2
Y
Absolute acceleration, m/s^2
X1
y"
x"1
butter
Random Number
Analog Filter Design
m1
1/m1
z"1
1/s
z'1
z1
Z1
Relative deflection, m
c1
k1
Clock
t
To Workspace1
Impact force
zr
z'r
z1-z2
z'1-z'2
du/dt
Impact Force
y"
m2
1/m2
z"2
z'2
z2

Figure 5.4. Simulink diagram for studying impact damper (single-mode model PCB)

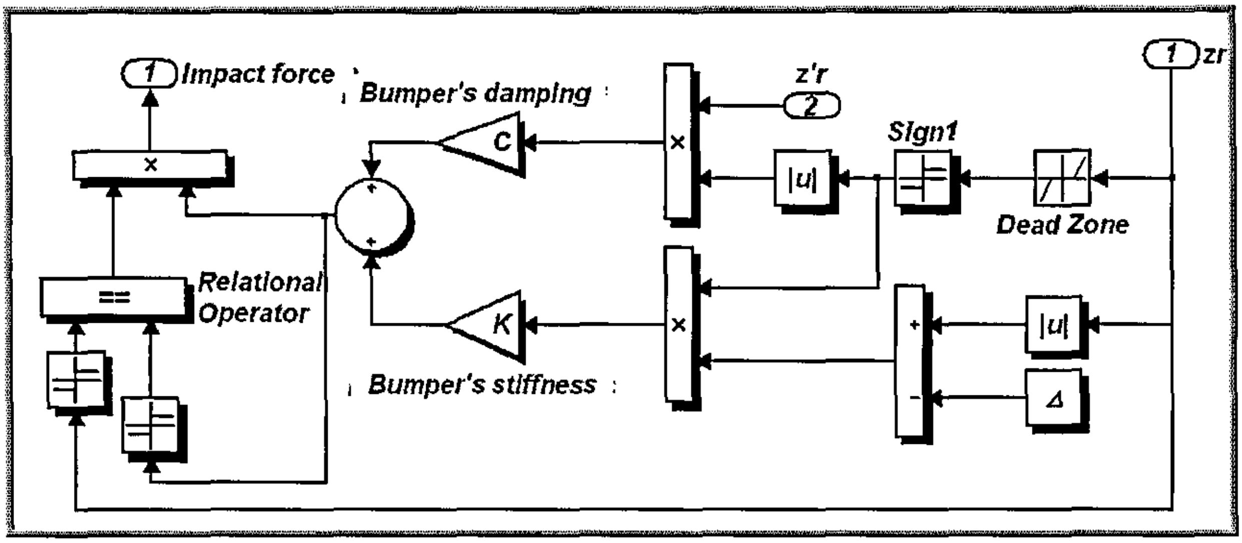
1
Impact force
Bumper's damping
C
×
z'r
2
Sign1
1
zr
|u|
Dead Zone
Relational
Operator
==
×
K
×
+
+
+
-
|u|
Δ
Bumper's stiffness

Figure 5.5. Impact force subsystem

An impact damper is conceptually a relative simple device. However, the behaviour of the impact damper is highly nonlinear and energy dissipation is derived from the shape of impact force (peak value and impact duration), a combination of loss factor and stiffness of the visco-elastic limiter. Such a contact force can be seen in Figure 5.6. It seems that the numerical simulation based on the theory of visco-elastic impact is the most adequate choice of producing such a peak value of impact force and absolute acceleration whereas the numerical simulation base on momentary impact these peak values are infinite when collisions occur. It should be noted that the peak of contact force could be infinite if a very high stiffness value of visco-elastic limiter were introduced. This configuration is likely to contribute to a higher noise level.

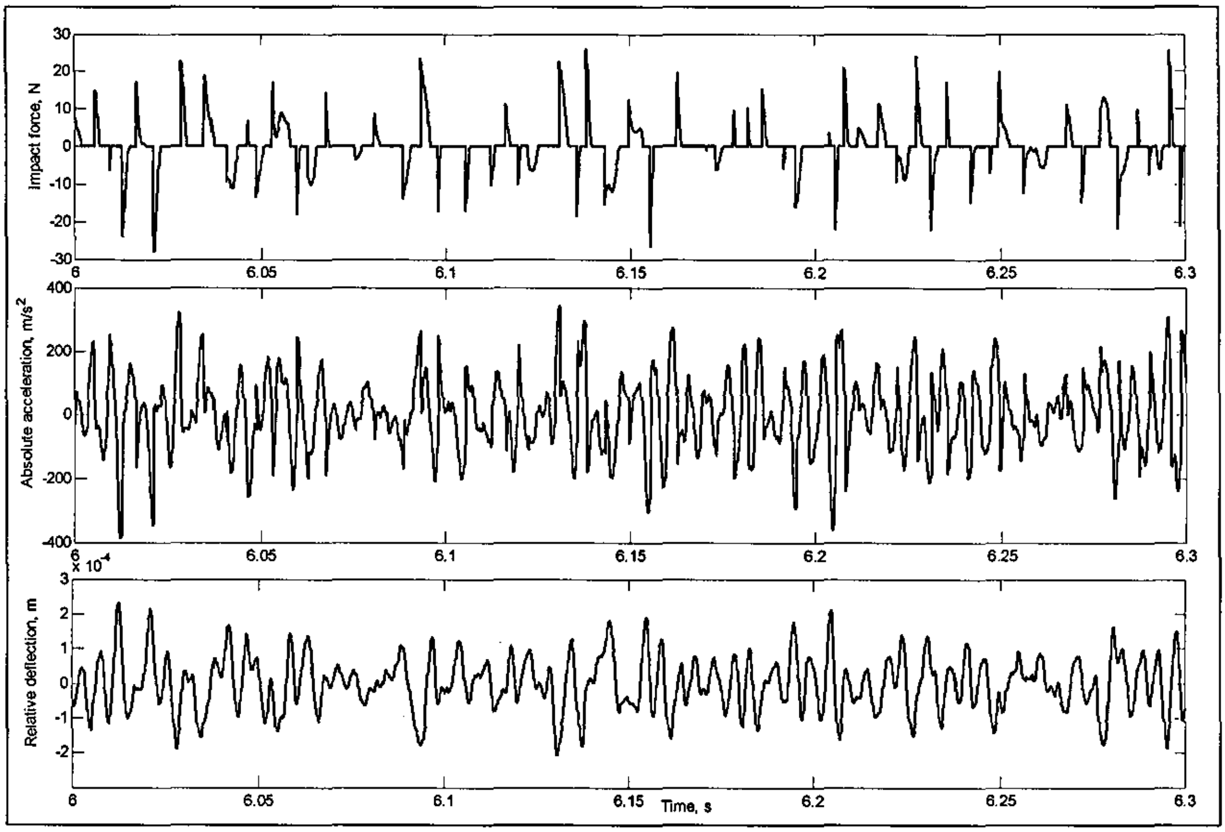

Figure 5.6. Time history of impact damper under random vibration excitation

5.2.2 Minimising the overall relative deflection of the PCB

Under random vibration the overall relative deflection response is of primary concern, an optimal design would involve many possible combinations of the secondary mass m_2, the visco-elastic limiter's parameters (Ω and ξ) and clearance Δ. Therefore, a Matlab m-file is written to run the above simulation model for all the possible combinations of these variables under restricted limits. These are:

Mass ratio of impact damper: $\frac{m_2}{m_1} \in [0,1]$

Visco-elastic limiter: $\frac{\Omega}{2\pi} \in [0,5000]Hz, \quad \xi \in [0,1],$

Clearance: $\Delta \in [0,1]mm.$

For each simulation run, these values are collected along with overall relative deflection using the **var** command.

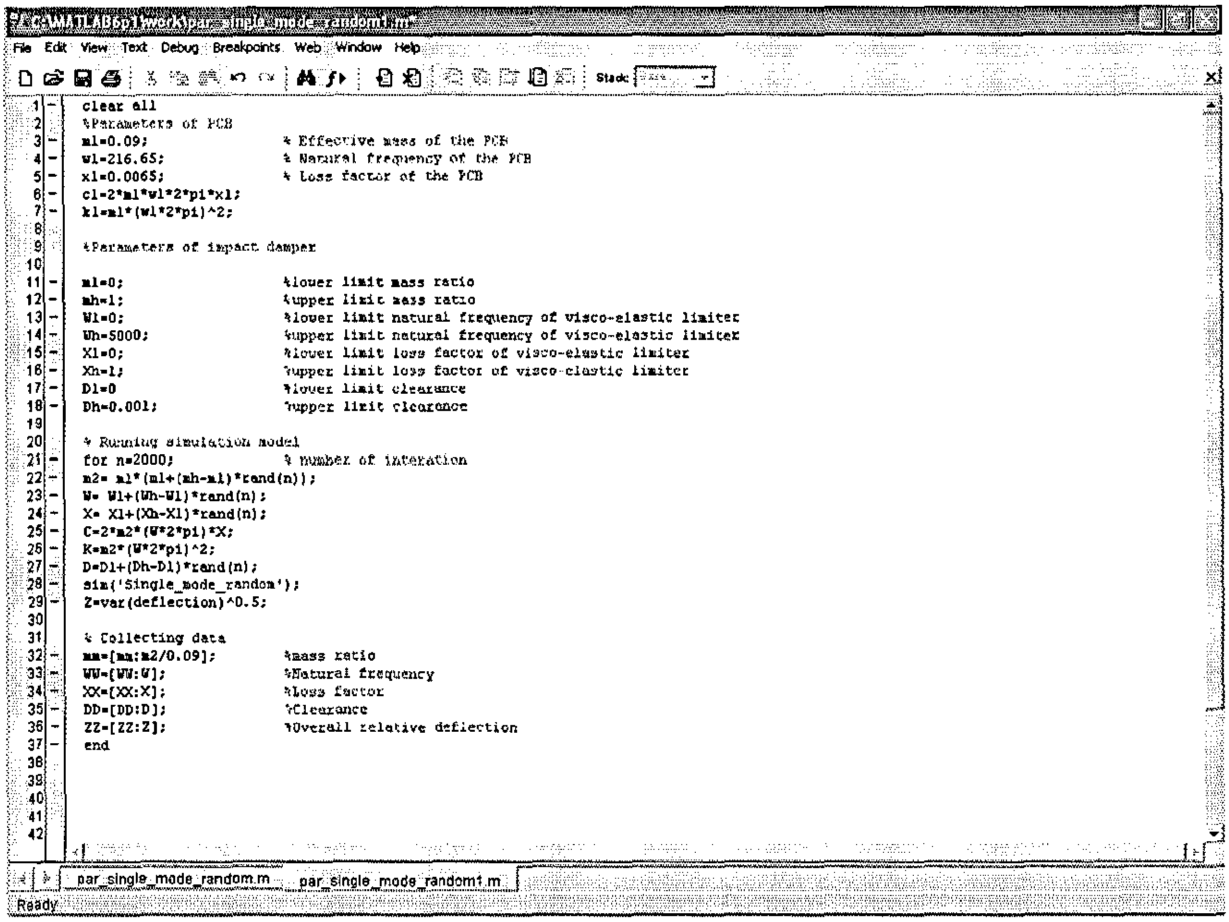
C:\MATLAB6p1\work\par_single_mode_random1.m*
File Edit View Text Debug Breakpoints Web Window Help
Stack:
par_single_mode_random.m
par_single_mode_random1.m
Ready

```
clear all
%Parameters of PCB
m1=0.09;                    % Effective mass of the PCB
w1=216.65;                  % Natural frequency of the PCB
x1=0.0065;                  % Loss factor of the PCB
c1=2*m1*w1*2*pi*x1;
k1=m1*(w1*2*pi)^2;

%Parameters of impact damper

ml=0;                       %lower limit mass ratio
mh=1;                       %upper limit mass ratio
Wl=0;                       %lower limit natural frequency of visco-elastic limiter
Wh=5000;                    %upper limit natural frequency of visco-elastic limiter
Xl=0;                       %lower limit loss factor of visco-elastic limiter
Xh=1;                       %upper limit loss factor of visco-elastic limiter
Dl=0                        %lower limit clearance
Dh=0.001;                   %upper limit clearance

% Running simulation model
for n=2000;                 % number of interation
m2= m1*(ml+(mh-ml)*rand(n));
W= Wl+(Wh-Wl)*rand(n);
X= Xl+(Xh-Xl)*rand(n);
C=2*m2*(W*2*pi)*X;
K=m2*(W*2*pi)^2;
D=Dl+(Dh-Dl)*rand(n);
sim('Single_mode_random');
Z=var(deflection)^0.5;

% Collecting data
mm=[mm:m2/0.09];            %mass ratio
WW=[WW:W];                  %Natural frequency
XX=[XX:X];                  %Loss factor
DD=[DD:D];                  %Clearance
ZZ=[ZZ:Z];                  %Overall relative deflection
end
```

Figure 5.7. Matlab script for random variable method

In Figure 5.8.a, dots show the overall relative deflection of the PCB against the mass ratio at different natural frequencies, loss factors of the visco-elastic limiter and clearances. The optimal curve obtained for the linear case is superimposed for reference. From Figure 5.8.a, the impact damper does not show any better results compared to the linear case at any mass ratio.

Further, Figure 5.8.b shows the overall relative deflection of the PCB against the loss factor of the limiters at different masses, natural frequencies of the visco-elastic limiter and clearances. The optimal curve obtained for the linear case is superimposed for reference. From Figure 5.8.b, the impact damper does show better results compared to the linear case at small values of loss factor.

Figure 5.8.c,d show the overall relative deflection of the PCB against the natural frequencies of the visco-elastic limiter at different masses, loss factors of the limiters and clearances. From Figure 5.8.c,d, the impact dynamic absorber again does show better results compared to the linear case in a wide range of natural frequencies.

From the above analysis, the performance of the vibroimpact dynamic absorber is lower as compared with the linear case. However, the sensitivity of vibroimpact dynamic absorber to the variation of critical parameters, such as loss factor and natural frequency of the dynamic absorber is smaller as compared with the linear case. Hence, the final tuning of the dynamic absorber may rely exclusively on the variation of the clearance.

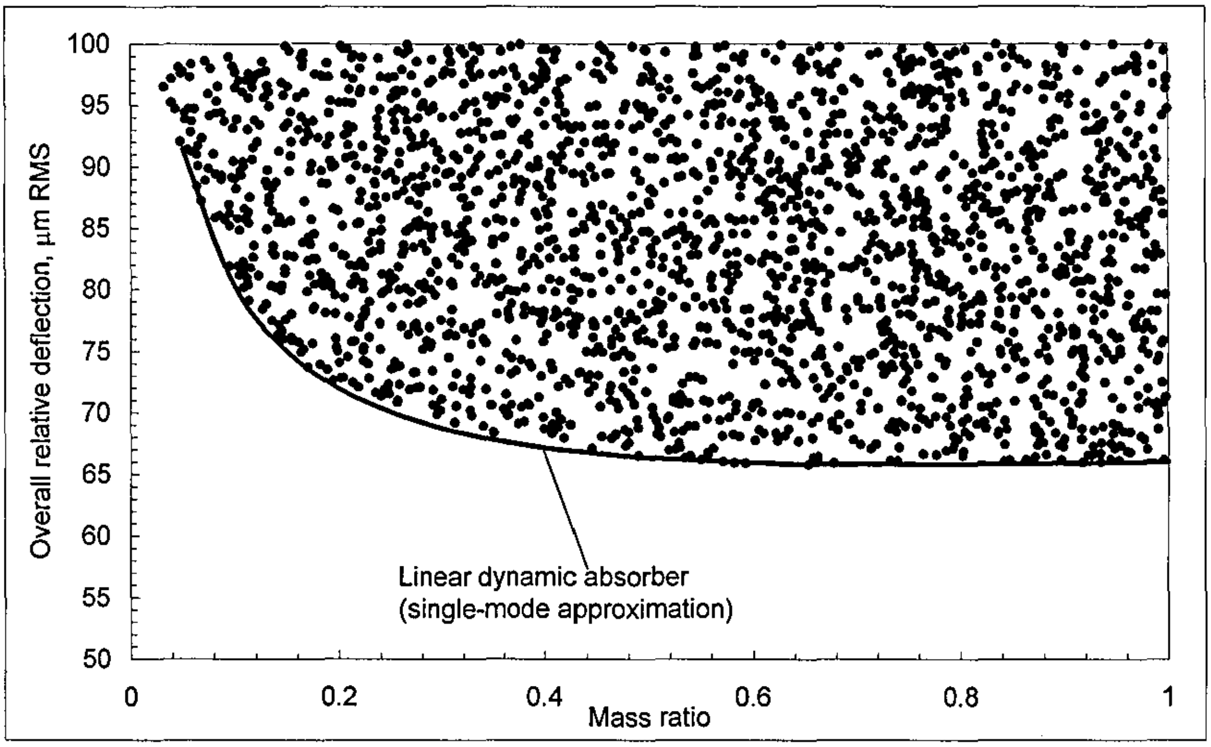

a)

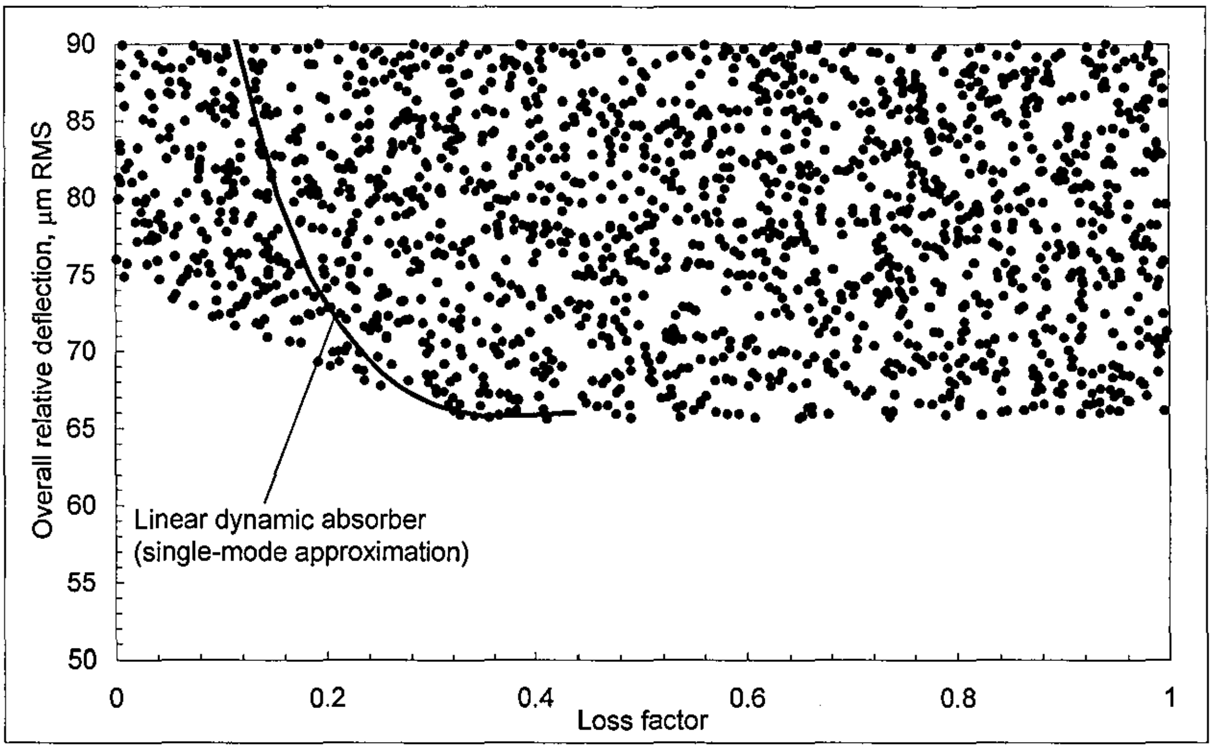

b)

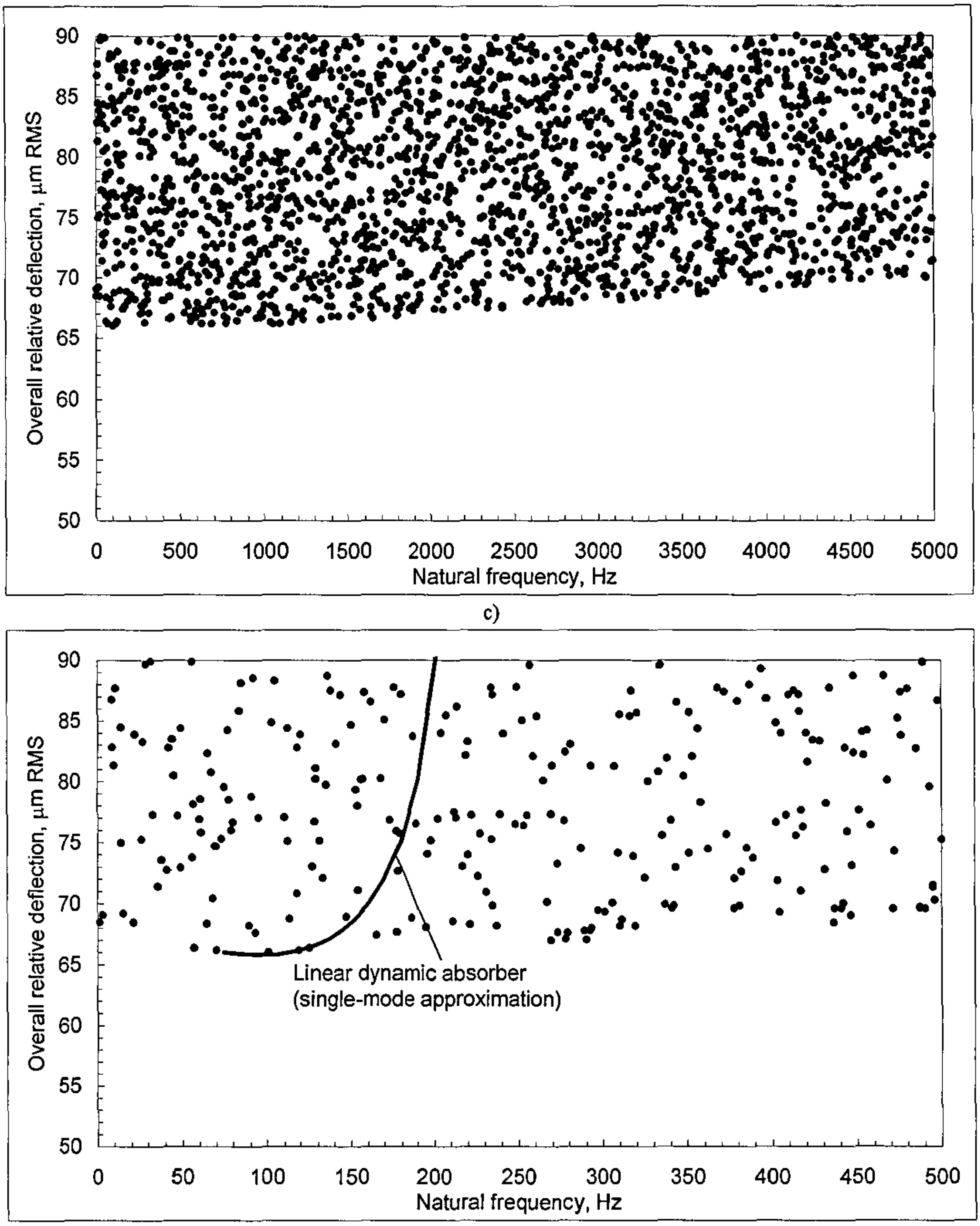

c)

d)

Figure 5.8. Overall relative deflection versus parameters of impact damper

To support the above findings, the simulation model is again run for the mass ratio 35% and 65% along with the loss factor and natural frequency of the visco-elastic limiter (optimal parameters set from linear absorber design) against a different clearance i.e.

$$\eta = 65\%,\ \frac{\Omega}{2\pi} = 106Hz,\ \xi = 0.35$$

$$\eta = 35\%,\ \frac{\Omega}{2\pi} = 144Hz,\ \xi = 0.267$$

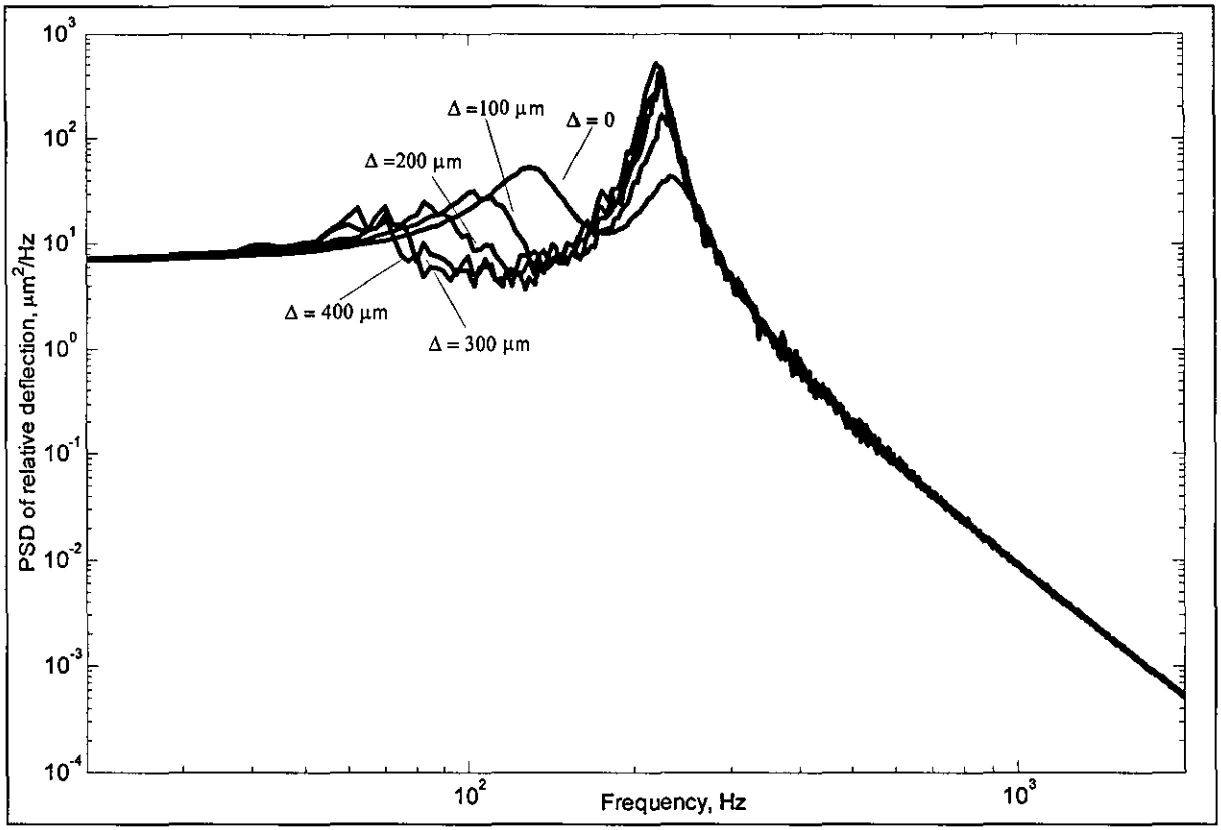

a) At 35% mass ratio

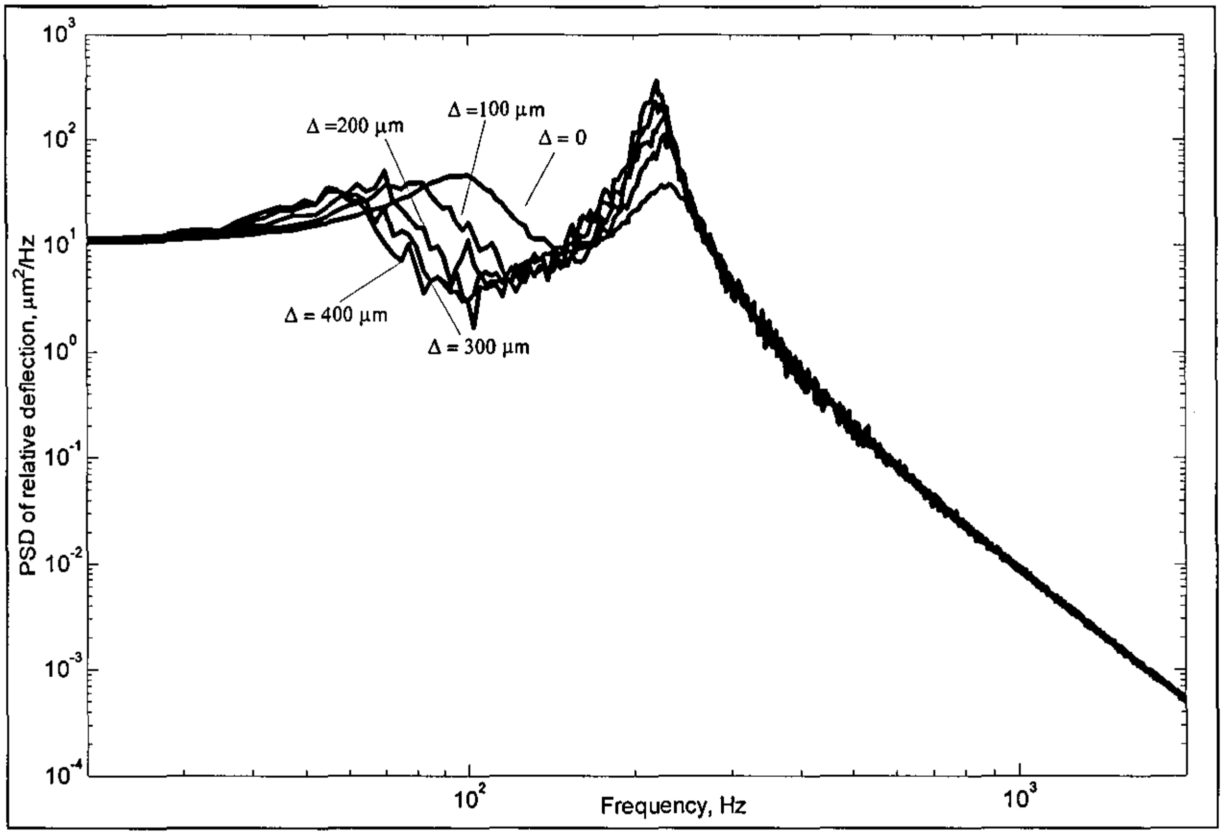

b) At 65% mass ratio

Figure 5.9. Simulated PSD of relative deflection of ruggedized PCB at different clearances

Figure 5.9 shows the corresponding PSD of relative deflection for each mass ratio, the transformation from time domain to frequency domain of these simulation curves are directly obtained with the help of the **Pwelch** command from Matlab. In these figures, the lowest overall relative deflection can be found when the gap is closed (Δ = 0) which correspond to the case of optimal linear absorber. It should be noted here, the response shape in these figures is almost similar to that sensitivity analysis on natural frequency of linear absorber (see Figure 3.7c from Section 3.2.2 for reference) even the stiffness of the visco-elastic limiter remains the same. This could be a new opportunity to ease the sensitivity of linear dynamic absorber outside its tuning range.

5.2.3 Sensitivity analysis

From the above simulation results, the superiority of an impact damper is its immunity to changes of loss factor and natural frequency of visco-elastic limiter as long as the clearance is not too tight. Therefore, in this section, we deal with the sensitivity analysis, similarly to the linear analysis the mass ratio 65% and loss factor of the symmetrical visco-elastic limiter is fixed at 0.35 whilst the natural frequency is varied from 50 Hz to 2000 Hz. As an additional parameter, the clearance is introduced in different values.

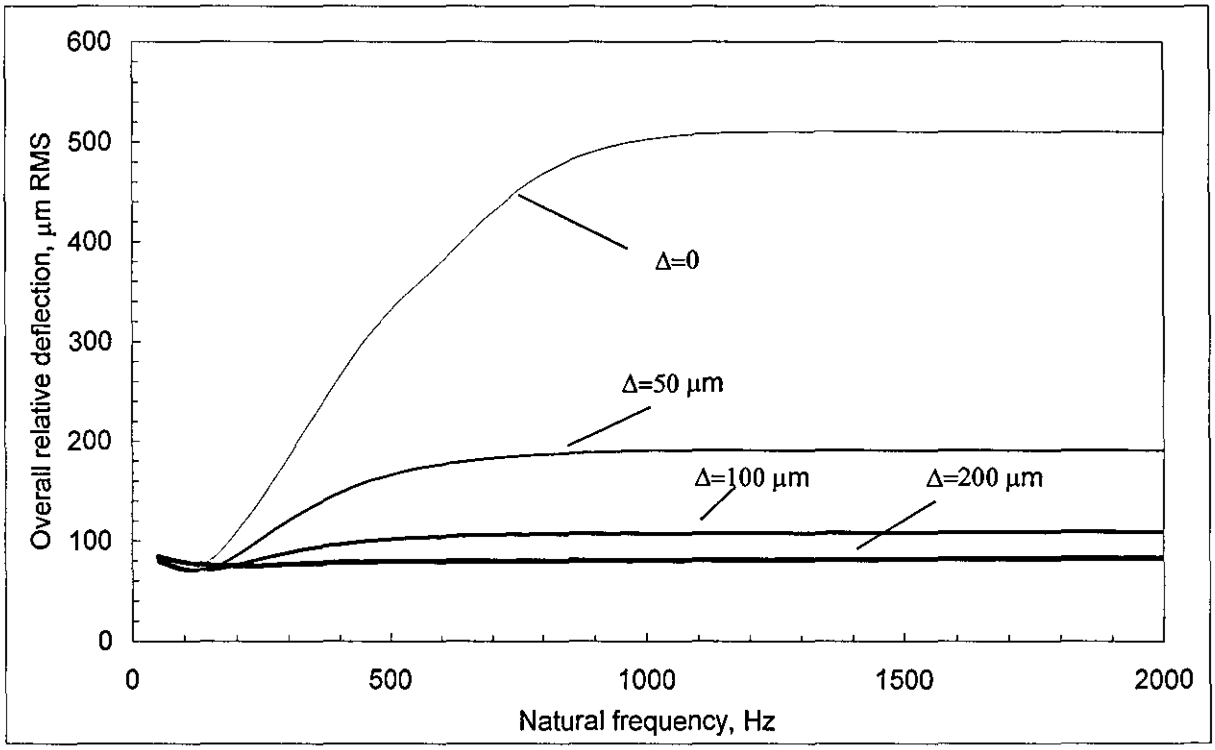

Figure 5.10. Sensitivity analysis of natural frequency dependence on clearance

Figure 5.10 highlights the results. As can be clearly seen the system is very sensitive when the gap is closed, particularly at high frequency range. Under this condition, the influence of linear dynamic absorber deteriorates the original response of the PCB. With the presence of clearance, the sensitivity of the system is, somehow, reduced significantly.

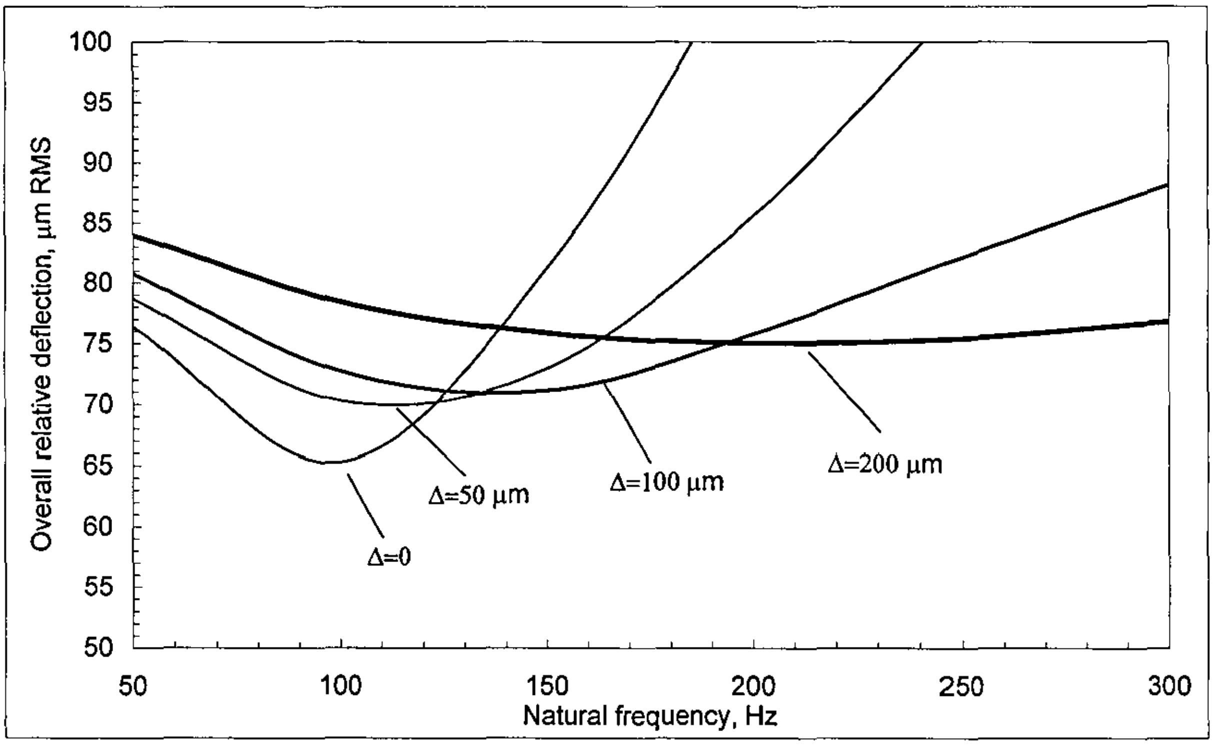

Figure 5.11. A closer look of sensitivity analysis on natural frequency

Figure 5.11 shows the overall relative deflection in "zoom in" area of natural frequency (50-300 Hz) which corresponds to Figure 5.19. In this vicinity, the performance of linear case (Δ=0) at 100 Hz is much better than other nonlinear cases. However, it is very sensitive to a small variation in natural frequency.

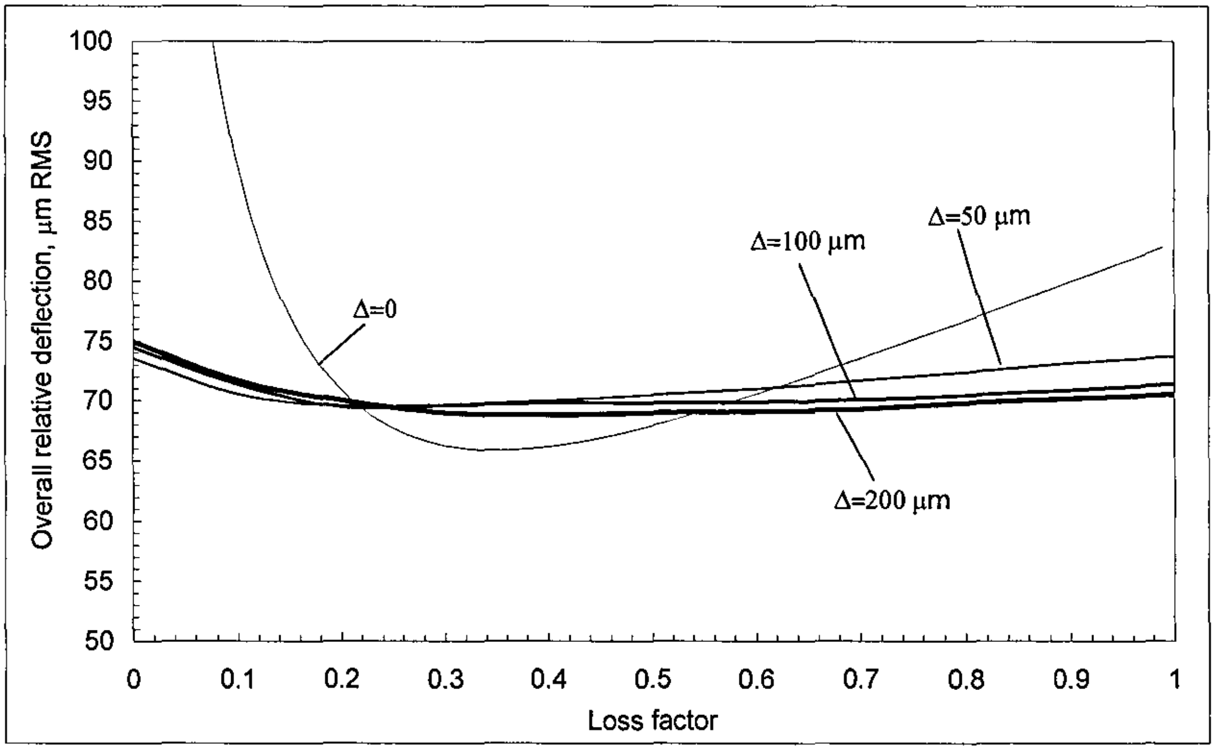

Figure 5.12. Sensitivity analysis of loss factor dependence on clearance

Figure 5.12 shows the sensitivity analysis on different loss factors and clearances of impact damper where 65% mass ratio and natural frequency of the symmetrical visco-elastic limiter 106 Hz are fixed while its loss factor is varied from 0 to 1. As can be seen again, the optimal linear response (see the curve labelled as $\Delta = 0$) is very sensitive to variation in loss factor, particularly outside its tuning value whereas the performance of impact damper is practically the same for any value of loss factors of the symmetrical visco-elastic limiter as long as the gap is not closed.

The sensitivity analysis for 35% mass ratio was carried in the similar manner, the obtained results were almost similar to the 65% mass ratio case in which the natural frequency and loss factor have little impact on the performance where as the clearance is more critical.

From sensitivity analysis, the desired performance of impact damper does not require any specific value of natural frequency or loss factor of the symmetrical visco-elastic limiter for any mass ratios whereas the clearance is more important. The assumption from [27] could, however, apply for the above results. This means that at any given set of parameters (m_2, Ω and ξ) at a constant level of excitation and G-load environment, the clearance can be tuned in order to produce a best performance. In addition to this statement, the impact damper seems to be insensitive to the natural frequency and loss factor of the visco-elastic limiter if the clearance is not too tight. In practice, this could be a new technique of reducing the sensitivity of linear absorber outside its tuning range. However, in airborne application the external parameters are not always constant in nature, the optimal tuned clearance does not always provide the best performance. Therefore, it is necessary to carry out further the sensitivity analysis on clearance for the mass ratio of 35% and 65% where the loss factor and natural frequency of the symmetrical visco-elastic are chosen as 0.5 and 200 Hz, respectively.

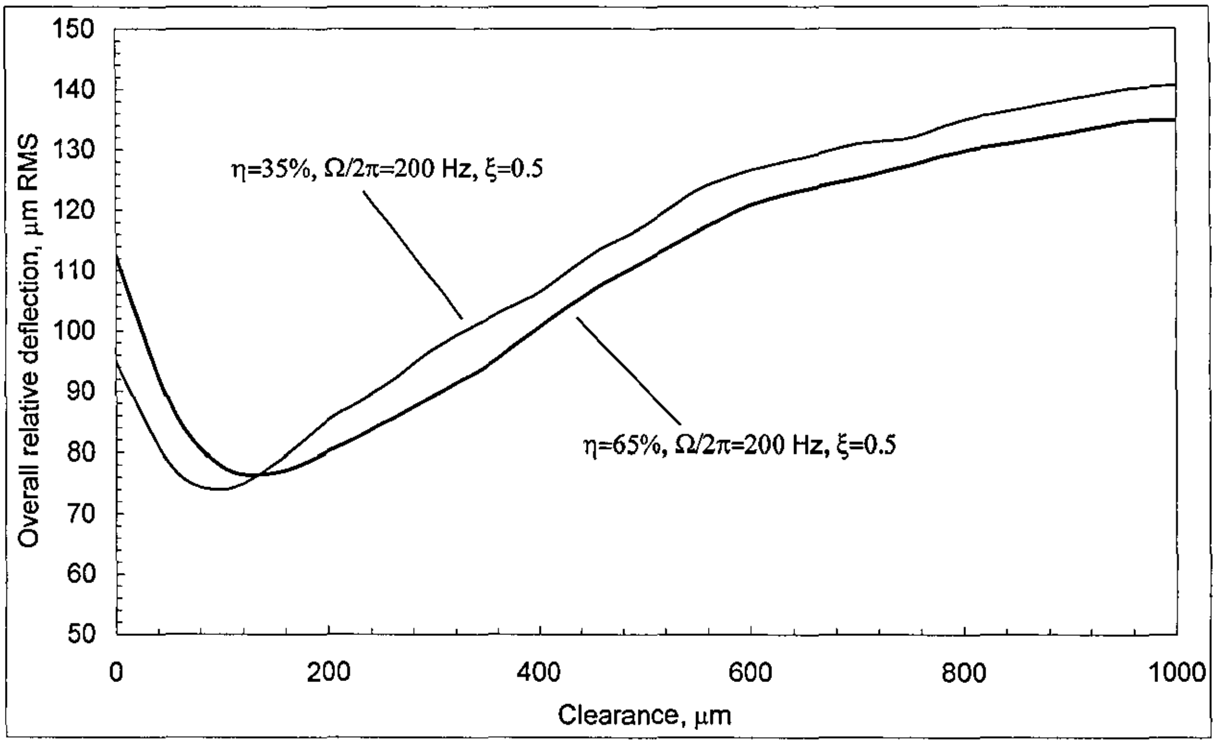

Figure 5.13. Sensitivity analysis on clearance

In this case, the optimal clearance is found for each mass ratio with the same parameters set which provides the lowest overall response (see appropriate label in Figure 5.13). Reasonably small changes of clearance have a small impact on the desired performance.

From Figure 5.13, 35% mass ratio provides a better performance than 65% mass ratio at its optimal clearance. It could mean that the performance of a lighter mass is better than a heavier one. However, these optimal performances only apply for this specified loss factor and natural frequency. Additionally, these differences can be significantly altered with a small increment of clearance. In a worse situation, a combination of high G-loads and maximum vibration level, then the impact damper will lock to the primary system and vibrate as untuned linear 2DOF system. Sometimes, the impact damper does not provide any means of vibration control if the external disturbance is not in critical condition. In a general conclusion, the comparison of the performance for the above mass ratios may prove inconsistent.

Since impact damper is less sensitive than linear dynamic absorber and its universal design, an illustration of time domain and hence frequency domain for 35% mass ratio with implementation of the visco-elastic limiter's propertied ($\Omega = 200$ Hz, $\xi = 0.5$) at $\Delta = 150$ μm is shown in Figure 5.14. The relative deflection and absolute acceleration have shown a significant improvement compared to its original response and about the same reduction ratio compared to the linear absorber at the same mass ratio, this can be clearly seen from its PSD response in Figure 5.15.

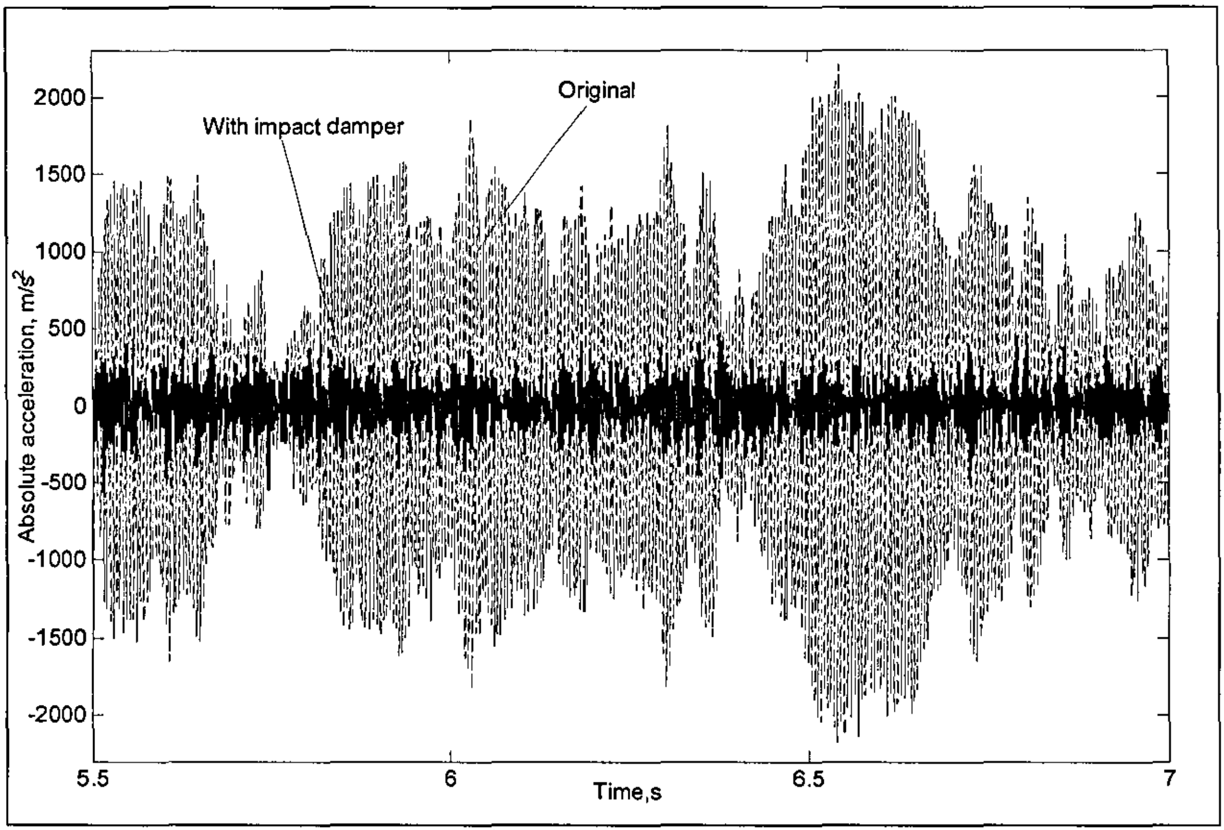

a) Absolute acceleration

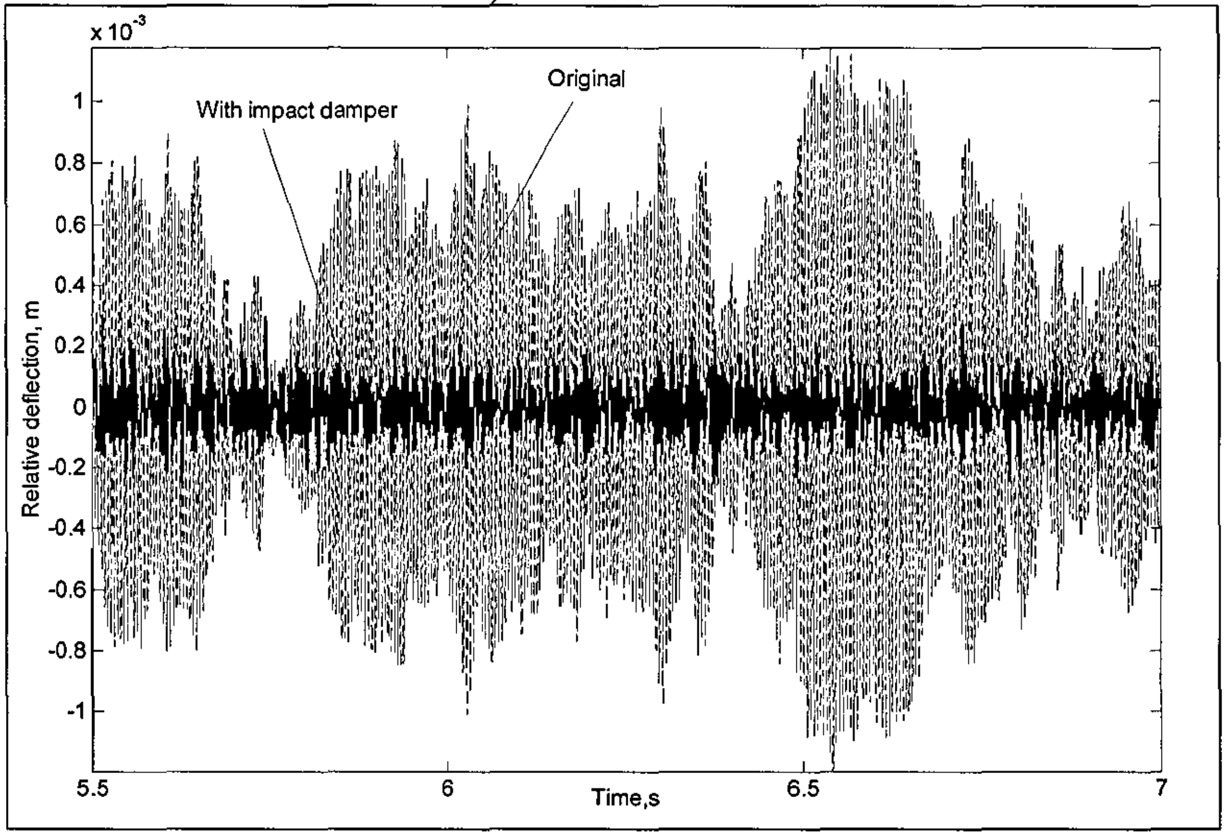

b) Relative deflection

Figure 5.14. Simulated time response of original and modified PCB

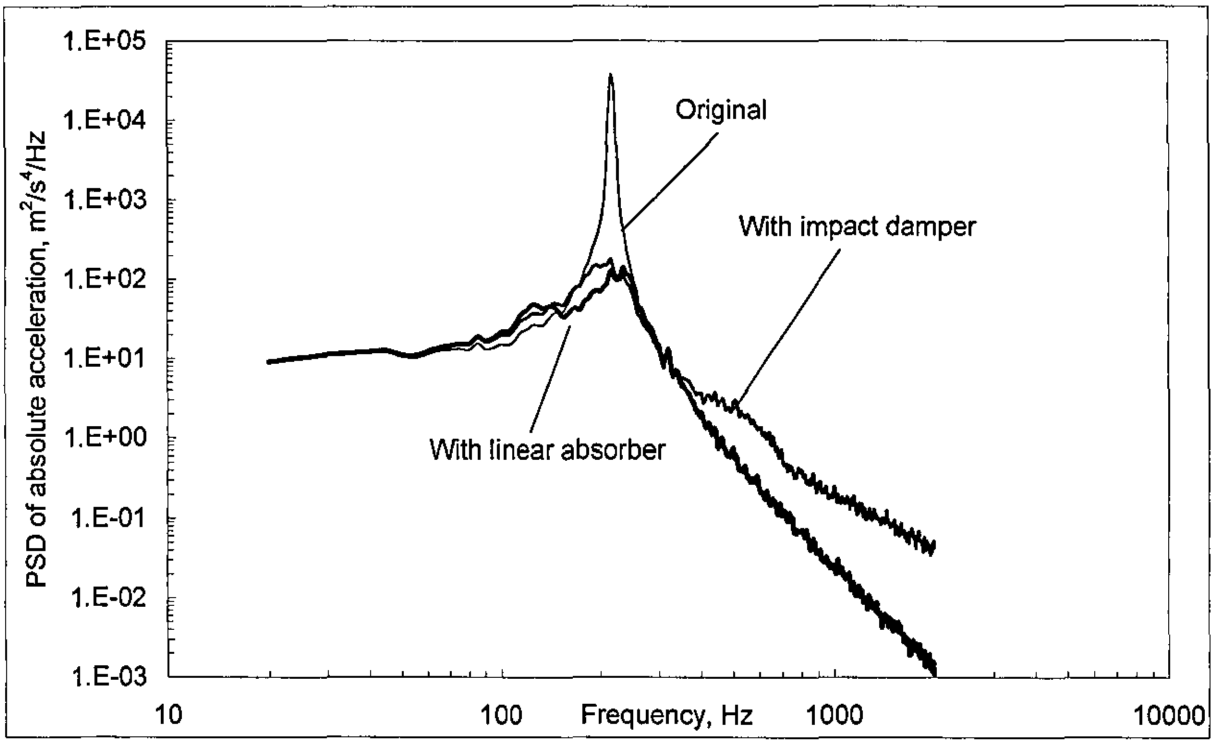

a) Absolute acceleration

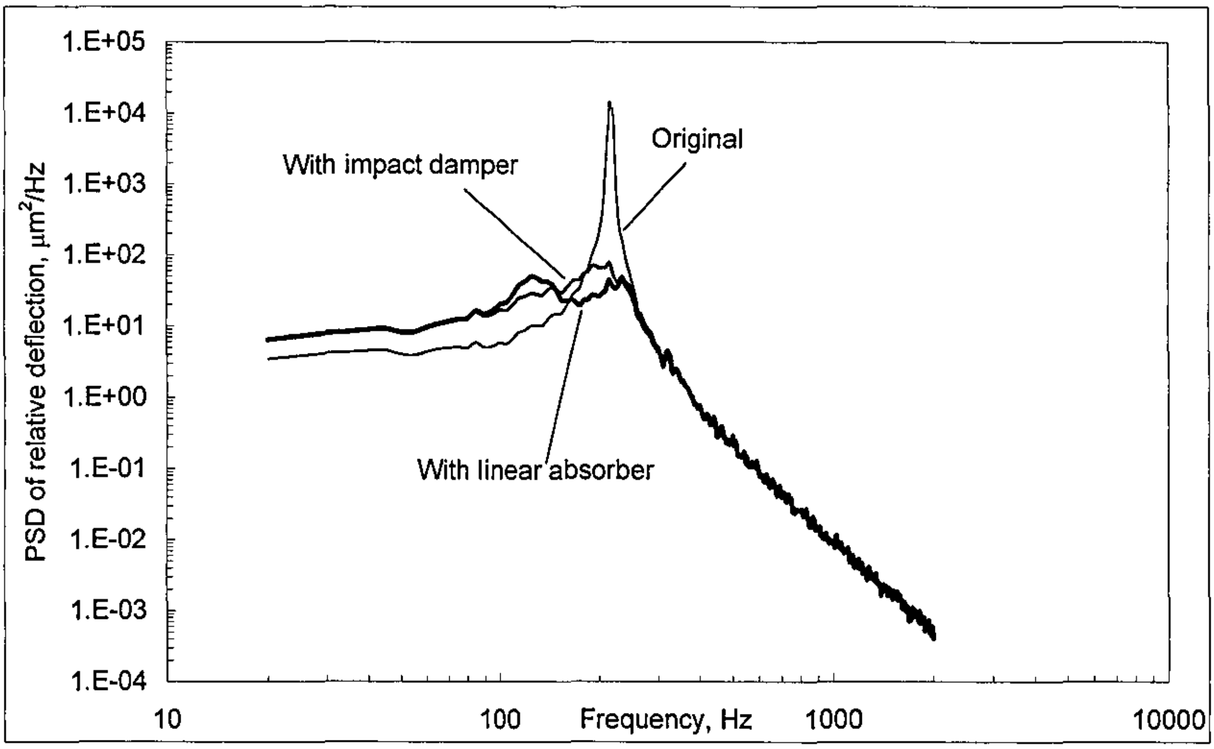

b) Relative deflection

Figure 5.15. Simulated PSD of original and modified PCB

The differences between nonlinear PSD curves and linear ones of the modified PCB are really small. However, maintaining this desired result still entirely depends on its chosen device and level of excitation.

Similarly, at a mass ratio of 65% with the same visco-elastic limiter's properties ($\Omega/2\pi = 200$ Hz, $\xi = 0.5$) at $\Delta = 150$ μm, the time history of absolute acceleration and relative deflection can be seen in Figure 5.16 with reference to its original response. Again, the differences of performance between them and the linear case at the same mass ratio can be distinguished in Figure 5.17.

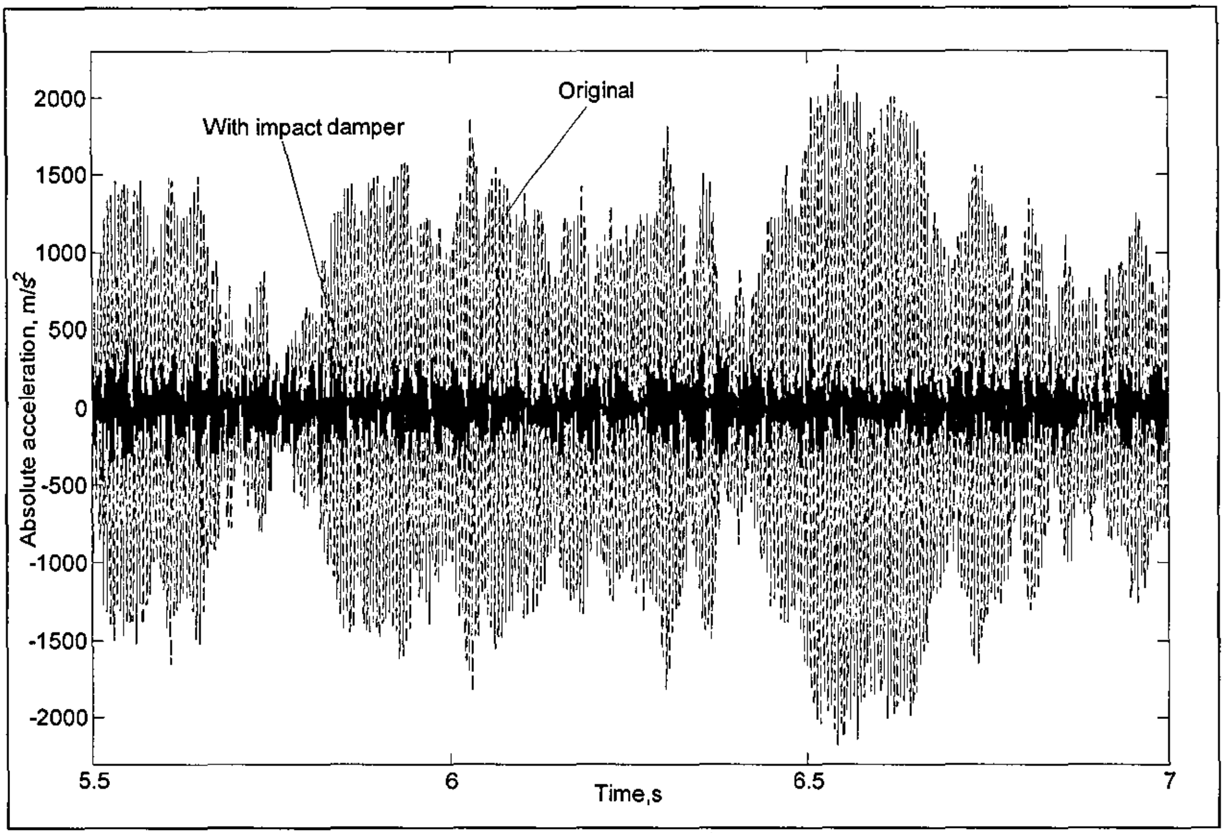

a) Absolute acceleration

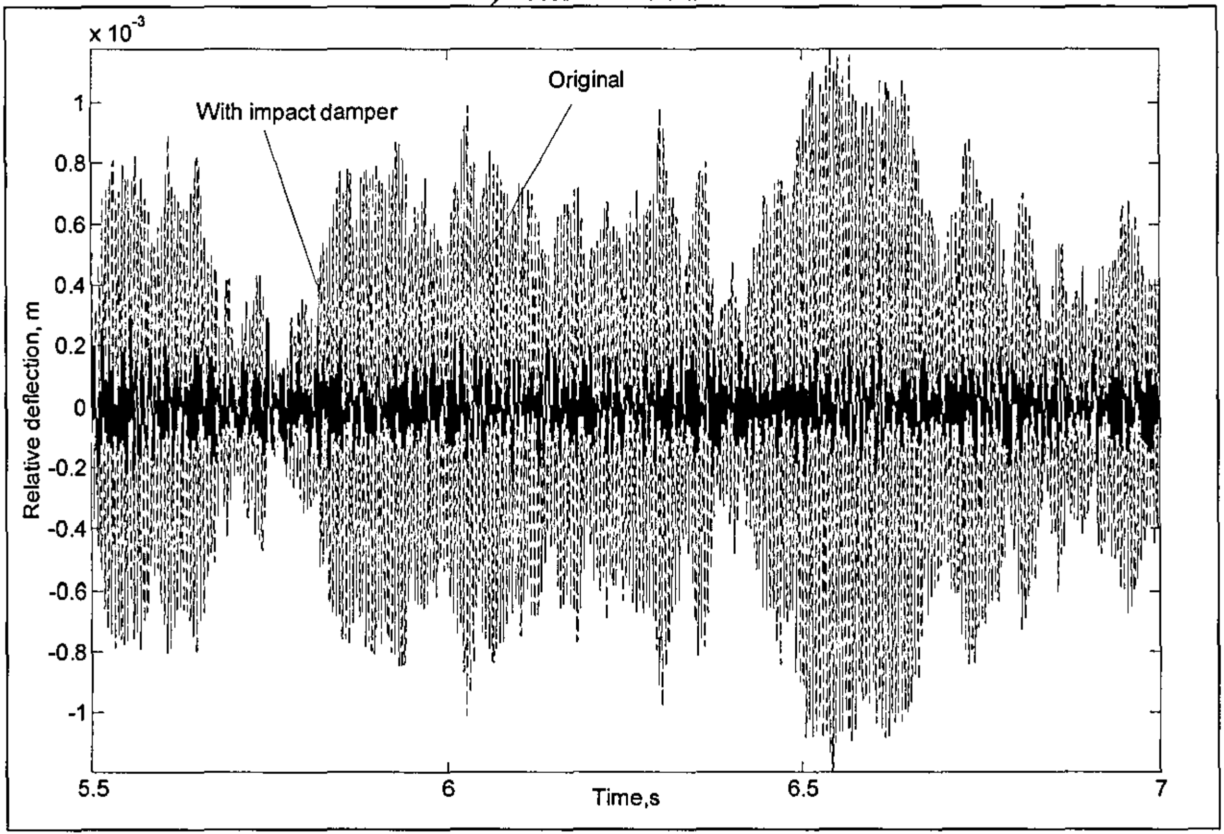

b) Relative deflection

Figure 5.16. Simulated time response of original and modified PCB

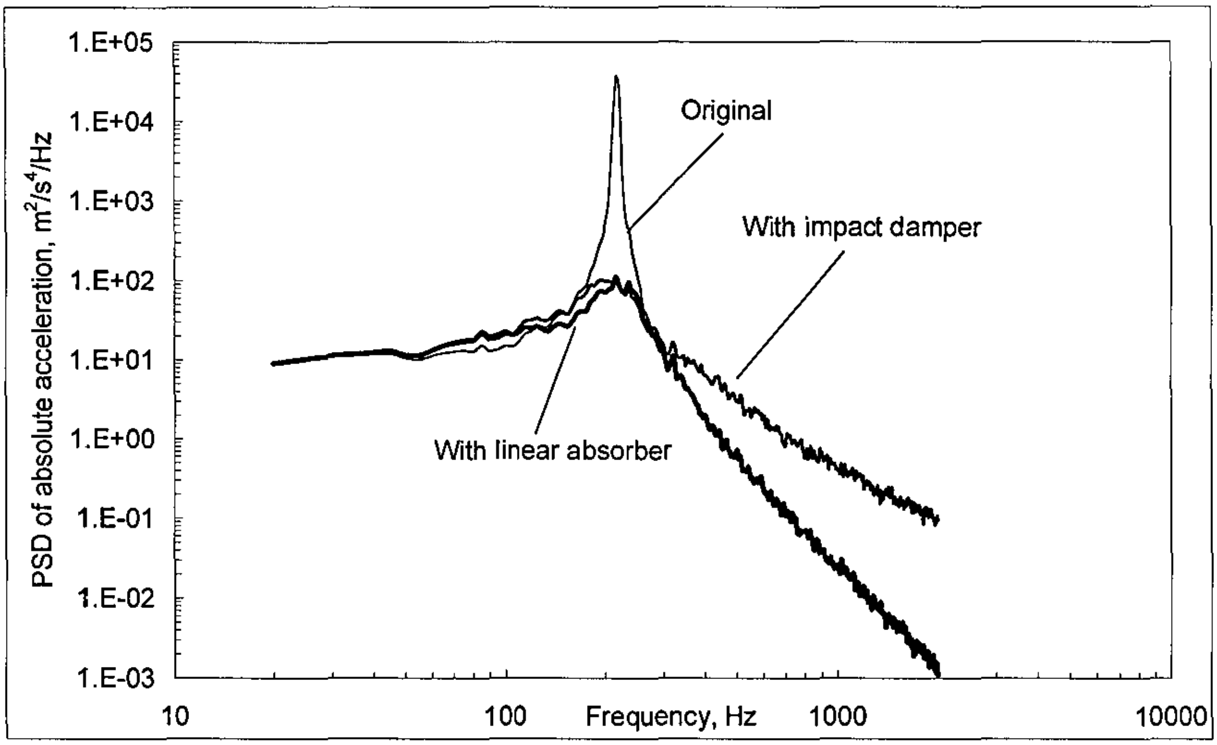

a) PSD of absolute acceleration

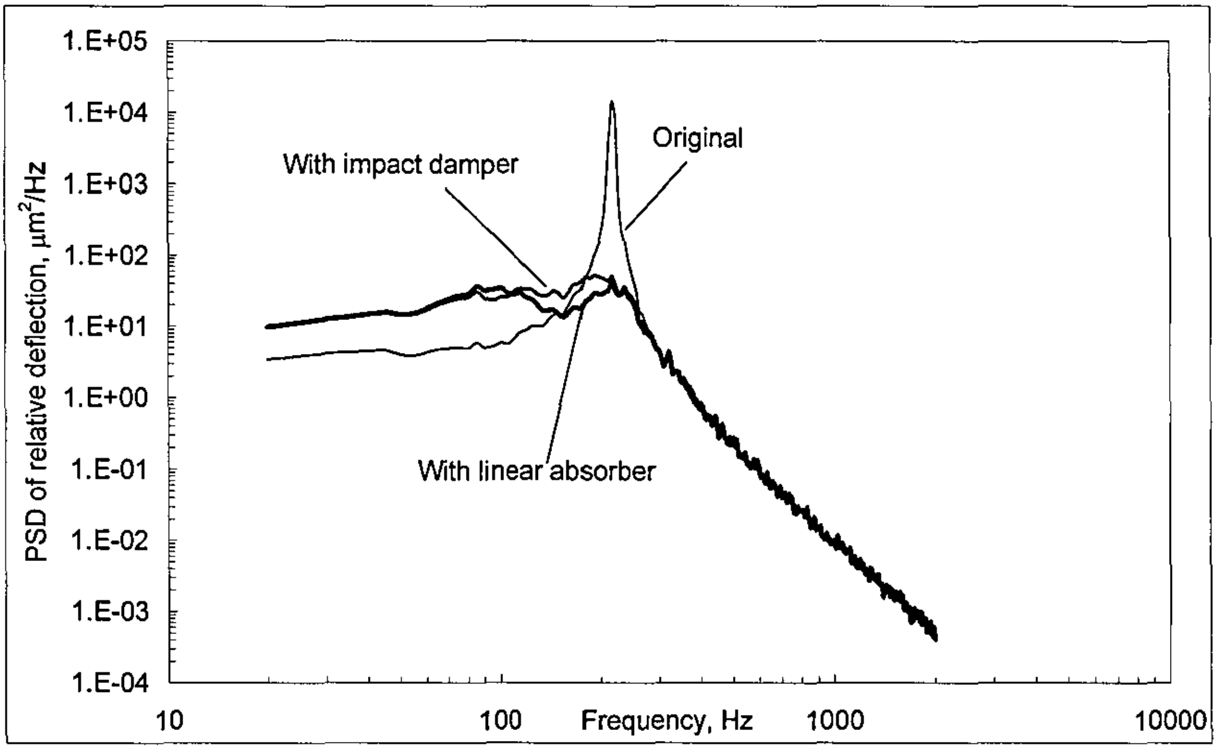

b) PSD of relative deflection

Figure 5.17. Simulated PSD of original and modified PCB

The performance between impact damper and optimal linear absorber at the same mass ratio is similar. It should be noted that any values of loss factor or natural frequency of the visco-elastic limiter could also produce a similar curve as shown in Figure 5.17 as long as the clearance is tuned. However, for the linear case, the natural frequency and loss factor of the dynamic absorber must be simultaneously tuned at a given mass ratio in order to produce an optimal performance, thus, it narrows the freedom of design. As a general conclusion, the impact damper technique only shows its superiority in terms of universal design and application as far as it has a "tuneable" clearance characteristics.

5.2.4 PCB with impact damper (full-mode model)

The emphasis of many impact damper analyses has been considered the primary system as a SODF system. In the "real-world" a SDOF system does not seem to exist in many complex dynamic structures. Therefore, there is little known about the dynamic behaviour of these devices in the MDOF system under random vibration. Using numerical simulation of the full-mode model of PCB, it is possible to justify the effect of such a technique in terms of vibration suppression.

The Simulink model used in studying of linear absorber, Figure 4.16 is now implemented for studying the impact damper in which the value of k_2 and c_2 are set equal to zero. Similarly, the **Impact Force** subsystem is "wired" at the relative motion of the PCB and the impact damper mass. Figure 5.18 portrays the corresponding Simulink model

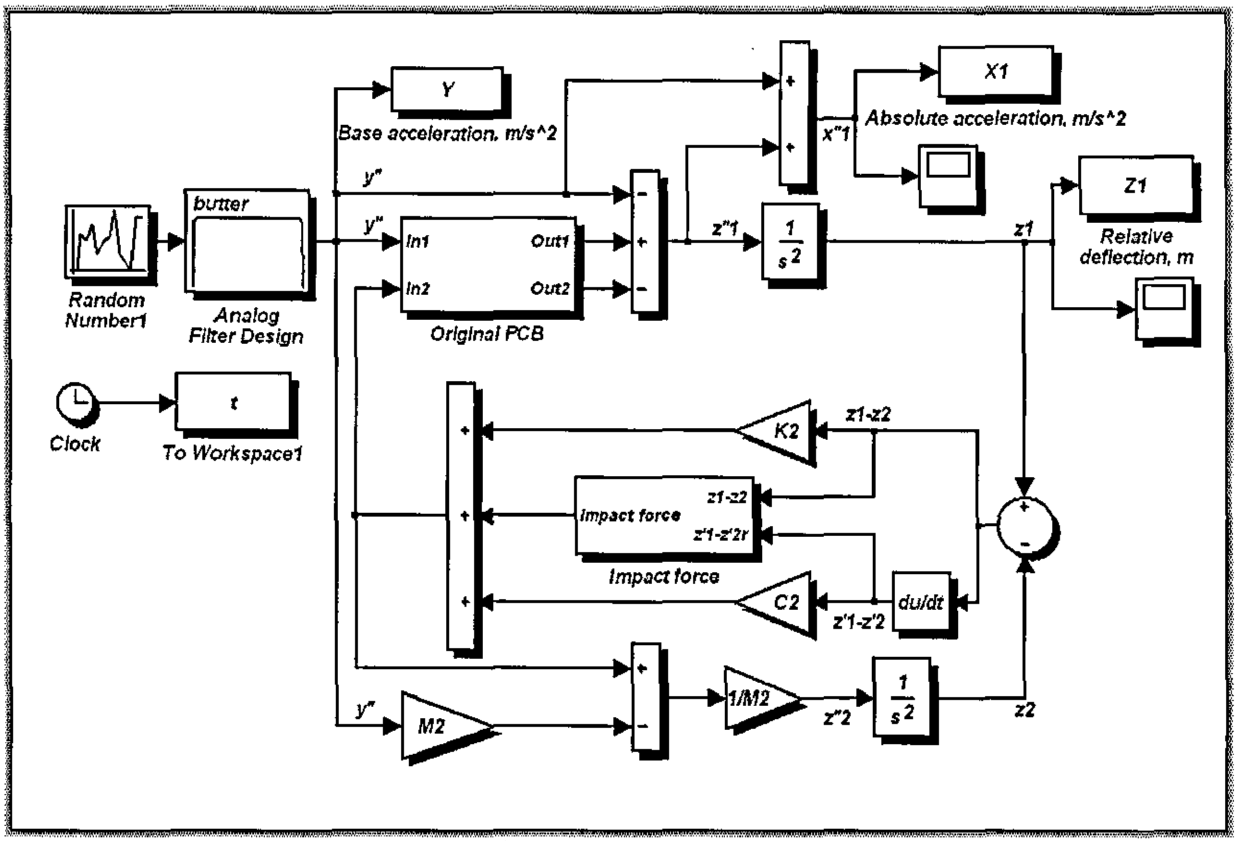
Y
Base acceleration, m/s^2
y"
X1
Absolute acceleration, m/s^2
x"1
Z1
Relative deflection, m
butter
Random Number1
Analog Filter Design
In1
Out1
In2
Out2
Original PCB
z"1
1/s2
z1
Clock
t
To Workspace1
K2
z1-z2
Impact force
z1-z2
z'1-z'2r
Impact force
C2
du/dt
z'1-z'2
1/M2
z"2
1/s2
z2
M2

a) Simulink model of impact damper (full-mode model of PCB)

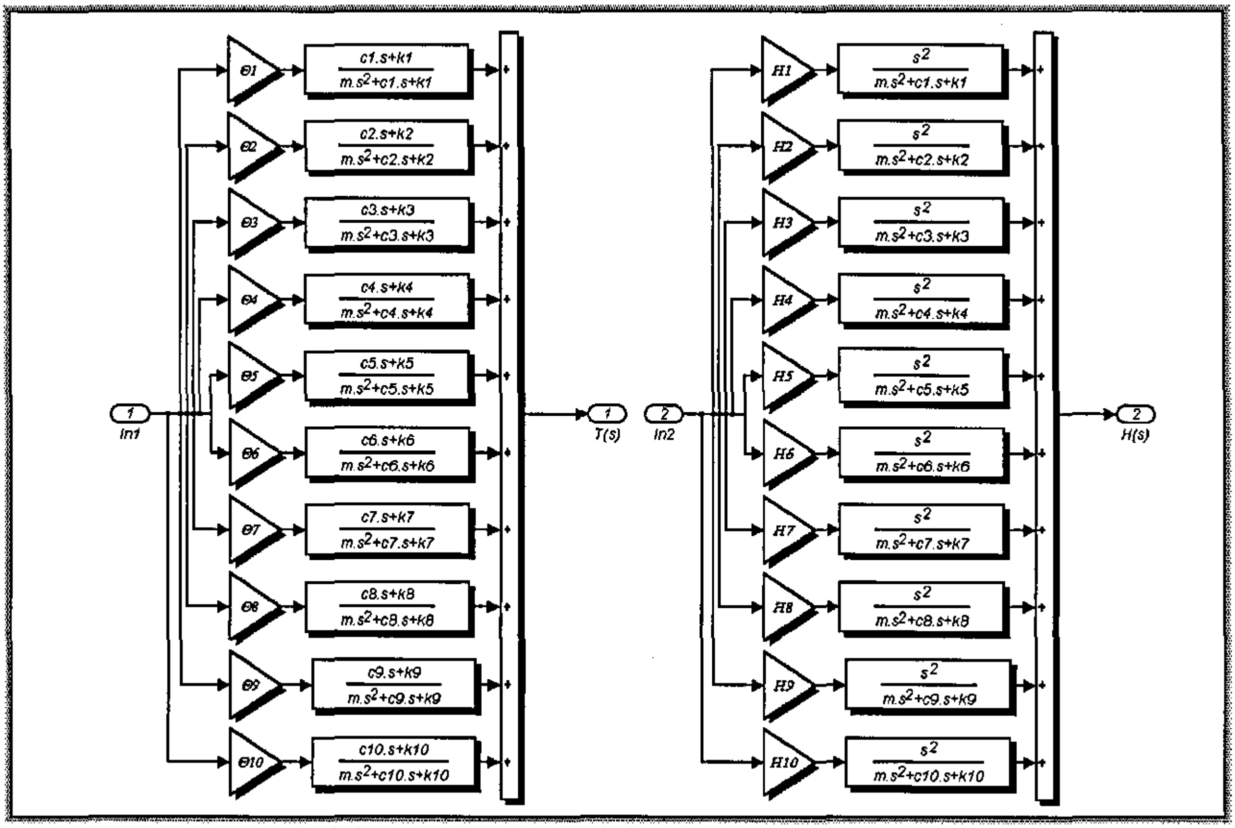
In1
θ1 … θ10
c1.s+k1 / m.s2+c1.s+k1 … c10.s+k10 / m.s2+c10.s+k10
T(s)
In2
H1 … H10
s2 / m.s2+c1.s+k1 … s2 / m.s2+c10.s+k10
H(s)

b) Subsystem Simulink block diagram of the original PCB

Figure 5.18. Simulink model for random vibration

This numerical model, could, however, run interactively with M-file to find optimal performance of many independent combinations of m_2, Ω, ξ and Δ. However, due to a large algorithm presence in the sub-system, the task of finding an optimal parameters set was abandoned. It should be noted that the impact damper is a highly dissipative energy device, it might control the resonant frequencies of the PCB but also at the same time it will destroy all antiresonant notches. Thus, the overall performance is not very impressive compared to linear absorber under random vibration.

The sensitivity analysis for this approach would not be carried out since the performance of single-mode and full-mode model of the PCB is dictated by the first resonant frequency and major influence of vibration suppression would take place at the first vibration mode. Additionally, from the sensitivity analysis of the single-mode approximation, the implementation of impact damper does not require any specific natural frequency or loss factor of the symmetrical visco-elastic limiter, therefore the parameters set of symmetrical limiter ($\Omega/2\pi$ = 200 Hz, ξ = 0.5) at Δ = 150 μm in accompany with 65% mass ratio are chosen to illustrate the principle of nonlinear vibration suppression for MDOF system. It should be noted that these parameters have been used in the single-mode approximation.

Figure 5.19 shows the superimposed absolute acceleration and relative deflection, respectively, of the original and modified PCB and correspondingly with PSD response as shown in Figure 5.20 and also the superimposed optimal PSD that was obtained from the linear case at the same mass ratio of 65%.

As can be seen from Figure 5.20a, the influence of the impact damper suppresses almost all resonant frequencies of the PCB at the same time it destroys all antiresonant notches, thus the overall performance in terms of absolute acceleration is less impressive compared to the linear case.

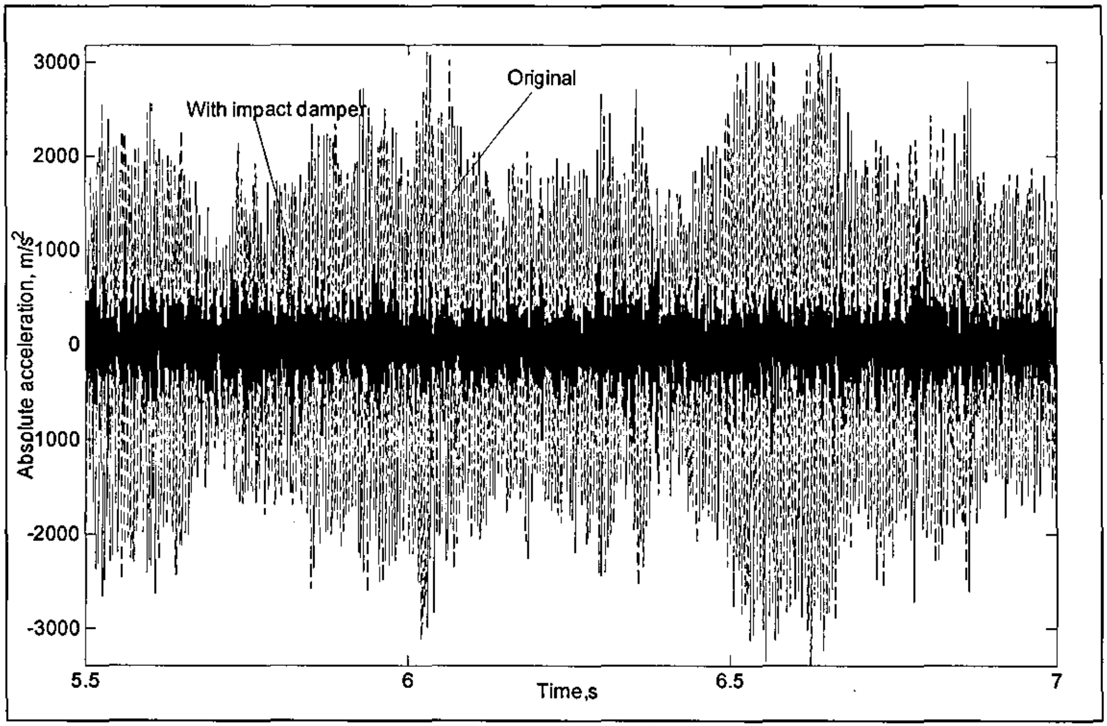

a) Absolute acceleration

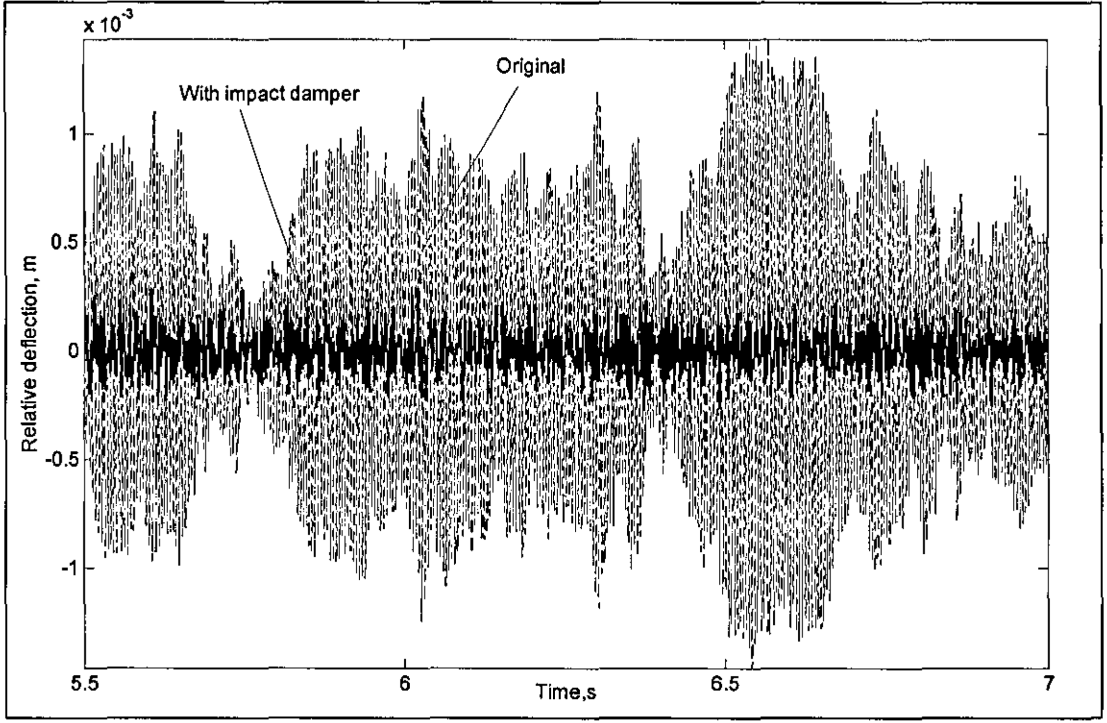

b) Relative deflection

Figure 5.19. Simulated time response of original and modified PCB (η=65%)

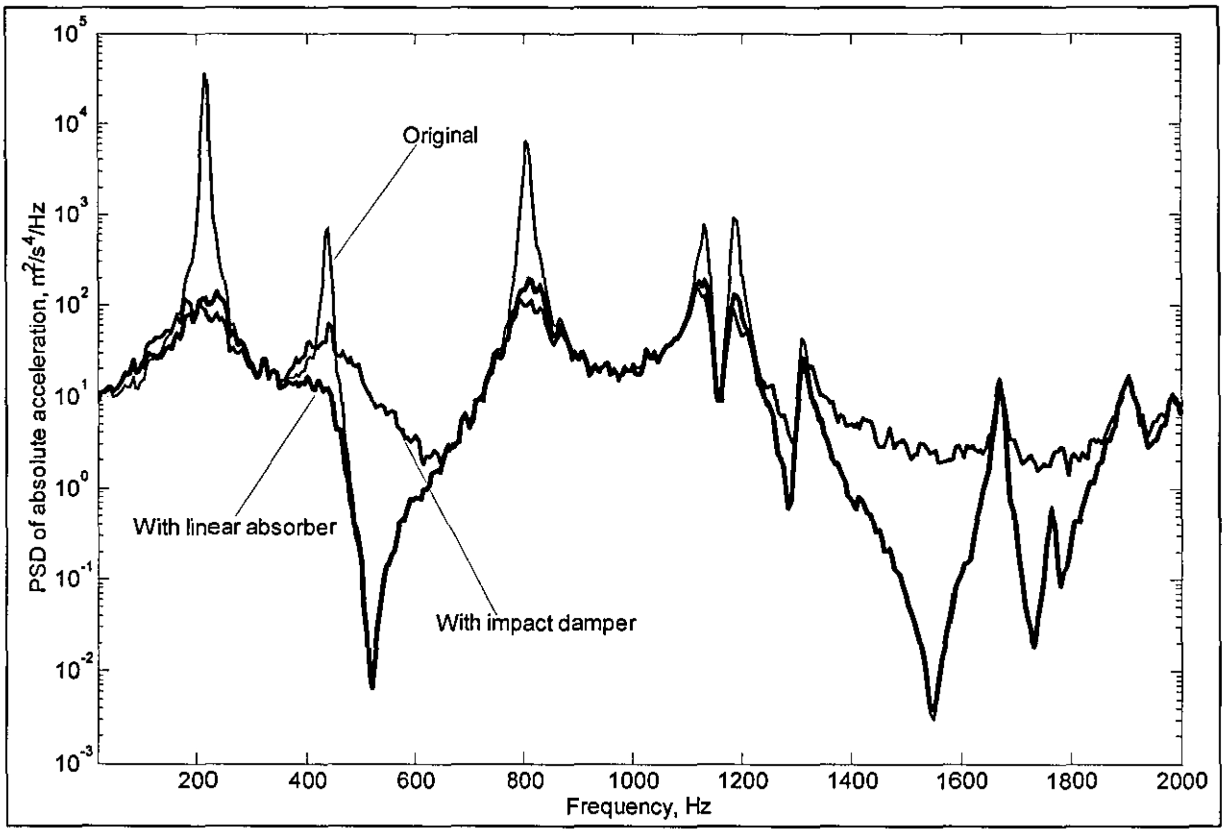

a) PSD of absolute acceleration

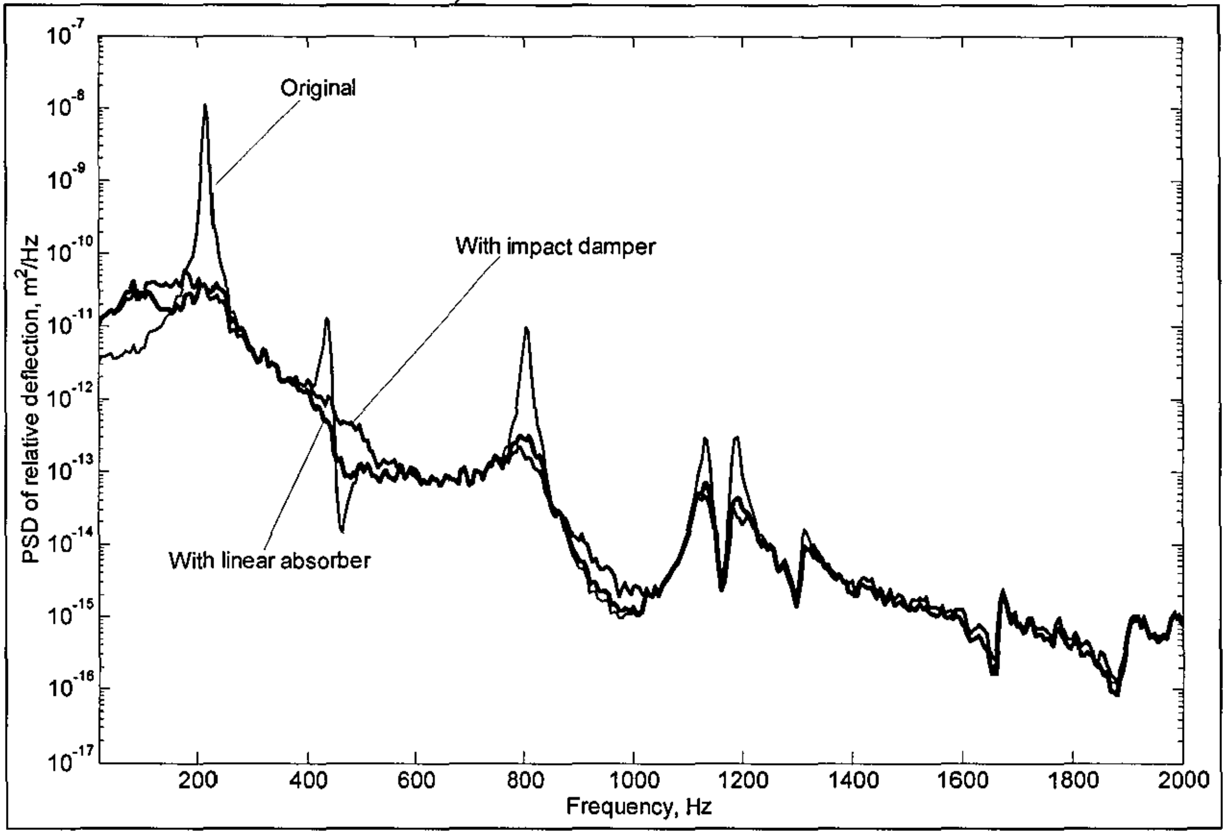

b) PSD of relative deflection

Figure 5.20. Simulated PSD of original and modified PCB (η=65%)

However, the overall relative deflection is of primary concern where the performance of the impact damper for this particular case produces 90 μm RMS whereas the performance of the optimal linear case gives 78 μm RMS, see Figure 5.20b for reference. This difference is partly due to the alternation of antiresonances at a higher frequency range.

Similarly, at 35% mass ratio with the same parameters set of symmetrical visco-elastic limiter ($\Omega/2\pi = 200$ Hz, $\xi = 0.5$) at $\Delta = 150$ μm. The time history of absolute acceleration and relative deflection with the reference of original response can be seen in Figure 5.21. The nonlinear PSD of absolute acceleration has the same characteristics as the 65% mass ratio in which all resonant frequencies are suppressed and antiresonances are destroyed (see Figure 5.22a for reference). In terms of vibration suppression, at this mass ratio the overall relative deflection 89 μm RMS is found to be about 9 μm RMS higher compared to the optimal linear case at 35% mass ratio (see Figure 5.22b for reference). Again, the desired response of the nonlinear case does not have to be dependent on the above chosen parameters set of the visco-elastic limiter whereas the clearance is more critical. For the linear case, the optimal response can be altered significantly if there is small variation of its optimal natural frequency of loss factor of the dynamic absorber.

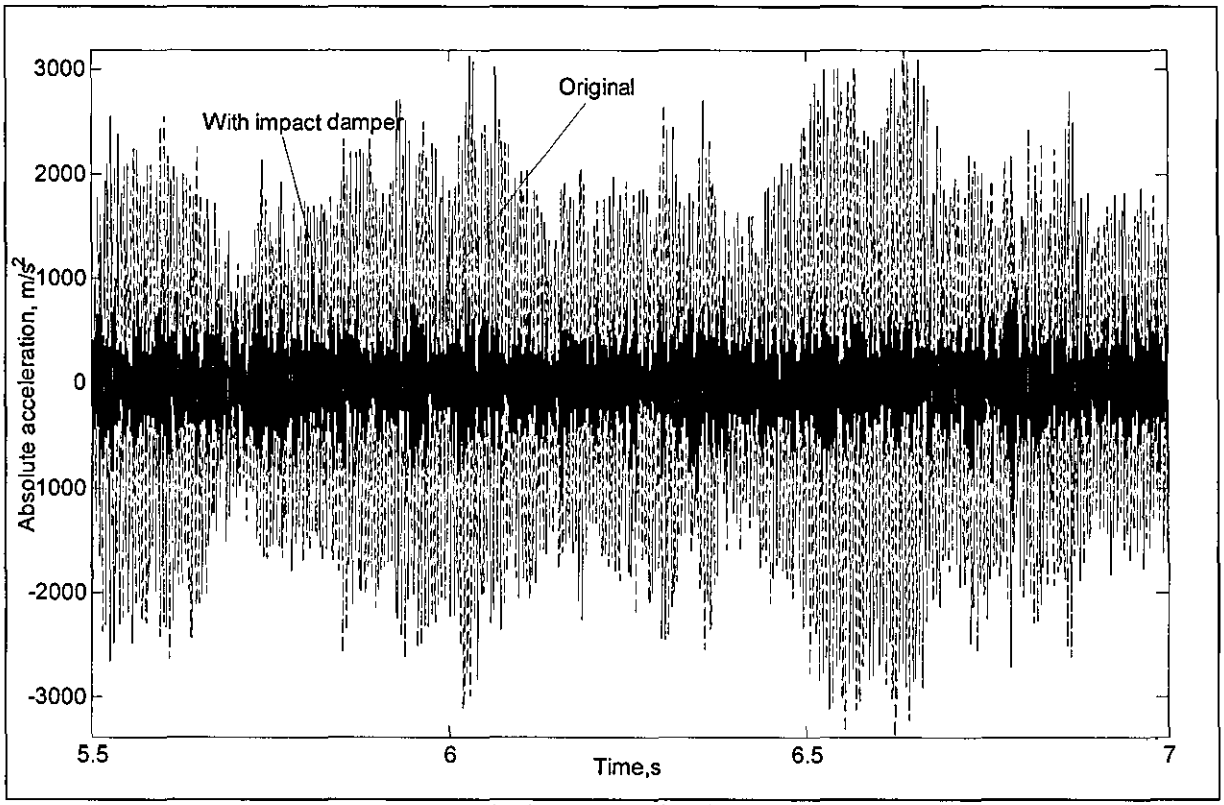

a) Absolute acceleration

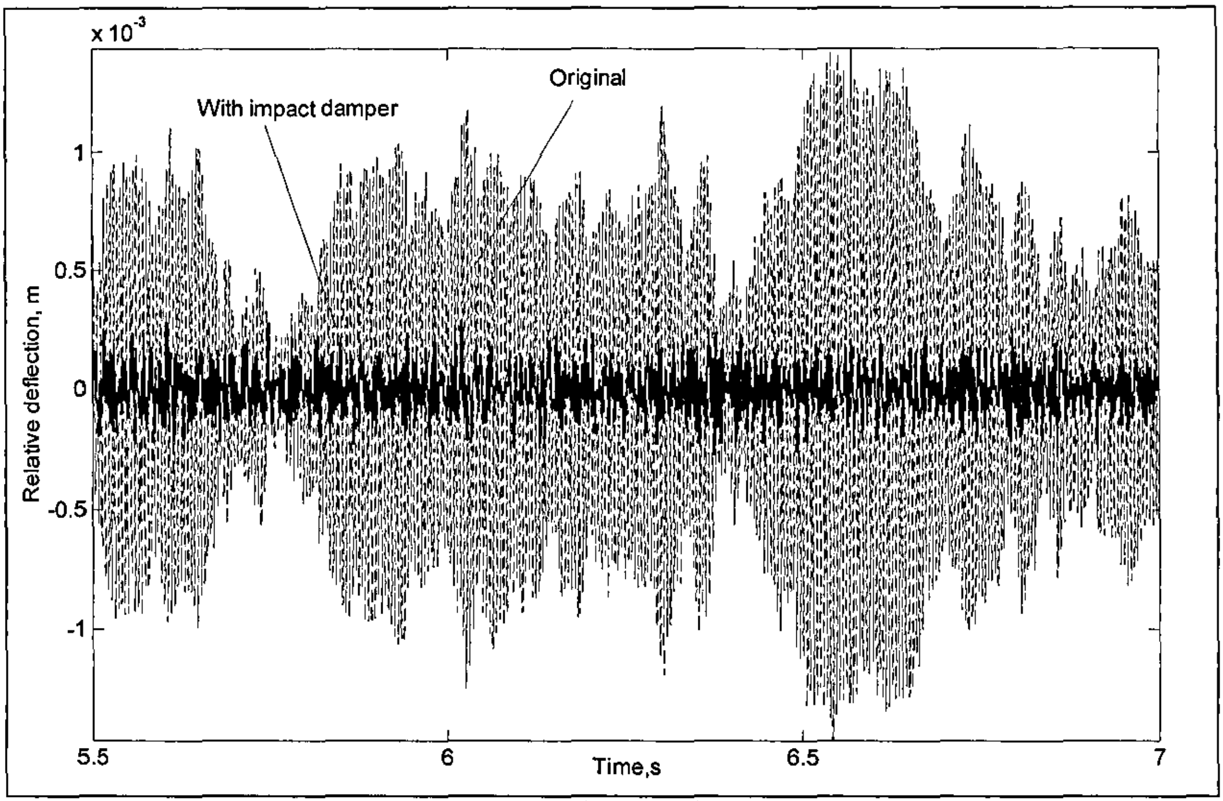

b) Relative deflection

Figure 5.21. Simulated time response of original and modified PCB (η=35%)

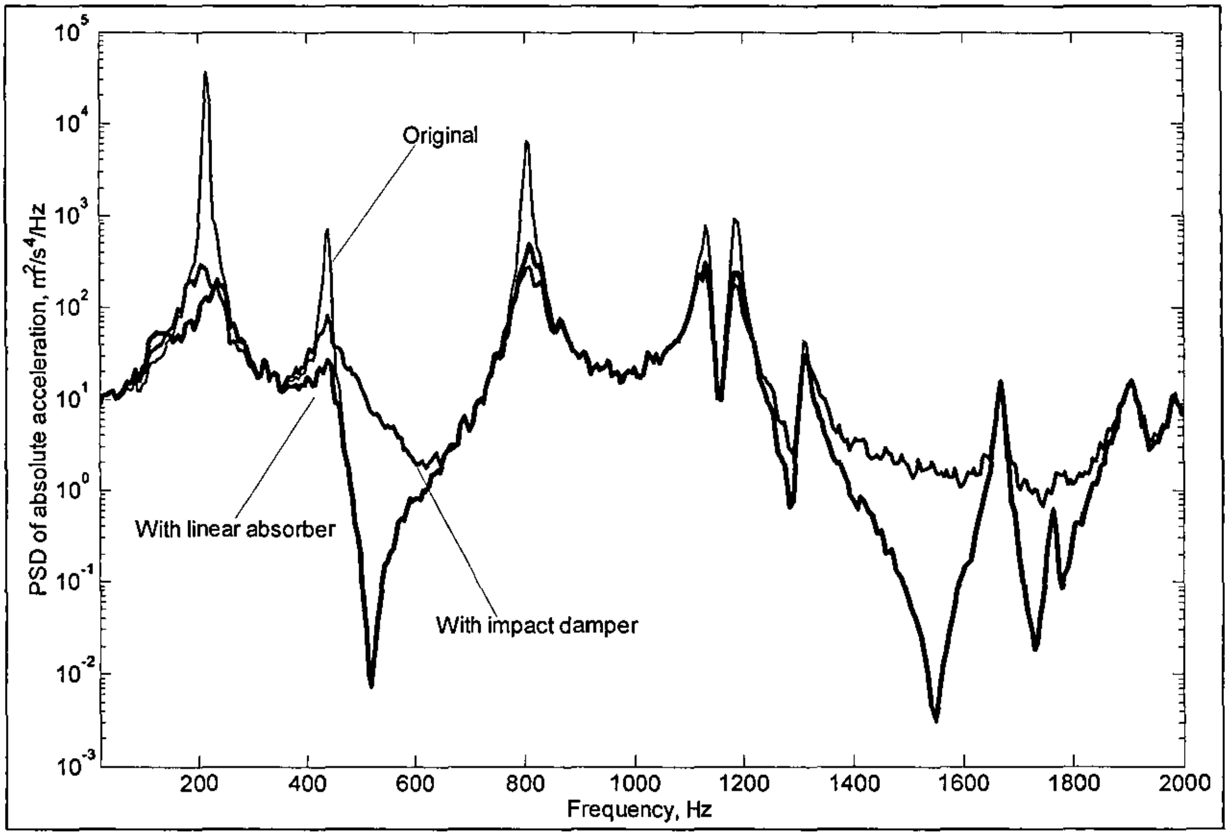

a) PSD of absolute acceleration

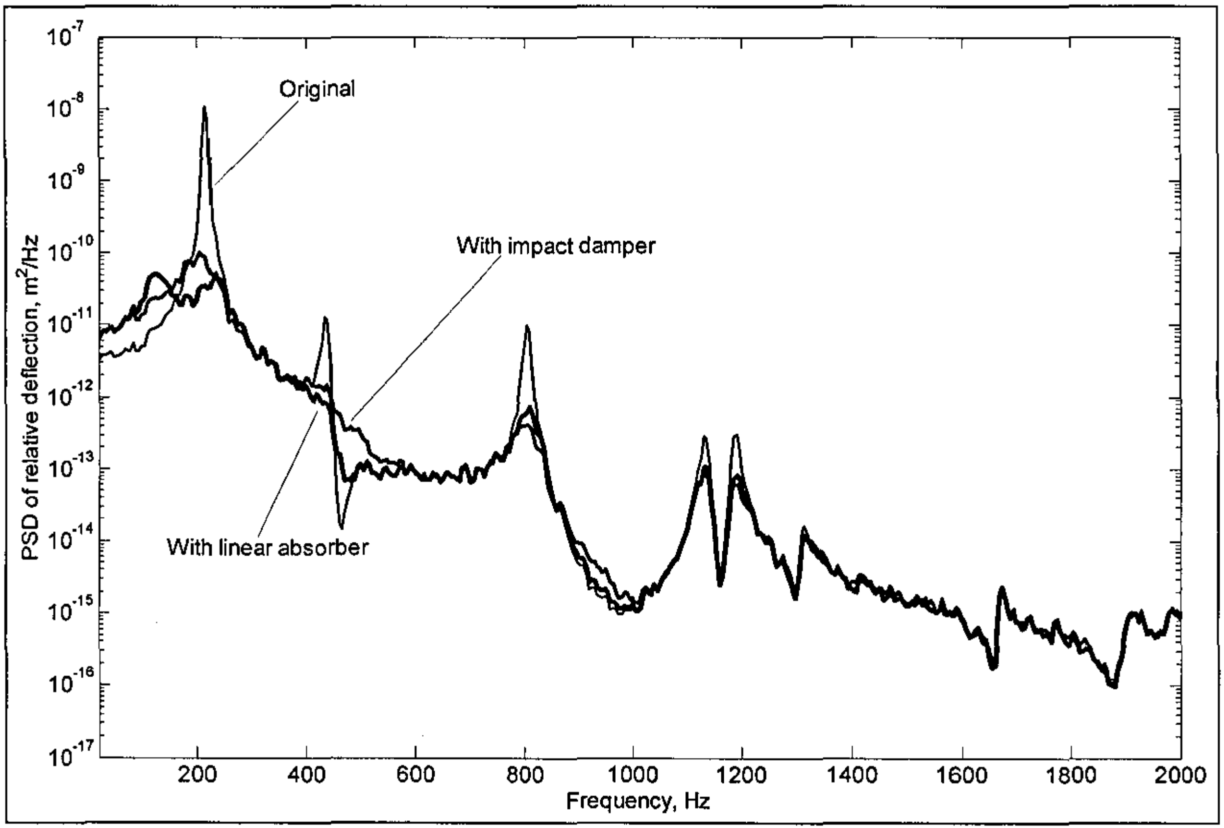

b) PSD of relative deflection

Figure 5.22. Simulated PSD of original and modified PCB (η=35%)

Generally, the differences in performance of impact damper between 35% and 65% mass ratio under random vibration is really small. This would allow a lot of choices when selecting a real device for vibration control of the PCB, the only drawback is its performance compared to the linear dynamic absorber but not much in terms of reduction ratio compared to the original response of the PCB. However, the parameters of the linear dynamic absorber are impossible to maintain at their optimal values due to manufacturing tolerances or temperature variations, with a small variation, the optimal performance can be altered significantly. This could explain why the impact damper is more superior in terms of sensitivity and design purposes.

The principle of the impact damper is the exchange of momentum phenomena in which every collision is involved on the free distance travel between the masses and elasticity of the limiter. The harder the limiter, the higher the impact force and eventually the higher the noise level. However, the overall relative deflection is a major concern which increases the possibility of using an "all-metal" impact damper for vibration suppression of the PCB.

5.3 Sine vibration

Random vibration is of primary concern in the process of designing a new vibration control method for this typical PCB. Since the performance of the impact damper does not show any better result compared to the optimal linear absorber, an optimal design for swept-sine application is no longer of interest. In addition, using numerical simulations to find optimal parameters set for nonlinear system under a swept-sine application will entail laborious tasks and require computational resources for either single-mode approximation or full-mode model of PCB. Unlike random vibration study, each simulation run will take time to sweep up from 0 to 500 Hz for each parameter set, also there are too many possible combinations that can produce a desirable performance, even though the sweep-rate can step up, the degree of accuracy is reduced. If, however, a better performance can be found under the swept-sine application, it does not apply to random or shock environment due to inconsistency in the excitation level and its sensitive nature. Thus, designing for a better universal performance using impact damper technique does not seem to exist in this study. Therefore, in this study, we analysed further the sensitivity of such a technique for the single-mode approximation instead of repeating the optimisation routine.

The numerical model is similar to that in Figure 4.28 in our linear vibration study in which the **Impact Force** subsystem is positioned at the relative motion of the primary system and the secondary system as shown in Figure 5.23 whereas in this case, the gain blocks c_2 and k_2 are excluded in which the impact dynamic absorber is a free mass as has been configured for random vibration case. For a better result, the sweep rate is still used to be 1 Hz/s to sweep up from 0 to 500 Hz and its amplitude is 10g.

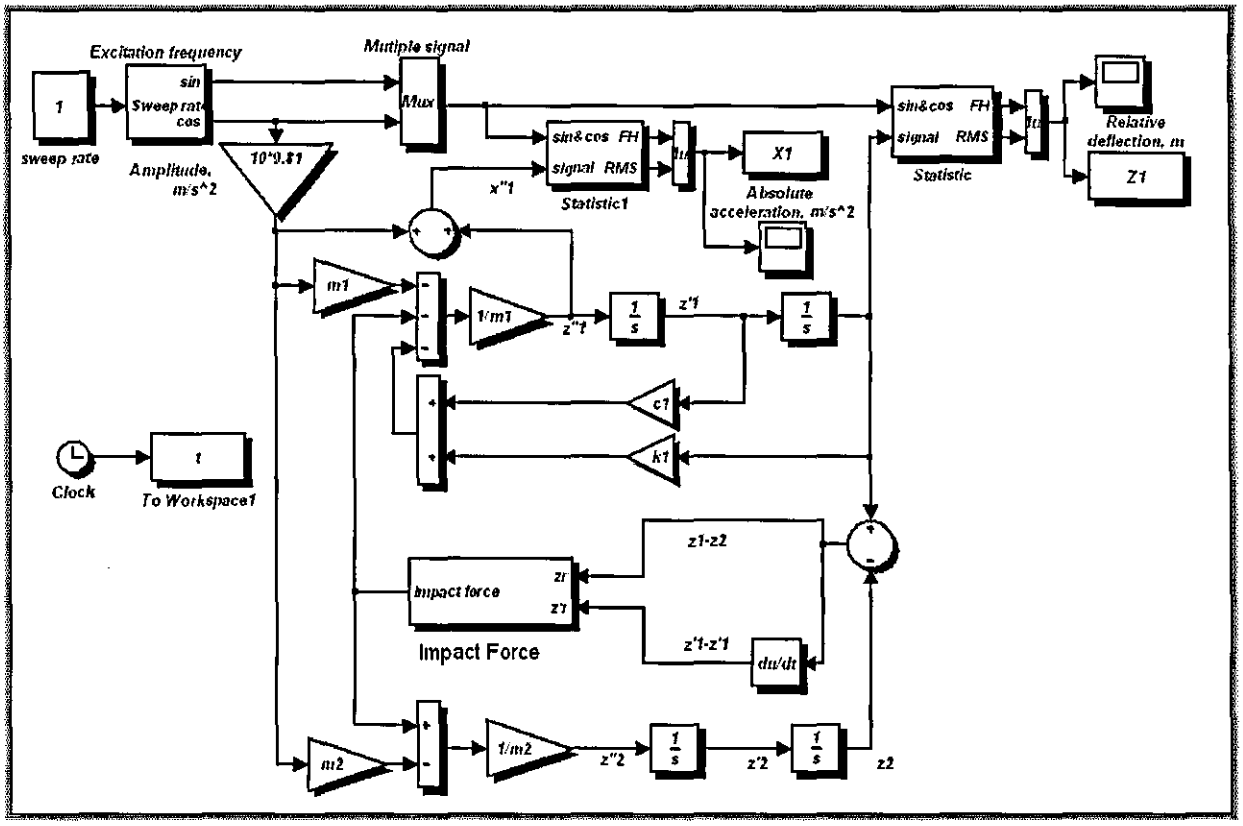
Excitation frequency
1
sweep rate
sin
Sweep rate
cos
Amplitude, m/s^2
10*9.81
Mutiple signal
Mux
sin&cos FH
signal RMS
Statistic1
x"1
X1
Absolute acceleration, m/s^2
sin&cos FH
signal RMS
Statistic
Relative deflection, m
Z1
m1
1/m1
z"1
1/s
z'1
1/s
c1
k1
Clock
t
To Workspace1
z1-z2
Impact force
zr
zr
Impact Force
z'1-z'1
du/dt
m2
1/m2
z"2
1/s
z'2
1/s
z2

Figure 5.23. Simulink diagram for swept-sine excitation

Figure 5.24 shows a typical time history of impact force and acceleration under swept-sine excitation, in this case the impact process occurs in a periodic manner, 2 impacts per cycle of excitation. The chaotic behaviour from this system can be examined by either varying the clearance or its excitation frequency but it is not our intention. In general, a full detailed analysis of nonlinear responses in time domain can be relied in this numerical simulation. Nevertheless, the entire impact process is well presented by a fundamental harmonic in which the envelope of time histories. This particularly holds true for the symmetrical impact system behaving in a periodic manner (see Figure 5.24 with appropriate label). The magnitude of absolute acceleration and relative deflection signals in frequency domain can be readily obtained via **statistic** subsystem.

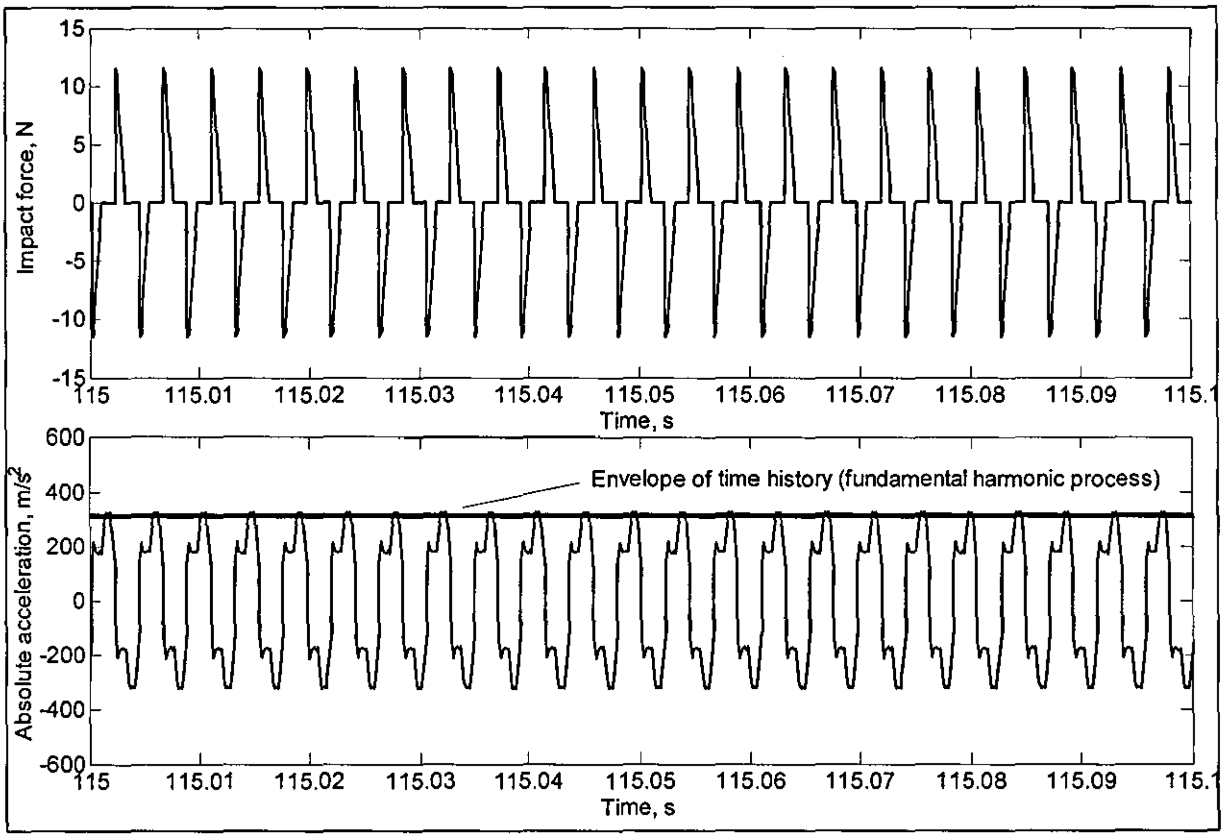

Figure 5.24. Time history of impact damper under swept-sine excitation

5.3.1 Sensitivity analysis

The sensitivity analysis is carried out for the mass ratio of 65% on loss factors and natural frequencies of the symmetrical visco-elastic limiter at different clearances, this would reflect on the performance and sensitivity of impact damper as compared to the linear case under swept-sine excitation. Firstly, this is done by fixing the loss factor to 0.35 (as it was used in linear case for 65% mass ratio) and natural frequency is varied from 50 Hz to 2000 Hz. Similar to Section 5.1.4, the clearance is introduced in different values.

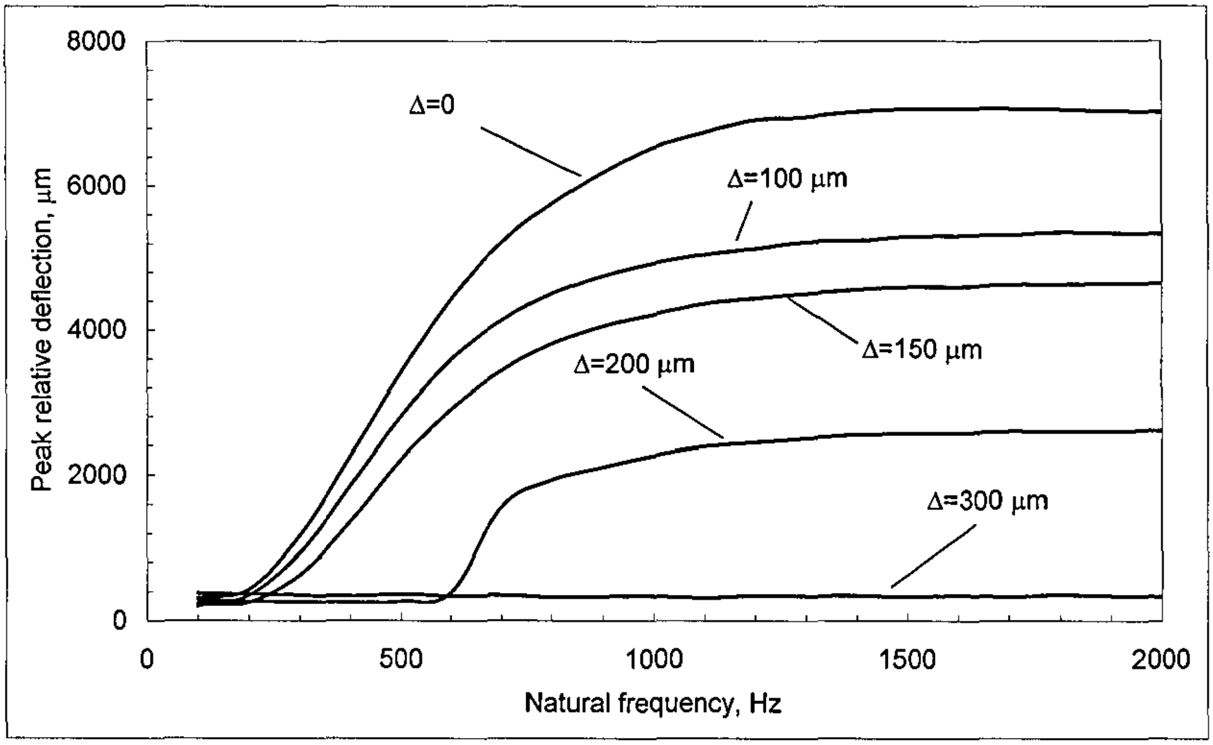

Figure 5.25. Sensitivity analysis on natural frequency

Figure 5.25 shows the variation of peak relative deflection against natural frequency of the symmetrical visco-elastic limiter, the curve labelled as (Δ=0) which corresponds to the linear case, as here, the sensitivity of the modified PCB is increased proportionally with the natural frequency of linear dynamic absorber. With the presence of clearance, the sensitivity outside its tuning has reduced significantly, in this case, when Δ=300 μm, the natural frequency of the visco-elastic has no effect on the desired peak relative deflection.

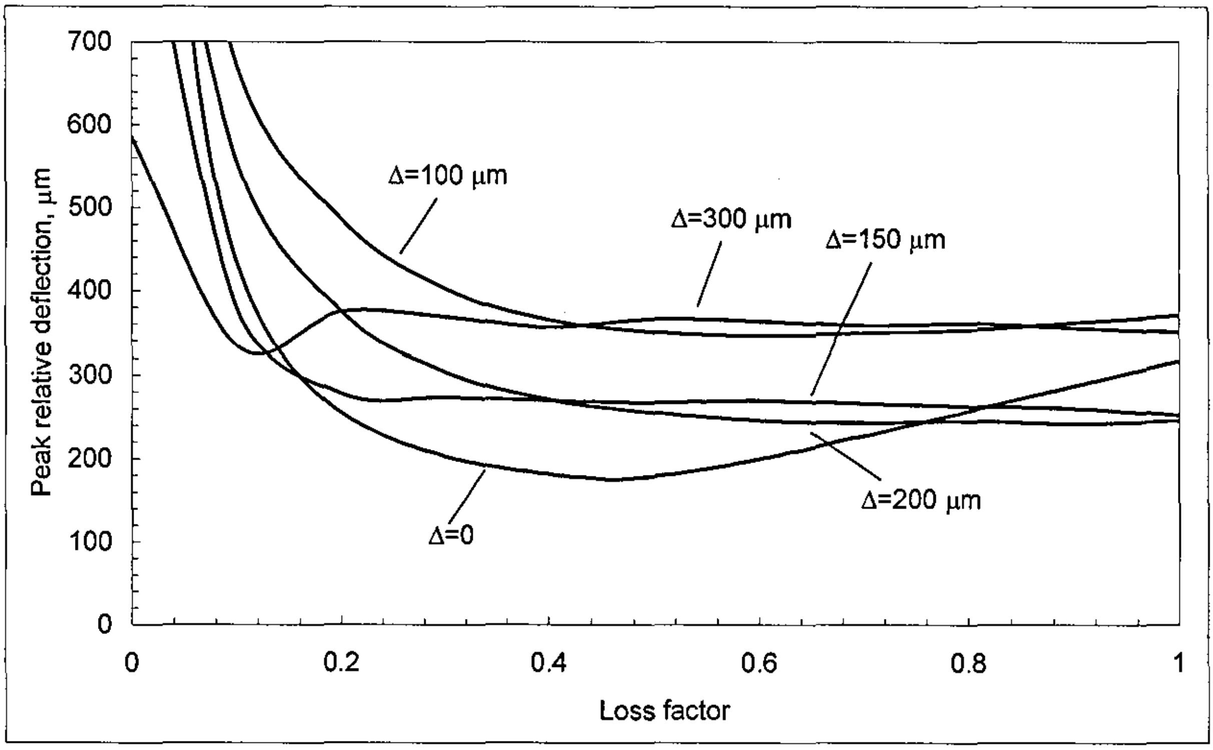

Figure 5.26. Sensitivity analysis on loss factor

Figure 5.26 shows the variation of peak relative deflection on loss factor whilst the natural frequency is fixed at 106 Hz. In this figure, the curve labelled Δ=0 is from the linear case which give the lowest value of relative deflection when it is tuned. However, this optimal value applies only for its optimal natural frequency of 106 Hz. The performance of the impact damper does not show any specific value of loss factor as its clearance is increased, the higher value of loss factor is the most appropriate one.

From sensitivity analysis, the desired performance of impact damper under swept-sine application at 65% mass ratio does not require any specific value of loss factor or natural frequency of the visco-elastic limiter. For this reason, we implement the parameter sets that chosen for random vibration application into swept-sine application i.e.

$$\eta=65\%,\ \Omega = 200\ \text{Hz},\ \xi = 0.5\ \text{at}\ \Delta = 150\ \mu\text{m}$$

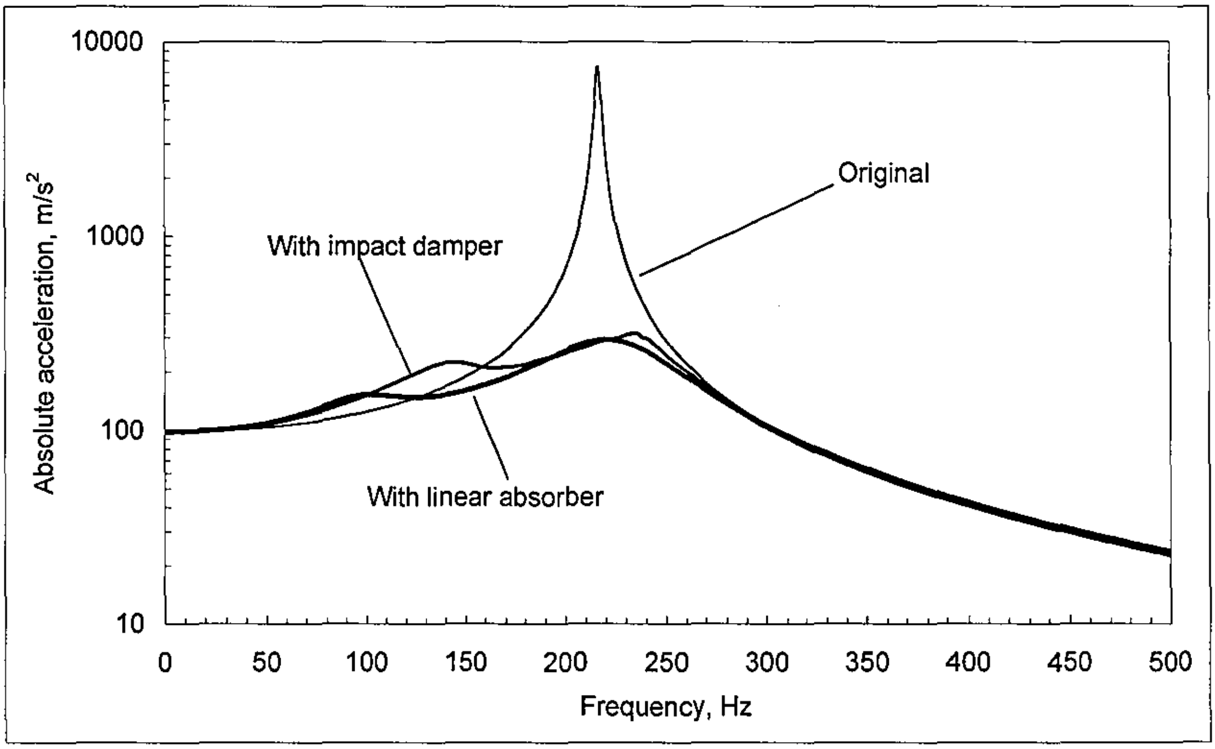

a) Absolute acceleration

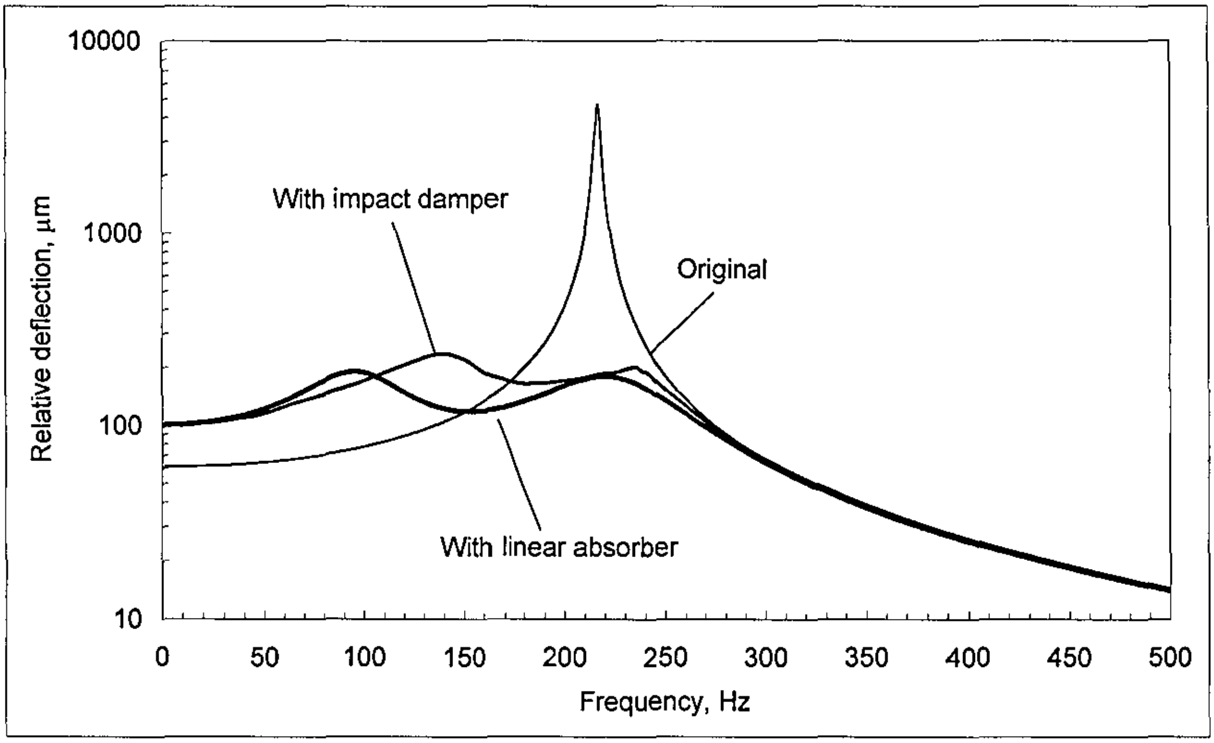

b) Relative deflection

Figure 5.27. Simulated dynamic response of original and modified PCB (η=65%)

Figures 5.27 shows the superimposed absolute acceleration and relative deflection, respectively, of the original and modified PCB also the linear optimal response is superimposed for reference. For the nonlinear performance, the peak relative deflection is found to be 260 μm, this is about 70 μm higher than that of the optimal linear case (190 μm) at the same mass ratio. This seems to be an acceptable performance compared to the original design in which the reduction ratio is about 19 times.

Similarly, at a mass ratio of 35% with the same the visco-elastic limiter's properties ($\Omega/2\pi$ = 200 Hz, $\xi = 0.5$) at Δ = 150 μm, the absolute acceleration and relative deflection can be seen in Figure 5.28 with reference to its original response and the optimal response of linear case at the same mass ratio.

For this particular parameters set, the performance between linear and nonlinear cases is almost the same in which the peak relative deflection of both cases are found to be 210 μm. It should be noted here, the nonlinear performance of 35% mass ratio is better than 65% with the same parameters set, but it seems to be insignificant. Keeping in mind that these differences only apply for this specific clearance, loss factor and natural frequency of the visco-elastic limiter.

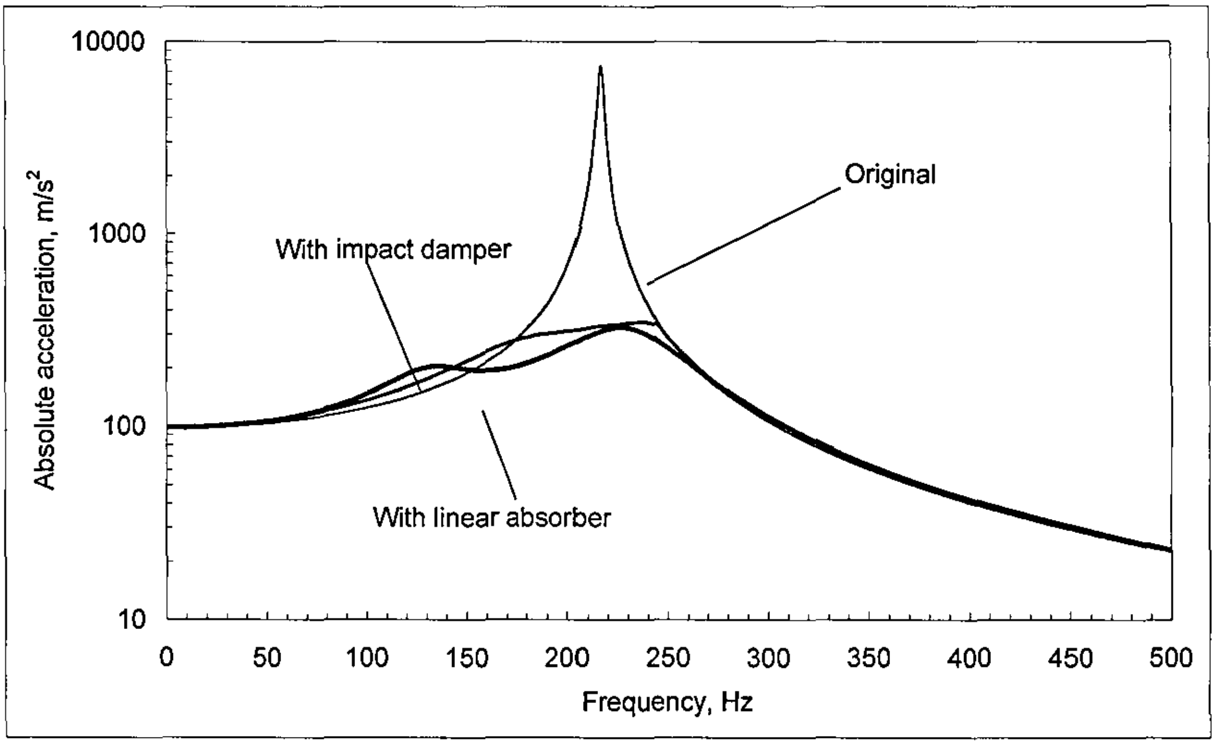

a) Absolute acceleration

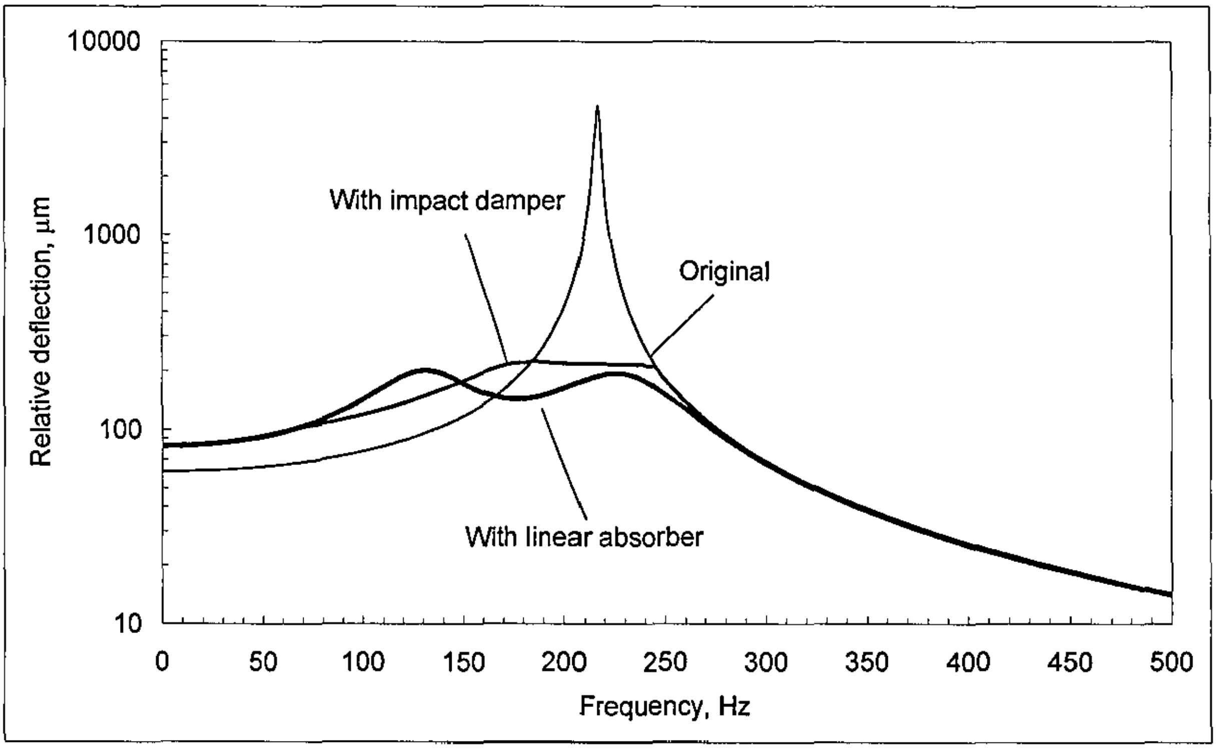

b) Relative deflection

Figure 5.28. Simulated dynamic response of original and modified PCB (η=35%)

From this study, the same dynamic properties of the visco-elastic limiter and clearance that was chosen for the random vibration is still suitable for swept-sine application, and also suitable for both mass ratios.

In swept-sine application, the peak relative deflection the PCB in the frequency range of 20-500 Hz is of primary concern, therefore the analysis in the single-mode approximation would be sufficient to reflect the performance of the full-mode model of the PCB in terms of reduction ratio. In addition, impact damper technique does not require any specific natural frequency or loss factor of the visco-elastic limiter. With this positive feature, the degree of accuracy is not required, therefore, the analysis of the full-mode model of PCB might not be relevant.

5.4 Shock

An impact damper could be an alternative method for vibration suppression of the PCB in random and swept-sine vibration. It shows that the chosen impact damper is suitable for both applications although its universal performance is so far a little less than target. The method of carrying out the investigation relied on numerical simulation which was based on a realistic model, the results of the finding proves to be consistent. As with the linear absorber study, the completion of this investigation is to consider the MIL-STD-810 shock test (half-sine shock pulse at 200g peak @ 3 ms) to see the influence of the impact damper on the PCB with the above parameters set s i.e.

$$\Omega/2\pi = 200, \text{Hz}, \ \xi = 0.5 \text{ at } \Delta = 150\ \mu\text{m},$$

for both mass ratios.

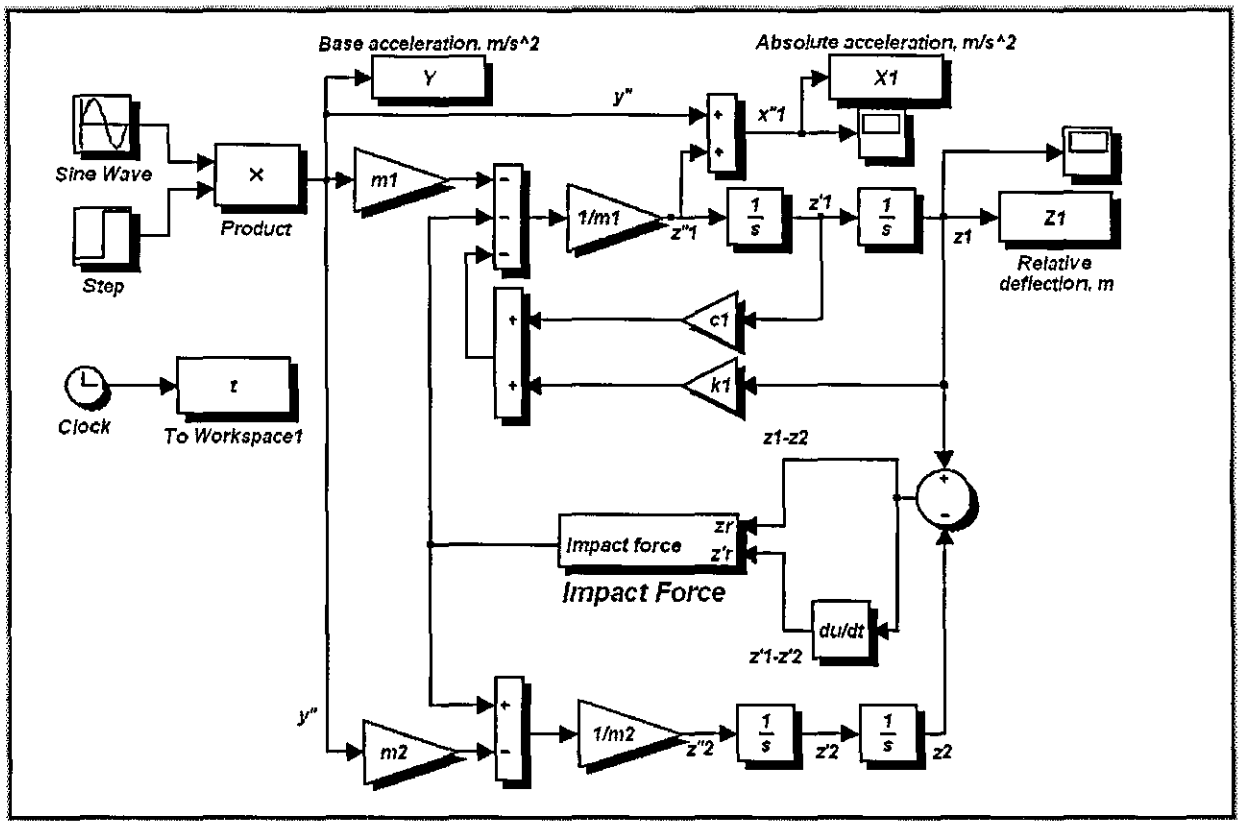
Base acceleration, m/s^2
Y
Absolute acceleration, m/s^2
X1
y"
x"1
Sine Wave
Product
m1
1/m1
z"1
1/s
z'1
1/s
z1
Z1
Relative deflection, m
Step
c1
k1
Clock
t
To Workspace1
z1-z2
zr
Impact force
z'r
Impact Force
du/dt
z'1-z'2
y"
m2
1/m2
z"2
1/s
z'2
1/s
z2

Figure 5.29. Simulink diagram for shock excitation

For consistency, the numerical simulation of the single-mode model of PCB with the impact damper that used for the random vibration is now implemented for shock excitation in which all the necessary external features are connected to the internal structure of the Simulink model as shown in Figure 5.29. Again, this simulation model could be used for optimising the system subjected to shock but this was not our intention. However, the main concern of this simulation was to see the influence of the impact damper on the PCB with the above chosen parameters in which the time histories of absolute acceleration and relative deflection of the PCB are of primary interest

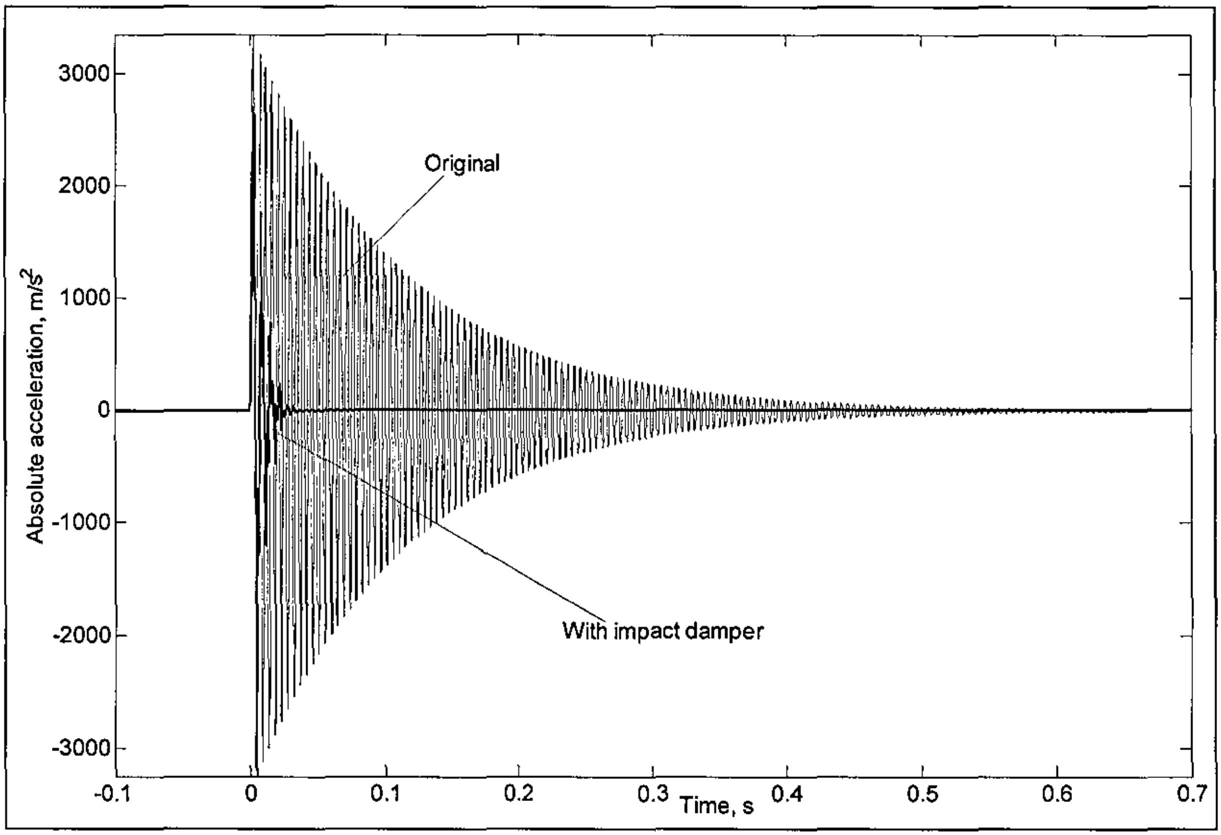

a) Absolute acceleration

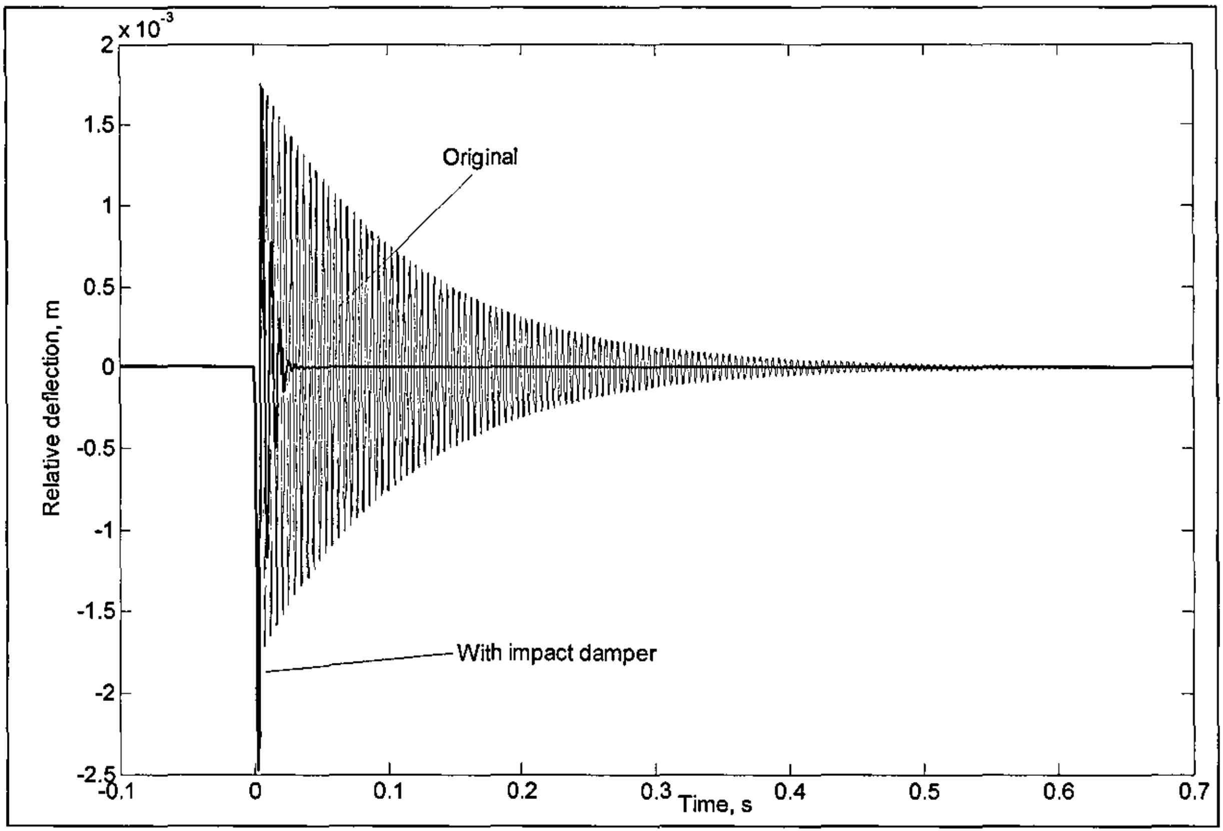

b) Relative deflection

Figure 5.30. Shock response of original and modified PCB (η=65%)

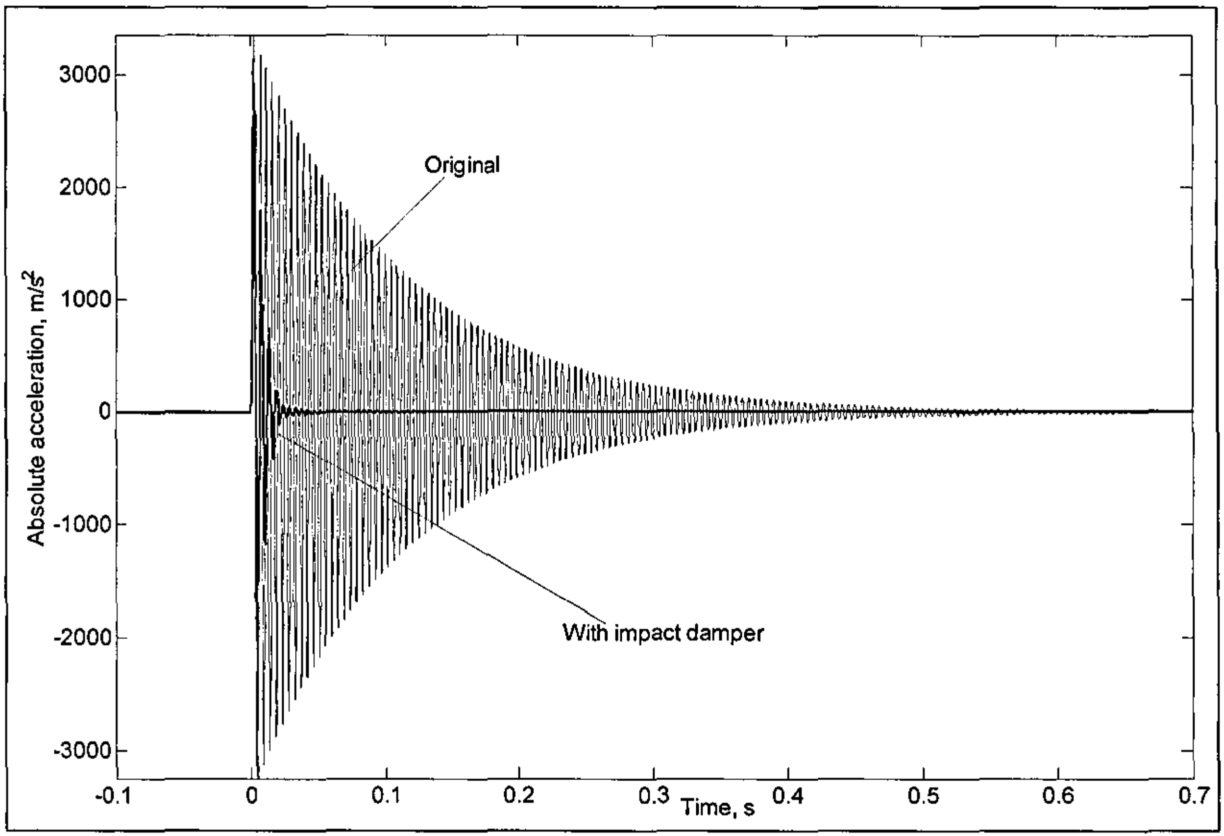

b) Absolute acceleration

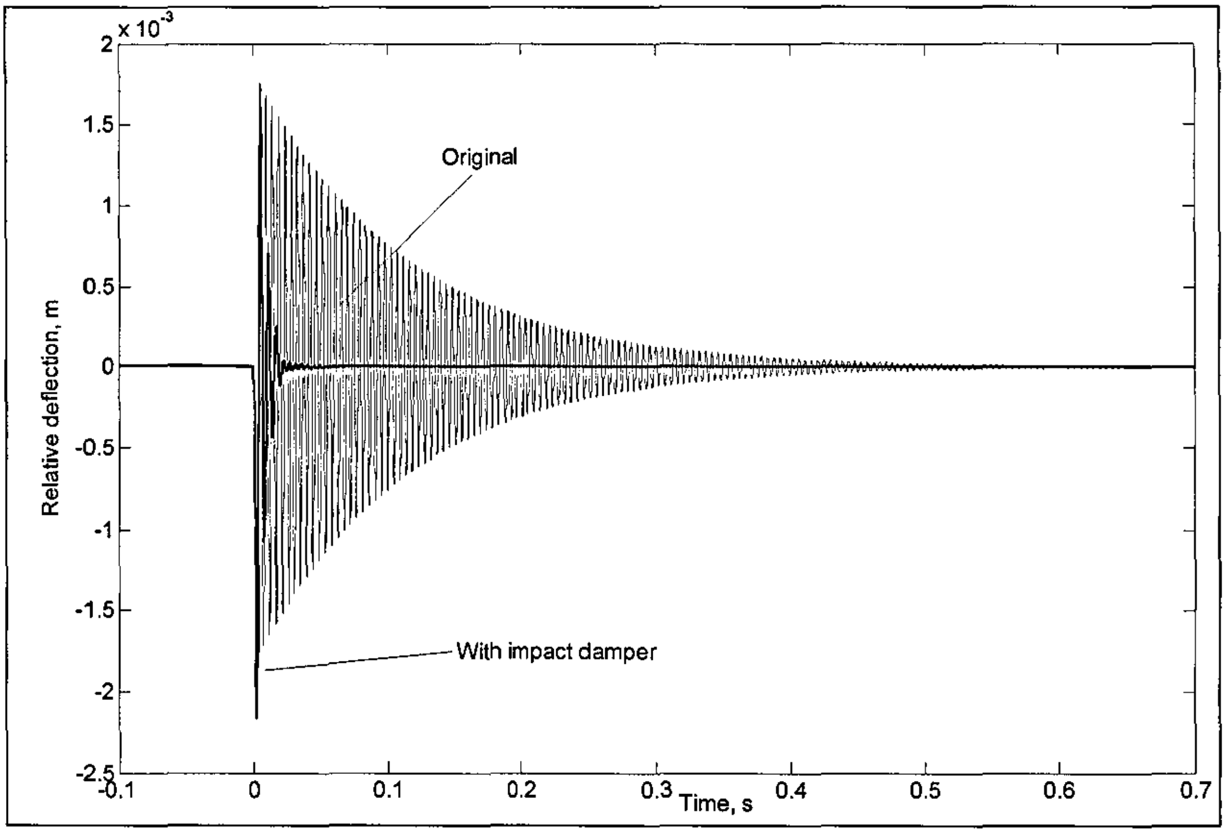

b) Relative deflection

Figure 5.31. Shock response of original and modified PCB (η=35%)

The performance of impact damper under shock excitation is almost similar to that of linear dynamic absorber at the same mass ratio in which the overall absolute acceleration, relative deflection and time settling show a significant improvement compared to the original response of the PCB, see Figure 5.30 and 5.31 for reference.

5.5 Concluding remarks

- In our nonlinear vibration study, the technique of building all Simulink models is almost similar to that of a corresponding linear case where all the necessary external disturbances and techniques of obtaining relevant signals practically remain the same
- With the presence of the **Impact Force** subsystem, the numerical simulation have made several contributions to the state-of-the-art and, as such, identified a number of unresolved issues of the vibroimpact system
- There is no optimal mass ratio to be found in the process of designing an impact damper. Strictly speaking, the differences of dynamic behaviour between the linear absorber and impact damper is clearance, it has an ability of reducing the sensitivity of the linear dynamic absorber beyond its tuning range

- At any given parameters set, an attainable universal performance would be found by tuning the clearance, this means that the impact damper that is designed for random vibration is suitable for swept-sine application and also suitable for shock excitation
- In practice, this could be an easier approach because many potential devices are available

Chapter 6

6.0 Experimental validation

During the initial stage of this study, a concise explanation of the full-mode model and single mode-model of PCB were addressed with respect to the root cause of the vibration. The search for an optimal dynamic absorber was entirely based on the original dynamic response of the chosen PCB and experimental measuring.

The fabrication and testing of the prototype dynamic absorber was the second stage. Taking into account that the dynamic absorber that was to be used was not available off-the-shelf, the design and manufacturing phase based on the optimal dynamic characteristics of the dynamic absorber and PCB was essential.

The third stage included the fabrication and installation of the optimal dynamic absorber on the real PCB and testing. Also, at this stage the main objective of this research was met through the experimentally measured data of the combined system per Mil-STD test.

6.1 Dynamic properties of dynamic absorber

To put the theory into practice, this dynamic absorber has to be designed and manufactured based on the dynamic characteristics of the PCB. Therefore, the important feature of dynamic ruggedizer is the capability of "tuning" its properties. In application, the dynamic absorber consists of visco-elastic grommet ① providing for damping and stiffness required (see Figure 6.0a). The heavy washer ② is used for inertia. The adjustment of frequency and loss factor of dynamic absorber relies on tightening the nut ③ and squeezing the grommet. In our experiments, suitable EAR ISODAMP® visco-elastic grommet and Tungsten washer (for compactness) were used. The above visco-elastic grommet is available off-the-shelf and the material used is capable of maintaining the persistent mechanical properties over a wide temperature range (see EAR data sheets from http://www.earsc.com/grommets). The two washers of mass 58.5 gr and 31.5 gr were manufactured. These two masses correspond to the mass factors of 65% and 35%, respectively, which gives 30% and 18% as compared to the actual mass of the PCB (175.5 gr). Strictly speaking, these dynamic absorber's size are really small which can be conveniently mounted on the upper-face of the PCB if necessary.

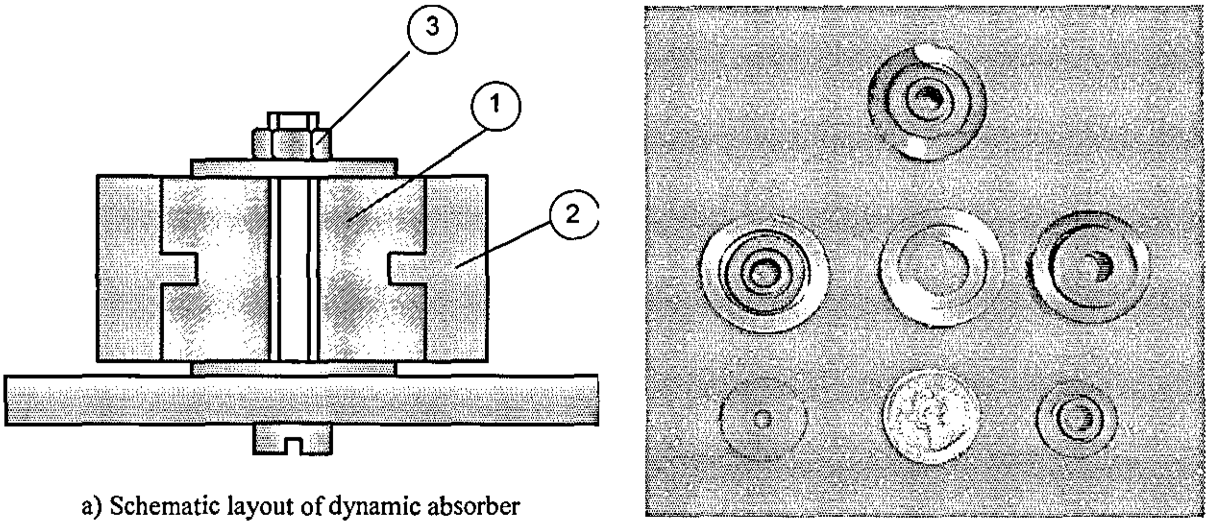

a) Schematic layout of dynamic absorber

b) Detailed assembly

Figure 6.0. Dynamic absorber

Before carrying out the experiment on the PCB with dynamic absorber attached, it is necessary to test the dynamic properties of the dynamic absorber separately. The dynamic absorber parameters are the most important factor contributing to the performance of the PCB and probably the most critical choice. For this purpose, the dynamic absorber is mounted on the fixture, which is rigidly attached to the shaker; the experimental set-up and apparatus is the same as in Figure 2.1 where it provided measurement of universal absolute and relative transmissibilities the dynamic absorber as shown in Figure 6.1.

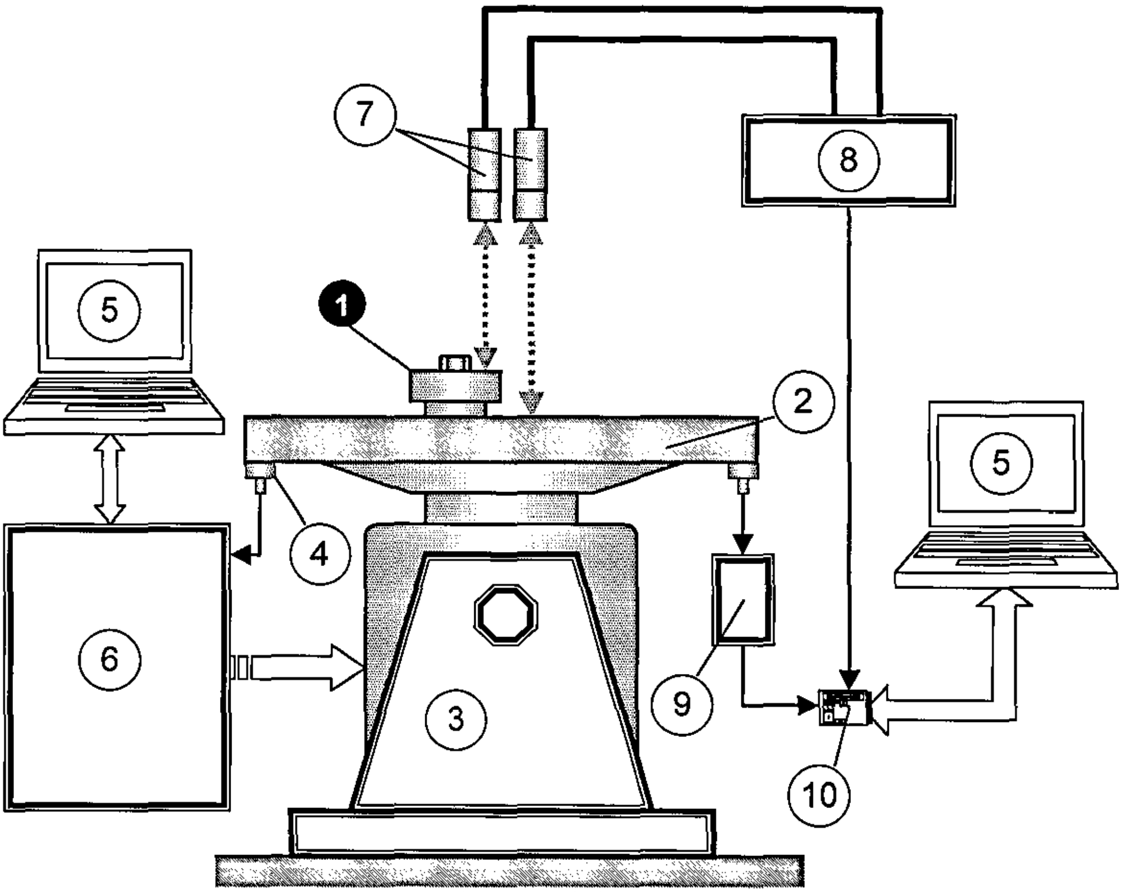

a) Schematic layout

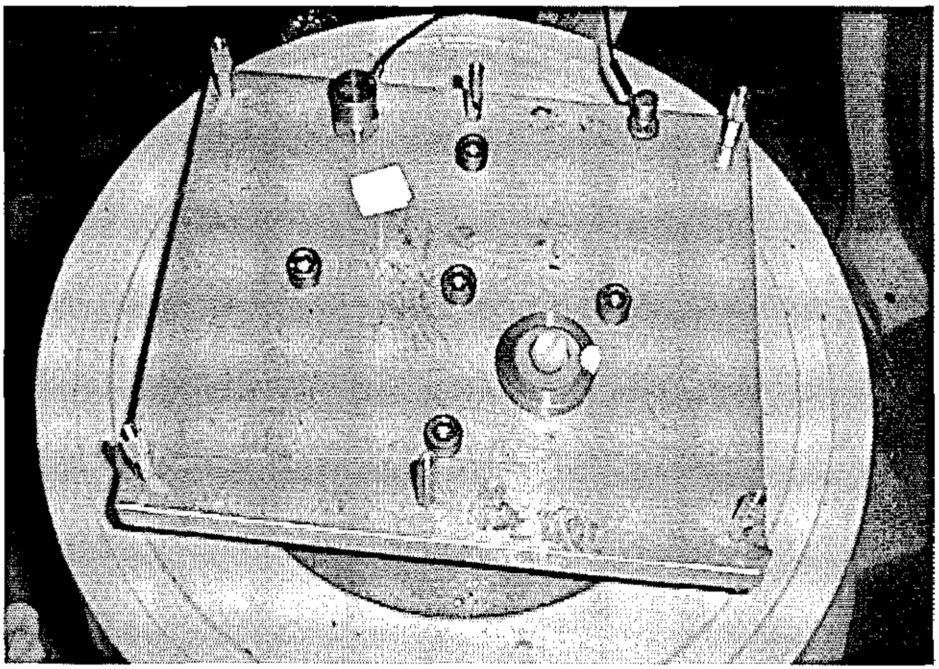

b) Dynamic absorber mounted on shaker

Figure 6.1. Experimental rig for tuning dynamic properties of dynamic absorber

The dynamic absorber mounted on the shaker is thought of as a SDOF system with base support motion. The modulus of absolute universal transmissibility of which may be expressed in terms of undamped natural frequency Ω_2 and loss factor ξ_2:

$$\left|T_a(j\omega)\right| = \sqrt{\frac{\Omega_2^4 + 4\omega^2\xi_2^2\Omega_2^2}{\left(\Omega_2^2 - \omega^2\right)^2 + 4\omega^2\xi_2^2\Omega_2^2}}. \tag{6.0}$$

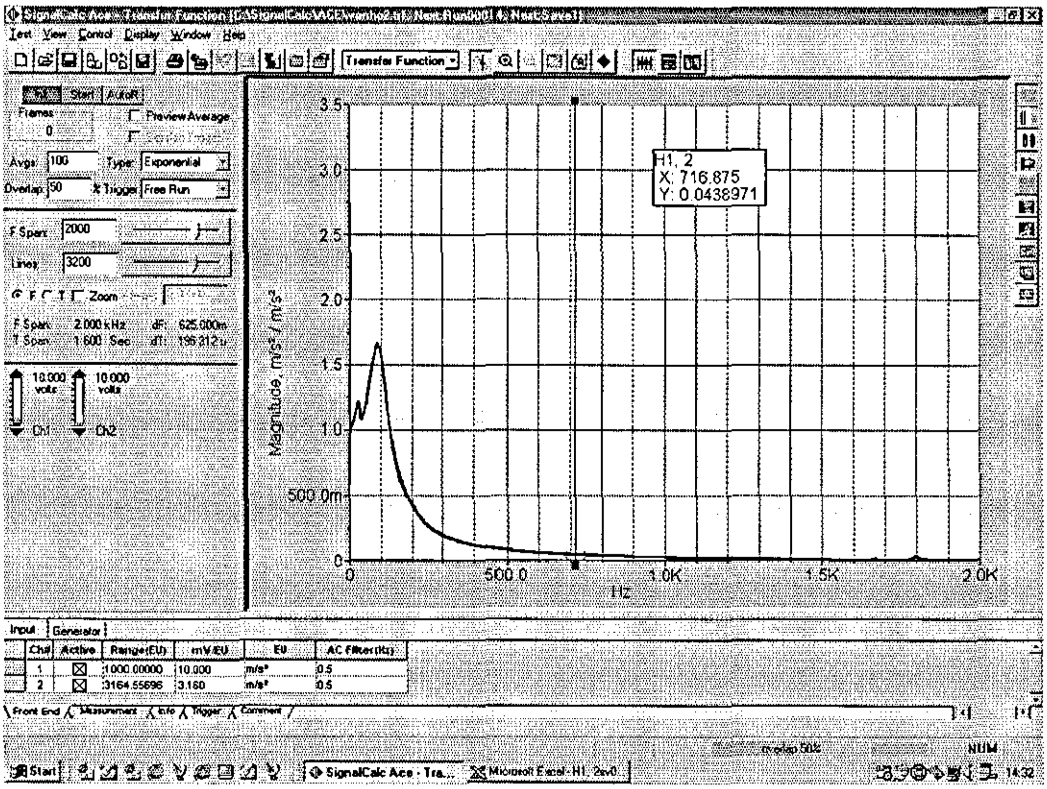

Test View Control Display Window Help
Transfer Function
Start
AutoR
Preview Average
Magnitude, m/s² / m/s²
3.5
3.0
2.5
2.0
1.5
1.0
500.0m
0
500.0
1.0K
1.5K
2.0K
Hz
Input
Generator
Front End
Measurement
Info
Trigger
Comment
Start
SignalCalc Ace - Tra...
Microsoft Excel - H1, 2av0
NUM
14:32

Frames 0

Avgs: 100 Type: Exponential

Overlap: 50 % Trigger: Free Run

F Span: 2000

Lines: 3200

● F ○ T ☐ Zoom

F Span: 2.000 kHz dF: 625.000m

T Span: 1.600 Sec dT: 195.312 u

Ch1 10.000 volts

Ch2 10.000 volts

H1, 2
X: 716.875
Y: 0.0438971

Chn#	Active	Range(EU)	mV/EU	EU	AC Filter(Hz)
1	☒	1000.00000	10.000	m/s²	0.5
2	☒	3164.55696	3.160	m/s²	0.5

overlap 50%

a) Analyser screenshot of absolute transmissibility of 58.5 gr dynamic absorber

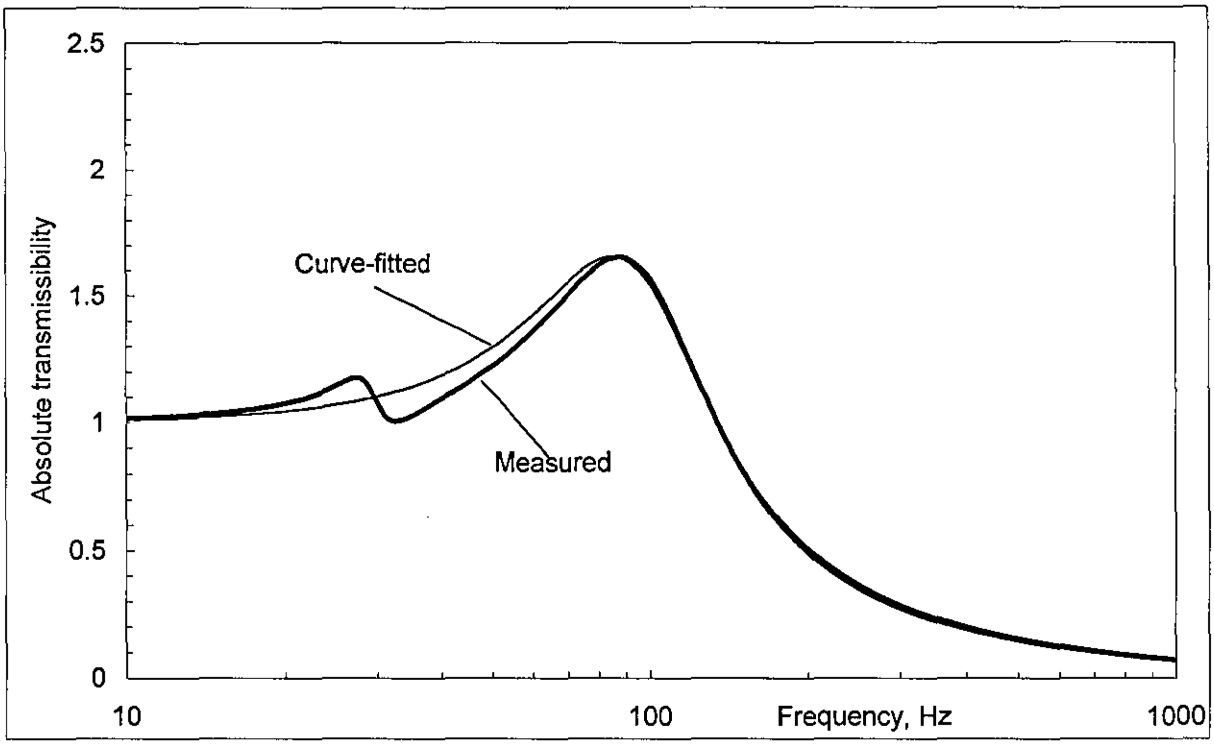

b) Absolute transmissibility of dynamic absorber (58.5 gr)

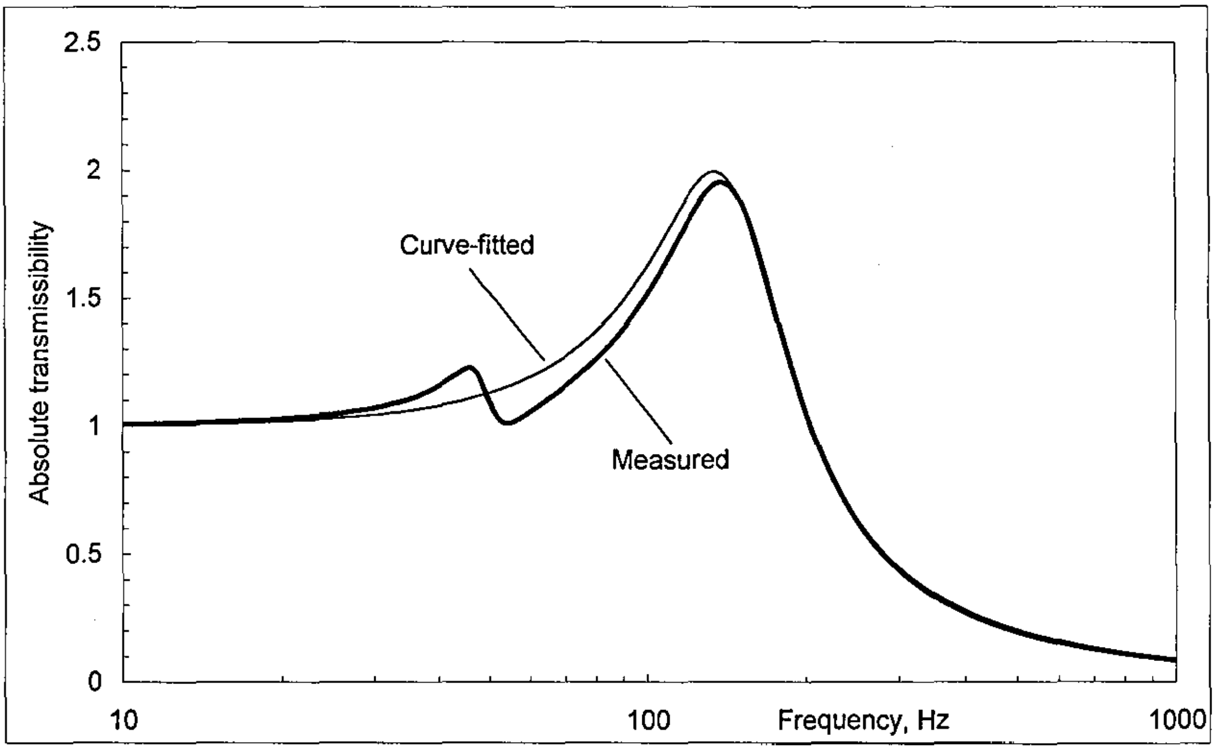

b) Absolute transmissibility of dynamic absorber (31.5 gr)

Figure 6.2. Comparison of absolute transmissibility of optimal dynamic absorbers

Figure 6.2 shows the absolute transmissibility of the chosen dynamic absorber. From curve-fitting with Equation 6.0 involved, the following modal parameters were identified: $\xi_2 = 0.39$, $\Omega_2 = 96.7$ Hz, for the mass of 58.5 gr and $\xi_2 = 0.287$, $\Omega_2 = 150$ Hz, for the mass of 31.5 gr, which are fairly close to the desired optimal values. Additionally, the above dynamic absorbers have the "tuneable" characteristics and they don't pose any nonlinearities at different excitation levels. From sensitivity analysis, better accuracy is most probably not required

6.2 Combined system

The objective of this experiment is to measure the dynamic response of the PCB with dynamic absorbers attached per MIL-STD test to back up its analytical study. The apparatus set-up for this experiment were similar to that in Figure 2.1, and are shown in Figure 6.3. For a better match result between the prediction and experimental measures, the dynamic absorber is now attached on the PCB at point ⓪ through a lightweight plastic screw as it was the main concern in the early stage of analysis. Additionally, this location of the dynamic absorber ensures that the major nodal points will not be involved.

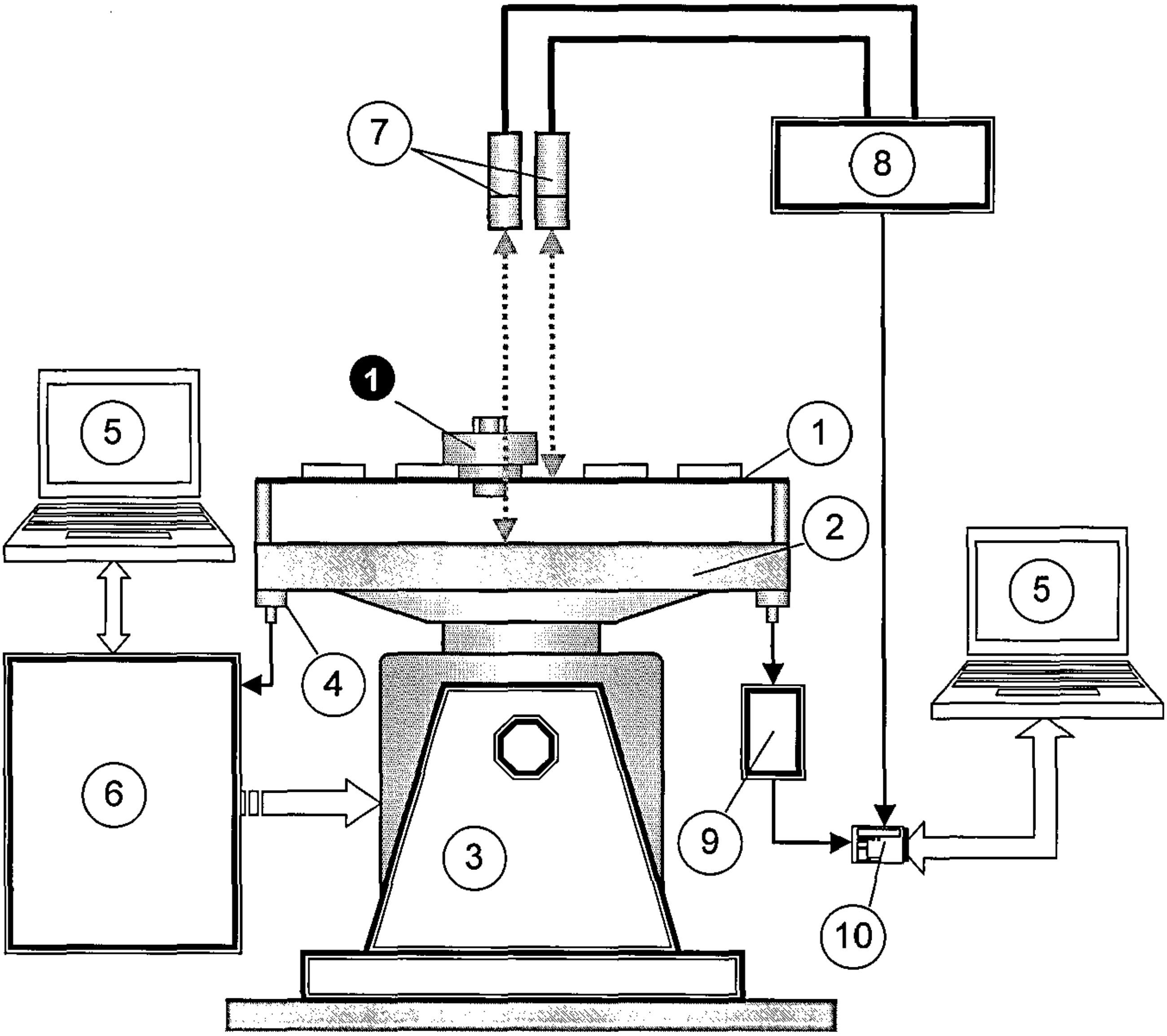

a) Schematic layout

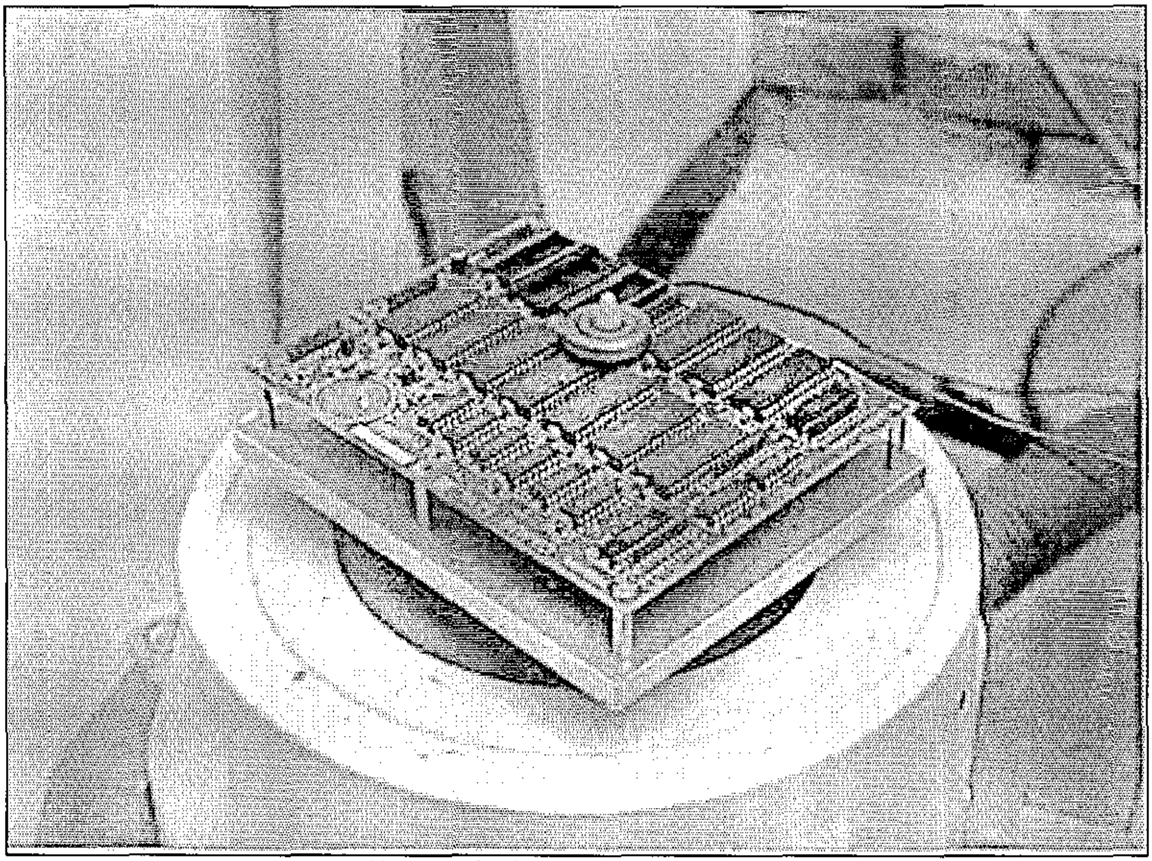

b) Dynamic absorber mounted on PCB

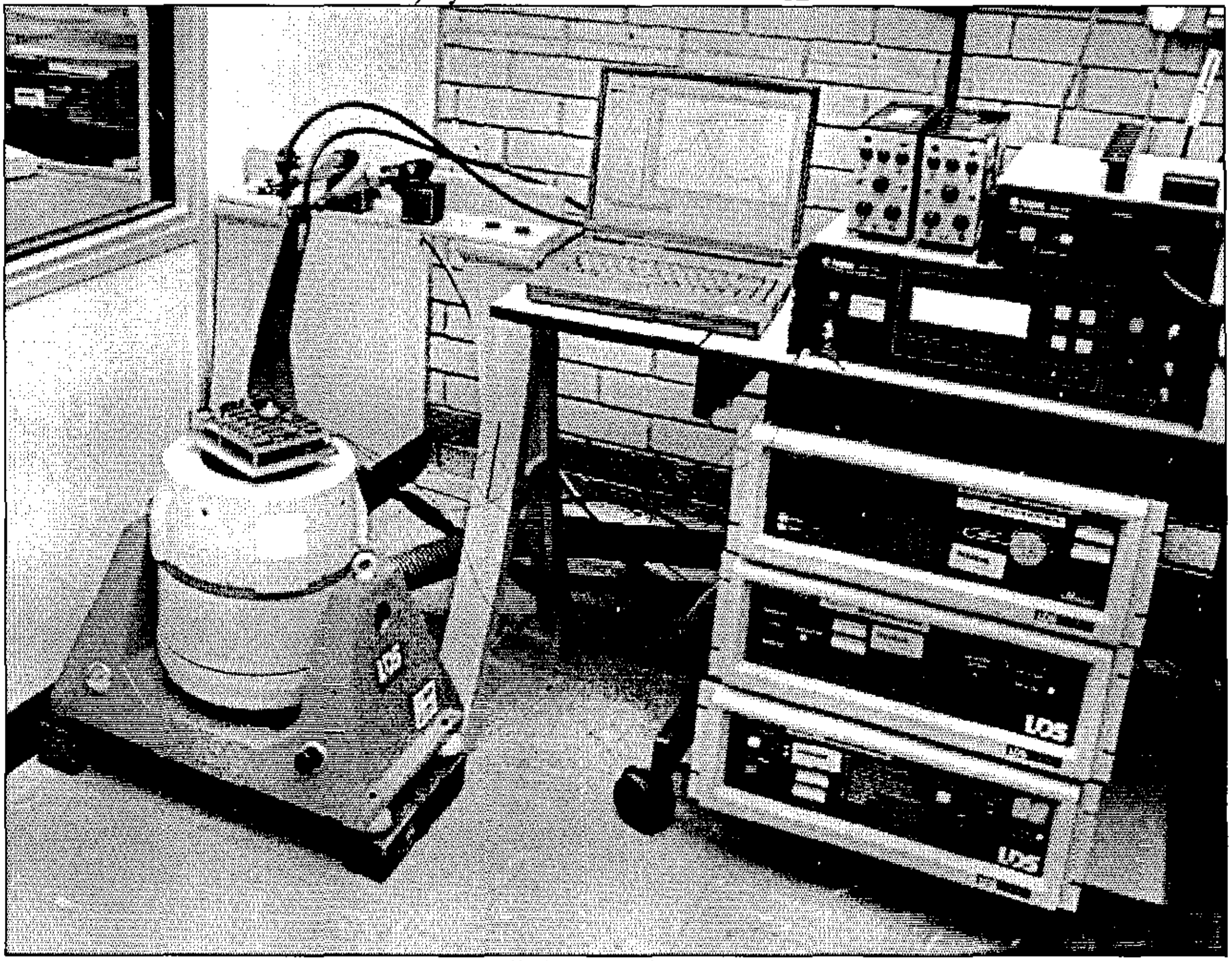

c) Overall view experimental set-up

Figure 6.3. Experimental rig for studying dynamic of PCB combined with dynamic absorber

6.2.1 Random vibration

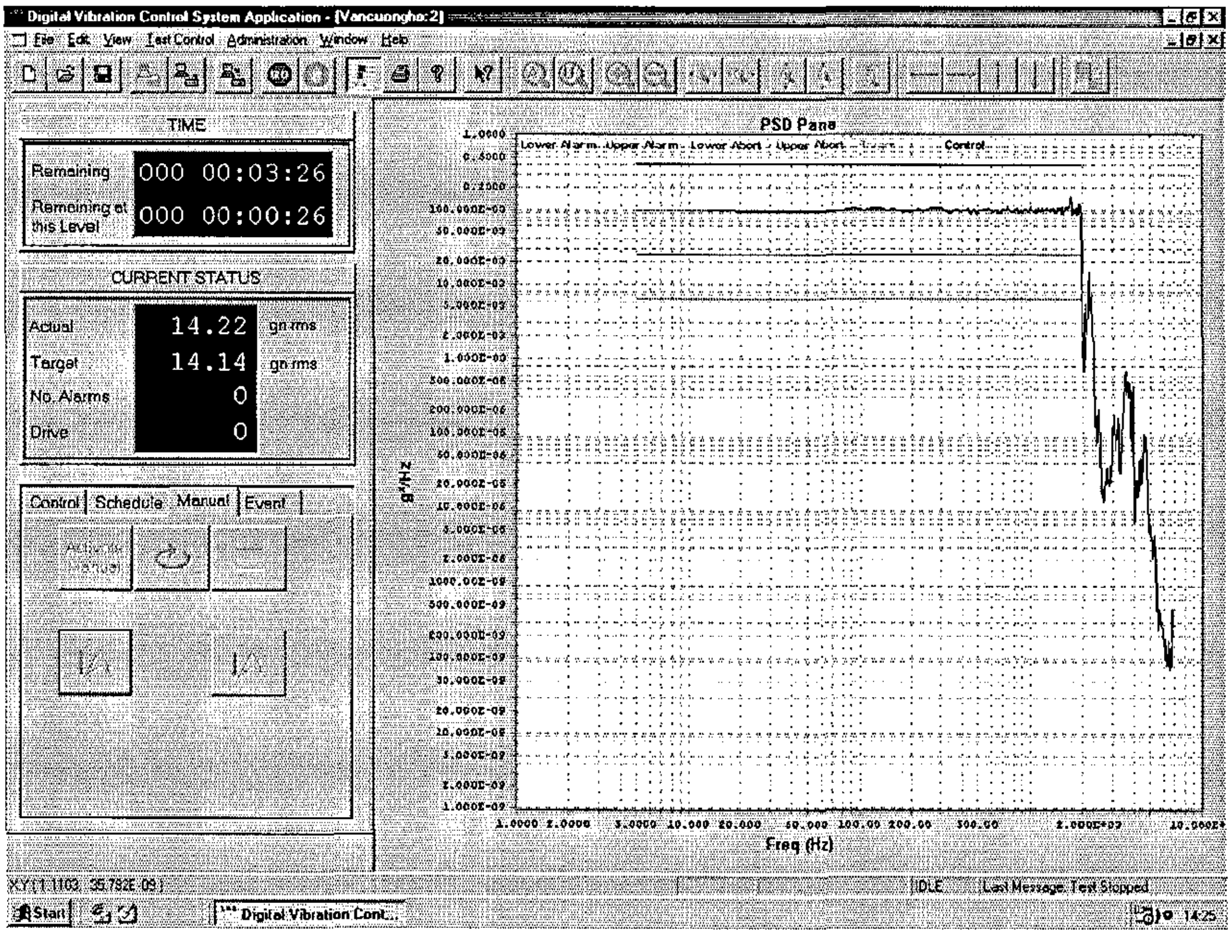

Digital Vibration Control System Application - [Vancuongho:2]

TIME

Remaining 000 00:03:26

Remaining at this Level 000 00:00:26

CURRENT STATUS

Actual 14.22 gn rms

Target 14.14 gn rms

No. Alarms 0

Drive 0

XY (1.1103, 35.782E-09)

IDLE

Last Message: Test Stopped

File
Edit
View
Test Control
Administration
Window
Help
Control
Schedule
Manual
Event
Activate Manual
PSD Pane
Lower Alarm
Upper Alarm
Lower Abort
Upper Abort
Control
1.0000
0.5000
0.2000
100.000E-03
50.000E-03
20.000E-03
10.000E-03
5.000E-03
2.000E-03
1.000E-03
500.000E-06
200.000E-06
100.000E-06
50.000E-06
20.000E-06
10.000E-06
5.000E-06
2.000E-06
1000.00E-09
500.000E-09
200.000E-09
100.000E-09
50.000E-09
20.000E-09
10.000E-09
5.000E-09
2.000E-09
1.000E-09
g²/Hz
1.0000
2.0000
5.0000
10.000
20.000
50.000
100.00
200.00
500.00
2.000E+03
10.000E+
Freq (Hz)
Start
Digital Vibration Cont...
14:25

a) Random vibration profile from vibration control screen

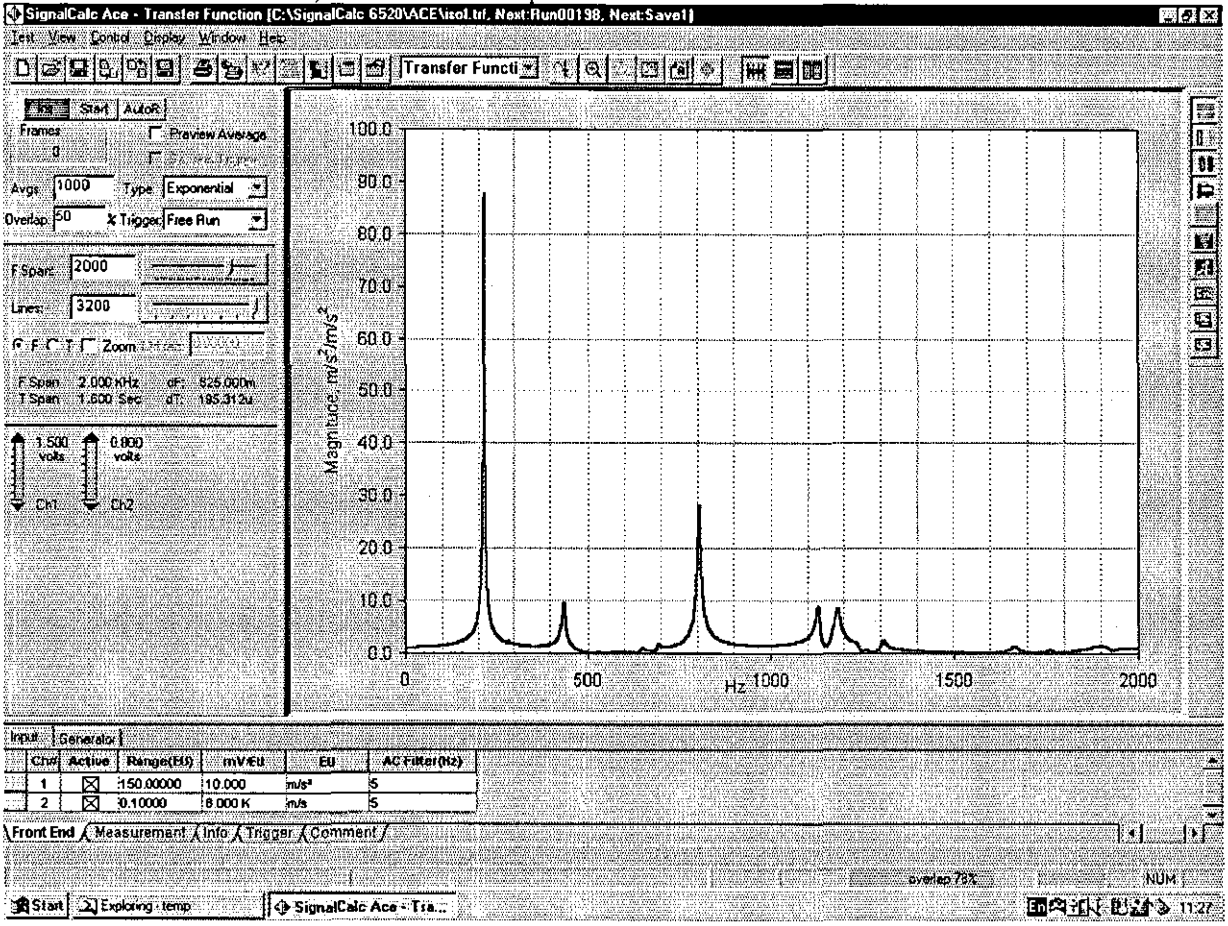

SignalCalc Ace - Transfer Function [C:\SignalCalc 6520\ACE\isol.trf, Next:Run00198, Next:Save1]

Frames 0

☐ Preview Average

Avgs 1000

Type Exponential

Overlap 50 % Trigger Free Run

F Span: 2000

Lines: 3200

● F ○ T ☐ Zoom

F Span 2.000 kHz dF: 625.000m

T Span 1.600 Sec dT: 195.312u

1.500 volts Ch1

0.800 volts Ch2

Ch#	Active	Range(EU)	mV/EU	EU	AC Filter(Hz)
1	☒	150.00000	10.000	m/s²	5
2	☒	0.10000	8.000 K	m/s	5

overlap 78%

Test
View
Control
Display
Window
Help
Transfer Functi
Start
AutoR
100.0
90.0
80.0
70.0
60.0
50.0
40.0
30.0
20.0
10.0
0.0
Magnitude, m/s²/m/s²
0
500
1000
1500
2000
Hz
Input
Generator
Front End
Measurement
Info
Trigger
Comment
NUM
Start
Exploring - temp
SignalCalc Ace - Tra...
11:27

b) Original

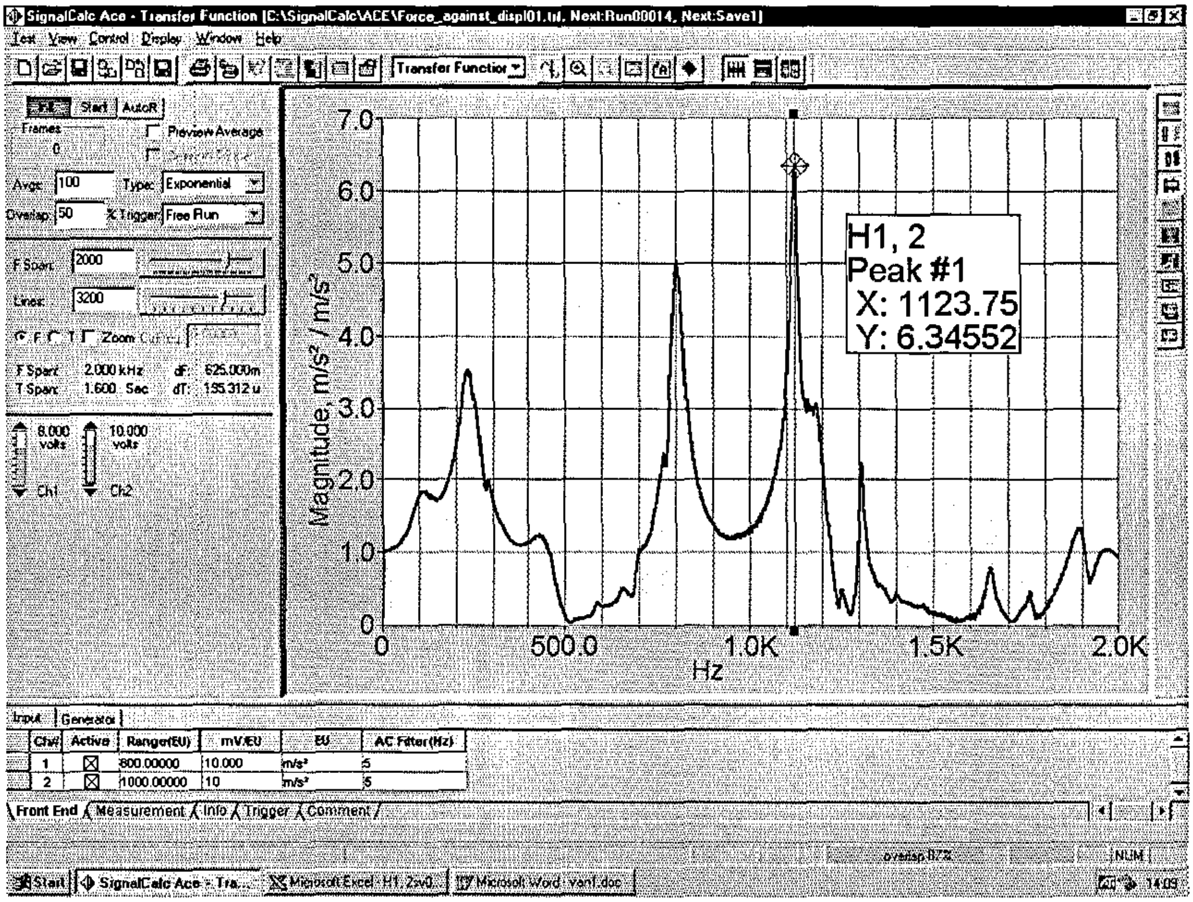
SignalCalc Ace - Transfer Function [C:\SignalCalc\ACE\Force_against_displ01.trf, Next:Run00014, Next:Save1]
Test View Control Display Window Help
Transfer Function
Start AutoR
Frames
Preview Average
Magnitude, m/s² / m/s²
7.0
6.0
5.0
4.0
3.0
2.0
1.0
0
500.0
1.0K
1.5K
2.0K
Hz
H1, 2
Peak #1
X: 1123.75
Y: 6.34552
Input Generator
Front End Measurement Info Trigger Comment
overlap 87%
NUM
Start SignalCalc Ace - Tra... Microsoft Excel - H1_2sv0... Microsoft Word - van1.doc
14:09

Frames: 0
Avgs: 100 Type: Exponential
Overlap: 50 % Trigger: Free Run
F Span: 2000
Lines: 3200
F Span: 2.000 kHz dF: 625.000m
T Span: 1.600 Sec dT: 195.312 u
8.000 volts Ch1
10.000 volts Ch2

Ch#	Active	Range(EU)	mV/EU	EU	AC Filter(Hz)
1	☒	800.00000	10.000	m/s²	5
2	☒	1000.00000	10	m/s²	5

b) With 65% mass ratio

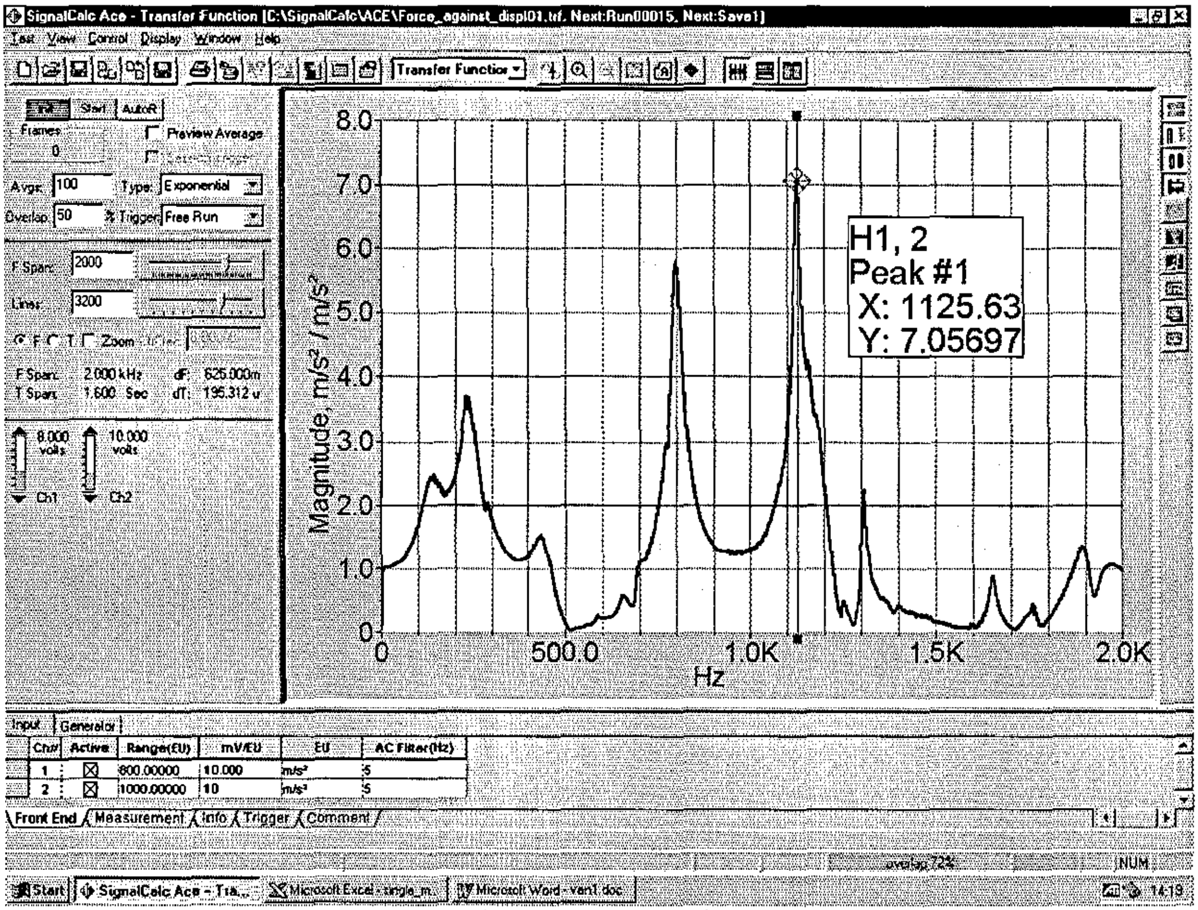
SignalCalc Ace - Transfer Function [C:\SignalCalc\ACE\Force_against_displ01.trf, Next:Run00015, Next:Save1]
Test View Control Display Window Help
Transfer Function
Start AutoR
Frames
Preview Average
Magnitude, m/s² / m/s²
8.0
7.0
6.0
5.0
4.0
3.0
2.0
1.0
0
500.0
1.0K
1.5K
2.0K
Hz
H1, 2
Peak #1
X: 1125.63
Y: 7.05697
Input Generator
Front End Measurement Info Trigger Comment
overlap 72%
NUM
Start SignalCalc Ace - Tra... Microsoft Excel - single_m... Microsoft Word - van1.doc
14:19

Frames: 0
Avgs: 100 Type: Exponential
Overlap: 50 % Trigger: Free Run
F Span: 2000
Lines: 3200
F Span: 2.000 kHz dF: 625.000m
T Span: 1.600 Sec dT: 195.312 u
8.000 volts Ch1
10.000 volts Ch2

Ch#	Active	Range(EU)	mV/EU	EU	AC Filter(Hz)
1	☒	800.00000	10.000	m/s²	5
2	☒	1000.00000	10	m/s²	5

c) With 35% mass ratio

Figure 6.4 Analyser screenshot of absolute transmissibility of the original and ruggedized PCB at different mass ratio and their input excitation

The dynamic absorber with mass ratios of 65% and 35% was attached to the PCB individually for experimental purpose. The universal transmissibilities are first to be measured, as the excitation level will not necessary be the same as the design excitation level. However, the input spectrum will be the same shape as the design-input spectrum (14g RMS) and is shown in Figure 6.4a. Firstly, the measurement was taken at point ◎, the analyser screenshot of the absolute transmissibility for both mass ratios is shown in Figure 6.4c and 6.5d together with the original response Figure 6.4b for comparison purposes. The measured magnitude response of the modified PCB is of primary concern, this information would be sufficient for to validate the analytical solution, therefore, the phase response will be necessary presented in this work.

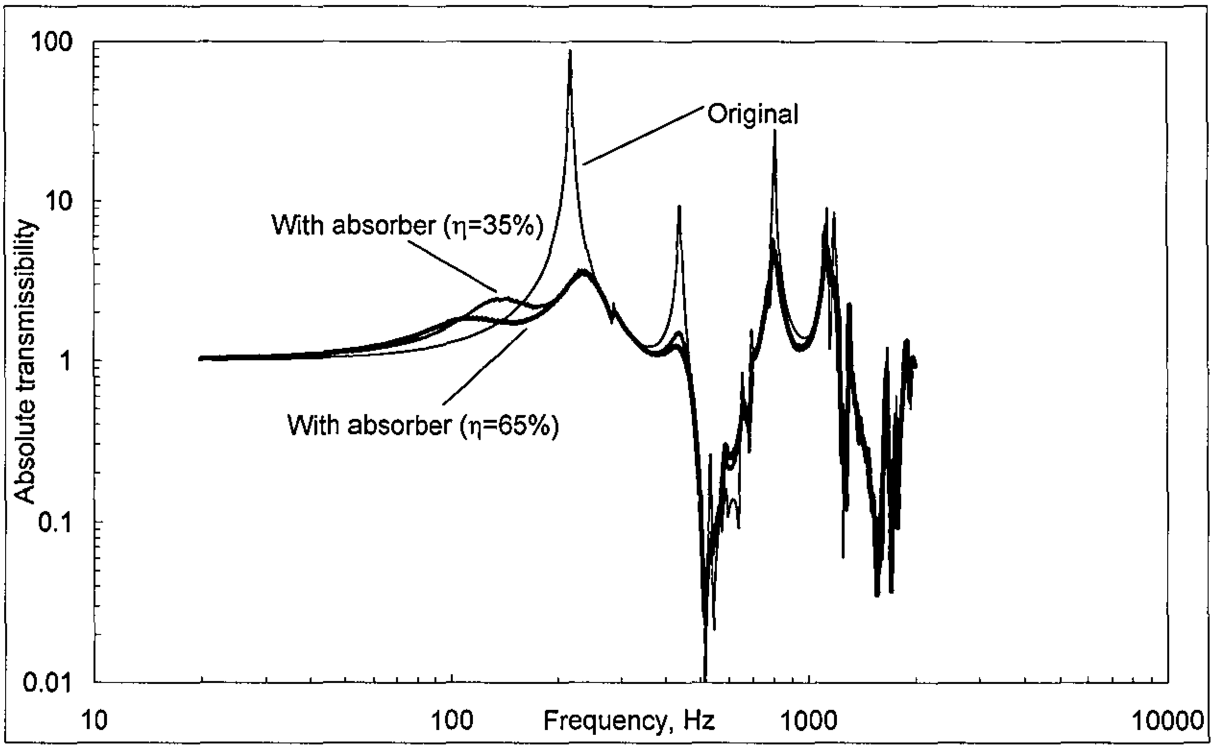

Figure 6.5. Experimentally measured absolute transmissibility of PCB with different mass ratios

Figure 6.5 shows the optimal absolute transmissibility of the PCB with different dynamic absorbers. In terms of absolute transmissibility, both cases provide similar characteristics as compared to the original response. From Figure 6.5, the influence of the dynamic absorber is that almost all resonances of the original PCB are significantly suppressed, while the antiresonant notches remain practically unaffected, as theoretically predicted above. This is an important feature of vibration suppression.

In terms of random vibration, the absolute acceleration of the PCB is normally expressed in RMS values. Generally, the measuring of RMS value would be calculated through the experimentally measured PSD. Table 6.0 highlights the results of overall absolute acceleration between prediction and experimentally measured data at the same level of excitation, 14 g RMS.

	Single-mode model of PCB (prediction)	Full-mode model of PCB (prediction)	Experimentally measured
Original	51.10 g RMS	70.18 g RMS	70.18 g RMS
35% mass ratio	11.18 g RMS	25.21 g RMS	25.10 g RMS
65% mass ratio	10.13 g RMS	22.93 g RMS	23.11 g RMS

Table 6.0. Comparison between measured and predicted results

The theoretical values of overall absolute acceleration (for full-mode model of PCB) are very close to its experimentally measured value. Both mass ratios of dynamic absorber produce a reduction ratio close to 3-fold vibration suppression compared to the original PCB design.

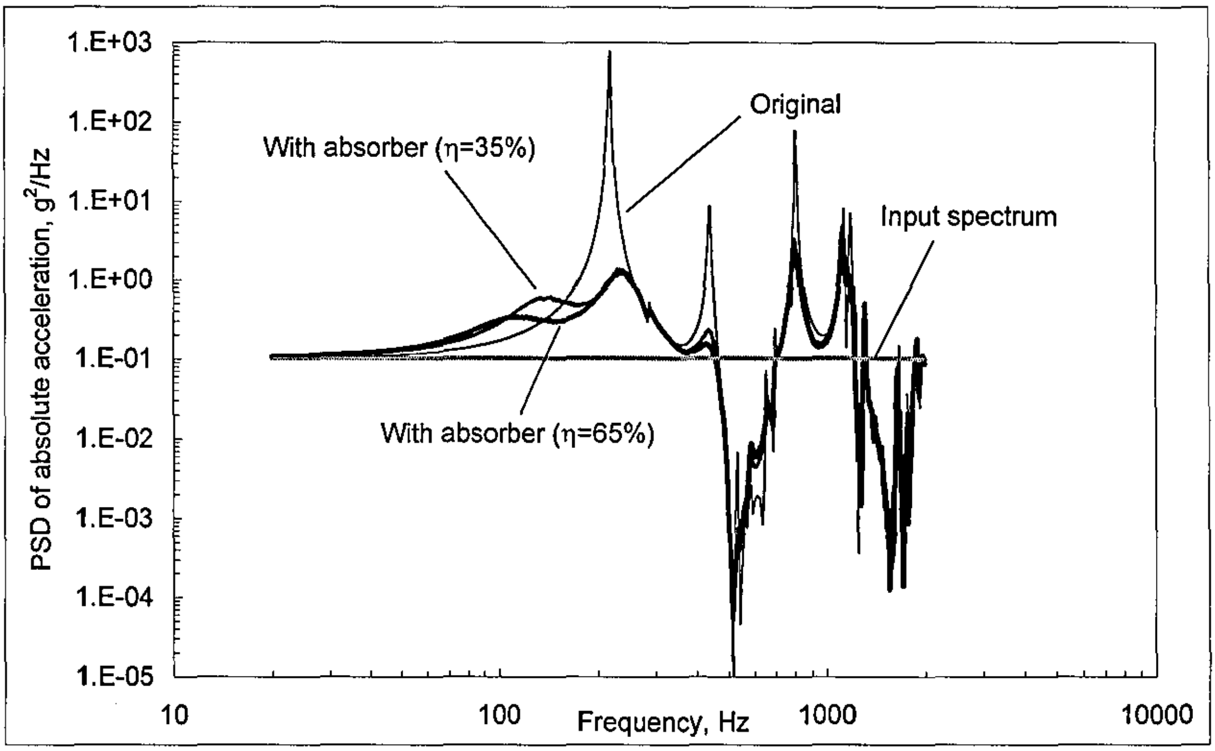

Figure 6.6. Experimentally measured PSD of absolute acceleration of PCB with different mass ratios

The reduction ratio between the original and ruggedized PCB in terms of overall absolute acceleration was calculated. This was best done by graphically representing the actual PSD curve as shown in Figure 6.6 which corresponds to measured data.

Figure 6.7 shows the superimposed PSD of the relative deflection of the dynamically ruggedized PCB (experiment) at mass ratios 65% and 35%in which the overall relative deflection 77.6 μm RMS and 79.2 μm RMS are found, respectively.

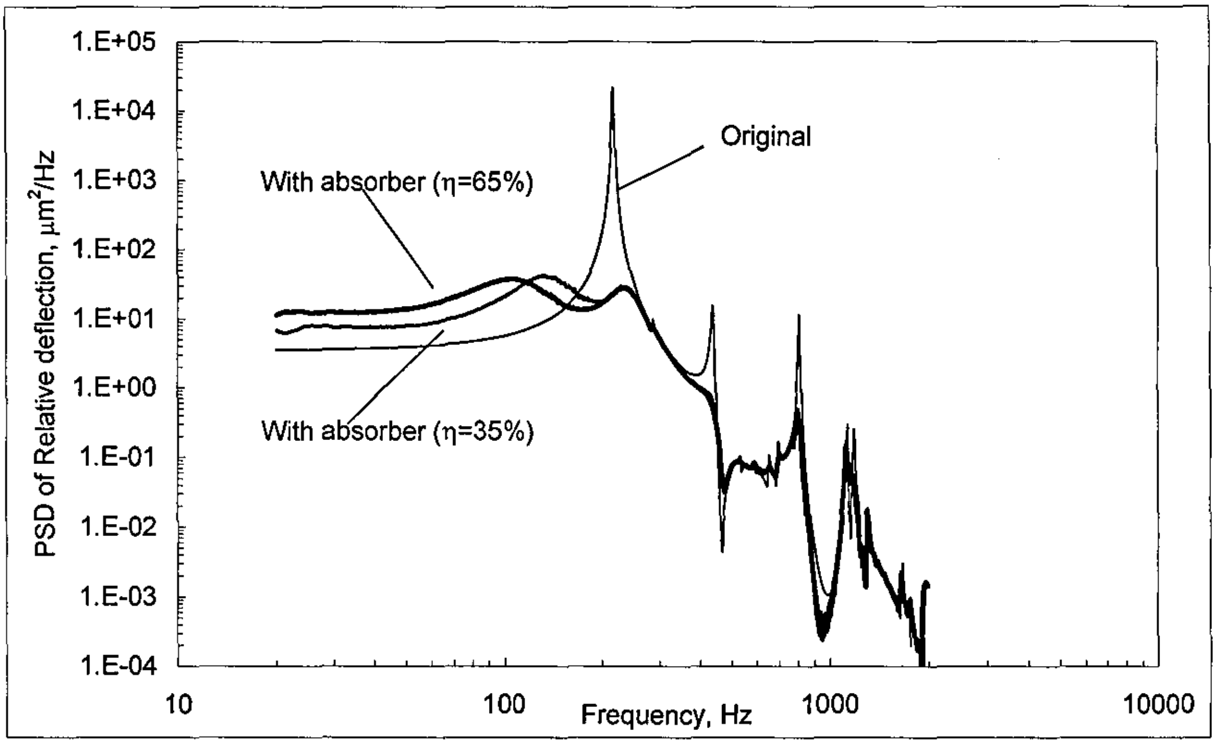

Figure 6.7. Experimentally measured PSD of relative deflection of original and ruggedized PCB at different mass ratios

Figure 6.8 shows the superimposed PSD of the relative deflection of the dynamically ruggedized PCB (experiment vs. theory) at a mass ratio 65% and 35%, respectively. Experimental results are in fair agreement with the analytical solution.

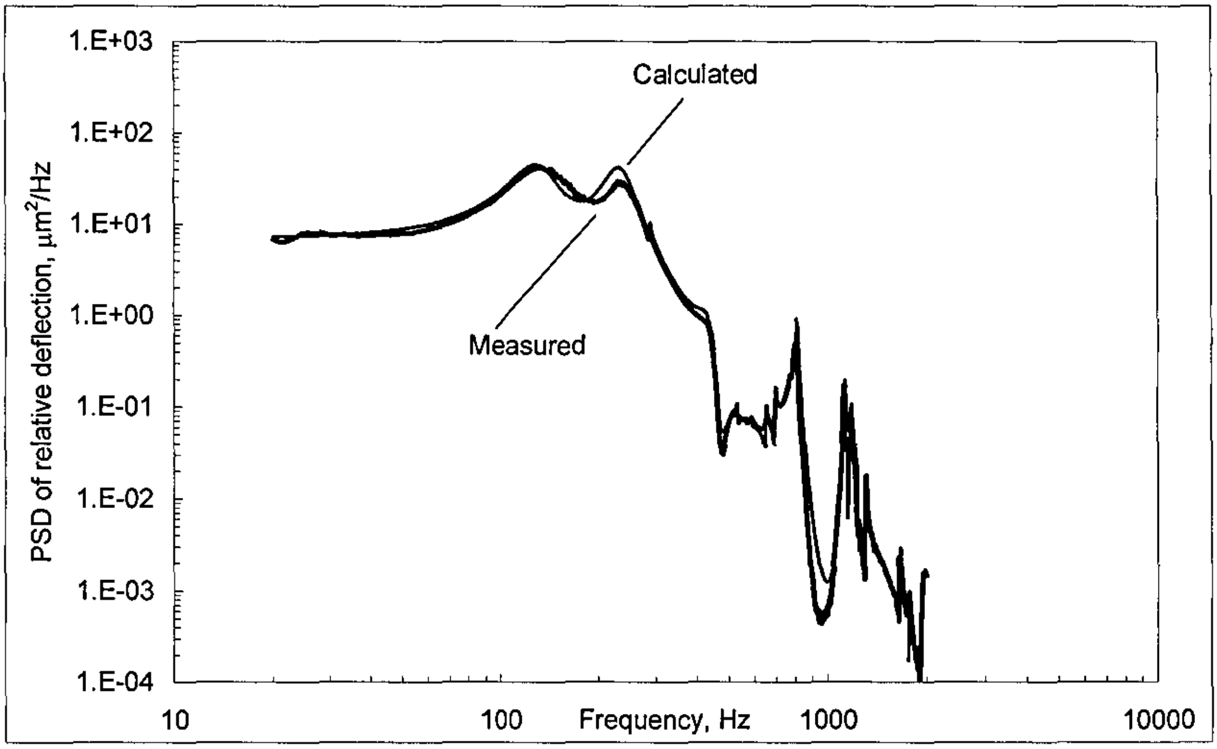

a) With 35% mass ratio

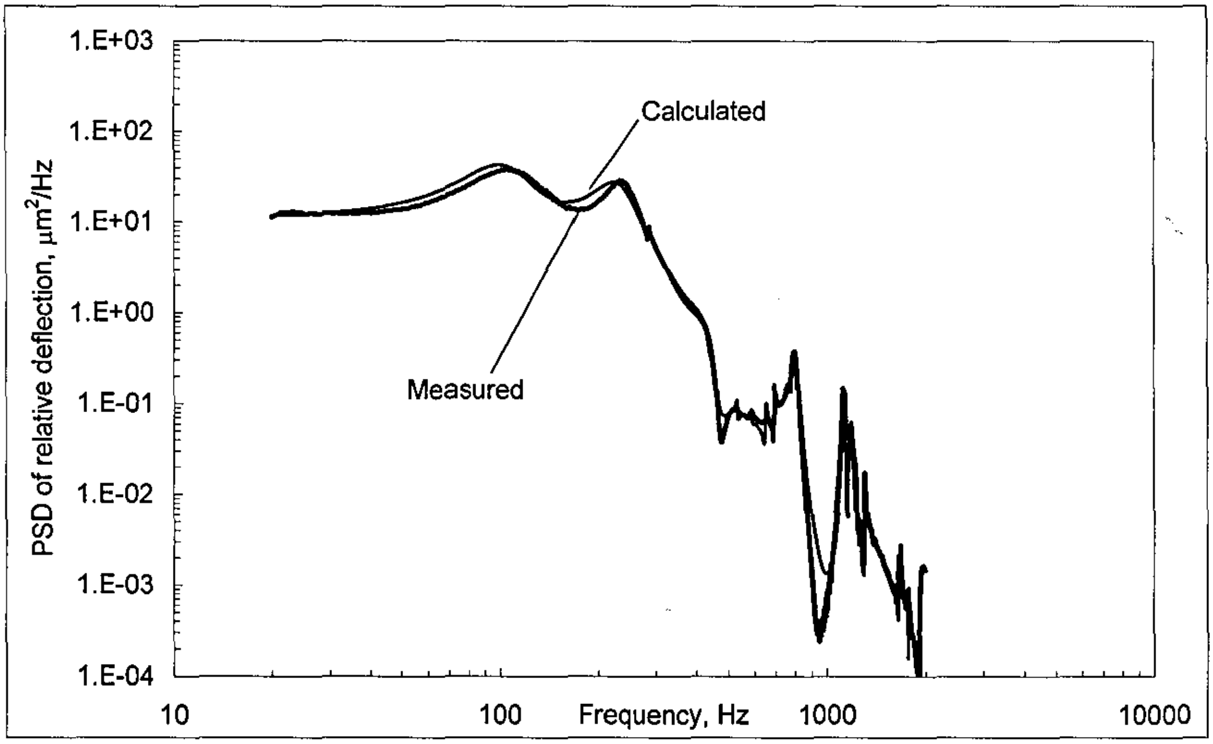

b) With 65% mass ratio

Figure 6.8. Comparison of PSD of relative deflection of ruggedized PCB at different mass ratios

Table 6.1 illustrates the comparison of the optimal performance found in the single-mode and full-mode model of PCB. The calculation shows that the lifetime of the ruggedized PCB will be increased by several thousand times compared to its original design.

Analysis	Predicted (full-mode)		Predicted (single-mode)		Measured	
Mass Ratio, η	35%	65%	35%	65%	35%	65%
Overall RMS reduction factor	4.0	4.1	3.9	4.05	3.95	4.07
Improvement in Endurance limit (times)	6,982	8,615	6,040	7,721	6,579	7,969

Table 6.1. Comparison between measured and predicted results

Additional measurement

To validate the analytical solution for other observation points on the PCB and also compare the performance of dynamic absorber with the existing vibration controls (damping and stiffening) the experimental PSD of absolute accelerations of those corresponding points are measured as shown in Figure 6.9 in conjunction at full level (14g RMS) excitation. The PSD of accelerations are being measured, obviously this would give a general view of reduction ratio as compared to its original PCB design. Additionally, these results would be best to represent the influence of dynamic absorber as compared to other vibration protection in terms of frequency response for the entire structure.

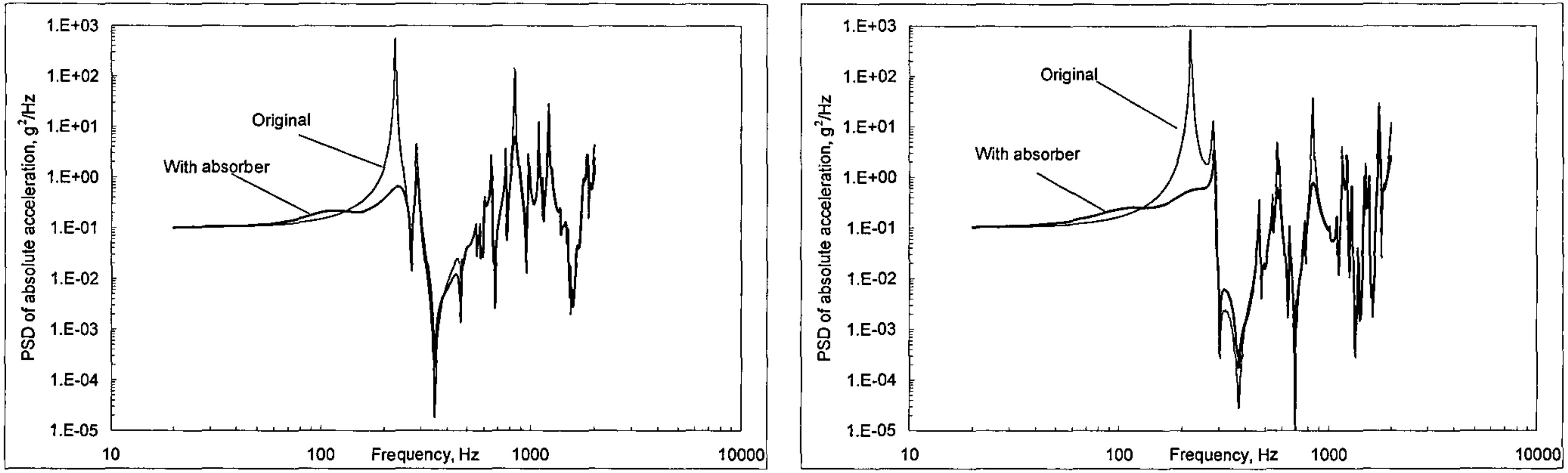

a) At observation point ① b) At observation point ②

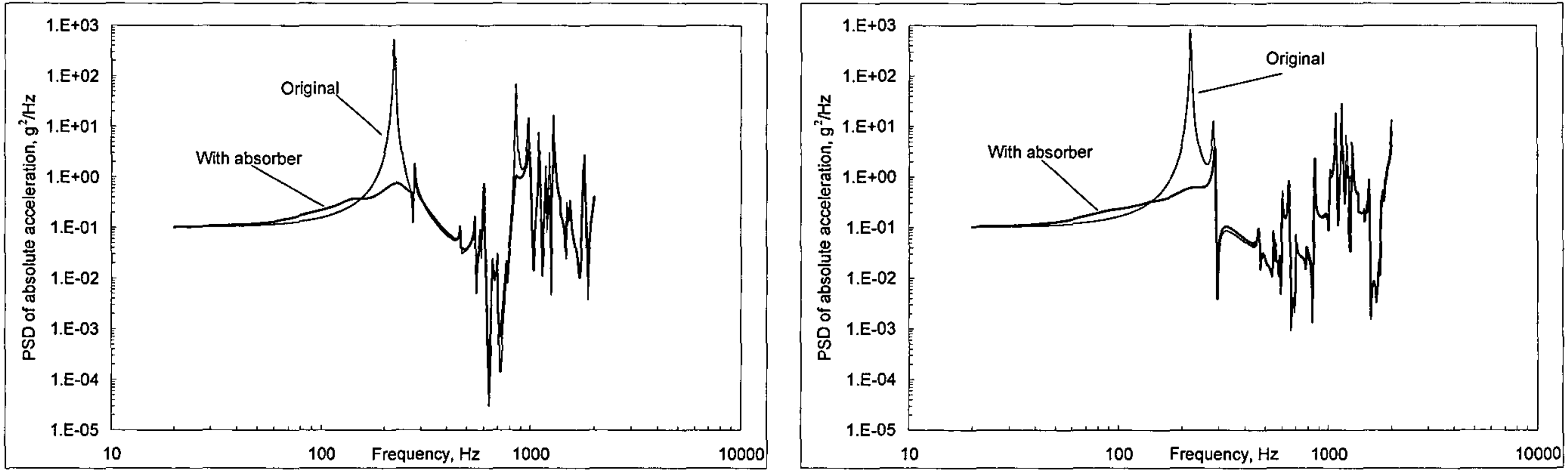

c) At observation point ③ d) At observation point ④

Figure 6.9. Experimentally measured absolute transmissibility of original and ruggedized PCB at different observation points

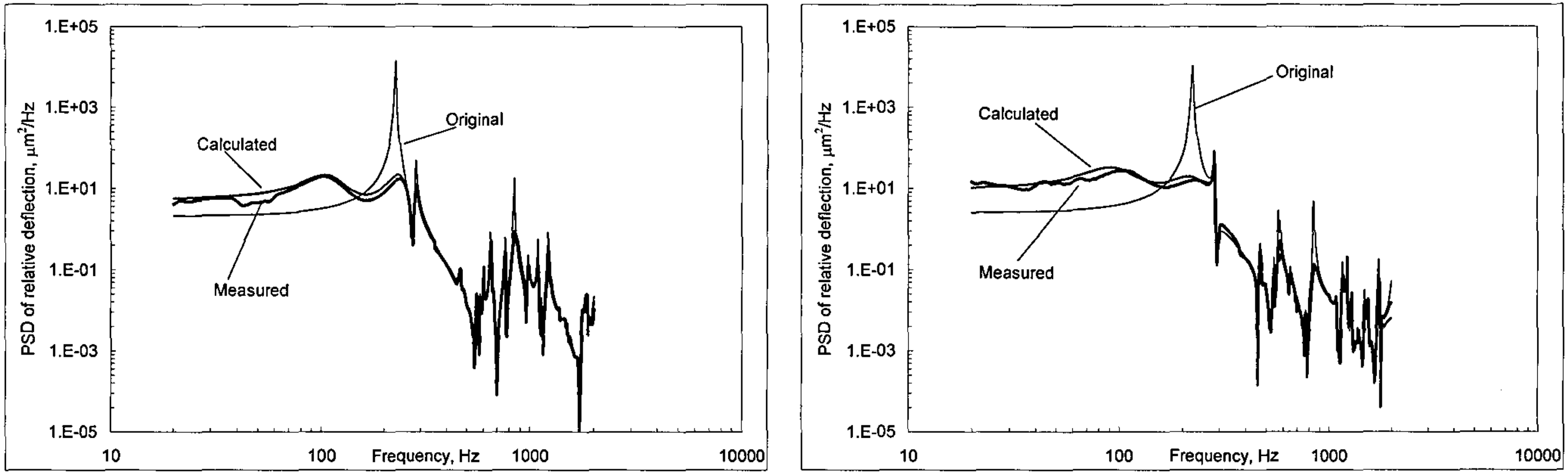

a) At observation point ①   b) At observation point ②

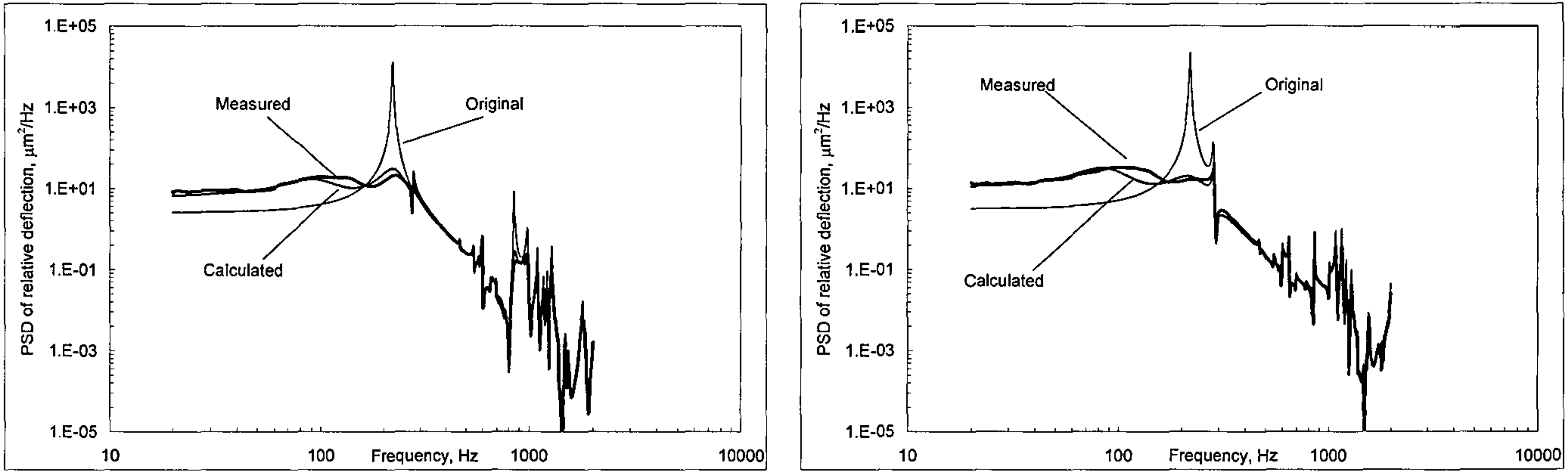

c) At observation point ③   d) At observation point ④

Figure 6.10. Comparison of PSD of relative deflection of original and ruggedized PCB at different observation points

Figure 6.9 shows the superimposed absolute transmissibility of the original and ruggedized PCB with application of optimal dynamic absorber (η=65%). Again, the influence of the dynamic absorber is that almost all resonances of the original PCB are significantly suppressed. It is obvious that the optimal dynamic absorber shows its superiority as compared to damping and stiffening by the means of controlling all major frequency resonances without creating new one and shifting the fundamental resonant frequency of the PCB.

The overall relative deflection of those observation points can be calculated through experimental PSD of relative deflection. The experimental results are shown in Figure 6.10 together with the corresponding theoretical curve and the original response of the PCB for comparison.

The comparison of the PSD of relative deflection for the experimentally and analytically obtained results are shown in Figures 6.10. They show how the analytical model is a close approximation to the true system. The insignificant differences between analytical and experimental curves can be distinguished by comparing the overall relative deflection in Table 6.2

	Observation point ①	Observation point ②	Observation point ③	Observation point ④
Original, μm RMS	234.43	260.82	301.31	305.45
Calculated, μm RMS	56.84	65.74	71.42	72.58
Measured, μm RMS	57.93	66.31	72.50	73.69

Table 6.2. Comparison between measured and predicted results

6.2.2 Sine vibration

The second test is carried out for the combined PCB and the above dynamic absorbers under sine vibration. Since the tuned characteristics of the dynamic absorbers are close to the optimal condition and do not pose any degree of nonlinearities, the Electrodynamic Shaker is programmed to perform the swept-sine test from 10 to 500 Hz at a constant magnitude of acceleration 10g with linearly sweep rate of 5 Hz/s, as normally recommended for electronic manufacturers [3]. Figure 6.11 shows the screenshot from the controller, the typical vibration pattern in which the PCB was exposed.

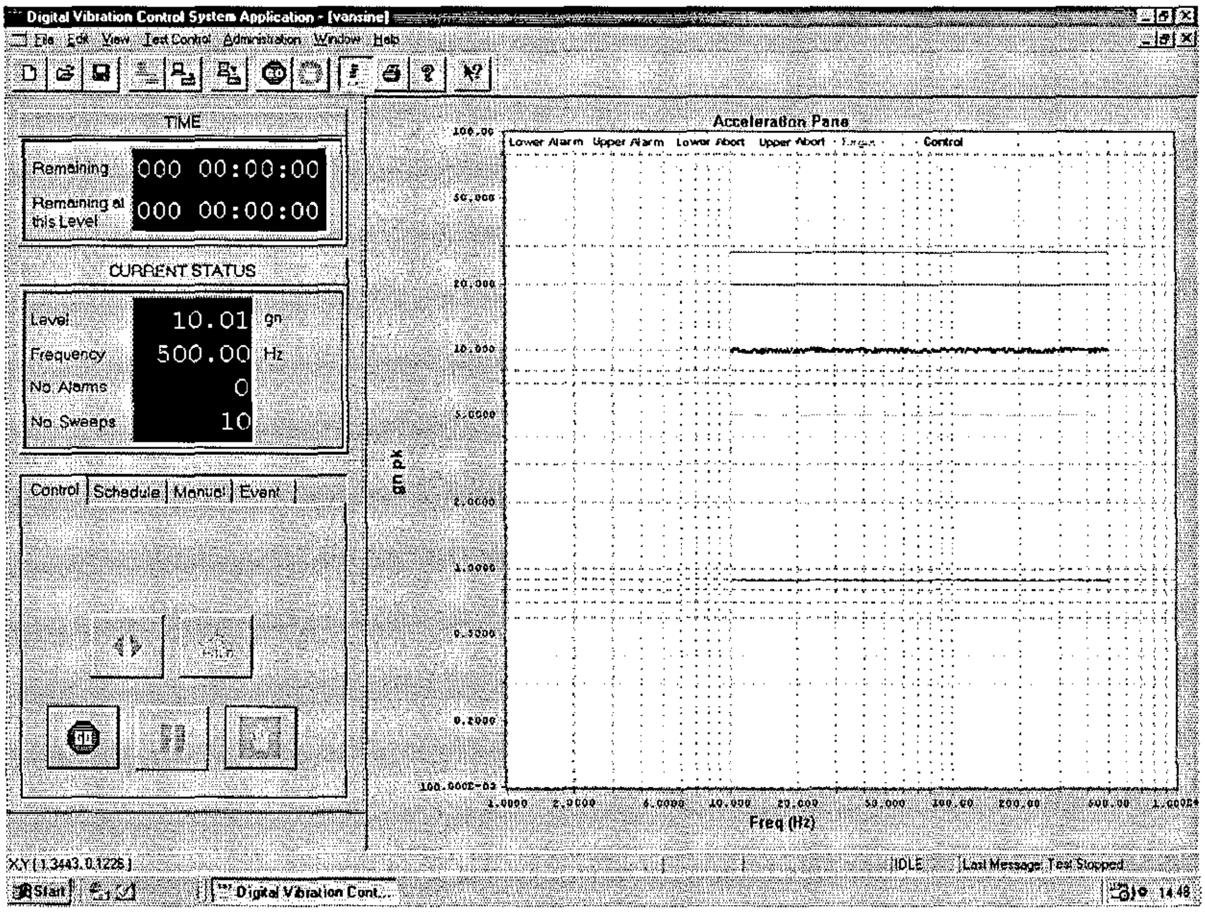
Digital Vibration Control System Application - [vansine]
File Edit View Test Control Administration Window Help
TIME
CURRENT STATUS
Control Schedule Manual Event
Acceleration Pane
Lower Alarm Upper Alarm Lower Abort Upper Abort Target Control
gn pk
100.00
50.000
20.000
10.000
5.0000
2.0000
1.0000
0.5000
0.2000
100.000E-03
1.0000
2.0000
4.0000
10.000
20.000
50.000
100.00
200.00
500.00
1.000E+
Freq (Hz)
Start
Digital Vibration Cont...
14:48

Remaining 000 00:00:00
Remaining at this Level 000 00:00:00

Level 10.01 gn
Frequency 500.00 Hz
No Alarms 0
No Sweeps 10

X,Y (1.3443, 0.1226)

IDLE

Last Message: Test Stopped

Figure 6.11. Swept-sine vibration profile from vibration control screen

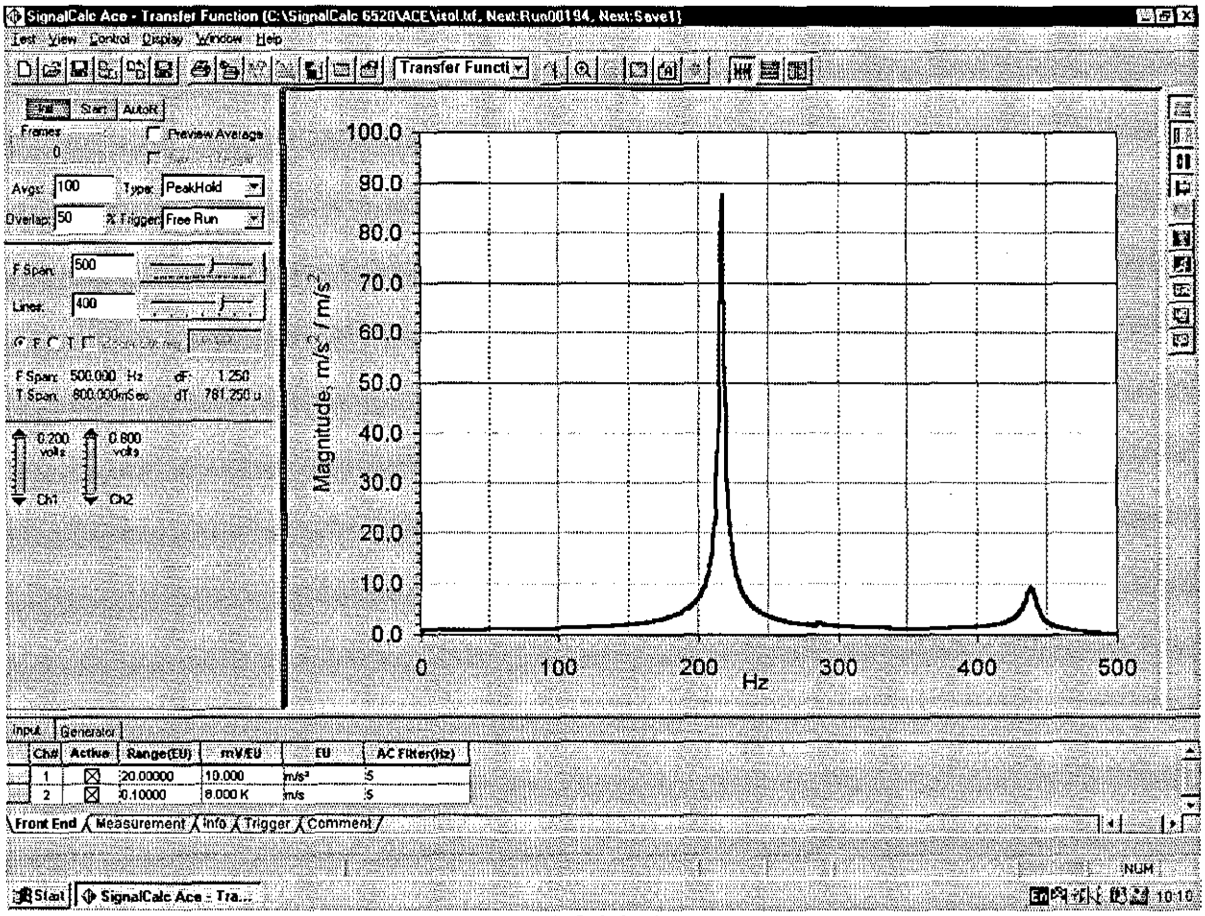
SignalCalc Ace - Transfer Function (C:\SignalCalc 6520\ACE\isol.tf, Next:Run00194, Next:Save1)
Test View Control Display Window Help
Transfer Functi
Init Start AutoR
Preview Average
Magnitude, m/s² / m/s²
100.0
90.0
80.0
70.0
60.0
50.0
40.0
30.0
20.0
10.0
0.0
0
100
200
300
400
500
Hz
Input Generator
Front End Measurement Info Trigger Comment
NUM
Start
SignalCalc Ace - Tra...
10:10

Frames 0

Avgs: 100 Type: PeakHold

Overlap: 50 % Trigger: Free Run

F Span: 500

Lines: 400

● F ○ T

F Span: 500.000 Hz dF: 1.250

T Span: 800.000mSec dT: 781.250 u

Ch1 0.200 volts

Ch2 0.800 volts

Ch#	Active	Range(EU)	mV/EU	EU	AC Filter(Hz)
1	☒	20.00000	10.000	m/s²	.5
2	☒	0.10000	8.000 K	m/s	.5

a) Original

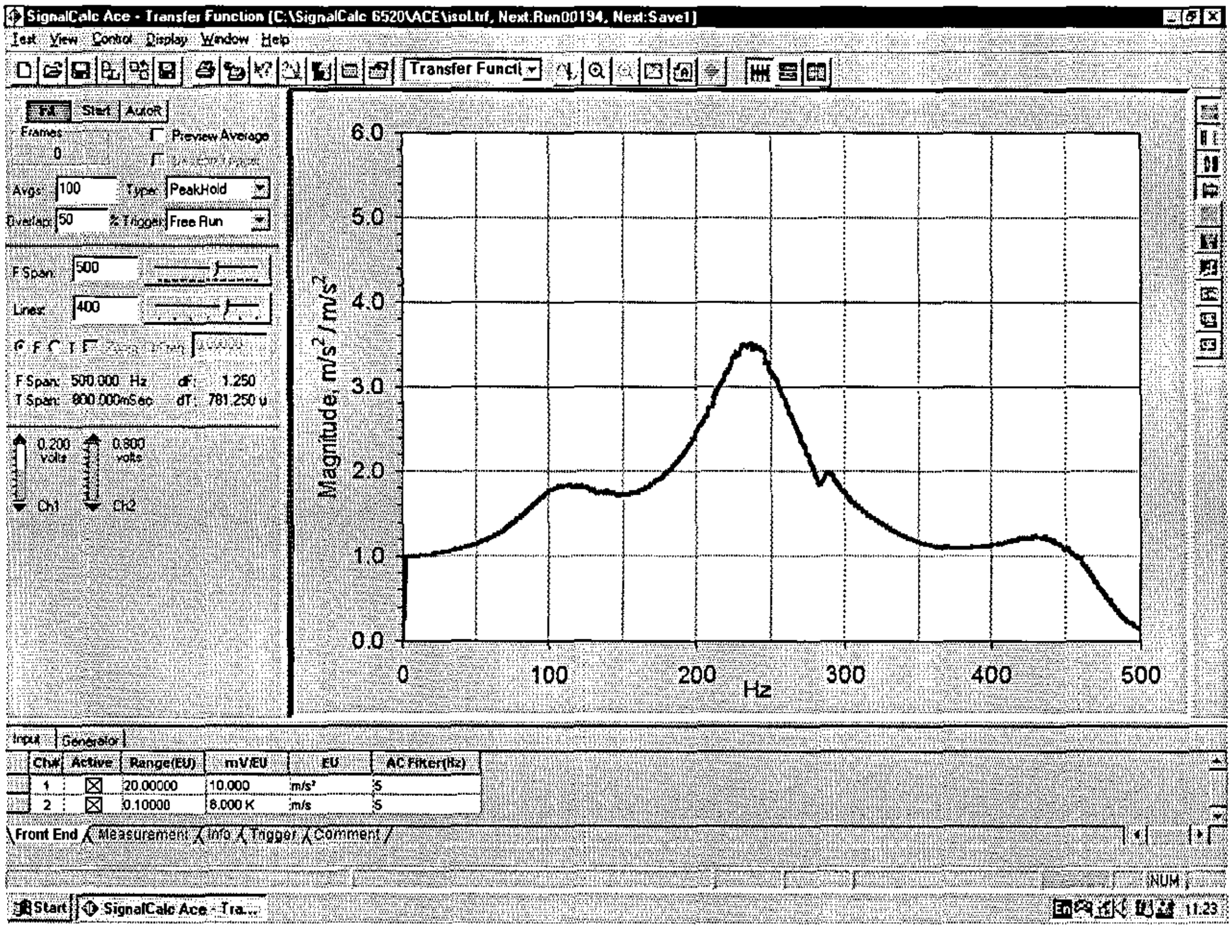
SignalCalc Ace - Transfer Function [C:\SignalCalc 6520\ACE\isol.tf, Next:Run00194, Next:Save1]
Test View Control Display Window Help
Transfer Functi
Fill Start AutoR
Preview Average
6.0
5.0
4.0
3.0
2.0
1.0
0.0
Magnitude, m/s² / m/s²
0
100
200
300
400
500
Hz
0.200 volts
0.800 volts
Ch1
Ch2
Input Generator
Front End Measurement Info Trigger Comment
NUM
Start
SignalCalc Ace - Tra...
11:23

Frames: 0

Avgs: 100 Type: PeakHold

Overlap: 50 % Trigger: Free Run

F Span: 500

Lines: 400

F Span: 500.000 Hz dF: 1.250

T Span: 800.000mSec dT: 781.250 u

Ch#	Active	Range(EU)	mV/EU	EU	AC Filter(Hz)
1	☒	20.00000	10.000	m/s²	.5
2	☒	0.10000	8.000 K	m/s	.5

a) At 65% mass ratio

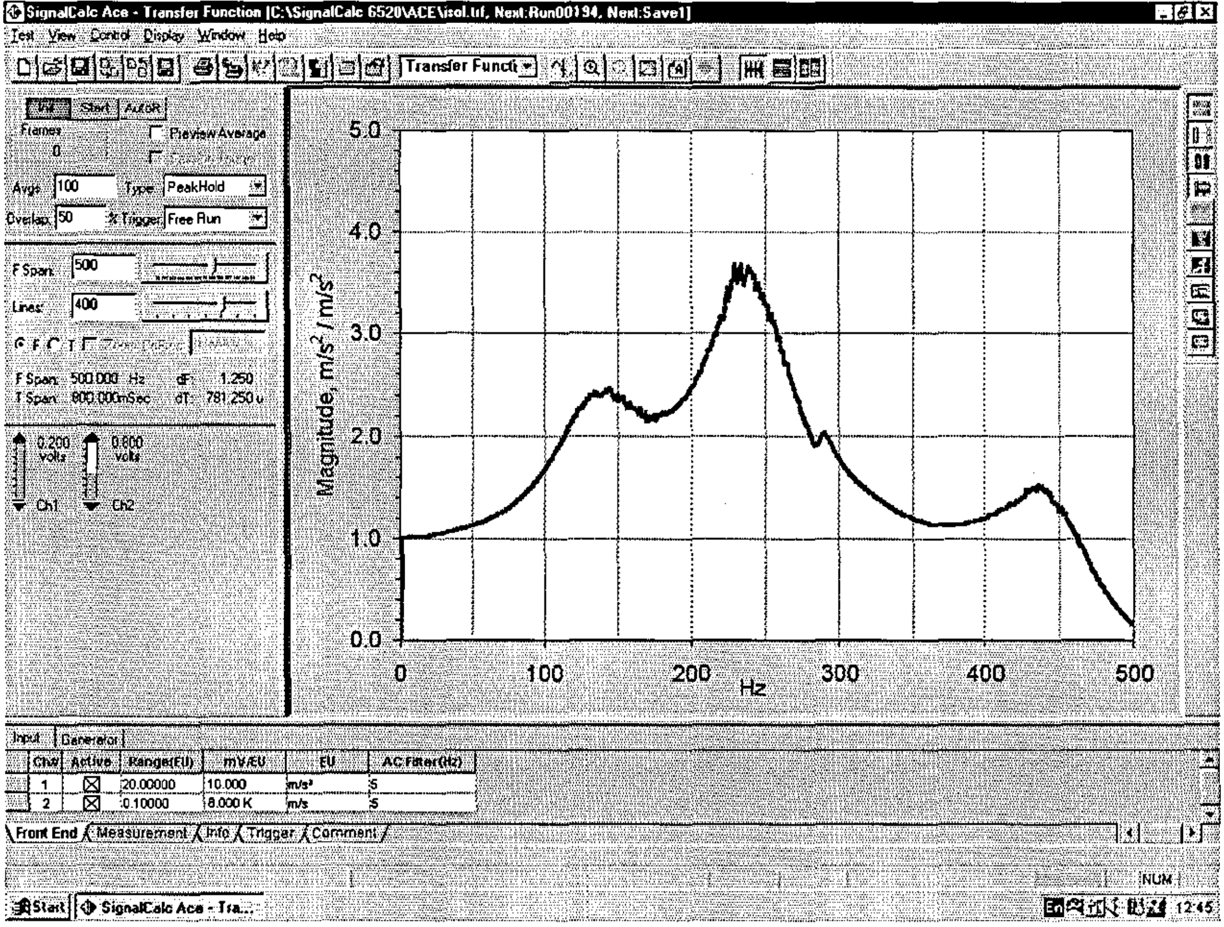
SignalCalc Ace - Transfer Function [C:\SignalCalc 6520\ACE\isol.tf, Next:Run00194, Next:Save1]
Test View Control Display Window Help
Transfer Functi
Fill Start AutoR
Preview Average
5.0
4.0
3.0
2.0
1.0
0.0
Magnitude, m/s² / m/s²
0
100
200
300
400
500
Hz
0.200 volts
0.800 volts
Ch1
Ch2
Input Generator
Front End Measurement Info Trigger Comment
NUM
Start
SignalCalc Ace - Tra...
12:45

Frames: 0

Avgs: 100 Type: PeakHold

Overlap: 50 % Trigger: Free Run

F Span: 500

Lines: 400

F Span: 500.000 Hz dF: 1.250

T Span: 800.000mSec dT: 781.250 u

Ch#	Active	Range(EU)	mV/EU	EU	AC Filter(Hz)
1	☒	20.00000	10.000	m/s²	.5
2	☒	0.10000	8.000 K	m/s	.5

b) At 35% mass ratio

Figure 6.12. Analyser screenshot of absolute transmissibility of original and ruggedized PCB

Figure 6.12 shows the analyser screenshot of universal absolute transmissibility of the ruggedized PCB with the above individual dynamic absorber.

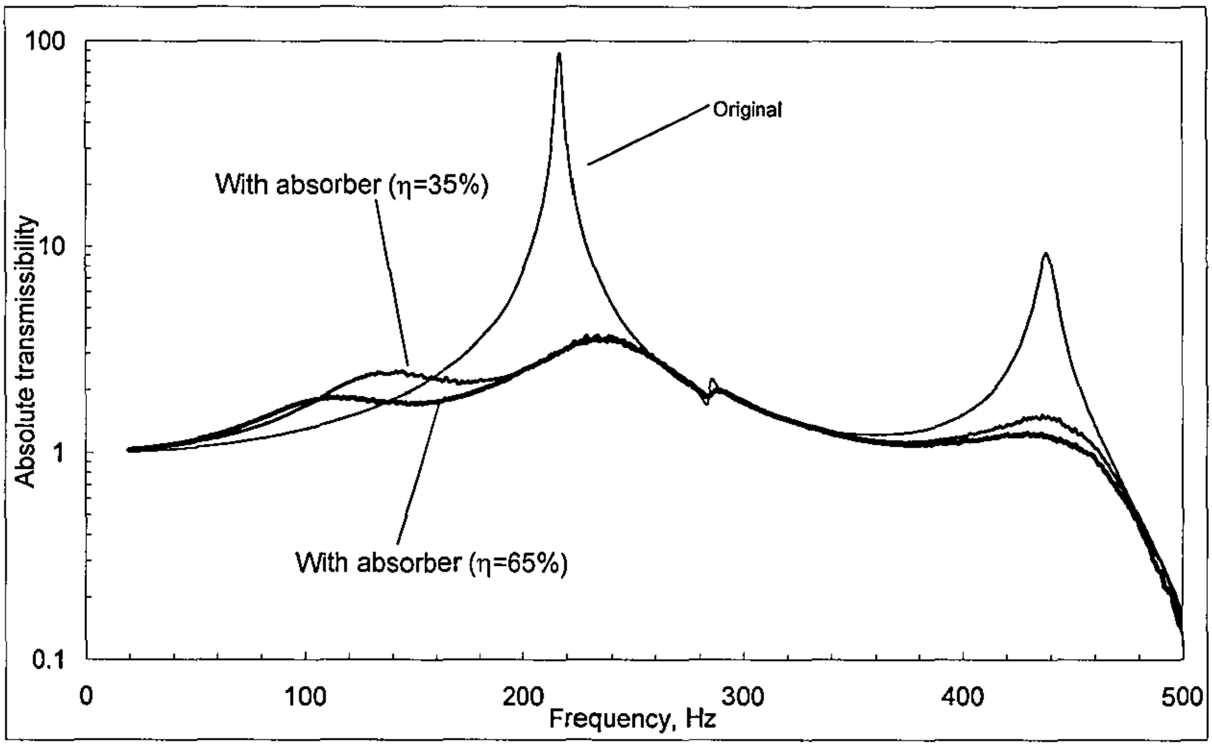

a) Absolute transmissibility

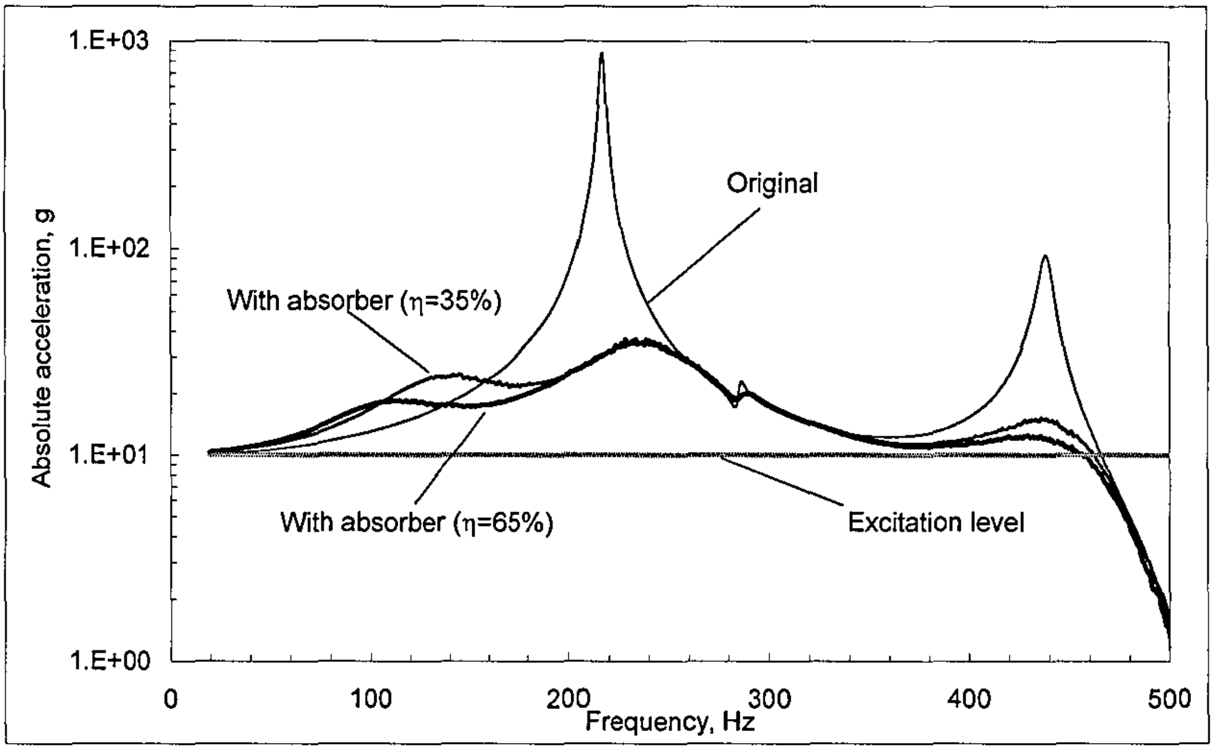

b) Absolute acceleration

Figure 6.13. Experimentally measured absolute transmissibility and acceleration of original and ruggedized PCB

Figure 6.13 shows the experimental absolute transmissibility and acceleration of the original (curve labelled **Original**) and dynamically ruggedized PCB at mass ratios of 65% and 35% (see corresponding curves). From the acceleration in Figure 6.13b, both dynamic absorbers should provide for about a 23-fold vibration suppression at resonant frequency.

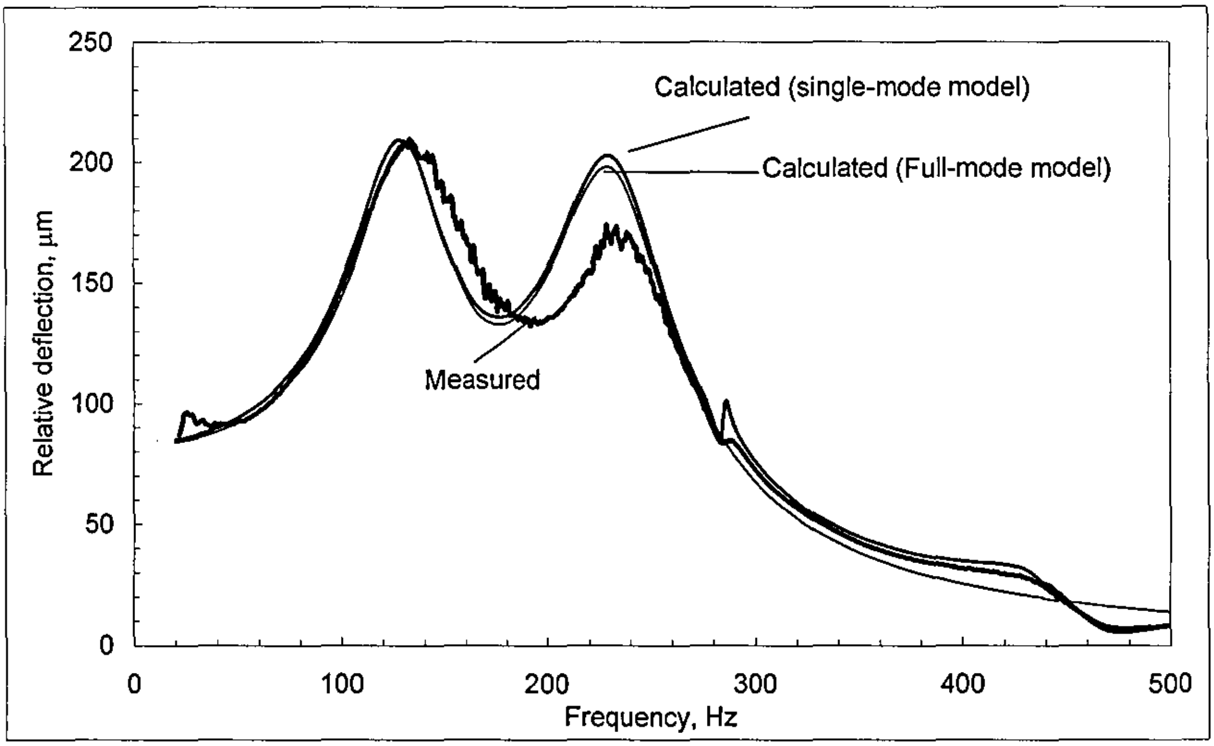

a) With 35% mass ratio

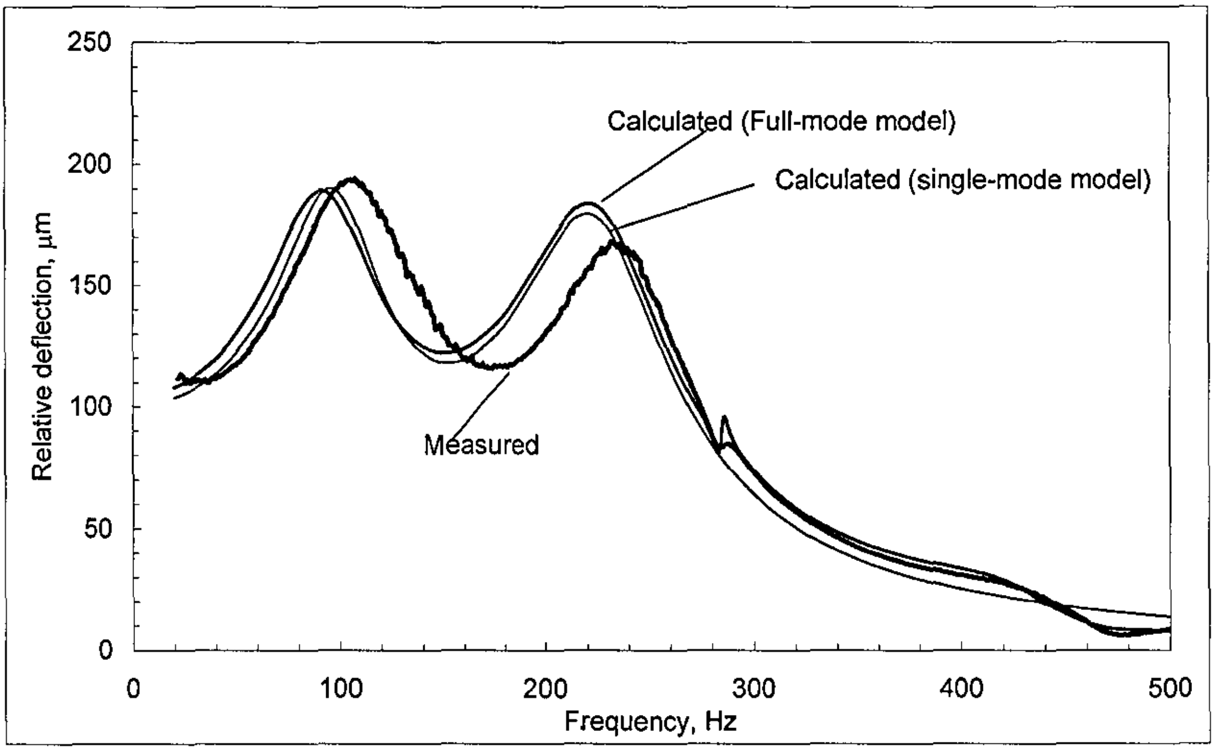

b) With 65% mass ratio

Figure 6.14. Comparison of relative deflection of ruggedized PCB at different mass ratios

Figure 6.14a compares the experimentally and analytically obtained relative deflection of the ruggedized PCB at different mass ratios. As can be seen, the analytical prediction which is based on single-mode and full-mode models yield a peak relative deflection of 190 µm. The experimentally obtained peak relative deflection of 195 μm is in close agreement with analytical prediction.

Figure 6.14b shows the comparison between analytical and experimental relative deflection of the ruggedized PCB at 35% mass ratio. The predicted peak relative deflection of both full-mode and single-mode models are 210 μm, whereas the experimental peak relative deflection is 209 μm which is close to the predicted value, see appropriate curves for reference.

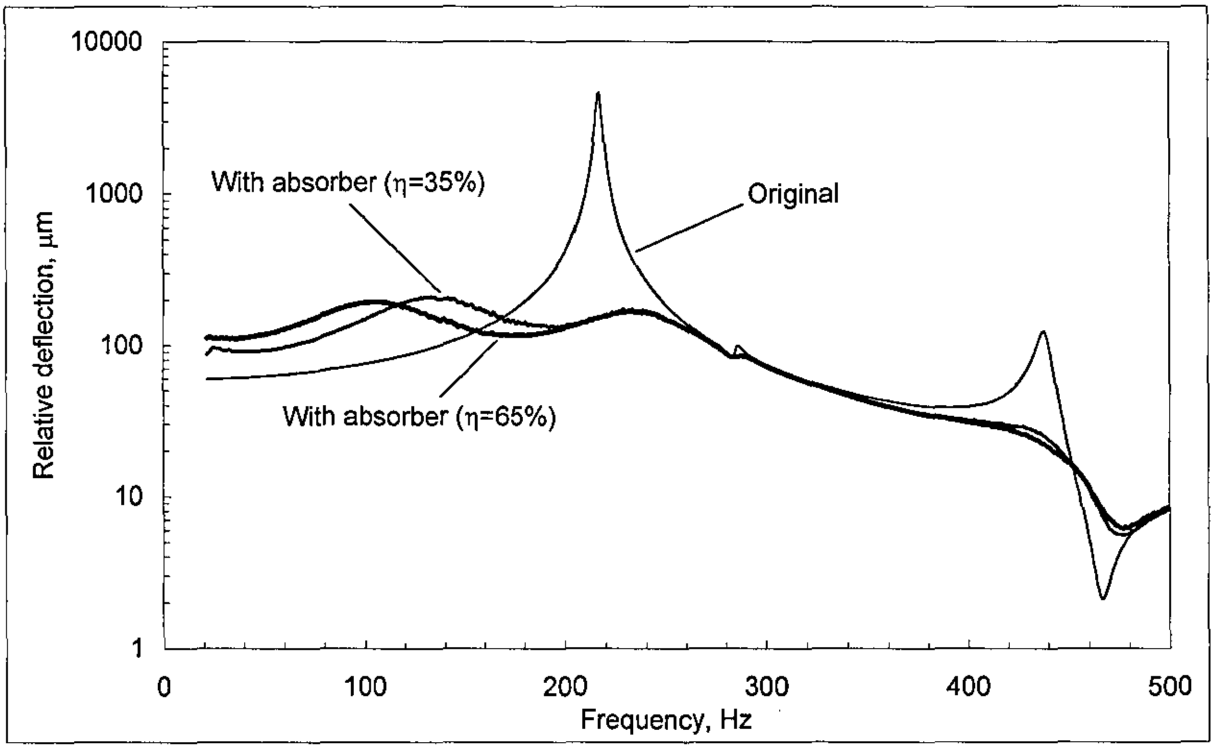

Figure 6.15. Experimentally measured relative deflection of original and ruggedized PCB

Figure 6.15 compares the obtained experimentally the dynamic responses of the original system showing a peak relative deflection of 4617 μm, and those for the dynamically ruggedized system at mass ratios of 35% and 65%, showing peak relative deflections of 209 μm and 195 μm, respectively.

This experimental work addresses the problem of the optimal design of a dynamic absorber for the PCB subjected to sinusoidal vibration with variable frequency. Using single-mode and then full-mode approximations for the PCB, from the handy numerical procedure for optimising the properties of a dynamic absorber. They have shown by example that an optimal dynamic absorber is capable of essential 24-fold suppression of the peak resonant response as compared with the case of the original PCB under the typical swept-sine tests. The results of analytical prediction are in close agreement with the experiment, which has shown the 23-fold suppression of the peak resonant response.

The work proves that the same dynamic absorber is equally suitable to effectively suppress the dynamic responses of PCB under wide-band random and sine excitation with a variable frequency.

6.2.3 Shock

To complete the experimental study of this new radical vibration protection for the sensitive PCB, the Electrodynamic Shaker is programmed a half-sine (200 g peak @ 3ms) as shown in Figure 6.16 to carry out a shock test on the original and ruggedized PCB. Also, to validate the numerical solution, the above chosen dynamic absorbers are individually mounted on the PCB.

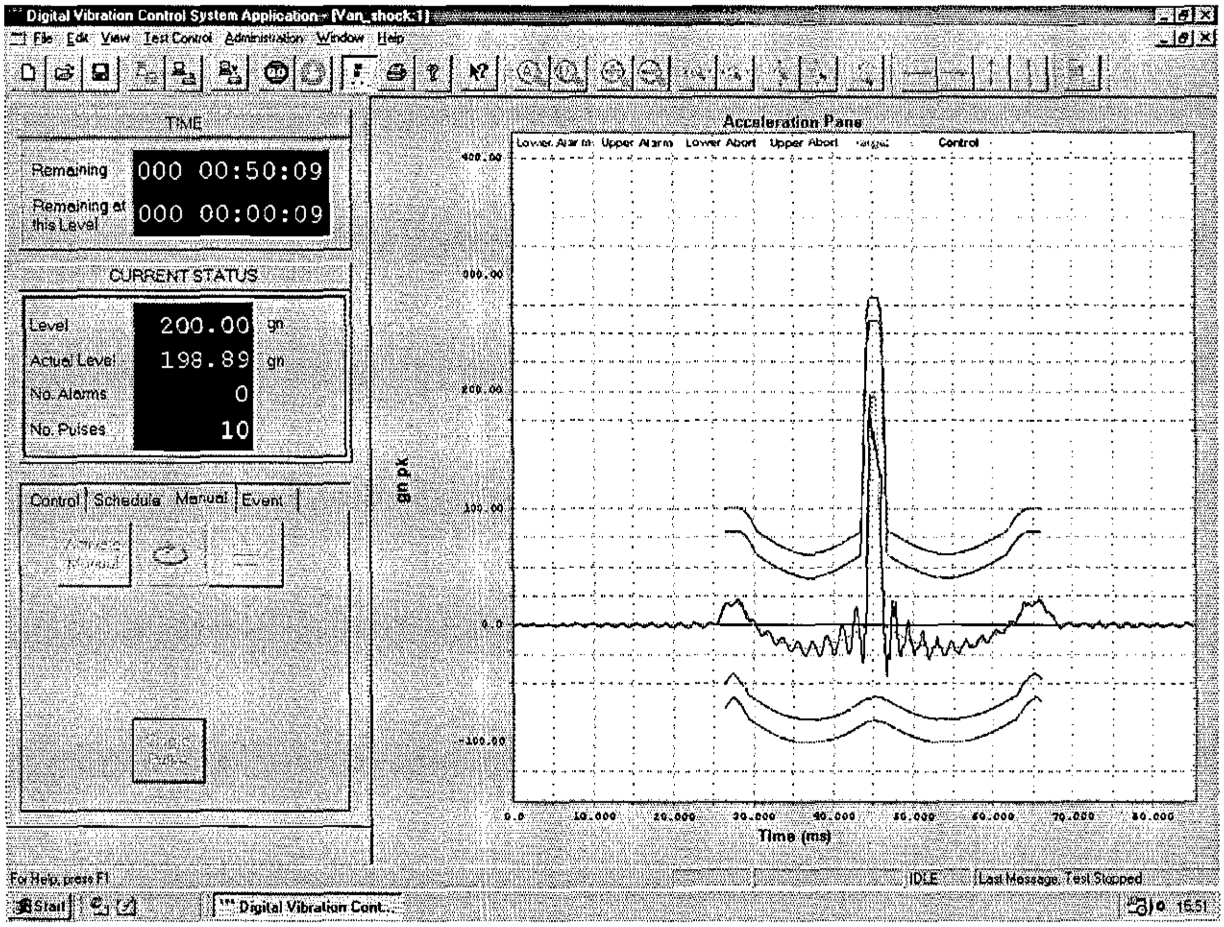
Digital Vibration Control System Application - [Van_shock:1]
File
Edit
View
Test Control
Administration
Window
Help
TIME
CURRENT STATUS
Control
Schedule
Manual
Event
Acceleration Pane
Lower Alarm
Upper Alarm
Lower Abort
Upper Abort
Control
400.00
300.00
200.00
100.00
0.0
-100.00
gn pk
0.0
10.000
20.000
30.000
40.000
50.000
60.000
70.000
80.000
Time (ms)
Start
Digital Vibration Cont...
15:51

Remaining 000 00:50:09
Remaining at this Level 000 00:00:09

Level 200.00 gn
Actual Level 198.89 gn
No. Alarms 0
No. Pulses 10

For Help, press F1
IDLE
Last Message: Test Stopped

Figure 6.16. Shock profile from vibration control screen

Figure 6.17 shows the analyser screenshot of absolute acceleration of the original PCB response. The peak value is measured to be about 300g which shows the amplification ratio to be 1.5 compared to its 200g input peak value and time settling is about 0.5 s, this shows a very close result with numerical simulation.

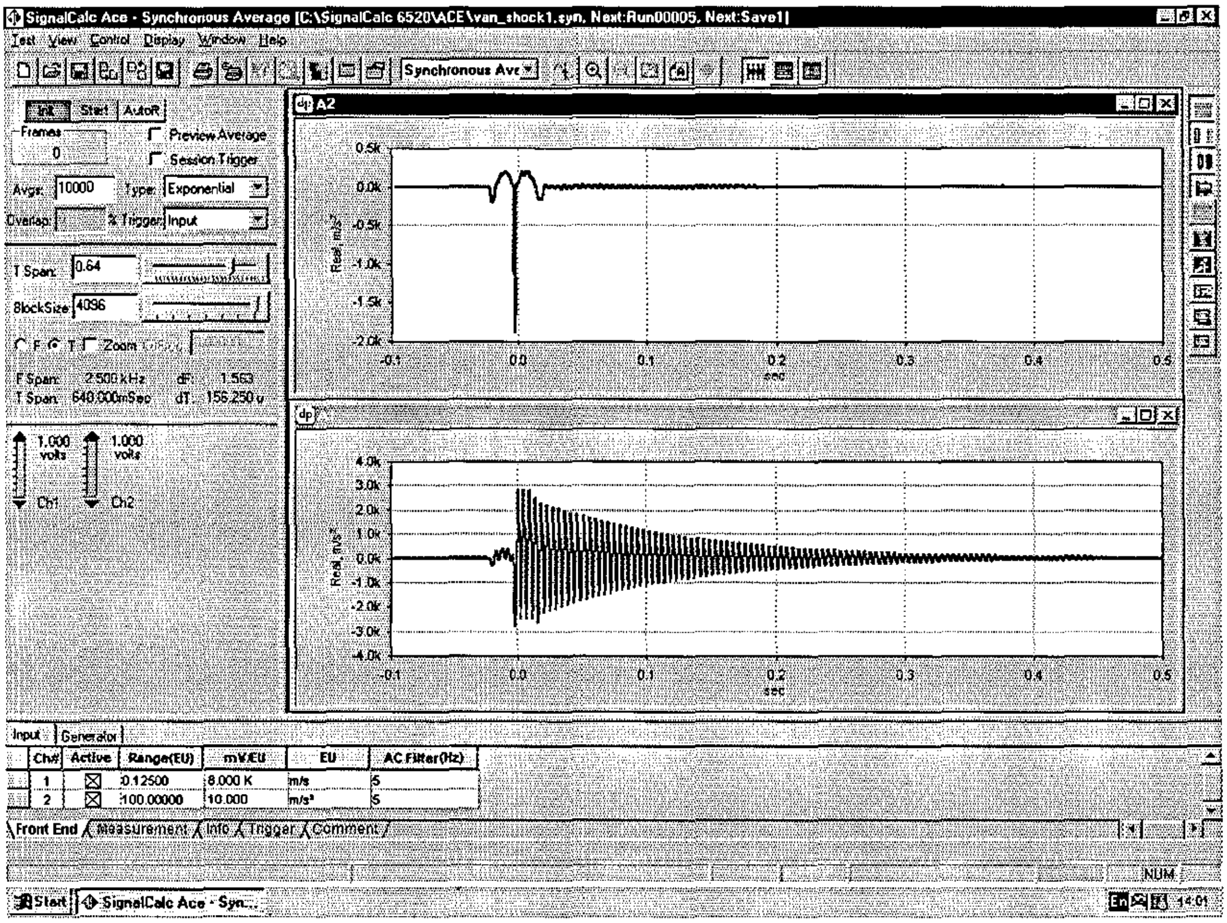
SignalCalc Ace - Synchronous Average [C:\SignalCalc 6520\ACE\van_shock1.syn, Next:Run00005, Next:Save1]
Test View Control Display Window Help
Synchronous Ave
Init Start AutoR
A2
0.5k
0.0k
-0.5k
-1.0k
-1.5k
-2.0k
Real, m/s²
-0.1
0.0
0.1
0.2
0.3
0.4
0.5
sec
dp
4.0k
3.0k
2.0k
1.0k
0.0k
-1.0k
-2.0k
-3.0k
-4.0k
Real, m/s²
-0.1
0.0
0.1
0.2
0.3
0.4
0.5
sec
1.000 volts Ch1
1.000 volts Ch2
Input Generator
Front End Measurement Info Trigger Comment
NUM
Start SignalCalc Ace - Syn...
14:01

Frames: 0
☐ Preview Average
☐ Session Trigger
Avgs: 10000 Type: Exponential
Overlap: % Trigger: Input
T Span: 0.64
BlockSize: 4096
○ F ● T ☐ Zoom
F Span: 2.500 kHz dF: 1.563
T Span: 640.000mSec dT: 156.250 u

Ch#	Active	Range(EU)	mV/EU	EU	AC Filter(Hz)
1	☒	0.12500	8.000 K	m/s	5
2	☒	100.00000	10.000	m/s²	5

Figure 6.17. Analyser screenshot of absolute acceleration response of original PCB

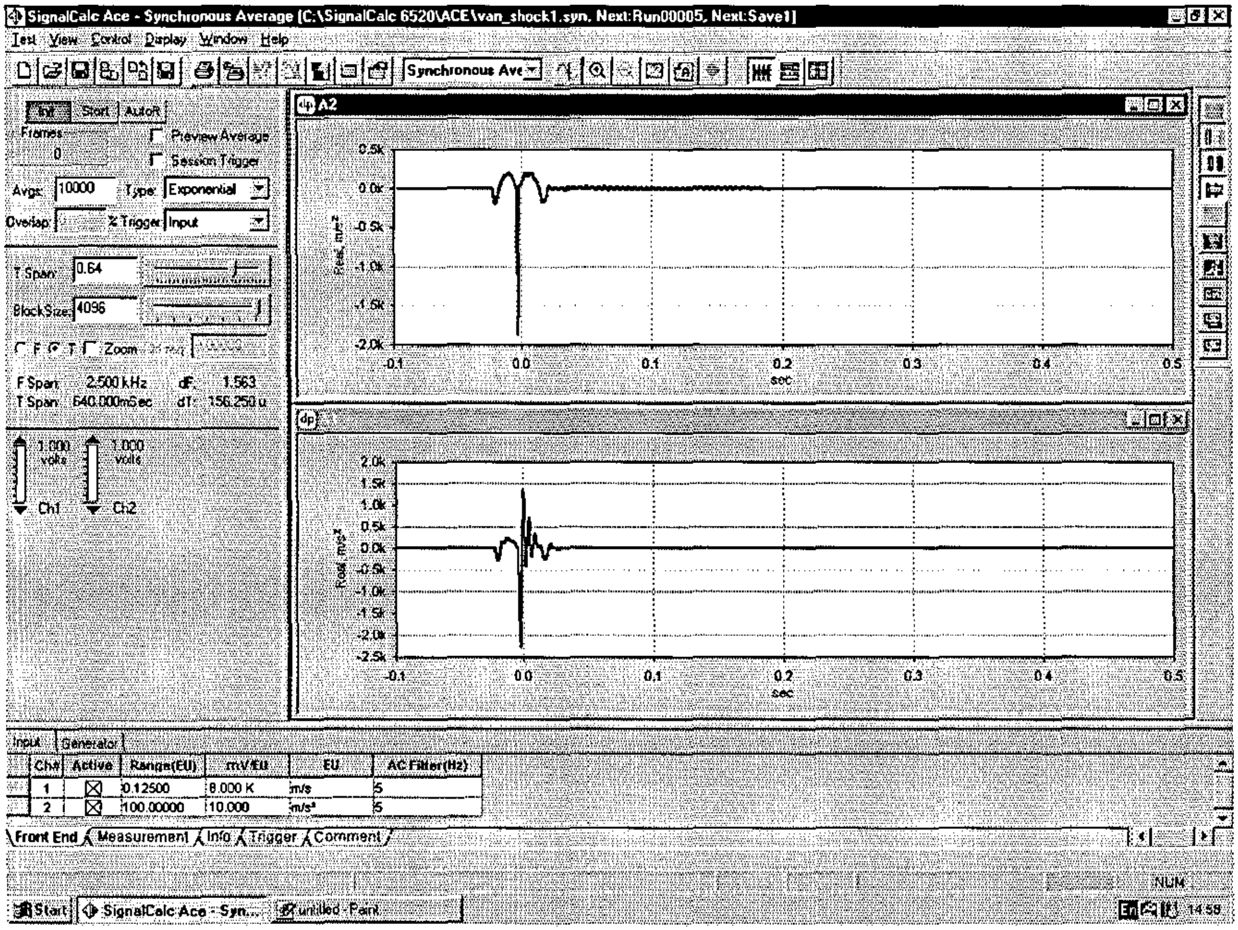
SignalCalc Ace - Synchronous Average [C:\SignalCalc 6520\ACE\van_shock1.syn, Next:Run00005, Next:Save1]
Test View Control Display Window Help
Synchronous Ave
Init Start AutoR
A2
0.5k
0.0k
-0.5k
-1.0k
-1.5k
-2.0k
Real, m/s²
-0.1
0.0
0.1
0.2
0.3
0.4
0.5
sec
dp
2.0k
1.5k
1.0k
0.5k
0.0k
-0.5k
-1.0k
-1.5k
-2.0k
-2.5k
Real, m/s²
-0.1
0.0
0.1
0.2
0.3
0.4
0.5
sec
1.000 volts Ch1
1.000 volts Ch2
Input Generator
Front End Measurement Info Trigger Comment
NUM
Start SignalCalc Ace - Syn... untitled - Paint
14:59

Frames: 0
☐ Preview Average
☐ Session Trigger
Avgs: 10000 Type: Exponential
Overlap: % Trigger: Input
T Span: 0.64
BlockSize: 4096
○ F ● T ☐ Zoom
F Span: 2.500 kHz dF: 1.563
T Span: 640.000mSec dT: 156.250 u

Ch#	Active	Range(EU)	mV/EU	EU	AC Filter(Hz)
1	☒	0.12500	8.000 K	m/s	5
2	☒	100.00000	10.000	m/s²	5

a) With 65 % mass ratio

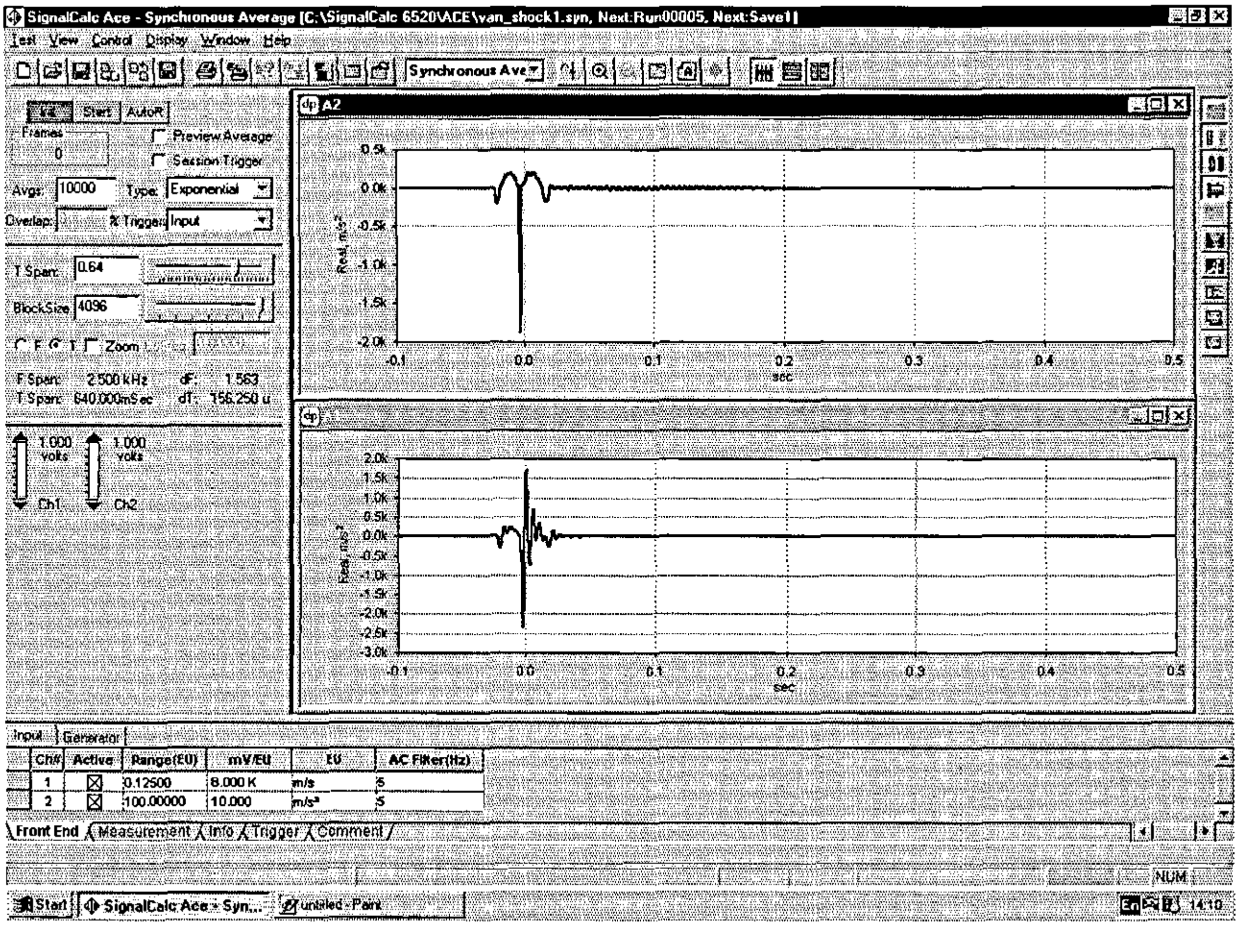
SignalCalc Ace - Synchronous Average [C:\SignalCalc 6520\ACE\van_shock1.syn, Next:Run00005, Next:Save1]
Test View Control Display Window Help
Synchronous Ave
Start
AutoR
A2
0.5k
0.0k
-0.5k
-1.0k
-1.5k
-2.0k
Real, m/s^2
-0.1
0.0
0.1
0.2
0.3
0.4
0.5
sec
2.0k
1.5k
1.0k
0.5k
0.0k
-0.5k
-1.0k
-1.5k
-2.0k
-2.5k
-3.0k
Real, m/s^2
-0.1
0.0
0.1
0.2
0.3
0.4
0.5
sec
Input
Generator
Front End
Measurement
Info
Trigger
Comment
NUM
Start
SignalCalc Ace - Syn...
untitled - Paint
14:10

Frames: 0
☐ Preview Average
☐ Session Trigger
Avgs: 10000 Type: Exponential
Overlap: % Trigger: Input
T Span: 0.64
BlockSize: 4096
○ F ● T ☐ Zoom
F Span: 2.500 kHz dF: 1.563
T Span: 640.000mSec dT: 156.250 u
1.000 volts Ch1
1.000 volts Ch2

Ch#	Active	Range(EU)	mV/EU	EU	AC Filter(Hz)
1	☒	0.12500	8.000 K	m/s	5
2	☒	100.00000	10.000	m/s²	5

b) With 35 % mass ratio

Figure 6.18. Analyser screenshot of absolute acceleration response of the ruggedized PCB with different mass ratios

Figure 6.18 shows the absolute acceleration response of the ruggedized PCB combined with the individual dynamic absorber. As can be clearly seen, the response of the ruggedized PCB is almost instantly dies out after the shock pulse disappears

The best way to represent the influence of dynamic absorber subjected to shock is to superimpose the corresponding experimentally measured absolute acceleration and relative deflection into the original PCB response. These comparison results can be seen in Figure 6.19 and 6.20, respectively.

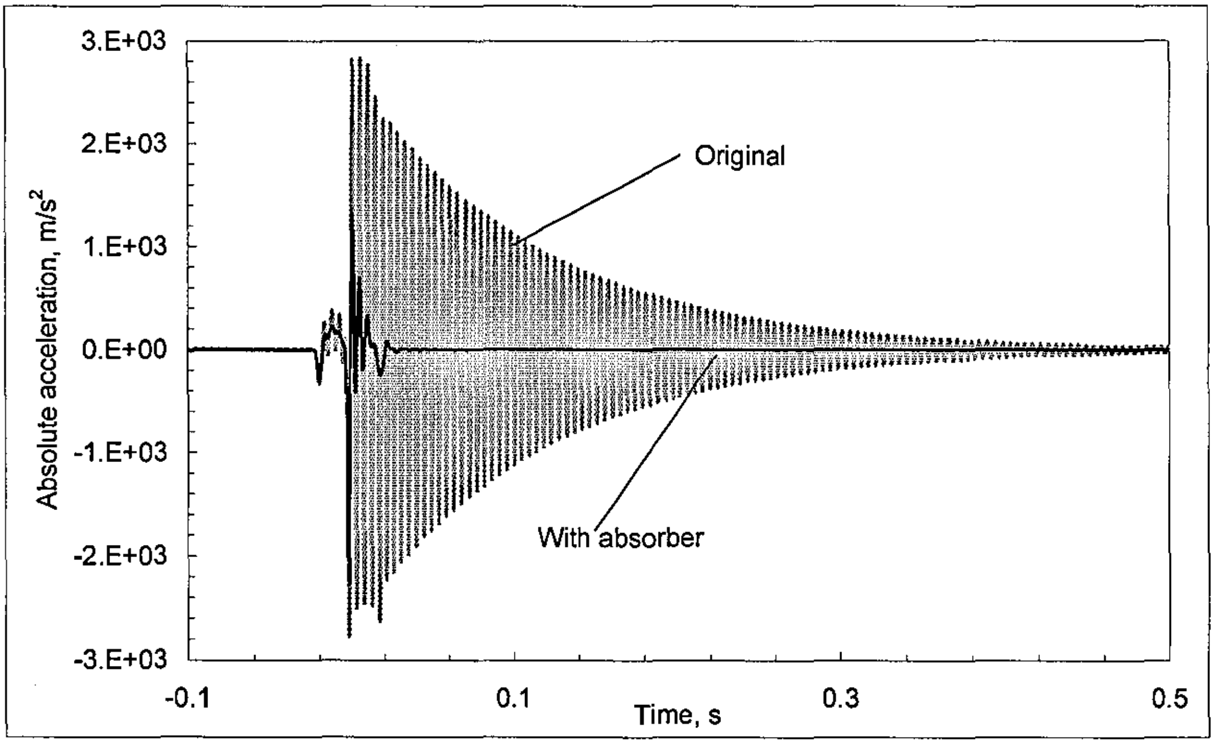

a) Absolute acceleration

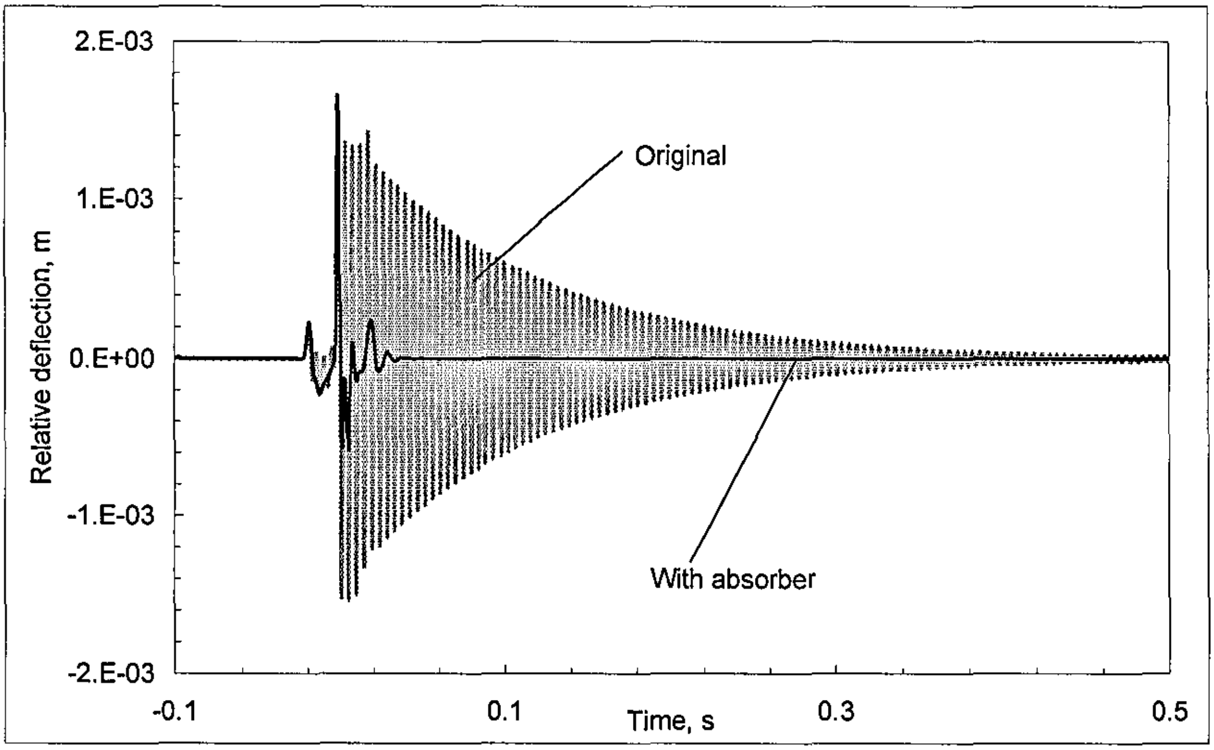

b) Relative deflection

Figure 6.19. Experimentally measured of original and ruggedized PCB with 65% mass ratio

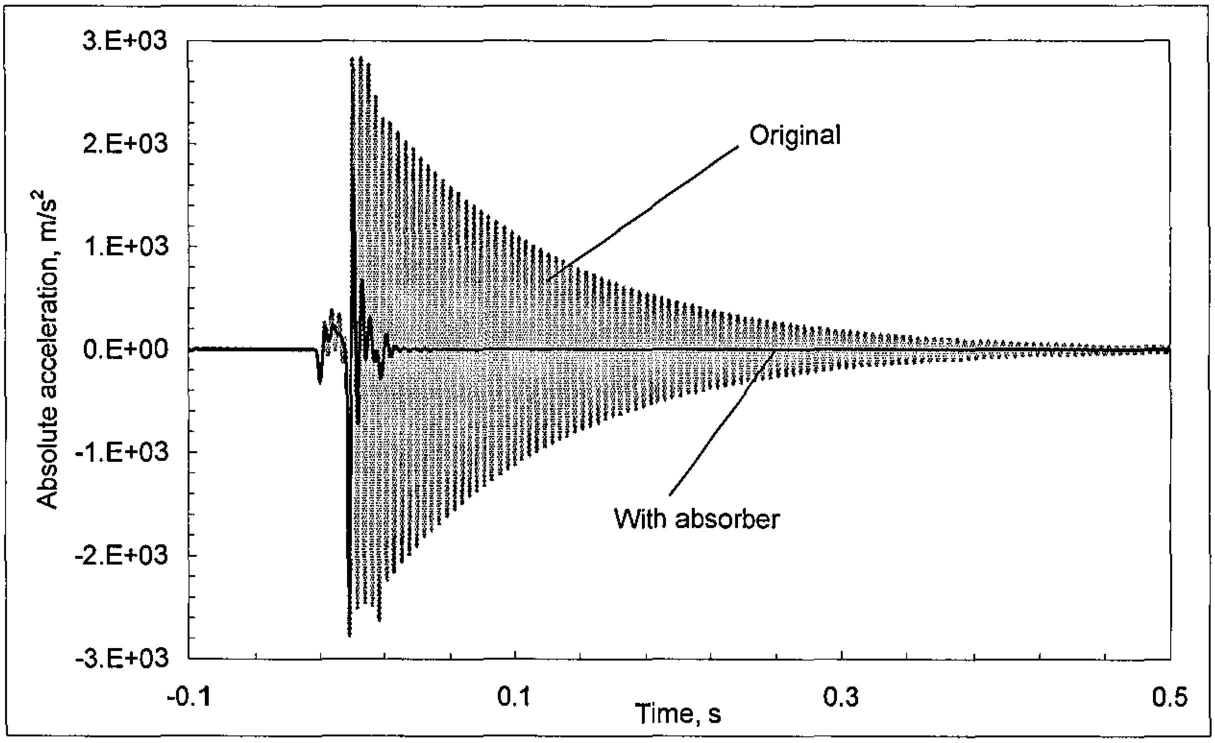

a) Absolute acceleration

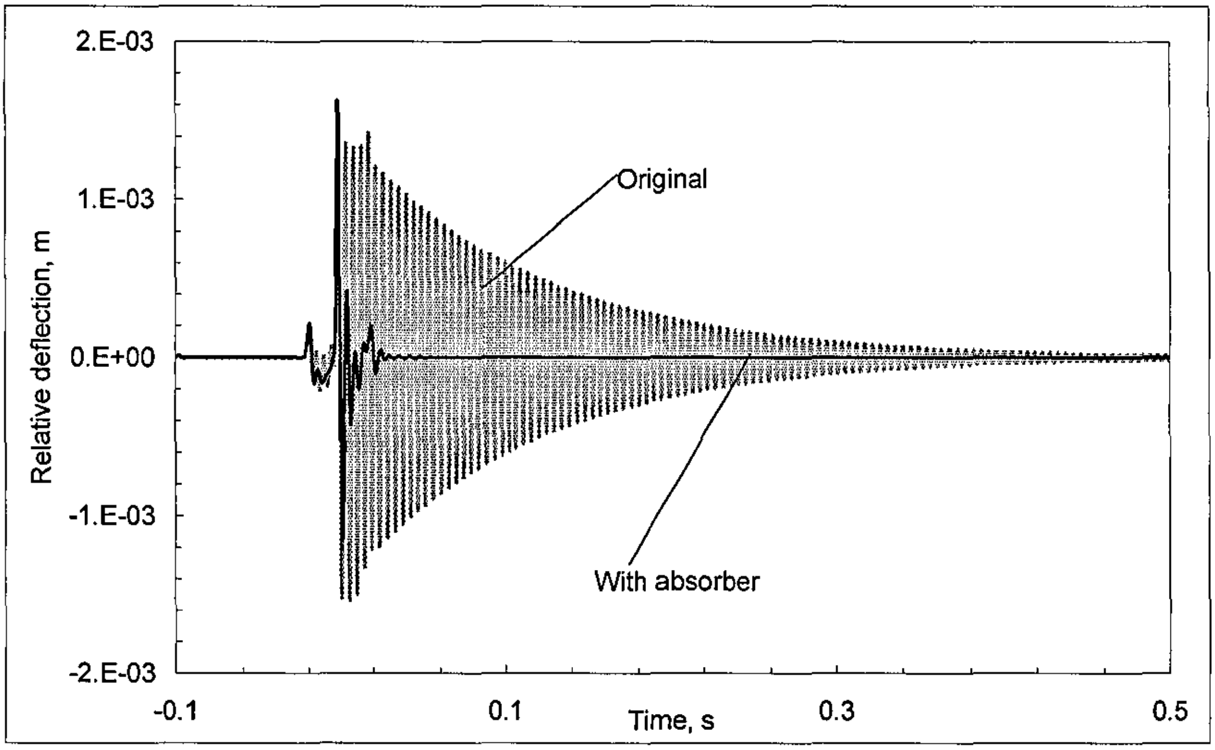

b) Relative deflection

Figure 6.20. Experimentally measured of original and ruggedized PCB with 35% mass ratio

Similar results were found in the relative deflection and absolute acceleration response for both optimal dynamic absorbers in shock test, in terms of vibration suppression both dynamic absorbers produce a similar factor compared to original PCB design.

6.3 Concluding remarks

This experimental work has clearly demonstrated the effectiveness of using a dynamic ruggedizer to minimise the dynamic response of sensitive components for military electronic equipment operating in harsh environmental conditions. Implementation of dynamic ruggedizer does not require drastic modification or redesign of internal components or mounting configurations, only slight modification is required.

Close correlation of the experimental and the theoretical results indicated accurate modelling of an actual system. Hence, optimisation of dynamic absorber properties and their impact on PCB response can be pre-determined theoretically before actual implementation. Although η_{opt} is an optimal point, a smaller dynamic absorber design will be highly possible within the constraint for allowable space. This clearly illustrates the effectiveness of reducing the mass ratio to 35%, which increases the natural frequency, but reduces the loss factor, and actual mass as established in the theoretical prediction. Although this shows greater improvement in terms of size, and demonstrates the same vibration protection analogy, the only drawback is in terms of performance of the PCB, but it seems to be insignificant in this experimental study.

6.4 Some practical considerations

- Dynamic absorber design must have the "tuneable" characteristics in accordance with the dynamic properties of the original PCB.
- The design of a dynamic absorber has to be compact and flat.
- The PCB has to be designed to allow attachment of a dynamic absorber somewhere in the centre of the PCB away from edges-guide and connectors.
- Such a dynamic absorber may by used for flat screens, walls of cabinets and enclosures instead of stiffening ribs and damping treatment.

However, it is known that the widely used visco-elastic grommets tend to stiffen and gain damping at low temperatures and soften and lose damping at elevated temperatures. These variations make it impossible to keep optimised configuration in actual airborne applications. Most probably, the all-metal design, such as Metal & Mesh Bushing (see http://barrymounts.com) are the only feasible solutions. These are especially designed to withstand the serve environmental conditions while showing the persistence of the visco-elastic parameters in a wide temperature range (-400°F to + 700°F). Upon the completion of this experimental work, the all-metal dynamic absorber was manufactured and tested. The design phase of this dynamic absorber is similar to that of the grommet design and is shown in Figure 6.21. This dynamic absorber has almost the same characteristics as from the above dynamic absorber, however, it exhibits a small degree of nonlinearities at different excitation levels as shown in Figure 6.22, but this does not seem to have much influence on the optimal performance of the PCB, say, sensitivity analysis.

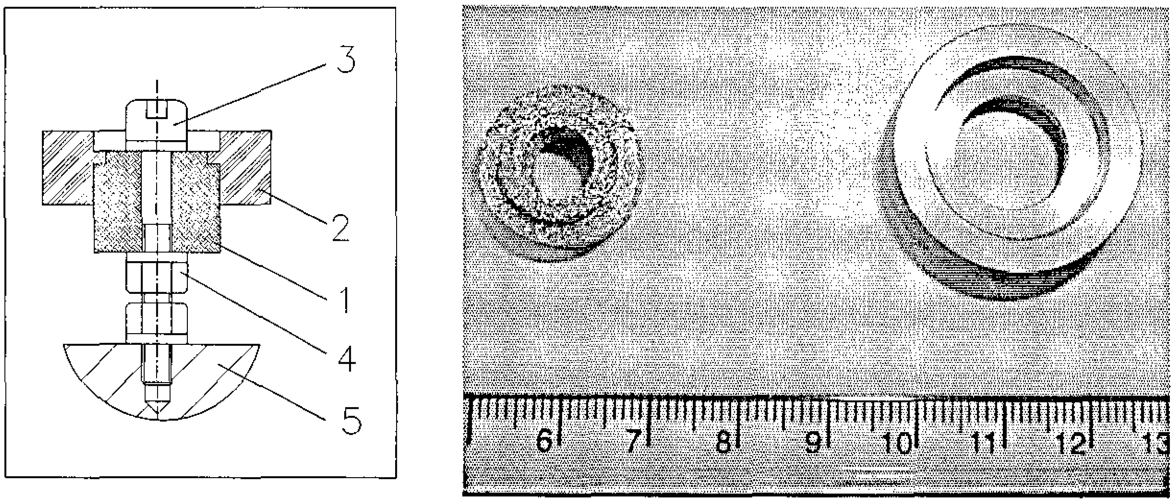

a) Schematic layout of dynamic absorber
(① wire mess bushing, ② inertia,
③ bolt, ④ nut, ⑤ fixture)

b) Detailed assembly

Figure 6.21. All-metal dynamic absorber

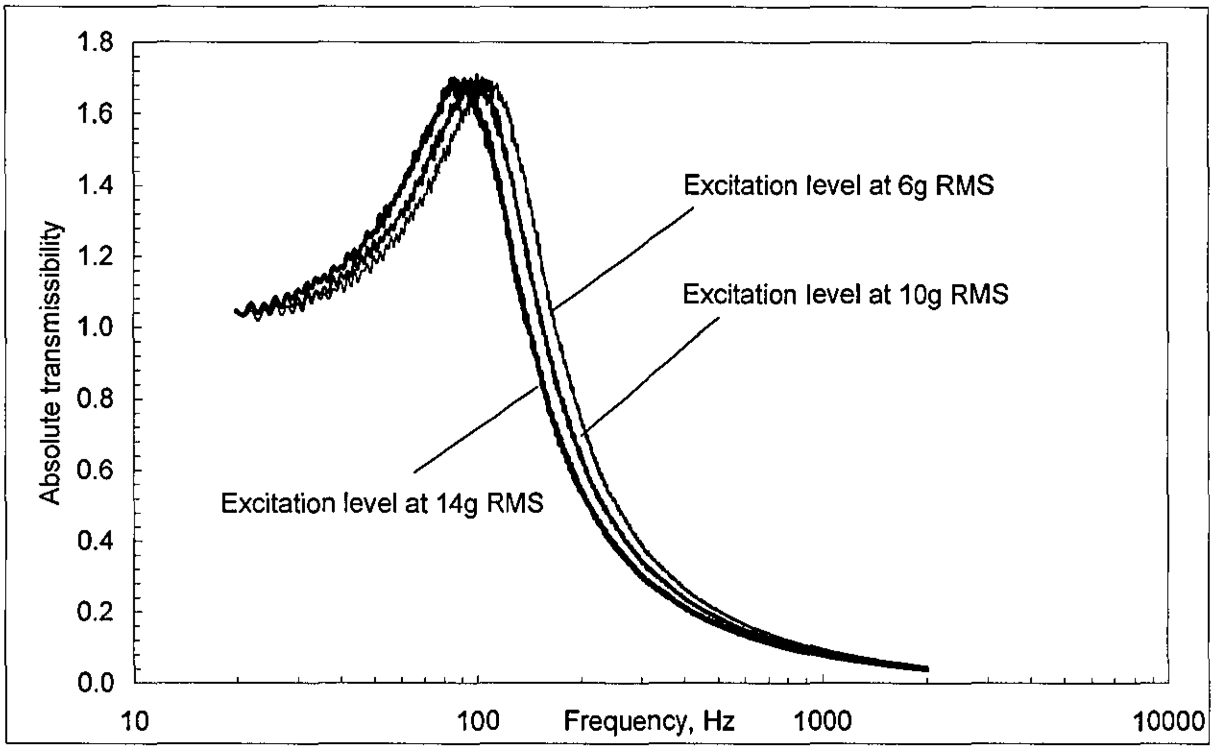

Figure 6.22. Absolute transmissibility of all-metal dynamic absorber

The experimental work for the combined system was carried in the same manner as compared to Section 6.2. Similarly, the all-metal dynamic absorber was attached on the PCB at point ⓪ and experienced at the random vibration level (14g RMS). As a result, the dynamic response of the modified can be seen in Figure 6.23, also in this figure the response of the original PCB and that modified PCB using the visco-elastic grommet absorber are superimposed for reference. As can be seen, at a similar mass ratio (η_{opt} = 65%) both absorbers have the same ability to suppress almost critical resonant frequencies of the original PCB except the level of "smoothness".

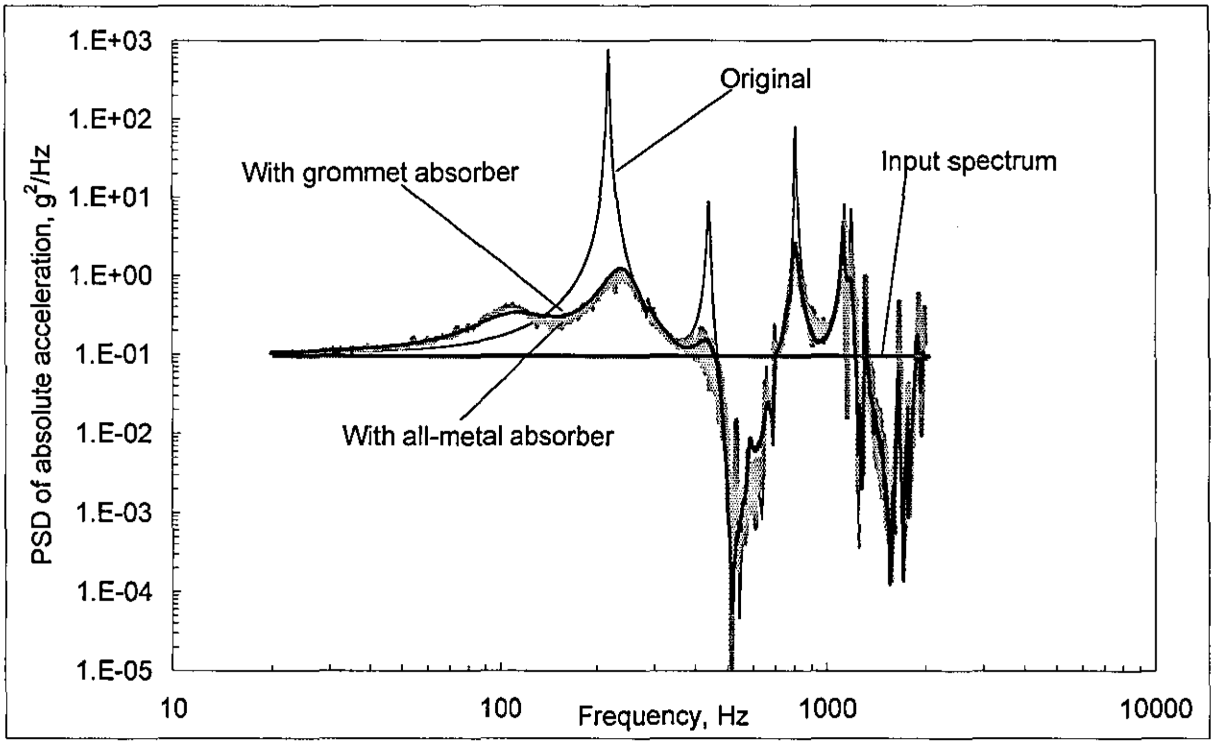

a) PSD of absolute acceleration

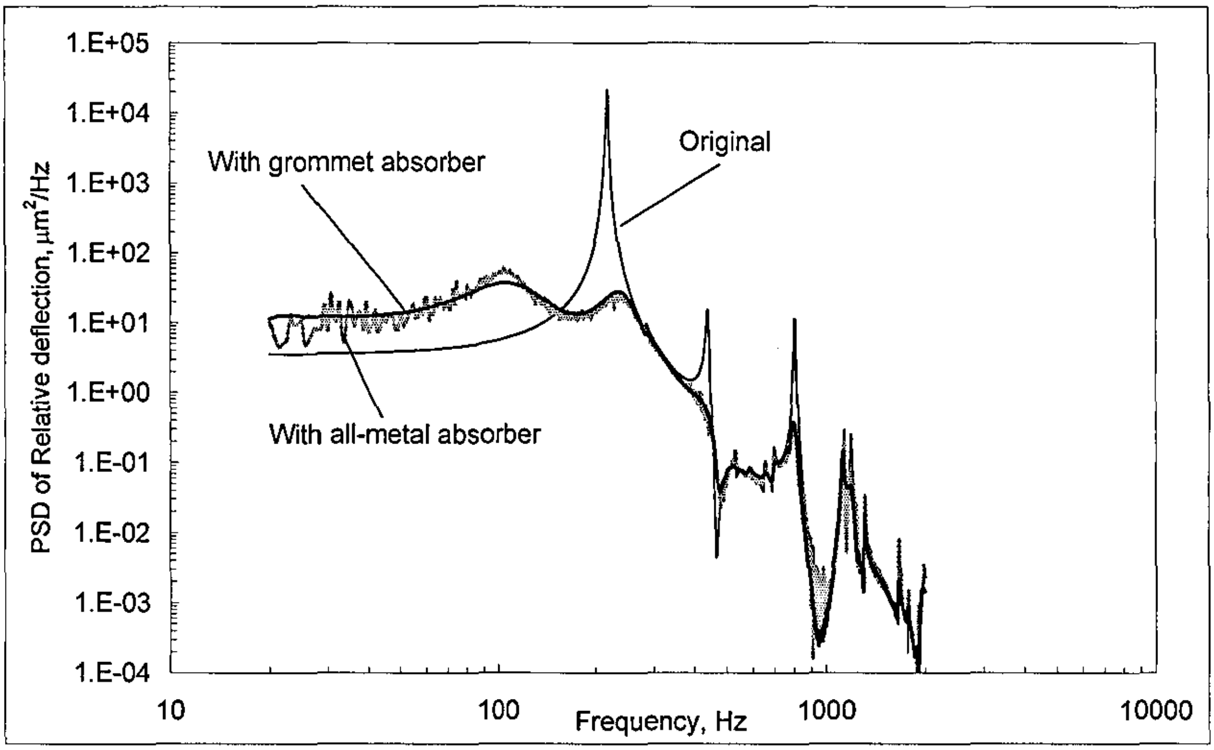

b) PSD of relative deflection

Figure 6.23. Comparison of dynamic response of the modified PCB in the case all-metal and grommet dynamic absorber

Further experimental work could be carried using the all-metal absorber, typically, under shock and swept-sine excitation. However, this would lead to excessive work due to the fact that both dynamic absorbers have almost the same characteristics at ambient temperature.

6.5 Experimental validation for impact damper

To support the impact damper study, the experiment is carried out with the use of a "rattling" ball bearing (approximately 40 gr) which provides an adequate clearance, inertia and low restitution ratio, the essential ingredient of impact damper device, beside, it provides the lowest cost solution and is widely available. However, the accuracy value of these dynamic properties is impossible to determine through experimentally measured absolute transmissibility alone or by any means of standard measurement technique. Indeed, this device can be considered a "black box" and totally immune to temperature variation. Since the dynamic behaviour of the bearing is classified as a loose mass and is highly sensitive to the level of excitation, it might lead to some difficulties of deciding on the "right" parameters, also the accuracy of these parameters are not required whereas the clearance is critical, say, sensitivity analysis. In order to avoid these problems, the experimental work is carried out directly in where the inner ring of the bearing is rigidly clamped on the PCB, at observation point © as shown in Figure 6.24.

The dynamic behaviour of the combined system is now highly nonlinear. The experimentally measured universal transmissibility between random and swept-sine tests would be in different response shapes. For this reason, the Electrodynamic Shaker is firstly programmed with random vibration at level (14g RMS) in the frequency range of 20-2000 Hz with "flat" PSD spectrum. Finding an optimal clearance and hence performance (if the gap is too large) can be achieved by tightening the copper wire which runs between the inner and outer ring (see Figure 6.25). This technique would, somehow, produce an additional friction feature between components, which was a beneficial factor for vibration suppression.

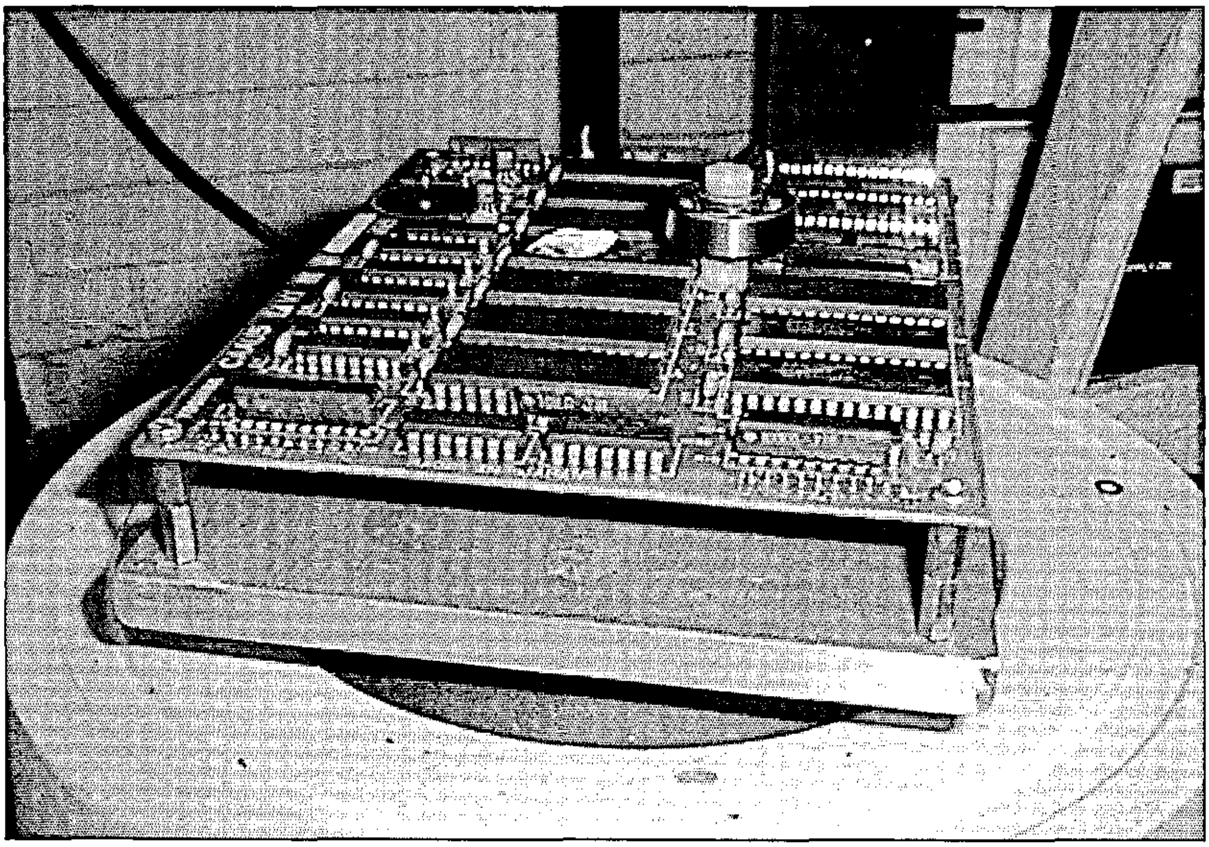

Figure 6.24. Ball bearing mounted on PCB for studying impact damper behaviour

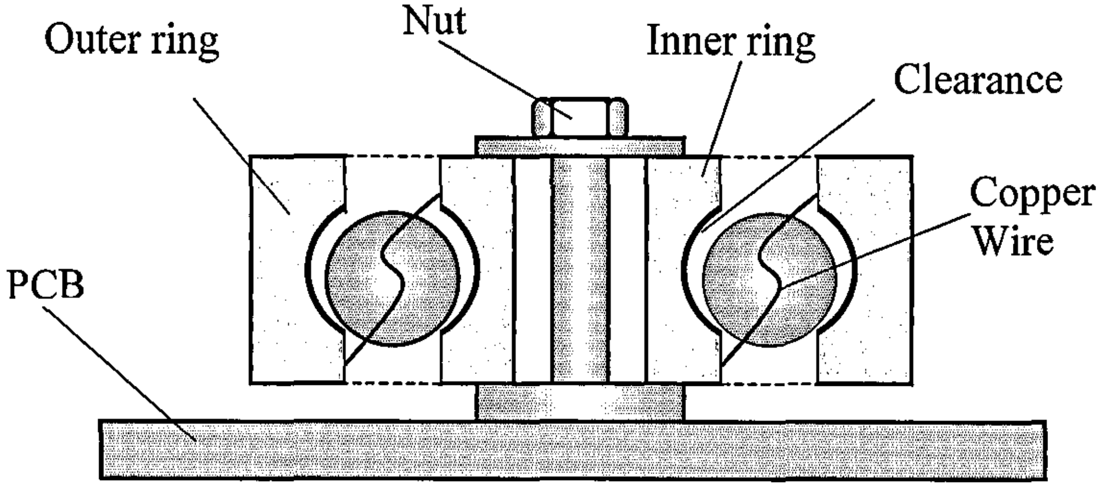
Outer ring
Nut
Inner ring
Clearance
Copper Wire
PCB

Figure 6.25. All-metal impact damper

Figure 6.26b shows the experimental analyser screenshot of absolute transmissibility of the combined system. As can be seen, the response signal is highly contaminated with noise, particularly at antiresonant notches although the frequency resolution is stepped up to 2.5 Hz. Indeed, contact between components can be classified as hard collision.

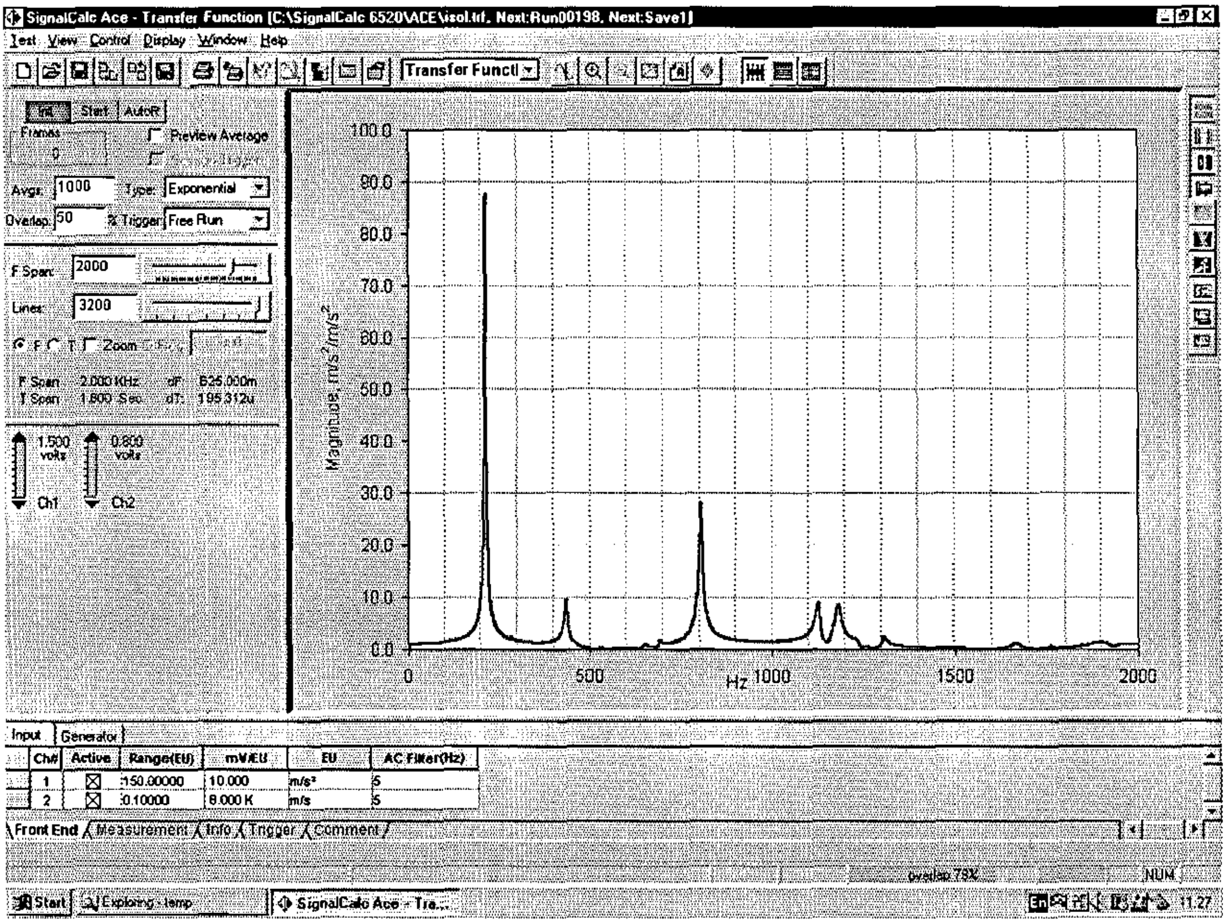

SignalCalc Ace - Transfer Function [C:\SignalCalc 6520\ACE\isol.trf, Next:Run00198, Next:Save1]

Frames 0

Avgs: 1000 Type: Exponential

Overlap: 50 % Trigger: Free Run

F Span: 2000

Lines: 3200

F Span 2.000 KHz dF: 625.000m

T Span 1.600 Sec dT: 195.312u

1.500 volts Ch1

0.800 volts Ch2

Ch#	Active	Range(EU)	mV/EU	EU	AC Filter(Hz)
1	☒	150.00000	10.000	m/s²	5
2	☒	0.10000	8.000 K	m/s	5

Test View Control Display Window Help
Transfer Functi
Init
Start
AutoR
Preview Average
F
T
Zoom
Input
Generator
Front End
Measurement
Info
Trigger
Comment
overlap 78%
NUM
Start
Exploring - temp
SignalCalc Ace - Tra...
11:27
Magnitude, m/s²/m/s²
100.0
90.0
80.0
70.0
60.0
50.0
40.0
30.0
20.0
10.0
0.0
0
500
Hz 1000
1500
2000

a) Original PCB

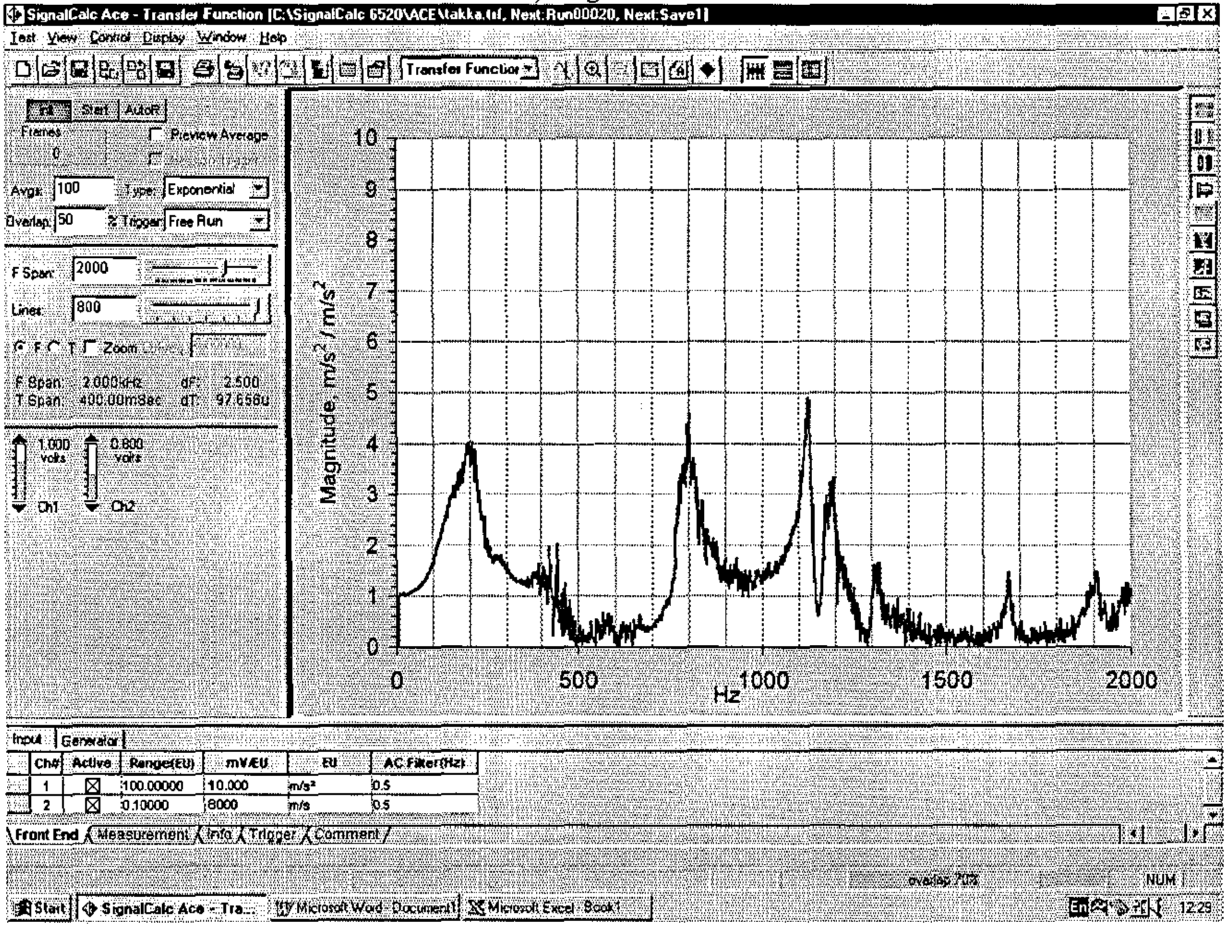

SignalCalc Ace - Transfer Function [C:\SignalCalc 6520\ACE\takka.trf, Next:Run00020, Next:Save1]

Frames 0

Avgs: 100 Type: Exponential

Overlap: 50 % Trigger: Free Run

F Span: 2000

Lines: 800

F Span: 2.000kHz dF: 2.500

T Span: 400.00mSec dT: 97.656u

1.000 volts Ch1

0.800 volts Ch2

Ch#	Active	Range(EU)	mV/EU	EU	AC Filter(Hz)
1	☒	100.00000	10.000	m/s²	0.5
2	☒	0.10000	8000	m/s	0.5

Test View Control Display Window Help
Transfer Function
Init
Start
AutoR
Preview Average
F
T
Zoom
Input
Generator
Front End
Measurement
Info
Trigger
Comment
overlap 70%
NUM
Start
SignalCalc Ace - Tra...
Microsoft Word - Document1
Microsoft Excel - Book1
12:29
Magnitude, m/s² / m/s²
10
9
8
7
6
5
4
3
2
1
0
0
500
Hz 1000
1500
2000

b) Modified PCB

Figure 6.26. Analyser screenshot of absolute transmissibility under random vibration

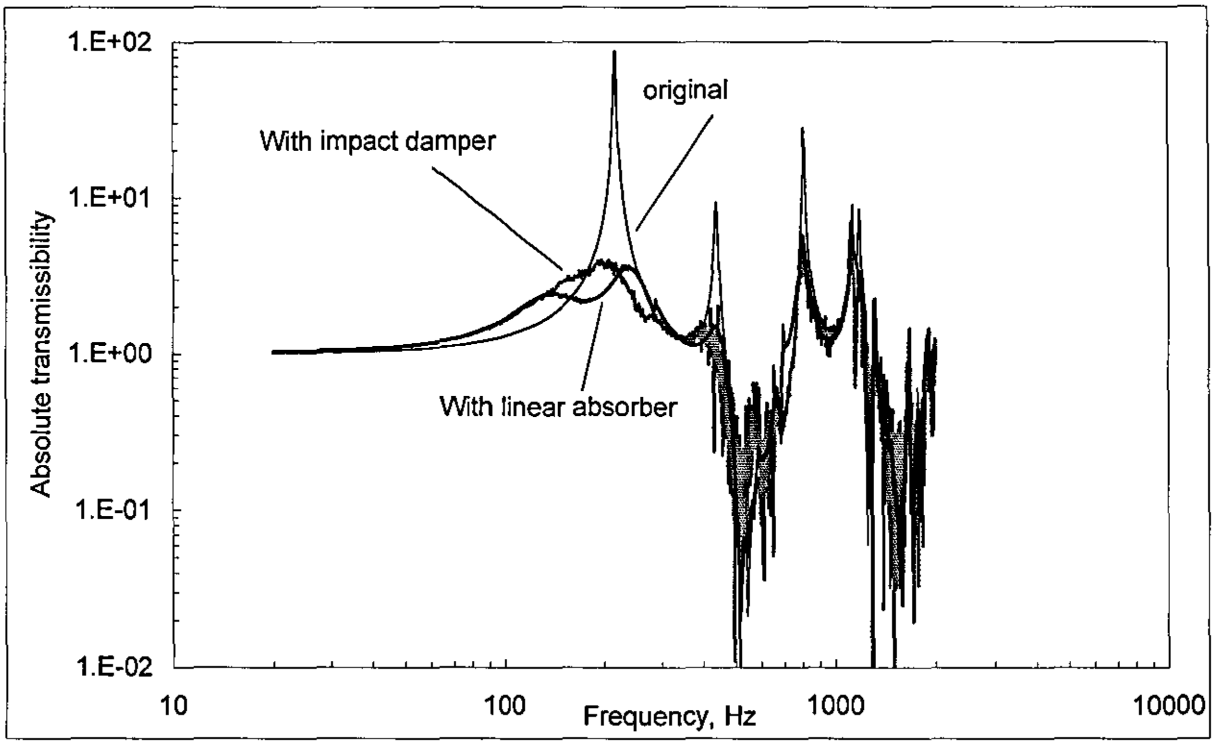

Figure 6.27. Experimentally measured absolute transmissibility of original and modified PCB

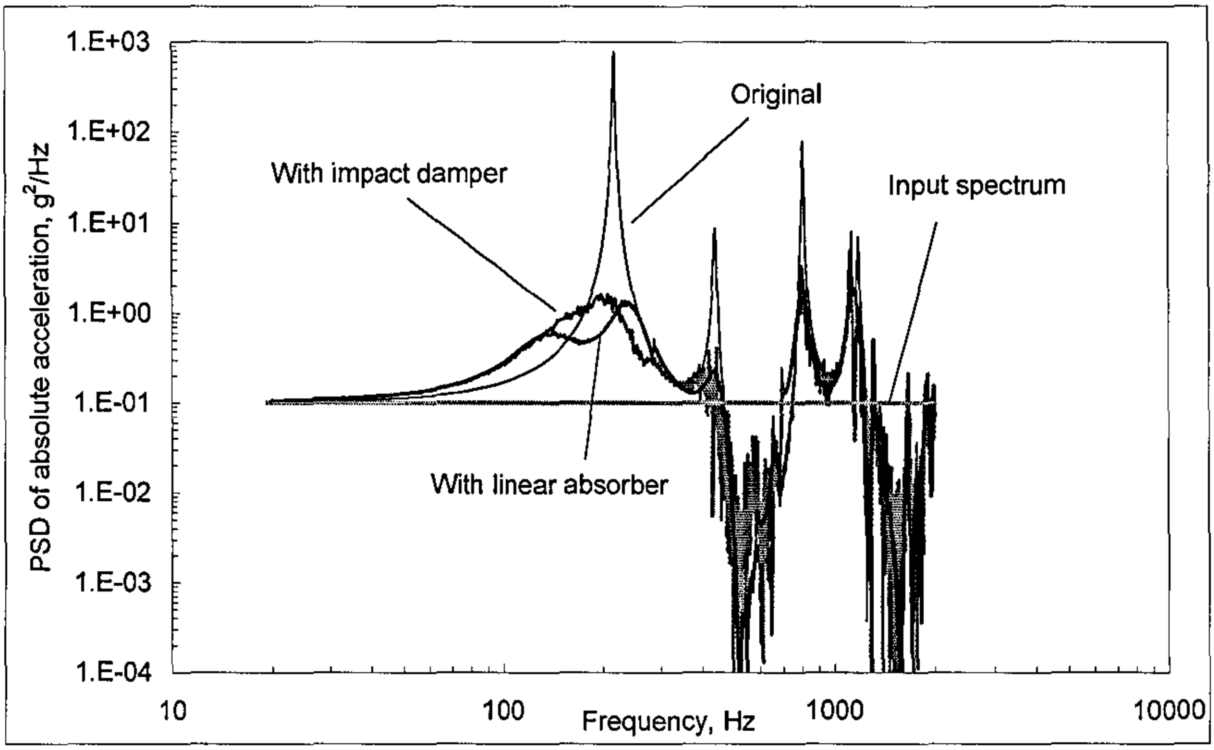

Figure 6.28. Experimentally measured PSD of absolute acceleration of original and modified PCB

Figure 6.27 shows the superimposed experimentally measured absolute transmissibility of the original and modified system. As shown, the impact damper has the capability of suppressing the first resonant peak of the PCB as well as its neighbour resonant frequencies while "filling" the antiresonant notches with noise as numerically predicted. The experimental absolute transmissibility of the ruggedized PCB with the use of linear dynamic absorber (31.5 gr) is superimposed for reference. It clearly shows that both techniques equally well suppress all resonances of the original PCB except the noise level.

For comparison purposes, an appropriate nonlinear PSD is measured, since the system is under full level of excitation (14g RMS), as has been used for linear case, therefore, it is reasonable to superimpose its corresponding PSD curve to those obtained in linear dynamic absorber case at a similar mass ratio. The result of PSD of absolute acceleration between linear dynamic absorber and impact damper together with the original PCB can be seen in Figure 6.28. Both techniques produce a similar reduction ratio close to 3-fold vibration suppression as compared to the original PCB design.

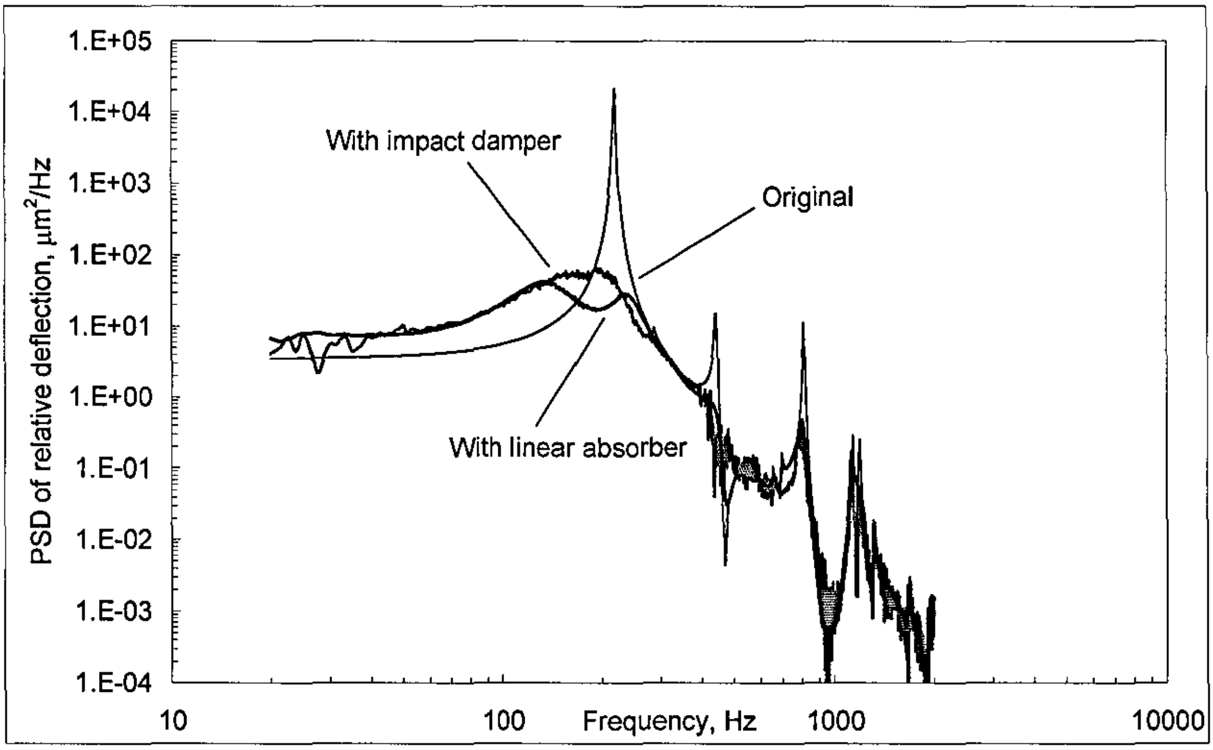

Figure 6.29. Experimentally measured PSD of relative deflection of original and modified PCB

Figure 6.29 shows the PSD of relative deflection of modified PCB which produced an overall value of 95 μm RMS, about 3.3 reduction factor compared to the original response, 312 μm RMS and 15.8 μm RMS higher than linear case (79.2 μm RMS) at about the same mass ratio, see the curve labelled as **Original** and **With linear dynamic absorber** reference.

Providing the desired clearance of the impact damper device. The Electrodynamic Shaker is programmed to perform the swept-sine test from 10 to 500 Hz at a constant magnitude of acceleration 10g with linearly sweep rate of 5 Hz/s. This allows further study of the influence of such a device on the PCB in sine vibration environment. The analyser screenshot, Figure 6.30b is best to represent the dynamic response of the combined system under such a test.

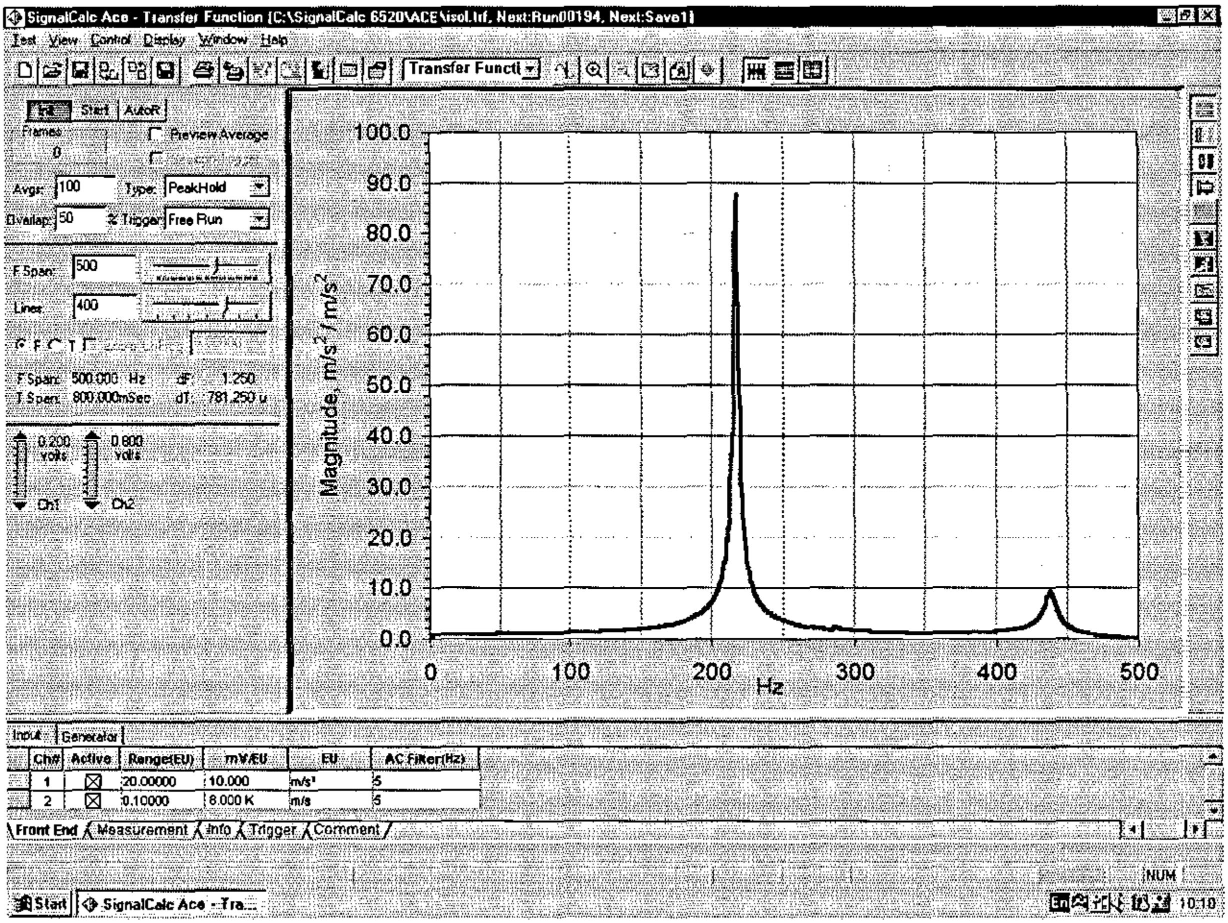

SignalCalc Ace - Transfer Function [C:\SignalCalc 6520\ACE\isol.trf, Next:Run00194, Next:Save1]

Frames: 0

☐ Preview Average

Avgs: 100 Type: PeakHold

Overlap: 50 % Trigger: Free Run

F Span: 500

Lines: 400

F Span: 500.000 Hz dF: 1.250

T Span: 800.000mSec dT: 781.250 u

0.200 volts Ch1

0.800 volts Ch2

Ch#	Active	Range(EU)	mV/EU	EU	AC Filter(Hz)
1	☒	20.00000	10.000	m/s²	5
2	☒	0.10000	8.000 K	m/s	5

Test
View
Control
Display
Window
Help
Transfer Functi
Start
AutoR
Magnitude, m/s² / m/s²
100.0
90.0
80.0
70.0
60.0
50.0
40.0
30.0
20.0
10.0
0.0
0
100
200
300
400
500
Hz
Input
Generator
Front End
Measurement
Info
Trigger
Comment
NUM
Start
SignalCalc Ace - Tra...
10:10

a) Original

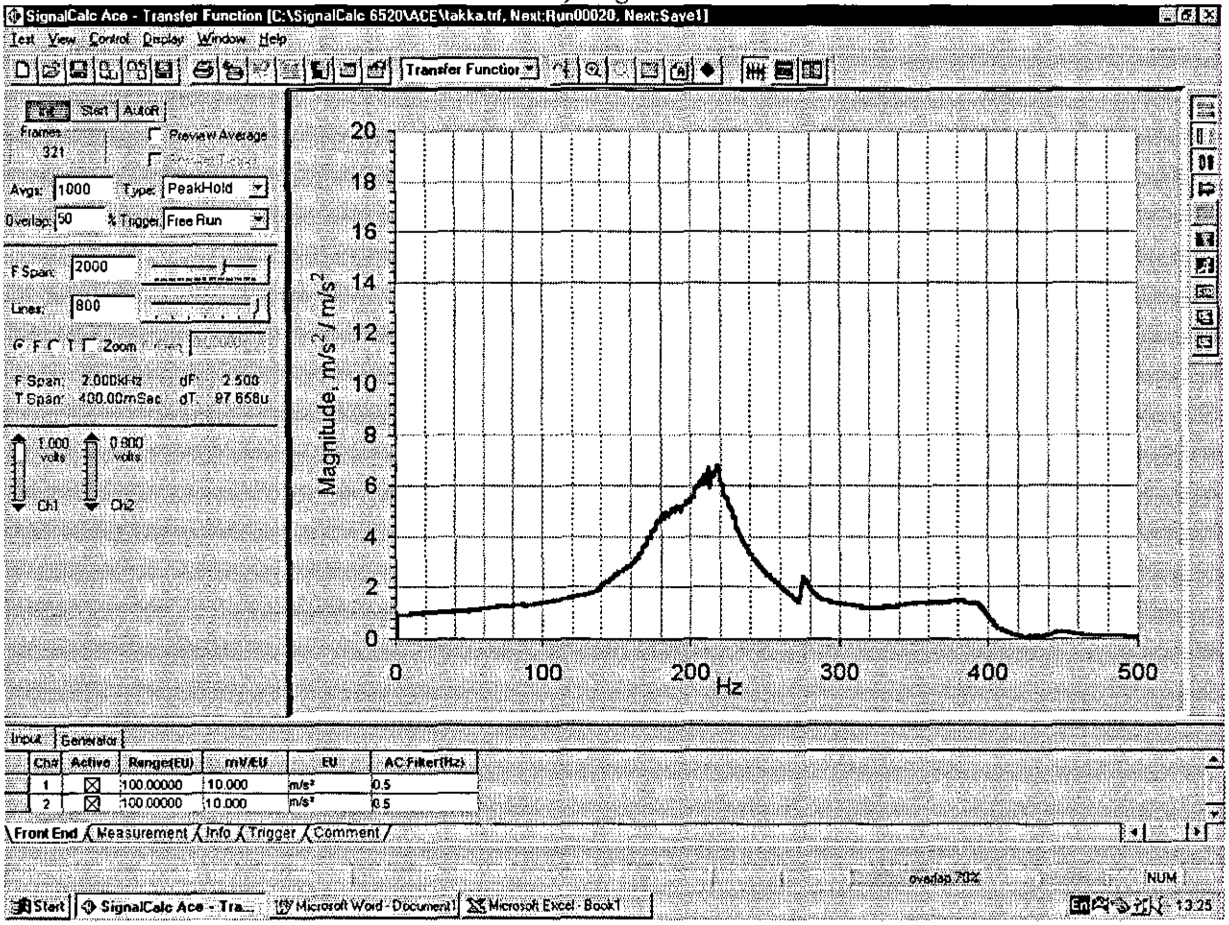

SignalCalc Ace - Transfer Function [C:\SignalCalc 6520\ACE\takka.trf, Next:Run00020, Next:Save1]

Frames: 321

☐ Preview Average

Avgs: 1000 Type: PeakHold

Overlap: 50 % Trigger: Free Run

F Span: 2000

Lines: 800

F Span: 2.000kHz dF: 2.500

T Span: 400.00mSec dT: 97.658u

1.000 volts Ch1

0.800 volts Ch2

Ch#	Active	Range(EU)	mV/EU	EU	AC Filter(Hz)
1	☒	100.00000	10.000	m/s²	0.5
2	☒	100.00000	10.000	m/s²	0.5

Test
View
Control
Display
Window
Help
Transfer Function
Start
AutoR
Zoom
Magnitude, m/s² / m/s²
20
18
16
14
12
10
8
6
4
2
0
0
100
200
300
400
500
Hz
Input
Generator
Front End
Measurement
Info
Trigger
Comment
overlap 70%
NUM
Start
SignalCalc Ace - Tra...
Microsoft Word - Document1
Microsoft Excel - Book1
13:25

b) Modified

Figure 6.30. Analyser screenshot of absolute transmissibility of original and modified PCB under swept-sine vibration

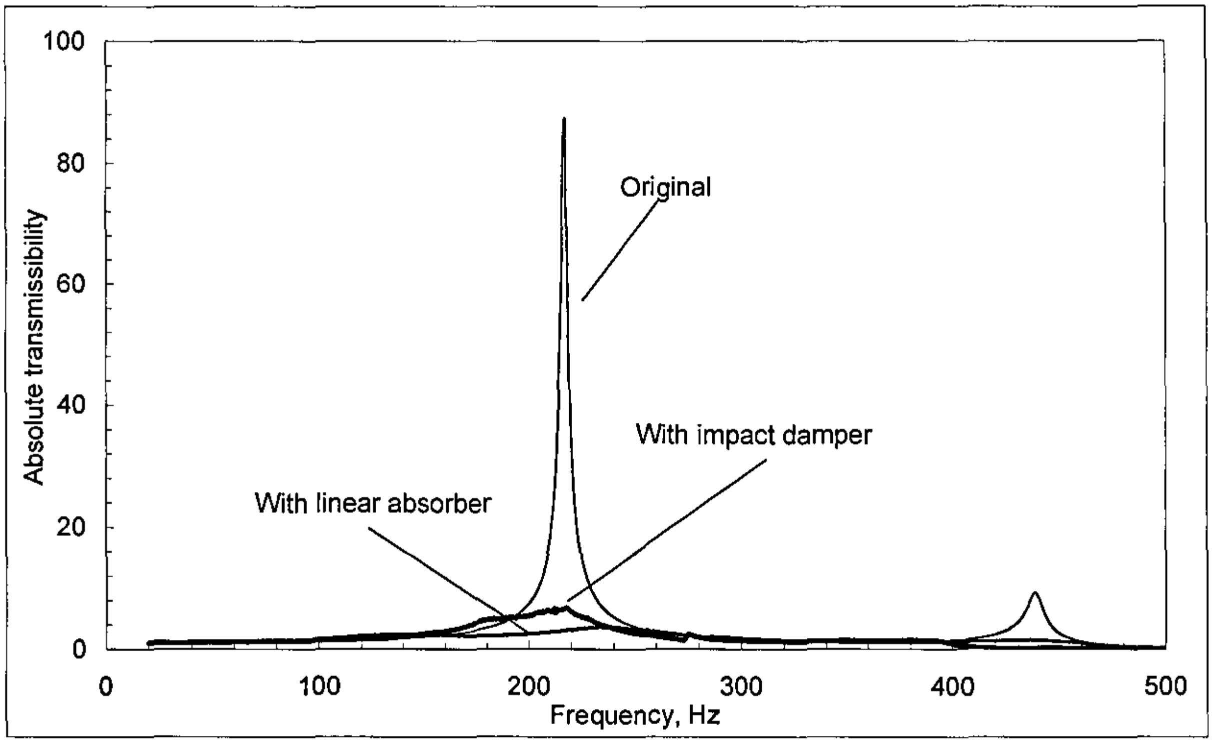

a) Absolute transmissibility

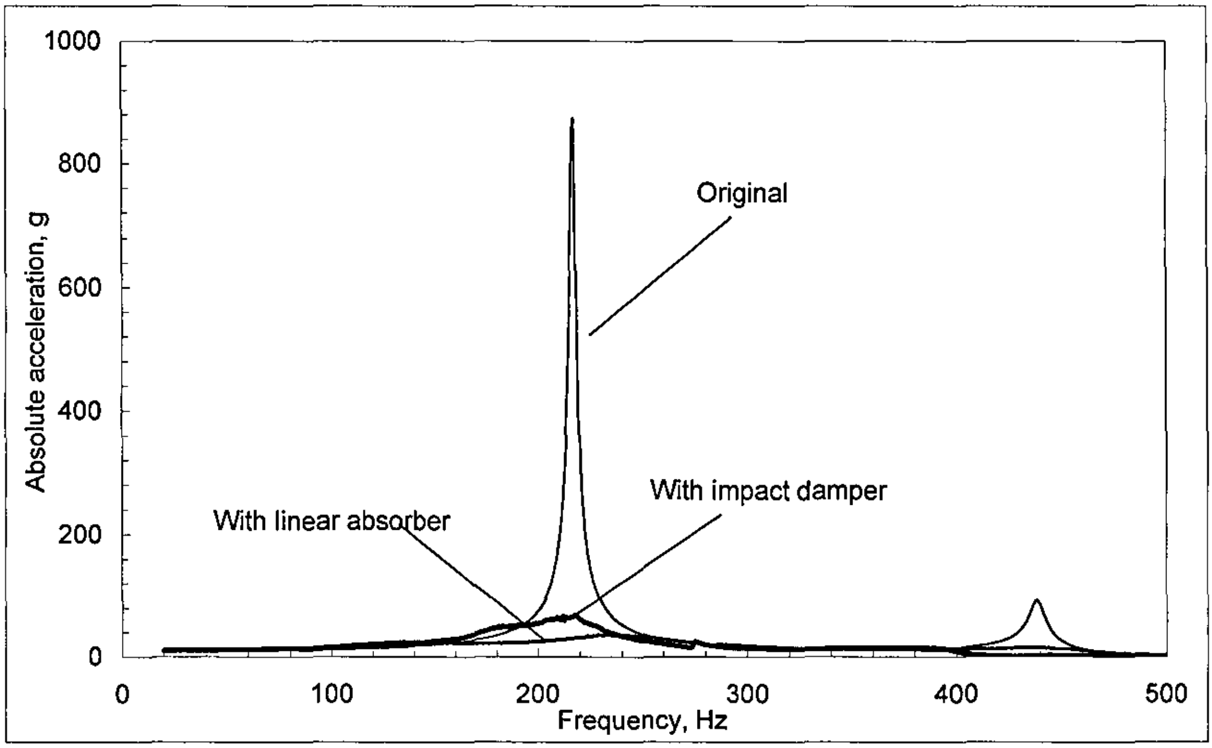

b) Absolute acceleration

Figure 6.31. Experimentally measured absolute transmissibility and acceleration of original and modified PCB

Figure 6.31 shows the superimposed absolute transmissibility and acceleration of original and modified PCB, respectively, the application of impact damper produces 15-fold vibration suppression at resonant frequency as compared to its original design. However, unlike linear systems, this reduction ratio does not remain constant in varied excitation level.

The described situation from above would also apply for relative deflection of the modified PCB. Nonetheless, at this fixed level of excitation a similar value, 15-fold vibration suppression is found for relative deflection, see Figure 6.32 for reference.

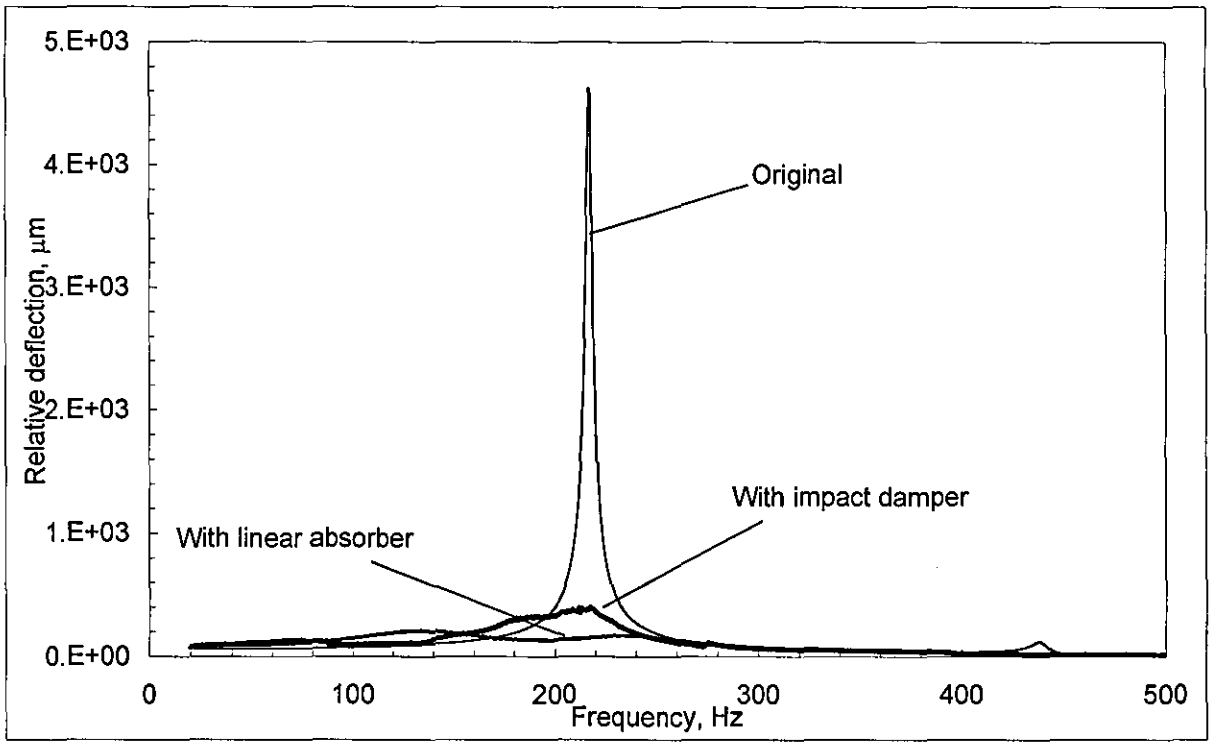

Figure 6.32. Experimentally measured relative of original and modified PCB

It is interesting to notice that there is no "jump phenomena" and "frequency pulling" occurring in the system response during frequency sweep-up this is due to the critical choice of clearance and probably from the contribution of low restitution ratio and friction between components.

Since, it is impossible to have massless inner ring of the ball bearing. Therefore the natural frequency of the modified system is slightly shifted to the left as shown in the result of the experimental data, Figure 6.32. If we then consider this alternative approach for vibration suppression it is necessary to have a smaller mass of inner ring.

This experimental work mainly addressed the principle of impact damper as part of vibration protection. The attainable performance of the PCB was achieved by adjusting the clearance of the "broken" ball bearing, providing the fixed vibration condition. Under extreme condition, say, temperature variation or considering cost effective solution and survivability, this could be an alternative method to protecting the PCB. However, the drawback is its sensitive performance.

7.0 Conclusions

This project has clearly demonstrated the effectiveness of using dynamic ruggedizing technique to minimise the response of sensitive components in military airborne equipment under harsh vibration environment. The solution proposed utilising dynamic absorber and impact damper against harsh vibration involving the reduction of vibration was considered in depth. It has clearly illustrated the elimination to an acceptable amount of vibration in which the cost is also compromised.

The author has shown theoretically and experimentally that the optimised linear damped and nonlinear vibroimpact dynamic absorbers can essentially suppress the dynamic responses and, therefore, increase the life of sensitive commercially-off-the-shelf PCBs operating in harsh environmental conditions under shock, wide-band random and swept sine vibration. From the conducted analysis, the optimal linear and nonlinear absorbers yield almost similar dynamic performance.

Implementation of such dynamic absorbers does not require a drastic increase in mass and dimensions, modification or redesign of commercially-off-the-shelf PCBs along with their mounting configuration and might be thought of as a prospective alternative/supplement to the existing methods of increasing reliability of sensitive electronic equipment. Further efforts should be aimed at developing compact, cheap and easily tuneable dynamic absorbers maintaining the consistent properties over a wide range of ambient temperatures and lifetime.

The choice of the all-metal design, Metal & Mesh Bushing type dynamic absorber (available off-the-shell offers significant improvements over the use of conventional rubber or plastic dynamic absorber. In particular, the non-temperature dependence of the dynamic properties so such material eliminates problems associated with the extreme temperature range of operation, and the vastly improved fatigue life minimises maintenance costs.

In general, the optimal linear absorber can be considered one of the best candidates of vibration suppression for sensitive electronic equipment harsh vibration environment. Due to the constraint in the electronic box, the dynamic absorber with a smaller mass ratio was designed and it was offered similar improvement over the optimally designed absorber that governs the same vibration protection analogy. The miniature dynamic absorber would be able to perform well in a small space.

The proposed optimising technique for linear dynamic absorber is very simple, there were no mathematical complication involved. The optimal dynamic absorber design has shown its superior as compared to the traditional one in term of performance, as shown, for a specific application such as the PCB, the design performance is improved by 5% in term of overall relative deflection under random vibration and 32% in peak relative deflection under swept-sine vibration. Therefore, using a common method for solving optimal dynamic absorber may not be relevant for any specific application even it is a simple device.

The novel optimising technique with the used of MS®Excel and its Solver may prove to be the most advantage technique to solve linear complex dynamic systems, typically to those systems with the unknown original mathematical model, only a set of measurement data is required. Further more, this package has shown its ability to obtain all modal parameters of a complex dynamic system such as the PCB whereas the traditional approach may prove to be complexity.

Numerical simulation using Matlab/Simulink proves to be very powerful and consistent to solve linear and nonlinear dynamic systems, additionally, it does not require solving complex mathematics only a simple set equations of motion are required.

The original objective of the Thesis–to provide recommendation for the design of a passive shock and vibration protection system-has been achieved through the analysis carried out. The design steps can be followed through for any similar system or environmental loading and the dynamic absorber's properties re-optimised. In fact when the spreadsheet described has been set up, it is a trivial matter of changing three or four numbers and running the Solver to optimise any combination system.

8.0 Suggestions for further work

The main objective of this study was design an dynamic absorber for optimal overall relative deflection of the PCB, as a result, the reduction ratio with a factor 4 was achieved whereas the overall absolute acceleration with a factor of 3 was obtained under a typical random vibration. This significant difference indicates the absorber may not be at its "best" universal performance. In some cases, it would be desirable to design a dynamic absorber that equally well suit both applications which would give a same reduction ratio as compared to its original design. By carrying out the analysis above, based on the principle outlined, the dynamic characteristics of the dynamic absorber would differ to match the optimal point of for any environmental condition. In this particular, the theory full-mode model and novel optimising technique may be the best case for designing such a dynamic absorber.

The use of absorbers for the vibration protection of PCBs has been validated by this project. The methods used to achieve this can be readily adapted for a multitude of other tasks. There are opportunities to use this technique in the protection of other sensitive components. Strictly speaking, hard disk drive is very susceptible towards shock and vibration. It would be desirable to perform testing on hard disk drive with the application of dynamic absorber.

9.0 References

1. E. JASSON 2000 COTS Journal. Shock and Vibration Isolator for COTS equipment, http://www.rtcgroup.com/cotsjournal.
2. D. S. STEINGBERG 1988 *Vibration analysis for electronic equipment.* New York: John Wiley and Sons, Inc.
3. Military Standard, Environmental Test Methods, MIL–STD-810E 1988 *Department of Defence, Washington, DC.*
4. Shock and Vibration : http://www.chassis-plans.com/html/shock_and_vibration.html. .
5. A.M.VEPRIK & V. I. BABITSKY *2000 Journal of Sound and Vibration* 298, 22-30, Vibration protection of sensitive electronic equipment from harsh harmonic vibration.
6. A.M.VEPRIK & V. I. BABITSKY *2000 Journal of Shock and Vibration.* Vibration Isolation of Infrared Package.
7. C. STAHLE 1989 *Pioneering Damping in Space*, Proceeding of Damping 89. Flight Dynamic Laboratory of Air Force Wright Aeronautical Laboratories.
8. D. J. MEAD 1999 *Passive vibration control.* New York: John Wiley and Sons, Inc.
9. C. SNOWDON 1977 *Vibration and Shock in Damped Mechanical System.* New York: John Wiley and Sons, Inc.
10. STRAZNICKY Nov/Dec 2000 *COTS journal* Designing Harsher Environment Circuit Boards *http://www.rtcgroup.com/cotsjournal* .
11. V. ROGOV AND B. DAVISON March 2001 *COTS journal.* Vibration Test and Analysis, Test & Screening, , *http://www.rtcgroup.com/cotsjournal* .
12. S LA MALFA, P.A.A LAURA, C.A. LROSSIT AND O. ALVAREZ 2000 *Journal of Sound and Vibration*, 230 721-724. Use of dynamic absorber in the case of a vibrating printed circuit board of complicated boundary shape.
13. J. ORMONDROYD and J.P.DEN HARTOG 1928 *Transaction of ASME* 50, 9-22. Theory of the dynamic absorber.
14. G. B. WARBURTON AND E.O. AYORINDE 1980 *Earthquake Engineering and Structure Dynamic* 8, 197-217. Optimal absorber parameters for simple system.
15. Y. Z. WANG & S.H. CHENG 1989 *Applied Acoustic* 28, 67-78. The optimal design of dynamic absorber in the time domain and the frequency domain.

16. B.G. KORENEV AND L.M.REZNIKOVE 1993 *Dynamic Vibration Absorber*. Theory and Technical Application. Chichester: John Wiley and Sons, Inc.

17. H. NISHIMURA, K. YOSHIDA AND T.SHIMOGO 1989. JSME *International Journal* 32, 373-379. Optimal dynamic vibration absorber for multi-degree-of-freedom system (Theoretical consideration in the case of random input).

18. L. KITIS, P. B WANG AND W. D. PILKEY 1983 *Journal of Sound and Vibration* 89, 559-569 Vibration reduction over a wide frequency range.

19. DOMINGOS AND S. VALDER 2000 *Mechanical System and Signal Processing* 14, 679-690. Optimisation of Dynamic Vibration Absorber Over a Frequency Band.

20. V I BABITSKY 1998 *Theory of Vibro-Impact system and applications*; Springer; Translated from Russian (Nauka, Moscow, 1978) by N. Birket.

21. C N BAPAT AND C BAPAT 1988 *Journal of Sound and Vibration*, 120(1):53-61. Impact-pair under periodic excitation.

22. T. KOTERA 1996; Chaotic motion in a vibro-impacting system; EUROMECH - 2nd European Nonlinear Oscillation Conference, Prague, Sept 9-13; Vol 1 p223-8.

23. C N BAPAT AND S SANKAR 1985 *Journal of Sound and Vibration*, 99(1):85-94. Single unit impact damper in free and forced vibration.

24. S. CHATTERJEE, A K MALLIK AND A GHOSH 1995; *Journal of Sound and Vibration, 187(3):403-420.* On impact dampers for non-linear vibrating systems.

25. S. F. MASRI 1967. *Journal of Engineering for Industry, Transactions of ASME*, 89:658-660. discussion on 'An investigation of an impact vibration absorber' by Egle (1967a).

26. M. M. NIGM AND A. A. SHABANA 1983 *Journal of Sound and Vibration*, 89(4):541-557. Effect of an impact damper on a multi-degree of freedom system.

27. S E SEMERCIGIL, N POPPLEWELL AND R TYC 1988 *Journal of Sound and Vibration*, 122(1):178-184. Impact damping of random vibrations.

28. L. PAGET 1937. *Engineering143:305-7*. Vibration in steam turbine buckets and damping by impact.

29. R. S. HAHN. 195. Trans. Am. Soc. Mech. Engrs; 67, 523-30. Design of Lanchester damper for elimination of metal cutting chatter.

30. M. VEPRIK AND V.I. BABITSKY 2000 *Journal of Sound and Vibration,* 239(2): 335-356. Non-linear correction of vibration protection system containing tuned dynamic absorber.

31. D. INMAN 1996 *Engineering Vibration*: Prentice Hill Inc.

32. S. H. CRANDAL 1986 *Random Vibration*. New York: Academic Press.

33. J. L. SLOAN 1985 *Design and Packaging of Electronic Equipment*. New York. Van Nostrand Reinhold Company Inc.

34. V.V. BOLOTIN 1999 *Mechanics Of Fatigue,* CLC Press, pp 7, 30, 235.

35. W.T. Thomson 1993 *Theory of Vibration with Applications.* Chapman and Hall.

36. M. H. RICHARDSON AND D. L. FORMENTI 1985 *IMAC conference, Orlando, Fl.* Global curve fitting of frequency response measurement using the rational fraction polynomial method.

37. D.J. EWINS 1984 *Model testing. Theory and Practice*. (Taunton: Research Press).

38. B. STANBRIDGE AND D. J. EWINS 1995 *Proc. In. Forum on Aeroelasticity & Structure Dynamic, Manchester*. Structure modal analysis using a scanning laser Doppler vibrometer.

39. R. J. ALLEMANG, D. L. BROWN AND R. W. ROOT 1984 *Proceeding of the* 2^{nd} *International Modal Analysis Conference*. Multiple input estimation of frequency response functions.

40. V.I. BABITSKY, 1991 *Dynamic absorption of vibration*, in the handbook *Vibration and Impact Protection*, Ed. K.V. Frolov, *Vibration in Engineering*, Vol.6, Mashinostroenie, Moscow, (in Russian).